IJERT

ESDST - 2017

International Conference On Eco-sensitive Developments In Science And Technology

20th - 21st January, 2017

Organized by :

Baba Banda Singh Bahadur Engineering College

Conference Proceedings

Published By

International Journal of Engineering Research and Technology (www.ijert.org)

Slurry Erosion Wear Behavior of Stainless Steel SS-410 Coated with WC-12co by Detonation Gun Process

Ashish Kumar
JRF, Department of Mechanical Engg
Baba Banda Singh Bahadur Engineering College,
Fatehgarh Sahib

Manpreet Kaur
Associate Professor,
Department of Mechanical Engg
Baba Banda Singh Bahadur Engineering College,
Fatehgarh Sahib

Jasbir Singh Ratol
Workshop Superintendent
Baba Banda Singh Bahadur Engineering College,
Fatehgarh Sahib

***Abstract*- In the current investigation, cermet coating Tungsten carbide (WC-12Co) was deposited on hydro turbine stainless steel SS-410 by Detonation gun (D-gun) thermal spraying process. Subsequently, the slurry erosion behavior of the coated and bare steels was investigated using a Jet Type Erosion Test Rig. Silica sand was used as the abrasive media. Effects of concentration (ppm), particle sizes, jet velocity and impact angle on the slurry erosion behavior of coated and bare steels under different experimental conditions was studied. The weight of each specimen was measured before and after experimentation using electronic weighing machine. The analysis of slurry erosion behavior of samples was done by using Taguchi's methodology. The average weight reduction due to slurry erosion of coated samples is reduced by 70% from uncoated samples.**

Keywords: Erosion, Wear, Detonation gun process

I. INTRODUCTION

Erosion corrosion is a severe and complex degradation process in which mechanical and electrochemical events interact, causing material loss and component failure. The total material loss results from the sum of the individual contributions of mechanical and electrochemical degradation components and an additional term knows as synergistic or additive effect [1, 2]. Erosion and corrosion of materials cost a very high economic loss to every country. Slurry erosion is a serious problem in a number of Indian hydro power stations especially those located in Himalayan region. Therefore, due to heavy economic losses associated with slurry erosion, this problem has attracted the attention of the researchers worldwide [3]. Slurry erosion occurring as a result of high-velocity impact of hard and angular abrasive particles carried by water is a very common problem faced by the most of the hydropower plants. This problem becomes more severe during monsoon season for hydropower plants situated in the Himalayan region in India and often leads to shutdown [4, 5]. Thermal spray techniques are versatile means of developing a wide variety of coatings to enhance the performance and durability of engineering components exposed to the above said form of wear [6, 7]. Detonation gun (D-gun) spray process is a thermal spray coating process which gives an extremely good adhesive strength, low porosity, coating surface with compressive residual stresses, low oxide contents, and high inter splat strength [8, 9]. The D-gun spray process involves the entrainment of powdered materials with the high-velocity combustion products of a detonation wave as it propagates through a water-cooled barrel. The two-phase mixture of molten particles and detonation products exits the barrel and impinges against a target substrate, where the hot particles bond in overlaying platelets [10]. The evaluation of slurry erosion under actual service conditions is often a difficult task, because of interactive effects of different parameters, such as slurry concentration, velocity, and properties of abrasive medium on wear rate. Accelerated erosion testing of materials can be performed by increasing load, velocity, and other operational parameters in a laboratory test rig where real contact conditions can be simulated [11].

The aim of the current work is to investigate the slurry erosion behavior of D-gun-sprayed WC-12Co coatings on SS-410 steel under the hydro accelerated conditions by means of a jet erosion test rig, to explore the possibility of use of this coating system in actual hydraulic turbines.

II. EXPERIMENTATION

A. Substrate Material

SS-410 stainless steel, which is commonly used in hydropower plants, was selected as a substrate material for the research work These steels received in as cast form were machined and samples of size 15mm*15mm*5mm were prepared. The chemical composition of SS-410 in weight % is 0.15 C, 1 2.0 Si, 1.0 Mn, 0.45 Cr, 0.3 Ni, 18-20 P, 8-12 S and remaining Fe.

B. Coating Deposition

The WC-12Co powder was deposited onto hydro turbine steel using the commercially available detonation gun facility at SVX Powder M surface Engineering Private Limited, Noida, India. The thickness of coating is approximate 200 microns. Before the coating deposition, the polished steel samples were grit blasted using alumina particles of grit size 80.

C. Erodent

For testing purpose, silica sand particles were used as a erodent because silica sand is very hard. Silica sand of three particle sizes (BSS NO. 30, 45, 60) was taken.

D. Slurry-Erosion Testing

Slurry-Erosion Testing was done on a jet type slurry erosion test rig. It is a recirculating-type rig as shown in Figure 2.1.The measured quantities of water and sand are mixed in the tank to obtain the required concentrations of the slurry. The pyramidal-shaped tank does not provide any space for the sand particles to sediment as shown in Figure 2.1. In pyramidal shape tanks, the particles are easily facilitated to flow under gravity. The centrifugal pump used for slurry transportation is driven by a 7.5 H.P./1440 rpm electric motor. Slurry from the tank, sucked through a 100-mm G.I. pipe with the help of a pump, is delivered to the nozzle through 25-mm pipe with a set of control valves. Using these valves, the amount of slurry to pass through the 8-mm nozzle can be controlled easily. An electromagnetic- type flow meter is placed upstream to the nozzle to measure the amount of slurry passing through the nozzle. By using continuity expression, the relation between the velocity of the jet and the discharge indicated by flow meter was established. The holder used to hold the sample has been designed in such a manner to facilitate the variation of impact angle between the slurry jet and sample surface within an accuracy of ±1 deg. Using this specimen holder, it is possible to mount the sample at a desired impact angle ranging from 15 deg to 90 deg. The standoff distance between the nozzle and the specimen was kept fixed at 90 mm for all tests.

To measure the amount of erosion, the weight loss of the samples was measured using a precision weighing balance with 0.1 mg accuracy. All the samples were cleaned carefully with acetone prior to each weight measurement.

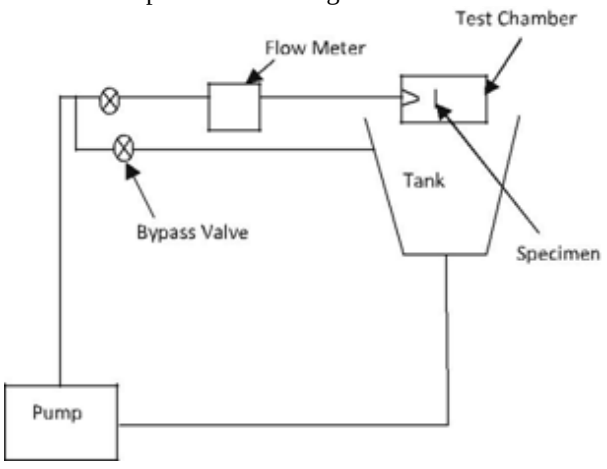

Fig. 2.1. Slurry erosion test rig developed for the current experimentation

E. Design of Experiment

The design of the experiment is a powerful tool that helps in interpreting more meaningful results with the minimum number of experiments using statistical methods for the analysis of data. It also helps in modeling and analyzing the influence of control factors on the performance output. The most important stage in the design of experiment lies in the selection of the control factors. The literature on the slurry erosion behavior of different materials reveals that operating parameters, viz., impact velocity, impingement angle, particle size, and slurry concentration, influence the erosion rate of materials largely. The effect of these four parameters was studied using the L9 (34) orthogonal array of Taguchi's methodology. In the conventional full factorial experimental design, it would have required 34 = 81 runs to study the effect of four factors each at three levels, whereas Taguchi's experiment approach reduces it to only 9 runs. This provides a greater edge in terms of the experimental time and cost. The operating conditions under which erosion tests were carried out have been presented in Table I. Two samples were tested at each combination of factors given by the orthogonal array L9 illustrated in Table II. Each test was run for 60 minutes with weight measurements taken at an interval of every 15 minutes. The analysis of variance (ANOVA) of the results was conducted using ''smaller is better'' quality characteristics. Randomization of the runs was ensured.

Table I Operating Conditions

Control Factor	Levels			
	I	II	III	
Velocity	15	30	45	m/sec
Impact Angle	30	45	90	deg
Concentration	5000	12000	30000	ppm
Particle Size(BSS no.)	30	45	60	BSS

Run No.	Velocity (m/sec)	ImpactAngle (deg)	Concentration (ppm)	PS (BSS)	Response
1	1(15)	1(30)	1(5000)	30	R1
2	1(15)	2(45)	2(12000)	45	R2
3	1(15)	3(90)	3(30000)	60	R3
4	2(30)	1(30)	2(12000)	60	R4
5	2(30)	2(45)	3(30000)	30	R5
6	2(30)	3(90)	1(5000)	45	R6
7	3(45)	1(30)	3(30000)	45	R7
8	3(45)	2(45)	1(5000)	60	R8
9	3(45)	3(90)	2(12000)	30	R9

Table II Orthogonal array L9

III. RESULTS AND DISCUSSION

For each run of coated and uncoated specimens the weight loss pattern curves were shown below. Along X-axis time was taken and along Y-axis weight of specimen was taken. Graphs from figure no. 3.1 to 3.9 show weight loss pattern curves for uncoated material and graphs from figure no. 3.10 to 3.18 show weight loss pattern for coated material.

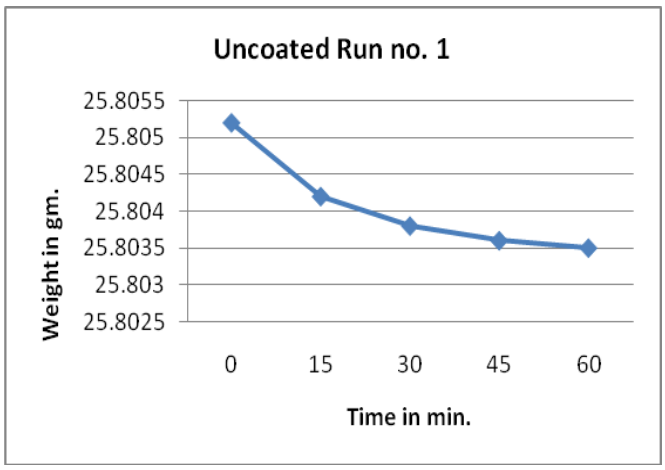

Figure no. 3.1:-Variation of weight change with time in min. for uncoated SS-410 steel for Run no. 1

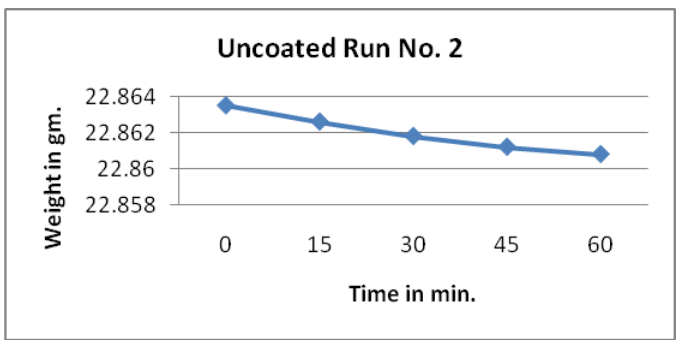

Figure no. 3.2:-Variation of weight change with time in min. for uncoated SS-410 steel for Run no. 2

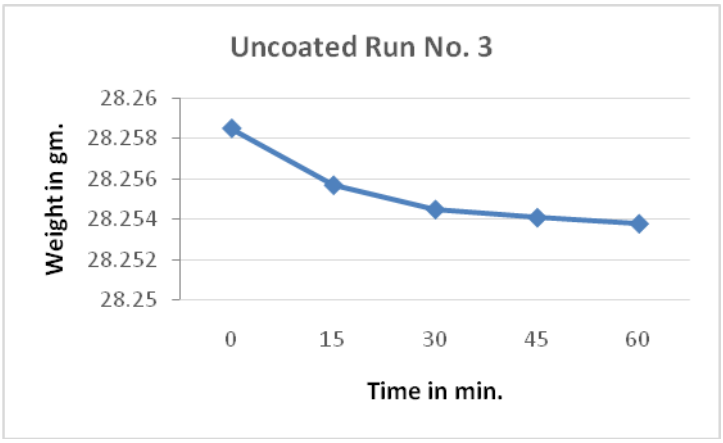

Figure no. 3.3:-Variation of weight change with time in min. for uncoated SS-410 steel for Run no. 3

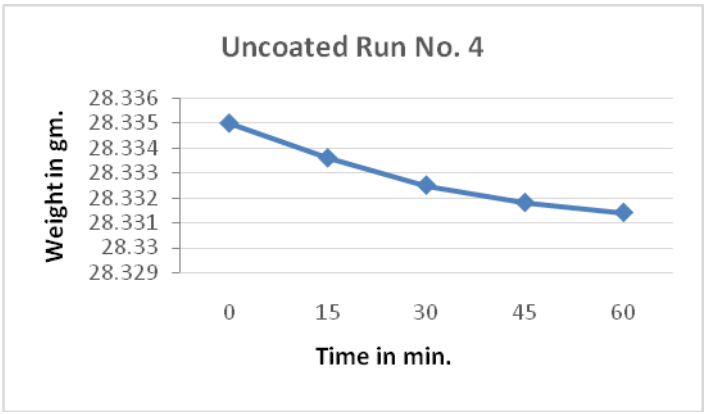

Figure no. 3.4:-Variation of weight change with time in min. for uncoated SS-410 steel for Run no. 4

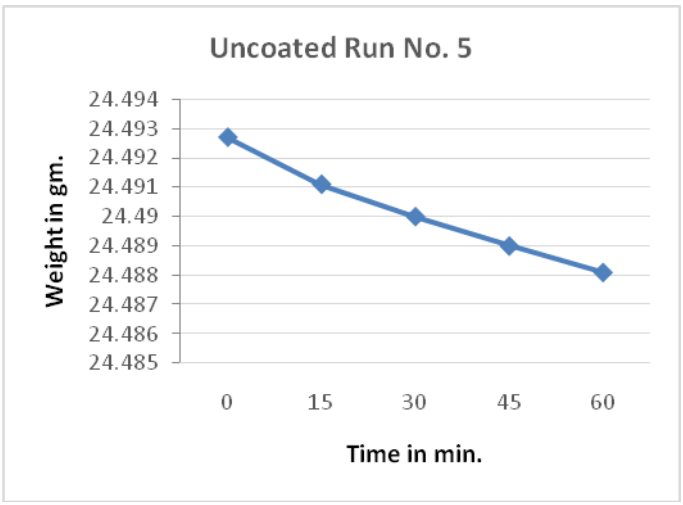

Figure no. 3.5:-Variation of weight change with time in min. for uncoated SS-410 steel for Run no. 5

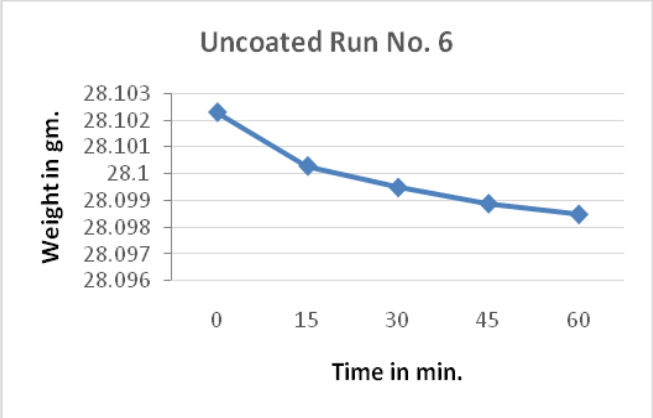

Figure no. 3.6:-Variation of weight change with time in min. for uncoated SS-410 steel for Run no. 2

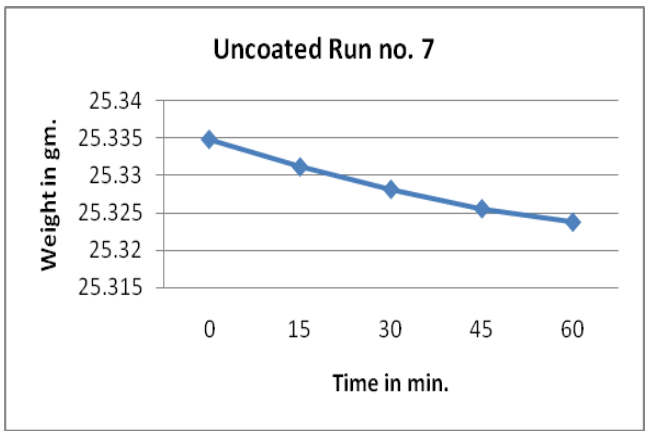

Figure no. 3.7:-Variation of weight change with time in min. for uncoated SS-410 steel for Run no. 7

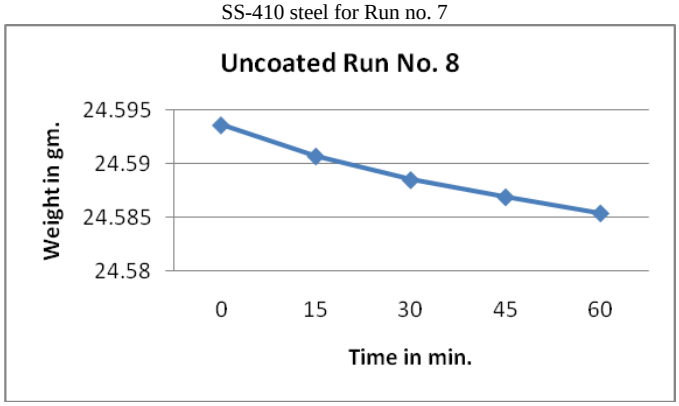

Figure no. 3.8:-Variation of weight change with time in min. for uncoated SS-410 steel for Run no. 8

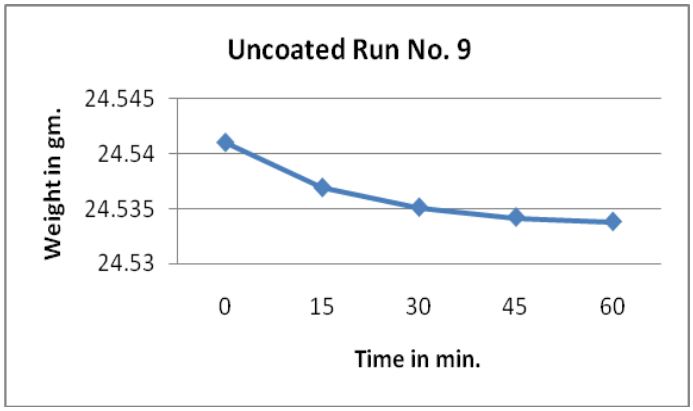

Figure no. 3.9:-Variation of weight change with time in min. for uncoated SS-410 steel for or Run no. 9

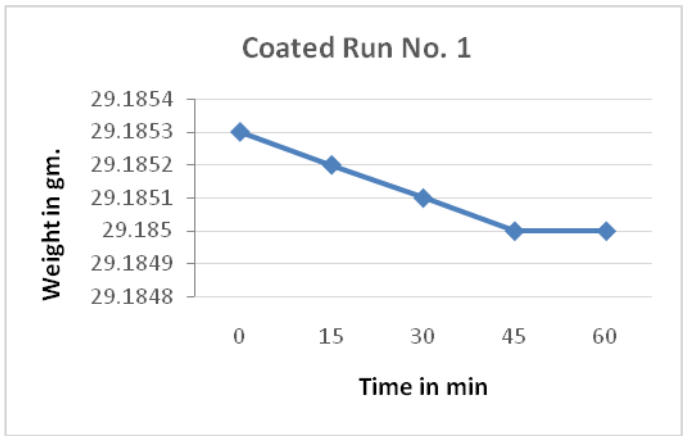

Figure no. 3.10:-Variation of weight change with time in min. for coated SS-410 steel for Run no. 1

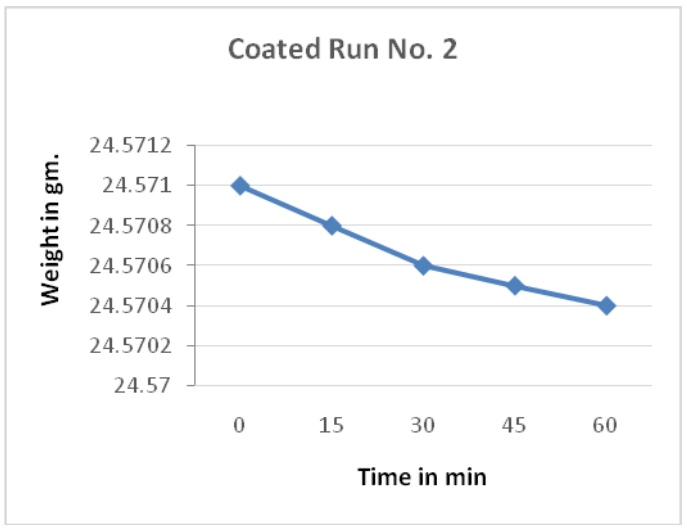

Figure no. 3.11:-Variation of weight change with time in min. for coated SS-410 steel for Run no. 2

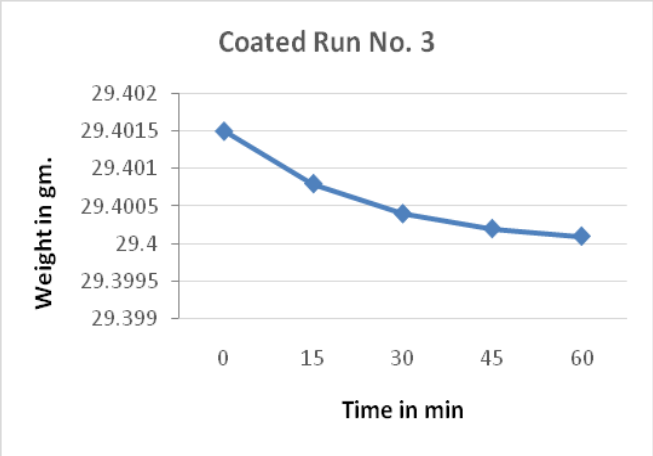

Figure no. 3.12:-Variation of weight change with time in min. for coated SS-410 steel for Run no. 3

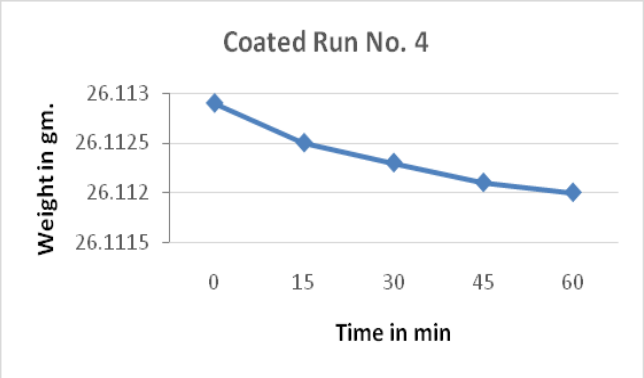

Figure no. 3.13:-Variation of weight change with time in min. for coated SS-410 steel for Run no. 4

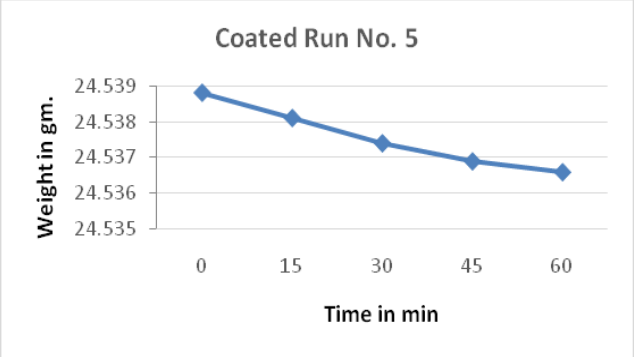

Figure no. 3.14:-Variation of weight change with time in min. for coated SS-410 steel for Run no. 5

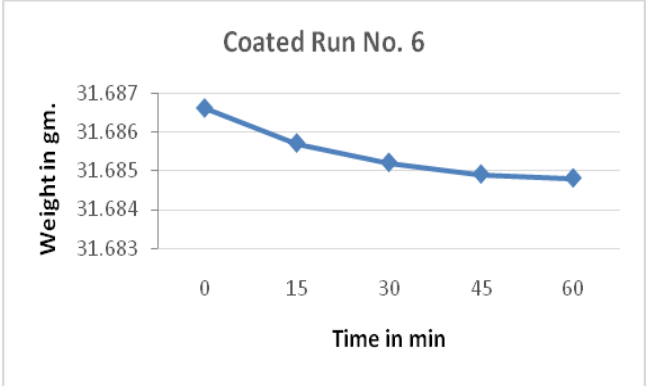

Figure no. 3.15:-Variation of weight change with time in min. for coated SS-410 steel for Run no. 6

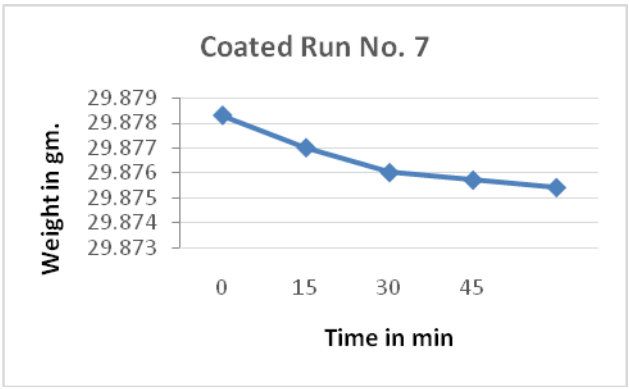

Figure no. 3.16:-Variation of weight change with time in min. for coated SS-410 steel for Run no. 7

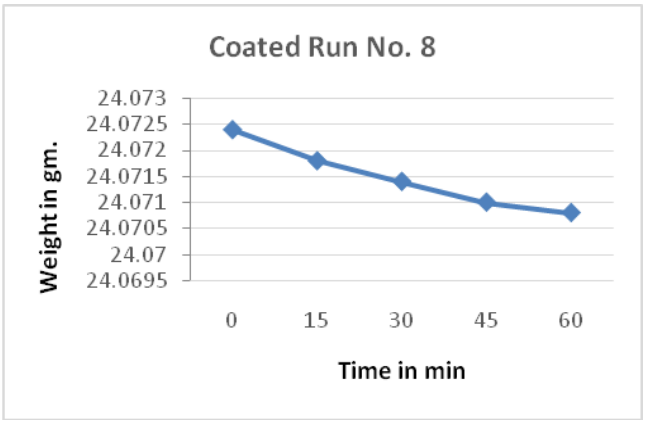

Figure no. 3.17:-Variation of weight change with time in min. for coated SS-410 steel for Run no. 8

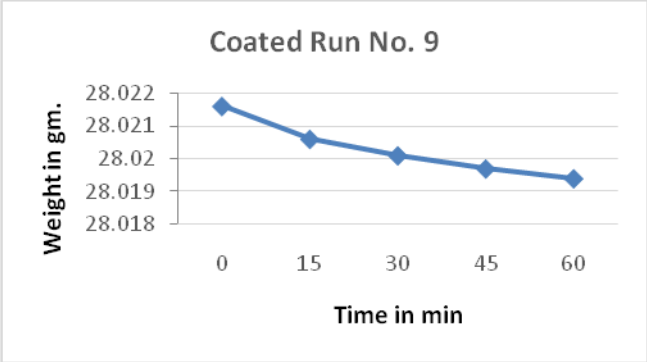

Figure no. 3.18:-Variation of weight change with time in min. for coated SS-410 steel for Run no. 9

From these graphs it was observed that there was decrease in erosion rate of coated specimens than the uncoated specimens. The total average reduced weight of uncoated specimens due to slurry erosion during experiments is 0.011525gm and that of coated specimens is 0.00345gm .The slurry erosion of coated samples is reduced by 70% from uncoated samples. The effect of four parameters on slurry erosion rate of both coated and uncoated specimens is given below:

A. Effect of velocity

The rate of slurry erosion depend upon the velocity of impinging particles in water. The weight loss pattern curve for both uncoated and coated material is given below.

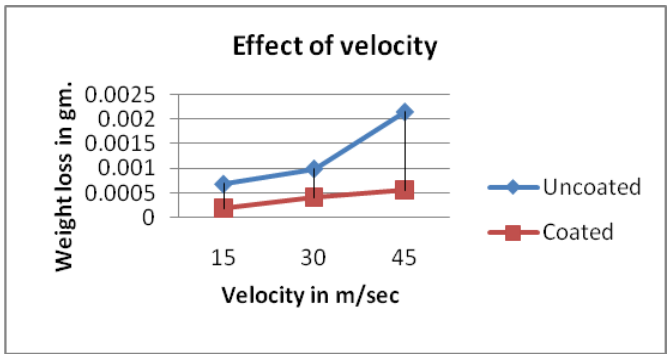

Figure no. 3.19-Variation of loss of weight for coated as well as uncoated SS-410 w.r.t velocity

It was observed that for both specimens with increase in velocity the slurry erosion rate is increased. But the rate of slurry erosion for coated specimens is less than uncoated specimens. It was observed that there is rapid increase in rate of slurry erosion from 15m/s to 30m/s but there is less increase in rate of slurry erosion from 30m/s to45m/s. Because at high speeds the sand particles strike with each other due to which energy of particles is reduced.

B. Effect of impact angle

The rate of slurry erosion depends upon the angle of specimen with the jet of slurry. The weight loss pattern curve for both uncoated and coated material is given below.

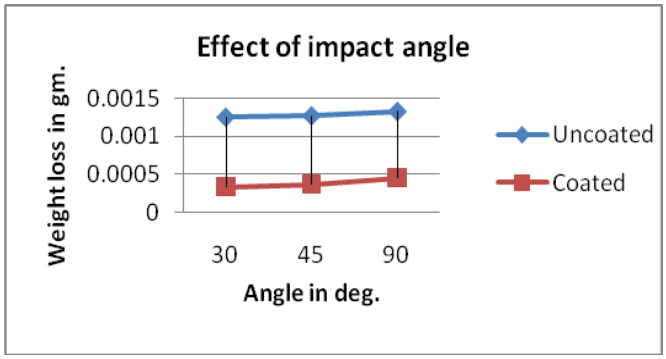

Figure no. 3.20:-Variation of loss of weight for coated as well as uncoated SS-410 w.r.t impact angle

It was observed that highest rate of slurry erosion is at 90 deg because at 90 deg maximum sand particles strikes with the surface of specimen.

C. Effect of concentration

The rate of slurry erosion depends upon the concentration of slurry in the water. The weight loss pattern curve for both uncoated and coated material is given below:

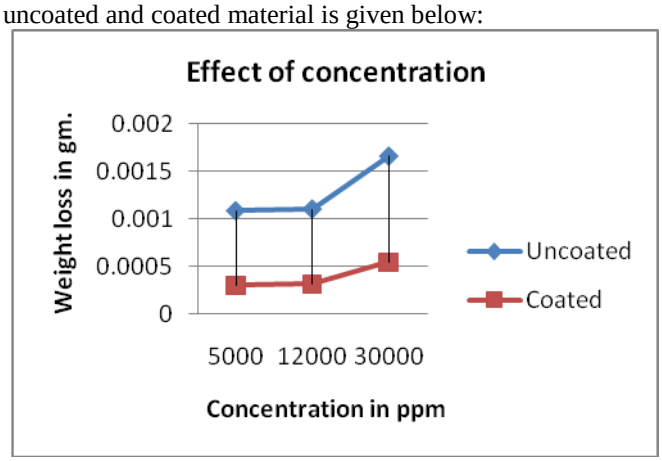

Figure no. 3.21:-Variation of loss of weight for coated as well as uncoated SS-410 w.r.t ppm

It was observed that with inrease in concentration of slurry the rate of slurry erosion is increased. But we see that there is less increase in rate of slurry erosion from 12000ppm to 30000ppm. Because at higher concentrations sand particles collide with each other due to which the energy is reduced and sand particles strike with surface of specimen with less momentum and slurry erosion rate is decreased.

D. Effect of particle size

The rate of slurry erosion depends upon the particle size of the silica sand. The weight loss pattern curve for both uncoated and coated material is given below.

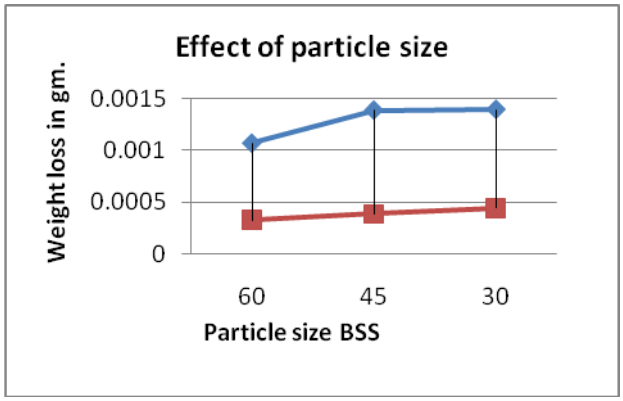

Figure no. 3.22:-Variation of loss of weight for coated as well as uncoated SS-410 w.r.t particle size

It was observed that with increase in particle size , the rate of slurry erosion is increased. We see that the rate of slurry erosion of coated specimens is less than the rate of slurry erosion of uncoated specimens.

IV. CONCLUSIONS

(a) D-gun-sprayed WC-12Co coatings can reduce the erosion rates of the SS-410 steel.

(b) During the slurry erosion of SS-410 steel, slurry concentration and jet velocity were found to more be dominant factors in comparison with average particle size. In the case of D-gun-sprayed WC-12Co coatings, average particle size was found to be more dominant factor in comparison with slurry concentration and jet velocity. Thus, D-gun-sprayed WC-12Co coatings can be used in high-speed hydro turbines and with high concentration slurries.

REFERENCES

[1] H.X. Guo, B.T. Lu, and J.L. Luo, “Interaction of Mechanical and Electrochemical Factors in Erosion-Corrosion of Carbon Steel”, Electrochim. Acta, 2005, 51(2), p 315–323

[2] A. Neville, F. Reza, S. Chiovelli, and T. Revega, “Assessing Metal Matrix Composites for Corrosion and Erosion-Corrosion Application in the Oilsands Industry”, Corrosion, 2006, 62(8), p 657–675

[3] A.P. Harsha and D.K. Bhaskar, Solid Particle Erosion Behaviour of Ferrous and Non-ferrous Materials and Correlation of Erosion Data with Erosion Models, Mater. Des., 2008, 29(9), p 1745-1754

[4] D.P. Sharma and S. Singh, Operational Problems of Water Turbine in U.P.—With Special Reference to Tiloth Power Station, Proceedings of All India Seminar on Metallurgical Problems in Power Projects, 30-31 Oct. 1987 (Lucknow), p 18-35

[5] B. Rajasekaran, S. Ganesh Sundara Raman, S. Joshi, and G. Sundararajan, Influence of Detonation Gun Sprayed Alumina Coating on AA 6063 Samples Under Cyclic Loading With and Without Fretting, Tribol. Int., 2008, 41(4), p 315-322

[6] P.M.J. Vuoristo, K. Niemi, and T. Mantyala, “On the Properties of Detonation Gun Sprayed and Plasma Sprayed Ceramic Coatings, Thermal Spray”, International Advances in Coatings Technology, C.C. Berndt, Ed., ASM International, Metals Park, OH, 1992, p 171-175

[7] B.S.K. Naidu, Developing Silt Consciousness in the Minds of Hydropower Engineers, Proceedings of 1st International Conference on Silting Problems in Hydropower Plants, CBIP, 13-15 Oct.1999 (New Delhi), p 1-36

[8] S.V. Joshi and R. Sivakumar, “Protective Coatings by Plasma Spraying”, Trans. Indian Ceram. Soc., 1991, 50, p 50-59

[9] K.G. Budinski, Surface Engineering for Wear Resistance, Prentice Hall, New York, 1988, p 15-48

[10] J. Knapp, “Fine-Particle Slurry Wear Resistance of Selected Tungsten Carbide Thermal Spray Coatings”, Tribol. Int., 1997, 30(3), p 225-234

[11] SanjeevBhandari, Harpreet Singh, Harmesh Kumar, and VikasRastogi (2012),” Slurry Erosion Performance Study of Detonation Gun-Sprayed WC-10Co-4Cr Coatings on CF8M Steel Under Hydro-Accelerated Conditions”, Journal of Thermal Spray Technology, Vol. 21(5), pp. 1054—1064

Characterization and High Temperature Corrosion Study of FSPed C70 Steel

Aayush Bawdekar
Department of Automobile Engineering
Chandigarh University
Mohali, India

Supreet Singh
Department of Automobile Engineering
Chandigarh University
Mohali, India

Manpreet Kaur
Associate Professor,
Department of Mechanical Engg
Baba Banda Singh Bahadur Engineering College,
Fatehgarh Sahib

Prabhjot Singh
Department of Mechanical Engineering
Chandigarh Group of Colleges
Mohali, India

Iqbal Singh
Department of Mechanical Engineering
Chandigarh Group of Colleges
Mohali, India

***Abstract*— In the present work C70 steel which is used in the manufacturing of automobile connecting rods and bearings was friction stir processed with defined parameters and investigations were made based on microstructure, mechanical properties and high temperature corrosion studies, for comparison unprocessed C70 Steel was also investigated under similar set of conditions. Friction Stir Processing has revealed to be feasible tool for enhancing the mechanical properties of materials like micro hardness, fine grain structures, high tensile strength, improved yield strength, improvement in elongation, and increased corrosion resistance. In detail characterization of both processed and unprocessed steel was carried out using a Scanning Electron Microscope (SEM), an Optical Microscope (OM), and Vickers Micro-Hardness testing. High Temperature Corrosion Studies were conducted for both at 900^{0}C for 50 cycles to see the influence of different parameters on corrosion rate. The microstructure refinement of processed C70 reveals that FSP have contributed to the considerable increase in the microhardness values at 2400 rpm and 60mm/min feed rate with plunge depth of 0.8mm.**

Keywords*— *Friction Stir Processing; medium carbon steel; microhardness; grain refinement

I. INTRODUCTION

C70 are extensively used in the sector of automobile engineering for the fabrication of connecting rods and bearings and shows potential in the field of shipbuilding industries. Friction Stir Processing (FSP) a contemporary surface engineering technique imitated from Friction Stir Welding is being widely used in naval and automobile industry. A non-consumable tool hold on CNC operated milling machine is penetrated inside the specimen of metal or alloys and it is made to rotate on its surface in a stirring motion and in transverse direction. Figure 1 shows the process of FSP. Tools are designed with a pin or pin less usually made up of tungsten carbide (WC) and polycrystalline cubic boron nitride (PCBN) used for FSPed of steel. Studies on a range of materials confirmed that the quality of Friction stir processing generally depends on base material properties as well as tool material, shape and dimensions also on process parameters like rotational speed, transverse speed, axial force, cooling system and feed rate. Frictions stir processing changes the properties of the specimen through intense localized plastic deformation, which results in process mixing the material without changing the phase and creates a microstructure with fine grain and increased hardness.

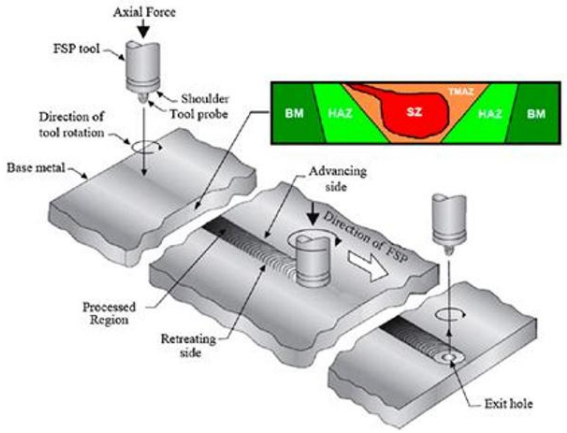

Figure 1 Process for FSP

The attainment of elevated temperatures plays an important role in the development of civilization for many countries [1]. Equipments in many cutting edge high technology areas have to work under elevated temperatures, high pressure and corrosive environment [2]. So, materials are prone to face problems at high temperatures in several high tech industries. Connecting rods in Automobile industry, Gas turbines in aircraft, fossil fueled power plants, refineries, and petrochemical industries, and heating elements for high temperature furnaces are some examples where corrosion limits their use or reduces their life, considerably affecting the efficiency [1].

Friction Stir Processing is the new and fast developing technique which is nowadays used for subsurface structural modification of different materials including not only aluminum and magnesium alloys but steels and other alloys also [3]. Friction stir processing is used for localized modification and control of microstructures in near-surface layers of processed metallic components for specific property enhancement [4]. It has proven to be an effective treatment to achieve major microstructural refinement, densification and homogeneity at the processed zone, as well as elimination of defects from the manufacturing process. Processed surfaces have shown an improvement of mechanical properties, such as hardness and tensile strength, better fatigue, corrosion and wear resistance [5].On the other hand, fine microstructures with equiaxed recrystallized grains improve superplasticity behavior. [6-8]

The main objective of the current investigation is to achieve strengthening of C70 through microstructural refinement by Friction Stir Processing (FSP) and analyze the effect of the same on high temperature corrosion behavior. The high temperature corrosion performance of the unprocessed and the FSPed specimens shall be evaluated in the Na_2SO_4-82%Fe_2 $(SO_4)^3$ molten salt environments in the laboratory and in the actual boiler environments so as to ascertain the usefulness of the FSP technique. The microstructure, mechanical properties, and corrosion resistance of the unprocessed and FSPed materials will be evaluated. The in-depth characterization analysis with an aim to propose mechanisms behind high temperature corrosion behavior of the coating.

II. EXPERIMENTAL PROCEDURE

A. Friction Stir Processing

Friction Stir Processing and preparing samples for metallographic analysis

The unprocessed base material C70 Steel plates with dimensions 76 x 50 x 5 mm were friction stir processed. The varying parameters are shown in table 1.

In the process to minimize the tool wear, selection of tool material i.e. Pin less Tungsten Carbide of 12mm diameter was selected with the sole purpose to minimize wear resistance used for working at high temperature.

The fixture for FSP was mounted on Jyoti VMC 640 CNC operated machine; the tool was held rotating there for about 10 seconds to soften the material and was allowed to travel along the slot. . The chemical composition and mechanical properties of C70 steel is shown in table 2 and table 3. After the procedure, specimens were cooled with dry ice at room temperature.

Table 1 Process parameters for FSP

Process Parameter			
Rotational Speed (RPM)	Transverse Speed (mm/min)	Plunge Depth (mm)	Passes
900	60	0.8	1
1600	60	0.8	1
2400	60	0.8	1

Table 2 Chemical Composition of C70

C	Mn	P	S	Fe
0.65 to 0.75 %	0.6 to 0.9 %	0 to 0.040 %	0 to 0.050 %	98.3 to 98.8 %

Table 3 Mechanical Properties of C70

Mechanical properties	Value
Density	7.8 g/cm³ (490 lb/ft³)
Elastic (Young's, Tensile) Modulus	210 GPa (30 x 10^6 psi)
Strength to Weight Ratio	82 to 97 kN-m/kg
Tensile Strength: Ultimate	640 to 760 MPa
Tensile Strength: Yield	410 to 570 MPa
Thermal Expansion	12 µm/m-K
Modulus of Resilience	400 to 770 kJ/m³
Poisson's Ratio	0.29

The specimens were cross-sectioned at 90 degree angle to the FSP direction and prepared for metallographic analysis, cut in 5 x 5 x 5mm pieces, hot mounted using mount press machine and polished on SiC emery paper ranging from 220 to 2000 grades followed by velvet cloth polishing as shown in figure 2.

Characterizations of the microstructure were examined by optical microscopy, scanning electron microscopy (SEM). The specimens were etched in a solution containing 98% HNO3 and 2% ethanol. Mechanical characterizations were evaluated using Vickers hardness.

Figure 2 Sample for Metallographic analysis

B. High Temperature Corrosion

a) Sample Preparation

The specimens to be tested were cut and made to specified dimensions of 13 x 10 x 5 mm plates. All six faces of the specimen were polished on Radical DPM-33 double disc polishing machine using SiC emery paper ranging from 200 to 2000 grades and on velvet cloth. The specimen were made dirt free by cleaning them with ethanol and dried, their area was measured using digital vernier caliper and were accurately weighted on Citizon CY 204 electronic balance machine so as to plot weight gain per unit area vs. number of cycle graph.

b) Preheating of Alumina boats and Samples

The alumina boats to be used were preheated in universal oven at 250^0C for 4 hours gradually followed by 20 minutes of cooling at room temperature and again heated in Digital programmable industrial muffle furnace at 900^0C for 2 hour as shown in figure 3 to completely remove moisture from the boats. Samples along with boat were preheated in universal oven at 150^0C for 2 hour and afterwards their weights were measured.

Figure 3 Preheating in Oven

c) Salt mixture Coating and hot corrosion studies

Mixture of salt containing [Na_2SO_4- 82%$Fe_2(SO_4)_3$] was prepared with distilled water and coated on the specimen with salt ranging from 3.0-5.0 mg/cm^2 and further heated in oven at 250^0C for 2.5 hour and weight along the boat were measured. Specimens were then kept in muffle furnace at 900^0C along with boat for 1 hour followed by 20 minutes of immediate cooling at room temperature and weight was calculated on electronic balance as shown in Figure 4. The oxidation cycles were carried out 50 times for each and every sample and their weight was calculated at the end along spalled scale and visual inspections were also made.

Figure 4 High Temperature Corrosion in Industrial Muffle Furnace

III. RESULTS & DISCUSSION

A. Microstructure

The Microstructures of the specimens were studied on leica inverted microscope available at IIT Ropar. There was a significant decrease in the grain size as the rotational speed was increased with similar feed rate. The images obtained for the different samples are shown in Figure 5.

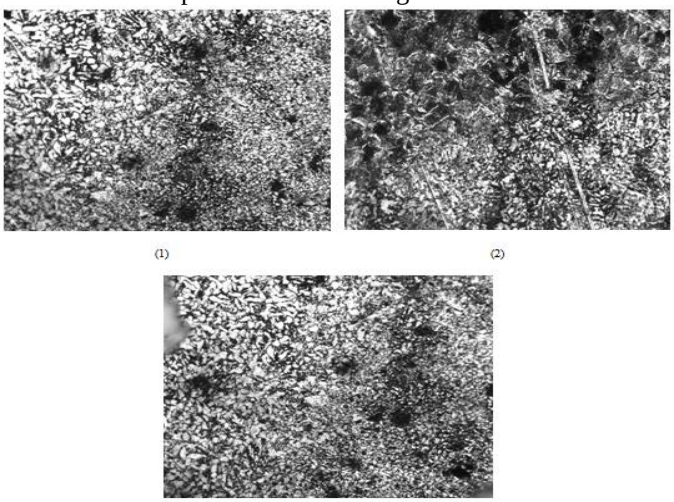

Figure 5 Microstructural developments of FSPed Samples (1) S1 (2) S2 (3) S3

B. Hardness

Hardness values of FSPed C70 specimens were measured on Vickers micro-hardness tester at a load of 0.3kgf. It is observed that grain refinement and reduction in grain size might have contributed to increased hardness value. Beside with grain size refinement, the existence of sub-micron sized precipitates may have also contributed in increasing the hardness of the C70. The microhardness profiles of Friction stir processed C70 along the cross-section as a function of distance from the FSPed interface are plotted in Figure 6. The critical hardness values of the Base Metal were found to be 180 HV. In the case of the FSPed samples, the microhardness

values for the FSP Sample 1 named as S1 with defined parameters lie in the range of 427-450 HV. The microhardness values for the sample S2 with defined parameters lie in the range of 490-515 HV. The microhardness values for the sample S3 with defined parameters lie in the range of 559-586. A maximum value of hardness was shown by S3 Friction Stir Processed sample, whereas a minimum of Sample S1.

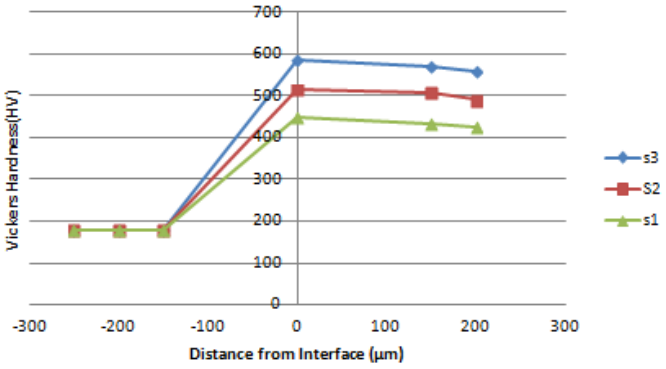

Figure 6 Hardness VS Distance Profile of Sample S1, S2, S3

C. *Scanning Electron Microscopy*

Scanning Electron Microscope analyzer (Jeol JSM -6610 LV) was used to obtain the micrographs and characterize the grain structure and transition zone of the samples at three different varying RPM's. Figure 7 (1), (2), (3) shows the micrograph of specimen at 900 RPM, 1600RPM, 2400 RPM in which the transition zone of ultrafine grain can be seen.

The average grain size of the specimens were observed to be around 2-3µ. The transition zone can be clearly seen in the micrographs.

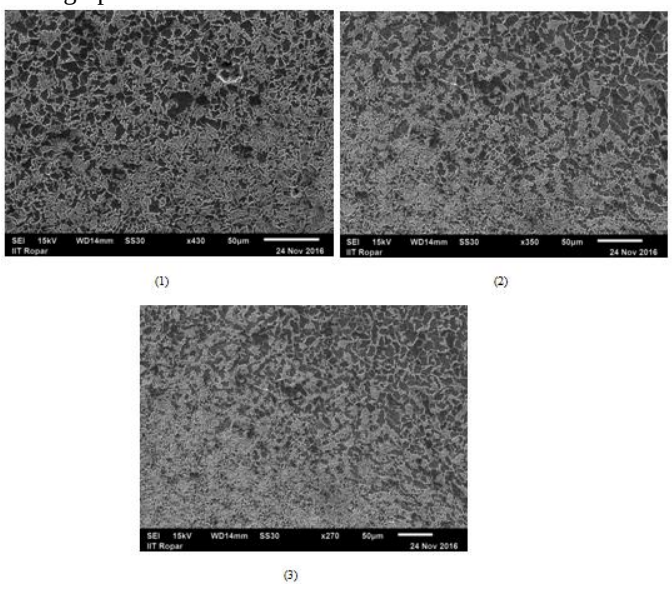

Figure 7 SEM Micrographs of Ultrafine grain of FSPed C70 Specimen (1) S1, (2) S2, (3) S3

D. *High Temperature Corrosion At 900 °C*

(a) Visual Examination

In the case of Sample 1 (S1) steel shown in Fig. 5.1 (a), it was observed that the surface of steel turned dark black with some spots on it after first cycle. The sample turned grayish black after second cycle. Few Minor cracks appeared on the top surface by the end of 5th cycle and remained there till the end of 50 cycles. After 10th cycle separation in fragments from top and sides were seen with a drastic increase in weight. By the end of 25th cycle lustrous layer was seen on the surface.

In the case of Sample 2 (S2) steel shown in Fig. 5.1 (b), the color of the sample changed from black to light gray after the second cycle and later to dark gray by the completion of 10th cycle. Apart from the change in colour, many small cracks started appearing by 13th cycle. Formation of pits with some spallation from the sides were observed by 20th cycle and remained there throughout 50th cycle.

In the case of Sample 3 (S3) steel shown in Fig. 5.1 (c) the color changed from black to grey after 3rd cycle. Some major changes were observed after 20th cycle which includes some cracks and lustrous appearance. The overall weight gain by the end of 50th cycle was least in the case of S3.

(b) Weight Change Data

The weight Gain VS No of cycles graph plot for the base and S1, S2, S3 at 900 °C for 50 cycles. The weight change data is usually used to establish the kinetics of the corrosion process. A higher weight gain represents higher rates of corrosion. In the case of S1 C70 steel, the rate of weight gain was slow for the first 15 cycles. Thereafter weight gain rate continued to increase at a comparatively higher rate till the end of cyclic studies. So from weight gain data it can be inferred that corrosion rate increased after the 15 cycles of study. The S2 C70 steel has shown the tendency to gain weight without showing any indication of steady state corrosion rate comparable to S3, which has shown the tendency to become uniform with least increase in weight.

It can be inferred from the plots that the parameters for Friction Stir Processing of Sample 3 showed protection in high temperature corrosion testing as the weight gain values for the Sample 3 C70 steel is significantly smaller than S2 and S3.

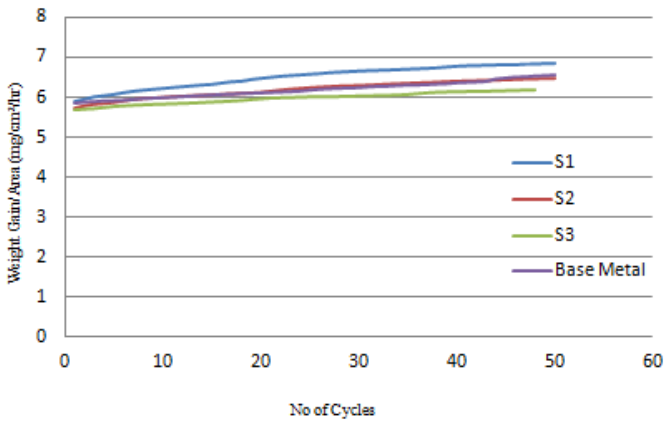

Figure 8 Weight Gain VS No of Cycles Graph for Specimen S1, S2, S3 and Base Metal

E. HALL PETCH EQUATION

Intense heat generation due to friction plastically deforms the metallic material thus resulting in ultra fine grain structure and enhanced mechanical properties such as tensile strength and hardness. To corroborate the relationship between ultrafine grain structure and enhanced mechanical properties Hall-Petch equation is determined to validate the findings.

The grain structure got considerably refined as a result of FSP. The average grain size of S1, S2 and S3 was found to be 8.7 µm, 7.2 µm and 3.9 µm respectively.

According to Hall-Petch, equation, as in (1)

$$\sigma = \sigma_0 + kd^{-1/2}, \quad (1)$$

Where σ is the yield strength, σ_0 is the stress for dislocation movement, k is the strengthening coefficient of material and d is the diameter of average grain size. This equation can be stated for hardness, as in (2)

$$H = H_0 + k_H d^{-1/2}, \quad (2)$$

Where H_0 and k_H are constants

The Hall-Petch equation is usually helpful in determining relationship between grain size and hardness of the material, as the grain size is reduced there is an increase in the hardness of the material.

Experimental values of hardness and observed average grain size of FSPed specimens clearly shows the relationship between both in accordance to Hall-Petch Equation.

Figure 9 (a), (b), (c) shows graphically the relationship between hardness values and grain size of C70 Steel.

The results thus obtained clearly shows that at higher RPM FSP helps in enhancing the mechanical properties of C70 Steel by creating superfine grain structure and increasing the hardness by three times that of base metal.

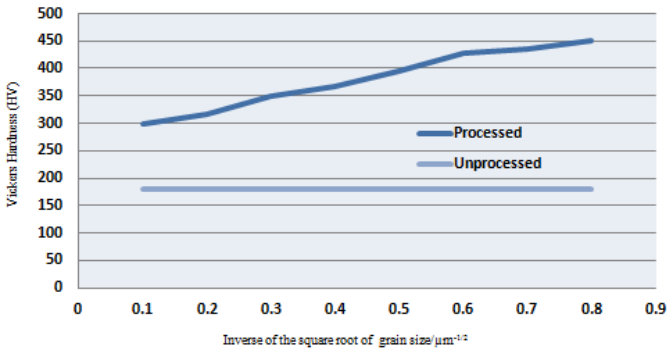

Figure 9(a) Hardness VS Grain Size Graph for S1

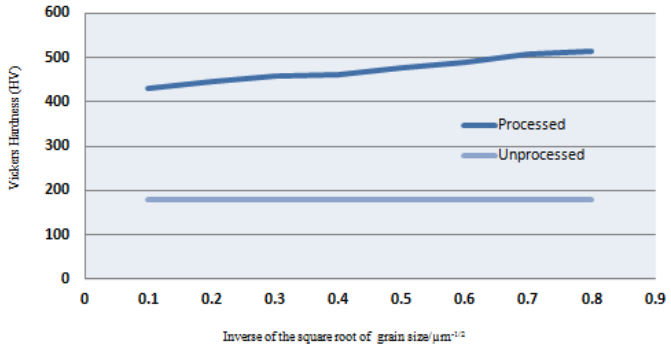

Figure 9(b) Hardness VS Grain Size for S2

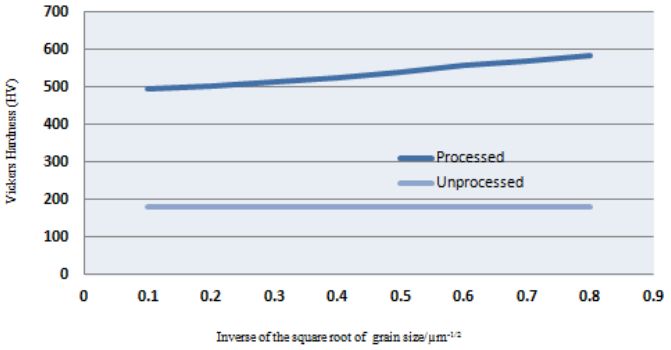

Figure 9(c) Hardness VS Grain Size for S3

V. CONCLUSIONS

The grain structure got considerably refined as a result of FSP. The average grain size of S1, S2 and S3 was found to be 8.7 µm, 7.2 µm and 3.9 µm respectively. It can be inferred from

the plots that the parameters for Friction Stir Processing of Sample 3 showed protection in high temperature corrosion testing as the weight gain values for the Sample 3 C70 steel is significantly smaller than S2 and S3. The microhardness values for the sample S3 with defined parameters lie in the range of 559-586. A maximum value of hardness was shown by S3 Friction Stir Processed sample, whereas a minimum of Sample S1.Hence FSP is successful on C70 materials in reference to above results.

REFERENCES

[1] Khanna A.S., (2002): "Introduction to high temperature oxidation and corrosion", ASM International, ISBN 0-87170-762-4, and SAN: 204-7586, pp.1-322.
[2] Ananthapadmanabhan P.V., Sreekumar K.P., Muraleedharan K.V., Venkatramani N.,(1991) "Plasma-sprayed composite coatings for high temperature applications", Surface & Coating Technology, Vol. 49, pp. 62-66.
[3] Nicholas E.D. (2003): "Friction Processing Technologies Welding in the World", Vol. 47, No. 11-12, pp. 2-9.
[4] Ma, Z.Y. (2008): "Friction stir processing technology: A review", Metallurgical and Materials Transactions A, Vol. 39A, pp.642–58.
[5] Karthikeyan, L., Senthilkumar, V.S., Balasubramanian V. and Natarajan, S. (2009): "Mechanical property and microstructural changes during friction stir processing of cast aluminum 2285 alloy", Materials and Design, Vol. 30, pp.2237–42.
[6] Mishra, R.S., Mahoney, M.W., McFadden, S.X., Mara, N.A. and Mukherjee, A.K. (2000): "High strain rate superplasticity in a friction stir processed 7075 Al alloy", Scripta Materialia, Vol .42, pp.163–168.
[7] Ma, Z.Y., Mishra, R.S. and Mahoney, M.W. (2004): "Superplasticity in cast A356 induced via friction stir processing", Scripta Materialia, Vol. 50, pp. 931–5.
[8] Ma, Z.Y., Liu, F.C. and Mishra, R.S. (2010): "Superplastic deformation mechanism of an ultrafine ne-grained aluminum alloy produced by friction stir processing", Acta Materialia, Vol. 58: pp. 4693-704.

Studies in Magnetic Abrasive Finishing of Internal Surface of Stainless Steel Tubes Using Pole Rotation System

Randhir Singh
Research Scholar,
BBSB Engg College, Fatehgarh Sahib

Lakhvir Singh
Professor and Head, Mechanical Engg Dept
BBSB Engg College, Fatehgarh Sahib

Abstract: **Magnetic Abrasive Finishing (MAF) is a renowned polishing technique widely used for operations requiring ultra finishing operations such as finishing of PCB's, balls, rollers, shafts, complex work pieces. This paper analyses the effect of MAF on the SS 307 tubes by using pole rotation system on aluminium based sintered magnetic abrasives. Input parameters have been selected on the basis of literature review and preliminary investigation. Experimentation have been carried out by varying the input parameters such as working gap, rotational speed of poles, size of magnetic abrasive particles (MAP's), Abrasive weight and keeping the other parameters fixed like machining time, lubricant type and quantity.**

Keywords: ***MAF, MAP, PISF, sintered magnetic abrasives, SS 307, surface finish***

1. INTRODUCTION

MAF is popular for utilizing controlled magnetic force having small magnitudes which is almost impossible in the conventional machining processes. The material removal is done with the help of magnetic abrasives.

Shinmura et al. (1985) conducted an experimental study on plane work and found that the surface roughness value decreases with increasing finishing time up to a certain limit of time beyond which no further improvement was noticed. Adding machining fluid (such as stearic acid, straight oil type of grinding fluid) to unbounded MAPs has shown remarkable effects on stock removal and surface roughness.

Shinmura et al. (1992) utilized iterations through uniformly mixing the diamond abrasives with iron to form diamond magnetic abrasives. They concluded that finishing efficiency increased with diamond magnetic abrasives with increase of speed of tool. Results showed that machining depth increases with increase of mixing weight percentage of iron particles.

Takeo Shinmura et al. (1994) prepared new type of abrasive material to study the magnetic abrasive machining of ceramics. They mixed small size diamond magnetic abrasives with large size ferromagnetic particles.

It was found that in the plane finishing, the magnetic force on the surface and rigidity of magnetic abrasive brush are most influenced by the diameter of the magnetic abrasives. He also showed that the use of ferromagnetic particles mixed with diamond magnetic abrasives not only improves the finishing efficiency but also multiplies the magnetic field density.

Kremen et al.(1999) performed experiments on ceramic cylindrical parts and silicon wafers using different grain size of magnetic abrasives to study their effect on material removal rate and surface roughness. their result showed variation of grain size has no effect on surface finish obtained in both cases. But material removal rate increase with increase of size of the diamond grain size of magnetic abrasives.

Dhirendra et al. (2005) analyzed microscopic changes in the surface texture resulting from the MAF process to distinguish the behaviour of abrasive particles during finishing. The observed surface texture indicated that the process creates micro scratches having width less than 0.5µm on the finished surface. Moreover, the surface is finished by the shearing of peaks resulting in circular lays formed by the rotation of the flexible abrasive magnetic brush (FMAB).

Jae-Seob Kwak (2009) improved the magnetic flux density in magnetic abrasive polishing process for non ferrous materials. To increase the flux density he installed a permanent magnet at the opposite side of the work piece. He concluded that the optimal conditions for the MAF of the magnesium alloy were an applied current of 2.0A, working gap of 1mm rotational speed of 800rpm and the amount of powder (Fe + boron nitride powder) of 0.7 g.

Singh et al. (2012) utilized mechanical alloying followed by heat treatment to prepare magnetic abrasives. The MAF is used effectively to remove tool marks, burrs and plastic deformation.

Shukla et al. (2013) stated that current and machining gap are most influencing factor. For optimization response genetic algorithm is used. Equations of response parameters are given by RSM. Sum of energies is depicted by a formula.

Yamaguchi et al. (2014) established relationships between surface conditions of AlTiN-coated round tools, cutting forces, and wear and their characteristics were clarified by milling of Ti-6Al-4V alloys.

Choopani et al. (2016) found that the magnetic force on the abrasive particles and strength of magnetic brush depends upon the type, shape and size of abrasive particle.

Saraeian et al. (2016) derived results which indicated that the parameters of working gap, rotational speed, and abrasive particle size influence the surface roughness from the most to the least respectively.

2. EXPERIMENTATION

The magnetic abrasive finishing process for the current experimentation is used for finishing internal surface of cylindrical work pieces using a magnetic pole system. Magnetic abrasives introduced in the work piece are conglomerated at the finishing zone by a magnetic field, generating the finishing force against the contact surface of the work piece. These particles join each other to form a flexible magnetic abrasive brush (FMAB) which pushes against the work piece surface and develops finishing pressure. The tangential force developed by FMAB is the major cutting force responsible for micro chipping. During the finishing operation rotary motion is given to the magnets and the work piece is stationary.

Since the magnitude of machining force caused by the magnetic field is controllable, a mirror like surface finish (R_a value in the range of nano-meter) is obtained.

2.1 Preparation of magnetic abrasive using sintering

Sintered Magnetic abrasives were prepared in following 4 steps:

- Uniformly mixing of aluminium oxides and iron powder
- Preparation of compacts
- Sintering of compacts
- Crushing and sieving of crushed sintered Compacts to prepare magnetic abrasives

2.2 Response Variable:

The response variables chosen for the present research is surface roughness. The initial surface roughness is not identical for all the work pieces (it varied between 1.70 µm to 1.90 µm R_a). A ratio of decrease of surface roughness to the initial roughness is considered as the response variable during this experimentation. It is called percentage improvement in surface finish and is given by

$$\text{PISF}(\mu m) = \frac{\text{Initial Surface Roughness - Final Surface Roughness}}{\text{Initial Surface Roughness}} \times 100$$

2.3 Independent Variables:

Selection of independent variables is mainly governed by the findings from literature and earlier experimentation.

2.3.1 Magnetic Gap:

The magnetic force generates finishing pressure on the work piece surface during MAF. Depending upon the limitation of set up the machining gap and size of work piece selected, the gap is selected in the range of 0.5 to 2.5 mm.

2.3.2 Rotational speed:

The poles are rotated to obtain surface finish. Material removal increases with rotational speed and after some value of speed jumbling of abrasives starts which decreases surface finish. In the present study five levels ranging from 100 to 300 rpm were selected for poles of the permanent magnet as it is clear from the initial experimentation that the abrasives start rolling over the surface due to higher value of tangential force.

2.3.3 Size of MAP:

It refers to the size of Sintered Magnetic abrasive prepared for the experimentation. It is understood that smaller MAP grains tend to give better surface finish, whereas the larger grains apply excessive force on the work piece and tend to deteriorate the surface finish. In the present experimentation, MAP grains with intermediate size were chosen so that the five levels of grain size of MAP lie between 60µm–450 µm.

2.3.4 Percentage of iron in magnetic abrasives:

In most of the cases iron percentage is varied from 60 to 90% of the abrasive volume. So in the present study the sintered magnetic abrasives were prepared by varying iron percentage from 75 to 95 % of the abrasive volume.

2.3.5 Constant Parameters:

Machining Time of 2 Hrs, Percentage of abrasive used in MAP: 20% by weight, Quantity of Lubricant was 1ml for 5 gm wt. of MAPs and SUS 307 stainless steel work piece having dimensions

3. RESULTS AND DISCUSSION

Initially the R_a values of work pieces were measured. The sintered magnetic abrasive powder, which is prepared just before each test by adding the lubricant, was placed in the stainless steel tube mounted in the magnetic chuck. After experiment, cleaning the specimen with ethanol, its surface finished was measured using a Mitutoyo surface roughness tester having a least count of 0.001µm (cut off length = 0.8mm).

The experiment was designed on the basis of Response Surface Methodology (RSM) using Central Composite Design (CCD). The practical deployment of CCD often arises through the sequential experimentation. In the present CCD, the total number of experimental runs came out to be 30. So to complete the entire experimentation 30 experiments were performed in random order. The 3D graphs were plotted with the help of software showing the composite effects of two input parameters on the response parameter.

The 3D plot (Fig. 1) shows the effect of simultaneous variation of Rotational Speed and Working Gap on PISF. At minimum rotational speeds, with the decrease in working gap the PISF increases noticeably. When at maximum rotational speeds, the PISF increases sharply with decrease in the working gap. The PISF increases slightly with increase in rotational speed when the gap is kept at minimum value. When the gap is maximum, the PISF decreases by 5 % with increase in the rotational speed.

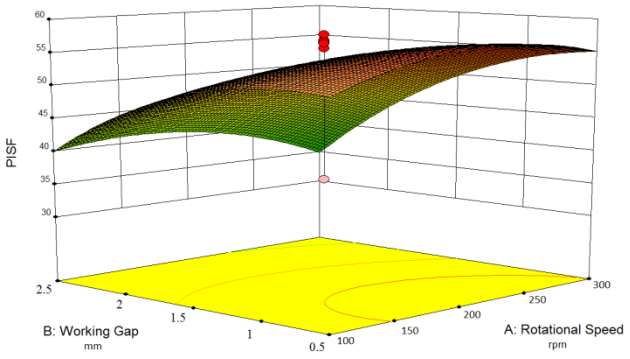

Fig. 1 Interaction effects of Rotational Speed (A) and Working Gap (B)

Fig. 2 shows the relationship between the rotational speed and magnetic abrasive particles size. As the size of MAP's increase by keeping the rotational speed at maximum value,

the PISF increases pointedly. As the MAP's size decreases at minimum rotational speed, the PISF increases acutely. The PISF increases steadily when the size of MAP's is kept minimum by decreasing the rotational speed. Using the maximum MAP's size, by increasing the rotational speed the PISF increases abruptly.

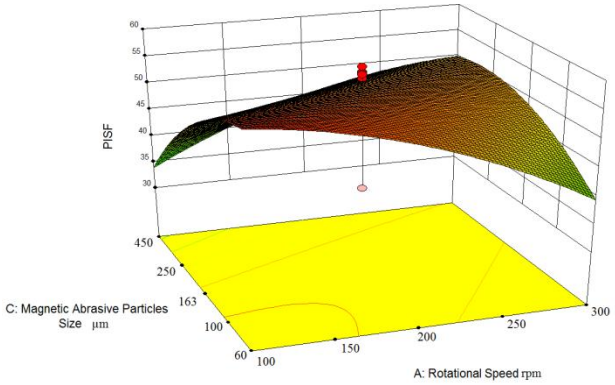

Fig. 2 Interaction effects of Rotational Speed (A) and MAP Size (C)

Fig. 3 shows the relationship between the rotational speed and abrasive weight. At lowest rotational speed, by decreasing the abrasive weight, the PISF increases while approaching the mid value of abrasive weight and then decreases afterwards. At higher rotational speeds, upon decreasing the abrasive weight, the PISF increases slightly.

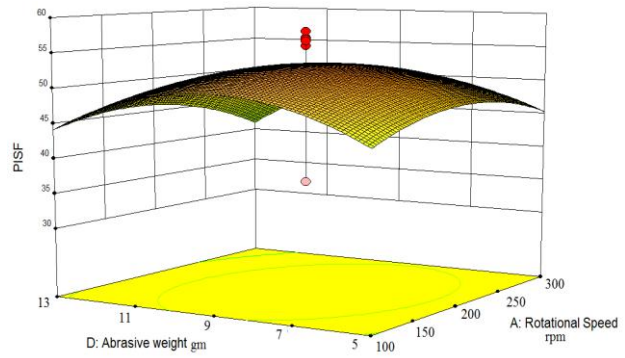

Fig. 3 Interaction effects of Rotational Speed (A) and Abrasive Weight (D)

As the rotational speed decreases by utilizing maximum abrasive weight, the PISF increases minutely. By using minimum abrasive weight, the PISF increases till midpoint value of the rotational speed and decreases afterwards.

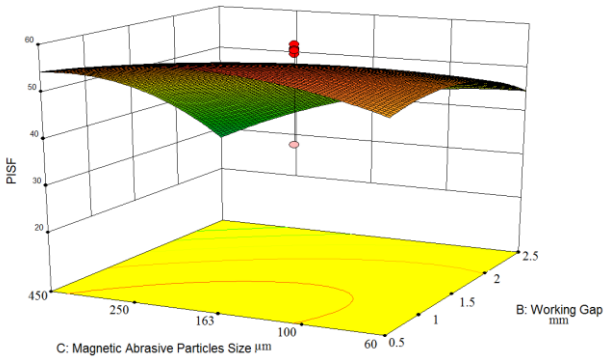

Fig. 4 Interaction effects of Working Gap (B) and MAP Size (C)

Fig. 4 shows interaction effect of working gap and magnetic abrasive particles size. With decrease in working gap by using maximum particle size the PISF increases abruptly. By using minimum particle size and decreasing the working gap, the PISF increases slightly. At minimum gap, the PISF increases minutely by increasing the abrasive particle size. At maximum working gap, by decreasing the particle size, the PISF increases sharply.

Fig. 5 shows the interaction effects of working gap (B) and abrasive weight (D) on the PISF. The PISF increases sharply with decrease in the gap by using abrasive weight as 13gm. When the gap is maximum, the PISF increases noticeably as the abrasive weight decreases. When the gap is minimum, the PISF increases gradually as the weight increases. By using minimum abrasive weight, the PISF increases till midpoint value of the working gap and decreases afterwards.

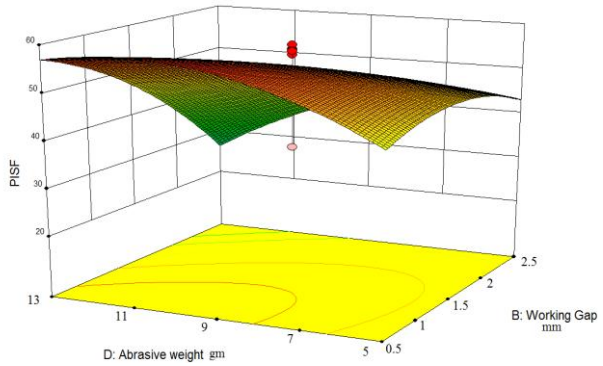

Fig. 5 Interaction effects of Working Gap (B) and Abrasive Weight (D)

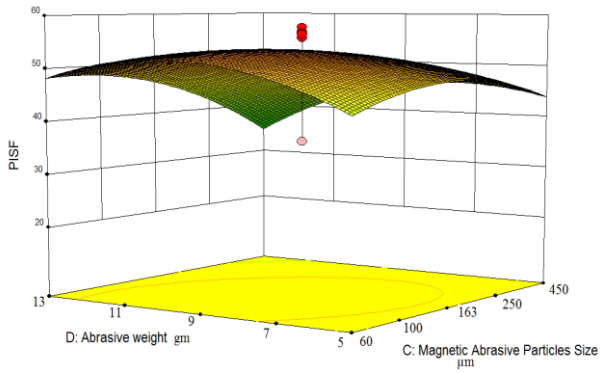

Fig. 6 Interaction effects of MAP Size (C) and Abrasive Weight (D)

Fig. 6 show 3Dgraph plots for the effects of magnetic abrasive particles size (C) and abrasive weight (D) on the PISF. It is observed that PISF decreases pointedly using large size MAP's as the abrasive weight increases. Whereas, PISF increases slightly using small size MAPs as the abrasive weight increases. Keeping minimum abrasive weight, the PISF improves using middle sized MAPs. At maximum abrasive weight value the PISF increases sharply as the MAP size decreases.

4. CONCLUSIONS

In the current research work, the machining of non-magnetic steel (SS307 grade) tubes by MAF process utilizing alumina based sintered magnetic abrasive particles was performed. The conclusions drawn are summarized as follows:

1. The working gap and size of abrasives have predominant effect on the percent improvement in surface finish.
2. The percent improvement in surface finish starts decreasing as the rotational speed of work piece increases.
3. The interaction effect of Rotational Speed (A) and MAP Size (C) had significant effect on PISF.
4. The SEM analysis shows that the tool marks are completely removed by MAF.
5. The process yielded best results at gap = 2mm, speed = 150 rpm, MAP size = 250 µm and weight = 11 gm for PISF on SS 307 grade tubes and surface finish (Ra) of about 0.16 µm.

REFERENCES

[1] Shinmura T, Takazawa K, Hatano E, "Study on magnetic abrasive process-application to plane finishing", Bull Japan Soc Precision Engineering, vol.19, no. 4, 1985,pp.289–291.

[2] Shinmura T, Yamaguchi H, and Shinbo Y, "A New Internal Finishing Process of Nonferromagnetic Tubing by Applying a Rotating Magnetic Field", Int'l Japan Society of Precision Engineering, vol.26, no. 4, 1992, pp.302–304.

[3] Shinmura T, Feng Hui Wang and Toshio Aizawa, "Study on a new Finishing Process of Fine Ceramics by Magnetic Abrasive Machining" , Int .J. Japan Society of precision Engineering, Vol.28 , No. 2, 1994.

[4] Kremen, G.Z, Elsayed, E.A,Feygin S and Igelshteyn L., "Material removal rate and surface roughness of Magnetic Abrasive Process" presented at 3rd international machining and grinding conference Cincinnati, Ohio, 1999.

[5] Dhirendra K. Singh, V. K Jain, V. Raghuram, R. Komanduri, "Analysis of surface texture generated by a flexible magnetic abrasive brush", wear, vol.259, 2005, pp. 1254-1261.

[6] Kwak J.S, "Enhanced magnetic abrasive polishing of non ferrous metals utilizing a permanent magnet", International journal of machine tools and manufacture, vol.49, 2009, pp.613-618.

[7] Shukla A., Singh D.K., "Modelling and optimization of Magnetic Abrasive Finishing Process", International Journal of Engineering Research & Technology (IJERT), ISSN: 2278-0181, 2(9), 2013.

[8] Yamaguchi H., Srivastava A.K., Tan M., Hashimoto F., "Magnetic Abrasive Finishing of cutting tools for high-speed machining of titanium alloys", CIRP Journal of Manufacturing Science and Technology, 7, 2014, pp. 299–304.

[9] Choopani, Y., Razfar, M. R., Saraeian, P., & Farahnakian, M., "Experimental investigation of external surface finishing of AISI 440C stainless steel cylinders using the magnetic abrasive finishing process," *The International Journal of Advanced Manufacturing Technology Int J Adv Manuf Technol*, *83*(9-12), 2016, pp. 1811-1821.

[10] Saraeian P., Mehr H.S., Moradi B., Tavakoli H., Alrahmani O.K., "Stu dy of Magnetic Abrasive Finishing for AISI321 stainless steel", Materi als and Manufacturing Processes. doi:10.1080/10426914. 2016.114019 5, 2016.

Review on Wear Behavior of Magnesium Matrix Composites

Amandeep Singh
Research Scholar
IKG PTU, Jalandhar, Pb, India

Niraj Bala,
Associate Professor,
Mechanical Engg. Dept.
BBSB Engg College Fatehgarh Sahib, Pb, India

Abstract—**In the last decades, light-weight materials such as magnesium matrix composites have become hot topic for material research due to their excellent mechanical and physical properties. But relatively very less work has been done related to the wear behavior of these composites. Magnesium metal matrix composites have wide applications in automobile and aerospace sector. In this review, attempt has been done to collect the literature related to wear behavior of magnesium matrix composites fabricated through various processing techniques. Effect of different reinforcements, reinforcement content, reinforcement size, wear load, sliding speed and time have been studied by different researchers in detail. Wear mechanism under different experimental condition has been reviewed in detail. From the literature it has been observed that wear rate can be decreased with the addition of different reinforcement particles and with their varying percentage. In most of the cases wear rate increases with increase of load.**

Keywords: Magnesium matrix composites, Rreinforcement, Hardness, Wear.

I. INTRODUCTION

Magnesium and its alloys are gaining more attention now days, because of their low density and high strength to weight ratio. But, the applications of these alloys are restricted due to their low wear resistance [1]. In order to enhance wear resistance of magnesium and its alloys, magnesium matrix composites have been developed by adding various reinforcement such as SiC particles, Al_2O_3 particles, fly ash cenospheres (FAC) and TiC[2-8]. These magnesium matrix composites are preferred for many applications such as aerospace and automotive industry.Alminium matrix composites (AMCs) have also been used in specific tribologicalapplications such as brake rotors, piston rings andcylinder liners in automobiles [10]. Different fabrication methods such as stir casting, powder metallurgy, friction stir processing (FSP) and squeeze infiltration technique have been used to make these MMCs [2-8].Magnesium matrix composites (MMCs) can be a better alternative to the AMCs in near future because of their low density, high specific strength, as well as high wear resistance. In spite of the potential ofMMCs, limited work has been done. Very less literature is available related to tribological behavior of MMCs. Wear is a critical problem in the industry which leads to the replacement of engineering components. During the last decade, research has been carried out to understand the wear behaviour of AMCs but a limited work is done on MMCs. The effect of reinforcement content on wear rate, during sliding wear of MMCs has proved that the wear rate of the composite can be enhanced significantly [10]. Based on the literature survey, it has been concluded that the wear resistance is mainly affected by the reinforcement, its volume percentage, reinforcement size, applied load, sliding speed and sliding distance. Considering the potential of magnesium matrix composites as advanced wear resistant material, it is essential to review the wear behavior of different MMCs under various experimental conditions.

II. RELATED WORK OF WEAR STUDIES OF MAGNESIUM MATRIX COMPOSITES

Gertsberg et al. [2] fabricated AZ91/SiC magnesium matrix composites using high-pressure die casting. AZ91D ingots were melted in steel crucible up to 640 ^{0}C under the protection atmosphere of 99.5% CO_2 + 0.5% SF_6.Preheated 700^0 C SiC reinforcement particles were added through spill immersed in the melt. After the addition of the particles while stirring the melt, the stirring was stopped and the melt was held for 2 h in order to enhance wetting between particles and melt. Following this the stirring was resumed for 15 min again. The wear tests on MMC were conducted on a block-on ring type wear resistance testing machine using sliding speed 300 rpm, sliding time 60 min and loads 5-120 N. The weight losses before and after wear test were calculated. The wear surfaces of composite showed that at high loads the material removed from the surface of composite specimens occurred due to the higher level of porosity, while the worn surfaces of base metal were relatively smoother.

Yu and Huang [3] investigated the effects of the applied load, the wear time, diameter and the fly ash cenosphere (FAC) content on the wear behavior of the AZ91D/ fly ash cenosphere composites fabricated through stir casting method. Four different diameters of FAC ie. 40, 80,100 and 150µm were used for composite fabrication.Wear tests were performed on pin-on-disk wear test machine under dry sliding condition. The rotational speed of the disk used was 60 rpm. The applied load was 5, 10, 20, and 30 N, respectively and the wearing time was 10, 20, 30, and 50 min, respectively. Results indicated that AZ91D/ 6 wt.% FAC composites were more wear resistant than AZ91D under above testing conditions.

Under the same applied load, the wear resistance of the composites is excellent when FAC diameter is moderate ie 100µm. If FAC diameter is more than 100um the wear of the composites decreased again. The wear resistance of the composites decreased with the increase in the applied load.

Nonlinear relationship was observed between the worn mass loss and the applied load. The mass fraction of FAC in the composites has also important effect on the wear resistance of the composites. With the increase in the mass fraction of FAC worn mass loss of composites decreased. The wear resistance of the composites is excellent when the mass fraction of FAC is 6 Wt.% which is also confirmed from surface morphology of composite.

Abbasi et al. [4] developed surface composites on the surface of AZ91 magnesium alloy by application of FSP. Two types of surface composites were prepared using SiC and Al_2O_3 particles separately as reinforcements. The results showed that wear properties of FSPed samples were better than AZ91. The results indicated that by increment of FSP pass upto 4 number wear rate decreased. The results also showed that particle type did not have significant effect on wear rate. Microscopic images show that grooves in base metal are deeper than those in processed samples. This can be correlated to the lower hardness of as-received material as compared to processed samples.

Chen et al. [5] successfullyprepared a surface composite layer reinforced by SiC particles on the thixoformed (TF) AZ91D alloy by FSP and the corresponding tribological properties were investigated. The microstructural evolution of the thermomechanically affected zone (TMAZ) could be clearly observed during FSP of the thixoformed AZ91D alloy. The main mechanisms of grain refinement during FSP include thermodynamic recrystallization and mechanical separation. The thixoformed AZ91D alloy with the composite surface possessed good tribological properties which were because of the presence of SiCp. Compared with the corresponding permanent mould casting alloy and the TF alloy without composite surface, the composite surface showed the highest wear resistance and lowest friction coefficient.

Reddy et al. [6] fabricated surface composites using friction stir processing. ZM21 magnesium alloy was used as matrix. Silicon carbide and boron carbide powders are used as reinforcement. Composites were characterized by metallography, hardness and pin-on-disc testing. Results show fine and uniform distribution of carbide particles in Mg matrix. Processed composites exhibited excellent wear resistance and which was attributed to grain boundary pinning and dispersion hardening caused by carbide particles. Composite prepared with boron carbide was found to possess better wear resistance than composites made with silicon carbide. This was attributed to formation of very hard surface layer of boron carbide reinforced composite. The wear behaviour of surface composite layer on ZM21 Mg alloy with that of conventionally used engineering materials such as mild steel and austenitic stainless steel was also compared. Jo et al. [7] investigated the effect of SiC particle size on the wear properties of AZ91 hybrid metal matrix composites reinforced with Saffil short fibers and SiC particles prepared through squeeze infiltration process. Different particle sizes of SiC 1, 7, and 20 μm, respectively, were used. The volume fractions of Saffil short fibers and SiC particles used in the hybrid composites fabrication were 15 and 5%, respectively. Ball-on disk wear test were conducted under loads of 5, 15, and 30 N and at sliding speeds of 0.1 and 0.2 m/s. The results indicated that the composite reinforced with large-sized SiC particles had better wear resistance compared with the smaller sized particles. At a low sliding speed and under lower loads of 5 and 15 N, the dominant wear mechanism of the composites observed was abrasive/adhesive. With the increase of load to 30 N a transition from abrasive/adhesive to severe abrasive wear occurred. A mechanically mixed layer was formed on the surface of the composite, at a higher sliding speed, which helped to increase wear resistance of the hybrid composites. The main mechanism under this condition was delamination wear. The effect of SiC particle size on wear properties in composites was found to be negligible under conditions of abrasive/adhesive or delamination wear mechanisms. However, the wear behavior of composites was largely influenced by their SiC particle size when the abrasive mechanism was severe.

Narayanasamy et al. [8] studied the effect of hybridizing MoS_2 on the tribological behavior of Mg–TiC Composites. A magnesium–TiC–MoS2 hybrid composite was developed by powder metallurgy route. The results indicated that the Mg–TiC–MoS_2 hybrid composites possess better hardness, higher wear resistance and lower coefficient of friction when compared with Mg, Mg–TiC and Mg–MoS_2 composites. The increase in hardness was attributed to the presence of hard TiC particles. Hardness was slightly decreased with addition of MoS2 when compared to Mg–TiC composite. The wear behaviors of these composites were investigated by pin-on-disc wear testing apparatus under dry sliding condition. The wear resistance of the composites improved considerably as compared to that of the magnesium matrix due to the courteous effect of both the reinforcements. The best tribiological performance was seen in composite with 10 wt% TiC and 5 wt% MoS_2. It was observed that wear loss and coefficient of friction increased with increase of either load or sliding distance or both, whereas wear loss and coefficient of friction decreased with increase of speed. The worn surfaces of various composites showed that abrasive wear and delamination were the major wear mechanisms.

Huang et al. [9] studied the effects of silicon carbide particle size on wear behavior of AZ91D /SiCp composite prepared by the melt stirring technique. Results indicated that the of SiC

TABLE1: SUMMARY OF RESEARCH WORK DONE BY VARIOUS RESEARCHERS' RELATED TO WEAR OF MAGNESIUM MATRIX COMPOSITES

S. NO.	INVESTIGATORS	MATRIX USED	REINFORCEMENT USED	TECHNIQUE USED	IMPORTANT RESULTS
1.	Gertsberg et al. [2]	AZ91D	SiC average particle size 10 µm 5 and 10 wt.%	high-pressure die casting	• Lesser wear rate of reinforced composites in comparsion to unreinforced alloy. • Increase in wear rate with increase of load.
2.	Yu and Huang [3]	AZ91D	Fly ash cenosphere 6 wt.%	Stir casting	• Better wear resistance of fabricated composites in comparsion to Mg alloy. • Excellent wear resistance of the composites achieved with moderate FAC diameter. • Wear resistance of the composites decreased with the increase in the applied load.
3.	Abbasi et al. [4]	AZ91	SiC 30 nm. Al2O3 30 nm.	FSP	• Wear rate of base metal found greater than other composites. • With increase in FSP pass hardness increases which lead to decrease in wear rate. • Processed composites using SiC and Al_2O_3 particles have nearly the same wear resistance.
4.	Chen et al.[5]	AZ91D	SiC	Permanent mould casting FSP composites	• Good tribological properties obtained in the composite surface of thixoformed AZ91D alloy. • The friction coefficient and wear rate found to be minimum in case of surface composite as compared to permanent mould casting, thixoformed alloy. • For surfaced composites increase in hardness lead to decrease in wear rate.
5.	Reddy et al. [6]	ZM21	SiC and B4C	Friction stir processing (FSP)	• Surface composites prepared with B4C obtained superior wear resistant as compared to those made with silicon carbide. • Improvement in the hardness of composite layer with the addition of carbides. • FSP with boron carbide powder significantly improved the wear resistance over the base metal.
6.	Jo et al. [7]	AZ91	Saffil short fibers SiC particles particle sizes of 1, 7, and 20 µm 15 and 5%	Squeeze infiltration	• At low sliding speed and loading conditions, the dominant wear mechanism of the hybrid composites was found to be abrasive/adhesive. • With increase of load, mechanism changed from abrasive/adhesive to severe abrasive. • At a high sliding speed, wear resistance of the hybrid composites increased and wear mechanism involved in this condition was delamination wear. • No effect of SiC particle size on wear properties in composites.
7.	Narayanasamy et al. [8]	magnesium powder (99.8 % purity)	TiC and MoS_2	Powder metallurgy	• Hybrid composites Mg–TiC–MoS_2 possess better hardness and higher wear resistance as compared to Mg, Mg–TiC and Mg–MoS_2 composites. • Best tribological performance of composite observed at 10 wt% TiC and 5 wt% MoS_2. • Abrasive wear and delamination are the major wear mechanisms seen on worn surface of composites.
8.	Huang et al. [9]	AZ91D	SiC volume fraction of 3% 5, 11, and 15 lm	Melt-stirring	• Improved in wear resistance with the addition of SiC. • The coefficient of friction increased with increasing particle size of SiC. • The specific wear rate decreased with increasing particle size of SiC. • Under different load, wear mechanism of composites was abrasion, oxidation, and delamination.

9.	Xiu et al. [10]	AZ91	5, 10 and 15 wt.% TiC	TiCp–Al master alloy process combined with mechanical stirring.	• Hardness and wear resistance of the composites improved significantly as compared to base metal. • The wear resistance of the composite increased with increase of the TiC content. • Wear volume loss increased with increase of applied loads or wearing time. • The wear mechanism was mainly ploughing, adhesion and oxidation.
10.	Yao et al. [11]	AZ91	TiC	Spray deposition.	• Wear resistance of composites improved with the addition of TiC. • At a lower load, wear rate of composites decreased with increasing TiC content, and the dominant wear mechanism was oxidation. • At a higher load, Mg composites showed excellent wear resistance and the dominant wear mechanism was delamination.
11.	Saravanan and Surappa [12]	Pure magnesium	SiC 30 Vol.%	Melt stir technique	• Cast composites showed significant decrease in wear rate in comparison to pure Mg
12.	Asadi et al. [13]	AZ91	nanosizedSiC and Al2O3 particles	FSP	• Increase in wear resistance in composites as compared to the base metal. • Better wear resistance obtained with SiC reinforcement.. • Wear mechanism was twofold in specimen reinforced with SiC particles, while in the specimen with Al_2O_3 particles, delamination wear occurred.

addition could improve the wear resistance of AZ91D matrix alloy for most of the sliding conditions. The superior wear resistance was exhibited under lower and moderate sliding condition. The hardness of composites after wear tests was measured and observed that it increased with increasing particle size of SiC both for 10 and 50 N loading conditions at low sliding speed of 250, 1000, and 1500 rpm. The specific wear rate decreased with increasing particle size of SiC for moderate sliding conditions at any specific sliding speed of 250 and 1000 rpm, except for 10 and 50 N at the severe sliding condition of 1500 rpm. The wear mechanism under 10N load was moderate abrasion, moderate oxidation, and slight delamination and slight abrasion, moderate oxidation, heavy delamination, and moderate adhesion and moderate softening/melting types for load of 50 N.

Xiu et al. [10] investigated the the sliding wear behavior of TiC/AZ91 magnesium matrix composites. Different weight % of TiC (5, 10 and 15 wt.%) particulates were used to fabricate TiCp–Al master alloy process combined with mechanical stirring. The effect of TiC particulate content, applied load and wearing time on the sliding wear property of the composites was studied. Results indicate that the hardness and wear resistance of the composites improved significantly as compared to AZ91 alloy. The wear resistance of the composites increases with increase of the reinforcement content, on the other hand friction coefficient of the composites decreased with increase of reinforcement content. The wear volume loss and friction coefficient of the composites as well as the base material increased with increase of applied load or wearing time, but the increase rates of the reinforced composites in two performance was found to be lower than those of the unreinforced AZ91 matrix alloy. Wear behavior mechanism observed in the unreinforced AZ91 matrix alloy and the composites was ploughing, adhesion and oxidation.

Yao et al. [11] studied wear mechanism of TiC particles reinforced AZ91 magnesium matrix composites fabricated by a melt in situ reaction spray deposition method. The dry sliding wear tests were performed under different load conditions 10, 20, 30, 40, and 50 N. Results showed that the composites had much better wear-resistance than the AZ91 alloy. The wear behavior of the composites was dependent on the TiC content in the matrix and the applied load. At a minimum load, the wear rate of fabricated composites decreased with increasing TiC content, and the dominant wear mechanism was an oxidative mechanism. At maximum loads, composites exhibited superior wear resistance to the AZ91 magnesium alloy, and the dominant wear mechanism involved was delamination.

Saravanan and Surappa [12] fabricated pure magnesium-30 vol.% SiC particle composite by melt stir technique without the use of a flux or protective atmosphere. Hot extrusion was done on cast composites with an extrusion ratio of 13. Pin-on disc machine was used for wear testing under loads in the range 5–50 N and at a sliding speed of 0.5 m/s. Results indicate that Magnesium composites show a wear rate lower by two orders of magnitude when compared to pure Mg. Improvement in wear resistance was attributed to the presence of SiC particles and to the improved strength of the composite.

Asadi et al. [13] studied the effects of particle types and number of friction stir processing passes on the magnesium-based nanocomposite produced by Friction Stir Processing. Two different nanosized particulate reinforcements (SiC and Al_2O_3) were added to as-cast AZ91 magnesium alloy.Thenanocomposite prepared with SiC particles showed smaller grain size and higher hardness and wear resistance in

comparison to nanocomposites prepared with Al_2O_3 particles. The wear resistance increased with the addition of reinforcing particles. In the composites fabricated with SiC particles, the wear mechanism is twofold, while in the composites with Al_2O_3 particles, delamination occurs due to the low integrity between alumina clusters and the magnesium matrix. Results showed that with the increase in FSP passes hardness and wear resistance improved due to grain refinement. Table1. has been prepared for quick review of the wear studies related to magnesium matrix composites.

III. CONCLUSIONS

Magnesium matrix composites have become excellent material in comparison to magnesium and its magnesium alloys. In last decades, some studies have been carried out to understand microstructure and mechanical properties of these composites to prop up their application in the automobile and aerospace industries. However, very less effort have been done to understand wear behavior of these composites. In this paper wear behavior of magnesium matrix composites fabricated using different techniques has been reviewed. From above studies it was concluded that wear rate of composites can be improved with the addition of different reinforcements such as SiC, Al2O3, TiC, FAC and B4C. In most of the cases wear rate increased with increase of load except for flyash reinforcement, in which a marginal decrease in wear was observed by the researcher. The wear resistance of the composite increased with increase of the reinforcement content in general. In surface composites with increase in FSP pass hardness increased which further lead to decrease in wear rate. Under different wear conditions dominant wear mechanisms observed in different composites was abrasive/adhesive, oxidation, and delamination. Hence it may be concluded that Mg matrix composites can be used for specific applications in automotive sector where wear resistance is major concern.

REFERENCES

[1] L. Chen and Y. Yao (2014), "Processing, Microstructures, and Mechanical Properties of Magnesium Matrix Composites: A Review", Acta Metall. Sin. (Engl. Lett.), 27(5), pp 762–774.

[2] G. Gertsberg, E. Aghion, A. Kaya, and D. Eliezer (2009), " Advanced Production Process and Properties of Die Cast Magnesium Composites Based on AZ91D and SiC", Journal of Materials Engineering and Performance,18(7),pp 886–892

[3] S.R.Yu and Z.Q. Huang (2014), "Dry Sliding Wear Behavior of Fly Ash Cenosphere/AZ91D Mg Alloy Composites", Journal of Materials Engineering and Performance, 23(10), pp 3480–3488.

[4] M. Abbasi, B. Bagheri, M. Dadaei, H. R Omidvar. and M. Rezaei (2015)), " The effect of FSP on mechanical, tribological, and corrosion behavior of composite layer developed on magnesium AZ91 alloy surface", Int J AdvManuf Technology, 77, pp 2051–2058.

[5] T. Chen, Z. Zhu, Y. Ma, Y. Li and Y. Hao (2010), "Friction Stir Processing of Thixoformed AZ91D Magnesium Alloy and Fabrication of Surface Composite Reinforced by SiCps",Journal of Wuhan University of Technology-Mater. Science, 25(2), pp 223-227.

[6] G. M. Reddy, A. S. Rao and K.S. Rao (2013), "Friction Stir Processing for Enhancement of Wear Resistance of ZM21 Magnesium Alloy", Trans Indian InstMet , 66(1), pp13–24

[7] S. K. Jo, W. J. Lee, Y. H. Park and I. M. Park (2012), "Effect of SiC Particle Size on Wear Properties of Al2O3.SiO2/SiC/Mg Hybrid Metal Matrix Composites", TribolLett, 45, pp101–107.

[8] P. Narayanasamy, N. Selvakumar and P. Balasundar (2015), "Effect of Hybridizing MoS2 on the TribologicalBehaviour of Mg–TiCComposites"Trans Indian Inst Met. DOI 10.1007/s12666-015-0530-z

[9] S. J. Huang, Y. R. Jeng, V. I. Semenov and Y.Z. Dai (2011), " Particle Size Effects of Silicon Carbide on Wear Behavior of SiCp-Reinforced Magnesium Matrix Composites" TribolLett, 42, pp79–87

[10] K. Xiu, H. Y. Wang, H. L. Sui, Y. Wang, C. L. Xu, J. G. Wang and Q. C. Jiang (2006), "The sliding wear behavior of TiCp/AZ91 magnesium matrix Composites" Journal Mater Sci, 41, pp7052–7058

[11] J. Yao, W. Li, L. Zhang, F. Wang, M. Xue, H.Jiang and J. Lu(2010)' "Wear Mechanism for In Situ TiC Particle Reinforced AZ91 Magnesium Matrix Composites" , TribolLett , 38, pp 253–257

[12] R.A Saravanan. and M.K. Surappa. (2000)," Fabrication and characterisation of pure magnesium-30 vol.% SiCP particle composite", Materials Science and Engineering A276, pp108–116

[13] P. Asadi, G.Faraji, A. Masoumi, and M.K. BesharatiGivi (2011), "Experimental Investigation of Magnesium-Base Nanocomposite Produced by Friction Stir Processing: Effects of Particle Types and Number of Friction Stir Processing Passes", Metallurgical and Materials Transactions A, ,42A, pp 2820—2832.

Investigation Related to Wear Behaviour of HVOF Sprayed Carbide based Coatings

Gaganjot Singh
Assistant Professor
Baba Banda Singh Bahadur Engineering College
Fatehgarh Sahib

Niraj Bala
Associate Professor
Baba Banda Singh Bahadur Engineering College
Fatehgarh Sahib

Avtar Singh
Assistant Professor
Baba Banda Singh Bahadur Engineering College
Fatehgarh Sahib

Jatinder Singh
M.tech. student
Baba Banda Singh Bahadur Engineering College
Fatehgarh Sahib

***Abstract*- Structure components such as boilers fail in high-temperature situationsbecause of contact of the atmosphere with the material, resulting in erosion, wear and successiveenhanced degradation, or to unintentional overheating due to reduced process control. To overcome this problem, three carbide based coatings namely WC-Co, CrC-NiCr and WC-Co-Cr coating were effectively deposited on ASTM-SA213-T11 boiler tube steel by HVOF thermal spray method. In the present work, wear testing was done to examine the performance of the coating. Wear testing was approved on pin on disc wear test set up by means of two different loads 2kg and 3kg and two disc speeds 500rpm and 800rpm. Wear resistance was determined from the weight loss outcomes.The outcomes of the coated steels have also been equated with the uncoated substrate steel. The samples were categorized by SEM analysis.Coating of CrC-NiCr showed maximum resistance through wear testing.**

Keywords: Wear; HVOF Spray; WC-Co, CrC-NiCr, WC-Co-Cr; Boiler Steel

I. INTRODUCTION

Workable engineering elements have todepend on their majority material properties along with the design and features of their surface. This has been seen in wear resistance elements because their surface must accomplish lot of engineering functions in a range of difficult environments. The study of the material is then greatly reliant onthe surface of the material, surface contact area and the atmosphere under which the material must work[1].The metallic material surface is comprised up of a matrix of individual grains, which fluctuate in size and bond strength reliant on the resources by which the material was produced and on the elements used to make those grains [1]. Structure components as boilers fail in high-temperature situations can be because of contact of the atmosphere with the material, causing in erosion, weardue to reduced process control. Wear is linked to communications between surfaces and more precisely the elimination and deformation of material on a surface as a effect of mechanical action of the reverse surface [2]. Erosion is well-defined as the wear produced by hard particles striking a surface, passed by a gas stream, or entrained in a flowing liquid medium [3]. Solid particle erosion (SPE) for the electric power industry is a main issue, costing an about US$150 million a year in productivity loss, repair costs [4]. At high temperatures, erosion is a main issue in lot of engineering systems, taking steams and jet turbines, boilers [5].Wear because of abrasion mostly rely on the surface of the material visible to the fluid and on the properties of the particles passed with the fluid [6].T11and SA516 substrate steels are commonly used in hydroelectric power plants becauseof their superior erosion properties and tolerable resistance to solid particle erosion.Thermal spraying method is one of the commonlyadaptable hard-facing techniques offered for the use of coating materials to guard components from abrasive wear, adhesive wear,erosive wear[7].The coating material shall be in the form of a powder, wire, ceramic-rod, or molten materials [8]. Thermal sprayed coatings are applied to enhance the wear characteristics of surfaces as they combine different attractive features i.e. resistance to abrasion, high temperature, erosion and corrosive atmospheres [9]. This issue of wear and erosion at high temperatures in boilers can be resolved out by various thermal spray coatings. In the present work HVOF spraying technique has been appliedto deposit coatings on T11 substrate. High-velocity oxy-fuel (HVOF) spraying is a rapidly emerging thermal spray technology for deposition of surface coatings. This is because of the attainment of higher kinetic energy of the particulates and lower melting degrees which empower particle flattening in the plastic state [10]. Components coated by the HVOF method include pump impellers and casings, valve bodies and pipe systems [11].Other benefits of these coatings include the ease of application[12].The process has been most effective for deposition of cermets materials (WC–Co, etc.) and corrosion-resistant alloys (stainless steels, nickel-based alloys, aluminium etc. [13]. Powder particles of the preferred coating material are fed axially into a hot gas stream, thereafter into a spray gun, where they are liquefied and propelled to the work piece surface to be coated [14].T11 substrate steel is mostly used in boiler power plants because of their brilliant resistance to solid particle erosion and wear resistance properties. In this work testing will be carried out on the coated and uncoated T11 steel. Various powders used for

deposition of carbide based coatings are WC-CO-Cr, CrC-NiCr and WC-CO. Wear testing is carried out at different loads and disc speeds. The SEM analysis will also be carried out for various specimens.

II. EXPERIMENTAL PROCEDURE

A. Substrate and Feedstock Powder

Substrate material choosen for the current study is T11 steel designated as ASTM-SA213-T11 steel with chemical composition (weight %) C 0.15, Mn 0.3-0.6, S 0.03 max, P 0.03 max, Si 0.5-1, Cr 1-1.5, Mo 0.44-0.65 and rest is Fe. It was procured from Cheema Boilers Limited, Ban Majra, Kurali (India). For wear testing specimens were cut in cylindrical form each measuring 20mm x 5mm x 5mm approximately. The specimens were polished and grit blasted by Al_2O_3 (Grit 60) before the deposition of the coatings. Three types of carbide based coating powder compositions were deposited on the given steel by the HVOF spraying, which include WC-CO, CrC-NiCr and WC-CO-Cr powder.

B. Deposition Technique and Equipment

HVOF spraying was applied for deposition of coatings. HVOF spray coatings were deposited at Metalizing Equipment Private. Ltd, Jodhpur. The various parameters used during HVOF spraying have been given in Table 1.

Table 1-Process parameters for the HVOF spray process

Process gas	Oxygen
Air pressure	6 Kg/cm^2
Process gas pressure	10 Kg/cm^2
Powder feed rate	40g/min
Carrier gas flow	18 kg/hr
Spray distance	6 inches
Coating thickness	225-250µm

C. Wear Experiments

Wear tests were executed on the pin specimens that had flat surfaces in the contact regions. The pin was held static against the counter face of a rotating disc made of En-32 steel at 100 mm track diameter. En-32 steel is a plain carbon steel; case hardened 62 to 65 HRC as provided with the pin-on-disc machine.

After that SEM analysis on Sophisticated Analytical Instruments Laboratories, Punjabi University, Patiala (Punjab) was done on all samples.

III. RESULTS AND DISCUSSIONS

A. Hardness Analysis

Hardness analysis was prepared for all the coated and uncoated specimens of T11 steel. Hardness values for substrate T11 steel is shown in Table 2. From all the specimens, T11 steel having CrC-NiCr coating indicated maximum hardness and T11 steel having WC-CO coating indicated minimum hardness. Sequence based upon overall hardness values for the coated and uncoated T11 steel was as follows:

CrC-NiCr>WC-Co-Cr>WC-Co>Uncoated T11 steel.

Table 2-Hardness values for substrate T11 steel

S.No.	Coating	Hardness values (HRA)
1.	Uncoated T11	216
2.	WC-CO coating on T11	228
3.	WC-CO-Cr coating on T11	235
4.	CrC-NiCr coating on T11	236

The results presented that maximum hardness was obtained by CrC-NiCr coating. Further addition of Cr to WC-Co increases its hardness value and has higher contiguity [15].

B. Wear Testing

T11 steel was examined for wear testing on the pin on disc wear test set up. The wear rate of the uncoated and coated steels was carried out at two loads i.e. 2kg and 3kg and at two disc speeds i.e. 500rpm and 800rpm.The test was conducted using disc track diameter 80mm. For each sample six reading were taken and the time interval for each reading was 2mins.

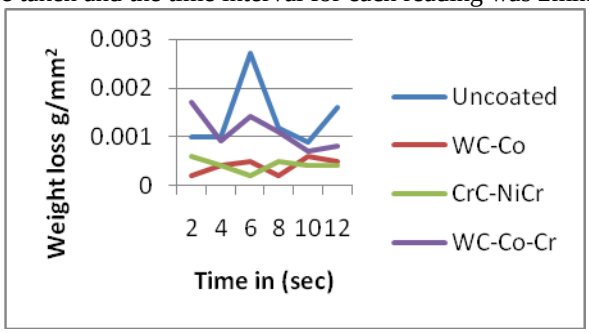

Figure 1- Wear rate for coated and uncoated T11 steels at 2kg load and 500rpm

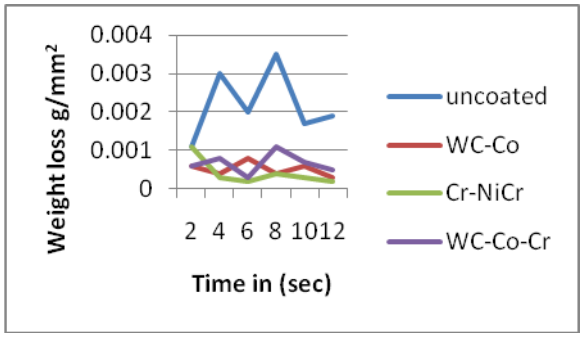

Figure 2- Wear rate for coated and uncoated T11 steels at 2kg load and 800rpm

Weight loss after each cycle (g/mm^2) at both loads 2kg and 3kg and at both speeds 500rpm and 800rpm during wear testing has been reported in Table 3 and 4. It can be inferred from the plots that the necessary

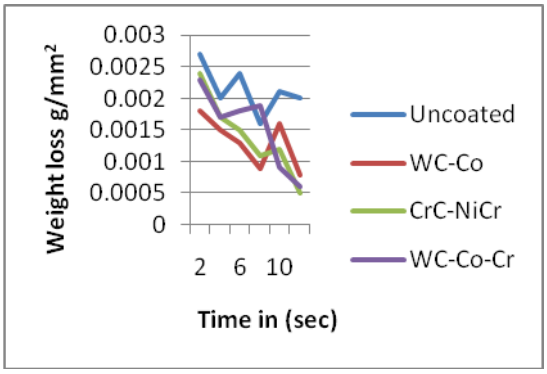

Figure 3- Wear rate for coated and uncoated T11 steels at 3kg load and 500rpm

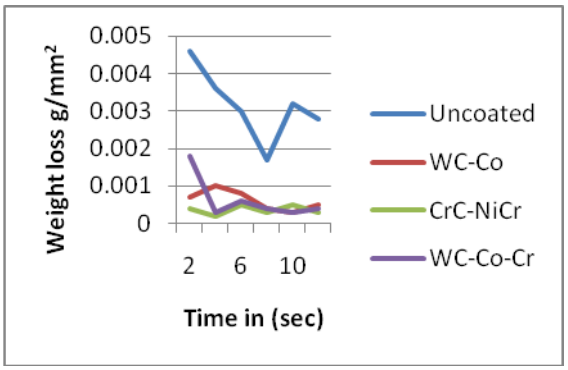

Figure 4- Wear rate for coated and uncoated T11 steels at 3kg load and 800rpm

protection against wear has been provided by all the coatings as the weight loss values for the coated steels are smaller than those for the uncoated steel.

It can be clearly seen from the figure 1-4that uncoated T11 steel conceived higher weight loss than all the coated T11 steels. It can be observed that T11 steel having coating WC-Co was least resistant and coating CrC-NiCr was most resistant to wear rate in comparison to other coatings. Sequence of the wear resistance based upon overall weight loss for the coated and uncoated T11 steel at 2kg and 3kg load for speed 500 rpm and 800 rpm was as follows:

CrC-NiCr>WC-Co-Cr>WC-Co> Uncoated T11 steel

The results presented that maximum resistance to wear was obtained by CrC-NiCr coating. It is known that addition of Cr to WC–Co increases binding of the metallic matrix with the WC grains and provides better wear resistant coating. Thus, WC–Co–Cr is considered to be a potential wear resistant coating material as compared to WC–Co coating [16].

C. SEM analysis of wear tested samples

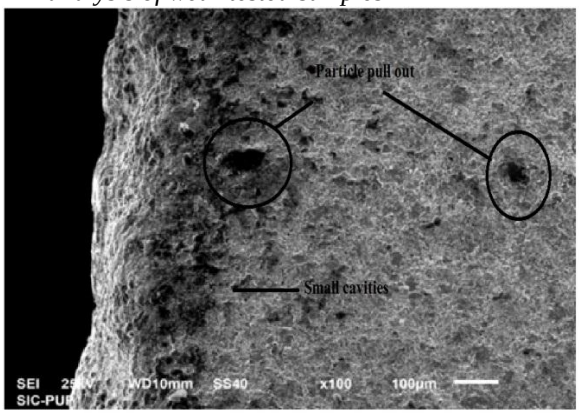

Figure 5- SEM micrograph of WC-Co coated T11 steel after wear testing

From the SEM micrograph (figure 5) it can be seen that WC-Co coated T11 steel after wear testing shows the presence of particle pull out and small cavities are showing material removal. The blackish area at the sides of specimen represents deformation ofmaterial in the form of cavities. From the SEM micrograph (figure 6) of WC-Co-Cr coated T11 steel after wear testing, presence of grooves and cavities shows the deformation of material during wear testing. Some areas also show delamination. From the SEM micrograph (figure 7)of CrC-NiCr coated T11steel after wear testing it can be clearly observed that this coating possess uniform and least wear loss than all other coatings with very small cavities and grooves.

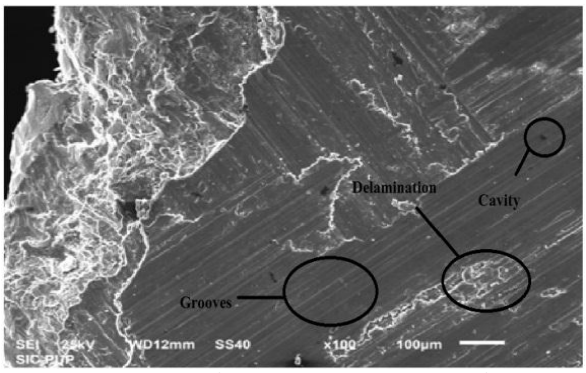

Figure 6- SEM micrograph of WC-Co-Cr coated T11 steel after wear testing

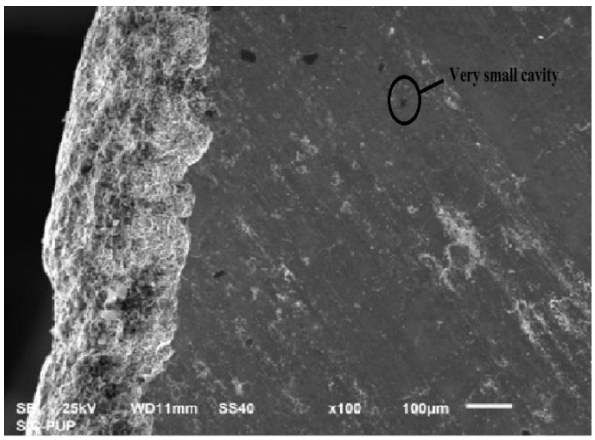

Figure 7- SEM micrograph of CrC-NiCr coated T11 steel after wear TESTING

IV. CONCLUSIONS

Conclusions from the present study have been summarized as given below.

- Uncoated substrate T11 possessed higher weight loss in comparison to coated T11 substrates at both loads i.e. 2kg and 3kg and at both speeds i.e.500rpm and 800rpm during wear testing.
- During wear testing, at both 500rpm and 800rpm at same load 2kg, CrC-NiCr coating possessed least weight loss in comparison to the WC-Co-Cr and WC-Co coatings, which showed that, CrC-NiCr possess the least wear rate.
- During wear testing, at both 500rpm and 800rpm at same load 3kg, WC-Co coating possessed highest weight loss in comparison to the CrC-NiCr and WC-Co-Cr coatings, which showed that, WC-Co possesses the highest wear rate.
- At both speeds 500rpm and 800rpm and at both loads 2kg and 3kg,during wear testing CrC-NiCr coating possessed least weight loss in comparison to the WC-Co and WC-Co-Cr coatings, which showed that, CrC-NiCr possess the lowest wear rate.

REFERENCES

[1] Herman, H. and Sampath, S., 2007. “Thermal spray coatings”, The Thermal Spray Laboratory Department of Material Science and Engineering, State University of New York Stony Brook, pp.11794-2275.

[2] Hawthorne, H.M., 1999.“Comparison of slurry and dry erosion behaviour of some HVOF thermal sprayed coatings”, Wear, vol.225–229, pp.825-834.

[3] Hutchings, I.M., 1992. “Tribology-friction and wear of engineering materials”, Arnold, Pans.

[4] Stein, S.S., Marder, 1999. “Erosion of thermal spray MCr-CrC Cermet coatings,” wear, vol.224, pp. 153-159.

[5] Hidalgo, J.B, Menendez, S.P., 2001. “High temperature erosion wear of flame and plasma sprayed nickel-chromium coatings under simulated coal-fired boiler atmospheres”, wear, vol.247, pp. 214-222.

[6] Alam, S., Sasaki, S., Shimura, H., 2001. “Friction and wear characteristics of aluminum bronze coatings on steel substrates sprayed by a low pressure plasma technique”, Wear, vol.248, pp.75–81.

[7] Ishikawa, K., Shi, G.Y., 1993. “Journal of the Japan Welding Society”,vol.6, pp.11.

[8] Frank, J. and Hermanek, 2001.“Thermal Spray Terminology and Company Origins”, ASM International, Materials Park, OH.

[9] Xu, H., Luo, X., 1998. “Proceedings of the 19th IAHR Symposium on Hydraulic machininery Cavitation”, vol.2, pp.544–555.

[10] Planche, M.P., Normand, B., Liao, H., Rannou, G., Coddet, C.,2003. “Comparison of HVOF and plasma sprayed alumina / titatia coatings–microstructure, mechanical properties and abrasion behavior”, Surface and Coatings Technology, vol. 167, Issue 1, pp. 68-76

[11] Dallare, S., (2001) “Hard Arc-Sprayed Coating with Enhanced Erosion and Abrasion Wear Resistance”, Journal of Thermal Spray Technology, vol. 10(4), pp. 511-519.

[12] Mack, R., Drtina, P., Lang, E., (1999) “Numerical Prediction of Erosion on Guide Vanes and In Labyrinth Seals in Hydraulic Turbines”, Wear, pp. 685-691.

[13] Rajasekaran, B., Mauer, G., Vaben, R., A. Röttger, Weber, S., Theisen, W. (2010) “Thick tool steel coatings using HVOF spraying for wear resistance application”, Surface and Coatings Technology, vol. 205, Issue 7, pp. 2449-2454

[14] Brandl, W.D., Toma, H., Grabke, J., (1998) “The characteristics of alumina scales formed on HVOF sprayed MCrAIY coatings”, Surface and Coatings Technology, vol. 108–109, pp. 10-15.

[15] Jonathan, W., Susanne,N., Hans, O. A,(2009) “Effect of V, Cr and Mn additions on the microstructure of WC–Co”, International journal of refractory metals and hard materials, vol.27, issue 5, pp. 817-822.

[16] J.K, Murthy, D.S, Rao, B,Venkataraman, 2007. “Effect of grinding on the erosion behaviour of a WC–Co–Cr coating deposited by HVOF and detonation gun spray processes”, vol.249, issue7, pp.592-600.

A Comparative Study of Fuzzy C-Means and Possibilistic Fuzzy C-Means Algorithm on Noisy Grayscale Images

Sachin Singla
M.Tech IT Student
Department of Computer Science & IT
BBSBEC, Fatehgarh Sahib

Baljit Singh Khehra
Associate Professor
Department of Computer Science & IT
BBSBEC, Fatehgarh Sahib

***Abstract*— Grouping is used to organize graphical data in the cluster's unsupervised learning methods. Grouping is used in the field of image processing to identify objects that have the same characteristics in an image. Clustering can be categorized into Hard and Fuzzy clustering scheme. This paper deals with the study of clustering soft (Fuzzy) algorithm outputs such as Fuzzy C-Means (FCM) and Possibilistic Fuzzy C-Means (PFCM). These algorithms are used to segment and analyze standard and colored images, but this research work involves noisy images in gray levels. PSNR, MSE and SSIM are used as an evaluation parameter to compare the FCM and PFCM results. Finally, the experimental results proved that PFCM favorable on FCM.**

***Keywords*— Image segmentation, Clustering, FCM, PFCM.**

I. INTRODUCTION

Image segmentation is an important step behind image understanding and image analysis, such as positioning objects and boundaries, machine vision and medical imaging. The purpose of segmentation is to divide the image into a set of different, visually distinct, uniform and significant areas based on certain characteristics such as intensity, color, and texture. Many different segmentation techniques have been discovered and can be seen in [1-3]. Image segmentation is divided into four techniques, namely, threshold, edge detection, grouping and extraction. However, this paper only deals with image segmentation based on method Clustering.

Clustering is used to process similar items, based on their respective data in the data set being grouped into groups. Assembling the data elements into clusters depends on the principle of maximizing similarity dissimilarity and reduces the similarity of things. The data items are assigned to the eligible cluster based on the minimum distance of the data item. The quality of clusters depends on low interclass and high intraclass similarity [4]. Clustering can be divided into hard and fuzzy clustering schemes, and each person has their own characteristics. Hard clusters limit each data point to exactly one cluster. Therefore, the use of hard clustering is a very difficult task in which the image has poor contrast, overlapping intensity, noise, and the like.

Another clustering scheme is fuzzy clustering based on the membership of each data item. In fuzzy clustering, fuzzy C-means is a widely used algorithm, in which each data item has a certain degree of membership value, which is used to determine the proximity of data items to clusters [5,6]. In Fuzzy C, each data item can belong to one or more clusters. FCM has a problem, it creates noise.

To avoid this problem, Krishnapuram and Keller proposed a new fuzzy clustering model called c-mean probability (PCM) [7, 8]. PCM uses typical values instead of member values, but PCM has the problem of overlapping clusters. PFCM is a better clustering algorithm because it has the potential to give members or typical values more value [9]. PFCM inherits the properties of PCM and FCM and generally avoids various problems such as cluster matching and noise sensitivity. Section II discusses the FCM, Section III discusses the PFCM, Section IV presents the experimental results which include some of the evaluation parameters, comparing FCM and PFCM, and Section V concludes the paper.

II. FUZZY C –MEANS (FCM)

Fuzzy C-means clustering is a part of two or more groups of data items and allows Dunn developed in 1973 [10]. This standard is widely used in pattern recognition and image, such as medical, geological and satellite images. In K-Means each data point belonging to the cluster or not, that is, belongs to the class of single cluster, but fuzzy clustering extends this concept, based on the membership function for each data point is assigned two or more groups. In K-means, each data point a value of 0 or 1, but diffuse, each data point is a percentage value between 0 and 1, which shows the amount of data pointing to a cluster. It is bound by the information sum for each data point, the value of all cluster members to be a [9,11,12]. Calculate the member function, and the value of each data element with the highest number of all cluster members are associated. The purpose of the algorithm is to minimize the following objective function:

$$X(A;U;B) = \sum_{c=1}^{i}\sum_{r=1}^{n}(\mu_{cr})^{m}\|a_r - b_c\|^2 \qquad (1)$$

Where, X is the objective function, μ_{cr} are the membership values, m fuzziness factor whose value must be greater than 1, a_r is the r^{th} data point, b_c is the c^{th} cluster centroid and $\|a_r - b_c\|^2$ is Euclidean distance.

Let A is the dataset, $A_r = \{a_1, a_2, \dots, a_n\}$ and list of cluster centers represented by $B_c = \{b_1, b_2, \dots, b_c\}$. Algorithmic steps for Fuzzy C-Means:

1. Provide the number of cluster i.e. i
2. Randomly set cluster centroids.
3. Randomly initialize membership value to $U = [\mu_{cr}]$ between 0 and 1.
4. Compute fuzzy membership $[\mu_{cr}]$ using:

$$\mu_{cr} = \frac{1}{\sum_{j=1}^{i}\left(\frac{\|a_r - b_c\|}{\|a_r - b_j\|}\right)^{\frac{2}{m-1}}} \quad (2)$$

Here, $1 \le c \le i, 1 \le r \le n$

5. Compute center Vector b_c using:

$$b_c = \frac{\sum_{r=1}^{n} \mu_{cr}^{m} b_r}{\sum_{r=1}^{n} \mu_{cr}^{m}} \quad (3)$$

Here, $1 \le c \le i$

6. Stop, if $\|U_{r+1} - U_r\| < \delta$, otherwise go to step 3.
7. Here 'δ' is termination criteria between [0,1] and $U = [\mu_{cr}]$ is a fuzzy membership matrix.

III. POSSIBILISTIC FUZZY C-MEANS (PFCM)

FCM has problems in handling noise and outliers. PCM has the problem of coincident clustering, and FPCM has difficulty when the data set is large because the typical value will be very small. The obvious problem with all FPCMs is that they impose constraints on the typical values (the sum of the typicalities for all data points for a particular cluster is 1). We relax the constraints on the typical values, but leave the column constraint on member values. In 1997, J. C. and N. R. Bezdek Pal suggested PFCM is a good clustering algorithm for performing classification tests because it has the ability to be more important to the canonical or membership value. The PFCM is a hybrid of PCM and FCM, which generally avoids the various problems of PCM, FCM and FPCM. The purpose of this algorithm is to minimize the following objective function:

$$\min_{(U,T,B)} \{X(A,U,T,B) = \sum_{c=1}^{i}\sum_{r=1}^{n}\left(a\mu_{cr}^{m} + bt_{cr}^{\eta}\right)\|a_r - b_c\|^2 + \sum_{c=1}^{i}\gamma_c \sum_{r=1}^{n}(1 - t_{cr})^{\eta}\} \quad (4)$$

Subject to constraint $\sum_{c=1}^{i}\mu_{cr} = 1 \; \forall \, r$, and $\mu_{cr} \ge 0$, $t_{cr} \le 1$. Here b>0, a>0, η>1, m>1 and γ_c> 0 are user defined constants. The constants a, b are used to define the relative proportions of the values of the typicality and membership values. In above objective function $U = [\mu_{cr}]$ is a membership matrix analogous to FCM and $T = [t_{cr}]$, a typicality matrix analogous to PCM algorithm. If giving more importance to the membership values that PFCM work closer to the FCM algorithm and if giving more importance to the values of typicity than PFCM work closer to PCM.

Let A is the dataset, $A_r = \{a_1, a_2, \dots, a_n\}$ and list of cluster centers represented by $B_c = \{b_1, b_2, \dots, b_c\}$. Set the various parameters b>0, a>0, η>1, m>1. Algorithmic steps for PFCM:

1. Provide the number of cluster i.e. c
2. Randomly set clusters centroids.
3. Run FCM Algorithm described in section II.
4. With the help FCM algorithm results, the penalty parameter γ_c is computed for eeach cluster using following equation and put K=1.

$$\gamma_c = K\frac{\sum_{r=1}^{n}\mu_{cr}^{m}\|a_r - b_c\|^2}{\sum_{r=1}^{n}\mu_{cr}^{m}} \quad (5)$$

5. Compute membership values $U = [\mu_{cr}]$ if distance between image pixel and its centroid is greater than 0. Membership values calculated using (2).
6. Compute typicality values T= $[t_{cr}]$ if distance between image pixel and its centroid is greater than 0. Typicality values calculated using following equation:

$$t_{cr} = \frac{1}{1+\left(\frac{b}{\eta}\|a_r - b_c\|^2\right)^{\frac{1}{(\eta-1)}}} \quad (6)$$

Here, $1 \le c \le i, 1 \le r \le n$

7. Calculate the center Vector $v_i$using:

$$b_c = \frac{\sum_{k=1}^{n}(a\mu_{cr}^{m} + bt_{cr}^{\eta})a^r}{\sum_{k=1}^{n}(a\mu_{cr}^{m} + bt_{cr}^{\eta})} \quad (7)$$

8. Stop, if error is less or equal to $\|B_{r+1} - B_r\| < \delta$, otherwise go to step 6.

Now, it's possible to determine the cluster using membership and typicality values.

IV. EXPERIMENTAL RESULTS

In this paper, several noise gray scale images are tested to show the results obtained from the clustering algorithm. An image is acquired from a database of still images. Noise is added to the original grayscale image using matlab's default Gaussian noise function. Matlab also has the function of parameters PSNR, MSE and SSIM to check the image quality of grayscale images [13]. Based on the above parameters, this study summarizes which clustering algorithm is more suitable for noise gray-scale image segmentation.

In this work, the size of the noise gray-scale image is 255 * 255, and the K-Means, FCM and PFCM algorithms are tested with different initial conditions and output shown in Figure 1.

A. FCM

- Total cluster taken: 2
- Centroid randomly initialized
- Maximum iteration: 200
- Membership matrix assigned randomly
- Parameter values are m=2, Epsilon $\delta = 0.0001$

B. PFCM

- Total cluster taken: 2
- Centroid randomnly initialized
- Maximum Iteration: 200 and Epsilon δ=0.0001
- Typicality and Membership matrix initialized randomly
- PFCM checked for various parameter values are
  - a=1, b=1, m=2, η=2
  - a=2, b=1, m=2, η=2
  - a=1, b=2, m=2, η=2

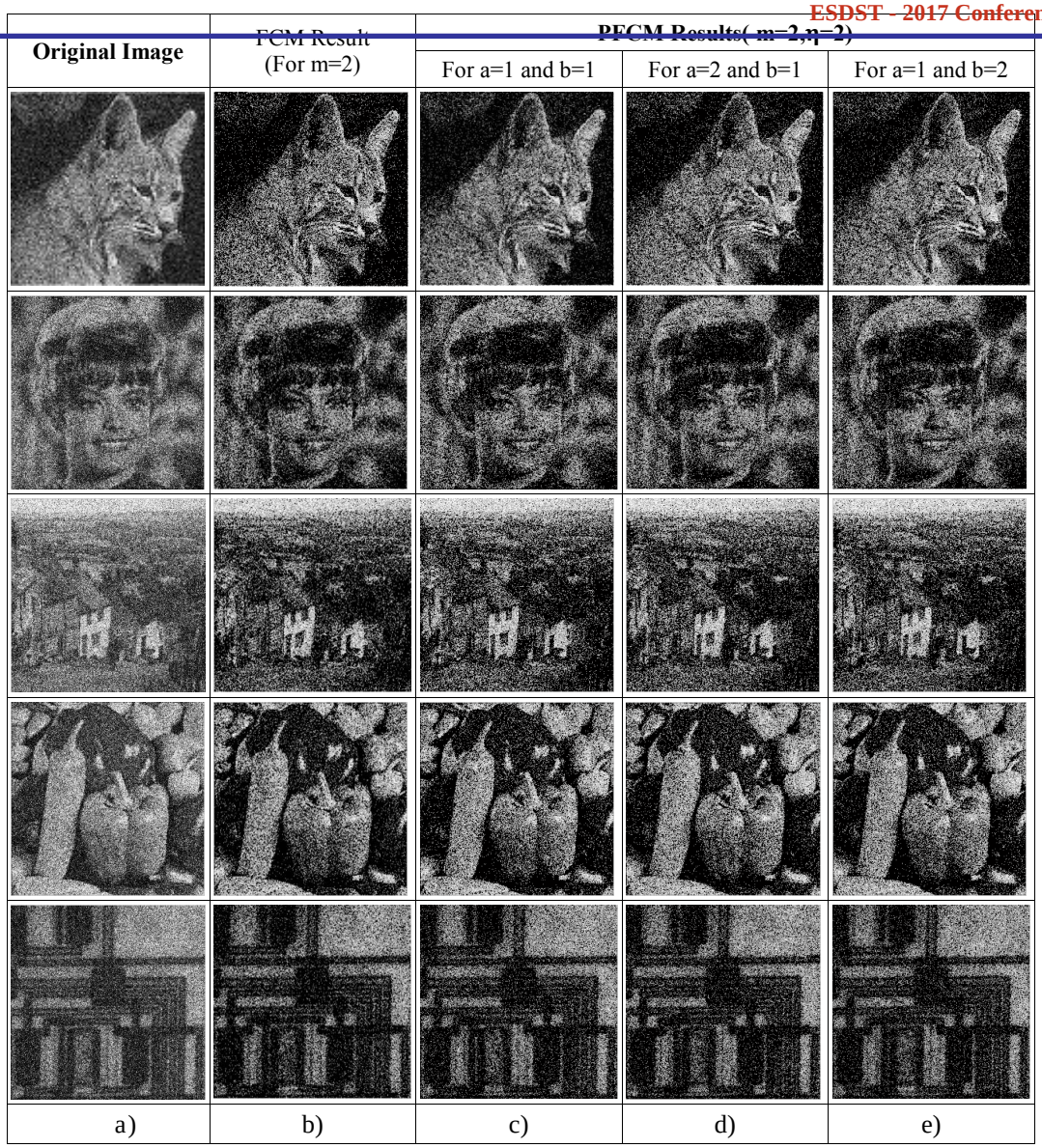

Fig. 1. Comparative results for different noisy grayscale images named *cat, zelda, house, pepper* and *circuit*, a) The original Images, b) FCM results, (c-e) PFCM results for various parameter values.

TABLE 1. MSE VALUES FOR SEGMENTED IMAGES BY FCM AND PFCM ALGORITHM

Original Image Name	FCM (m=2)	PFCM (m=2,η=2)		
		For a=1 and b=1	For a=2 and b=1	For a=1 and b=2
Cat	0.0293	0.0223	0.0231	0.0224
Zelda	0.0327	0.0281	0.0283	0.0285
House	0.0461	0.0409	0.0428	0.0420
Pepper	0.0355	0.0316	0.0316	0.0307
Circuit	0.0260	0.0191	0.0205	0.0192

TABLE II. PSNR VALUES FOR SEGMENTED IMAGES BY FCM AND PFCM ALGORITHM

Original Image Name	FCM (m=2)	PFCM (m=2,η=2)		
		For a=1 and b=1	For a=2 and b=1	For a=1 and b=2
Cat	63.4675	64.6429	64.4870	64.6232
Zelda	62.9790	63.6491	63.6197	63.5750
House	61.4936	62.0107	61.8198	91.9016
Pepper	62.6247	63.1403	63.1390	63.2545
Circuit	63.9811	65.3209	65.0041	65.3025

TABLE III. SSIM VALUES FOR SEGMENTED IMAGES BY FCM AND PFCM ALGORITHM

Original Image Name	FCM (m=2)	PFCM (m=2,η=2)		
		For a=1 and b=1	For a=1 and b=1	For a=1 and b=1
Cat	0.9977	0.9983	0.9982	0.9983
Zelda	0.9974	0.9978	0.9977	0.9978
House	0.9961	0.9965	0.9964	0.9965
Pepper	0.9971	0.9975	0.9974	0.9975
Circuit	0.9978	0.9984	0.9984	0.9985

C. *Evaluation Parameters*

1) MSE: By all pixels and summing the squared difference divided by the total number of pixels, pixel by pixel to calculate the mean square error Let's assume an Image A= $\{a_1, a_2, \ldots\ldots, a_m\}$ and Image B= $\{b_1, b_2, \ldots\ldots, b_m\}$ with 'm' no. of pixels then,

$$MSE(A,B) = \frac{1}{\mathrm{m}}\sum_{\mathrm{i}=1}^{\mathrm{m}}\|a_{\mathrm{i}} - \mathrm{b_i}\|^2 \qquad (8)$$

The smaller the MSE value, the better the image quality. Table 1 shows the FCM and PFCM results between the real and reconstructed images of each algorithm.

2) PSNR: The peak signal-to-noise ratio is described in decibels (dB) as the maximum value of the maximum signal power of the MSE, which is assumed to be the noise power. Let's assume an Image A= $\{a_1, a_2, \ldots\ldots, a_m\}$ and Image B= $\{b_1, b_2, \ldots\ldots, b_m\}$ with 'm' no. of pixels then PSNR is given by,

$$PSNR(A,B) = 10Log_{10}\left(\frac{Max\ Signal\ Power^2}{MSE(A,B)}\right) \qquad (9)$$

For 8-bit grayscale images, the maximum value is 255. The higher the value of the peak signal to noise ratio, the better the image quality. Table 2 shows the results of the calculation of the FCM and PFCM between the real and reconstructed images for each algorithm.

3) SSIM :Structural similarity indices measure the structural similarity between real and reconstructed images. Its value is between -1 and 1. When the two images are equal, the SSIM approaches 1. The SSIM evaluation index is based on the calculation of three terms, namely, brightness, contrast, and structural terms. The overall SSIM exponent is then the product of the above three terms as follows:

$$SSIM(A,B) = \frac{(2\mu_{\mathrm{A}}\mu_{\mathrm{B}}+K_1)(2\sigma_{\mathrm{AB}}+K_2)}{(\mu_{\mathrm{A}}^2+\mu_{\mathrm{B}}^2+\mathrm{K}_1)(\sigma_{\mathrm{A}}^2+\sigma_{\mathrm{B}}^2+K_2)} \qquad (10)$$

Where, $K_1 = (0.01 * L).\hat{}2$ *and* $K_2 = (0.03 * L).\hat{}2$ is the regularization constants and L is dynamic range value, μ_{A}, μ_B is the local means and σ_A, σ_B is the standard deviation, σ_{AB} is cross variance.

The higher the SSIM value, the better the image quality. In this work, the matlab function SSIM is used to check the quality of the image. Table 3 shows the FCM and PFCM results between the real and reconstructed images of each algorithm.

Table (1-3) shows that PFCM has a lower MSE value, higher PSNR and SSIM value, which proves that PFCM produces better results for noise gray scale image.

V. CONCLUSION

In this work, the Gaussian noise function is used to add artifacts to different gray-scale images to demonstrate that PFCM provides better results in noise-gray images than FCM. After analysis of the results obtained for the PSNR, MSE, and SSIM of the noise gray scale image, it is shown that the PFCM is effective and robust. The results obtained from the PFCM algorithm are closer to the FCM algorithm and require more computation time than the FCM. Therefore, future work needs to develop new methods or improve which are beneficial to noise gray-scale images and provide better image quality.

ACKNOWLEDGMENT

The author would like to express his sincere gratitude to all faculty and staff of Baba Banda Singh Bahadur Engineering Institute and Fatehgarh Sahib for their invaluable advice on research.

REFERENCES

[1] R. C. Gonzalez, R. E. Woods, "Digital Image Processing", 3rd ed., Prentice Hall, New Jersey (2008).
[2] K. S. Fu, "A survey on image segmentation", Pattern Recognition, Vol. 13, pp. 3–16(1981).
[3] N.R. Pal, S.K. Pal, "A review on image segmentation Techniques", Pattern Recoginition, Vol. 26, pp. 1277-1294(1993).
[4] S. Ghosh, S.K. Dubey, "Comparative Analysis of K-Means and Fuzzy C-Means", International Journal of Advanced Computer Science and Applications (IJACSA), Vol. 4, No. 4(2013).
[5] J. C. Bezdek, "Pattern Recognition With Fuzzy Objective Function Algorithms", New York: Plenum (1981).
[6] D.C. Park, "Intuitive fuzzy C-means algorithm for MRI segmentation", IEEE International Conference on Information Science and Applications (ICISA), pp. 1-7(2010).
[7] R. Krishnapuram, J. M. Keller, "Apossibilistic approach to clustering", IEEE Trans. Fuzzy Syst.,Vol. 1, No. 2, pp. 98–110(1993).
[8] R.J. Almeida, J. M. C. Sousa," Comparison of fuzzy clustering algorithms for classification", IEEE International Symposium on Evolving Fuzzy Systems, pp. 112-117(2006).
[9] N.R. Pal, K. Pal, J.M. Keller, J.C. Bezdek, "A Possibilistic Fuzzy c-Means Clustering Algorithm", IEEE Trans. on Fuzzy Systems, Vol. 13, No. 4, pp. 517-530(Aug. 2005).
[10] J. C. Dunn, "A fuzzy relative of the ISODATA process and its use in detecting compact well-separated clusters", Journal of Cybernetics, 3(3), pp. 32-57(1973).
[11] L.A. Zadeh, "Fuzzy sets, Information and control", 8(3), 338-353(1965).
[12] Yong Yang, "Image Segmentation By Fuzzy C-Means Clustering Algorithm with a novel penalty term", Computing and informatics, Vol. 26, pp. 17-31(2007).
[13] Yusra, A. Y. AI-Najjar, Dr. Der Chen Soong, "Comparison of image quality assessment: PSNR, HVS, SSIM, UIQI", International Journal of Scientific and Engineering Research, 3(3), 1-5(2012).

A New Method for Face Recognition Using Wavelet

Manjinder Kaur
Department of Computer Science
K.C. College of Engineering. & IT
Karyam, SBS Nagar, Punjab (India)

Sumit Chopra
Department of Computer Science
K.C. College of Engineering. & IT
Karyam, SBS Nagar, Punjab (India)

***Abstract*—Content-Based Image Retrieval (CBIR) allows to automatically extracting target images according to objective visual contents of the image itself. Representation of visual features and similarity match are important issues in CBIR. In this paper an attempt is made to review a wide range of methods used for face recognition comprehensively. This include PCA, LDA, ICA, SVM, Gabor wavelet tool for recognition .This review investigates all these methods with parameters that challenges face recognition like illumination, pose variation, facial expressions.**

***Index Terms*— CBIR, Wavelet, Principal Component Analysis (PCA), Linear Discriminant Analysis (LDA), Independent Component Analysis (ICA).**

I. INTRODUCTION

Content-Based Image Retrieval (CBIR) is the process of retrieving desired images from huge databases based on extracted features from the image themselves.[1] CBIR provide access of multimedia databases that deal with text, audio, video and image data, which could provide us with enormous amount of information. CBIR is a technique, which uses visual contents (features), to search images from large-scale image databases according to users' requests in the form of a query image. There are so many different algorithms for face recognition which have different human face recognition rate with different database sets and different variation of poses. Face recognition algorithms are basically principal component analysis (PCA), 2DPCA (2-Dimensional), Sub-pattern recognition algorithm, Linear Discriminant analysis (LDA), Independent component analysis (ICA), Line edge map (LEM), Radial basis function (RBF), Elastic bunch mark graph(EBGM). [4] There are various applications of the face recognition such as Human - Computer interface, matching of photographs in static manner; security based video surveillance, Biometric based security, Image and video processing, Attendance system etc. There are various challenges in face recognition. These are Automatically locate the face, Identify similar faces(twins), Recognize the face from a general view point under different illumination conditions, facial expressions, and aging effects, variation in poses, Cartoon faces.

II. LITERATURE REVIEW

Sukhija P. et. al (2016) proposed a genetic algorithm based approach for face recognition. The proposed algorithm recognizes an unknown image by comparing it with the known training images stored in the database and gives information regarding the person recognized [2] .Given G. H. et al. (2013) proposed new opportunity for the application of statistical methods driven by growing interest in biometric performance evaluation [3] .Aman R.Chadha et. al (2011) discussed a face recognition technique for local and global features using discrete cosine transform. DCT is applied to whole face for local features and global features such as nose, mouth, and eyes are also extracted [4]. Jayshree Ghorpade et. al (2011) Discussed the use of PCA and SOM in face . In this paper author combines both PCA and SOM. For dimensionality reduction of human face image and for feature extraction and also tries to enhance these techniques.[5] Kulkarni A. Bormane D. (2013) Tells about a face recognition algorithm based on principal component analysis that is already implemented [6].

III. FACE RECOGNITION TECHNIQUES

For recognizing the face there are many commercial systems and new algorithms have been developed and proposed. Most of the systems use the Principal Component Analysis (PCA) as a base technique to recognize the face. There are different face recognition algorithms example principal component analyses, 2-dimensional principal component analysis (2DPCA), independent component analysis (ICA), line edge map (LEM), radial basis function (RBF), Linear Discriminant Analysis (LDA), elastic bunch graph matching (EBGM). These are the different techniques that are used to recognize the faces, each of this method has own performance rate for recognition the face.

A. Principal Component Analysis (PCA)

The term "Eigen faces" basically belongs to the PCA that is face recognition approach. Generally, refers to the use of "Eigen faces". PCA is used to remove the information which is not useful and therefore reduce the dimension data and accurately decompose the dimensions of face into components of orthogonal principal that are called as "Eigen faces". The results of covariance matrix are decreased by calculating the S^TS matrix rather than SS^T same as the covariance matrix. Where S is the matrix that is containing all vectors of an image. This deduction is balanced by multiplication of images T with the images S with Eigen vectors of the S^TS matrix. At last, results into the Eigen faces, these are the basic vectors and works as the matrix of projection. [3] For the compression of image and for the recognition of face PCA is used. In case of data of high dimension, for the ruling pattern, this is the commonly used technique. Different concepts of mathematics,

like standard deviation, covariance, eigenvectors and Eigen values will be used in PCA so they are discussed first as these concepts provide grounding on which this PCA is based.

B. 2-Dimensional Principal Component Analysis

2 Dimensional principal component analyses method to recognise the face is the enhanced algorithm from PCA. Computational cost of PCA is more than computational cost of 2DPCA. To reduce the computational cost, 2 D principal component analyses (2DPCA) was proposed. As vectors, images are treated in PCA, but in 2 D PCA the form of matrix, images are treated. To analyse the 2 D principal component analyses and principal component analyses effectiveness, there Eigen values of face images were obtained and that produced Eigen values are compared. To show the comparison of the 2 D principal component analyses and principal component analyses, result displayed in graphical in terms to show the accuracy and effectiveness. 2 D principal component analyses is easy for implementation on a digital computer in any programming language. 2D principal component analyses algorithm, from results shows that more effective and accurate**.[7]**

C. Independent Component Analysis (ICA)

In PCA image, with the Gaussian filter distribution images element treated as random variables and to minimize the statistics of second order. For any non-Gaussian distribution, PCA basis vectors, largest variances would not correspond. But independent Component Analysis method of face recognition minimizes both dependencies of higher order and second-order dependencies in the input data and which the statistically independent data tries to find on the basis of that. Bartlett had given two architectures of face recognition that are, 1st architecture- independent statistically basis on images and 2nd architecture given – representation of factorial code. In earlier technique, to perform ICA, to reduce the dimensionality, PCA is used.[8]

D. Linear Discriminant Analysis (LDA)

Same as PCA, LDA approach is also based on principles of some statistical features. In space of facial features or can say vectors find the underlying vectors that is between the classes of individual would maximized the variance and then within the classes find the maximized variance and then within the classes find the minimum variance between the sample of that same person. If this algorithm's efficiency increased, then to recognize the human face images of individual unknown, then this algorithm between the individual face images, would be able to discriminate and minor changes in expression. This algorithm has a training set.[9]

E. Elastic Bunch Graph Matching (EBGM)

EBGM technique uses the concept of small blocks of numbers that are called Gabor filters, once the related small area of an image, to produce the numbers that are called jets, by multiplying and adding the small selected blocks with pixels, to accommodate minor variations these minor variations these selected blocks location can be adjusted. In fact that, the Gabor filters are used to remove the variability in images, due to variation in contrast and lightning against deformations and small shifts. They are robust at the same time. To increase the dimensions in the space of face features with representation of Gabor filters. New technique to enhance significantly with new technique for normalization in illumination, the discriminating the ability of Gabor filters. [10]

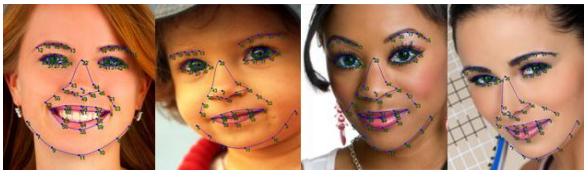

Fig.1. Elastic Bunch Graph Approach

F. Line Edge Map (LEM)

In its pre-processing phase, the technique makes use of hybrid LEM feature-based and template-based eye detection. The eye detection algorithm produces 100% result on the Caltech database [11], for a normalized error of 0.1.8 the face recognition technique is also implemented block-wise with face LEM and I-face LEM. Face recognition results of I-LEM and block-wise implementation show an improvement of 6-7%, and thus look promising.[11]

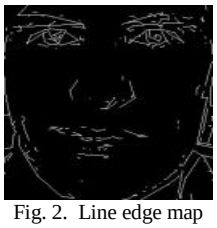

Fig. 2. Line edge map

G. Radial Basis Function (RBF)

To train the neural networks of RBF, an algorithm proposed that is hybrid learning algorithm. System's excellent performance achieves. Simulation result shows, both in terms of rate of occurring errors of learning efficiency and classification. From the information of gray scale, features vectors of face images are extracted. Most of face features extracted from spatial texture and gray scale information both. But to detect the face and recognition of face systems to use in real time are currently under construction. [11]

IV. ORL DATABASE

ORL database was actually given by OLLIVETTI RESEARCH LABORATORY. ORL database of contains the set of face images. These images were captured between 1992 and 1994 April at the lab of Cambridge University. In this data base, there are 400 images of faces. This data base is standard data base that is used in various types of face recognition study systems and used in various applications like vision, robotics and speech group of engineering department of university of Cambridge.

There are 10 different poses of one person. For some faces, images were captured at different times, with different poses or at different angles, different face expressions (eyes/closed eyes, smiling/ not smiling), with different style (glasses/ without glasses), changes in lighting conditions. All the images were captured against background that is homogenous dark with different position upright and frontal

position. Visibility of images of faces from data base is available.

All the images are in BMP format. Each face image has size pixels of 92 x 112with per pixel 256 gray levels and images are stored in folders. In 40 folders, images of 40 persons with 10 different poses are stored. Names of folders in sX form. In data base X indicates the numbers of folder starting from 0 to 9. S denotes the subject number that starts from 1 to 40. In these folders there are ten different poses of one person, which have names as Y.bmp, where Y is the image number between 1 and 10 for each person. Table-1 the following table shows description of images in ORL Database.

V. HAAR WAVELET

Wavelet decomposition using HAAR wavelet transforms that is used to compress an image and to extract the features from face image. To complete image, HAAR wavelet transform is applied. In these pixels, images are divided into N/2 x N/2 blocks. LL Sub band contains the maximum information of an image. In this work, LL sub band is used to extract the features. Let say, X be an input image matrix given below:

$$X = \begin{bmatrix} a & b \\ c & d \end{bmatrix}$$

Then the HAAR wavelet transform (Y) of X is given by the below matrix transform:

$$Y = \frac{1}{\sqrt{2}} \begin{bmatrix} (a+b+c+d) & (a-b)+(c-d) \\ (a+b)-(c+d) & (a-b)-(c-d) \end{bmatrix}$$

These are the different operations performed correspond to sub-bands:

i. Top left : Low-Low Sub-band 2-D low pass filter.
ii. Top right : High-Low Sub-band horizontal high pass, vertical low pass filter.
iii. Lower left : Low-High Sub-band horizontal low pass, vertical high pass filter.
iv. Lower right : High-High Sub-band 2-D high pass filter.

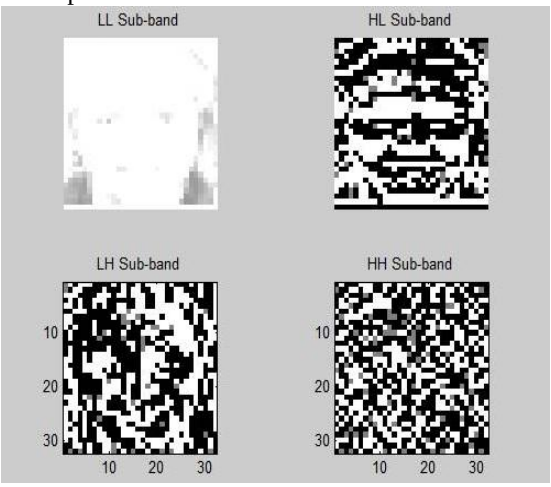

Fig.3. HAAR Wavelet decomposition of original image

The energies of all four sub images in Fig. 1 having values

Lo − Lo	Hi − Lo
88.2%	4.0%
Lo − Hi	Hi − Hi
6.3%	1.5%

As can be seen above, the maximum energy lies in the LL sub-band, therefore, LL sub band image is taken for face recognition purposes and taken for Euclidean distance vector generation.

VI. PROPOSED METHODOLOGY

These are the steps of this proposed work using HAAR Wavelet and correlation coefficient:-

1. Enter the group photograph as an input image, in which human faces must be present.
2. From the group photograph given as an input image, segment the individual faces using Viola Jones algorithm for further processing and select one image for recognizing the image
3. Using the wavelet transform decompose the detected face which have been selected for testing from the group photograph into sub bands and select the Low – Low sub band which contains the maximum frequency component of the face image.
4. The selected sub band is used to extract the features from the image. The image is now represented by feature vector which is one dimensional.
5. Load the ORL Database of human faces for processing.
6. Wavelet transform is used to obtain the four sub bands to test the face image on ORL database stored images and take the component containing the maximum frequency.
7. The maximum frequency component is used to extract the features from the face image. And then, reshape it for converting 2D matrix into feature vector which is one dimensional.
8. Correlation coefficient is calculated between test image and images of the stored database.
9. After calculating the correlation coefficient between the test image and stored database images, matching is performed based on the maximum value of correlation coefficient.
10. After matching the features, Ranking of different poses of similar face images is performed based on ascending order of value of correlation coefficient.
11. Display all the matched images.

ALGORITHM FOR FACE RECOGNITION USING EIGEN VALUES

Step1: Convert the acquired image into Grey scale image.
Step2: Compute the Eigen values.
Step3: Compute the mean of the acquired images.
Step4: Find out the difference of each image from the mean.
Step5: Form a covariance matrix and calculate its Eigen values and Eigen vectors.
No. of Images -->

EV	E1	E1	E1	T1
	E2	E2	E2	T2
	E3	E3	E3	T3
	E4	E4	E4	T4

Step6: Sort the Eigen values in descending order and choose the highest values.
Step7: Calculate the Eigen values using Eigen faces.
Step8: Find out projected train images using Eigen faces.
Step9: Take another image which is a test image and repeat the 1st step for this image.
Step10: Then project this image with the previous projected images and reshape them.
Step11: Find out the difference of the reshaped image from mean and then find out the projected test image with the help of difference image and Eigen faces.
Step12: Then find out the Euclidean distance between projected train images and projected test image.
Step13: Face recognition will be done on the bases of minimum Euclidean distance, minimum the Euclidean distance; image will be the best match.

VII. EXPERIMENTAL RESULTS

We have given a group image as input to face detection module. There are number of faces in group image. Then, using the viola-Jones algorithm, that faces are detected from group photograph. From that detected images, select one image for testing. We have used ORL database, there are 400 images of 40 persons with 10 distinct poses of one person. In this proposed work, we have taken 390 images that are stored in database for proceeding.

Fig.4. Group Photograph (Different faces are grouped in one image taken from ORL Database)

Fig.5. Single Faces are detected from group image

Fig.6. Test Image

We have selected one single image to give as query/test image. Then apply HAAR wavelet transform on that image and then that is converted into four sub-bands take LL-band that has maximum information. LL-sub band would be of 2-D that would be converted into reshaped into 1D format for find 1D-correlation to matching the features of face with stored database.

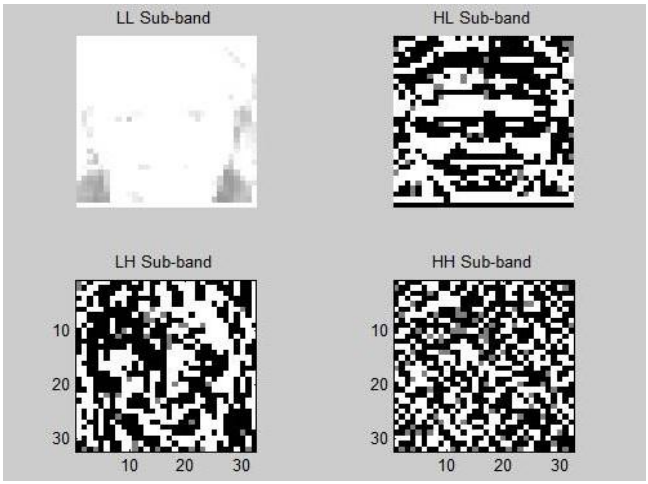

Fig.7. HAAR Wavelet Sub-Bands (LL, HL, LH, HH Sub-Bands)

Fig.8. Recognized Image at variation of pose

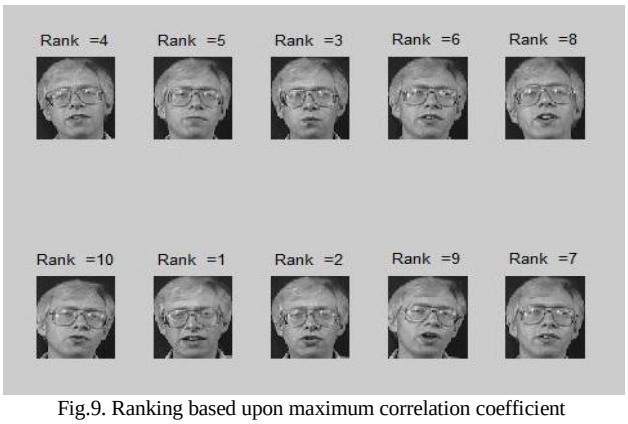

Fig.9. Ranking based upon maximum correlation coefficient

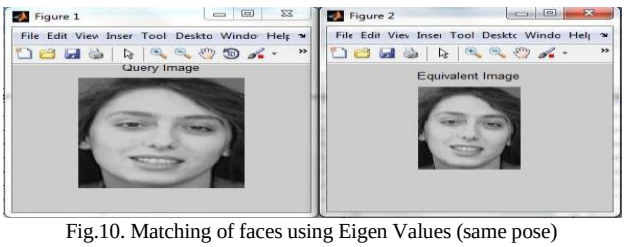

Fig.10. Matching of faces using Eigen Values (same pose)

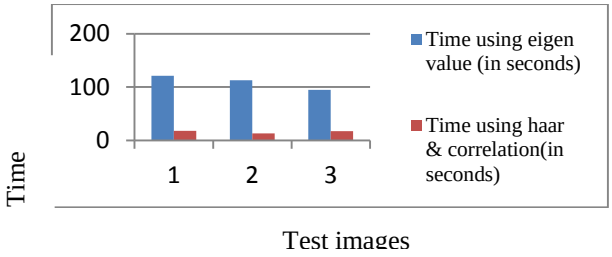

Fig.11. Graph shows the comparison between face using Eigen value and using HAAR Wavelet &1D correlation.

VIII. CONCLUSION AND FUTURE SCOPE

In Face recognition system, challenging to detect the face from group photograph & recognize the faces at different poses. In the proposed work, we have done the detection of human face from group photograph using Viola-Jones algorithm. From the detected faces, we have selected one face image from group photograph's detected faces as a test image. Using HAAR Wavelet and correlation coefficient, we have recognized the face at different poses. Matching of face features based on maximum correlation coefficient Index. Ranking of similar faces at different poses is done in this system. That is based upon ascending order of maximum correlation coefficient index and we have compared proposed system with face recognition using Eigen values. In proposed system, system is more accurate to recognize the face at different poses and speedy. Big difference came in time. Processing Time between Eigen value and proposed system is ~110 seconds and ~15 seconds respectively to recognize one face at a time. Face Recognition with Eigen values is less accurate to recognize the different pose as compared to proposed work.

Process to recognize the face is under construction. This proposed work can be applied to images of different type color format example RGB color format. This proposed work can be applied to real time images. This proposed approach can be used in biometric system. Attendance in schools, institutions and colleges can be taken using this system. This system is fast and accurate as compared to others.

REFERENCES

[1] Sneha R. Madane, Prof. S.T.Khandare, "A Survey on Face Recognition in Present Scenario" International Journal of Modern Communication Technologies& Research (IJMCTR),Vol. 3, pp. 6-10,2015.
[2] Sukhija P. , Behal S. , Singh P. " Face recognition using Genetic Algorithm" , Proc. International Conference on Computational Modelling and Security", Vol. 85, pp. 410-417.2016.
[3] Given G. H. , Beviridge J. R. , Philips P. J. , Draper B. , Bolme D. " Introduction to face recognition and evaluation of algorithm performance" , Proc. Computational Statistic and Data Analysis , Vol. 67, pp. 236-247,2013.
[4] Aman R. Chadha et. al, "Face Recognition Using Discrete Cosine Transform For Global And Local Features", International Conference On Recent Advancements In Electrical, Electronics And Control Engineering, vol. 6, pp. 210-216,2011.
[5] Jayshree Ghorpade et. al, "Signal Processing, Image Processing and Pattern Recognition", Communications in Computer and Information Science, vol. 260, pp 215-224,2011.
[6] Kulkarni.A, Bormane.D, "An Improved Hybrid Face Recognition Based on PCA and Subpattern Technique", International Journal of Innovative Technology and Exploring Engineering, vol. 2, pp. 215-218, 2013.
[7] Das D. et. al, "Comparative Analysis Of PCA And 2DPCA In Face Recognition" International Journal Of Emerging Technology And Advances Engineering, vol. 2, pp. 330-336, 2012.
[8] Bajwa u. et. al, "A Multifaced Independent Performance Analysis Of Facial Subspace Recognition Algorithms", Science Direct, vol. 5, pp. 35-54, 2010.
[9] Aleix M. Martinez et. al, "Recognizing Imprecisely Localized, Partially Occluded, And Expression Variant Faces From A Single Sample Per Class", pattern analysis and machine intelligence, IEEE, transactions vol. 24, pp. 748-763, 2002.
[10] Sujata G. Bhele1 and V. H. Mankar, "A Review Paper on Face Recognition Techniques "International Journal of Modern Communication Technologies & Research (IJMCTR) , vol.3, pp. 339-346, 2015.
[11] Sneha R. Madane, Prof. S.T. Khandare, "A Survey on Face Recognition in Present Scenario" International Journal of Modern Communication Technologies & Research (IJMCTR) , vol. 3, pp.6-10, 2015.
[12] Yi-Qing Wing et. al , "An Analysis Of Viola-Jones Algorithm", Image Processing On Line, vol. 90, pp. 128-148, 2014.
[13] Tripti G. et. al. , "Comparative Analysis of Various Illumination Normalization Techniques For Face Recognition", International Journal Of Computer Applications, vol. 28, pp. 81-88, 2011.
[14] Virendra P., Vishwakarma et. al , "Illumination Normalization Using Fuzzy Filter In DCT Domain For Face Recognition", International Journal Of Machine Learning And Cybernetics, vol. 78, pp. 245-251, 2013.
[15] Phalguni G. et. al , "An Efficient Pose Invariant Face Recognition System", International Conference On Soft Computing For Problem Solving, vol. 15, pp. 449-460 ,2011.
[16] Prabu U. et. al , "Unconstrained Pose-Invariant Face Recognition Using 3D Elastic Models" IEEE Transactions On Pattern Analysis & Machine Intelligence, vol. 33, pp. 1952-1961, 2011.
[17] Rishiwal V., Gupta A. , "Improved PCA Algorithm for Face Recognition" International e-Conference on Computer Engineering, vol.2, pp. 55-59, 2012.
[18] M. Parisa B. et. al, "Face Recognition Using Appearance Based Approach: A Literature Survey", International Conference & Workshop On Recent Trends In Technology, vol. 25, pp. 16-21, 2012.
[19] Neerja et. al, "Face Recognition Using Improved Fast PCA Algorithm", Image And Signal Processing, vol. 1, pp. 554-558, 2008.
[20] Ohil K. et. al, "Two Faces Are Better Than One: Face Recognition In Group Photographs", IEEE International Joint Conference On Biometric Compendium, vol. 62, pp. 1-8, 2011.
[21] Onsen T. et. al, "Multiple Classifier Implementation Of A Divide And Conquer Approach Using Appearance-Based Statistical Methods For Face Recognition", Science Direct, vol. 25, pp. 1421-1430, 2004.
[22] Pengfei S. et. al, "Image PCA: A New Approach For Face Recognition", IEEE Acoustics, Speech And Signal Processing, vol.72, pp. 1241-1244, 2007.
[23] Kulkarni.A, Bormane.D, "An Improved Hybrid Face Recognition Based on PCA and Subpattern Technique", International Journal of Innovative Technology and Exploring Engineering, vol. 2, pp. 215-218, 2013.
[24] Lu H., Plataniotis K., "MPCA: Multilinear Principal Component Analysis of Tensor Objects", IEEE Journal Of Pattern Recognition, vol. 44, pp. 1540-1551, 2008.
[25] Mandeep k. et. al, "Recognition Of Facial Expressions With Principal Component Analysis And Singular Value Decomposition", International Journal Of Computer Applications, vol. 9, pp. 36-40, 2010.
[26] M. Parisa B. et. al, "Face Recognition Using Appearance Based Approach: A Literature Survey", International Conference & Workshop On Recent Trends In Technology, vol. 25, pp. 16-21, 2012.
[27] Neerja et. al, "Face Recognition Using Improved Fast PCA Algorithm", Image And Signal Processing, vol. 1, pp. 554-558, 2008.
[28] Kresimir D. et. al, "Independent Comparative Analysis Study of PCA, ICA, And LDA on the FERET Data Set", International Journal Of Advance Computer Information Engineering, vol. 26, pp. 70-79, 2006.
[29] Furl N. , Philips P.J. , Toole A.J.O. ," Face recognition algorithms and other race – effect : computational mechanisms for a development contact hypothesis", Elsevier Cognitive Science , Vol. 26, No. 6, pp. 797- 815, 2002.
[30] Vishwakarma et. al, "A Novel Approach For Face Recognition Using DCT Coefficients Re-Scaling For Illumination Normalization", IEEE International Conference On Advanced Computing And Communications, vol. 167, pp. 535-539,2005.

An Approach to Detect Clones in Class Diagram Based on Suffix Array

Amandeep Kaur,
Computer Science and Engg. Department,
BBSBEC Fatehgarh Sahib, Punjab, India.

Manpreet Kaur ,
Computer Science and Engg. Department,
BBSBEC Fatehgarh Sahib, Punjab, India.

Harjot Kaur,
Computer Science and Engg. Department,
BBSBEC Fatehgarh Sahib, Punjab, India.

***Abstract*— Copy-paste is becoming a very usual practice in software development. Copying a code in one or more place without any change is mainly known as software cloning and the pasted part of code is called clone. Clones in code increase the maintenance cost, resource requirements and make code more error prone. So detection and removal of clone is very important for source code. Models are also affected by the cloning problem. Model Driven Engineering now becomes a standard and important framework in software research area. Unpredicted copy of model elements leads to various difficulties. Models consists design level similarities and are in the same way harmful for software maintenance as code clones are. Therefore, clones are required to be identified from models. Class diagram is the main aspect of modeling and used to describe the static view of an application. Class diagram contains redundant elements which increase complexity of the class diagram as well as maintenance effort. Code quality can be improved if clones are detected from the class diagram. Current work aims to find clones in class diagram using an approach based on suffix array. Firstly, diagram is encoded as XML file and then tokens are extracted. Suffix array is used to compare tokens and matched tokens are known as clones.**

Keywords— clone; code clones; model clones; class diagram; complexity; Suffix array.

I. INTRODUCTION

According to Rattan et al. [15] and Roy and Cordy [19], repeating existing code and pasting them with or without changes into different sections of code is a common process in software system development. The copied code is termed as code clone and therefore the process is named code cloning.

Code clones have high impact on software quality. Biggest difficulty in code clones is that, these are only linked by their similarity and do not have any implicit or explicit link between them which makes software code clones difficult to detect [10]. When we make changes or updations at one place, other similar things remains unchanged accidently that deteriorates the code quality. Therefore, it is very important to find related fragments. However, Storrle [20] had mentioned code duplication or cloning as a form of software reuse and had concluded that software code can be shrinked to a percentage on doing exact matching. In today's technology, software reuse is highly supported by open source software.

A. Reasons for Software clones

There are various reasons due to which clones occurs. Rattan et al. [15] and Roy and Cordy [19] mentioned different reasons as follows:

- Lack of time: Programmers are bound to do copy-paste to meet hard time constraints.
- System's Complexity: Adopting a new system or understanding a complex system only promotes coping existing functionality, code and logic.
- Language loopholes: Due to limitations in programming language, programmers are forced to do copy paste. Many of the languages lack inherent support for code reuse. These loopholes become limitations of a programmer.
- Fear of adaptability of fresh code: Rattan et al. [15] identified that for programmer adopting a new ideas always have fear of getting wrong and lengthy code, which will again lead to reuse of existing code.
- Lack of abstraction: Programmer ignores or avoids abstraction of program due to time limits. Delay refactoring will give rise to high maintenance cost.

B. Advantages and disadvantages of clones

There are some positive points considered by Rattan et al. [15] and Storrle [20] to have clones:

- Sometimes use of templates are encouraged in programming paradigms.
- Hard time constraints have only option to use the existing functionalities.
- Overhead of procedure calls promotes code duplication.

Rattan et al. [15] and Storrle [20] had mentioned problems associated with clone presence, some of them are following:

- High maintenance cost and efforts.
- Increased probability of bug propagation.
- Wrong effect on design.
- Wastage of resources.
- Bad impact on system understanding.

The rest of the paper is organized as follows. Section II presents the background. In Section III, we have described the methodology to detect clones in class diagram using suffix array. In Section IV results are discussed. Section V gives the related work and Section VI concludes the current work and gives future directions.

II. BACKGROUND

A. *Cloning in Models*

According to Storrle [20] and Roy and Cordy [18], as the source code clone detection is large problem for code based development, the same problem also occurs for copied parts of models in model based development. Due to significant difference between programming languages code and models, clone notations and algorithms are difficult to directly transfer between them. Unexpected overlaps and duplications in models are termed as model based clones [11].

The various challenges in detecting model clones mentioned by Storrle [20] are:

- To derive a practical definition of model clone.
- To develop and implement an algorithm to detect model clones.

B. *Code Clones versus Model Clones*

- Identification: Source code are easily identified by names and procedures used whereas models use internal identifiers which are equal but not identical.
- Structure: Code is represented as a directory tree of text files or long characters of tokens, on other side models have graph like structure. Tools are used to represent models, so it is important to consider tool-specific representation into account.
- Type Categorization: Roy et al. [17] and Storrle [20] mentioned different types of clones as given in Table 1.

Table1. Types of code clones and model clones

Code Clones		Model Clones	
Type I: Exact Clone	A copy that is identical except most of changes in whitespaces and comments.	Type A: Exact model clone	A copy that is identical except from secondary notations or internal identifiers.
Type II: Renamed Clone	A copy with consistent changes to identifiers, variables types or functions names.	Type B: Modified model clone	A copy with changes to the element names attributes and parts.
Type III: Parameter clone	A copy allowing changes, additions or removal of statements.	Type C: Renamed model clone	A copy that allows actual changes in additions or removal of parts.
Type IV: Semantic clone	A copy of code that performs same function but different syntactic variants are used.	Type D: Semantic model clone	A copy in content, those are due to model part copying or language constraints.

C. *Various Clone Detection Techniques*

There are various clone detection techniques available. The only difference between these techniques is the granularity level of clone. Rattan et al. [15] and Roy et al. [17] proposed some of them as follows:

1) Text-Based Clone Detection: In this technique, the source program is taken as sequence of lines. As discussed by Roy et al. [17], two code fragments which are similar in terms of texts or strings are known as code clone. Tools available for text based detection are: Duploc, DuDe(line based comparison), Simian(detection in different programming languages), SDD (Clone detection in large systems), NICAD (Hybrid clone detector with high precision and recall).

2) Token-Based Clone Detection: Tokens are considered better for comparison according to Roy and Cordy [23]. Source program is transformed into sequence of tokens for comparison. Suffix tree and Suffix array is used mostly as data structure in token based detection. Suffix arrays are considered prior to suffix tree in term of space requirements. CCFinder is a tool which uses suffix tree to find similar tokens. CP-Miner is another token based tool that detects structural clones with high abstraction repeated tokens. Suffix array is widely accepted by many other tools like SHINOBI.

3) Tree Based Clone Detection: Rattan et al. [14, 15] mentioned that tree based clone detection transforms the source code into tree structure. Similar subtrees in the tree are searched using tree matching techniques and reported as clones. Addition or removal of sub-parts i.e. Type 3 clones are easily detected by tree based clone detection.

4) Graph Based Clone Detection: Pham et al. [12] and Rattan et al. [15] mentioned that the semantic information of source code is represented by Program Dependency Graph (PDG). On obtained PDG, subgraph isomorphism is applied to detect similarity. Duplix and PDG-DUP are the tools for finding similar subgraphs.

5) Metrics based clone detection: Various similarity based metrics are applied to suitable form of data structures to perform clone detection. CLAN uses metrics obtained from AST of source code [15].

III. RESEARCH METHODOLOGY

Class diagram is created using UML modeling tool MagicDraw. The model is converted to XML document. The document is parsed to extract the tokens (i.e meaningful information) which are then matched using suffix array. Similar tokens are categorized as clones. Clone analysis is carried out to get numbers of clones and number of instances of each clone. Clusters, the group of clones repeated, are also reported with their occurrence value. Clone coverage and percentage of class similarity is also calculated from the clone detection results. Fig.1 gives the overview of methodology followed.

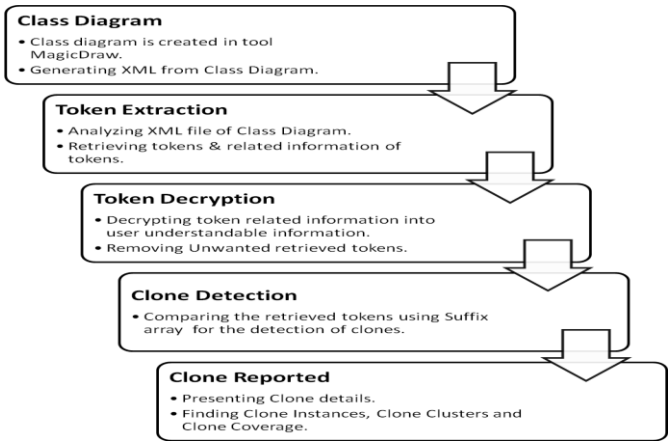

Fig.1 Steps of the Methodology

Fig.2 shows us with the interface of our tool. In step 1, we browse the XML file which is representation of class diagram from which we want to detect clones. Then using button 'Start Clones Detection', clone detection process is started. To check the report, button named 'View Report' is used. 'Exit' button can be used to exit the tool.

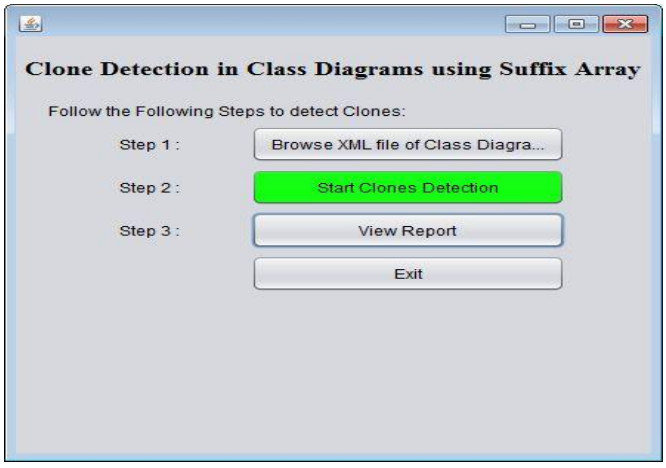

Fig.2 Interface of tool

IV. EXPERIMENTAL RESULTS AND DISCUSSIONS

This section discusses the results obtained after clone detection in UML class diagram. The methodology is explained in section 3. The class diagram of library management system is taken as a subject system which has 31 classes with 271 attributes and 62 operations. This UML class diagram is given as input to the clone detection approach based on suffix array. The clone detection results are presented on the basis of following parameters:

a) Clone Candidates and their instances.
b) Clone Clusters
c) Clone Coverage
d) Class Similarity
e) Memory
f) Runtime

A. Candidates

This parameter gives the number of clones detected from class diagram. The tokens are extracted from XML file of class diagram of library management system which are compared using clone detection approach based on suffix array. Similar tokens are reported as clones.

Clone Candidates: 65

1) Clone Instances: Clone instances parameter specifies the total number of occurrences of each clone which are present in various classes. Fig.3 shows the clones with their respective instances. Clones are differentiated from each other by using clone id. Clone id is an integer number assigned to each detected clone to give unique identification. Fig.3 shows clone with clone id 50 has maximum number of instances i.e. 26

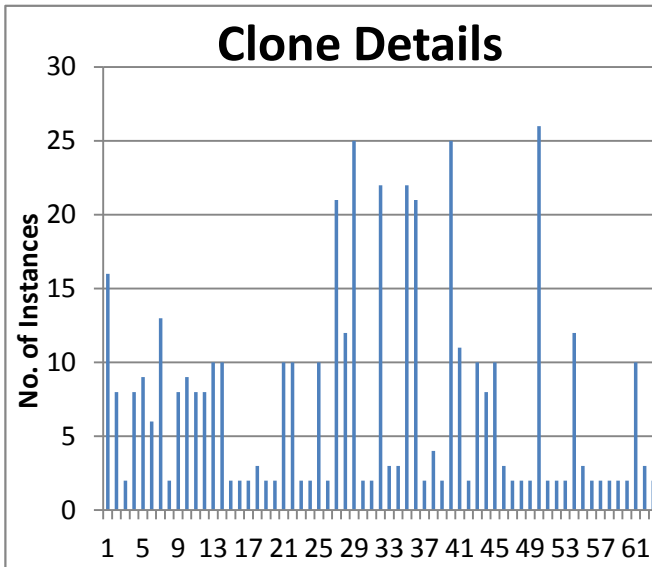

Fig.3 Instances of various Clones

Table 2 provides us information about clones and their instances exist in various ranges. It has been clearly shown that 36 clones have 2 to 6 instances and there are 7 clones having more than 17 instances.

Table 2. Number of Clones and their Instances

Clone Instances	No. of Clones
2-6	36
7-11	18
12-16	4
>17	7

B. Clone Clusters

Clone cluster defines the group of clones repeating together in various classes. Clusters are helpful to find maximum similarity in the classes. Table 3shows various clusters with their Id's, length (number of clones in the cluster) and instances (number of occurrences). Results show that the biggest cluster having 14 elements is repeated in two classes. Most of the clusters are of length two. Cluster having Cluster id 20 is of length three which is repeating in 25 classes. Cloned elements present in clone cluster can be put into super class to remove the redundancy in various classes. Fig.4 shows graph representation of clone clusters.

Table 3.Clone Cluster Details

Cluster ID	Cluster Length	No. of Instances
1	14	2
2	8	2
3	3	2
4	4	2
5	2	2
6	7	2
7	2	2
8	11	2
9	2	2
10	2	3
11	2	3
12	3	3
13	13	8
14	2	8
15	8	8
16	7	9
17	6	10
18	2	21
19	2	22
20	3	25

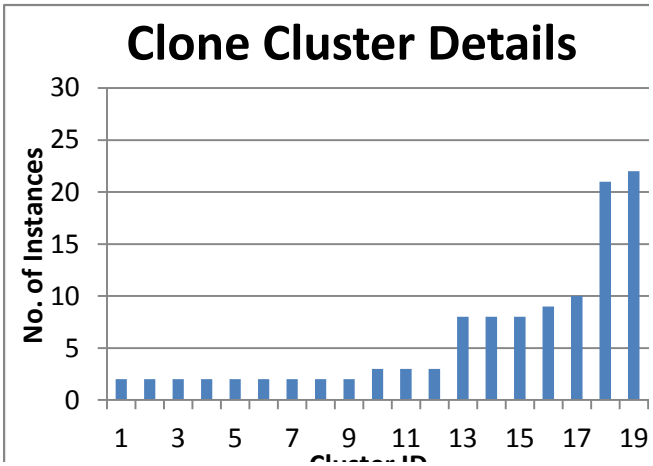

Fig.4 Clone clusters with their instances.

C. Clone Coverage

Clone coverage parameter gives the percentage of clones associated with a class. This parameter helps us to know the extent of cloning in various classes of our subject system. Table 4 shows clone coverage of each class. Clone coverage is calculated from cloned elements to the total elements of the class.

Results of clone coverage, as shown in Table 4 report maximum clone coverage i.e. 90% in the class having class id 7 and minimum clone coverage .04% in class with class id 27. It has been shown that there are four classes without clones i.e 0% clone coverage. Clone coverage helps us to check the extent of cloning in each class.

Table 4. Clone Coverage

Class ID	Clone Coverage
1	53%
2	57%
3	34%
4	48%
5	85%
6	62%
7	90%
8	76%
9	35%
10	69%
11	70%
12	72%
13	72%
14	72%
15	69%
16	76%
17	86%
18	52%
19	62%
20	73%
21	64%
22	73%
23	64%
24	71%
25	54%
26	72%
27	.04%
28	0%
29	0%
30	0%
31	0%

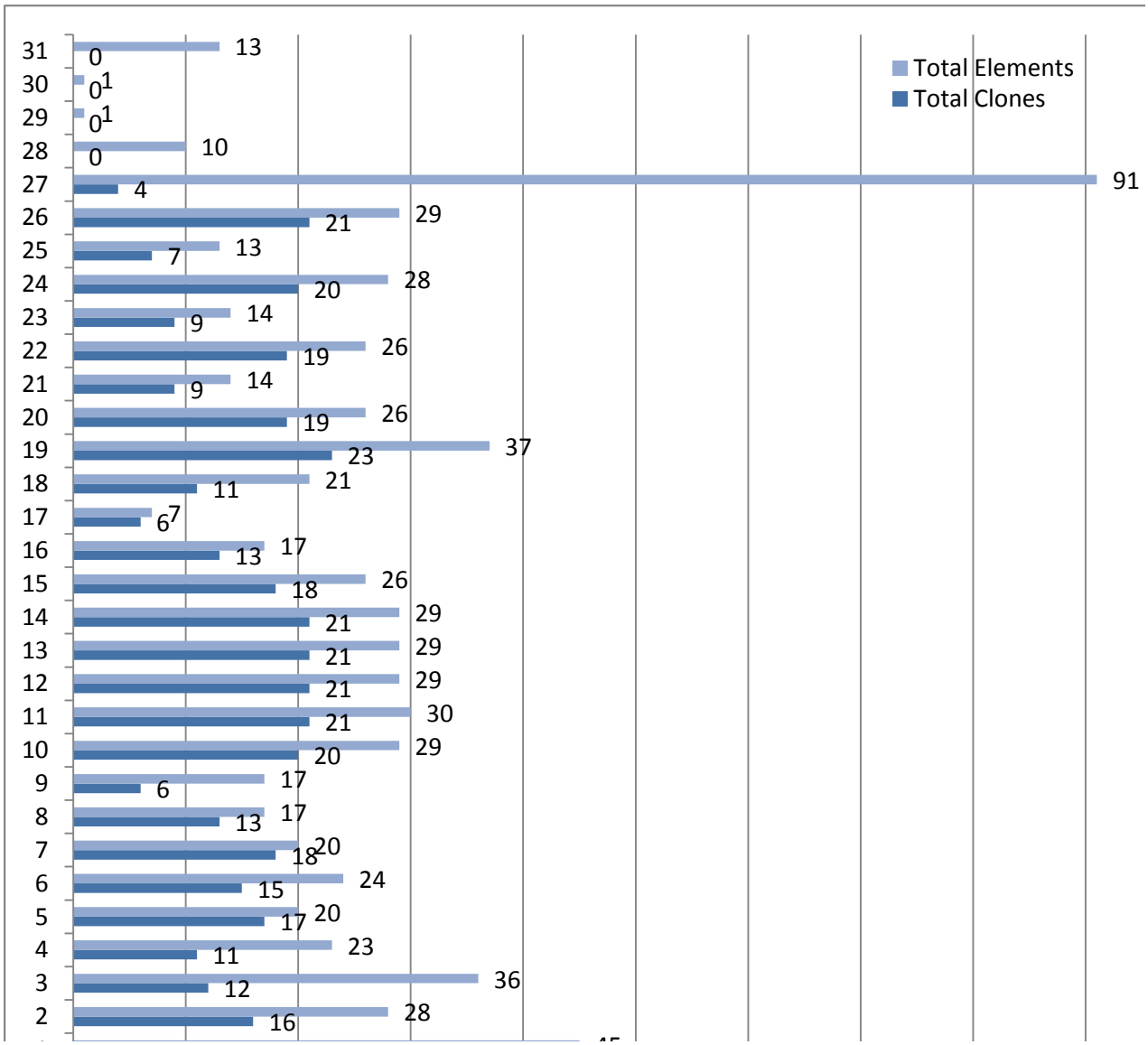

Fig.5 Details of cloned elements w.r.t. total number of elements of class.

D. Class Similarity

Class similarity parameter defines the percentage of similar tokens between two classes. Table 5 gives the detail about percentage of similarity and number of classes lying in that percentage. Maximum numbers of classes are 70 to 80 % similar to each other. There is no class which is having more than 90% similarity.

Table 5.Class Similarity between classes

Class Similarity	No. of Classes
51% - 60%	7
61% - 70%	13
71% - 80%	21
81% - 90%	6
91% - 100%	0

Fig.7 Results summary

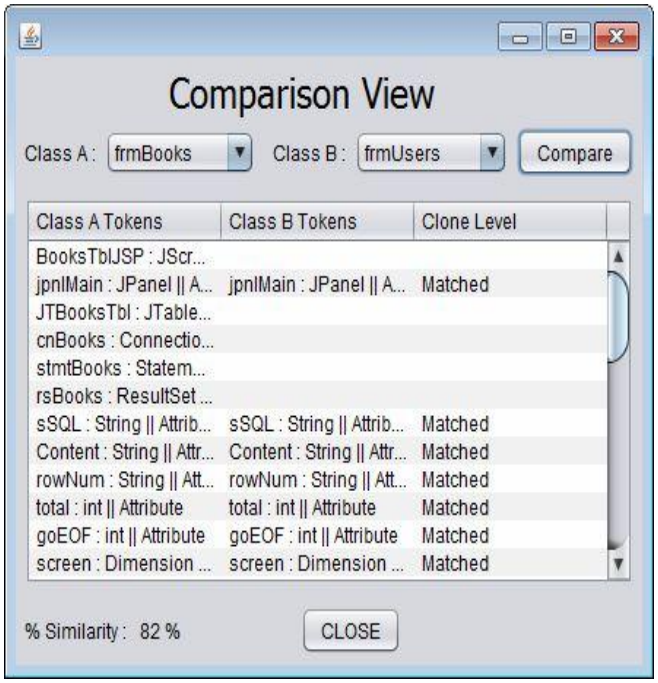

Fig.6 Class Comparison View

Fig.6 is the class comparison view showing the token comparison between two classes and the matched tokens i.e. clones between them.

E. Result Summary

As shown in interface of tool, after completing the clone detection phase, report of results are prepared. Fig.7 is the summary of result showing all the important fields. It presents us with the number of clones, clone ID`s, number of clone instances of each clone, Clusters with their elements and number of instances. The report is very useful to summarize the results.

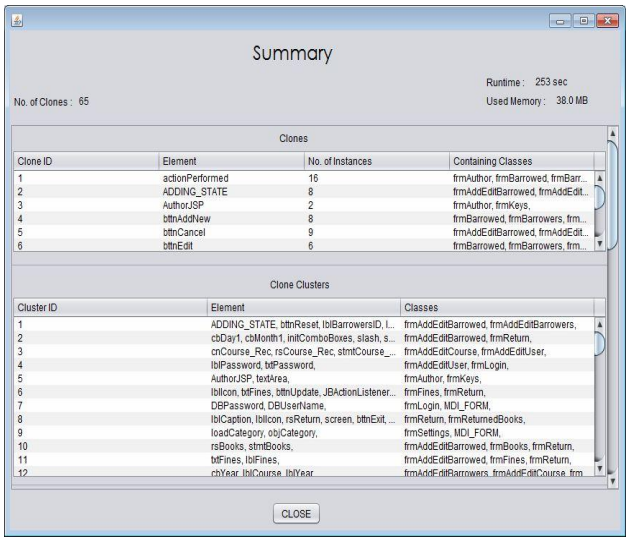

Fig.7 Results summary

F. Memory

This parameter specifies the space used by the clone detection approach.

Used memory: 38 MB.

G. Runtime

This parameter specifies the time taken by the clone detection approach to give various results.

Run time: 253 sec.

V. Related Work

Storrle [20] presented a formal definition of model clones, fragments and clone group. He proposed a clone detection algorithm for UML domain models. According to him, as code clones are problem for code base development, model clones are also increasing problems in model based development. He proposed a model element heuristics and clone detection algorithm based on detailed study of actual model structures. He implemented the approach in MQ_{lone} tool. According to the approach, UML models are seen as a set of heavy nodes that carry major information not similar as graphs with light nodes. Therefore, graph based clone detection cannot be applied to the UML domain model.
He defined four heuristics to find the similarity. First is the Name approach that looks for name similarity only but not provides good detection results. Second heuristic is Name2, it performed best in terms of quality and run time comparing all kind of attributes not just name. Third is INDEX, that defines similarity heuristics to apply on model elements but with shorter identifier but it will not work for long identifiers and XMI models. Last, INDEX-2 is defined which replace all the identifiers with their element name before heuristics are applied. In nutshell, NAME-2 provides the best result in terms of precision and false positives. The study can be applied to all kinds of UML models (e.g. Class diagrams, state machines, activity diagrams). Small and medium sized models works well with the approach, large models are yet to be run on the approach.

Clones exist in software due to copy paste and hard time constraints. Rattan et al. [15] presented the standard literature review on code clone detection. Empirical evaluation of clone detection tools and technique is presented with comparison. They presented the study with nine different types of clones, thirteen intermediate representations and twenty four match detection techniques. The emphasis of the study is to increase awareness of the potential benefits of software clone management. The presented study firstly defines the current status of clone detection in software field. They describe various intermediate representations or transformation techniques with code granularity levels e.g. set of statements, set of tokens, set of methods, set of blocks, set of procedures. Also various match detection techniques are defined with clone granularity level. The most frequently occurring match detection techniques are suffix tree, suffix array, metric and feature vector clustering.

They presented the list of tools with the methodology adopted e.g. (CCFinder takes tokens as input and matching is carried out with suffix tree). Comparison and evaluation of various clone detection tools and techniques are done to identify an efficient clone detector. They enlisted the tool comparison with the outcome or results in terms of precision, recall, no. of candidates, true negatives, false position, rejected candidates. They have extended the study from code clone detection to model based clone detection.

UML models are also affected by cloning. Rattan et al. [16] introduced an approach to detect clones in UML models. According to them, the motive behind this work is to attain high level of abstraction in model driven software process to avoid complexity and high rate of duplication in models due to increasing size of models and to support the study of clone detection in UML models. They have defined the definition, background and general theories on model clones and model clone detection. According to them, reasons of clones in models are copy/paste, language limitation, complexity and time constraints. Their proposed technique is scalable to implement and only relevant tokens are extracted from XMI file and are stored in tree. Only relevant clones are reported as we are storing key elements of UML diagram. Future scope of the study is to extend the prototypical implementation and display the results of clone detection in more user friendly manner. The proposed technique can be extended to large class diagrams, state chart diagrams and activity diagrams [16].

Deissenboeck et al. [4] proposed an approach to automatically identify duplicates in graphic models. The proposed tool is applied on case study of BMW group. They have illustrated various challenges raised when model clone detection is carried out and also presented methods to address these challenges. They proposed model clone detection algorithm, which reports full names of affected model elements. The Clone groups are inspected and accessed to find out the relevance output.

The tool provides the model clone detection with the integrated environment having visualizing effect of detection results. Clone group is easily inspected and highlighted clone instances with their location and extent are shown. They have presented the technique to improve scalability of subsystem, to improve relevance of the detected clones by providing specific ranks and easy clone inspection.

Deissenboeck et al. [5], presented an approach for the automatic detection of clones in large models. Their approach is based on graph theory and is applied to graphical data flow languages. They have taken the industrial case study MIN and demonstrate the applicability of their approach on Matlab/Simulink models. Matlab/Simulink models are widely used in model-based development of embedded systems in the automotive domains. In the case of embedded systems, main part of the code is generated from the domain-specific modeling languages. To support model based development and maintenance, it is very essential to detect clones in models. They proposed solution for the increasing size and complexity of products that relies on model-based development methods. Their technique contains an algorithm and corresponding tool to identify similarity in a model based graphs having weight based filtering heuristics that provide relevant output. Future work is proposed to improve the results by fine tuning the tool and algorithm. Further implementation have to be carried out on larger case studies to get better understanding of strengths and weakness of proposed algorithm.

VI. CONCLUSION AND FUTURE SCOPE

Large adaptability of model based development in software field is promoting model based clone detection. In this work, we are detecting clones in class diagram by using suffix array and analyzing various results of clone detection.

The present work reports that class diagram contains number of redundant elements. Similar attributes or operations present in two different classes are known as clones. The result has shown that there are number of clones present at multiple places in the class diagram. These clones can affect quality of source code generated from that class diagram and hence increases maintainability. The result has shown that there are clone clusters present in class diagram. Clusters are helpful to get idea of clones repeated always together. These clone clusters are good candidates for making super class so that unnecessary redundancy can be removed from class diagram. We report clone coverage which helps to know the extent of cloning in various classes. Maximum clone coverage is 90% and there are 4 classes having no clones. Class similarity is also being calculated which reports that 21 classes of the subject system are 71-80% similar.

So we can conclude that finding redundancy or clones from the class diagram will help the developer to know the extent of cloning in class diagram and clones can be removed to improve the maintenance effort because maximum developers interact with the system through diagrams only. Awareness of clones will help in developing reusable mechanism. Hence it is concluded that detecting clones in models reduces clones in codes which reduces error and maintenance cost.

In future, our present work can be used to explore clone detection in state chart, activity diagram and sequence diagrams. We can also rate reported clones as relevant or irrelevant so that maintainer can have more useful information. Class diagram with large number of classes can also be taken to check the working of our approach. Categorization of clones into various types can also be done.

REFERENCES

[1] H.B. Abdul and S. Jarzabek, “Detecting Higher-level Similarity Patterns in Programs” ESEC-FSE’05, ACM, Lisbon, Portugal, 2005.
[2] H.B. Abdul, S.J. Puglisi, W.F. Smyth, A. Turpin and S. Jarjabek, “Efficient Token Based Clone Detection with Flexible Tokenization” , ESEC/FSE’07, ACM, Cavtat Croatia, 2007.
[3] E.P. Antony, M.H. Alafi and J.R. Cordy, “An-Approach to clone detection in Behavioral Models” Queen’s university, Kingston, Canada, AAC-WCRE, 2013.

[4] F. Deissenboeck, B. Hummel, E. Juergens, M. Pfaehler and B. Schaetz, "Model Clone Detection in Practice", IWSC`10, Cape Town, South Africa, pp.37-44, 2010.
[5] F. Deissenboeck, B. Hummel, E. Juergens, B. Schatz, S. Wagner, J.F. Giard and S. Teuchert, "Clone Detection in Automotive model-Based Development" ICSE` 08,ACM, Leipzig,Germany.pp.603-612, 2008.
[6] R. Falke, R. Koschke and P. Frenzel, "Empirical Evaluation of Clone Detection Using Syntax Suffix Trees", Empirical Software Engineering, vol. 13, no. 6, pp. 601-643, 2008.
[7] B. Hummel, E. Juergens, and D. Steidl, "Index-Based Model Clone Detection", Proceedings of 5th International Workshop on Software Clones, Honolulu, USA, pp-21-27, 2011.
[8] H.J. Lin and L.F. Peng, "Quick Similarity Measurement of Source Code based on Suffix Array", International Conference on Computational Intelligence and Security" ,DOI 10.1109/CIS.2009.175, 2009.
[9] H. Liu, M. Zhiyi, L. Zhang and W. Shao, "Detecting Duplications in Sequence Diagrams Based on Suffix Trees" Software Institute, School of Electronics Engineering and Computer SciencePeking University, Beijing , China.
[10] M. Kaur, D. Rattan, R. Bhatia and M. Singh, "Comparison and Evaluation of Clone Detection Tools: An Experimental Approach" CSI journal of computing, vol.1, no. 4, pp. 44-55, 2012.
[11] M. Kaur, D. Rattan, R. Bhatia and M. Singh, "Clone detection in Models : an Empirical Study" , 3rd IBM Collaborative Academia Research Exchange(I-CARE), New Delhi, India, Oct 2011.
[12] N.H. Pham, A. H, T.T. Nguyen, J.M. Nguyen, Kofahi and T.N. Nguyen," Complete and Accurate Clone Detection in Graph-based Models", ICSE'09,Vancouver,Canada, IEEE, 2009.
[13] H. Petresen, "Clone Detection in Matlab Simulink Models", IMM-M.Sc, Berlin, 2012.
[14] H.C. Purchase, L. Colpoys, M. McGill, D. Carrington and C. Britton, "UML class diagram syntax: an empirical study of comprehension", Australian Symposium on Information Visualization, Sydney,vol.9, 2001.
[15] D. Rattan, R. Bhatia, and M. Singh, "Software clone detection: A systematic review", Information and Software Technology vol.-55, pp.1165-1199., 2013.
[16] D. Rattan, R. Bhatia and M. Singh, " Model Clone detection based on tree comparison", IEEE , 2012.
[17] C.K. Roy, J.R. Cordy and R. Koschke, "Comparison and Evaluation of Code Clone Detection Techniques and Tools: A Qualitative Approach", Science of Computer Programming, vol.74, no. 7, pp. 470-495, 2009.
[18] C.K. Roy, J.R. Cordy and R. Koschke, "An Empirical Study of Function clones in Open Source Software Systems", Proceedings of 15th Working conference on Reverse Engineering, pp-81-90, 2008.
[19] C.K. Roy, J.R. Cordy and R. Koschke, "A Survey on Software Clone Detection Resarch", Technical Report 2007-541, Queen's University at Kingston Ontario, Canada, 2007.
[20] H. Storrle, " Towards Clone Detection in UML domain models", DOI:10.1007/s10270-011-0217-9.
[21] T. Yamashina, K. H.Uwano, Y.Kamei. Fushida, M. Nagura, S. Kawaguchi and H. Lida, "Shinobi: A Real Time Code Clone Detection Tool for Software Maintenance", nasa institute of science and technology.

Impact of Refactoring on Software Quality

Prabhjot Kaur
Computer Science and Engg. Department
Punjab Technical University
Jalandhar, India

Puneet Mittal
Computer Science and Engg. Department
Baba Banda Singh Bahadur Engineering College
Fatehgarh Sahib, India

***Abstract*— Refactoring is the process of transformation of software. It changes its internal structure of software without affecting its external behavior. Bad smells means there are potential problems in the code, which we have to refactor. In this paper, we use two tools for bad smells detection on object oriented open source software are PMD and JDeodrant. Then after refactoring bad smells, we analyze the impact of refactoring on external quality attribute of software.**

***Keywords*— Refactoring, Metrics, Quality of Software**

I. INTRODUCTION

A. Refactoring

Refactoring code is the process of reorganizing code with the intent of simplifying both design and structure while not changing the functionality of the code [4]. By refactoring, we makes the code clean. It enhances the quality of software by removing potential problem in code. It minimizes the chances of introducing of bugs in the code.

B. Bad Smells

Bad smells are the defect in design of the software. Code smells are called as Bad smell. It is an indication of flaws in code which to be removed by applying appropriate refactoring technique. Fowler [16] given 22 bad smells and their respective 72 refactoring techniques to remove these bad smells. There are various tools to detect the bad smells. We detect 6 bad smells in the code. JDeodrant tool will detect 4 bad smells are- God class, Long method, Feature envy and Type Checking. Bad smell detected by PMD are- Dead code and Long parameters list.

- God Class- means a large class. Too many functions in one class so it's difficult to understand functionality of class.
- Long Method-means very long method in a class.
- Feature envy-means a class that is more interested to use function or methods of another class.
- Type Checking-it is switch statement bad smell. It has more duplication of code. So it is best to use polymorphism instead of switch statements.
- Dead Code- means variable, methods and classes that does not perform any functionality in software.
- Long Parameter List-means too many parameters are passed in parameter List.

C. Refactoring Techniques

Technique used for refactor the bad smells are called as Refactoring Techniques. These are the set of procedures to remove bad smell or clean the code. There are some refactoring techniques [16] used are-

- Extract Method - means extracting the set of statements into a new method.
- Extract Class – means extracting the set of methods and statements into a new class from the old class.
- Move Method – means methods from one class to another more relevant class.
- Remove or Delete – means delete the unused imports, local variables, unused private methods.
- Replace Conditional with Polymorphism- means replace switch conditional statements with polymorphism.
- Introduce Parameter Object–means replace parameter with an object.
- Replace Parameter with Method Call – means replace parameter passing function with value getting code inside the class.

D. Tools Used

- Eclipse- It is an Java based open source Integrated Development platform. It is designed in such a way that it can be extensible using plugins. It supports various languages C, C++, JAVA, PHP and COBOL. We can integrate bad smell detection plugins and refactoring tools into eclipse for refactoring the code.
- JDeodrant Plugin- is an eclipse plugin which are used for detecting and removing bad smells in the code. It can detect four bad smells are –Feature envy, God Class, Type Checking and Long Method. It detects bad smells in java based code.
- PMD Plugin-is a static java source analyze. It can be integrated into eclipse as a plugin. It can detect bad smells are- Dead code, Long Parameter List and Duplication Code.
- Metrics 1.3.6 Plugin- is a quality calculation tool. It can calculates No. of attributes, Lines of code, No. of classes, Weighted methods per Class, Cohesion and Coupling.

E. Quality Attributes

Software Quality Attributes are the characteristics of software by which quality is described and evaluated. It is divided into two groups- Internal Quality Attributes and External Quality Attributes. Internal Quality is measured directly from the

code. External quality attributes are measured with the help of internal quality attributes.

Internal Quality Attributes are-

- Lack of Cohesion
- Coupling
- Depth of Inheritance
- Number of Classes
- Lines of Codes
- Weighted Method per Class
- Abstractness

External Quality Attributes are-

- Understandability
- Reusability
- Functionality
- Effectiveness
- Flexibility
- Extendibility

II. LITERATURE SURVEY

Fowler et al. [16] describes the 22 bad smells and their 72 respective techniques to refactor bad smells. They mention duplicate code as a serious kind of bad smell. It increases maintenance cost of software. Due to increasing use of open source software and its variants, there is also increased use of code reuse. Due to Code reuse, it results in duplication of code.

Bansiya and Davis [10] presented a QMOOD (Quality Model for Object Oriented Designed) that access quality attributes like reusability, functionality, extendibility, flexibility, understandability, effectiveness. QMOOD relates low level design properties such as encapsulation, coupling and cohesion to high level quality attributes. It weighted quality attributes accordance to their influence and importance in the system.

Alshayed [1] investigate the effect of refactoring on software quality attributes. He focused on quality attributes like adaptability, maintainability, understandability, reusability and testability. They apply refactoring on three open source software- UML tool, terpPaint, Rabtpad. But after refactoring, he concludes that it does not necessary that refactoring improve the quality attributes of software.

Kannangara and Wijayanaka [21] investigate the impact of refactoring on internal quality attributes are maintainability, DIT, LOC, coupling. They compare quality attributes of nonrefactored code with refactored code. After study, they get result that only maintainability is improve, other attributes does not show any positive effect.

Tsantalis et al. [15] presented a tool, JDeodrant which is implemented as a plugin in Eclipse that automatically indentifies God class. They remove these smells by extract class refactoring. They also indentify the application of extract class refactoring in bad smells removal.

Kaur and Kaur [14] provide a review on bad smell detection tool PMD and JDeodrant using eclipse. They discuss and compare the bad smell detected by PMD and JDeodrant and their refactoring. They apply refactoring techniques on Online Exam System which is written in java. They refactor 6 bad smells using tools.

III. PROBLEM FORMULATION

To maintain the poorly design system is difficult and tough work. Software goes through various evolutionary development lifecycle, and then its quality attributes degrade. So it becomes difficult for developer to maintain the understandability, extensibility and reusability of the software. So refactoring is a way to maintain overall functionality and behavior of the system. So we proposed to detect the bad smells in object oriented open source java software and remove these by refactoring techniques. Then after refactoring, we analyze the impact of refactoring on external quality attributes of the software.

- To find different bad smells in an open source softwares.
- To analyze various refactoring techniques.
- To clean code by removing these bad smells through refactoring.
- To analyze the impact of refactoring on software quality before and after refactoring.

IV. RESEARCH METHOLOGY

A. Methodology

JDeodrant and PMD are bad smells detector. Object oriented open source software are JChart 2D (3.2.1),GhantProject(9.11) and RabtPad(0.1).

1. Measure internal quality attributes of the software.
2. Detect code bad smell by using PMD and JDeodrant tools in the software.
   a. Indentify the type of bad smell detected.
   b. Indentify location of bad smell detected.
   c. Refactoring techniques to be applied to it to refactor bad smell.
   d. Check, is there any error occur during refactoring, if not then move to next step to find next bad smell, otherwise rollback refactoring and applied another refactoring technique to refactor bad smell.
3. Then after removing bad smells in the codes, measure the internal quality attributes of software.
4. Calculates the external quality attributes of software with the help of internal quality attributes. Compare the external quality attributes of software before and after refactoring to analyze the impact of refactoring.

B. External Quality Attributes.and Internal Qualiy Attributes

TABLE I. Shows the external quality attributes given by bansiya[12]

External QA	Formula Used for Calculation
Reusability	-0.25*Coupling+0.25*Cohesion+0.5* Messaging+ 0.5*Design Size.
Flexibility	0.25*Encapsulation - 0.25*Coupling + 0.5*Composition + 0.5* Polymorphism.
Understand-ability	-0.33*Abstraction+0.33*Encapsulation-0.33*Coupling+0.33* Cohesion-0.33*Polymorphism-0.33*Complexity-0.33*Design Size.
Functionality	0.12*Cohesion + 0.22*Polymorphism + 0.22*Messaging + 0.22*Design Size +0.22*Hierarchies.
Extendibility	0.5*Abstraction - 0.5*Coupling + 0.5*Inheritance +0.5* Polymorphism.
Effectiveness	0.2*Abstraction + 0.2*Encapsulation + 0.2*Composition+ 0.2* Inheritance+ 0.2*Polymorphism.

TABLE III. Shows the Intenal Quality Formula

Design Property	Metrics used by Bansiya	Metrics we Used
Design Size	Design Size in Classes (DSC)	Number of Classes
Hierarchies	Number of Hierarchies (NOH)	Depth of Inheritance Tree
Abstraction	Average Number of Ancestors (ANA)	Abstractness
Encapsulation	Data Access Metrics (DAM)	(Total no. of attributes –static Attributes) / (Total no. of attributes + static Attributes)
Coupling	Direct Class Coupling (DCC)	Instability
Cohesion	Cohesion Among Methods of Classes(CAM)	1/Lack of Cohesion of Methods
Composition	Measure of Aggregation (MOA)	Number of Overridden Methods
Inheritance	Measure of Functional Abstraction (MFA)	No. of Overridden Methods /Number of Methods
Polymorphism	Measure of Polymorphic Methods (NOP)	Number of Overridden Methods
Messaging	Class Interface Size (CIS)	Number of Methods
Complexity	Number of Methods (NOM)	Weighted Methods per Class

V. RESULTS

Number of bad smells detected is shown in table IV. Table V and table VI shows the internal quality attributes before and after refactoring respectively. Then table V and table VI shows the external quality attributes values before and after refactoring respectively.

TABLE IV. Show the number of bad smell detected in software

Bad smells	RabtPad	JChart2D	GhanttProject
God Class	10	8	33
Feature envy	5	9	34
Long method	27	16	150
Type Checking	6	-	6
Dead Code	31	5	70
Long Parameter List	-	2	3

TABLE V. Shows Internal Quality Attributes of Software Before Refactoring

Softwares / Metrics	RabtPad	JChart2D	Ghantt Project
Coupling	0.252	0.406	0.397
Cohesion	2.551	2.463	0.2595
Messaging	7.581	3.991	6.189
Design Size	1.824	9.727	9.211
Encapsulation	0.4819	0.1797	0.5288
Composition	8.581	1.411	4.709
Polymorphism	0.258	0.467	0.417
Abstraction	0.044	0.0851	0.206
McCabe Complexity	18.871	8.533	15.034
Inheritance	0.966	0.882	0.937
Hierarchies	2.744	3.636	2.166

TABLE VI. Shows Internal Quality Attributes of Software After Refactoring

Softwares / Metrics	RabtPad	JChart2D	Ghantt Project
Coupling	0.296	0.623	0.397
Cohesion	3.164	2.898	0.2595
Messaging	10.12	4.236	6.189
Design Size	2.941	12.727	9.211
Encapsulation	0.4903	0.337	0.5288
Composition	5.38	1.543	4.709
Polymorphism	0.34	0.350	0.417
Abstraction	0.077	0.0865	0.206
McCabe Complexity	17.44	7.786	15.034
Inheritance	0.967	0.9174	0.937
Hierarchies	2.18	3.043	2.166

TABLE VII. Shows External Quality Attributes of Software Before Refactoring

External Quality Attributes	RabtPad	JChart2D	GhanttProject
Reusability	5.277	7.373	7.665
Flexibility	4.476	0.882	2.595
Understandability	-6.011	-5.469	-8.077
Functionality	3.042	4.216	3.987
Extendibility	0.508	0.514	0.581
Effectiveness	2.066	0.604	1.359

TABLE VIII. Shows External Quality Attributes of Software After Refactoring

External Quality Attribute	RabtPad	JChart2D	GhanttProject
Reusability	7.247(↑)	9.050(↑)	11.431(↑)
Flexibility	2.908(↓)	0.875(↓)	1.731(↓)
Understandability	-5.755(↑)	-6.051(↓	-7.469(↑)
Functionality	3.807(↑)	4.826(↑)	5.710(↑)
Extendibility	0.544(↑)	0.365(↓)	0.662(↑)
Effectiveness	1.450(↓)	0.646(↑)	1.000(↓)

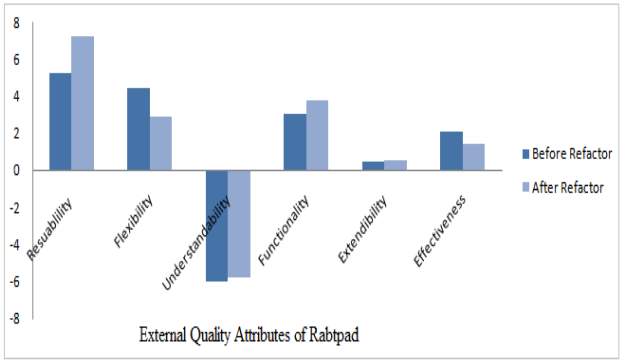

Fig. 1. Shows External Quality Attributes of RabtPad before Refactoring and after Refactoring.

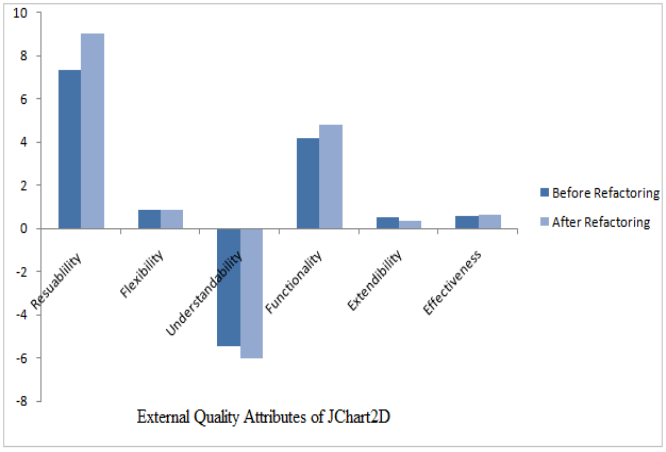

Fig. 2. Shows External Quality Attributes of JChart2D before Refactoring and after Refactoring.

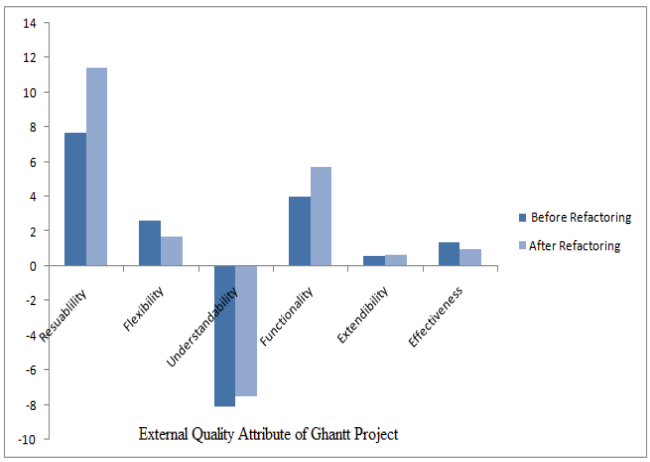

Fig. 3. Shows External Quality Attributes of GhanttProject before Refactoring and after Refactoring.

VI. CONCLUSION

In this paper, we notice the impact of refactoring of refactoring on external and internal quality attributes. It shows that reusability and functionality of all three shows an postive impact. But other external attributes like extendibility, understandability and flexibility shows negative impact on software after refactoring. So conclude from the experiment that group of refactoring techniques have postive and negative impact on software.

In future work, we can detect more bad smells and then apply more refactoring techniques to software to refactor these smells in a code. Then, after refactoring analyze the impact on quality.We can also check impact of refactoring on other quality attributes like testability.

REFERENCES

[1] M. Alshayeb, “Empirical Investigation of Refactoring Effect on Software Quality”, Information and Software Technology, ELSEVIER, 2009.

[2] W. Opdyke, “Refactoring Object-Oriented Frameworks”, PhD thesis, University of Illinois at Urbana-Champaign, 1992.

[3] A. Rani and H. Kaur, “Refactoring Methods and Tools”, International Journal of Advanced Research in Computer Science and Software Engineering, vol.2, No. 12, 2012.

[4] D. Jonsson, “Detecting Code Smells in Educational Software: an in-depth study by David Jonsson”, March 2013.

[5] D. Roberts, “Practical Analysis for Refactoring”, PhD thesis, Department of Computer Science, University of Illinois at Urbana-Champaign, 1999.

[6] S. Kaur and S. Singh, “Spotting and Elimination Type Checking Code Smells using Eclipse Plug-in: JDeodorant”, International Journal of Computer Science and Communication Engineering, v.5, No.1, 2016.

[7] EMF Metrics Plugin, URL – Retrieved from http://sourceforge.net/projects/metrics/.

[8] PMD, URL--Retrieved from http://pmd.sourceforge.net/eclipse/.

[9] ISO/IEC9126,”Software product evaluation- Quality characteristics and guidelines for their use”, 9126 Standard, Information technology, 1991.

[10] J. Bansiya and C.G. Davis, “A Hierarchical Model for Object-Oriented Design Quality Assessment,” IEEE Transactions on Software Engineering, vol. 28, no. 1, pp. 4-17, 2002.

[11] JDeodorant, URL - Retrieved from https://marketplace.eclipse.org/content/jdeodorant.

[12] K.O. Elish and M. Alshayeb, ” A Classification of Refactoring Methods Based on Software Quality Attributes”, Arabian Journal for Science and Engineering, Springer, 2011.

[13] K.O. Elishand M. Alshayeb, “Investigating the Effect of Refactoring on Software Testing Effort”, 16th Asia-Pacific Software Engineering Conference,IEEE, 2009.

[14] S. Kaur and S. Kaur, “Review on Identification and Refactoring of Bad Smells using Eclipse”, International Journal for Technological Research in engineering, v.2, Issue 7, March 2015.

[15] N. Tsantalis, M. Fokaefs and E. Stroulia, “JDeodorant: Identification and Application of Extract Class Refactoring”, ICSE ‘11, USA, 2011.

[16] M. Fowler, K. Back, J. Brant, W.Opdyke and D.Roberts. “Refactoring: Improving the Design of Existing Code”, Addison-Wesley, New York, 1999.

[17] M. Mantyla,“Bad Smells in Software – a Taxonomy and an Empirical Study”, Master Thesis, Department of Computer Science, Helsinki University of Technology, 2003.

[18] A. Chatzigeorgiouand A. Manakos, “Investigating the Evolution of Bad Smells in Object-Oriented Code”, International Conference on the Quality of Information and Communications Technology, IEEE, 2010.

[19] N. Tsantalis and A.Chatzigeorgiou, “Identification of move method refactoring opportunities”, IEEE Transactions on Software Engineering, pp.347–367, 2009.

[20] N. Kumari and A. Saha, ”Effect of Refactoring on Software Quality “, Academy and Industry Research Collaboration Center, v.4, pp.37-46, 2014.

[21] S.H. Kannangara and W.H.J.I Wijayanaka, “An Empirical Evaluation of Impact of Refactoring on Internal and External Measures of Code Quality”, International Journal of Software Engineering and Applications, v.6, No.1, 2015

[22] A. Sharma and S.K. Dubey, “Comparison of Software Quality Metrics for Object-Oriented System”, International Journal of Computer Science & Management Studies (IJCSMS), ISSN (Online): 2231 –5268, vol. 12, 2012.

Scrutinizing Punjab Elections Scenario via Big Data and Map Reduce Technology

Kulwinder Singh
Yadavindra College of Engineering
Talwandi Sabo Bathinda, Punjab (India)

Balkrishan Jindal
Assistant Professor, CE Department
Yadavindra College of Engineering
Talwandi Sabo Bathinda, Punjab (India)

***Abstract*—In this paper, structured database related to different political parties and political leaders of Punjab state elections in Comma separated value (CSV) or Tap separated value (TSV) is created. This database is undergone a mining process using map-reduce algorithm using Apache Hadoop framework. No one can get desired result by writing different scripts and passing numerous queries on the database and can get final results in graphical form or any different visualization. It will help the voters to select the right party and candidate in their assembly in lok Sabha elections.**

Keywords*—Big Data, Hadoop, MapReduce, structured data, unstructured data.

I. INTRODUCTION

Big data refers to the data sets that are too big to handle using the offered database management tools in many significant applications, such as Internet search, industry informatics, social networks and social medium and genomics and meteorology. In simple words it can be thought that some data which challenges the currently existing techniques for handling data is referred as big data. Big data present a grand challenge for folder and data analytics research. Gone are the days when remembrance was used to be considered in conditions of GigaBytes, TeraBytes or PetaBytes. Today even larger units are been used to measure memory like ExaBytes, ZettaBytes and Yotta Bytes. Big Data is not a single technology, technique or initiative. Rather, it is a trend across many areas of business and technology [2, 3]. Talking about technologies enabling the use of Big Data, there are three fundamental technological strategies for storing and providing fast access to large data sets [1, 7, 13, 14].

- Superior hardware presentation and capacity: make use of faster CPUs, make use of more CPU cores (require parallel/threaded operations to take advantage of multi-core CPUs), increase disk capacity and data transfer throughput, increased network throughput Massively Parallel Processing (MPP) [14].
- Reducing the size of data accessed: Data compression and data structures that, by design, boundary the amount of data required for queries. E.g. bitmaps and column-oriented databases (NoSQL) Not Only SQL [15].
- Distributing data and parallel processing: putting data on more disks on the way to parallelize disk I/O, set slices of data on separate work out nodes that can work on these less important slices in equivalent, use extremely distributed architectures with importance on fault lenience and presentation monitoring with higher-throughput network to improve data transfer among nodes Hadoop and Map Reduce.

A. Challenges of Big Data

Big data also has its own unique set of obstacles such as: [2, 4, 6]

- Information Growth-Over 80 percent of the data in the activity consists of shapeless data, which tends to be growing at a much faster pace than traditional relational information. This massive information threatens to swamp all but the well prepared IT organizations.
- Dispensation power- The expected approach of using a single, expensive and powerful computer to moment of truth information just does not scale for Big Data. Because we soon see the method to go is dividing and conquers using commoditized hardware and software via scale out.
- Physical storage- Capturing and managing all this information can chomp through enormous resources, outstripping all budgetary prospects. Data issues: Lack of data mobility, proprietary formats, and interoperability obstacles can all make working with Big Data complicated.
- Cost-Extract, change, and load (ETL) processes for Big Data can be expensive and time consuming, particularly in the absence of specialized well-designed software.

B. Big Data Use in Politics

The President Barack Obama is the first man on the planet earth to use the Big Data in elections [2]. In U.S.A., right here 2008 the elected birthday party used huge statistics just earlier than analyze the general public feeling which helped it with appropriate outcomes inside the election. It analyzed big public records and engineered social television and different media retailers to create a focused operation to win over younger voters for the elections. The movement proved beneficial in grasp states anywhere Democrats won a booming success. Within the big information evaluation additionally certified Democrats to fix to marketing campaign electorate which enabled them to generate over $1 billion in profits. Data was not effectively shared to be truly effective in analyzing potential voters. The fund raising lists differed from the get out the vote lists causing problems for the movement office as well as voters During in the establishing stages of the operation the records analytics team understand that the diverse departments together with the manner workplace website department and location departments have been running considering the fact that exclusive units of facts. The analytics group helped to create a great single gadget that can act as a central shop for information.

This records shop enabled the Democrats to gather facts from fieldworker's or fundraisers and public consumer databases for evaluation. This centralized save up helped the marketing campaign office to locate citizens and to create centered campaigns to get their recognition. Analytics on the large datasets certified the fight workplace to find out what exactly appealed to the voter in a particular section. It allowed campaigner to expect which citizens had been likely to provide online. It enabled them to peer who had cancelled their subscription from their campaign lists. This indicated voters which may also have switched to their political rival. It also allowed them to evaluate a thing which includes how the human beings could react to a nearby unpaid helper making a call as distinct to a person from a non-swing nation. The facts indicated that the individuals who had signed up for the short bestow application were 4 instances much more likely to offer than others. This record enabled them to create a stepped forward gift machine where people could make a contribution with lots much less annoy main to higher finances.

Barack Obama campaign had a devoted team of workers of over hundred people with over 50% of them in a special analytics department to research the information and 30% in the area to take the results. With reference to era they rate Hadoop for using the huge records analytics engine but they have been not able to do so because it required notably specialized skills to increase packages to apprehend the big records. Some other trouble that they facade turned into that Hadoop in its first variations changed into now not designed to deal with actual-time query. The crew sooner or later used straight up a huge records appliance that turned into scalable and easy to put into effect. Vertical is a column orientated database that gives a standardized interface and sq. equipment to get right of entry to the facts, as a result existing gear and users can effortlessly work with it without specialized skill units. The crucial statistics storehouse for the campaign was created on directly up, which enabled the analysts to get a 360-diploma view.

The problems that the Democratic motion faced with era are very commonplace with different following campaigns around the world. Humans may not have the assets to assemble an analytical engine much like that used by the Democratic campaign. Everywhere in the global humans may have records that they hope to apply now not simply to influence electorate but also to perceive problem regions for their own constituencies. Lease a large analytics group and developing a records computation facility isn't feasible in maximum instances. Elections in India until currently comprised heat, dirt, theatre, fixed expertise, opinion polls, speech, procession, door-to-door visit or sweat and toil. Two irreparable tendencies that had been sign in 2014 parliamentary elections were dreadfully huge younger voter base and use of era to its excellent. In 2014 Lok Sabha elections in India are well lead via virtual social media technologies. In 2008 USA presidential drive for Barack Obama is started with the use of Social Media and 2012 bring huge data Analytics to front role. One method for predicting the results of upcoming elections is via exit poll. The most valuable information regarding campaigns and their affect on general public is provided by citizens themselves.

Data analysts develop models based on this information and perform predictions regarding winning and losing chances of any political party and any political leader. If such results are properly harnessed, they could gain sizeable gains. Elections in India have always comprised issues based on caste, religion, sentiments, traditional wisdom, opinion polls and rallies. But 2014 Lok Sabha elections witnessed the use of technology to its very best by political parties. All this idea was actually borrowed by the way Barack Obama contested his elections in America and raise to power in 2008 and 2012. In an extraordinary attempt to engage digitally literate electorates of India Google and some other social platforms started a forceful digital information campaign. Google India launched one such hub related to elections where electorates can search for political candidates or political parties and election platforms and voting related information in their regions. They even launched one site on the counting date which updated about live status of results on the day of counting. It changed into discovered that Narendra Modi constantly topped the quest traits while as compared to different applicants. For conduct 2014 Lok Sabha elections 543 Parliamentary constituency and 4120 assembly constituency were set up. All over India total of 9 lakh 30 thousand polling booths be set up for conducting just elections. Voter rolls were ready in 12 different languages and total of 9 lakh pdf files which amounted to 2.5 crore pages were translate. The genuine challenge was removal of voter info from these 2.5 crore PDF pages and transliteration of the similar into English to merge with other source.

II. HADOOP AND MAP-REDUCE TECHNIQUE

Hadoop is a java based framework that is well-organized for processing large data sets in a distributed computing environment [11, 12]. Hadoop is sponsored by Apache Software Foundation. The maker of Hadoop was Doug wounding and he named the framework after his child's swollen toy elephant. Applications be made run on systems with thousands of nodes making employ of thousands of terabytes via Hadoop. Dispersed file system in Hadoop facilitate fast data transfer among nodes and allows continuous operations of the system even if node failure occurs. This concept lowers the risk of disastrous system breakdown even if multiple nodes become out of action. The inspiration behind working of Hadoop is Google's Map reduce which is a software framework in which application under consideration is busted behind into number of small parts [5, 6]. Hadoop is a framework which comprised of six components [4].Every component is assigned a particular job to be performed.

- HDFS – Hadoop distributed file system are distributed cages where all animals live i.e. where data resides in a distributed format.
- Apache HBase – It is a well-groomed and large database.
- Zookeeper- Zookeeper is the person responsible for managing animals play.

Pig – Pig allows playing with data from HDFS cages.

Hive- Hive allows data analysts play with HDFS and makes use of SQL.

- HCatalog helps to upload the database file and automatically create table for the user.

Map Reduce is a framework originally developed at Google that allows for easy large scale disseminated computing from corner to corner a number of domains [8]. The Apache Hadoop software library is a framework that allows for the distributed processing of large data sets from corner to turn clusters of computers with easy programming models. It is planned to range up from only servers to thousands of machines, every offering local computation and storage space. Hadoop MapReduce includes several stages, all with a key put of operation selection to get to your purpose of getting the answer you need from big data. The method starts with a user request to run a MapReduce program and continues until the results are written back to the HDFS.

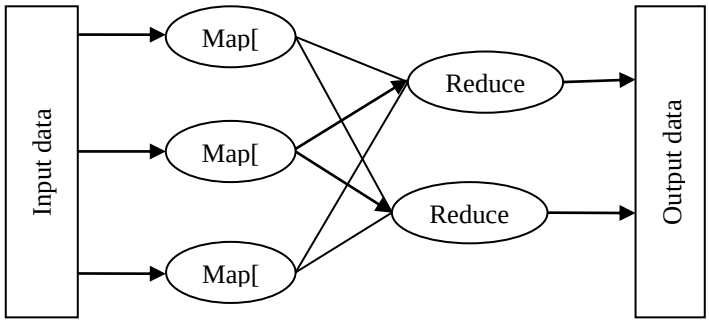

Fig. 1 Working of Map Reduce Technology

MapReduce is an architectural model for parallel processing of tasks on a distributed computing system. This algorithm is first described inside a paper "MapReduce easy Data Processing going on Large Clusters," by Jeffery Dean and Sanjay Ghemwat from Google. This algorithm allows split of a single computation task to various nodes or computers for distributed processing.

As an only task can be broken down into many subparts, each handled by a separate node the number of nodes determines the processing rule of the system. There are a choice of commercial and open-source technologies that implement the MapReduce algorithm as a part of their internal architecture. A popular implementation of MapReduce is the Apache Hadoop, which is used for data processing in a distributed computing environment. As MapReduce is an algorithm, it can be written in any programming language [17,18].

The initial part of the algorithm is used to split and 'map' the sub tasks to computing nodes. The 'reduce' part takes the results of individual computations and combines them to get the final result.

In the MapReduce algorithm, the mapping function reads the input data and generates a set of intermediate records for the computation. These intermediate records generated by the map function take the form of a key, data pair. As a part of mapping function, these records are distributed to different computing nodes using a hashing function. Individual nodes then perform the computing operation and return the results to the reduce function. The reduce function collects the individual results of the computation to generate a final output.

III. PROPOSED WORK

Snap shot of database created in the proposed method is shown in Figure 2. It involves 15 different attributes which are related to elections conducted in Punjab 13 Lok Sabah sheets. It involves both string values and integers.

	A	B	C	D	E	F	G	H	I	J	K	L	M	N	O
1	NAME	AGE	EDUCATION	SEX	PARTY	PARTY TYPE	VOTES IN FAVOUR	OF VOTES IN FAVOU	CRIMINAL CASE	ASSETS	LIABILITIES	STATUS	WINNING CHANCES	onstituency Nam	Year
2	Harsimrat Kaur Badal	47	10th	Female	SAD	State	514727	46.09	0	100 Crore	41 crore	Crorepati	Bright	BATHINDA	2014
3	preet Singh S/O Gurdas Si	52	Graduate	Male	INC	National	495332	44.35	0	42 Crore	4 Crore	Crorepati	Bright	BATHINDA	2014
4	Jasraj Singh Longia	40	Graduate	Male	AAP	National	87901	7.87	0	31 Lac	Nil	Lakhpati	Average	BATHINDA	2014
5	Kuldeep Singh	32	10th	Male	BSP	National	13732	1.22	0	80 Lac	Nil	Lakhpati	Poor	BATHINDA	2014
6	Ashish	25	10th	Male	IND	Independent	6626	0.59	3	10 Thousanc	Nil		Poor	BATHINDA	2014
7	Bhagvant Singh Samaon	36	8th	Male	CPI	National	5984	0.53	0	2 Lac	15 Thousand	Lakhpati	Poor	BATHINDA	2014
8	Satish Arora	51	12th	Male	IND	Independent	5936	0.52	0	1 Crore	Nil	Crorepati	Poor	BATHINDA	2014
9	preet Singh S/O Gurdev S	33	10th	Male	IND	Independent	4618	0.413	0	7 Lac	Nil	Lakhpati	Poor	BATHINDA	2014
10	Shaminder Singh	34	12th	Male	JKKNPP	National	4610	0.412	0	33 Lac	2 Lac	Lakhpati	Poor	BATHINDA	2014
11	Geeta Rani	50	5th	Female	ABSR	National	4380	0.39	0	Nil	Nil		Poor	BATHINDA	2014
12	Sanjeev Kumar Thapar	34	10th	Male	IND	Independent	2833	0.253	0	26 Lac	2 Lac	Lakhpati	Poor	BATHINDA	2014
13	Makhan Lal	43	8th	Male	BSP(A)	National	2507	0.221	0	11 Thousanc	Nil		Poor	BATHINDA	2014
14	Vijay Kumar	44	10th	Male	IND	Independent	2258	0.202	2	6 Lac	Nil	Lakhpati	Poor	BATHINDA	2014
15	Swaran Singh	45	Graduate	Male	IND	Independent	2077	0.185	0	1 Crore	Nil	Crorepati	Poor	BATHINDA	2014
16	Rajinder Singh	34	10th	Male	SAD(A)	State	1960	0.175	0	26 Lac	Nil	Lakhpati	Poor	BATHINDA	2014
17	Navneet	42	12th	Male	SHS	National	1893	0.169	0	17 Thousanc	5 Lac		Poor	BATHINDA	2014
18	Jagdeep Singh Gehri	39	10th	Male	IND	Independent	1665	0.149	0	1 Lac	Nil	Lakhpati	Poor	BATHINDA	2014
19	Bhupesh Kumar	36	Graduate	Male	IND	Independent	1487	0.133	0	6 Lac	Nil	Lakhpati	Poor	BATHINDA	2014
20	Gurdeep Singh	44	Illiterate	Male	IKL	National	1404	0.125	0	5 Lac	Nil	Lakhpati	Poor	BATHINDA	2014
21	Gurmeet Singh Ranghreta	44	12th	Male	PLP	National	1386	0.124	1	35 Lac	1 Lac	Lakhpati	Poor	BATHINDA	2014
22	Sushil Kumar Jindal	31	10th	Male	IND	Independent	1330	0.119	0	1 Lac	Nil	Lakhpati	Poor	BATHINDA	2014
23	Jagdish Rai Sharma	57	ost Graduate	Male	NBDP	National	1248	0.111	1	95 Lac	3 Lacs	Lakhpati	Poor	BATHINDA	2014
24	Sukhwinder Singh	33	12th	Male	BMP	National	1086	0.097	0	2 Lac	Nil	Lakhpati	Poor	BATHINDA	2014

Fig. 2 This Snapshot show the structured database of Punjab

In this snapshort shows the all candidate details like 15 different attributes name, age, education, sex,party, party_type, votes_in_favour, % votes_in_favour, criminal_case, assets, liabilities, status, winning chance, constituency type, year.

IV. RESULTS AND DISCUSSION

In this section results of the proposed method are presented and discussed. The result obtained from the database after running appropriate queries are shown in the form of visualization as below using Apache Hadoop Framework.
In this database first query Select * from kulwinder65; is used to display all the attributes in the table.

Table 1.Query result generated in the proposed work on created table 'kulwinder65' using query 1.

S. no	Name	Age	Education	Sex	Party	Party Type	Votes In Favor	% of votes	Criminal case	Assets In crore	Liabilities in crore's	status	Winning chance	Constituency name	Year
1	Harsimrat Kaur Badal	47	10th	F	SAD	State	514727	46.09	0	100	41	Crorpati	Bright	Bathinda	2014
2	Manpreet Singh S/o Gurdas Singh	52	Graduate	M	INC	National	495332	44.35	0	42	4	Crorpati	Bright	Bathinda	2014
3	Kuldeep Singh	40	Graduate	M	AAP	National	87901	7.87	0	0.31	Nill	Lakhpati	Average	Bathinda	2014
4	Ashish	32	10th	M	BSP	National	13732	1.22	0	0.80	Nill	Lakhpati	Poor	Bathinda	2014
5	Bhagwant Singh Samaon	25	10th	M	IND	Independent	6626	0.59	3	0.80	Nill		Poor	Bathinda	2014
6	Satish Arora	36	8th	M	CPI	National	5984	0.53	0	0.2	0.15	Lakhpati	Poor	Bathinda	2014
7	Manpreet Singh S/o Gurdev singh	51	12th	M	IND	Independent	5936	0.52	0	1	Nill	Crorpati	Poor	Bathinda	2014

In this table different attributes like name, age, education, sex, party, party_type, votes_in_favour, % of votes in favors, criminal_case, assets, liabilities, winning chance, constituency_name, year of all candidate consist in election of Punjab state in show table 1.

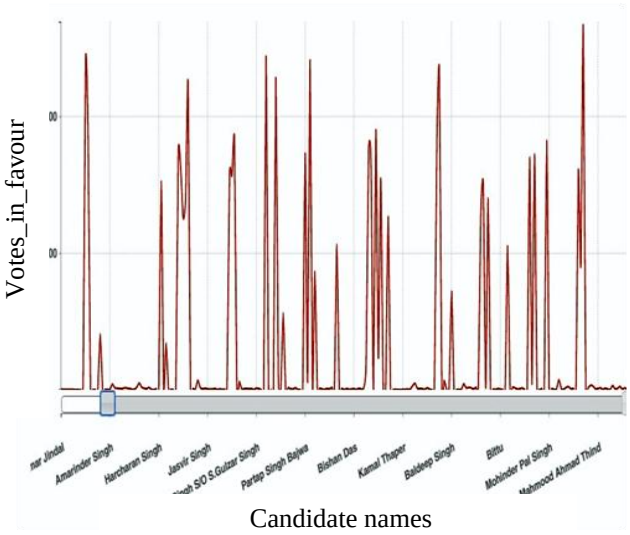

Fig. 3 visualization result of the proposed method

In Fig 3 is show the information about the 473 candidate's information for consists the election in Punjab from the fig. It will help the people to judge which candidate of most lead in past or wanted to elect their leader in future.

Use 2nd Query Select * from kulwinder65 where criminal_case>=2; to show the criminal case retails of all candidates.

Table 2 Result obtained using Query2.

Name	Age	Education	Party	Criminal Case
Ashish	25	10th	Ind	3
Vijay Kumar	44	10th	Ind	2
Captain Amrinder Singh	72	Graduate	Inc	3
Arun Kumar Joshi	40	12th	Ind	3
Dr.inder Pal	52	Graduate Professional	Ind	2
Balwinder Singh	57	Post Graduate	Ind	2
Gurdeep Singh Kahlon	42	Graduate professional	Ind	2
Simrjeet Singh bains	43	Graduate	Ind	2

Table 2 shows that number of candidates registered against then 2 or more criminal cases.

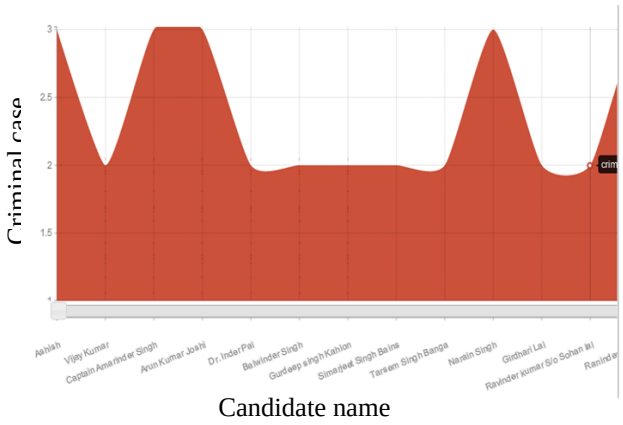

Fig.4 visualization result of the proposed method

The information about the candidate against under who have more than 2 criminal cases registered in past show in fig 4.

Use 3rd Query Select * from Kulwinder65 constituency_name="Fridkot"; to show all the candidates of district Fridkot.

Table 3 Query generated in this proposed work on created table kulwinder65using query 3.

S.no	Name	Age	Education	Sex	Party	Party Type	Votes in Favors
0	Sukhwinder Singh Danny	32	Post Graduate	M	INC	National	395692
1	KauhalChamanbhaura	60	Graduate	M	CPI	National	19459
2	Parmjit Kaur gulshan	60	Post Graduate	F	SAD	State	457734
3	Resham Singh	56	Doctorate	M	BSP	National	34479
4	Gurmeet Singh	39	12th	M	PLP	National	1243
5	Jasvir Singh	35	8th	M	MB	National	910
6	Pritam Singh	70	5th	M	RPI	National	812
7	Prem Singh	63	8th	M	SP	National	3133
8	Raj kaur	60	Literate	F	AIDWC	National	1041

Table 3 is show of candidate who belongs to district Fridkot and their education, age, sex etc.

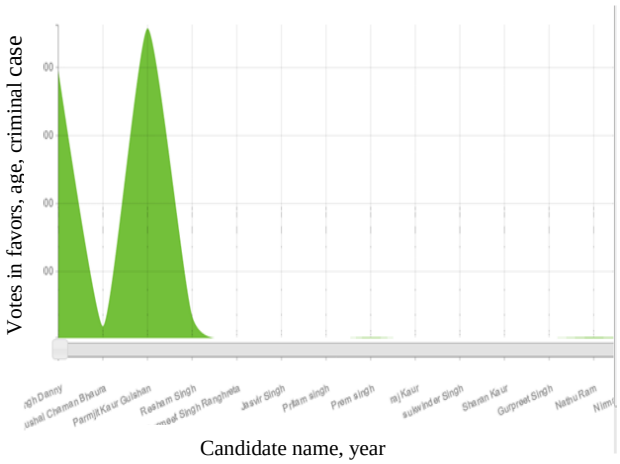

Fig.5 visualization results of the proposed method

In this Fig 5 show the information about the Fridkot district constituency in all candidates.

```
State Postal,County Name,FIPS,Obama vote,Obamaper,Romney vote,Romneyper
AK,Alaska,0,"91,696",41.6,"121,234",55
AK,Alaska,2000,"91,696",41.6,"121,234",55
AL,Alabama,0,"793,620",38.4,"1,252,453",60.7
AL,Autauga,1001,"6,354",26.6,"17,366",72.6
AL,Baldwin,1003,"18,329",21.6,"65,772",77.4
AL,Barbour,1005,"5,873",51.3,"5,539",48.3
AL,Bibb,1007,"2,200",26.2,"6,131",73.1
AL,Blount,1009,"2,961",12.3,"20,741",86.5
AL,Bullock,1011,"4,058",76.3,"1,250",23.5
AL,Butler,1013,"4,367",46.1,"5,081",53.6
AL,Calhoun,1015,"15,500",33.5,"30,272",65.5
AL,Chambers,1017,"6,853",47.1,"7,596",52.2
AL,Cherokee,1019,"2,126",21.8,"7,494",76.8
AL,Chilton,1021,"3,391",19.5,"13,910",79.8
AL,Choctaw,1023,"3,785",47.5,"4,150",52.1
AL,Clarke,1025,"6,317",45.7,"7,463",54
AL,Clay,1027,"1,770",26.7,"4,802",72.3
AL,Cleburne,1029,971,15.4,"5,269",83.6
AL,Coffee,1031,"4,899",24.8,"14,638",74.2
AL,Colbert,1033,"9,160",39.2,"13,931",59.6
AL,Conecuh,1035,"3,551",50.6,"3,434",49
AL,Coosa,1037,"2,188",41.7,"3,028",57.8
AL,Covington,1039,"3,155",20.5,"12,148",78.8
AL,Crenshaw,1041,"2,048",31.9,"4,326",67.5
AL,Cullman,1043,"4,855",14.6,"27,930",84.2
AL,Dale,1045,"5,283",28.5,"13,105",70.6
AL,Dallas,1047,"14,599",69.7,"6,284",30
AL,DeKalb,1049,"5,235",22,"18,316",76.8
AL,Elmore,1051,"8,940",25.2,"26,223",74
AL,Escambia,1053,"5,476",36.9,"9,263",62.5
AL,Etowah,1055,"12,792",30.1,"29,102",68.5
AL,Fayette,1057,"1,803",22.8,"6,034",76.3
AL,Franklin,1059,"3,171",29.2,"7,567",69.7
AL,Geneva,1061,"2,039",18,"9,173",81
AL,Greene,1063,"4,514",84.7,799,15
AL,Hale,1065,"5,401",62.6,"3,205",37.1
AL,Henry,1067,"3,046",35,"5,605",64.4
AL,Houston,1069,"12,348",29.5,"29,214",69.8
```

Fig.6 Unstructured database Obama and Romney of USA Elections

We have compare my structured database with unstructured database and found that results are obtained in less time in case of structured database as compared to unstructured database. The four parameters considered are time in milliseconds, number of mappings, number of reductions and average R/W operation done.

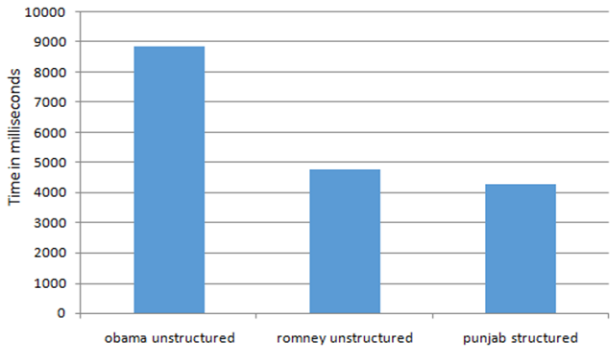

Fig.7 Comparison Obama unstructured, Romney unstructured and Punjab structured

The figure 7 below shows the pictorial representation of the comparison conducted. The two parameters considered are Database and Time in milliseconds for creation of the graph below. I have considered database taken from US elections. The first database has been related to Barrack Obama status and second to Romney status during elections. Later third database is that of Punjab elections. The third database is structured database and the results obtained after executing these databases are shown in the figure below.

Table 4 Time in milliseconds

Database	Time in milliseconds
Obama Unstructured	8830
Romney Unstructured	4750
Punjab Structured	4260

In this table 4 show of the comparison of structured database Punjab and unstructured database of USA elections.

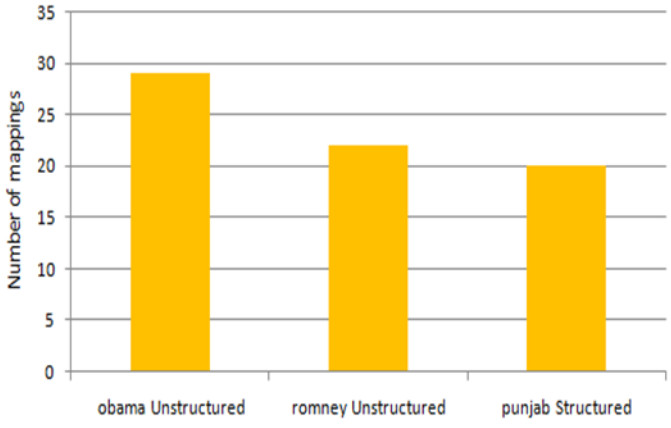

Fig.8 Comparison Obama unstructured, Romney unstructured and Punjab structured chart number of mappings.

In this proposed work the figure 8 shows the pictorial representation of the comparison conducted. The two parameters considered are Database and Number of mappings for creation of the graph below. I have considered Punjab election database taken from US elections. The first database has been related to Barrack Obama status and second to Romney status during elections. Later third database is that of Punjab elections. The third database is structured database and the results obtained after executing these databases are shown in the figure below.

Table 5 Number of mappings

Database	Number of Mappings
Obama Unstructured	29
Romney Unstructured	22
Punjab Structured	20

In this table show of the comparison of structured database Punjab and unstructured database of USA.in number of mappings and show the values.

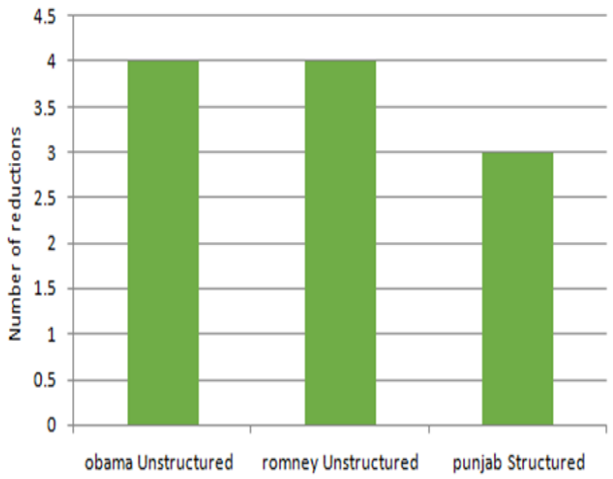

Fig.9 Comparison of Obama unstructured, Romney unstructured and Punjab structured database show the number of reductions.

The pictorial representation of the comparison conducted. The two parameters considered are Database and Number of reductions for creation of the graph below. I have considered database taken from US elections. The first database has been related to Barrack Obama status and second to Romney status during elections. Later third database is that of Punjab elections. The third database is structured database and the results obtained after executing these databases are shown in the figure 9 below.

Table 6 Number of reductions

Database	Number of reductions
Obama Unstructured	4
Romney Unstructured	4
Punjab Structured	3

This table show of the comparison of Obama unstructured, Romney unstructured database of USA elections and Punjab structured database .in number of reductions and show the values.

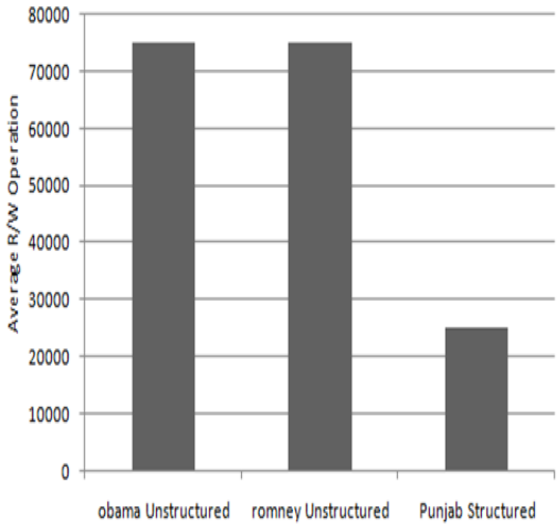

Fig.10 Comparison of Obama unstructured, Romney unstructured And Punjab structured database.

In this proposed work figure10 shows the two parameters considered are database and average read and writes operations for creation of the graph below.

Table 7 Average R/W operation

Database	Average R/w operation
Obama Unstructured	75153
Romney Unstructured	75153
Punjab Structured	24891

In this proposed work table 7 shows the two data base comparison values.

V. CONCLUSION

It has been concluded that big data will act as a backbone for the next elections and may be path breaker in the way it's fought. It could turn into a massive data gathering exercise where unique databases (for e.g. voter registration, social media, subscription data, transaction profile, mobile records, television viewership and channel bouquet, work profile, location, etc.) are integrated together and analyzed with zeal to find correlations and patterns. It has been predicted that about 160 million of those unsure about who to vote could be reached through mobile phones and about a 100 million through television. These people are waiting to hear the right message to make that choice of which party to vote for and may be the right message is hidden somewhere waiting to be uncovered. Advanced big data analytics could be the key to uncover the winning mantra for the candidate as well as political party.

REFERENCES

[1] Marz, N and Warren, J. "Big Data: Principles and best practices of scalable realtime data systems". Manning Publications,pp.1-32, 2013
[2] Smolan, R and Erwitt, D. "The Human Face of Big Data.Sterling" Publishing Company Incorporated, 2012.
[3] Gntz, J. and Reinsel, D. IDC: The Digital Universe in 2020: Big Data, Bigger Digital Shadows, and Biggest Growth in the Far East. pp. 1-11, 2012.
[4] Taylor, R., "An overview of the Hadoop/Map Reduce/HBase framework and its current applications in bioinformatics," BMC Bioinformatics article, 11(12):pp.1-7, 2010.
[5] Jagdev, G., Singh, B. and Mann, M., "Big Data Proposes an Innovative Concept for Contesting Elections in Indian Subcontinent. International journal of scientific and Technical Advancement, 1(3): pp. 23-28, 2015
[6] Krzywinski, M., Birol, I., Jones, S. and Msarra,M., "Hive plots-rational approach to visualizing networks," Briefings in Bioinformatics, View · 13(5):pp. 627–644, 2012.
[7] Katal, A., Wazid, M. and Goudar, R., "Big Data: Issues, Challenges, Tools and Good Practices"Proc. of the IEEE24th conference on contemporary computing, 33(2):pp. 404-409, Noida, 2013.
[8] Dean, Jeffery, and Ghemwat Sanjay. "MapReduce: Simplified Data Processing on Large Clusters.pp.1-14, 2004.
[9] Kaisler, S., Armour, F., Espinosa, J.A., and Mony, W., "Big Data issues and Challenges Moving Forward. International conference on system Sciences" Proc. of the IEEE 46th Hawaii international conference on system science: pp.995-1004, 2013
[10] Umasri.M.L, Shyamalagowri.D ,Suresh Kumar.S"Mining Big Data:- Current status and forecast to the future" 4 (1): pp. 5-11,2014
[11] Mukherjee, A., Datta, J., Jorapur, R., Singhvi, R., Haloi, S., Akram, W., "Shared disk big data analytics with Apache Hadoop"IEEE 18-22 Dec, 2012.
[12] Aditya B, Manashvi Birla andUshmaNair,"Addressing Big Data Problem Using Hadoop and Map Reduce",2012
[13] Harshawardhan and Prof. DevendraGadekar, JSPM's Imperial College of Engineering & Research, 4(10):pp.1-7, Wagholi, 2014.
[14] Mrigank.M, Akashdeep. K, Snehasish. D and Kumar. N "Analysis of Bidgata using Apache Hadoop and Map Reduce" 4 (5):pp.67-78, 2014.
[15] Kyong.H"Parallel Data Processing with Map Reduce: A Survey" SIGMOD Record, 40(4):pp.445-478, 2011.
[16] Chen. H, "Matchmaking: A New Map Reduce Scheduling" in 10th IEEE International Conference on Computer and Information Technology, pp. 2736–2743, 2010.
[17] R. Ahmed and G. Karypis, "Algorithms for Mining the Evolution of Conserved Relational States in Dynamic Networks," Knowledge and Information Systems, 33(3): pp. 603-630, Dec. 2012.
[18] M.H. Alam, J.W. Ha, and S.K. Lee, "Novel Approaches to Crawling Important Pages Early," Knowledge and Information Systems, 33(3): pp.707-734, Dec. 2012.

Comparative Analysis of Various Image Compression Techniques

Gaganjot Singh
M-Tech Student
Department of CSE
AIET Faridkot, Punjab, India

Jasneet Singh Sandhu
Assistant Professor
Department of CSE
AIET Faridkot, Punjab, India

Abstract: **- Image compression is a process to remove the redundant information from the image so that only essential information can be stored to reduce the storage size, transmission bandwidth and transmission time. The essential information is extracted by various transforms techniques such that it can be reconstructed without losing quality and information of the image. In this paper, comparative analysis of image compression is done by Hybrid (DWT-DCT) Transform. MATLAB programs are written for each of the above methods and conclusions based on the results obtained by hybrid DWT-DCT algorithm performs much better than the standalone JPEG-based DCT, DWT algorithms in terms of peak signal to noise ratio (PSNR), as well as visual perception at higher compression ratio. The wavelet transform, which is part of the new JPEG 2000 standard, claims to minimize some of the visually distracting artifacts that can appear in JPEG images.**

I. INTRODUCTION

The increasing demand for multimedia content such as digital images and video has led to great interest in research into compression techniques. The development of higher quality and less expensive image acquisition devices has produced steady increase in both image size and resolution, and a greater consequent for the design of efficient compression systems. Although storage capacity and transfer bandwidth has grown accordingly in recent years, many applications still require compression.

Factors related to the need for image compression include:

- The large storage requirements for multimedia data
- Low power devices such as handheld phones have small storage capacity
- Network bandwidths currently available for transmission
- The effect of computational complexity on practical implementation.

A data compression system mainly consists of three major steps and that are removal or reduction in data redundancy, reduction in entropy, and entropy encoding. A typical data compression system can be labelled using the block diagram shown in Figure 1

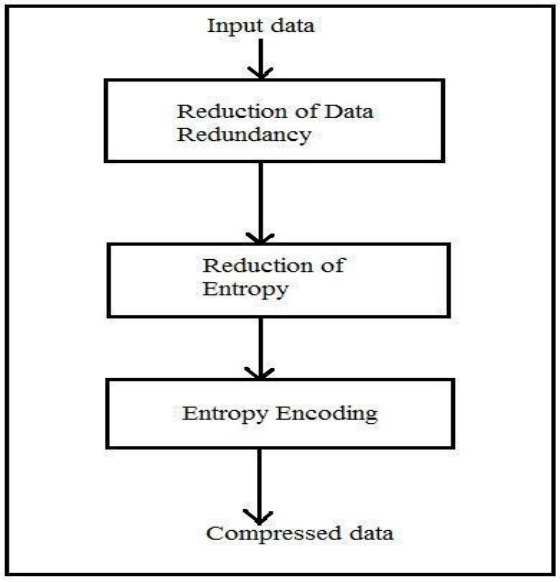

Fig.1: A data compression model

It is performed in steps such as image transformation, quantization and entropy coding. JPEG is one of the most used image compression standard which uses Discrete Cosine Transform (DCT) to transform the image from spatial to frequency domain. An image contains low visual information in its high frequencies for which heavy quantization can be done in order to reduce the size in the transformed representation. Entropy coding follows to further reduce the redundancy in the transformed and quantized image data.

A. Image Compression Based on Entropy

The principle of digital image compression based on information theory. Image compression uses the concept of Entropy to measure the amount of information that a source produces. The amount of information produced by a source is defined as its entropy. For each symbol, there is a product of the symbol probability and its logarithm. The entropy is a negative summation of the products of all the symbols in a given symbol set. Compression algorithms are methods that reduce the number of symbols used to represent source information, therefore reducing the amount of space needed to store the source information or the amount of time necessary to transmit it for a given channel capacity.

The mapping from source symbols into fewer target symbols is referred to as compression. The transformation from the target symbols back into the source symbols representing a close approximation form of the original information is called decompression. Compression system consists of two steps, sampling and quantization of a signal. The choice of compression algorithm involves several conflicting considerations. These include degree of compression required, and the speed of operation. Obviously if one is attempting to run programs direct from their compressed state, decompression speed is paramount. The other consideration is size of compressed file versus quality of decompressed image. Compression is also known as encoding process and decompression is known as decoding process. Digital data compression algorithms can be classified into two categories-

- *Lossless compression:* In lossless image compression algorithm, the original data can be recovered exactly from the compressed data. It is used generally for discrete data such as text, computer generated data, and certain kinds of image and video information. Lossless compression can achieve only a modest amount of compression of the data and hence it is not useful for sufficiently high compression ratios. GIF, Zip file format, and Tiff image format are popular examples of a lossless compression [30, 3]. Huffman Encoding and LZW are two examples of lossless compression algorithms. There are times when such methods of compression are unnecessarily exact.
  In other words, 'Lossless' compression works by reducing the redundancy in the data. The decompressed data is an exact copy of the original, with no loss of data.
- *Lossy compression:* Lossy compression techniques refer to the loss of information when data is compressed. As a result of this distortion, must higher compression ratios are possible as compared to the lossless compression in reconstruction of the image.
  'Lossy' compression technique sacrifices exact reproduction of data for better compression. It removes redundancy and creates an approximation of the original.

B. Redundancy

Redundancy different amount of data might be used. If the same information can be represented using different amounts of data, and the representations that require more data than actual information, is referred as data redundancy. In other words, number of bits required to represent the information in an image can be minimized by removing the redundancy present in it. Data redundancy is of central issue in digital image compression. If n1 and n2 denote the number of information carrying units in original and compressed image respectively, then the

$$CR = n1/n2$$

II. TECNIQUES USED

A. Discrete Cosine Transform

Discrete Cosine Transform (DCT) is an orthogonal transform, the DCT attempts to decorrelate the image data. After decorrelation each transform coefficient can be encoded independently without losing compression efficiency.

The DCT transforms a signal from a spatial representation into a frequency representation. The DCT represent an image as a sum of sinusoids of varying magnitudes and frequencies. DCT has the property that, for a typical image most of the visually significant information about an image is concentrated in just few coefficients of DCT. After the computation of DCT coefficients, the coefficients are normalized according to a quantization table with different scales provided by the JPEG standard computed by psycho visual evidence. Selection of quantization table affects the entropy and compression ratio. DCT has many advantages:

- It has the ability to pack most information in fewest coefficients.
- It minimizes the block like appearance called blocking artifact that results when boundaries between sub-images become visible.

An image is represented as a two dimensional matrix, 2D DCT is used to compute the DCT coefficients of an image. The 2D DCT for an N x N input sequence can be defined as follows:

$$D(i,j) = \frac{1}{\sqrt{2n}} C(i)C(j) \sum_{x=0}^{N-1} \sum_{y=0}^{N-1} P(x,y) \cos\left(\frac{(2x+1)i\pi}{2n}\right) \cos\left(\frac{(2y+1)j\pi}{2n}\right)$$

Where, P(x, y) is an input matrix image N x N, (x, y) are the coordinate of matrix elements and (i, j) are the coordinates of coefficients.

Limitations of DCT: For the lower compression ratio, the distortion is unnoticed by human visual perception. In order to achieve higher compression it is required to apply quantization followed by scaling to the transformed coefficient. For such higher compression ratio DCT has following two limitations. First is blocking artifacts is a distortion that appears due to heavy compression and appears as abnormally large pixel blocks. For the higher compression ratio, the perceptible blocking artifacts across the block boundaries cannot be neglected and second one is false contouring, occurs when smoothly graded area of an image is distorted by a deviation that looks like a contour map for specific images having gradually shaded areas. The main cause of the false contouring effect is the heavy quantization of the transform coefficients.

B. Discrete Wavelet Transform (DWT)

Wavelets are a mathematical tool for changing the coordinate system in which signals are represented to another domain that is best suited for compression. Wavelet based coding is more robust under transmission and decoding errors. Due to their inherent multi-resolution nature, DWTs are suitable for applications where scalability and tolerable degradation are important.

Wavelets are tool for decomposing signals such as images, into a hierarchy of increasing resolutions. The more resolution layers, the more detailed features of the image are shown, DWTs are localized waves that drop to zero. DWTs come from iteration of filters together with rescaling. Wavelet produces a natural multi resolution of every image, including the all-important edges. The output from the low pass channel is useful compression. Wavelet has an unconditional basis as a result the size of the wavelet coefficients drop off rapidly. The wavelet expansion coefficients represent a local component thereby making it easier to interpret. Wavelets are adjustable and hence can be designed to suit the individual applications. Its generation and calculation of DWT is well suited to the digital computer. DWTs are only multiplications and additions in the calculations of wavelets, which are basic to a digital computer.

III. PROPOSED METHOD

In this work comparative analysis of image compression is done by three transform methods, which are Discrete Cosine Transform (DCT), Discrete Wavelet Transform (DWT) & Hybrid (DWT+DCT) Transform. MATLAB programs were written for each of the above method and concluded based on the results obtained that hybrid DWT-DCT algorithm performs much better than the standalone JPEG-based DCT, DWT algorithms in terms of peak signal to noise ratio (*PSNR*), as well as visual perception at higher compression ratio.

A. Hybrid (DWT+ DCT) Transform

In heading II two different ways of achieving the goals of image compression, which have some advantages and disadvantages had been discussed, in this section there is a proposal of hybrid transform technique that will exploit advantages of DCT and DWT, to get compressed image. Hybrid DWT-DCT transformation gives more compression ratio compared to JPEG and JPEG2000, preserving most of the image information and create good quality of reconstructed image. Hybrid (DWT+DCT) Transform reduces blocking artifacts, false contouring and ringing effect.

a) *Compression procedure:* The input image is first converted to gray image from colour image, after this whole image is divided into size of 32 x 32 pixels blocks. Then 2D DWT applied on each block of 32 x 32 blocks, by applying 2D DWT, four details are produced. Out of four sub band details, approximation sub band is further transformed again by 2D DWT which gives four sub bands of 16 x 16 blocks. Above step is followed to decompose the 16 x 16 block of approximated detail to get new set of four sub band of size 8 x 8. The level of decomposition depends on size of processing block obtained initially, i.e. there is a division of 32 x 32. Hence the level of decomposition is 2. After getting four blocks of size 8 x 8, proposed method uses the approximated details for computation of discrete cosine transform coefficients. These coefficients are then quantize and send for coding. The complete coding scheme is explained in Figure 2.

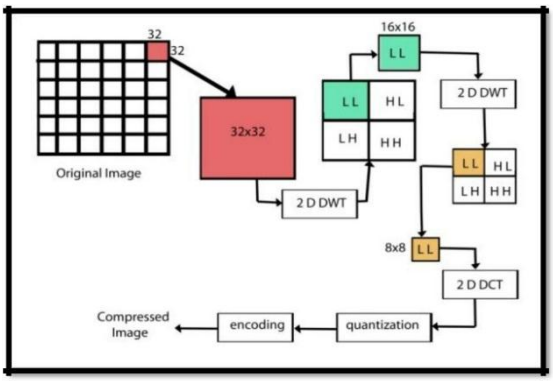

Fig. 2. Compression technique using Hybrid transform

b) *Decompression procedure:* At receiver side, the algorithm decodes the quantized DCT coefficients and the inverse two dimensional DCT (IDCT) of each block is calculated. Then block is de quantized. Further applying inverse wavelet transform on the de quantized block. Since the level of decomposition while compressing was two, here also inverse wavelet transform is taken two times to get the same block size i.e. 32 x 32. This procedure followed for each block received. When all received blocks are converted to 32x 32 by following decompression procedure, explained above. The algorithm arranges all blocks to get reconstructed image. The complete decoding procedure is explained in Figure 3. The hybrid DWT-DCT algorithm has better performance as compared to stand alone DWT and DCT in terms of Peak Signal to Noise Ratio (PSNR) and Compression Ratio (CR). In standalone DCT, the entire image/frame is divided into 8 X 8 block in order to apply 8 point DCT.

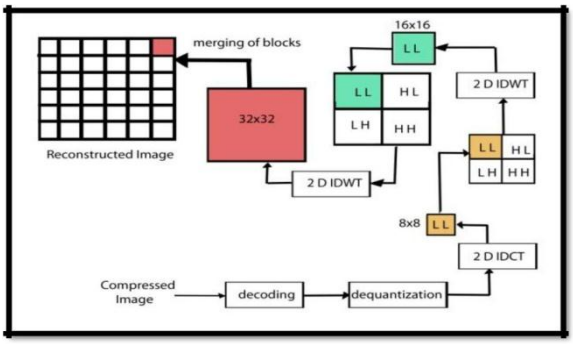

Fig. 3: Decompression technique using Hybrid transform

IV. PERFORMANCE MEASUREMENT PARAMETERS

In this work prominence were given on the amount of compression used and how good the reconstructed image similar to the original. Analysis was done on the basis of the amount of distortion, which was calculated using important distortion measures: mean square error (MSE), peak signal-to-noise ratio (PSNR) measured in decibels (dB) and compression ratio (CR) measures were used as performance indicators. A good compression algorithm would reconstruct the image with low MSE and high PSNR

a) Mean Square Error (MSE): The MSE is the cumulative squared error between the compressed and the original image. A lower value of MSE means lesser error. In general, it is the average of the square of the difference between the desired response and the actual system output. As a loss function MSE is also called squared error loss. MSE measures the average of the square of the error. For an unbiased estimator, the MSE is the square root of the variance, known as the standard error.

$$MSE = \frac{1}{m*n}\sum_{y=1}^{m}\sum_{x=1}^{n}[I(x,y) - I'(x,y)]^2$$

Where, I(x, y) is the original image and I'(x, y) is the reconstructed image and m, n are the dimensions of the image. Lower the value of MSE, the lower the error and better picture quality

b) Peak Signal to Noise Ratio (PSNR): PSNR is a measure of the peak error. Many signals have very wide dynamic range, because of that reason PSNR is usually expressed in terms of the logarithmic decibel scale in (dB). Normally, a higher value of PSNR is good because it means that the ratio of signal to noise is higher. Here, a signal represents original image and noise represents the error in reconstruction. It is the ratio between the maximum possible power of a signal and the power of the corrupting noise. PSNR decreases as the compression ratio increases for an image. The PSNR is defined as:

$$PSNR = 10 * \log_{10}\left\{\frac{MAX_1^{\,2}}{MSE}\right\}$$

PSNR is computed by measuring the pixel difference between the original image and compressed image. Values for PSNR range between infinity for identical images, to 0 for images that have no commonality

c) Compression ratio (C_R): Compression ratio (*CR*) is a measure of the reduction of the detailed coefficient of the data. In the process of image compression, it is important to know how much detailed (important) coefficient one can discard from the input data in order to sanctuary critical information of the original data. Compression ratio can be expressed as:

$$C_R = \frac{Uncompressed\ Image}{Compressed\ Image}$$

d) Normalized cross correlation (NC): For image-processing applications in which the brightness of the image and template can vary due to lighting and exposure conditions, the images can be first normalized. This is typically done at every step by subtracting the mean and dividing by the standard deviation. That is, the cross-correlation of a t(x,y) template, with a sub image f(x,y) is

$$\frac{1}{n}\sum_{x,y}\frac{(f(x,y)-\bar{f})(t(x,y)-\bar{t})}{\sigma_f\sigma_t}$$

V. PERFORMANCE EVALUATION AND SIMULATION RESULTS

This chapter evaluates the performance of the various image compression algorithms. The studied algorithms are applied on several types of medical images. These benchmark images are the standard image generally used for the image processing applications. The results of the meticulous simulation for images and are presented in this section. Comparison of the results of MSE, CR and PSNR are shown in Table I, Table II and Table III respectively.

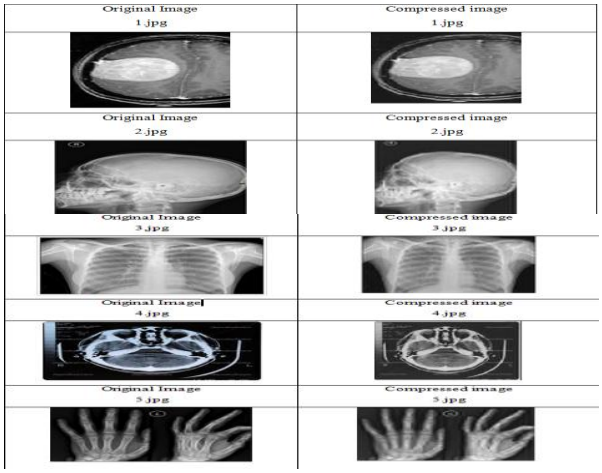

Fig.4: Experimental snapshots of original and compressed images

TABLE I
Comparison results of MSE

IMAGES	DWT+DCT	Ref. no [4]
1.jpg	0.37679	1.8295
2.jpg	0.309242	0.4567
3.jpg	1.45876	0.1561
4.jpg	0.705212	0.7350
5.jpg	0.126074	2.0095
Average	0.5952156	1.03736

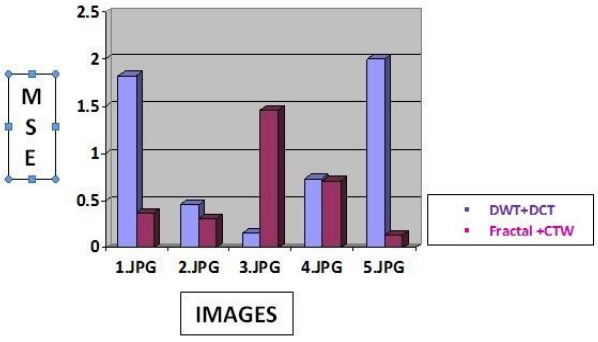

Fig. 5 graphical representation of MSE

TABLE II Comparison results of CR

IMAGES	DWT+DCT	Ref. no [4]
1.jpg	55.9256	49.4178
2.jpg	56.7836	55.4447
3.jpg	50.0468	60.1073
4.jpg	53.2034	53.3783
5.jpg	60.6804	49.0103
AVERAGE	55.32796	53.47168

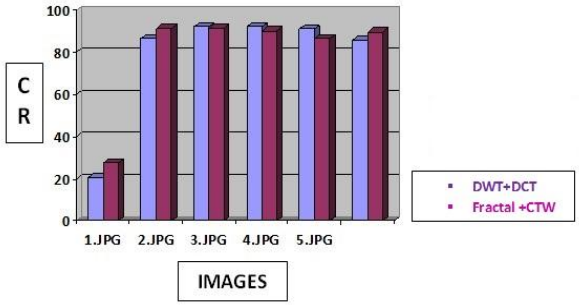

Fig. 6 graphical representation of CR

TABLE III Comparison results of PSNR

IMAGES	DWT+DCT	Ref. no [4]
1.jpg	91.1978	86.4319
2.jpg	91.094	91.9231
3.jpg	90.0612	91.9231
4.jpg	86.5355	90.8100
5.jpg	89.5468	85.7119
AVERAGE	89.68	89.36

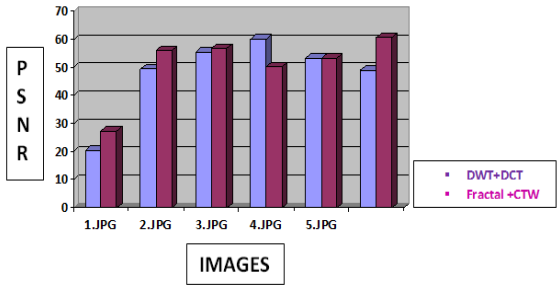

Fig. 7 graphical representation of PSNR

TABLE IV (a)

	Images	MSE	PSNR	CR
Gray Scale Images	l.jpg	037679	55S256	91.1978
	2.jpg	0309242	563836	91.094
	3.jpg	1.45876	512034	90.0612
	4.jpg	0305212	512034	86.5355
	5.jpg	0126074	60.6804	893468
Colour Images	6.jpg	039438	514526	91.5454
	7.jpg	0.614927	543654	91.901
	8.jpg	0.970452	523802	816894
	9.jpg	0337986	533521	89393
	10.jpg	094879	52.6515	893447

TABLE IV (b)

	Images	CORRELATION	BER
Gray Scale Images	l.jpg	0991978	0.0178809
	2.jpg	099094	0.0176107
	3.jpg	0.980612	0.0199813
	4.jpg	0945355	0.0187958
	5.jpg	0.975468	0.0164798
Colour Images	6.jpg	0995454	0.0187082
	7.jpg	099901	0.0183266
	8.jpg	0.916894	0.0190186
	9.jpg	0.97793	0.0186039
	10.jpg	0.977447	0.0189928

VI. CONCLUSION

The algorithms for compression and decompression for various Image compressions methods such as DCT, DWT, and Hybrid are discussed. DCT requires less computational resources and can achieve the energy compaction property. However, for the higher compression ratio it introduces the blocking artifact and the false contouring effects while image reconstruction. DWT is the only techniques which has capacity of multi resolution compression. However, it requires higher computational complexity as compared to other techniques. Hence, in order to benefit from each other, hybrid DWT-DCT algorithm has been discussed for the image compression.

This hybrid approach speeds up the encoding time by reducing the number range- domain comparison with remarkable amount. Each method can be well suited with different images based on the user requirements.

In this work, analysis of various Image compression techniques for different images is presented based on parameters, compression ratio (CR), mean square error (MSE) & Peak signal to noise ratio (PSNR). This work gives higher compression ratio. DWT gives better compression ratio without losing more information of image. Pitfall of DWT is, it requires more processing power. DCT overcomes this disadvantage since it needs less processing power, but it gives less compression ratio. DCT based standard JPEG uses blocks of image, but there are still correlation exits across blocks. Block boundaries are noticeable in some cases. Blocking artifacts can be seen at low bit rates. In wavelet, there is no need to divide the image.

Hybrid transform gives higher compression ratio and for getting that clarity of the image. It is more suitable for regular applications as it is having a good compression ratio along with preserving most of the information.

REFERENCES

[1] A. K. Jain, "Fundamentals of Digital Image Processing", Prentice-Hall Inc, Englewood Cliffs, 1989.

[2] A. M. Raid, W.M. Khedr , M. A. El-dosuky and W. Ahmed, "Jpeg Image Compression Using Discrete Cosine Transform - A Survey", International Journal of Computer Science & Engineering Survey, Vol. 5, No. 2, 2014.

[3] C. S. Rawat and S. Mehar, "A Hybrid Image Compression Scheme using DCT and Fractal Image Compression" The International Arab Journal of Information Technology, Vol. 10, No. 6, 2013

[4] M. Kaur and V. Wasson, "ROI based Medical Image Compression for Telemedicine Application", Proceedings of the 4th International Conference on Eco-friendly Computing and Communication Systems, Procedia Computer Science, Vol. 70, pp. 579-585, 2015

[5] N. A. Dheringe and B.N. Bansode, "Genetic Algorithm Using Discrete Cosine Transform for Fractal Image Encode", International Journal of Soft Computing and Engineering, Vol. 3, Issue-6, 2014.

[6] N. K. More and S. Dubey, "JPEG Picture Compression Using Discrete cosine transform", International Journal of Science and Research, Vol. 2, Issue 1, 2013.

[7] P. K. Singh, N. Singh and K. N. Rai, "Comparative Study between DCT and Wavelet Transform Based Image Compression Algorithm", Journal of Computer Engineering, Vol. 17, Issue 1, pp. 53-57, 2015

[8] P. Kaur and G. Lalit, "Comparative Analysis of DCT, DWT & LWT for Image Compression", International Journal of Innovative Technology and Exploring Engineering, Vol. 1, Issue 3, 2012.

[9] R. C. Gonzolez, R. E. Woods, "Digital Image Processing second edition", Prentice Hall, 2002

[10] S. J. Bagul, N. G. Shimpi and P. M. Patil, "JPEG Image Compression Using Fast 2-D DCT Technique", International Journal of Advanced Research in Computer and Communication Engineering, Vol. 3, Issue 11, 2011.

[11] S. Sharma and S. Kaur, "Image Compression using hybrid of DWT, DCT and Huffman coding", International Journal for Science and Emerging Technologies, Vol. 5, No. 1, pp. 19-23, 2013.

Prioritization of Decision Variables for SMBE Cloud based Big Data Solutions Adoption

Prabhjot Singh Lamba
Industry Manager
Accenture, Noida

Ramita Kaur
Vice President
MARKIT, Noida

Somesh Kumar
Professor,
Department of CSE
NIT, Noida

Abstract: **Data is becoming the top asset for most organizations and is the key success factor for organizations who are market leaders. The phenomenal growth of Internet and its adoption by consumers has completely changed the market landscape. Consumers are more aware and have various ways of expressing their opinions, thoughts and concerns. Organizations can now no longer ignore these sources of consumer voice and have to be agile enough to use this data to understand the new consumer and his needs. With technological advancement and better business processes, also comes the ability to collect huge data which was never possible before. A typical organization has millions of data records related to functions like Production, Supply Chain, Finance, Customers etc which provide insights into system functionality and maturity.**

As a bottom line, Organizations have access to Big Data related to its internal processes and external environment which can be used to understand the evolving consumer needs and help these enterprises to move from old age reactive analytics to new proactive and better business interactions and data based business decisions.

Until recently only large organizations had the resources to collect access and crunch this data, providing them a competitive edge over others. But with the maturity of Cloud technology these capabilities are now available to the SMBE sector too. Small and medium business organizations can now use cloud based Big Data tools to move ahead and create a niche for themselves in the market irrespective of cost and technology skill barriers.

This empirical study looks at the Small and Medium Business Enterprise (SMBE) Sector and aims at identifying top five factors / attributes which influence SMBE adoption of Cloud based Big Data Solutions and ranking these factors based on importance.

Data is gathered from SMBEs using various market research techniques including questionnaires and detail interviews. Prioritization of these factors is done using Conjoint Analysis.

The result of this study can be leveraged by Big Data Solution vendors to create cloud offerings specific to SMBE sector.

CLOUD BASED BIG DATA SOLUTIONS (CBDS)

Cloud technology is a disruptive technology which is changing the way Business function and use IT resources. Using the metered service model (pay as per use), Cloud technologies have removed the entry barriers for cost, and IT skills for organizations who want to use expensive IT resources. Services are now hosted on Cloud vendor's infrastructure and clients simply use these over a network and are charged only for what they use. Vendors offer services like infrastructure, software, platform, database etc to clients relieving them of the overheads of setting up a complete IT center in house.

With the evolution, maturity and affordability of technology, there was a huge spike in the data generated through different sources. Whether these are consumers talking about products online or data tracked through Retail sales and consumer touch points or through internal end to end production to sale systems; organizations have a lot of data at their disposal. This data is the potential source of Business insights which can help enterprises evaluate their actual performance, understand the changing consumer needs, generate new ideas, better their business processes and identify new markets through innovation.

This huge data is now called Big Data and technologies which allow in gathering, storing, analyzing and presenting this data are called Big Data technologies. IDC defines Big Data solutions [1] as a generation of solutions, tools and architectures designed for extracting value economically from humongous volumes of a wide assortment of data by allowing high velocity capture, discovery and analysis.

In a recent whitepaper published by IDC, it was found that Big Data technology and services market globally will grow at a compound annual growth rate (CAGR) of 39.4% which is around seven times of the entire Information & Communication technology (ICT) market. It also states that enterprises which have started to embrace Big Data technology and processes are demonstrating that they can gain competitive advantage not by guesswork but by taking action based on timely, complete, accurate and relevant data insights [5, 7, 9].

Big Data and analytics is an exploding practice today. In the last few years, companies have devoted time and budgets to harness and understand the troves of data around them. This data includes, but is not limited to, social media data (Facebook, Twitter, blogs, Google search), mobile handset usage, digitally enabled processes and transactions, online news, and internal business related administrative records.

Until recently traditional platforms were used for managing Big Data but now specialized tools and techniques have emerged which specifically aim at Big Data and its efficient and real time analysis through new algorithms and paradigms. These technologies require expensive hardware installation and complex frameworks and could only be afforded by organizations with deep pockets and skilled resources. This acted like an entry barrier for smaller organizations that could greatly benefit from Big Data but could not afford the upfront investments.

Emergence and maturity of Cloud technologies and new offerings around Big Data tools has changed the game field. Now Cloud Based Big Data Solutions (CBDS) or Big Data as a service is the new trend which is leveling the market landscape and allowing all organizations to use these services at hardly any cost as compared to the initial infrastructure setup required before.

Cloud has made redundant the benefits of size, scale and scope previously held by a few large enterprises and opened up a new front for smaller companies to leverage the benefits of Big Data technologies. It has drastically cut down the investment arbitrage for new and small players.

CBDS AND SMBE SECTOR

Small and Medium Enterprises have grown exponentially with the spurt in technology adoption and new consumer mindset. Big players in all sectors are being threatened by the small and medium business strategies. The government has also come up with various policies to help the SMBE sector grow. Findings in a recent study the SMB Chamber of Commerce and Ministry of Micro, Small & Medium Enterprises, there are around 48 million small and medium business enterprises in India, contributing 45% of industrial output, 40% of total exports and 1.3 million yearly jobs [1]. In a recent survey by GreyHound Knowledge group [2] SMBEs in India are facing growth challenges out of which the biggest are unavailability of affordable technology, lack of infrastructure and availability of Finance. The affordability of Cloud based technology has come as a relief for SMBEs. SMBEs have realized the importance of adopting technology in business processes and decision making and now with the possibility of having Big data technology within reach through Cloud vendors, SMBEs increasingly are looking forward to integrating their business intelligence with these CBDS to leverage the strength information brings.

This study concentrates on three SMBE sectors.

1. Telecom Sector: Based on a report by Analysys Mason, it is forecasted that worldwide revenue from SMBEs for Information and Communication technology (ICT) sector will grow from $203 billion in 2012 to $226 billion in 2017. A lot of SMBEs are growing in this sector and big players are collaborating with these SMBEs. The telecom market in the Indian subcontinent is around $800 million out of which SMBEs contribute to almost one fourth of the market share (more than $200 million).
2. Retail: Small and Medium Business enterprises in Retail Sector are estimated to generate revenue of more than $450 Billion, and comprise of almost 95% of the overall Indian Retail sector. This sector is growing exponentially with better practices and government support. Also FDI is playing a major role in transforming the market landscape.
3. Health: Based on the research done by the rating agency Fitch, the Health sector in India is estimated to grow to $ 100 billion by 2015, with a 20% yearly growth [8]. With changing lifestyles, increase in medical tourism and an increasing need for quality and specialized health facilities, this industry is expected to jump to $ 280 billion by 2020.

SMBEs have yet to utilize the full potential of the Cloud technology and specially Big Data tools. The availability of huge transaction and customer data is now making SMBEs take a serious look at these CBDS technologies for business edge and growth. The cost advantages which Cloud brings by drastically reducing initial CAPEX and OPEX has made expensive infrastructure and solutions affordable and lucrative to these industries [10, 11, 12]. SMBEs which are mostly entrepreneurial or family based businesses and used to base business decisions mostly on personal networks and dated concepts and knowledge can now avail deep data insights which were not possible earlier leading to rapid time to market, better consumer understanding, accurate forecasting, sleek supply chains and better cash flows.

Despite the known advantages, the SMBE sector faces a lot of challenges in adopting cloud technologies [3] and Big Data frameworks due to various internal and external constraints like:

- Absence of clear technology driven business value chain benefits
- Vague understanding of technology and its integration in existing business processes
- Significant upfront technology investment
- Shortage of skilled personnel

In a previous research by the authors, ten satisfiers and ten dissatisfiers were identified based on interviews with various industry experts and SMBE leaders. These variables were found to influence the decision of cloud based big data adoption by small and medium business enterprises [4].

SATISFIERS:

1. *Cost Effective:*
Clients perceive benefits of upfront cost saving by adopting cloud solutions. Immediate CAPAX is saved on infrastructure costs and OPEX is saved on usage since Cloud models are based on utility payment models. The client only pays for the services it consumes.
Cloud vendors also provide different kinds of payment methods like one time pay, pay per use etc.

2. *Innovation:*
Big Data solutions allow enterprises to understand the real time changes in the business landscape and hence be nimble enough to look for new business opportunities or identify better business process or Innovate. Innovation sprouts from enterprises which are business focused and have business processes based on insights from real time data. Big Data gives deep and real insights on what is going on and what is needed.

3. *Location:*
Cloud services allow even the remotest of SMBEs to connect to the vendor services and avail access CBDS. This has been possible only because of successful deployment of Big Data tools on Cloud. Location and large distances are no longer a limitation for enterprises.

4. *Convenience:*
Cloud based Big Data tools have an inherent advantage of providing continuous and universal access to consumers. Data and tools can be accessed from anywhere, anytime on any device.

5. *Speed & Scales:*
SMBEs have the advantage of scaling up or down the services it avails based on business needs and pay only for what they consume saving immediate OPEX. Also the time lag between identifying a business need for Big Data and getting access to a Big Data tool is minimal as Cloud services can be made available almost immediately.

6. *Multiple Users, Mobility and Device independence:*
Cloud enables offerings to be device independent and be accessed by multiple users on the go anywhere. These services can range from a salesman entering data on a handheld device on the shop-floor to the senior managers sitting at remote locations making real-time decisions based on the insights generated by data analytics over cloud.

7. *Flexibility:*
CBDS allow enterprises to pick and choose services from a set of offerings provided by the vendor, based on current business maturity and need. Alternately in a non-cloud platform, complete platform needs to be deployed for using only a small part of it.

8. *Unlimited Storage Space andComputing power:*
Big Data analytics requires high storage and computing power for storing and analyzing data. Cloud platforms provide this computing power and storage which can be scaled based on needs.

9. *Customize Settings:*
Enterprises can dictate the vendors to tweak the services based on their unique business requirements. Cloud vendors allow consumers to cherry-pick and tailor what they need and also pay only for what they use.

10. *Software and Hardware Updates:*
The Cloud consumer is free of any overheads regarding maintaining the hardware or ensuring software updates and installing patches. This is the responsibility of the cloud vendor leaving the consumer to focus on its core business.

DISSATISFIERS:

1. *Data Security:*
Data is one of the biggest assets an organization can have and data security is a major issue. SMBEs have concerns in putting their critical and sometimes confidential data on cloud which may eventually reside on servers in remote locations under a risk of malicious access over the network.

2. *Data Privacy:*
Since data is now available on the network, there is a threat to the data which comes from internal employees and the way they access the tools. No matter how strong the vendor secures the data, a simple password misplaced by an employee can render all security useless.

3. *Data Availability:*
The cloud is dependent on a constant availability of the network. There is an inherent fear of not getting access to the cloud in case the network goes down due to uncontrollable reasons leaving the business separated from the data it needs.

4. *Vendor Lock In:*
Organization data may run into terabytes of information over time. This creates a situation where the consumer of cloud services becomes dependent on the cloud vendor simply because the cost of moving to a different vendor becomes more than the cost to continue with the current vendor creating a vendor lock in situation. This lock in may be because of many reasons like incompatibility with the underlying technology, data structures, application restrictions to user getting comfortable with the vendor framework.

5. *System and Process compatibility:*
SMBEs usually have an existing set of tools, either in-house or small third party, which are critical to the functioning of the business. Any decision to move to the

CBDS may result in compatibility issues between these solutions and the cloud offerings. There can also be a case of conflicts over the way business functions with the way the cloud vendor functions.

6. Location of Data:
Cloud benefits include providing solutions to anywhere in the globe, but this also means that organization data could be stored anywhere. This could result in export control (ITAR / EAR) issues for research data. Enterprises may also be uncomfortable in storing data in enemy countries or countries with security and accessibility laws different from their own.

7. Duration of Services:
Vendor service and the duration of the services offered have an important impact on the decision of partnering with a vendor. SMB organizations may be looking at a small term engagement and a cloud vendor which provides flexible options suiting SMBEs preferences and business needs will be rated higher than those who don't provide flexible service durations.

8. Responsibility for End Users:
SMBEs need to be educated on the service terms, policies and scope of the services offered. Typically SMB enterprises do not have the technical expertise to fully understand the terms and vendor's Acceptable use Policy (AUP) on the big data services and hence expectation mismatch could lead to failed implementations of cloud.

9. Ownership of Data:
SMBEs may be hesitant to move their critical data on vendor cloud due to ownership questions. Since the cloud is not in their control, a debate arises that who will own and be eventually responsible for the data and consequently the insights generated from this data since the vendor owns the infrastructure on which the data is stored and the tools which helped generate the insights. This brings the question of whether the cloud vendor can use Intellectual Property Rights (IPR) and use client data for personal use simply by the virtue of transactions.

10. Bandwidth, quality of service and data limits:
Since the Cloud is completely network dependent, there could be issues of outages due to network failures, slow connection speeds etc. resulting in unavailability of data and services to the client which may have a direct dollar impact.

Problem Formulation and Research Methodology
As per a study by The Economist in 2013 named "The hype and the hope"[3], it was found that firms in Asia Pacific which had implemented Big Data tools and solution reported limited success in implementation even when they did report that they had a huge and increasing opportunity to utilize Big Data. Two of the top reasons identified were:

- Lack of suitable software to suit the business requirement
- Lack of necessary skills to implement Big Data technology in the organization

This study clearly shows that understanding the correct technology required for the business and the right skillset to implement it has a major impact on Big Data implementation for an organization. For SMBEs are still worried and conscious of moving to Cloud based Big Data technology because of a vague understanding of the technology and its fitment. Cloud vendors need to be cognizant of the priorities of the SMBEs and the right tools and frameworks which suit these sectors and create offerings based on these. This paper takes a step in this direction.

The authors in a previous study identified top ten satisfiers and dissatisfiers for CBDS adoption by SMBE sector. These were grouped into four Gain drivers and Risk drivers. Interviews with industry leaders and sector experts were used to condense these four gains from the satisfiers and four risks from the dissatisfiers which were related to four independent and unrelated gain and risk drivers.

The satisfiers and dissatisfiers which integrate into each factor are tabulated and shown in Figures below:

Gain 01	Gain 02
Cost Saving Cost Effective Software and hardware Updates Flexibility Customize Settings Speed and Scales	Better Prediction Innovation Convenience

Gain 03	Gain 04
Consumer Insights Unlimited Storage Space and Computing Power	Accurate and Real Time Data Location Multiple users, Mobility and Device Independence

Figure 1 (a) four posited gains of cbds

Risk 01	Risk 02
Vendor Risk Vendor Lock in System and Process Capability Duration of Services Responsibility of End users Ownership of Data	Security Risk Data Security Data Privacy Location of Data

Risk 03	Risk 04
No Gain Risk of no gain from CBDS adoption or only Short term gain.	Efficiency Risk Data Availability Speed and Scales Bandwidth, quality of service and data limits

Figure 1 (B) Four Posited Risks Of Cbds

A sample space of 116 SMBE experts was chosen from a diaspora of Telecom, Retail and Health SMB Enterprises. These experts were divided between Telecom sector (34 respondents), Health sector (39 respondents) and Retail sector (43 respondents).

Most of the respondent population had not yet adopted CBDS significantly and hence the responses are purely based on the respondent perceptions of the gains and risks CBDS brings to their respective sectors and organizations.

Method

Big Data technology on Cloud not only enables SMBEs to save upfront investments as CAPEX and allocate capital to core Business functions, but also helps them in gaining market insights, perform better PR activities, faster time to market, uncover trends, accurate forecasting, streamline processes etc. The utility based payment model (pay as per use) of cloud computing technology is favorable to SMBEs which saves a lot of OPEX on skill and infrastructure maintenance. Thus cost saving is one of the first gain driver. Big Data technology also helps enterprises in understanding trends and forecasting. This is the main advantage of Big Data mining which helps uncover variables and trends which help organizations understand a behavior and predict what can happen. SMBEs can then plan product launches or better system processes based on these predictions. Similarly Vendor risk and security risk which are inherent to Cloud technology are two of the risk variables. SMBEs are wary of putting their data in external servers where a risk of data theft or loss is a possibility.

This research paper aims at identifying the preferences of SMB Enterprises on the decision variables involved in adopting Cloud Based Big Data Solutions in their business. These are anticipated or perceived preferences and not based on ex-post adoption feedback. We identify using conjoint analysis the relative priority of gain and risk variables which the SMBE sample space perceives is important to their sectors. This is done for Telecom, Health and Retail sectors separately.

- The sample space for the research consists of 116 SMBE leaders and industry/sector experts.
- These are from the Telecom, Retail and Health sectors.
  - Telecom sector: 34 respondents
  - Health sector: 39 respondents
  - Retail sector : 43 respondents
- This sample of respondents has not yet adopted CBDS significantly in their organizations and hence their responses are purely based on ex-ante perceptions and not on post adoption feedback.
- Conjoint Analysis has been used to rank the professed priority of drivers and inhibitors for CBDS adoption by SMBEs.
- Data Collection: Data was collected through an online questionnaire which was released to SMBEs all over India. The respondents were guided over audio and skype calls (wherever face to face meeting was not possible) to the context of the questionnaire.
- Questionnaire:
  - Respondent details: We gather the name and age of the respondent. Apart from basic response identification, these fields may also help us understand the difference in perceptions of the young or mature respondents.
  - Industry Sector: This field helps us understand the sector to which the organization belongs to. We also capture the name of the organization so that in case more details regarding the firm can be recovered if required.
- Drivers favoring CBDS Adoption: Following are the gain drivers.
  - Cost Saving: Perceived advantages of revenue increase and cost reduction. CAPEX gains due to cut in upfront investments in architecture and OPEX gains due to the utility model of payment inherent to cloud based services. It also includes no cost on software and hardware updates (as this falls in the vendor domain) and the services being offered in a-la-carte fashion allowing SMBEs to choose services they need and ignore others.
  - Better Prediction: Advantages of insights from Big Data which help uncover trends and variables which help SMBEs in building improved marketing strategy, launch of products and services, tweak and better business processes and help innovate and build next generation offerings. All this based on the convenience of having Big Data technology available over cloud for different departments with the data view they need for forecasting and prediction.
  - Consumer Insights: Big Data helps enterprises understand the voice of the consumer and hence brings them closer to the customer needs. Enterprises can then move from creating products and services designed for mass to personalized solutions for individual consumer unique to his/her needs. The advantage cloud offers is unlimited storage and raw computing power which enables organizations to store collect data from all relevant resources and then churn this data to generate real time insights.
  - Accurate and Real time Data: A key driver for successful business decision making is the availability of right information in the right way to the right people. Cloud and Big Data technology allow huge data to be

processed real time and made available anytime to the management in a location and device independent way.

- Drivers deterring CBDS adoption:
  - Vendor Risk: Risks associated with the specific vendor with which the SMBE deals with. This could be the risk of technology lock up wherein the data once stored in the vendor infrastructure is difficult to migrate to other vendor in case the SMBE wishes to change the vendor, to Vendor Lock in incompatibilities in the system and processes of the vendor. Also post implementation support, responsibilities of the customer, duration of services, ownership of data etc create a part of vendor risk.
  - Security Risk: Risks affecting organization data security, privacy, integrity, access. Data is a key winning asset for any organization and security of that data is a critical concern.
  - Efficiency Risk: Due to the inherent dependency of Cloud technologies on network, data availability and speed depend on the available network strength. Hence bandwidth, quality of data, download and upload speeds etc are a concern for efficient utilization of CBDS.
  - No Gain Risk: The fear that adopting CBDS will lead to no long term tangible gain for the organization. All effort and transformation will bring only marginal or no gain to the business process and decision making.

- The Gain drivers and the Risk drivers are grouped in combination of two's and the respondents were requested to rank these six combinations on a scale of 1-100 such that the total sum of ranks has to be equal to 100. Hence respondents were forced to rate their perceptions by allocating 100 points to each of the six combinations.
- This questionnaire was sent to SMBEs in three sectors: Telecom, Retail and Health.
- Post data gathering, conjoint analysis was run on the survey results to identify which Gain and Risk drivers were important to the SMBE for these three sectors.

Analysis

The aim of this research is to identify a ranked associativeness of the four decision variables on the decision by Small and Medium business enterprises for Cloud based Big Data Solution adoption. All the gain are important to the SMBE sector but ranking them helps understand the subtle differences between the three sectors on their perceptions about CBDS and priorities[6]. Tradeoff between these drivers helps understand patterns and eventually the fundamental working of these sectors.

Telecom Sector:

The ranking of the four gain drivers for telecom SMBE is given in **Figure 1** below. It can be clearly seen in the figure that Cost saving including both CAPEX and OPEX and availability of accurate and real time data take 63% of the gain perception spectrum of the SMBE in Telecom sectors. Better prediction and Consumer Insights take a lower ranking.

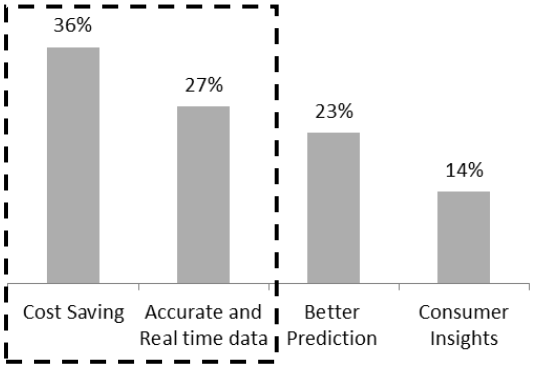

Figure 1: Gain Drivers for Telecom SMBE Sector

The ranking of the risk perceptors for telecom sectors can be seen in the Figure 2 below. Vendor risk seems to be the top concern for telecom sector. This is evident of the huge data that telecom companies capture leading to vendor locking risk perception. Efficiency is also a major concern. A lot of data in this sector is captured real time and availability of this data for analysis is key to business success. An interesting fact captured is that Security risk seems to be of less concern to Telecom SMBE sector. This could be attributed to the understanding that SMBEs do not have access to the confidential consumer data or such data is not planned to be moved on Cloud for analysis due to strong industry governance and laws.

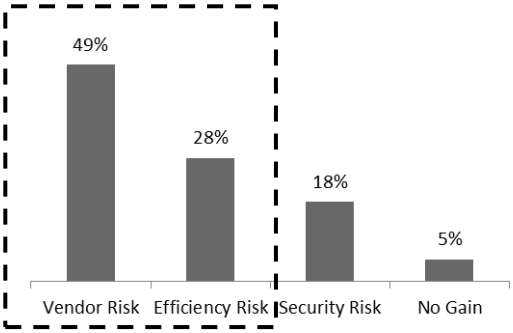

Figure 2: Risk Drivers for Telecom SMBE Sector

The ranking of the gain drivers is given below in Figure 3. Both the Cost Saving and Better prediction gain drivers take almost 70% of the perception spectrum. Consumer insights and Accurate and Real time data seem to be at a lower priority for Health sector. Health SMBEs usually have tight budgets and hence Cost saving seems to be the top logical gain driver. Further predicting consumer patterns seems to drive the CBDS adoption by Health SMBEs

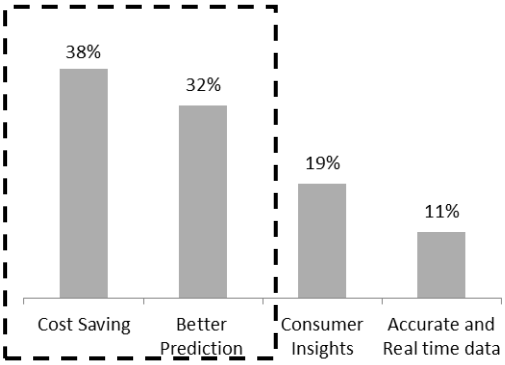

Figure 3: Gain Drivers for Health SMBE Sector

The risk driver ranking for Health sector is given below in **Figure 4**. A clear priority to Security and Efficiency risk is given which amounts to total 74%. Health records are confidential and SMBEs understand the risk of losing this data. Vendor risk and No Gain are of least priority.

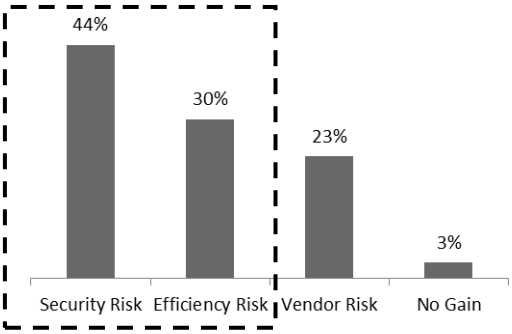

Figure 4: Risk Drivers for Health SMBE Sector

Retail Sector:

The ranking for Retail sector gain perceptors is given in the **Figure 5** below. It can be seen that Cost saving is the highest priority with 39% but Accurate and Real time data closely follows with 31% both making the 70% of Gain perception for Health SMBE sector. As a cash conscious sector, Cost saving is the logical top priority. Success in Retail sector is based on carefully monitored supply chain and availability and flow of real time accurate data between the various processes in the product life cycle. Prediction is also important by compared to availability of accurate data ranks less.

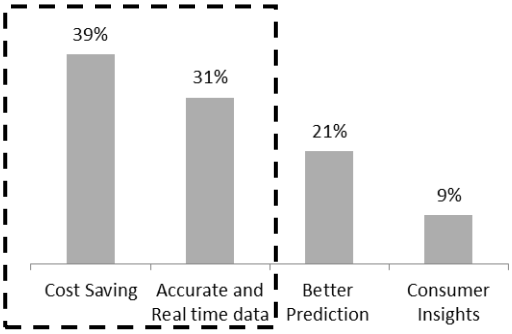

Figure 5: Gain Drivers for Retail SMBE Sector

The risk driver ranking for the retail sector is given in the Figure 6 below. Data security risk is the predominant risk for the Retail sector followed closely by Efficiency Risk. Both contribute to 70% of the risk perception spectrum. Vendor risk seems to be low priority with 19% of spectrum. Retail industry deals with financial information like credit card details leading to security concerns over data. Also in the extremely competitive Retail sector it is important to get real time information on sales and customers making efficient risk as second priority for retails enterprises.

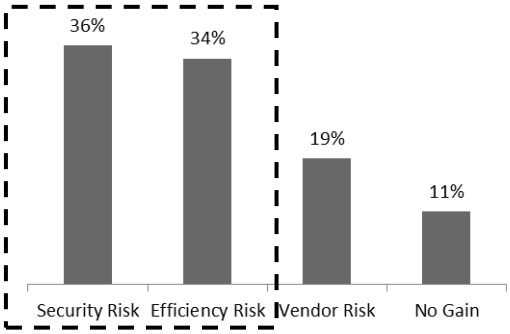

Figure 6: Risk Drivers for Retail SMBE Sector

Overall for all three sectors it if found that Cost Savings is the top gain driver for SMBEs. Cloud platforms and the Utility based payment methods has really attracted the SMBE sector which now has access to all the latest technology infrastructure and tools without the overheads of maintaining and upgrading these setups. The "How-to" of the process is effectively out-sourced to the cloud vendors thereby leaving the business to focus on "What-to" of their core business domain. The SMB enterprises which are usually strapped for cash focus on Cost saving as a major benefit. Coming to the next gain driver, the availability of accurate and real time data, except the Health sector, both the Telecom and Retail sectors view it as priority. This can be attributed to the fact that Telecom and Retail sectors need real time or near real time data from across its systems for business processes, for Telecom it could be network optimization or actual usage of services whereas for Retail it could be stock or product location control , accurate and real time information is key in success. Better prediction is the third driver which the Health Sector marks at a higher priority than the other two sectors. This may be due to real time customized package offers to walk in customers in health clinics based on predictive analysis of past medical tests and possible ailments.

Moving on to the risks, Security risk dominates the risk perception spectrum among Health and Retail sectors. This could be due to the sensitive financial and customer information these sectors have to handle. Telecom on the other hand does not consider this as a top risk may be due to already heavy regulations around the consumer data not allowing SMBEs to migrate it over cloud. Efficiency risk

has been ranked as second risk driver for all the three sectors. The decision to move on Cloud brings with it the risk of complete dependency on the available network. In case the network goes down or bandwidth is impacted, this could adversely affect the ongoing systems delivering a blow to the business. Hence the perceived problems with data transfer between the vendor and client to latency issues affect the SMBE decision to adopting CBDS in their organizations. Telecom sector ranks Vendor Risk as a top driver whereas the other two do not. Telecom SMBEs work with huge data and the risk of getting stuck with all this data overtime with a single vendor is real. Hence choosing a vendor has to be done taking in consideration a lot of vendor specifications. The No-Gain driver takes the least priority in the SMBE mind set. This clearly shows that all sectors see value in moving to Cloud platforms hosting Big Data technology. This perception is the reason we see mass SMBE migration to Cloud.

The aim of this research study is to aid cloud vendors in planning new offerings for the SMBE sector based on the right tools, price points, security processes and service levels. But the authors also understand that SMBE sector need to see more successes CBDS implementation, more case studies, proven technology frameworks and tool recommendations to feel comfortable and move to adopting Big Data on Cloud with confidence. Our study will pave way to a clear the fog of qualm surrounding the cloud offerings for the SMBE market.

RESULTS

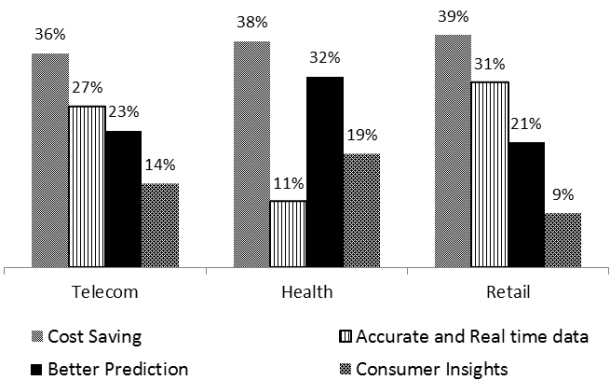

Figure 7: Gain Drivers for all three SMBE Sectors

1. As seen in Figure 7 above which shows the Gain drivers for all SMBE sectors, Cost savings are the top ranked gain drivers for all three sectors. All three sectors rate it close to 40% of the mindset spectrum
2. Since SMBEs are usually strapped for cash, Cost savings is the most attractive driver for CBDS adoption. Specifically the CAPEX savings inherent to Cloud, saving SMBEs from making huge upfront infrastructure investments before actually seeing the technology gains
3. Accurate and real time data is the next top gain driver for Telecom and Retail since both sectors rely decisions taken real time like network optimization and supply chain tracking
4. Better prediction capabilities of Big Data technology is the third driver which is rated higher in Health sector than other two sectors
5. Consumer Insights has been ranked the least important as compared to the other three drivers by all three sectors. This may be due to the perceived lack of maturity in Big Data technology for SMBE sector in generating meaningful consumer insights to actually show a dollar impact on the revenue

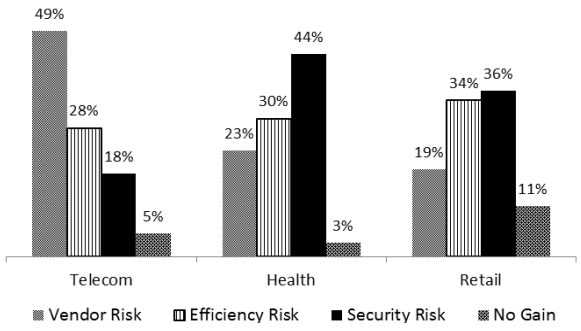

Figure 8: Risk Drivers for all three SMBE Sectors

1. All Risk drivers for three SMBE sectors is shown above in **Figure 8**. Vendor risk is the top rated risk in SMBE adoption of CBDS in Telecom sector. This encompasses
   a. Vendor Lock in due to technology binding
   b. Service durations and the available payment models
   c. Client responsibilities vs Vendor responsibilities
   d. Data ownership issues
2. Vendor risk is not the top risk as perceived by Retail and Health sectors.
3. Efficiency related risks take the second position in SMBE mindset for all three sectors.
4. Security risk is highest rated risk for Health and Retail sectors but not so much for Telecom.
5. Telecom is a heavily regulated sector and hence secure data is never planned to be moved to cloud. Health and Retail sector on the other hand have to look at data security issues before migrating.
6. SMBE sector has an understanding of the value CBDS could bring to the organizations and hence all three sectors rate No Gain as the least concern.

CONCLUSION

All organizations are experiencing a boom in the available data from various sources including external sources like social media platforms, online customer feedbacks, product purchase patterns to internal sources like system logs, data generated during production etc. With the onset of the Internet-of-Things (IOT) we are now looking at huge waves of data generated through systems and devices. All this data is growing exponentially leading to a situation where existing systems are overwhelmed or simply unable to store and analyze this data. On the other hand this data

beings with it information, patterns and insights which could mean a game changer for the SMB enterprises. Organizations now are moving away from reactive analytics to real time proactive customer touch points and interactions. Insights generated through this Big Data lead to competitive advantages and optimal returns. Cloud vendors now bring Big Data technology to their platforms leading to availability of these technologies to the SMBE sector bringing with it the inherent advantages of Cloud like Utility model of payment to almost zero CAPEX investments.

Through this paper we have looked at the perceived gains and risks of the SMBEs for Telecom, Retail and Health sectors. This helps cloud vendors in understanding the subtle differences in the needs of these sectors and create offerings targeting them.

Future Directions of Research

With a plethora of tools and technologies in the Big Data space available today, it is difficult for SMBEs to understand which suits their needs and priorities. Based on the findings of this paper, a further study of these tools can be done. They may be ranked based on the gain and risk drivers and specific offerings may be created by Cloud vendors for these sectors.

REFERENCES

[1] http://articles.economictimes.indiatimes.com/2013-06-09/news/39834857_1_smes-workforce-small-and-medium-enterprises
[2] http://firstbiz.firstpost.com/sme-report/pdf/Analysing-Indian-SME-perceptions-around-Union-Budget-2014-15_Final-new.pdf
[3] https://www.hds.com/assets/pdf/the-hype-and-the-hope-summary.pdf
[4] Prabhjot Singh Lamba et All, Decision Variables for SMBE Adoption of Cloud Based Big Data Solutions, International Journal of Advanced Trends in Computer Applications, 2395-3519
[5] E llaway RH, Pusic MV, Galbraith RM, Cameron T (2014) Developing the role of big data and analytics in health professional education. Med Teach 36(3):216-222
[6] E llaway RH, Pusic MV, Galbraith RM, Cameron T (2014) Developing the role of big data and analytics in health professional education. Med Teach 36(3):216-222
[7] Big data: The next frontier for innovation, competition, and productivity. James Manyika, Michael Chui, Brad Brown, Jacques Bughin, Richard Dobbs, Charles Roxburgh, and Angela Hung Byers. McKinsey Global Institute. May 2011.
[8] Seebode C, Ort M, Regenbrecht C, Peuker M (2013) BIG DATA infrastructures for pharmaceutical research. IEEE International Conference on Big Data, California.
[9] Bellini P, di Claudio M, Nesi P, Rauch N (2013) Tassonomy and review of Big data solutions navigation. In: Big Data Computing. Chapman and Hall/CRC, Boca Raton. p 57
[10] http://www.ey.com/Publication/vwLUAssets/EY-SMAC-the-next-growth-driver-for-SMEs-in-India/$FILE/EY-SMAC-the-next-growth-driver-for-SMEs-in-India.pdf
[11] Amit Singh Sisodiya, "SMEs in India – Future Perfect", Global CEO, April 2006, The ICFAI University Press

Sensor Deployment for Optimal Coverage: BFO Approach

Raminder Singh Uppal
Deptt. of ECE
BBSBEC, Fatehgarh Sahib

Karamjeet Singh
Deptt of ECE
BBSBEC, Fatehgarh Sahib

Daljeet Singh Bajwa
Deptt of ECE
BBSBEC, Fatehgarh Sahib

Abstract: **The placement of sensors in given physical space is a critical parameter to be considered while studying the effectiveness of sensing network. The sensors may be deployed in a determined or a random order according to the monitoring sense of coverage. The random deployment provides better coverage in case when sensors are to deployed in large physical space or when condition are harsh at target area. Optimal coverage to target area is provided by using efficient deployment algorithms based on optimization techniques. In this paper, two deployment approaches based on Genetic Algorithm and BFO Algorithm is proposed to optimize the coverage provide by sensors. These approaches minimize overlapping (fitness) amongst the sensors in order to increase the coverage. As the fitness value decreases the coverage percentage increases in both the approaches.**

Keywords: ***Deployment, Coverage, Genetic Algorithm, Bacterial Foraging Optimization (BFO) Algorithm***

I. INTRODUCTION

The information of the physical space is essential to build up valuable knowledge of the environment. In harsh environment, remote accurate observations are required for sensing natural parameters. Recent advances in electronics have led to development of sensors for their type of observations from which the information is derived. The process of analyzing the information to trace changes in the state of physical space over time is called monitoring and that depends on the accuracy of the parameters sensed in the physical space under study [20]. These sensor nodes deployed in the particular area to sense the information and to transmit this information to base station. These nodes have been deployed mainly in those areas in which human interaction is not possible. The sensors may be deployed randomly or in a determined order with taking into consideration the sense of coverage. As follows:

- *Target coverage* – When the number of targets, with existing locations are to be regularly observed, maximum sensors are stochastically deployed close to target [2].

- *Barrier coverage* – To observe movement on national border, sensors are deployed in a line along with the border to monitor every inch [2].

- *Blanket or full coverage* – Covering entire physical area that is every single point is in the sensing range [2].

In the blanket coverage, various approaches have been used to maximize coverage with the minimum number of sensors. The random deployment is carried out only in case of large physical space otherwise the sensors can be deployment in a determined manner. However, in case of random deployment a problem of hole formulation in the coverage is encountered that is solved by using efficient deployment algorithms [3] – [7].

The sensors may be deployed in static, dynamic or hybrid manner depending upon the situation of observation being sensed by the network. All nodes could be considered as mobile nodes to maximize the coverage in the first approach of hole formulation. In the second approach named as hybrid approach in which some node would be static (stationary) nodes and efficient algorithm would determine locations and number of mobile nodes to be deployed in order to get maximum coverage [18].

In WSN, the major issue is of the energy consumption, because in sensors utilized the battery energy for sensing the information, to transmit the information to neighbor nodes. Once the energy provided to the nodes is the net amount of energy that can be utilize no extra energy can be provided to the system.

In WSN, the sensed data from physical space is to be communicated to base station that is done with hop-by-hop link among the neighbor nodes, the failure of which would result in disconnected pieces of sensor network.

A. Communication Models of WSN

- *Unit Disc*: In the Unit Disc model, the communication among the nodes of the network depends on sole distance between the nodes [19].

- *Empirical Network (Instance Model):* Other factors such as radio, transmission power type and antenna height are significant [19].

B. Sensing Models

- *Boolean Sensing Model* – In this model, the sensing area of node is the area of the circle with radius isometric to the sensing range of the node. The effect of environment and other emitted signals at the time of detection are ignored [18].

- *Probabilistic Model* – In this model, the probability of detection of event depends on environmental factors.

The sensing ability of node is not uniform as it depends on the fading parameter. Elf's sensing and Shadow Feeding sensing model is a probabilistic model [18].

II. SOFT COMPUTING APPROACHES

- Deployment Approach based on GA

// Initialization
1 generate initial population of size PS randomly;each population IP represent (x,y) coordinate of n mobile sensor and all sets of population are represented PUSH
// Loop until the terminal condition
2 for i=1 to I; number of iterations
3 calculate the fitness of each population. fitness is given by overlapping area calculated by square matrix. Sort the populations as per fitness value is ascending order.
4. population with minimum fitness value are Selected and saved as IP the best population are saved for next iteration;
// Crossover
5 for j=1 to m do two solution from IP are picked randomly IPi and IPj;
6 generate IPq and IPr by one-point crossover to IPi and IPj;
7 IPq and IPr are saved to IP ;
8 end for
// apply mutation with probability Pm
9 for j=1 to m do
10 IPi is selected from IP;
11 Even bit of solution IPi is exchanged with odd bit and vice versa to produce new solution IPi(n) ′;
12 check feasibility of IPi(n) is unfeasible
13 if feasible update PUSH by replacing IP i with IPi(n);
14 endif
15endfor
// Updating
// Returning the best solution
16 return the best solution(x,y coordinates of mobile sensors) with minimum fitness value out of IP.

- Deployment approach based on BFO

[Step 1] Initialize parameters
Population(p),quantity of bacteria(S), step number (Nc), swim boundary (Ns), steps for reproduction (Nre), event count (Ned), Probability of elim./disp.(Pe) .

[Step 2] Elimination–dispersal loop: l = l +1
[Step 3] Reproduction loop: k = k + 1
[Step 4] Chemotaxis loop: M = M +1
a) For i=1to S; consider bacteria steps (chemotactic) as given below
b) Calculate weight of fitness function J (i, j, k, l). Assume M(i, j, k, l)=M(i, j, k, l) + Mcc(θ^i(j, k, l),P(j, k, l))
(i.e., nutrient concentration effected due to addition of cell attractant).
c) Assume M_{last}= M (i, j, k, l) to store the parmeter , since there are chances of finding better fitness value in another iteration.
d) Tumble:this step generates a vector (random) r Δ(i) € R^p with every element Δ_m (i), m = 1, to P
e) Move: Let

$$d^i(j+1,k,l) = d^i(j,k,l) + C(i)\times\Delta(i)/\sqrt{\Delta^T(i)\times\Delta(i)}$$

movement happens in the tumble direction with distance equal to step size
f) Compute J (i, j+1, k,l) and
let J (i, j+1, k,l)=J(i, j, k, l)+Jcc (θ^i (j+1,k,l),P(j+1,k,l))
g) Swim
i) Let m=0 (counter for swim length)
ii) While m < Ns (if have not climbed down too long)
• Let m = m+ 1
If J (i, j+1, k,l)<J_{last} (if doing better),
Let J_{last} = J (i, j, k, l)
& let

$$\theta^i(j+1,k,l) = \theta^i(j,k,l) + C(i)\times\Delta(i)/\sqrt{\Delta^T(i)\times\Delta(i)}$$

And use this □ i (j □1, k, l) to compute the new
M (i, j+1, k, l) is identical in step (f)

• Else, assume m = N_s. it indicates end of while loop

h) increment (i) .condition i ~=S . In order to proceed return to [b] which is next bacterium

[Step 5] If j< N_c, return control at step 4. If bacteria life is not over continue.
[Step 6] Reproduction
a) For the given k and l, and for each i=1,2,….S, let

$$J\ health^i = \sum_{j=1}^{N_c+1} J(i,j,k,l)$$

Value of J parameter indicates fitness of solution, sort solution J parameter and C(i) parameter in ascending.
b) S_r =S/2 solution (bacteria) with poor health J_{health} dies. Balance solution (bacteria) split into two bacteria.this process are carried at the location of parents.
[Step 7] return to step 3 condition k < N_{re} .
[Step 8] Elimination- Dispersal // return best solution
For i=1 to S apply elimination and dispersion to each solution (bacteria) with P_{ed} (given probability)
// helps in maitaing population size)
return to step 1 If l < N_{ed} .

III. PROPOSED WORK

- *Problem Definition*

In our work we consider circular coverage pattern with radius r as a range for all mobile sensors. Area covered for sensing is πr^2 for each sensor. Set of mobile sensors n is given by S = {S_1, S_2……., S_n} and each deployed at location having coordinates (x_i, y_i). The fitness value of

deployment is the overlapping amongst the deployed mobile sensors. This fitness value is calculated by square area matrix(AM)..each element of AM represents the overlapping among adjacent sensors e.g. A31 represents overlapping among sensor 3 and 1.

- *Proposed Solution*

Given a set of sensors, it is desired to compute the coordinates of sensors (x_i, yi), through the soft computing techniques, that minimizes the overlapping sensing range and maximizes the coverage of area A.

- *Mathematical Model*

In this model, for a two-dimensional physical space, each sensor's range is considered as circle and is placed at the centre say *(x, y)* of such circle with radius *r* of the circle as the sensing range of sensor. Thus, the sensing area is πr^2 , while its communication range is greater than *2r*. So, in a given two-dimensional physical space of area *A*, the *n* numbers of sensors are randomly deployed in said manner. The coordinates of centre of circles are denoted as:

(x_i, y_i), where i = 1,2, 3……., n

The area of overlapping between two nodes *i* and *j* is represented by A_{ij} and is calculated by

$$A_{ij} = 2r^2\cos^{-1}\left(\frac{d_{ij}}{2r}\right) - \left(\frac{d_{ij}}{2}\right)\left(\sqrt{4r^2 - \left(d_{ij^2}\right)}\right) \quad \text{.... (1)}$$

Where, d_{ij} represents distance between mobile node (i) and node (j) and given by

$$d_{ij} = \sqrt{(x_j - x_i)^2 + (y_j - y_i)^2} \quad \text{..... (2)}$$

Total Overlapping of Deployment = $\frac{1}{2}\sum_{i=1}^{n}\sum_{j=1}^{n} A_{ij}$ … (3)

For example, the area of overlying between two nodes, say p and q, is given by

$$Apq = 2r^2\cos^{-1}\left(\frac{d_{pq}}{2r}\right) - \left(\frac{d_{pq}}{2}\right)\left(\sqrt{4r^2 - \left(d_{pq^2}\right)}\right) \quad \text{..... (4)}$$

Amount of overlapping among two adjacent node is calculated and placed in a square matrix of order n which is shown as under :

$$\text{Area Matrix (AM)} = \begin{bmatrix} A_{11} & A_{12} & A_{13} \ldots A_{1n} \\ A_{21} & A_{22} & A_{23} & A_{2n} \\ A_{31} & A_{32} & A_{33} & A_{3n} \\ & & \vdots & \\ A_{n1} & A_{n2} & A_{n3} & A_{nn} \end{bmatrix}$$

IV. RESULTS & EXPERIMENTS

We have performed the experiments by using soft computing algorithms such as GA and BFO algorithms. These algorithms perform on the principal to find out best optimum solution to a given problem. Genetic algorithm computes best solution by using Crossover and mutation provinces. Bacterial Forging optimization approach use three operator's chemotactic steps, reproduction and elimination-dispersal to find best optimum solution in a single iteration. The parameter considered for simulation for GA and BFO are placed below in table 1 and table 2 respectively.

Table 1: Simulation Parameter (GA)

Parameters	Values
Number of rounds	10
Crossover probability	0.87
Mutation probability	0.13

Table 2: Simulation Parameter (BFO)

Parameters	Values
Number of rounds	12
Search space dimension (p_1 & p_2)	15
bacteria (s) quantity	6
Steps number (N_c)	10
Swims boundaries (N_s); limit length	6
Steps for reproduction number (N_{re})	6
Events count (N_{ed}) for elim/disp.	2
Probability (P_{ed}) of elim/disp.	0.25

Both these approaches are validated by simulation them in MATLAB using core i7@2.50 GHz processor with 8 GB RAM based computer running on Windows 7 platform. Both the approaches were simulated with the simulation parameter given the table 1 and table 2. Two network scenario simulated by these two approaches are mentioned in table 3

Table 3: Network Parameters

Scenario No.	Iteration	Sensors	Radius	Area of Deployment
1	2000	70	7m	100X100 m
2	2000	70	14m	200X200m

In order to compare the performance the average covered area by GA and BFO approach for 2000 iterations were recorded .Twenty five trails were carried out for each approach and results are placed in table 4

Table 4: Performance comparison of GA and BFO

Scenario No	GA Covered Area	BFO Covered Area
1	94.3760	95.3427
2	94.9204	95.2446

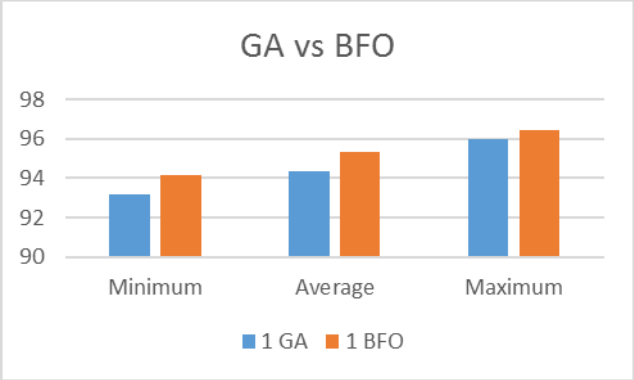

Scenario	Algorithm	Minimum	Average	Maximum
1	GA	93.2014	94.3760	95.9955
	BFO	94.1520	95.3427	96.4155
2	GA	93.8968	94.9204	96.7792
	BFO	94.4566	95.2446	96.3279

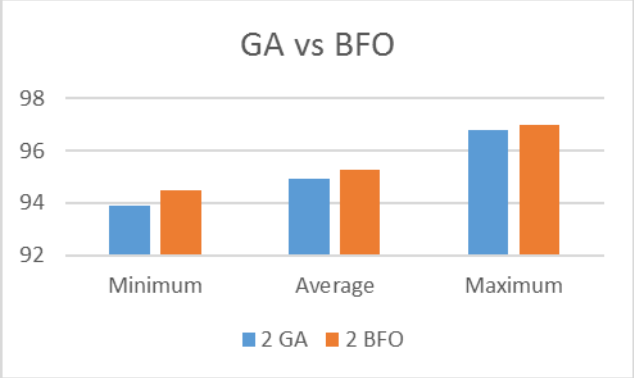

V. CONCLUSION

Wireless Sensor Network is utilized to sense the accurate observations from harsh environments. The network is deployed to sense the information from a particular defined area. To enhance the network coverage optimum positions of the nodes are to be determined. This problem reduced to NP hard problem in which the overlapping area amongst sensor is to be minimized. In the purposed work two deployment approaches were proposed based on Genetic Algorithm and Bacterial Forging Optimization algorithm. Genetic algorithm use crossover and mutation operators for generation of new Childs and on the basis of best fitness select the nodes. Bacterial Forging Optimization Technique utilize different chemotactic steps, reproduction and elimination-dispersal operators to compute best optimum solution.

These approaches are validated by simulation them in MATLAB using core i7@2.50 GHz processor with 8 GB RAM based computer running on Windows 7 platform. The average covered area by applying both approaches for two network scenarios for 25 trails were recorded. It is observed from the simulation results of table 4 that BFO approach provides better coverage as compared to GA approach. Conclusion could be drawn from the results that BFO approach could be used to find optimal sensor deployment in large target area having harsh environmental conditions

REFERENCES:

[1] Jie Jia, Jian Chen, Guiran Chang, and Zhenhua Tan," Energy efficient coverage control in wireless sensor networks based on multi-objective genetic algorithm", Computers and Mathematics with Applications, Vol. 57, pp. 1756-1766, 2009.

[2] A. Zahmatkesh and M. H. Yaghmaee, "A Genetic Algorithm-Based Approach for Energy-Efficient Clustering of Wireless Sensor Networks," International Journal of Information and Electronics Engineering, Vol. 2, No. 2, March 2012.

[3] Shiyuan Jin, Ming Zhou, Annie S. Wu, "Sensor Network Optimization Using a Genetic Algorithm," School of EECS, University of Central Florida Orlando, FL 32816.

[4] Yang SUN, and Jingwen TIAN, "WSN Path Optimization Based on Fusion of Improved Ant Colony Algorithm and Genetic Algorithm," Journal of Computational Information Systems, Vol. 6, Issue 5, pp. 1591-1599, 2012.

[5] S.M. Hosseinirad, and S.K. Basu, "Wireless sensor network design through genetic algorithm," Journal of AI and Data Mining Vol. 2, No. 1, pp. 85-96, 2014.

[6] Mohammad M. Shurman, Mamoun F. Al-Mistarihi, Amr N. Mohammad, Khalid A. Darabkh, and Ahmad A. Ababnah, "Hierarchical Clustering Using Genetic Algorithm in Wireless Sensor Networks," MIPRO 2013, May 20-24, 2013, Opatija, Croatia.

[7] Amol P. Bhondekar, Renu Vig, C Ghanshyam, Madan Lal Singla, and Pawan Kapur, "Genetic Algorithm Based Node Placement Methodology for Wireless Sensor Networks," Proceedings of the International Multi Conference of Engineers and Computer Scientists, Vol. 1, pp. 18–20, March, 2009, Hong Kong.

[8] Shiyuan Jin, Ming Zhou, Annie S. Wu, "Sensor Network Optimization Using a Genetic Algorithm," School of EECS, University of Central Florida Orlando, FL 32816.

[9] Naeim Rahmani, Farhad Nematy, Amir Masoud Rahmani, Mehdi Hosseinzadeh, "Node Placement for Maximum Coverage Based on Voronoi Diagram Using Genetic Algorithm in Wireless Sensor Networks," Australian Journal of Basic and Applied Sciences, Vol. 5, Issue 12, pp. 3221-3232, 2011.

[10] Seyed Mahdi Jameii and Seyed Mohsen Jameii, "Multi-Objective Energy Efficient Optimization Algorithm for Coverage Control in Wireless Sensor Networks," International Journal of Computer Science, Engineering and Information Technology (IJCSEIT), Vol. 3, No.4, August 2013.

[11] Omar Banimelhem, Moad Mowafi, and Walid Aljoby, "Genetic Algorithm Based Node Deployment in Hybrid Wireless Sensor Networks," Communications and Network, Vol. 5, pp. 273-279, November 2013.

[12] Yingyou Wen, Jie Jia, Jian Chen, Guiran Chang, and Jingping Song, "Multi-objective optimization for coverage control in wireless sensor network with adjustable sensing radius," Computers and Mathematics with Applications Vol. 57, pp. 1767-1775, 2009.
[13] Yong-Hyuk Kim and Yourim Yoon, "Efficient Genetic Algorithm for Maximum Coverage Deployment in Wireless Sensor Networks," IEEE Transactions on Cybernetics, Vol. 43, No. 5.
[14] Mohamed Younis and Kemal Akkaya, "Strategies and techniques for node placement in wireless sensor networks: A survey", Ad hoc Networks, Vol. 6, pp. 621-655, 2008.
[15] Passino KM, "Biomimicry of Bacterial Foraging", IEEE Control System Magazine, Vol. 22, pp. 52-67, 2002.
[16] Dang, J., et al.: Option model calibration using a bacterial foraging optimization algorithm. In: Giacobini, M., et al. (eds.) Evo Workshops 2008. LNCS, Vol. 4974, pp. 133–143. Springer, Heidelberg 2008.
[17] Das, S., Biswas, A., Dasgupta, S. and Abraham, A. Bacterial Foraging Optimization Algorithm: Theoretical Foundations, Analysis, and Applications, Vol. 203 of Studies in Computational Intelligence, Springer Berlin/Heidelberg, pp. 23–55, 2009.
[18] Hossain, A., Biswas, P.K.; Chakrabarti, S., "Sensing Models and Its Impact on Network Coverage in Wireless Sensor Network", industrial and Information Systems, IEEE Region 10 and the Third international Conference on, Kharagpur, pp. 1-5, 2008.
[19] Uribe, C., Grote, W., "Radio Communication Model for Underwater WSN", New Technologies, Mobility and Security (NTMS), 2009 3rd International Conference on, Cairo, pp. 1–5.
[20] J. Yick, B. Mukherjee, and D. Ghosal., "Wireless sensor network survey" Computer Networks, Vol. 52, Issue 12, 2008.
[21] S. Devi, M. Geethanjali, "Application of Modified Bacterial Foraging Optimization algorithm for optimal placement and sizing of Distributed Generation", Expert Systems with Applications, Vol. 41, Issue 6, pp. 2772-2781.
[22] J. Doyne FARMER and Norman H. PACKARD, Alan S. PERELSON, "The Immune System, Adaptation, And Machine Learning", Physical 22D, pp. 187-204 North-Holland, Amsterdam.
[23] Livjeet Kaur, Mohinder Pal Joshi, "Analysis of Chemotaxis in Bacterial Foraging Optimization Algorithm" International Journal of Computer Applications, Vol. 46, No. 4, 2012.
[24] Mary Saranya, Rajapandiyan A, Fathima K., Hema S, GeethaPriya S, Saravanan S, "A Power System Stabilizer for Multi-Machine Power Based on Hybrid BF0A-PSO", International Journal of Electrical and Computer Engineering, Vol. 5, No. 2, pp. 213-220.
[25] *Dac-Nhuong Le*, "GA and ACO Algorithms Applied to Optimizing Location of Controllers in Wireless Networks", Vol. 3, No. 2, pp. 221-229.

WSN – a Technology for Natural Resource Monitoring and Conservation- a Review

Kawalpreet Kaur
Department of Electronics and Communication Engineering
Baba Banda Singh Bahadur Engineering College
Fatehgarh Sahib, Punjab, India

Tripatjot Singh Panag
Department of Electronics and Communication Engineering
Baba Banda Singh Bahadur Engineering College
Fatehgarh Sahib, Punjab, India

***Abstract*- With rapid increase in globalization, the human activities have gradually affected the environment. So, environment monitoring is a vital issue and has attracted a lot of attention. A wireless sensor network (WSN) consists of a large number of tiny sensor nodes spread over a large geographical area (sensing field) where each node is a low-power device that incorporates computing, wireless communication, and sensing abilities. The WSNs are designed and implemented in a manner that they can withstand harsh environments and keep working for a long period of time. WSNs are very useful for monitoring and preserving the environment. These are used for various applications such as habitat monitoring and control, glacier monitoring, agricultural conservation, disaster forecasting, forest fire detection and detection of acid rains, computing of various activities in mines, plant protection for sustainable crop protection, water quality monitoring, ocean sensing and monitoring, earthquake detection etc. This paper presents a survey of applications of WSNs that contribute to the monitoring and conservation of environment.**

Keywords—WSN; Environment monitoring; glacier monitoring; habitat monitoring.

I. INTRODUCTION

Wireless Sensor Networks consist of randomly or spatially distributed sensors over a wide geographical area for measuring various environmental parameters like temperature, humidity, sound, pressure etc. The units collecting this data are called sensing nodes. The sensing nodes transmit this data to the sinks using single hop or multiple hop communication. The sink either uses the information locally or sends it to other networks through gateways [1].

The architecture of a wireless sensor node is shown in Fig. 1. Each node is equipped with a sensing unit, a transceiver, a processing unit and a power supply. A WSN node may also have some additional application-dependent equipment attached, such as the location finding system and mobilizer. These devices when combined into a small unit make it multi-functional. In other words, the structure and characteristics of sensor nodes depend not only on their electronic, mechanical and communication limitations but also on their application-specific requirements.

The fact that WSN comprises a large number of wireless sensing units that are scattered over a wide area and work in collaboration with each other to provide information about the entire area, makes them naturally suitable for monitoring wide geographical areas. The geographical area can be a farm field, a forest, a glacier, a mine etc. This paper presents a survey of the applications of WSN that contribute towards monitoring and conservation of natural resources.

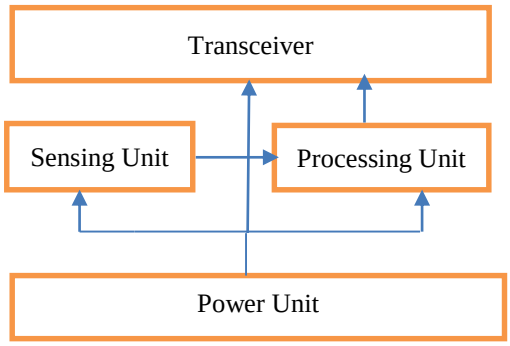

Fig.1. Architecture of a Wireless Sensor Node

The rest of the paper is organised as follows. Section II lists the design objectives for a WSN based environment monitoring system. The various characteristic features of WSNs are listed in section III. Section IV presents the various applications of WSN developed for environmental monitoring like agricultural monitoring, various methods for water and air quality monitoring etc. Finally, the paper is concluded in Section V.

II. DESIGN OBJECTIVES FOR A WSN BASED ENVIORNMENT MONITORING SYSTEM

A WSN based system designed for environmental monitoring must should the following objectives:

Autonomy: The system should be autonomous in terms of operation and control. It should have the capability of self-evaluating, self-calibrating and self-healing.

Reliability: It is important to maintain reliability in order to prevent packet loss during bad weather conditions.

Robustness: The network has to be robust to encounter problems related to hardware failure, and poor signal connectivity.

Flexibility: The system should be highly flexible so that the user may be able to add, move or change stations depending on the requirements of the stations.

III. CHARACTERSTIC FEATURES OF WIRELESS SENSOR NETWORKS

The wireless sensor networks are a special type of wireless networks. The characteristics that make them different from other wireless networks are listed below:

1) Lifetime: This is the most critical factor since the nodes are energy consuming. Energy efficient routing should avoid the loss of a node due to battery depletion. Many protocols were proposed to minimize the energy consumption on the forwarding paths, but if some nodes happen to be displaced, their lifetime will be reduced.
2) Maintenance: The desired form of maintenance in a network is the complete update of the program codes in the sensor nodes over the channel. All the sensor nodes should be updated.
3) Resilience: The sensor nodes in the network should be able to cope up with the node failures, if any.
4) Fault tolerance: The network functionality should be maintained even though the built in dynamic nature and failure of the nodes due to harsh environment, depletion of batteries, or external interference make networks prone to errors.
5) Security: The need for security in WSNs is evident, especially in health maintenance, safety and military applications. Most of the applications relay data that contain private or confidential data.
6) Production Cost: The number of nodes in WSNs is very high, and once the batteries of the nodes run out they are to be replaced by new ones. So, in order to make the deployments possible, the nodes should be of low cost.

IV. APPLICATIONS OF WSNs

In early times analogy mechanisms were used to measure physical environmental parameters. The old mechanisms included human help to download the recorded data. Then came digital data loggers. They were easy to operate but they had certain drawbacks. The digital data loggers solution, usually provided monitoring at one point only and in many cases multiple points were needed to be monitored. There was not a standard to store data and to communicate with the data logger, so several different solutions were used. Then came wireless sensors which made the work easier. Using a WSN, a number of sensors continuously monitor factors like temperature and luminosity, humidity and will process, store and transmit data co-operatively and wirelessly with other sensors to produce data that can then be collected and made accessible to users virtually anywhere on the globe.

A. Agriculture monitoring

WSN system [2] is made up of four fragments: sensor node, the sink, transmission networks and monitoring terminal. The data from the sensors can be stored, analyzed and transmitted via wireless radio channel to manager vehicle. In order to monitor agricultural activities we need environmental parameter sensors like humidity sensor, temperature sensor, CO_2 sensors etc. Based on this information the various parameters can be controlled and rectified. WSN can be used to determine the quantity of fertilizers to be used for crops, to determine the leaf chlorophyll content, leaf temperature, leaf area index, soil compaction, soil fertility, yield of grain, plant water status. WSN can be used to determine the optimum conditions for each crop, management of crop cultivation to know the exact condition in which plants are growing from your own home.

Various studies have been provided in the literature which provide us a great knowledge about the various advancements in the field of monitoring the agricultural environment.

In [3],Y. Zhu presented an agricultural environment monitoring system which included the sensor nodes design hardware and software which consist of the software flowchart. From the test performed, the system verified for consuming low power but provides high reliability, which can control real time monitoring for unprotected agriculture and environment

In [4], the authors presented a Zigbee-based agriculture monitoring system which proved to be a reliable and efficient system for efficiently monitoring the environmental parameters. Wireless monitoring of field not only allowed users to reduce the human power, but it also allows user to see accurate changes in it. This research focused basically on developing devices and tools for managing, displaying and alerting the weather/disaster warnings.

In [5],Yu et al. proposed a mixed architecture including WSN and wireless underground sensor networks (WUSN). An enactment framework was then developed for monitoring the real-time properties of soil. The influence of parameters of soil, depth of nodes, signal frequency and attenuation on transmission were studied. During data transmission reflection, scattering and diffraction may occur in the soil and at the soil–air interface. The research revealed that the frequency of the electromagnetic signals and the water content of soil affect the path loss. These system used a wireless transceiver chip based on ZigBee which was developed to gather soil terrestrial information.

In [6], the authors monitored a potato field in order to observe the climate: humidity, temperature and weather. This was done to reveal when the crop is at risk due to a disease called phytophtora.

In [7], Kim et al. developed a sensor network that used an independent robots with beacons to monitor and detect fires and air pollution in fields. The authors used a network tree topology with RF transceivers and microcontroller in order to monitor the temperature, gas, smoke, humidity and illumination.

In [8], the authors described the deployment of WSNs in an apple orchard with the main aim to monitor the moisture in top soil to analyse interaction with plant physiology. Numerous homogeneous sensors were deployed in a multi-hop mesh topology in order to minimize energy consumption.

In [9], the authors proposed a system to monitor crop fields where the system could detect and identify procedures of a WSN video surveillance system. The so designed system was able to monitor, detect, identify and transmit data over long distances. The system integrated video transmission to networks for only monitored crops. The system was, therefore, quite useful in cost reduction, increasing the lifetime of the devices and networks, and avoiding duplicate infrastructure.

1. Irrigation management

In the present era, people are working on effective irrigation techniques so as to preserve our water resources [10]. So, several efforts has been done for the preservation and effective use of water for irrigation and to provide some help in doing so, WSN are used. In [11], Peng proposed an intelligent irrigation system based on a WSN and neural fuzzy control. The objective was to solve issues of soil fertility loss and water wastage during irrigation. The system was composed of sensor nodes and the controller node. They consist of soil moisture sensors along with irrigation pipes, spray irrigation and irrigation control valves for deployment. The ZigBee network was adopted in the mesh network topology.

In [12], NesaSudha et al. proposed an automatic irrigation system with energy-efficient TDMA-based algorithm, a network with a star single- hop topology along with a MAC protocol was used to control energy consumption.

In [13], Zhang et al. proposed a WSN-based system to monitor the moisture of soil and to analyse the temporal and spatial variability of soil moisture for variable irrigation. The position of the deployed sensor nodes and the moisture sensors were measured with a GPS and both the sensors were waterproof to withstand harsh conditions. These sensors provided valuable information which further became the basis to make irrigation decisions.

In [14], a WSN soil moisture mapping and monitoring method was developed to provide irrigation scheduling information. In this the data in digital format was incorporated into VRI controlling software. The irrigation was by a centre pivot (CP) irrigator with VRI modification. Each sprinkler was controlled independently by digital maps that were uploaded to the dominant controller.

In [15], the authors presented a system that was intended to automate the irrigation process. The variability in the soil moisture was calculated and was used by the irrigation controller to initiate the irrigation actions. The sensor nodes deployed for this system were composed of ZigBee end devices (ZED) and ZigBee co-ordinator (ZC), where ZED collected soil moisture and temperature data and send it to ZC which in turn was sent to the Remote monitoring station (RMS) via cellular network. The opening and closing of irrigation valves depend on the values stored in the co-ordinator node.

2. Greenhouse management

The greenhouse effect occurs when solar radiation from sun are imprisoned by the gases in the earth's atmosphere and reflected back from the earth. Thus, it heats the surface of earth and hints to global warming. Therefore, greenhouse monitoring system is important to guarantee the stabilization of the environment. Monitoring and control of greenhouse can be divided into three main parts: Measuring, calculating and adjusting. The measured parameters of the greenhouse climate are first converted from analog to digital and then transmitted to the computer which is normally located outside because of the large moisture content in the greenhouse. Signals provided by the sensors are normally weak. Without signal amplifier, cabled sensor units cannot transmit the data correctly. Wireless sensor networks does not have such problems. Measured data can be sent directly to the gateway node which are inserted in to the computer or it can be transferred in a multi-hop means via router nodes, if the distance between the measuring nodes and the computer extends the length of a single radio link. Besides data collection and control calculation, the computer also represents the climate variable values and statistics on the screen for the user. The computer runs the algorithm for greenhouse climate control, and the new values for the control signals are computed in every 15-60 seconds. Each output is linked to electronic relay, which switches the tools under its control on or off via the second relay, which gives the input voltage needed for the device. A modern greenhouse system can consist of several parts which have their own local climate variable settings.

Various technologies has been emerged since now that are presented in the literature as below:

In [16], a greenhouse management system using a base platform, TinyOS to measure and monitor various environmental parameters including temperature, light and humidity. The parameter information is automatically collected and send to the system which ensures the system to become highly efficient.

A Greenhouse environment monitoring system based on ZigBee was implemented in [17] which use oretical analysis and experimental test methods to ensure system efficiency. The various greenhouse monitoring parameters are collected by the system, and the system demonstrate the nodes and network coordinator communications, perform network stabilization, and agree between theoretical data and real situations.

In [18], the author proposed a method to monitor greenhouse environment for various distances. It consists of various sensor and repeat nodes and a single main node, PC terminal, MYSQL database system, an alarm system and a web service. The system senses and monitors the temperature and humidity parameters and compare them with the values stored at the database and web service. A curve is drawn by the web server which depicts the differences from the sensing module. An alarm is triggered if the curve shows the abnormal changes in the temperature and the humidity which in turn helps to take a desired action.

In [19], the authors presented an automatic monitoring system for preventing dew condensation in greenhouse environment. The system consists of sensor nodes, base nodes and relay nodes for collecting, processing the data and for driving the devices inside the greenhouse environment respectively, for data storage and processing. They constructed a physical model which resembles the typical greenhouse to verify the performance of system with regard to control of dew condensation.

B. Water and air quality monitoring

Water quality monitoring includes analyzing the properties of water in dams, rivers, lakes & oceans, as well as underground water reserves. The use of these sensors helps in proper calculation of the status of water, its levels, the various elements like minerals or toxic compounds which are harmful for human as well as for animals and plants. WSN are also helpful in the measurement of the pollution level in the air. This can be done by collecting the readings from the nodes and transmitting them to a gateway and then by visualizing the

collected data using statistical and user friendly methods like tables and line graphs, reports can be generated on daily or monthly basis that represents the seriousness of air pollution. Various techniques are been laid in the literature for control of pollution levels in air and water.

The solution to the monitoring of indoor air quality is provided in [20]. In this search, various environmental parameters like temperature, humidity, pollutants, aerosols were determined to check the health of indoor space and represents them in Air Quality Index (AQI) and provides this as an input to the HVAC (Heating, Ventilation and Air Conditioning) System. A toolkit was developed to keep a check on the air quality of the deployed regions in form of graphs and numbers.

A multisensory system, SmartCoast for monitoring the quality of water is presented in [21]. This system aimed at providing a platform that aimed at meeting the monitoring requirements of Water Framework Directive (WFD) across EU. The various parameters included temperature, phosphate, dissolved oxygen, conductivity, pH, turbidity and water level. In this system, the WSN enabled the 'plug and play' capabilities at Tyndall for the integration of the sensors.

In [22], the authors proposed a group of intelligent sensors for observing the water level of the sea. In this system the authors used humidity sensors for accessing the water quality and the sea level. This system was also capable of measuring the humidity level of the sea water at the shores.

C. Glacier environment monitoring

With the constant advancements in wireless technology and miniaturization have made the deployment of sensor networks to monitor various aspects of the environment increasingly realistic. Unfortunately, due to the inventive nature of the technology, there are currently very few environmental sensor networks in operation that validate their value. Various methods or technologies has been developed which has provided a great share in the monitoring of the glaciers like NASA/JPL's project in Antarctica [23], and Huntington Gardens [24], Berkeley's habitat monitoring at Great Duck Island [25],Columbian river estuary described by CORIE project [26], deserts [27], volcanoes [28] and glaciers [29]. GlacsWeb, a sensor network was developed for operation in the hostile conditions underneath a glacier. The main aim of this system was to understand glacier dynamics in response to climate changes. Since the nodes are to be laid down in the glacial environment, they are subjected to constant immense strain and pressure from the moving ice. Therefore, a robust sensor design, integrated with high levels of fault tolerance and network reliability has to be developed

A research project for glacial monitoring, PermaSense which investigates the effect of climate changes on permafrost is well explained by the authors in [32]. It mainly aims at understanding the heat transport in frozen rock walls and its effects on the stability and large scale movements. The system consists of tiny nodes placed on the surface and a computer as a base station running on Linux OS.

N. Burriin [31] provided a MAC Layer (TDMA), topology control and a routing protocol, Dozer which provided nodes with precised wake-up schedules for all communications that only rely on local synchronization. In dozer, the clock drift compensation is the responsibility of receiver node and worst case guard times were used to guarantee a prior wake up of receiver before the transmission is started by the sender.

Elsaify introduced GWMAC, a centralized TDMA protocol in [32] especially designed for networks where contention is completely eliminated and control packets are minimized. This protocol reduces the duty cycle of the nodes to almost zero, allowing only few minutes for communication per day. It is used to synchronize the entire network during booting and each time a command packet is received.

D. Marine environment monitoring

With rapid development of economy and habitat and with their increasing human activities like tourism, urban development, industry, the marine environment has been gradually deteriorating. It is of vital importance and has attracted a great deal of research and development. For the past few decades, various marine environmental monitoring systems has been developed which used oceanographic research vessel which was quite expensive and time consuming. So, WSN has been considered as an alternative for monitoring the environment as it has numerous advantages like easy deployment, unmanned deployment, low cost and real time monitoring. In this deployment, various kinds of sensors are used to monitor and measure various physical and chemical parameters such as water temperature, pressure, wind direction and speed, salinity, turbidity, pH, chlorophyll levels and oxygen density. Various projects has been offered in the literature which aimed at monitoring the marine ecosystem with the use of different protocols like with the use of ZigBee ocean sensing and monitoring was carried out that included various parameters like temperature, pressure, salinity, nitrates, velocity with the use of LabVIEW based user interface using google maps. Some specific efforts has been also made for fish farm monitoring, coral beef monitoring, marine shellfish monitoring.

In [33], the authors presented a system that demonstrated the deployment of novel fiber optic based sensing platform which is capable of monitoring the minute changes in the impurity level of the water. Firstly, the system was validated for the oil in water and then with chlorophyll. Then this system was interfaced with SHIMMER mote to test whether the system was capable of alarming the user of the presence of pollutant in the water.

In [34], the authors proposed adaptive time piecewise constant vector quantization (ATPCVQ) compression algorithm to monitor the environment near the harbor so as to make nearby ships out of danger area. The system was capable of lowering the budget and increasing the lifetime of the sensors.

E. Wildlife

With growing population and search for new habitat, over exploitation of wildlife and forests is carried out. For covering a huge area like forests, we use mobile agents with WSN for multi hop communication. WSN can collect, transmit and store large volumes of environmental data which may be used in research or to refine wildlife management or monitoring. They can also be used in decreasing operational cost of terrestrial wildlife trapping. WSN system provides detailed tracks of targets inside the observed area. These can be used to study animal behavior in some crucial areas with the help of not only

cameras but also sensor networks deployed in the surrounding area. An example of WSN application is Zebra Net, used to track zebras on the fields by gathering dynamic data about zebra positions in order to understand their mobility patterns. WSN can be used for monitoring endangered birds in their habitat, to analyze the actual life time of the different species etc.

A. Tovarin [35], reports the study of applying a WSN using DTN (Delay Tolerant Network) to find the current status of White Tail Deer in WMU Area Ontario, North of Parry Sound District of Canada. System is so designed that it is able to obtain highest range with least number of sensors. Further the author simulated the system on Planet Lab Environment to create a DTN network for monitoring the wildlife habitat.

In [36], S. Gaikwad contributes mainly towards the devastating effect of smuggling or theft of forest trees especially sandal woods on the environment. The authors proposed a microcontroller along with WSN based anti-poaching system which is capable of monitoring the theft based on the vibrations produced during cutting of trees. A low power MSP430F5529 microcontroller is used along with Xbee RF modules based on Zigbee to communicate to a central server from a remote place. The data produced due to vibrations by various tests on trees and simulated using Labview.

S. A. Seboin [37] proposed dielectric caps used for wildlife protection. In this work, Fog chamber tests were used to check and to estimate the performance of six different wildlife protection caps, which were positioned on their insulators, and outfitted with the suitable connecting cables. During the evaluation phase, the insulators were exposed to salty fog which used deionized water with appropriate amount of salt added to it. The results showed that only two caps out of six satisfied the expectations.

F. Radiation sensor networks

Radiation Sensor Networks helps in radiation prevention by helping authorities and security forces to measure the levels of radiations due to mining activities, nuclear power plants High doses of radiations can be devastating for the environment. In animal's radiations cause's molecules to lose electrons, kill enzymes in the body, damages the DNA, and may even increase the chances of cancer. These radiations also adversely affect the marine life. High levels of UV can cause reduction in reproduction capabilities, reduce the amount of food and oxygen that the plankton produce, can result changes in pollination patterns etc.

In [38], a WSN was designed using a group of radiation detectors with different types of sensors. These sensors were scattered in different areas and each sensors transmits data through to the main control station. The design included Gsm module and GSM modem to determine the location of mobile and fixed station and to transmit the data respectively. In the main control system, GUI software was designed to show the information and status of stations to report any radiation leakages.

G. Habitat monitoring

Habitat monitoring is one of the essential part of environment monitoring. Habitat is a place where animals and plants reside and grow. So, habitat monitoring ensures that the species grow without any turbulences in their habitat so that there is no ecological disturbance for plants and animals due to pollution. Various studies show how a system can monitor the pollution affecting the lives of species.

In [39], they proposed a system architecture for seabird nesting and behaviour monitoring. The authors used wireless sensor nodes instead of performing their research physically, to collect the data online without disturbing the birds' life and routine.

In [40], the authors presented a new approach, a tonal region detector (TRD) using sigmoid function. This offered flexibility since the slope and the mean of the sigmoid function can be adjusted independently. After tonal region detection, recognition performance, noise immunity and energy consumption can be improved.

An experimental test-bed for real world Habitat Monitoring System (HMS) was presented in [41], that consist of stationary sensor nodes which were combined with Wi-Fi to collect the physical data of the environment. The test- bed described data monitoring, handling and storing. The sensors can be replaced with the test bed to calculate and monitor air population, forest fire detection, health care and water quality monitoring.

H. Natural environment protection

Wireless sensor nodes deployed in the environment helps in detection of forest fires. These nodes detect the flames, heat and gases which are used to identify the molecules of chemical compounds that are generated due to combustion. The networks can also acquire the daily values for temperature and humidity to determine the likelihood of fire. These send an alarm indicating the status of fire, the level and the area under fire.

In study [42], by J. Lloret proposed a fire detection system that uses a wireless local area network (WLAN) together with sensor node technology. The system fixed in wireless mesh network uses multi-sensor nodes with cameras which are IP based to detect the presence of fire. When a fire is discovered by the nodes, the sensor alarm propagate via wireless network to a central server. The closest wireless camera to the multi sensor is selected by the central server, and it transmits a message to it to retrieve real-time figures from the area under detection. The main benefit from this study is that it integrates sensory data with images.

In [43], K. Trivedi presented a technique for the faster detection of forest fires using a mobile agent with the minimum consumption of energy.

V. CONCLUSION

A review of various applications of the wireless sensor networks that contribute towards the monitoring and conservation of the environment and natural resources has

been presented. Many such wireless sensor networks based applications have been developed and are contributing to satisfy the cause. The inherent properties of the WSNs make them naturally suitable for such applications. Hence, in future many more such applications shall be coming up.

REFERENCES

[1] D. S. Deif and Y. Gadallah, "Classification of Wireless Sensor Networks Deployment Techniques," in IEEE Communications Surveys & Tutorials, vol. 16, no. 2, pp. 834-855, Second Quater 2004.
[2] M. R. M. Kassim and A. N. Harun, "Applications of WSN in agricultural environment monitoring systems," 2016 International Conference on Information and Communication Technology Convergence (ICTC), Jeju Island, South Korea, 2016, pp. 344-349.
[3] Y. Zhu, J. Song, and F. Dong, "Applications of wireless sensor network in the agriculture environment monitoring," Procedia Engineering, vol. 16, pp. 608-614, Jan. 2011.
[4] S. S. Patil et al, "Smart Wireless Sensor Network for Monitoring an Agricultural Environment," in (IJCSIT) International Journal of Computer Science and Information Technologies, 2014, Vol. 5, issue 3, pp.3487-3490.
[5] Xiao Q. Yu, Pu T. Wu, Wen T. Han, Zeng L. Zhang ," A survey on wireless sensor network infrastructure for agriculture," in Computer Standards & Interfaces, vol. 35, issue 1, pp.59–64, January 2013.
[6] M. R. MohdKassim, I. Mat and A. N. Harun, "Wireless Sensor Network in precision agriculture application," 2014 International Conference on Computer, Information and Telecommunication Systems (CITS), Jeju, 2014, pp. 1-5.
[7] Young-Duk Kim, Yeon-Mo Yang, Won- Seok Kang, Dong-Kyun Kim,"On the design of beacon based wireless sensor network for agricultural emergency monitoring systems," in Computer Standards & Interfaces, vol.36, issue 2, pp.288–299, February 2014.
[8] B. Majone, F. Viani, A. Bellin, et al. "Wireless sensor network deployment for monitoring soil moisture dynamics at the field scale," in Procedia Environmental Sciences, 2013, vol.19, pp. 426–435.
[9] A. Garcia-Sanchez, J. Garcia-Sanchez, F. Garcia-Haro, J. Garcia-Haro, "Wireless sensor network deployment for integrating video-surveillance and data-monitoring in precision agriculture over distributed crops," in Computers and Electronics in Agriculture, vol.75, issue 2, pp. 288–303, February 2011.
[10] B. Balaji Bhanu, M. A. Hussain and P. Ande, "Monitoring of soil parameters for effective irrigation using Wireless Sensor Networks," 2014 Sixth International Conference on Advanced Computing (ICoAC), Chennai, 2014, pp. 211-215.
[11] X. Peng and G. Liu, "Intelligent Water-Saving Irrigation System Based on Fuzzy Control and Wireless Sensor Network," 2012 Fourth International Conference on Digital Home, Guangzhou, 2012, pp. 252-256.
[12] Nesa Sudha, M. Valarmathi, M., & Babu, A. S. (2011). "Energy efficient data transmission in automatic irrigation system using wireless sensor networks," in Computers and Electronics in Agriculture, vol. 78, issue 2, pp. 215–221. September 2011.
[13] R. Zhang, J. Guo, L. Zhang, Y. Zhang, L. Wang, Q. Wang,"A calibration method of detecting soil water content based on the information-sharing in wireless sensor network," in Computers and Electronics in Agriculture 76, pp.161–168, Jan,2011.
[14] Hedley, C. Ekanayake, J., Roudier, P. (2012). "Wireless soil moisture sensor networks for precision irrigation scheduling." In L. D. Currie & C. L. Christensen (Eds.), Workshop abstracts, advanced nutrient management: Gains from the past-goals for the future. (p. 85), New Zealand: Massey University
[15] M. Mafuta, M. Zennaro, A. Bagula, G. Ault, H. Gombachika, &T. Chadza, "Successful deployment of a wireless sensor network for precision agriculture in Malawi," 2012 IEEE 3rd International Conference on Networked Embedded Systems for Every Application (NESEA), Liverpool, 2012, pp. 1-7.
[16] Rui Gao, Hong Zhou and Gang Su, "A wireless sensor network environment monitoring system based on TinyOS," Proceedings of 2011 International Conference on Electronics and Optoelectronics, Dalian, 2011, pp. V1-497-V1-501.
[17] L. l. Li, S. f. Yang, L. y. Wang and X. m. Gao, "The greenhouse environment monitoring system based on wireless sensor network technology," 2011 IEEE International Conference on Cyber Technology in Automation, Control, and Intelligent Systems, Kunming, 2011, pp. 265-268.
[18] Tongtong Yin, WenjieFeng and Zheying, "Temperature and humidity wireless sensing and monitoring systems applied in greenhouse," Proceedings of 2011 International Conference on Computer Science and Network Technology, Harbin, 2011, pp. 857-861.
[19] Dae-Heon Park, Jang-Woo Park, "Wireless Sensor Network- Based Greenhouse Environment Monitoring And Automatic Control System For Dew Condensation Prevention," in Sensors, Basel, 2011, vol.11, issue 4, pp. 3640-3651.
[20] S. Bhattacharya, S. Sridevi and R. Pitchiah, "Indoor air quality monitoring using wireless sensor network," 2012 Sixth International Conference on Sensing Technology (ICST), Kolkata, 2012, pp. 422-427.
[21] B. O'Flynn *et al*., "SmartCoast: A Wireless Sensor Network for Water Quality Monitoring," 32nd IEEE Conference on Local Computer Networks (LCN 2007), Dublin, 2007, pp. 815-816.
[22] Shahid Siddhik P and S. S. Kumar, "Sea water quality monitoring using smart sensor network," 2015 International Conference on Control, Instrumentation, Communication and Computational Technologies (ICCICCT), Kumaracoil, 2015, pp. 804-812.
[23] K.A. Delin, R.P. Harvey, et.al, "Sensor Web in Antarctica: Developing an Intelligent, Autonomous Platform for Locating Biological Flourishes in Cryogenic Environments," in 34th Lunar and Planetary Science Conference, 2003.
[24] http://sensorwebs.jpl.nasa.gov/resources/huntington_sw31.shtml.
[25] R. Szewczyk, et al., "Lessons from a Sensor Network Expedition," in Proceedings of the 1st European Workshop on Wireless Sensor Networks (EWSN '04), January 2004, Berlin, Germany, pp 307-322.
[26] D.C. Steere, et al., "Research Challenges in Environmental Observations and Forecasting Systems," in Proceedings ACM/IEEE International Conference on Mobile Computing and Networking (MOBICOMM), 2000, pp. 292-299.
[27] K.A. Delin, S.P. Jackson, D.W. Johnson, et.al, "Sensor Web for Spatio-Temporal Monitoring of a Hydrological Environmental," in 35th Lunar and Planetary Science Conference, League City, TX, 2004.
[28] K. Lorincz, D. Malan, Thaddeus R. F. Fulford-Jones, et.al, "Sensor Networks for Emergency Response: Challenges and Opportunities", in Special Issue on Pervasive Computing for First Response, IEEE, Oct-Dec 2004, pp.16-23.
[29] K. Martinez, J.K. Hart, R.Ong, "Environmental Sensor Networks. Computer," vol.37, issue 8, pp. 50-56.
[30] J. Beutel, S. Gruber. et.al, "The PermaSense Remote Monitoring Infrastructure," in International Snow Science Workshop Davos 2009.
[31] N. Burri, P. von Rickenbach and R. Wattenhofer, "Dozer: Ultra-Low Power Data Gathering in Sensor Networks," 2007 6th International Symposium on Information Processing in Sensor Networks, Cambridge, MA, 2007, pp. 450-459.
[32] Elsaify, Ahmed, Padhy, Paritosh, Martinez, Kirk, Zou and Gang, "GWMAC – A TDMA based MAC Protocol for glacial sensor network," in 4th ACMPE-WASUN 2007.
[33] E. O'Connell, M. Healy, S. OKeeffe, T. Newe and E. Lewis, "A Mote Interface for Fiber Optic Spectral Sensing With Real-Time Monitoring of the Marine Environment," in IEEE Sensors Journal, vol. 13, no. 7, pp. 2619-2625, July 2013.
[34] Y. Li, Z. Zhang, W. Huangfu, X. Chai, X. Zhu and H. Zhu, "Sea route monitoring system using wireless sensor network based on the data compression algorithm," in China Communications, vol. 11, no. 13, pp. 179-186, Supplement 2014.
[35] A. Tovar, T. Friesen, K. Ferens and B. McLeod, "A DTN wireless sensor network for wildlife habitat monitoring," CCECE 2010, Calgary, AB, 2010, pp. 1-5.
[36] S. Gaikwad, R. Patil, A. Khandare and A. Rai, "Design WSN node for protection of forest trees against poaching based on ZigBee," 2015 IEEE International Conference on Electronics, Computing and Communication Technologies (CONECCT), Bangalore, 2015, pp. 1-4.
[37] S. A. Sebo, R. Otte and J. A. Moore, "Improving the Performance of a Wildlife Protection Cap by the Use of Salt Fog Testing," 2008Annual Report Conference on Electrical Insulation and Dielectric Phenomena, Quebec, QC, 2008, pp. 259-262.
[38] M. Altayeb, M. Mekki, O. Abdallah, A. B. Mustafa and S. Abdalla, "Automobile and fixed wireless sensor network for radiation detection," 2015 International Conference on Computing, Control, Networking, Electronics and Embedded Systems Engineering (ICCNEEE), Khartoum, 2015, pp. 199-202.

[39] A. Mainwaring, J. Polastre, R. Szewczyk, and D. Culler, "Wireless Sensor Networks for Habitat Monitoring," Habitat, in Intel RsearchBerleley, June 2002, pp. 88-97.
[40] A. Boulmaiz, D.Messadeg, N. Doghmane, A. Taleb- Ahmed, "Robust acoustic bird recognition for habitat monitoring with wireless sensor networks," International Journal of Speech Technology, September 2016, vol. 19, issue 3, pp 631-645.
[41] A. More, S. Wagh and K. Joshi, "A test-bed for habitat monitoring system using Wi-Fi in Wireless Sensor Networks," 2015IEEE International Conference on Computational Intelligence and Computing Research (ICCIC), Madurai, 2015, pp. 1-6.
[42] J. Lloret, M. Garcia, D. Bri, and S. Sendra, "A wireless sensor network deployment for rural and forest fire detection and verification," Sensors (Basel, Switzerland), vol. 9, no. 11, Jan. 2009, pp. 8722-47.
[43] K. Trivedi and A. K. Srivastava, "An energy efficient framework for detection and monitoring of forest fire using mobile agent in wireless sensor networks," 2014 IEEE International Conference on Computational Intelligence and Computing Research, Coimbatore, 2014, pp. 1-4.

Survey on Maximizing Power Efficiency using Mac Protocol

Er. Jiwanjot Singh
Mtech Scholar,
Department of ECE,
Baba Banda Singh Bahadur Engineering College,
Fatehgarh sahib, 140406, Punjab (India)

Raju Sharma
Assistant Professor,
Department of ECE,
Baba Banda Singh Bahadur Engineering College,
Fatehgarh sahib, 140406, Punjab (India)

***Abstract*-Latest technological advances in sensors, low-power built-in circuits, and wireless communications have enabled the design of low-cost, miniature, lightweight, and smart physiological sensor nodes. Wireless physique area networks (WPANs) are emerging as predominant networks, relevant in various fields. Wireless body area network (WBAN) is a novel technology to furnish effective, easy and safe wellness, clinical and private amusement services however it still faces longstanding challenges in the application. A review on implementations, advantages and drawbacks of the vigor efficient routing protocols mannequin for the wireless body discipline community is made. This case gain knowledge of investigates energy efficient Mac protocol and offers an overview on the success and the possibility of the failure related to the protocol. This paper helps to understand additionally a assessment amongst the three routing protocols on the more than a few parameters which are viewed to be the most influential in physique area networks. The paper offers an insight on the parameters that must be taken care to make the entire process vigor-aware ,power-effective and energy efficient.**

Keywords-Wireless Body Area Network, Mac Protocol, routing protocols, Power Consumption, Energy efficiency

1. INTRODUCTION

Wireless Sensor Networks

A wireless sensor network (WSN) is a network containing a group of very small sized sensor nodes which are deployed in a field to monitor physical conditions autonomously. WSNs measure a great number of physical conditions like sound, pressure, temperature etc. Sensor nodes then pass this sensed data to a base station or sink. The current advance WSNs control the activity of sensor node and are bidirectional. Most of the advancements in WSN is shown in military applications. WSNs are deployed in many industrial applications to monitor industrial process, industrial control and monitoring health of machine. The WSN's are composed of 'sensor nodes' which can be few in numbers, hundreds or thousands in numbers. A sensor node in WSN is connected with other sensor node or with several sensor nodes. Components of sensor node are, a microprocessor or a microcontroller to control the operation of node, to interface sensors with power source, a radio transceiver to communicate and an electronic circuitry is used. Either energy is harvested from any available source or batteries are normally used as power source in these sensors. Sensor node size varies according to application, as sensor node can have a size of a tiny senor like dust grain or as big as a shoe box . Similarly the sensors have variable cost. The price of a sensor node may range from few dollars to hundreds of dollars as a node contain complex circuitry and advance features. Many of the topologies used in these networks are like simple star topology or advance multihop topologies [8].

II. CHALLENGES IN WBAN

A. Interoperability:-

To provide plug and play interaction between devices, the data must have to exchange across standards. The data of one standard has to transfer to another standard. The system would have to migrate from one network to another network and during this transfer the connectivity should not be interrupted. In addition, the system must have the capability to scale.

B. System devices:-

The WBAN sensors are mostly used for medical applications so the weight of these sensors must be small, so they can easily placed on the human body or implant inhuman body. Sensor would have to energy efficient as they have to run for several years to monitor patient. WBAN sensors must be reconfigurable and easy to use. In addition to that the patient data must be store in remote storage devices so that the medical specialist can view and analyze the data through internet.

C. System and device-level security:-

The patient's data is very important for its health monitoring so it must be secure. The standard must support security and accurate data transfer. It is highly required that the patient's data securely transfer to WBAN system coordinator and the data of one patient should not mix up with data of another patient. The data generated of a patient would have limited access and must be highly secure.

D. Invasion of privacy:-

The WBAN technology is used for human health monitoring, however some people consider that this technology may cause threat to freedom if the use of the technology cross the limits of secure medical use.

E. Sensor validation:-

The sensing node in WBAN technology must have reliable wireless communication link. These sensing devices have inherent communication limitations in form for limited energy source and interference. These inherited issues in WBAN may cause false data transmission back to user. For health care application or patient monitoring application, it is very important that the readings of the patient are valid and then securely transmitted to medical server. It can overcome false alarms.

F. Data consistency:-

The data of a patient sensed by wireless sensors must be gathered to analyze in smooth way. The vital data of a patient resides on multiple nodes and transmitted to other networked medical servers. This data must reach to medical specialist for further analysis, if not then the quality of patient's health care and monitoring process decays [10].

G. Interference:-

In WBAN technology the body sensors must have minimum interference in wireless link. The body sensors must increase peaceful existence with the other devices of network. It is required for implementation of large network [11]

H. Motivation:-

In current era of technology, applications of wireless sensor networks (WSNs) are rising in various fields. The deployment of WSNs for real life applications is greater than before. Still, the energy constraints remain one of the key issues; it prevents the complete utilization of WSN technology. Sensors typically powered with battery, which have insufficient life span. Even though renewable energy sources like solar energy or piezoelectric means are used as supplementary energy in WSNs, it is still some degree of reserve to consume energy judiciously. Proficient energy routing is thus a key requirement for a trustworthy design of a wireless sensor network.

Wireless body area network (WBAN) is an interesting application of sensor networks which can revolutionize our interaction with the outside world. WBAN like any other sensor network suffers limited energy resources and hence preserving the energy of the nodes is of great importance. Unlike typical sensor networks WBANs have few and dissimilar sensors. In addition, the body medium has its own propagation characteristic which means that the existing solution for preserving energy in wireless sensor networks might not be efficient in WBANs. The quality of the links between the nodes in WBAN is changing frequently due to the moving nature of the body. This can pose major problem especially in the energy efficiency merit. In this work we have proposed an opportunistic scheme to exploit the body movements during the walking to increase the life time of the network. The results show that comparing to the existing methods this work can increase the life time of the network.[1]

Wireless sensor networks represent a key technology enabler for enhanced health care and assisted living systems. Recent standardization efforts to ensure compatibility among sensor network systems sold by different vendors have produced the IEEE 802.15.4 standard, which specifies the MAC and physical layer behavior. This standard has certain draw backs: it supports only single-hop communication; it does not mitigate the hidden terminal problem; and it does not coordinate node sleeping patterns. The IEEE 802.15.4 standard design philosophy assumes that higher layer mechanisms will take care of any added functionality. Building on IEEE 802.15.4, this paper proposes Time zone Coordinated Sleep Scheduling (TICOSS), a mechanism inspired by MERLIN that provides multi-hop support over 802.15.4 through the division of the network into time zones. TICOSS is cross-layer in nature, as it closely coordinates MAC and routing layer behavior. The main contributions of TICOSS are threefold:

(1) it allows nodes to alternate periods of activity and periods of inactivity to save energy;

(2) It mitigates packet collisions due to hidden terminals belonging to nearby star networks;

(3) it provides shortest path routing for packets from a node to the closest gateway.

Simulation experiments confirm that augmenting IEEE

802.15.4 networks with TICOSS doubles the operational lifetime for high traffic scenarios. TICOSS has also been implemented on the Phillips Aquis Grain modules for testing and eventual deployment in assisted living systems.[2]Recent technological advances in sensors, low-power microelectronics and miniaturization, and wireless networking enabled the design and proliferation of wireless sensor networks capable of autonomously monitoring and controlling environments. One of the most promising applications of sensor networks is for human health monitoring. A number of tiny wireless sensors, strategically placed on the human body, create a wireless body area network that can monitor various vital signs, providing real-time feedback to the user and medical personnel. The wireless body area networks promise to revolutionize health monitoring. However, designers of such systems face a number of challenging tasks, as they need to address often quite conflicting requirements for size, operating time, precision, and reliability. In this paper we present hardware and software architecture of a working wireless sensor network system for ambulatory health status monitoring. The system consists of multiple sensor nodes that monitor body motion and heart activity, a network coordinator, and a personal server running on a personal digital assistant or a personal computer.[3]Recent technological advances in sensors, low- power integrated circuits, and wireless communications have enabled the design of low-cost, miniature, lightweight, and intelligent physiological sensor nodes. These nodes, capable of sensing, processing, and communicating one

or more vital signs, can be seamlessly integrated into wireless personal or body networks (WPANs or WBANs) for health monitoring. These networks promise to revolutionize health care by allowing inexpensive, non-invasive, continuous, ambulatory health monitoring with almost real-time updates of medical records via the Internet. Though a number of ongoing research efforts are focusing on various technical, economic, and social issues, many technical hurdles still need to be resolved in order to have flexible, reliable, secure, and power-efficient WBANs suitable for medical applications. This paper discusses implementation issues and describes the authors' prototype sensor network for health monitoring that utilizes off-the-shelf 802.15.4 compliant network nodes and custom-built motion and heart activity sensors. The paper presents system architecture and hardware and software organization, as well as the authors' solutions for time synchronization, power management, and on-chip signal processing.[4]Sensor networks have many potential applications in biology, physics, medicine, and the military. One major challenge in sensor networks is to maximize network life under the constraint of limited power supply. The paper addresses energy-efficiency in the context of routing and data gathering. A new protocol proposed: Hybrid Indirect Transmission (HIT). HIT is based on a hybrid architecture that consists of one or more clusters, each of which is based on multiple, multi-hop indirect transmissions. In order to minimize both energy consumption and network delay, parallel transmissions are used both among multiple clusters and within a cluster. This is made possible by having each sensor independently compute a medium access controlling TDMA schedule. The computation within each sensor is intelligent yet simple. Formal analysis shows that it requires O(n) space and O(n long) time complexities, and O(1) setup messages prior to the computation, where n is the total number of sensors. HIT does not require sensor nodes with CDMA capability, or the remote base station to compute a data gathering schedule. Performance is evaluated by simulating and comparing HIT with three other existing protocols, including Low Energy Adaptive Clustering Hierarchy (LEACH), Power Efficient Gathering for Sensor Information System (PEGASIS), and Direct Transmission. Results have shown that HIT greatly reduces both energy consumption and network delay; it also maintains longer network life compared to these three existing protocols. Security issues and a potential application of HIT in biomedical sensing technology are also rigorously discussed. This work is significant to the advancement of energy-efficient micro sensor networks; the proposed protocol is promising and would contribute to the use of wireless micro sensor networks in future biomedical sensing technologies.[5]we introduce a multi-tier telemedicine system and describe how we optimized our prototype WBAN implementation for computer-assisted physical rehabilitation applications and ambulatory monitoring. The system performs real-time analysis of sensors' data, provides guidance and feedback to the user, and can generate warnings based on the user's state, level of activity, and environmental conditions. In addition, all recorded information can be transferred to medical servers via the Internet and seamlessly integrated into the user's electronic medical record and research databases.[6] This paper presents an energy-efficient medium access control protocol suitable for communication in a wireless body area network for remote monitoring of physiological signals such as EEG and ECG. The protocol takes advantage of the static nature of the body area network to implement the effective time-division multiple access (TDMA) strategy with very little amount of overhead and almost no idle listening (by static, we refer to the fixed topology of the network investigated). The main goal is to develop energy-efficient and reliable communication protocol to support streaming of large amount of data. TDMA synchronization problems are discussed and solutions are presented. Equations for duty cycle calculation are also derived for power consumption and battery life predictions. The power consumption model was also validated through measurements. Our results show that the protocols energy efficient for streaming communication as well as sending short bursts of data, and thus can be used for different types of physiological signals with different sample rates. The protocol is implemented on the analog devices ADF7020 RF transceivers.[7]

III. ENERGY-EFFICIENT LOW DUTY CYCLE MAC PROTOCOL FOR WIRELESS BODY AREA NETWORKS

Ambulatory biomedical signal monitoring has been an area of rapid growth in recent years. With advancement in storage and wireless technologies has resulted in an increase in the number of recording devices available capable of monitoring patients outside of a clinical setting. With these devices, wireless communications are used to stream data from the patient to a central storage device. As a result of the power consumed for data transmission and the requirement for long battery lifetime, there is a strict limit on any further processing, which the device could perform. With a reduction in communication power, low power signal processing techniques could be employed in order to provide relevant information, reduce transmission and/or storage, and reduce the analysis workload on the medical staff. This will enable sensors to be smart by performing more signal analysis on the sensor side. Wireless body area networks (WBANs) have enabled the deployment of lightweight, portable

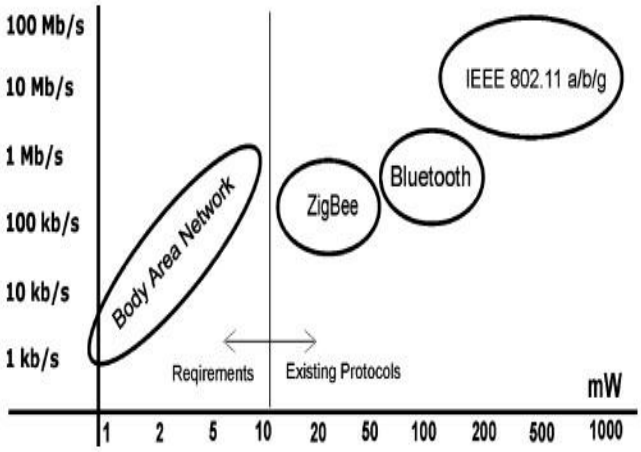

Figure 1. Data rates and power requirements for WBAN

From figure 1. it can be seen that BAN protocols should be more power efficient compared to existing commercial protocols [12].Sensors replacing the need for patients to spend long periods in hospital for routine monitoring. This enhances quality of life for patients and also has impact on medical care cost reduction. WBAN consist of a number of sensors that are either connected with a person's body or are small enough to be implanted. One of the main constraints for such systems is the power consumption since power supply is very limited.

These sensors need to transmit data at relatively wide range of data rates from 1 kbit/s to 1Mbit/s (body temperature, ECG, EEG, electromyography (EMG), movement, etc.). Fig. 1 shows that current technology meets the speed levels required for a body area network (BAN), but still does not meet the power requirement of less than 10 mW. While there has been some progress in this area, most devices used in WBAN applications store all the recorded data or transmit them to a monitoring station (MS) using IEEE 802.15.1 (Bluetooth) or
802.15.4 (ZigBee) protocols. These wireless standards are well documented and tested, but are not an ideal choice for the WBAN since they are targeted to more flexible networks than this and used for longer transmission ranges. This makes them not as energy efficient as the protocols that are specifically targeted at a BAN. A comparison and optimization of two popular WBAN technologies, Bluetooth and ZigBee, is given in the comparative study, in terms of design cost performance and energy efficiency.Table.1 differentiates the three Mac Protocols according to their operation, advantage and disadvantage [14].

Table.1. Classification of MAC Protocols

Power efficient Mechanism	Basic Operation	Advantage	Disadvantage
Contention based (CSMA/CA)	(CSMA/CA) have their nodes contended for channel access prior to transmission.	Collision of the data is avoided, Low delay, reliable communication.	Extra energy utilization for collision detection and collision avoidance
Schedule Based (TDMA)	Access to the channel is divided into time slots that are of fixed or variable duration	Collision free, low overhearing, Low duty cycle operations.	Need to pay an extra energy cost for time synchronisation, non-adaptability and scalability.
Low Power Listening (LPL)	Uses preamble sampling technique for communication between the nodes	Reduce idle listening using non-persistent CSMA and preamble sampling technique.	Sensitive to traffic rates which results in degradation of performance in the scenario of highly varying traffic rates.

2. ENERGY-EFFICIENT MULTI-HOP MEDICAL SENSOR NETWORKING

The ageing population in many developed countries highlights the importance of novel technology-driven enhancements to current health care practices. Recent technological developments in the fields of sensing, actuation, processing, wireless communication, and information management have fueled increased interest in technology-enhanced health care. For example, a wireless network of sensor and actuator node scan be deployed in an elderly person's home (with the person consent) to assist the person in living independently for as long as possible. Another example is the use of wireless sensor networks to monitor hospital patient vital signs to allow the patient's greater freedom of movement.

A major enabling technology of enhanced health care systems is wireless sensor networks (WSNs). The large scale adoption of WSN technology for health care systems will depend on the Quality-of-Service (QoS) provided by these networks, namely the reliability, latency, and efficiency. QoS provision in WSN's is tightly coupled with the medium access control (MAC) protocol. The MAC layer is responsible for coordinating channel access, such as transmission scheduling to maximize throughput and to avoid packet collisions. To ensure network longevity and acceptable end-to-end packet delay, MAC protocols for sensor networks target a balance between energy efficiency and end-to-end packet delay at the expense of data throughput.

Requirements of sensor network MAC protocols:

• Coordinated sleep states: recent studies revealed that the transceiver activity (transmitting and receiving) is one of the main sources of node energy consumption; therefore alternating periods of activity (radio on) to periods of inactivity (sleeping) can lead to significant reductions in energy consumption reduction. However, communication between neighboring nodes necessitates simultaneous node activity, so coordinated sleeping is necessary.

• Multi-hop communication: in order for a transmitter and receiver pair to communicate, the required transmitting power Pt changes exponentially with the distance D. Significant energy saving can be achieved by reducing the sensor transmitting power and by enabling multihop communication.

• Hidden node avoidance: Sensor network MAC protocols should provide mechanisms to avoid the hidden terminal problem (HTP) that is characteristic of distributed wireless communication networks. The recent IEEE 802.15.4 standard developed for energy efficient WSNs assumes that higher layers will handle the above requirements. The IEEE 802.15.4 standard only supports a single star-topology network, in which several child nodes communicate with a designated coordinator node.The communication performance seriously degrades when the system scales to a larger network which includes several nearby star-networks in the same area.

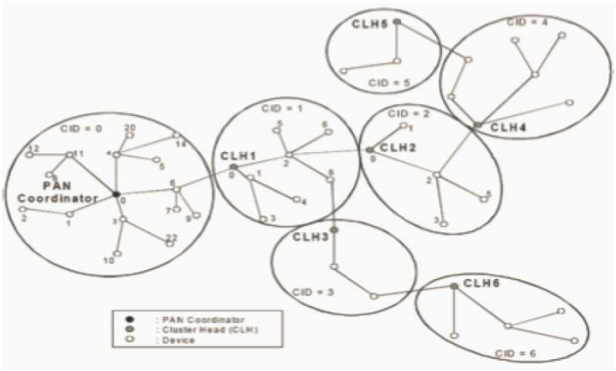

Figure 2: Cluster tree network

The Fig 2 defines different cluster zones nodes implementation and cluster-head formation [15].The IEEE 802.15.4 also cannot control the channel access within a multiple star topology network, leaving the resolution of multi-hop routing for higher layer protocols. Furthermore, the 802.15.4 standard does not provide any mechanism to avoid the HTP or to coordinate sleeping patterns in multi-hop peer-to-peer networks.

Building on the IEEE 802.15.4 standard, this paper proposes a mechanism called Time zone Coordinated Sleep Scheduling (TICOSS) that provides multi-hop support, HTP mitigation, and coordinated sleeping through the division of the network into time zones. The time zone concept adopted from the recent developed MERLIN mitigates the HTP by ensuring that nodes in neighboring zones do not transmit simultaneously. The time zones also provide coordinated sleeping, through the V-table scheduling, and shortest path multi-hop routing. The adoption of MERLIN is due to its earlier comprehensive evaluation in that presented a superior energy/delay performance than existing protocols for WSNs.

IV. CONCLUSION

The review paper is based on the study of various methods which are based on energy efficient wireless body area networks (WBAN). The purpose of study is to find the better sensor networks which are more energy efficient, the design of low-cost, miniature, lightweight, and smart physiological sensor nodes. In the paper named “Energy-Efficient Multi-hop Medical Sensor Networking“, a comparison of the network lifetime between 802.15.4 with and without TICOSS specification of more complex issues to upper layers. This paper has described improvements to the IEEE 802.15.4 standard by setting all nodes to FFDs then imposing a time zone coordinated sleeping mechanism named TICOSS to (1) save energy; (2) mitigate hidden terminal collisions through V- table scheduling; (3) provide configurable shortest path routing to the PAN coordinator. Whereas In the paper, “Energy-Efficient Low Duty Cycle MAC Protocol for Wireless Body Area Networks presented a novel low power reliable MAC protocol. Energy model was proposed and validated through measurements. WBAN with our protocol can be used in the EEG monitoring scenario. Reducing the power requirements for the communication part of the system allows allocation of more energy to more accurate DSP for seizure detection. The paper “Energy-Efficient Multi-hop Medical Sensor Networking” is dealing more efficiently with Mac protocols in WBAN. More hybrid methods can be a possibility to reduce energy consumption and increase power efficiency.

REFERENCES

[1] Maskooki, A., Soh, C.B., Gunawan, E. and Low, K.S., 2011, January. Opportunistic routing for body area network. In 2011 IEEE Consumer Communications and Networking Conference (CCNC) (pp. 237-241). IEEE.

[2] Ruzzelli, A.G., Jurdak, R., O'Hare, G.M. and Van Der Stok, P., 2007, June. Energy-efficient multi-hop medical sensor networking. In Proceedings of the 1st ACM SIGMOBILE international workshop on Systems and networking support for healthcare and assisted living environments (pp. 37-42). ACM.

[3] Otto, C., Milenkovic, A., Sanders, C. and Jovanov, E., 2006. System architecture of a wireless body area sensor network for ubiquitous health monitoring. Journal of mobile multimedia, 1(4), pp.307-326.

[4] Milenković, A., Otto, C. and Jovanov, E., 2006. Wireless sensor networks for personal health monitoring: Issues and an implementation. Computer communications, 29(13), pp.2521-2533.

[5] Culpepper, B.J., Dung, L. and Moh, M., 2004. Design and analysis of Hybrid Indirect Transmissions (HIT) for data gathering in wireless micro sensor networks. ACM SIGMOBILE Mobile Computing and Communications Review, 8(1), pp.61-83.

[6] Jovanov, E., Milenkovic, A., Otto, C. and De Groen, P.C., 2005. A wireless body area network of intelligent motion sensors for computer assisted physical rehabilitation. Journal of NeuroEngineering and rehabilitation, 2(1), p.1.

[7] Marinkovic, S.J., Popovici, E.M., Spagnol, C., Faul, S. and Marnane, W.P., 2009. Energy-efficient low duty cycle MAC protocol for wireless body area networks. IEEE Transactions on Information Technology in Biomedicine,13(6), pp.915-925.

[8] M. F. F. B. Ismail and L. W. Yie, “Acoustic monitoring system using wirelesssensornetworks,” Procedia Engineering, vol. 41, pp. 68–74, 2012.

[9] S.-D. Bao, Y.-T.Zhang, and L.-F. Shen, "Physiological signal based entity authenticationfor body area sensor networks and mobile healthcare systems," in Engineeringin Medicine and Biology Society, 2005. IEEE-EMBS 2005.27th AnnualInternational Conference of the, pp. 2455–2458, IEEE, 2005.

[10] R. Kaur, "Wireless body area network & its application," 2011.

[11] Wang and H. Liang, "Research and improvement of the wireless sensor networkrouting algorithm gpsr," in Computing, Measurement, Control and Sensor Network (CMCSN), 2012 International Conference on, pp. 83–86, IEEE, 2012.

[12] S. Drude, "Requirements and application scenarios for body area networks," in Proc. Mobile Wireless Commun. Summit, 2007, 16th IST, Jul. 1–5, pp. 1–5.

[13] JK.Murthy,V.Sambasiva Rao May 2013 "Improved Routing Protocol for Health Care Communication," in Open Journal of Applied Biosensor,2013, 2, 51-56.

[14] P Sinval,A K Rangra," A Review of Mac Protocols for Wireless Body Area Networks "IOSR Journal of Computer Engineering (IOSR-JCE) e-ISSN: 2278-0661,p-ISSN: 2278-8727, Volume 18, Issue 1, Ver. III (Jan – Feb. 2016), PP 55-65.

[15] IEEE Computer Society,"Wireless Medium Access Control (MAC) and Physical Layer (PHY) Specifications for Low-Rate Wireless Personal Area Networks (LR-WPANs)" IEEE Std 802.15.4™-2003.

Brain Tumor Extraction System using Fuzzy c-means

Arshpreet Singh
M-tech Student ,ECE Dept.
Baba Banda Singh Bahadur Engineering College,
Fatehgarh Sahib,Punjab ,India

Harpreet Kaur
Assistant Professor,ECE Dept.
Baba Banda Singh Bahadur Engineering College,
Fatehgarh Sahib,Punjab ,India

***Abstract*— Digital image processing is gaining attraction in field of research nowadays specially in medical science. For medical diagnosis scanning and inspection of inner organs of human body is possible by medical image processing technique. Brain tumor is naturaly serious and deadliest disease. Highly accurate methods are the need of the day than manual detection techniques. In this paper Brain Tumor is detected using Fuzzy c-means algorithm techniques having input from magnetic resonance imaging(MRI) . Main concern of the work is to obtain highly accurate ,less time consuming and fully automatic brain tumor detection system. It has been studied that algorithm Fuzzy c-means(FCM) gives the more accuracy. Human body is a combination of many organs and brain is the most vital and critical organ among all the other organs. It is observed that if the growth of brain tumor cells is increased rapidly than it become incurable that's why fast and accurate methods are preferred.**

Keywords*— *Tumor, Fuzzy c-means , segmentation and Magnetic Resonance .

I. INTRODUCTION

Now days doctors use smart mouted systems in which doctors study the MRimages of patients manually which results in lower accuracy ,more time consuming and higher Acumen difference. Human body is a combination of many organs and brain is most vital and critical organ among all the other organs. Cells of a brain tumor grow abundantly and take up all the nutrients from healthy tissues and cells. Cause of this abundant growth of brain tumor cells results in brain failure which leads to death of a patient[1]. Researchers are tried to overcome this problem and many methods and algorithms are given by them .In the Era of Technology we need a system which is totally automatic and does not need any type of Human interference to get the results .This paper gives the system which automatically read the MRImages. Due to the no Human Interference chances of acumen difference become totally negligible which causes higher accuracy and very less time consuming[2]. Brain tumor is naturaly serious and life aggressive disease. Highly accurate methods are more preferable than manual detection techniques. Main objective of this paper is to obtain highly accurate, less time consuming and fully automatic brain tumor detection system. It has been studied that algorithm Fuzzy c-means(FCM) gives the highest accuracy more than 90%. In the Era of Technology highly automatic systems are more preferred than manual or semi-automatic systems. This results is in accurate detection of the tumor and is also considered to be very time consuming. The main consequence of this approach is that the results are highly error prone due to perception difference [3].Furthermore, brain tumors tend to have different boundaries in the different contrasts . In the case of brain tumor segmentation, several techniques exist to separate the tumor from healthy tissue, such as locating outliers of the registration of healthy atlases to the tumor , or learning textural patterns that are common to tumors [4]. Accurate measurements in brain diagnosis are quite difficult because of diverse shapes, sizes and appearances of tumors. So these are the reasons for adopting automatic brain tumor detection system.

A. Problem Formulation

Abnormal growth and unmanaged division of cells in a brain is the main reason of brain tumor. Patients suffering from brain tumor having the results of tumor more than 50% than they were unable to cover from life altering disease and results are death of patients due to brain failure. So there are many problems incurred by doctors while reading MRI images of patients manually which results in higher inaccurate results with more time consumed. Problem can be tackled if brain tumor is detected at initial stage and accurately. Researchers are tried to overcome this problem and many methods and algorithms are given by them. In the present scenario, need is of automatic, fast system which is also free from human interference. Main objective of this paper is to obtain highly accurate,less time consuming and fully automatic brain tumor detection system.

B. Proposed Work

As technique for extraction or can say detection of brain tumor in medical images is needed so in this paper an application which will have the option of selecting different edge detection algorithms is considered. And on basis of that one can conclude that which technique is suitable for detecting Brain tumor form medical images[4].
In our proposed work a new technique for image segmentation of medical MR images has been developed. The proposed technique works on the basis of fuzzy C-mean. In fuzzy c-mean clustering each point have some specific probability of belonging to each cluster.

II. LITERATURE VIEW

A. Magnetic Resonance Imaging(MRI)

MRI machines uses powerful magnetic scanners to excite and polarize hydrogen nuclei which is single proton in a nucleus.

In an atom neutrons and protons of the nucleus forms spin on an angular momentum. Radio Frequency(RF) is the base of MRI.Machines sends the radio frequency pulses to the specific organs of the body which are to be examined[5].

B. Image Enhancement

MRImages which are taken from the MRI scanners sometimes found that are affected by additional noise or having the poorer visual clarity. This is the very solid reason for the need of use of image enhancement.
Enhancement technique in brain tumor detection systems is used first on MRImages. There are many methods to overcome from poor visual clarity and noise for further processing of image .In earlier techniques comparison is made between the taken image and the reference image for image enhancement to get out the result difference between the images[6].

C. Image Segmentation

Image segmentation refers to the decomposition scene into its components. In this paper image segmentation is used for boundry based approaches. In image segmentation technique image is segmented into no of segments using various techniques[6]. It helps in extraction of suspicious regions from MRimages. In Boundry based extraction techniques segment the objects on the basis of their profiles[7].

D. Morphological Analysis

Morphology is the study of medical images about their shapes and structures from a scientific view. Morphology works on the integral parts of the image. Binary morphology is used to complete the binary events which make extraction of objects from binary images. In Morphological analysis various techniques have been used such as Multiscale morphology and Fuzzy mathematical morphology (FMM). Erosion, Dilation ,open and close are the operators of morphology[8]. There are two fundamental operator in morphological Erosion and Dilation are one of them in image processing on which all morphological operations are based. These are originally defined for binary images and later being for gray scale images. On the other hand Opening removes the small objects from the foreground and closing removes the small holes from the foreground [9].

III. PROPOSED METHODOLOGY

A. Fuzzy c- Means

This technique is based on a fuzzy logic actually it is clustering technique used to segment the image. Clustering algorithm for fuzzy partition for optimal fuzzy. In mathematical principles fuzzy logic is used for knowledge representation based on binary logic classical degrees. For getting the intelligent human detection systems FCM allows methods in segmentation to perform the relevant tasks to approach the result. Fuzzy c-means is based on a clustering technique. In image segmentation Fuzzy c-means gives the higher accuracy among all another techniques. For the purpose of overcome the weakness of PCM method fuzzy c-means is used .Fuzzy is also called advanced version of K-means algorithms due to the assigning of objective functions[10].

B. FCM Parametres

Input unlabelled data set- x={x1,x2,x3-----xn}

n is the data point in x (1)

Main output

Partion of x, which is c*n matrix U (2)

Common additional Output

Set of vectorsV={v1,v2,v3,----vn} (3)

V1 is called cluster centre

From equation (1) input values are assigned and from equation (2) and (3) output are calculated[10].

IV. EXPERIMENTAL RESULTS

During experiment input is taken as MRimage from online respiratory in jpeg format of size(640*720). No of MRImages are taken for experimentation and good results are obtained.

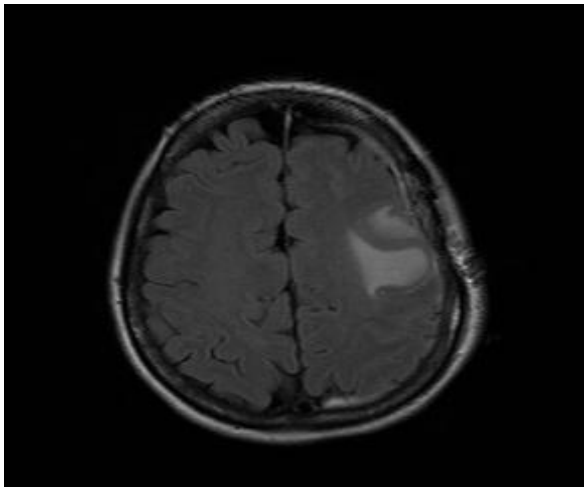

Fig.1. Input Image-1

In Fig.1 and Fig.2 represents input MRImage. By reading MRimages manually not clearer results are obtained about the size and type of Tumor. For experimentation two input images are taken to come to know about the location and type of tumor. Doctors take any type of MRImage but the condition is that format must be Jpeg.

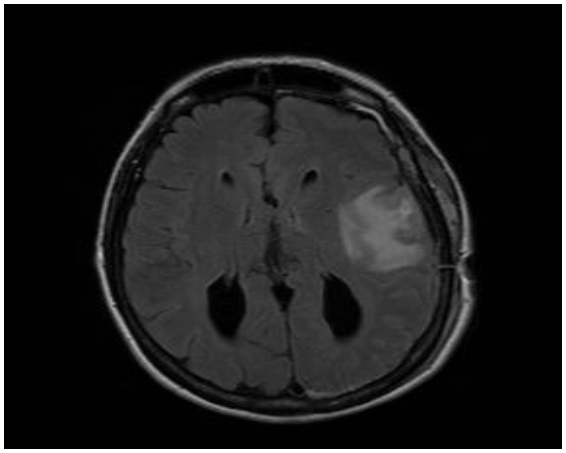

Fig.2. Input image-2

Input is given in the form of jpeg images by using command 'uigetfile' paper can browse image from any folder in the pc or laptop. There is no need to assign path manually in the MATLAB software. It is shown below in Fig-3 the MRimage chosen from a no of input images.

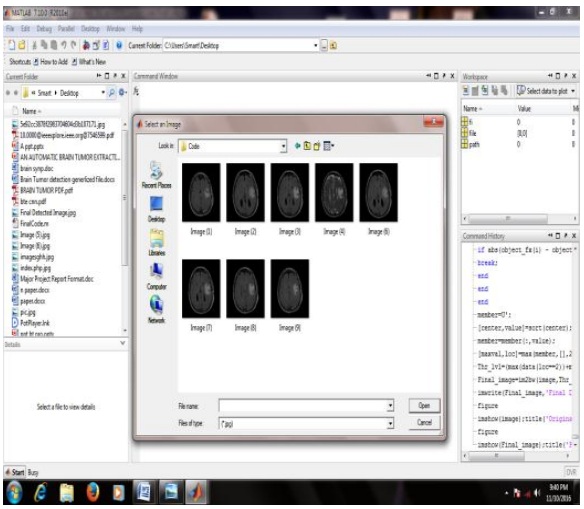

Fig.3. selection of MRImages

Maximum 999 iterations are performed for getting better results on a single MRImage. When objective function becomes constant and level of minimum improvement comes. Break command breaks the program execution and returns result in the form of accurate tumor detected with less time. In Fig.4, System performing iteration in Matlab software by running Matlab code. No of Iterations are mainly depends upon the type of input MRImage. By changing the value of impro command in Matlab code, no of iterations performed by the system can be increased or decreased. After performing iterations when objective function becomes constant output is obtained in the form of tumor detected having higher accuracy and less computational time. Which is shown in Fig.5 and Fig.6.

From the experimental results we obtain a system which is fully accurate, very less time consuming and and with negligible perception difference.

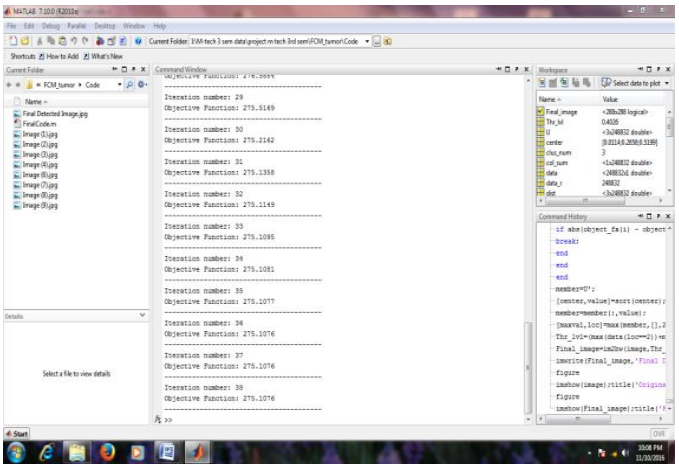

Fig.4. system performing iterations

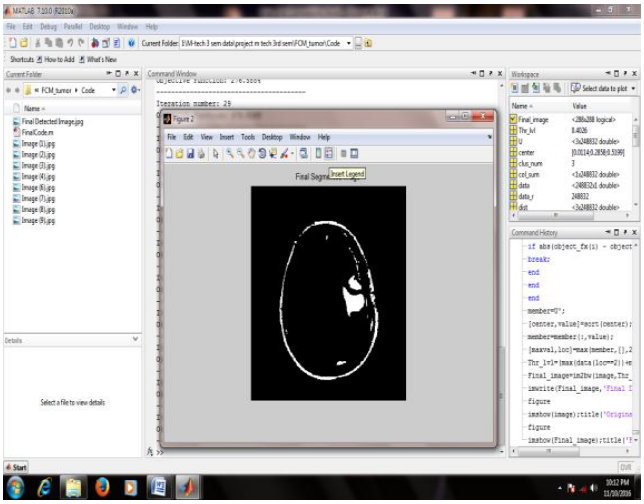

Fig.5. output of detected tumor of input image 1

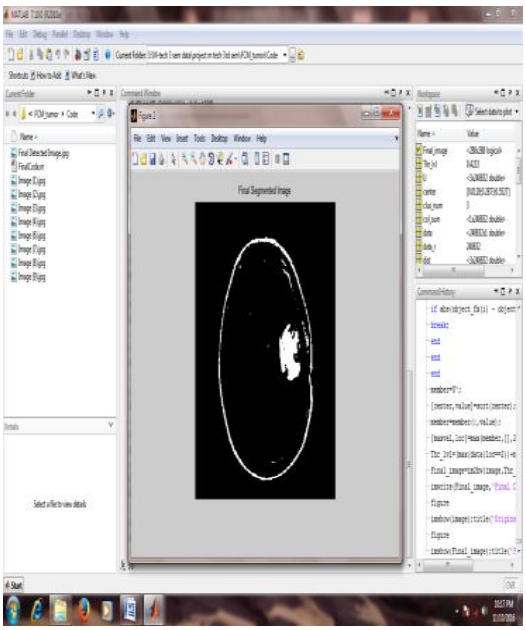

Fig.6. output of detected tumor of input image 2

V. CONCLUSION

Using the proposed technique a highly accurate method with less time consuming is found which also reduces the manual work to be done by doctors and with minimum human interference. So highly automatic system can be made in which chances of errors are less and acumen difference is fully negligible.

REFERENCES

[1] A. Kaur, "An Automatic Brain Tumor Extraction System using Different Segmentation Methods".Second International Conference on computational intelligence & communication technology,(2016 IEEE) pp 187-191.

[2] M.Karuna, A.Joshi, 2014**"**Automatic Detection And Severity Analysis Of Brain Tumors Using Gui In Matlab" International Journal of Research in Engineering and Technology, eISSN:2319-1163/pISSN:2321-7808, Volume 02 issue/oct -2013,pp586-593.

[3] S. Ben Chaabane, "Color Image Segmentation Using Automatic Thresholding and the Fuzzy C-means Techniques",Proceedings 14th IEEE Mediterranean Electro technical Conference, 2008, pp. 857-861.

[4] S. Agrawal , Prof. Dr. S. R Gupta., 2014**,** "Detection of Brain Tumor Using Different Edge Detection Algorithm" International Journal of Emerging Research in Management and Technology,(April 2014) pp85-89.

[5] N.Subbanna.,2014 "Iterative Multilevel MRF Leveraging Context and Voxel Information for Brain Tumor Segmentation in MRI"IEEE Pp 4321-4326" .

[6] P.K Srimani and S. Mahesh,2013 "A Comparative Study of Different Segmentation Techniques for Brain Tumor Detection" International Journal of Emerging Technologies in Computational and Applied Sciences,pp192-197.

[7] A. Singh , K. Kant Singh, "A Study Of Image Segmentation Algorithms For Different Types Of Images", International Journal of Computer Science Issues, vol. 7,Issue 5, pp 414-417,2010

[8] A.Hakeem Aejaz , 2013 "A New Approach to Image Segmentation for Brain Tumor detection Pillar K-means Algorithm", IJARCCE, Vol. 2, Issue 3, pp 1429-1436.

[9] K.Thapaliya, and G.Rak Kwon, "Extraction of Brain tumors based on morphological operations",. 8th International Conference on Computing Technology and Information Management (ICCM), 515-520, 2012.

[10] M.amiri. "Fuzzy c-means clustering course paper presentation", june 2003 sharif university of technology.

Comparative Analysis of Q-factor For Notch Filter Designing in Cardiological Signal Processing

Rohit Gupta
ME scholar
PEC University of technology
Chandigarh

Sulata Bhandari
Associate Professor
PEC University of technology
Chandigarh

Sandeep Kaur
Assistant Professor
PEC University of technology
Chandigarh

***Abstract* –Electrocardiogram is a signal which measures the electrical activity of the heart. Normal heart beat for human is 70 cycles per minute. Any change in natural sequence of activities of heart like beating too fast, too slow or erratically is Arrhythmia, and this can be detected by analyzing ECG of the subject. The recorded ECG potentials are usually contaminated by power-line frequencies which lie within the frequency spectrum of ECG signal making it difficult to extract useful information from it; this interference is suppressed using 50/60Hz notch filter. It has been shown that notch filter application deforms the QRS complex of the electrocardiogram. In this paper a comparative analysis of the impact for different values of Q-factor of the notch filter, on QRS complex of Electrocardiogram has been shown.**

***Keywords*- ECG, Q-factor, Notch filter, interference**

I. INTRODUCTION

Electrocardiogram (ECG) is the record of electrical activity of heart (Fig. 1). ECG machine is a device through which we record this electrical activity. This device is connected by wires to electrodes pasted on patient's chests at particular position [1]. Around 12 million deaths occur worldwide each year due to cardiovascular diseases as stated by the World Health Organization. Due to the insufficient supply of blood in the heart the clogging occurs and thus Coronary Heart Disease (CHD) takes place [2][3][4]. The cardiac arrhythmias accounts for ninety percent of the deaths due to cardiovascular diseases [5]. Arrhythmias are seen as an abnormal function of the heart.

There have been several researches in the field of arrhythmia detection. Adams and Choi [5] proposed a method based on ANN to classify different arrhythmias using the QRS complex as features of ECG. Another neural network based classification of ECG for Premature Ventricular Contractions using Wavelet transform was done by Inan et al [6] with an accuracy of 88%. Patel et al [7] proposed arrhythmia detection method based on peak detection of QRS complex. They concluded that QR S complex is an important feature for classification of arrhythmia. Rahman and Nasor [8] used the QRS complex to define and classify different types of arrhythmia. Li, Zheng an d Tai [9] detected ECG characteristic points using wavelet transforms for the detection of QRS, T, and P waves [10].

ECG signal consists of a P wave, a QRS complex, and a T wave (Table 1). Before contraction the electric currents due to atrial depolarization causes P, while the depolarization due to ventricle contraction causes QRS complex. During recovery of the ventricles from the state of depolarization the T wave is formed.

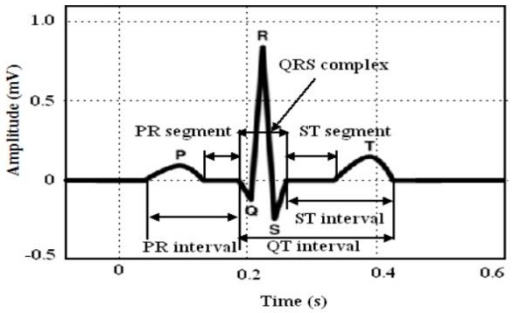

Fig. 1 Schematic representation of normal ECG waveform

Table 1 Amplitude and duration of waves, intervals and segments of ECG signal.

Sl. no.	Features	Amplitude (mV)	Duration (ms)
1	P wave	0.1-0.2	60-80
2	PR-segment	-	50-120
3	PR- interval	-	120-200
4	QRS complex	1	80-120
5	ST-segment	-	100-120
6	T –wave	0.1-0.3	120-160
7	ST-interval	-	320
8	RR-interval	-	(0.4-1.2)s

The T-wave is characterized as the wave of re-polarization. Fig. 1 shows a representation of an ECG with the waves [11].

II. NOISE IN ECG SIGNAL

Unfortunately the acquired ECG does not only consist of the components derived from the electrical functionality of the heart, but it is very often contaminated by artifacts that can interfere or interrupt the signal and result in loss of information. Sometimes, these artifacts might even present with similar morphology as the ECG [11]. The most commonly found artifacts in the ECG are:

1. Power-line interference, which is characterized by a frequency of 50 or 60 Hz depending on the country.
2. Steep voltage changes form the loss of contact between the electrodes and the skin.

3. Electrical activity from muscle contractions that varies from dc to10kHz.
4. Baseline drift which is usually caused from respiration at very low frequencies, around 0.1v 0.3Hz.

III. POWER LINE INTERFERENCES

In this paper we will deal with only Power line interferences that contains 60 Hz pickup (in U.S.) or 50 Hz pickup (in India) because of improper grounding.

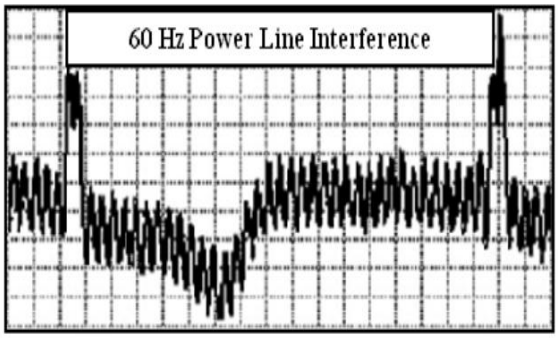

Fig.2 60 Hz Power line interference.

It is indicated (Fig. 2) as an impulse or spike at 60 Hz/50 Hz harmonics, and will appear as additional spikes at integral multiples of the fundamental frequency. Its frequency content is 60 Hz/50 Hz and its harmonics, amplitude is up to 50 percent of peak-to-peak ECG signal amplitude. A 60 Hz notch filter can be used remove the power- line interferences [11].

IV. CASE STUDY

For this study, the data used is publicly available MIT-BIH arrhythmia database at physionet.org [12] The complete data set consist of 48 sets each containing set of 2 channels. Each set is divided into normal and arrhythmia set. The length of each recording is 27.7 seconds. The sampling rate of data is 360 Hz. In most records, the upper signal is a modified limb lead II (MLII). The lower signal is usually a modified lead V1 (occasionally V2 or V5, and in one instance V4 [13]

V. NOTCH FILTER

The Notch Filter, (BSF) is another type of frequency selective circuit that functions in exactly the opposite way to the Band Pass Filter. The band stop filter, also known as a band reject filter, passes all frequencies with the exception of those within a specified stop band which are greatly attenuated.

If this stop band is very narrow and highly attenuated over a few hertz, then the band stop filter is more commonly referred to as a notch filter, as its frequency response shows that of a deep notch with high selectivity (a steep-side curve) rather than a flattened wider band.

Also, just like the band pass filter, the band stop (band reject or notch) filter is a second-order (two-pole) filter having two cut-off frequencies, commonly known as the -3dB or half-power points producing a wide stop band bandwidth between these two -3dB points.

Then the function of a band stop filter is to pass all those frequencies from zero (DC) up to its first (lower) cut-off frequency point f_L, and pass all those frequencies above its second (upper) cut-off frequency f_H, but block or reject all those frequencies in-between. Then the filters bandwidth, BW is defined as: $(f_H - f_L)$[14].

VI. NOTCH FILTER DESIGNING IN MATLAB

IIR NOTCH Second-order IIR notch digital filter is designed in MATLAB [15] as

[NUM,DEN] = IIRNOTCH (ωo,BW)

It designs a second-order notch digital filter with the notch at frequency ωo and a bandwidth of BW at the -3 dB level. The bandwidth BW is related to the Q-factor of a filter by

$$BW = \omega o/Q. \qquad [1]$$

VII. RESULTS & DISCUSSION

FFT spectrum of all the cases considered reflects almost equal suppression of power line frequency for all values of Q considered as shown in Fig. 3-6. Comparative analysis of filters with different values of Q shows that for higher value of Q the spectrum obtained (Fig. 7) is more close to the unfiltered signal (for frequencies other than power line frequency). Table 2 and 3 shows the change in position of peaks of QRS wave for different values of quality factor considered.

Removing 60Hz frequency Component

For Q=2

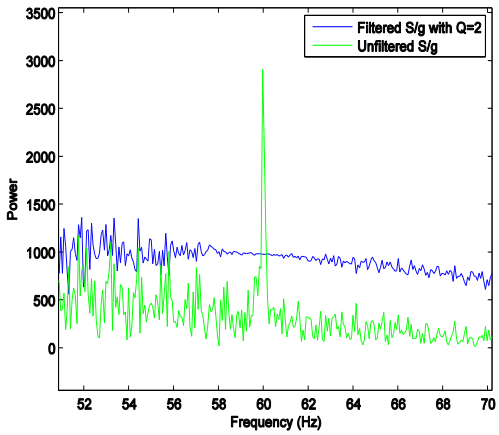

Fig.3 FFT spectrum of filtered and unfiltered ecg signal withQ=2

For Q=15

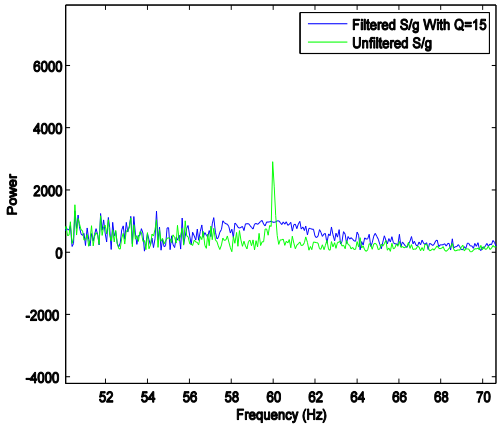

Fig.4 FFT spectrum of filtered and unfiltered ecg signal withQ=15

For Q=35

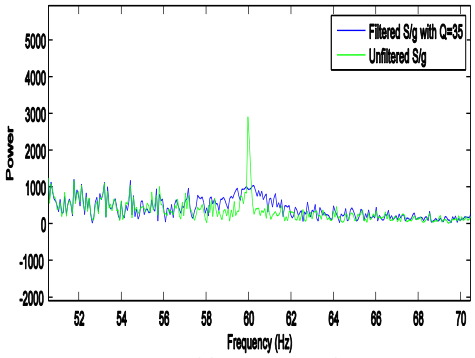

Fig.5 FFT spectrum of filtered and unfiltered ecg signal with Q=35

For Q=60

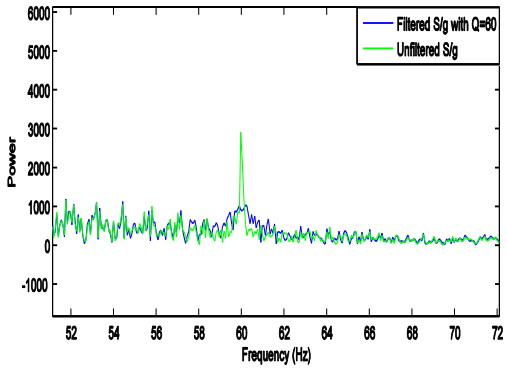

Fig.6 FFT spectrum of filtered and unfiltered ecg signal withQ=60

Comparison of notch filtered output of Q=35 and Q=15

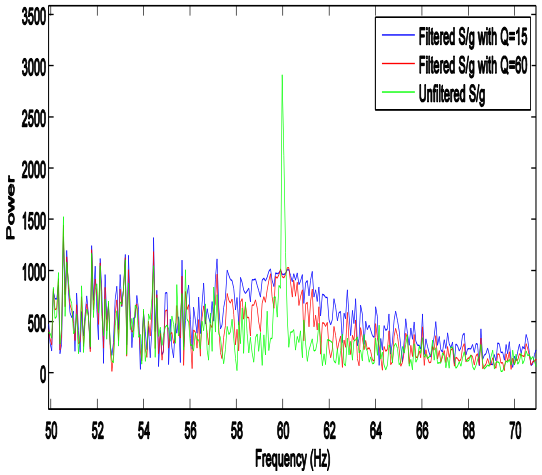

Fig.7 FFT spectrum Comparison of filtered ecg signal with Q=15 and 60

Table 2. Results showing Index no. of R-peak for Q-factor=2 and Q-factor=35

S.No.	Q Factor	Peak No	Index of R peak	Q Factor	Peak No	Index of R peak
1	2	1	5	35	1	
2	2	2	79	35	2	78
3	2	3	372	35	3	371
4	2	4	665	35	4	664
5	2	5	949	35	5	948
6	2	6	1233	35	6	1232
7	2	7	1517	35	7	1516
8	2	8	1811	35	8	1810
9	2	9	2044	35	9	2046
10	2	10	2404	35	10	2404

Table 3. Results showing percentage change in amplitude of R-peak for Q-factor=2 and Q-factor=35

S.No.	Peak No	Percentage change in amplitude
1	1	-
2	2	6.00785
3	3	1.225169
4	4	5.646113
5	5	4.500548
6	6	3.776180
7	7	5.628712
8	8	3.751535
9	9	2.838984
10	10	3.320069

VIII. CONCLUSION

For the filtering of power line frequency (60Hz for U.S.A and 50Hz for India) designing of notch filter is important step. Only after this we can extract various features from ECG signal i.e. R-R interval, Q and S peak, R peak etc. For notch filter designing the value of Quality factor is crucial. The FFT spectrum of filtered and unfiltered signal with different values of Q is shown above. As seen from the results, for low value of Q deformation of frequency spectrum is more as compared to the higher Q-factor. All the plots above reflect that for all values of Q, there is significant suppression of 60 Hz component. Results

shown in table1 and 2 clearly indicate towards the deformation of QRS complex due to the notch filter used for suppression of power line frequency. It can thus be concluded that deciding Q-factor for the notch filter plays important role in its implementation.

REFERENCES

[1] J. C. T. B. Moraes, M. M. Freitas, F. N. Vilani, E. V. Costa, "A QRS Complex Detection Algorithm using Electrocardiogram leads", Computers in Cardiology, 2002,Vol.29, pp 205-208.
[2] K. Kavitha, K. Ramakrishnan, M. Singh, "Modeling and design of evolutionary neural network for heart disease detection", IJCSI International Journal of Computer Science Issues 2010, 7(5), pp 272-283.
[3] S. Bulusu, M. Faezipour, M. Nourani, L. Tamil, and S. Banerjee, "Transient ST-segment episode detection for ECG beat classification", Life Science Systems and Applications Workshop (LiSSA), IEEE/NIH, 2011, pp 121-124.
[4] Y. Ozbay, B. Karlik, "A recognition of ECG arrhythmias using artificial neural networks", EBMS Proceedings23rd Annual Conference of IEEE at Instanbul, Turkey, 2001, pp1-5.
[5] E.R. Adams, A. Choi, "Using Neural Networks to Predict Cardiac Arrhythmias", IEEE International Conference on Systems, Man and Cybernetics at COEX, Seoul, Korea, October 14-17, 2012, pp 402-407.
[6] O. T. Inan, L. Giovangrandi, G. T. A. Kovacs, "Robust Neural-Network-Based Classification of Premature Ventricular Contractions Using Wavelet Transform and Timing Interval Features", IEEE Transactions on Biomedical Engineering, December 2006, Vol. 12, pp 2507-2515.
[7] P. G. Patel, J. S. Warrier, U. R. Bagal, "ECG Analysis And Detection Of Arrhythmia Using MATLAB", International Journal Of Innovative Research and Development, 2012, Vol.1, pp 59-68.
[8] M. Rahman, M. Nasor, "An Algorithm for Detection of Arrhythmia", International Journal of Biological Engineering,2012, 2(5), pp 44-47.
[9] C. Li, C. Zheng, C. Tai, "Detection of ECG Characteristic Points Using Wavelet Transforms", IEEE Transactions on Biomedical Engineering, January 1995, Vol. 42, pp 23-28.
[10] Y. U. Khan, N. Jain, U. Sharma and V. Chaudhary, "Arrhythmia detection based on derivative analysis of QRS complex,"*2016 3rd International Conference on Signal Processing and Integrated Networks (SPIN)*, Noida, 2016, pp. 112-115
[11] Sahoo, Jaya Prakash. Analyses of ECG signal for Detection of Cardiac Arrhythmias. Diss. MS Thesis, Department of Electronics and Communication Engineering, National Institute of Technology, Rourkela, India.
[12] A. L. Goldberger, L. A. N. Amaral, L. Glass, J. M. Hausdorff, P.Ch. Ivanov, R. G. Mark, J. E. Mietus, G. B. Moody, C. K. Peng, H. E. Stanley, "PhysioBank, PhysioToolkit, and PhysioNet: Components of a New Research Resource for Complex Physiologic Signals", June 2000, Circulation 101(23) :e215-e220.
[13] MIT-BIH Database Distribution, Massachusetts Institute ofTechnology, Cambridge, MA, 1998.
[14] http://www.electronics-tutorials.ws/filter/band-stop-filter.html
[15] https://in.mathworks.com.

Oil-Contaminated Soil Evaluation and Remediation

Ishatpreet Kaur,
Assistant Professor
Civil Engineering Department,
Baba Banda Singh Bahadur Engineering College,
Fatehgarh Sahib, India.

Manpreet Kaur,
Assistant Professor
Civil Engineering Department,
Baba Banda Singh Bahadur Engineering College,
Fatehgarh Sahib,India

***Abstract*— Humans are, unintentionally or intentionally contaminating soils from different sources. The contaminated soils are not only a challenge for the environmentalists but also for the geotechnical engineers. The surface and subsurface environment is becoming increasingly contaminated because of disposal of chemicals and waste materials produced as a result of rapid industrialization and various other human activities. All types of pollution have direct and indirect effect on soil/sub-soil. Hydrocarbon contaminated has not just affected the quality of the soil but will also alter the physical properties of oil-contaminated soil.**

Amongst the contaminants, the hydrocarbons are a major source of soil pollution; petrol and diesel being the chief contributors. A vast majority of the population use these two commodities. Amongst diesel and petrol, the consumption of diesel is higher. Therefore, diesel was selected as the pollutant and its effect on engineering properties soil (IS classification : (CL-ML) was studied and also study the effect of cement (as stabilizing agent at different percentages 3%, 7%, 11%) on the geotechnical properties of diesel contaminated soil. The soil used in the present work was obtained from Sir hind town (Punjab) and the pollutant i.e. diesel was obtained from local fuel outlet. It is apparent from the test results that the stabilization agents improved the geotechnical properties of the soil by way of cat ion exchange, agglomeration, and pozzolanic actions. UCS and CBR value of contaminated soil increased with increased cement content .This improvement in unconfined compressive strength and California bearing ratio of soil was due to neo-formations such as Calcium Silicate Hydrates (CSH, CSH_1) that coats and binds the soil particles.

Keywords—Unconfined Compressive Strength, Cement, Diesel, Soil, California bearing ratio.

I. INTRODUCTION

Contamination of land has arisen from kinds of human activity and is essentially a legacy of our recent industrial history. Sources of contamination include the deposition of waste products; industrial operations' spills and leakages, airborne contaminated dust and repeated raising and leveling of land as one industrial use supersedes another. Contaminants may be solid, liquid or gaseous and can adversely affect susceptible targets such as human, rivers, soil, sub-soil, buildings and the environment.
Hydrocarbon contamination is the most obvious concern of the industrial age. There are multiple causes for the same. The pendulum swings from oil exploration, production, processing and transportation from one end to refining, storage (surface and subsurface) transportation and distribution the other end. Petroleum contamination may also occur on right of way of the road due to leakage of diesel products from leaking oil tankers, spills due to vehicular accidents, buried pipelines, acquired properties such as rail yards an abandoned oil storage sites. The resulting environmental degradation is colossal. Not only the agricultural properties of the soil have been destroyed, the performance of soil as a construction material or as supporting material of engineering structures has been greatly affected. The detrimental effect of contaminants on properties of soil has also received attention but less than it deserves. Research has shown that leakage of hydrocarbon into sub soil directly affects the use and stability of supported structure. The unintended modification of soil properties due to interaction with contaminants can lead to various geotechnical problems (excessive settlements, loss of shear strength etc.) A sound understanding of fundamental principles of geotechnical engineering is needed to predict the behavior and performance of soil as a constructive material or as a supporting medium of engineering structures. To arrive at logical results the effect of contaminants on soil properties has got to be analyzed and studied before recommendations can be made for its employment as a constructive material/ supportive medium for structures.

By knowing the properties of such soil, applications, whether it is for structural use of as a supporting material/ medium can be decided upon economically. In India the scope of study in this field is very large. Whereas in Europe and America great strides have been made in this field, in India a concerted effort has to be made so that technologies can be developed to reclaim contaminated sites for their intended use.

II. LITERATURE REVIEW

In United States of America, US Environment Protection Agency (USEPA) carries out environment studies of selected sites. USEPA reviews all existing hydro geological aspects and can undertake test-drilling program me to define the

geology of study area. They use a variety of remote sensing techniques such as Ground Penetrating Rader and Electro Magnetic Conductivity. In the United Kingdom, the Department of Environment carries out survey of land sites. They only give the environmental impact viz water contamination details, presence of toxic material, and the harmful effect on living organisms. As far as geotechnical aspects are concerned, researchers have tackled specific issues and after carrying out field and laboratory investigations, explanations have been offered for behavior of contaminated soils. Some of the details of the investigations are given in succeeding paragraphs.

Rahman.et al. (2010) studied the Influence of Oil Contamination on Geotechnical Properties of Basaltic Residual Soil. This study presented the geotechnical properties of oil-contaminated soils as well as uncontaminated soils for comparison. Testing programs performed on the studied soils included basic properties, Atterberg's limit, compaction, permeability and unconsolidated untrained triaxial tests. The base soils used were originated from weathered basaltic rock of grades V and VI. Soil samples were artificially contaminated with 4, 8, 12 and 16% oil of the dry weight of based soils. The results showed that the oil contamination decreased the liquid limit and plastic limit values for both grades of weathered soils.
Gupta M.K et al.2010) study on Evaluation of Engineering Properties of Oil-contaminated Soils journal of the institution of engineering. The study was aimed t o investigate the impact of used engine oil, a hydrocarbon and also an organic contaminant, on important engineering properties of soils. Two cohesive soils (IS classification: CL, CH) were particularly chosen for the study. Index and engineering properties of virgin (uncontaminated) soils and soil samples artificially spiked with used engine oil (at 2%, 4%, 6% and 8% of the dry weight of the soil) were determined for comparison. It was found that the permeability increased with the increasing concentrations of contaminant for both the soils, while compression index values also increased but coefficients of consolidation values decreased. Unconfined compressive strength values were found to decrease for both the soils with the increasing oil content.

Habib-ur- rehman et al.,(2007) in his paper, has focused on Geotechnical behavior of oil-contaminated fine-grained soils The comparison between uncontaminated and crude oil-contaminated clay showed that there would be a significant change in the engineering behavior of the clay if it were contaminated by crude oil. The contaminated clay behaves more like cohesion less material, owing to the formation of agglomerates. The coarse-grained soil-like behavior was obvious in the strength behavior of the oil-contaminated clay. The contamination has affected the plasticity and the cation exchange capacity (CEC) of the investigated clay. The swelling pressure of the clay after contamination suffered three times reduction, while no change was observed in the percent swelling of the contaminated clay.

Amer Al-Rawas et al. (2005) carried out studies on Stabilization of oil-contaminated soils using cement and cement by-pass dust in Management of Environmental Quality. To investigate the effect of cement and cement by-pass dust (CBPD) as a stabilizer on the geotechnical properties of oil-contaminated soils resulting from leaking underground storage tanks, or soils surrounding petroleum refineries and crude oil wells. Oil-contaminated soil (untreated soil) and a soil treated by bio-remediation (treated soil) as well as a natural soil were obtained from Northern Oman. These soils were stabilized with cement and cement by-pass dust at 0, 5, 10, 15 and 20 percent, by dry weight of the soil, and cured for seven, 14 and 28 days. Compaction, compressive strength, direct shear, permeability and leaching tests were carried out on the stabilized soils. The results indicate that cement and cement by-pass dust improve the properties of oil-contaminated soils.
Shah et al. (2003) carried out the study on Stabilization of fuel oil contaminated soil. An attempt has been made to stabilize the contaminated soil using various additives viz., lime, fly ash and cement independently as well as an admixture of different combinations. It is apparent from the test results that the stabilization agents improved the geotechnical properties of the soil by way of cation exchange, agglomeration, and pozzuolanic actions. The best results were observed when a combination of 10% lime, 5% fly ash and 5% cement was added to the contaminated soil. The improvement in unconfined compressive strength (UCS), cohesion and angle of internal friction can be attributed to neo-formations such as Calcium Silicate Hydrates (CSH) that coats and binds the soil particles. Formation of stable complex between oil and metallic cations, results in reduction of each able oil .

III. MATERIALS & METHODS

PART –I EVALUATION OF DIESEL CONTAMINED SOIL

A. Materials: Soil

The experimental work was conducted with soil, procured from Sirhind at a depth one to two maters from ground surface. The soil is classified as silt and clay of low compressibility (CL-ML) and other geotechnical properties of the soil are listed in Table 1.

Table 1: Geotechnical Properties of soil

Properties	Value
Particle size	
Clay(%)	25.7
Silt(%)	48
Sand(%)	26.3
Consistency limits	
Liquid limit(%)	27
Plasticity Index(%)	6.615
Specific gravity	2.88
Compaction characteristics	
Optimum moisture content (OMC (%))	10.3
Maximum dry density (kN/m3)	17.658
Free swell index (%)	32.5
Unconfined compressive strength (Kpa)	140.96
Soaked CBR (%)	3.67

B. Methods

Procedure of Contamination**:** Initially, the soil is air dried and hand sorted to remove the pebbles and vegetable matter, if any. It is then oven dried, ground, pulverized and sieved through a 425µ sieve. The soil is then contaminated by Diesel oil in varying percentage i.e. 4%, 8% and 12% by weights and kept for one week period of time to ensure through absorption of contaminant in soil and tested to determine their physical and engineering properties. Evaluation of engineering properties of virgin soil and contaminated soils was done as per the relevant sections of IS: 2720. Some difficulties were encountered while doing experiments with the contaminated soil samples as the oil in soil pores together with water at times required patience and innovations. The aim of the investigation is to examine the effect of contaminant Following laboratory tests have been performed to study the geotechnical properties of soil before and after contamination.

C. Experimental Work

The experimental schedule for collecting data is shown in the following tables.

Table2: Test performed on Virgin soil and contaminated Soil

Test	Virgin soil	Contaminated soil		
		D_4	D_8	D_{12}
Atterberg's Limit	√	√	√	√
Free swell	√	√	√	√
M.D.D	√	√	√	√
O.M.C	√	√	√	√
Specific gravity	√	√	√	√
U.C.S	√	√	√	√
Soaked CBR	√	√	√	√

D=Diesel Oil, Suffix is percentage of contamination

D. RESULTS & DISCUSSION

The effect of Diesel oil contamination on geotechnical properties of (CL-ML) is shown in table 3.

Table 3: Various Geotechnical Properties of virgin soil and contaminated soil

Properties of soil	Virgin Soil	Contaminated soil		
		D_4	D_8	D_{10}
Specific Gravity	2.88	2.77	2.584	2.47
Liquid Limit (%)	27	34.2	35.7	36.7
Plastic Limit (%)	20.83	29.31	30.34	32.1
Free swell	32.5	55	52	50
Maximum Dry Density(KN/m^3)	17.658	16.97	16.677	16.48
Optimum Moisture Content (%)	10.3	9	8.75	8.00
Unconfined Compressive Strength(Kpa)	140.96	90.54	63.76	33.25
CBR % (Soaked)	3.67	2.71	1.85	1.515

E . Shear strength

Shear strength of the virgin soil and also of all the soil contaminant mixes was determined by unconfined compression strength (UCS) tests on remolded samples as per IS2720- part 10. The stress- strain relationship curves of soil corresponding to virgin state and for all the contaminant mixes are presented in figures 1. It is seen from the figure that the USC values decreased for the from soil from their virgin state with increasing percentage of contaminant. The maximum decreased for 4% oil was 50%. It is thus obvious that soil lost shear strength as the contaminant percentage increased.

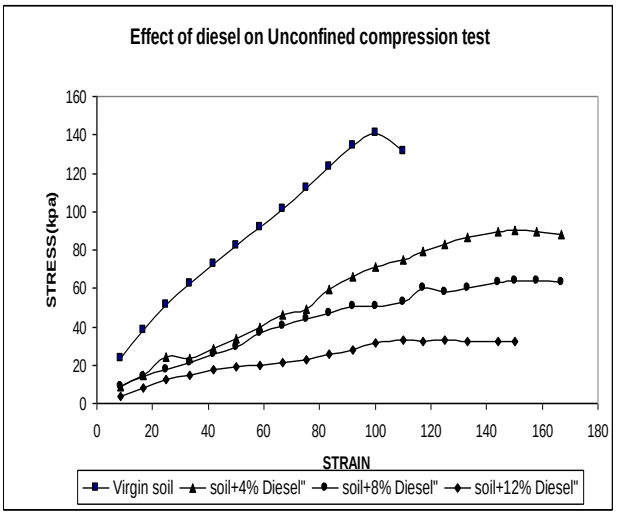

Fig -1 Effect of diesel on unconfined compression test.

F. California bearing ratio test

California bearing ratio of the treated soil samples were evaluated after curing the sample at room temperature for seven days. The CBR value (soaked) was seen to be decreasing as percentage of contaminant increased soaked CBR value reduce from 3.67% to 1.51%.

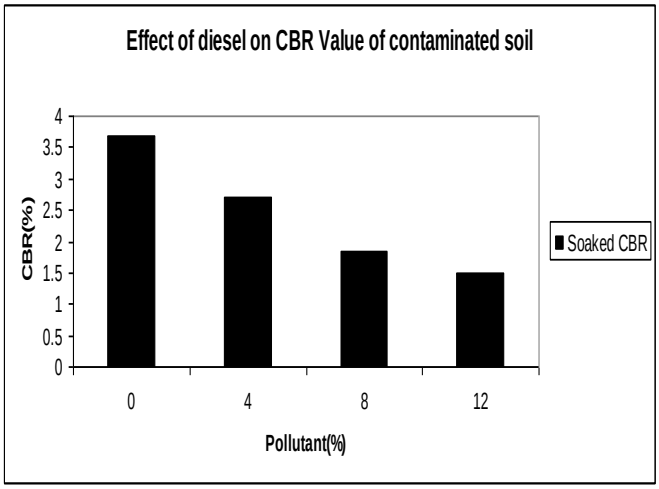

Fig -2 Effect of diesel on California bearing ratio test

PART:II REMEDATION OF DIESEL CONTAMINATED SOIL

A. *Soil Samples*

The experimental work was conducted with soil, procured from Sirhind at a depth one to two meters from ground surface. The soil is classified as silt and clay of low compressibility (CL-ML)

B. *Diesel Sample*

Diesel oil was used as contaminant. The soil was contaminated in the laboratory with varying percentage of Diesel oil as contaminant to study the contaminant's effect on various geotechnical properties of soils.

C. *Cement Sample*

The Ordinary Portland cement is obtained from ACC Cement Company with grade of 43 is used. Portland cement is one of the older materials used for stabilization. Cement stabilization differs somewhat from other forms of chemical stabilization. The cement hardens the soil material and structural strength is primarily obtained from the cementing action rather than from internal friction, cohesion, chemical ion exchange and/ waterproofing of the materials.

D. *Quantity of Diesel and Cement*

The contaminated soil with 0, 4,8,12 percentage of diesel was stabilized with cement at 0, 3, 7, and 11 percent, by dry weight of the soil. The contaminated soil was divided into 12 numbers of sets. Each set then treated with additive Portland cement at different weight percentages. Maximum amount of additives used did not exceed 20% by weight due to economic considerations. Atterberg's limits and strength parameters of the treated soil samples were evaluated after curing the sample at room temperature for seven days. Three samples were tested from each batch and the results are expressed as a mean value.

E. *Experimental programmed*

Table 4 Properties of diesel contaminated soil with cement

Soil Sample	OMC %	MMD (kn/m^3)	UCS (kpa)	CBR (soaked) (%)
S+0% D+3%C	10.6	17.91	1269.2	20.56
S+0%D+ 7%C	10.9	17.96	2280.1	36.56
S+0%D+11%C	11.3	18.09	2855.4	48.17
S+4%D+3% C	9.3	17.16	881.9	12.7
S+4%D+7% C	9.5	17.53	1390.8	22.5
S+4%D+11%C	10	17.75	1917.8	28.4
S+8%D+3% C	9	16.99	583.6	7.02
S+8%D+7% C	9.5	17.20	980.0	12.5
S+8% +11%C	10	17.36	1417.3	16.05
S+12%D+3%C	8.4	16.67	236.1	2.5
S+12%D+7%C	8.7	16.87	294.0	3
S+12%D+11%C	8.9	16.97	333.5	5.88

S=Soil D=Diesel C=Cement

F. *Unconfined Compressive Strength (UCS)*

Unconfined compressive strength test (confirming IS: 2720 (PART X) were conducted on cylindrical sample of 38mm diameter and 76mm height, prepared at maximum dry density and optimum moisture content. Each sample was cured for 8 days (7 days moist curing and one day water immersion).Samples was tested with strain rate of 1.25 m/minute. The results show that the addition of cement resulted in marked increase in UCS.

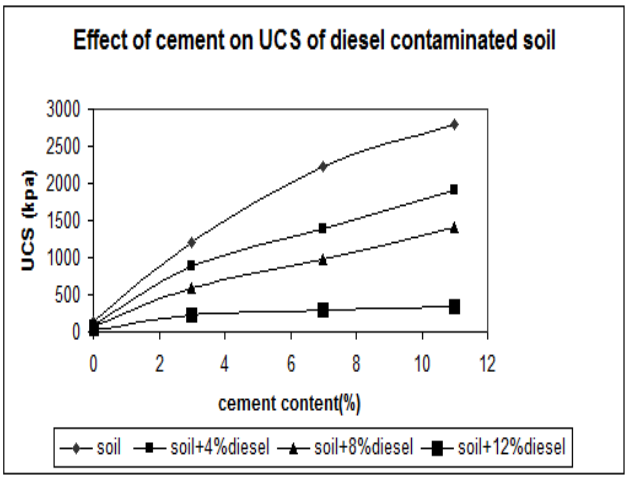

Fig 3 Effect of cement content on UCS of diesel Contaminated soil

G. *California Bearing Ratio Test*

As the most important engineering parameter to evaluate a sub grade or sub base material for pavement design is the California bearing ratio value of soil .The soaked C.B.R value of the diesel contaminated soil with different percentage of cement is determined. It is observed that the addition of cement increases the CBR value. From the results it is observe that when 3% of cement content, soaked CBR value of soil is 20.56% and soil + 4% diesel is treated with 7% cement and soil+ 8% diesel is improved with 11% cement the values respectively 22.5% and 16.05%.

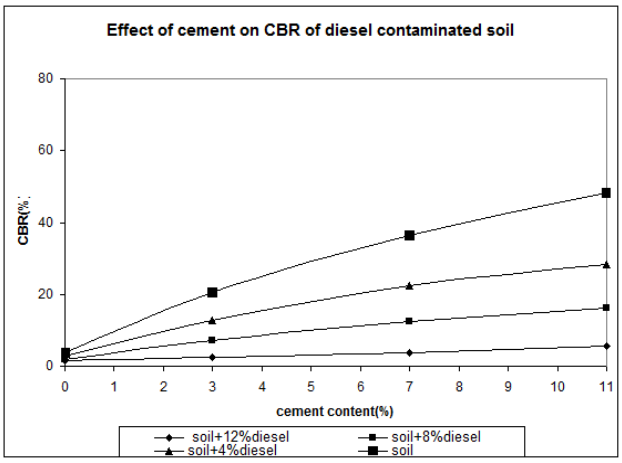

Fig 4 Effect of cement content on CBR of diesel Contaminated soil

IV CONCLUSION

In this study, the effects of oil contamination on some geotechnical properties are clearly observed. The Atterberg's limits of contaminated soils were lower than that of uncontaminated soils. The maximum dry density and optimum moisture content also dropped due to increase in oil content in contaminant soil. Similar behavior was also observed on shear strength and CBR value of soil. When stabilized with cement, the treated soil had the highest maximum dry density then non-stabilized samples. It appears that the specific gravity of un hydrated cement (3.1) relative to the soil tends to produce a higher density. Addition of cement resulted in marked increase in UCS. . The improvement in unconfined compressive strength (UCS) can be attributed to neo-formations such as calcium silicate hydrates (CSH, CSH-1) that coats bind the soil particles. It is observed that the addition of cement increases the CBR value. Soil+12%diesel not improved with this much of percentage of cement and improvement is uneconomical hence soil+12%diesel is improved by other method such as soil venting (volatilization), Soil air suction, and Bioremediation.

This study will be helpful to reuse the contaminated soil in construction application provides a safe and useful solution for the problem of the disposal of oil-contaminated soils.

REFERENCES

[1] A.R., Hossam, F. H., Ramzi, T., Abdulwahid, H., Bader, A.S., and Yahia, A.S. (2005), "Stabilization of oil-contaminated soils using cement and cement by-pass dust", International Journal 16**, 6,** 670-680.

[2] Determination of Unconfined Compressive Strength.' IS: 2720 Part-10, BIS, 1973

[3] Evgin, E., and B. M. Das (1992) "Mechanical Behavior of Oil Contaminated Sand," Environmental

[4] Gupta, M.K.,Srivastava, R.K.,(2010), "Evaluation of Engineering Properties of Oil-contaminated Soils", Journal of the Institution of Engineer India. Civil engineering 90, 37-42.

[5] IS 2720, Part 10 (1991), Indian Standard Specifications for Determination of Unconfined Compressive Strength of Soil, Indian Standard Institutions, (Publ.) New Delhi

[6] IS 1498 (1970), Classification and Identification of Soils, Indian Standard Institutions (Publ.), New Delhi.

[7] Puri, V.K., B.M. Das, E.C. Cook and E.C. Shin, (1994)."Geotechnical Properties of Crude Oil-Contaminated Sand". ASTM Special Technical Publication, 1221, 7 Y 5-88

[8] Rahman, Z.A., U. Hamzah and N. Ahmad, 2010."Geotechnical characteristics of oil-contaminated granitic and metasedimentary soils". Asian J. Applied Sciences, 3: 237-249.

[9] Sridhran, A. and Sivapulliah, "P. V.": Engineering behaviour of soils contaminated with different pollutants". In: Environmental Geotechnical, Balkema Press, Rotterdam, 1987.

[10] Rao, S.M.,Reddy,P.M.,"Collapse Behaviour of a Laboratory Contaminated Soil" Indian Geotechnical Congress 1995, Bangalore,December 1995**, 1**, Bangalore.

[11] Tuncan, A., Tuncan, M. and Koyuncu, H. (2000), "Use of petroleum contaminated drilling wastes as sub-base material for road construction", Waste Management and Research, **18**, 489-505.

[12] Yaji, R. K. (1995)."Effect of contamination by some chemicals on engineering behaviour of Shedhi soil", Indian Geotechnical Congress 1995, vol. 1, Bangalore,1995,pp.241.

[13] Young, R. N. and Warith, M. A. (1989), "Leaching effect of organic solution on geotechnical properties of three clay soils", Proc. of 2nd Symposium on Environmental Geotechnology,

Stabilizing Soils Incorporating Combinations of Rice Husk Ash and Cement

Ishatpreet Kaur,
Assistant Professor
Civil Engineering Department,
Baba Banda Singh Bahadur Engineering College,
Fatehgarh Sahib, India.

Manpreet Kaur,
Assistant Professor
Civil Engineering Department,
Baba Banda Singh Bahadur Engineering College,
Fatehgarh Sahib, India

***Abstract*— Rice husk ash (RHA) is a pozzolanic material which is readily available in an agricultural country like India. It can be used in soil stabilization, when rice husk is burnt under controlled temperature and 17%-25% of rice husk's weight remains ash. Soil is the basic construction material which supports the loads of superstructure .The existing soil at a particular location may not be suitable for the construction so may need an improvement in basic properties using cost effective practices like treating with industrial wastes and agricultural wastes like fly ash, rice husk ash etc which are having cementitious value. The focus of the paper is to study the effects of various proportions of rice husk ash – cement for enhancing the properties of soil. The objective of this study is to investigate the strength improvement of Soil: RHA: Cement mixtures in terms of strength properties of stabilized soils. Tests were conducted on different test specimens with varying ratios of contents at OMC and MDD. Locally available soil was mixed with 0%, 5%, 10% & 15% of RHA along with 0%, 6%, 8% & 10% cement.**

***Keywords*— RHA, Cement, Clayey Soil, UCS.**

I INTRODUCTION

The existing soil at a particular location may not be suitable for the construction due to its poor load carrying capacity and higher compressibility or even sometimes excessive swelling in case of expansive soils. The improvement of soil at a site is necessary due to rising cost of the land and huge demand for high rise buildings. There is a need to concentrate on improving properties of soils using cost effective practices like treating with industrial wastes and agricultural wastes like fly ash, rice husk ash etc which are in pozzolonic materials.Clays exhibit generally undesirable engineering properties. They tend to have low shear strengths and also lose shear strength further upon wetting or other physical disturbances. Some types of clay expand and shrink greatly upon wetting and drying which is the most undesirable feature. Also clays develop large lateral pressures and they tend to have low resilient modulus values. For these reasons, clays are generally poor materials for foundations. But, the engineering properties of clayey soils can be improved by using different stabilization techniques. Soil stabilization is a technique introduced many years ago with the main purpose to make the soil capable of meeting the requirements of the specific engineering projects (Cook, C.J. et al, (1989),Basha , E.A., Hashim, R. , Mahmud, H.B. &Muntohar , A.S., (2004), Jha, J.N. & Gill, K.S., (2006),Koteswara Rao. D et al., (2012).Several additives, which may be utilized for ground modification such as cement, lime and mineral additives such as fly ash, silica fume, rice husk ash, have been used under various contexts. Rice husk (RH) is one of the by-products obtained during milling of rice. This surrounds the paddy grain. It is reported that approximately 0.23 tons of rice husk (rice hull) is formed from every ton of rice produced. World rice production is approximately 500 million tons. Asian farmers produce rice about 90% of total production with two countries, China and India, growing more than half of the total crop. In certain countries, RH is sometimes used as a fuel for parboiling paddy in the rice mills and to power steam engines. The residual product obtained from burning of rice husk is called rice husk ash (RHA) which contributes to environmental pollution. It would be beneficial to the environment to recycle the waste to produce eco-materialhaving high end value. It is generally reported that in rice husk, silica is predominantly in inorganic linkages, but some of the silica is also bonded covalently to the organic compounds. This portion of the silica is un-dissolved in alkali and can withstand very high temperatures. It has been clear that once the organic part of RH is extracted, the inorganic residue may be relatively pure, forming a better source of silica. Characterizations by scanning electron microscopy (SEM), energy-dispersive X-ray analysis (EDX) etc., suggest that silica is present all over, but is concentrated on Protuberances and hairs (trichomes) on the outer epidermis, adjacent to the rice kernel. There is a significant variation in silica percentage. The silica is in hydrated amorphous form, either opal or silica gel. Disposal of rice husk ash is an important issue in the countries like India which cultivate large quantities of rice. Rice husk has a very low nutritional value and as they take very long to decompose, so are not appropriate for composting or manure. Therefore in the present investigations an effort has been made to utilize RHA for geotechnical purposes after mixing with soil and cement.

II MATERIALS AND METHODS

A. Soil**:** The soil sample used for this study was locally available soil near Rajpura, Punjab, using the method of disturbed sampling. The properties of the soil used in the investigation are given in Table 1. The overall geotechnical properties of the soil classified as Clay with low plasticity (CL) in the IS Soil Classification System. The soil collected from the site was pulverized with wooden mallet to break the

lumps and then air dried. Subsequently it was sieved through 2.36mm IS sieve and then dried in an oven at 105^0 C for 24 hours.

B. RH**A**: The rice husk ash (RHA) used in the investigation was collected from Vardhmann spinning Mills, Ludhiana. Processing of RHA was done on similar line as that of soil. Required quantity of soil was weighed and desired quantity of RHA and cement were added to get the uniform mix required for sampling**.**

C. ORDINARY PORTLAND CEMENT 43 GRADE**:** The Ordinary Portland cement obtained from Ambuja Cement Company with grade 43 was used in the study. Cement is a fine, grey powder. It is a material with adhesive and cohesive properties which is capable of bonding mineral fragments into a compact-solid.

D. Water**:** Locally available tap water was used for investigation.
The composition along with the physical properties of materials used is outlined in Table: 1, Table: 2, Table: 3 and 4 respectively.

TABLE 1 Physical properties of soil

S. No.	Parameters	Results
1.	Light compaction test	
	MDD (kN/m^3)	18.35
	OMC (%)	14.2
2.	Liquid limit (%)	29.6
3.	Plastic limit (%)	17.8
4.	Plasticity index (%)	11.8
5.	Specific gravity	2.64
6.	Indian soil classification	CL

TABLE 2 Physical properties of RHA

S. No	Properties	Values
1.	Specific Gravity	1.97
2	Grain Size Analysis	
	a) Gravel Size Fraction (%)	0.00
	b) Sand Size Fraction (%)	54.4
	c) Silt & Clay Size Fraction (%)	45.6
3.	Maximum Dry Density (kN/m^3)	9.25
4.	Optimum moisture content (%)	52.4

TABLE 3 Chemical Properties of RHA.

S. No	Component	%
1.	Silica (SiO2)	91.58
2.	Alumina (Al2O3)	1.95
3.	Iron Oxide (Fe2O3)	0.48
4.	Lime (CaO)	0.78
5.	Magnesia Oxide (MgO)	0.58
6.	Potassium (K2O)	2.92
7.	Other oxides	1.71

TABLE 4 Physical Properties of Cement used

Properties	Value
Grade	43
Initial Setting time (min)	30
Final Setting time (min)	300
Compressive strength	
3Days strength (MPa)	25.5
7Days strength (MPa)	36.7
28Days strength (MPa)	41.5

Specimen Preparation

The soil collected from the site was pulverized with wooden mallet to break the lumps and then air dried. Subsequently it was sieved through 2.36mm IS sieve and then dried in an oven at 105^0 C for 24 hours. Processing of RHA was done on similar line as that of soil. Required quantity of soil was weighed and desired quantity of RHA and cement were added to get the uniform mix required for sampling. A set of 16 specimens were prepared according to Indian Standard specifications. All the desired tests were conducted as IS methods. The test results reported are the average of three tests.

Method of Testing

In the strength tests, cylindrical specimens were prepared according to codal provisions for soil and soil + RHA + cement mixtures. One of the popular methods of evaluating the effectiveness of stabilization is unconfined compressive strength, the better the quality of stabilized material; higher will be the compressive strength. Each specimen used was compacted at optimum moisture content and dry density. Specimens were cured in groups of three in a controlled chamber before being tested in compression a curing period of 7 days was adopted and at least three specimens were tested for each case.

III TEST RESULTS & DISCUSSION

Compaction Characteristics

Fig. 1 & Fig. 2 shows the effect of the addition of cement, RHA, and cement–RHA mixtures on the compaction characteristics of the soil tested. The figure depicts that adding cement and RHA increased the OMC and diminish amount of the MDD correspond to increasing of cement and RHA percentage. The decrease in the MDD can be due to the replacement of soil by the RHA in the mixture. Also the decrease in the MDD may be considered due to RHA acting as filler in the soil voids with lower specific gravity. The increase in OMC is due to the addition of RHA, which decreases the quantity of free silt and clay fraction and coarser materials with larger surface areas. These processes need water to take place which implies that more water is needed in order to compact the soil-RHA mixtures as reported in Zhang et. al (1996).

Unconfined Compressive Strength

The effect of the addition RHA and cement on the unconfined compressive strength is shown in Fig.- 3.Unconfined compressive strength (UCS) results after 7 days curing for different mixes shows that with increase of cement, deformation goes on decreasing and unconfined compressive strength goes on increasing. The subsequent increase in the UCS is attributed to the formation of cementitious compounds

between the CaOH present in the soil and RHA and the pozzolans present in the RHA. The results showed that addition of RHA up to 10 % increases the UCS to maximum value and thereafter further addition does not contribute towards strength. The decrease in the UCS values after the addition of 10% RHA may be due to the excess RHA introduced to the soil and therefore forming weak bonds between the soil and the cementitious compounds formed.

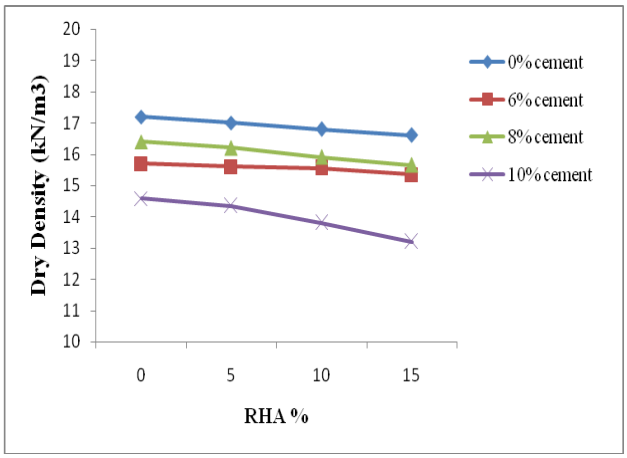

Figure 1: Variation of MDD with RHA Content

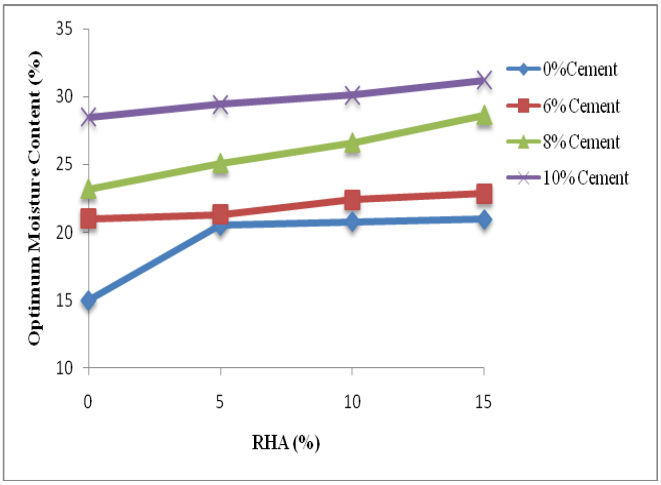

Figure 2: Variation of OMC with RHA Content

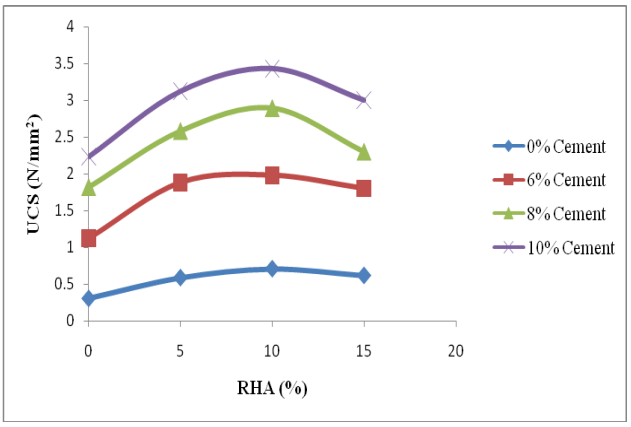

Figure 3: Combined Graph showing UCS of different proportions of Soil: RHA: Cement at 7days curing period

IV CONCLUSIONS

The following conclusions can be made on the basis of test results obtained from cement-RHA stabilized clayey soil:

1. Treatment with RHA and a small percentage of cement shows a general decrease in the MDD and increase in OMC with increase in the RHA content.
2. The UCS of 7 days cured samples shows an increasing trend up to 10% RHA for various proportions of cement and further increase in RHA content does not contribute much towards strength. It may be due to pozzolanic reaction between lime liberated from hydration reaction of cement and RHA to form secondary cementitious materials.
3. With increase in percentage of RHA the strength tends to increase and reaches a certain value and thereafter it starts decreasing but it is always higher than respective soil – cement mixture. Hence even in smaller amounts, RHA is beneficial in improving the properties of soils. The maximum value is obtained at an addition of 10% RHA.
4. RHA when used as an alternative or as a partial replacement along with cement in stabilizing clayey soils reduces the cost of material for construction as well as solving the disposal problem.

REFERENCES

[1] Arora, K.R "Soil Mechanics & Foundation Engineering" 4th Edition, 2013.

[2] Alhassan, Musa & Mohammed, Alhaji, "Effects of Rice Husk Ash on cement stabilized laterite Leonardo Electronic Journal of Practices and Technologies,April 2008, 11, 47-58.

[3] Basha, E.A., Hashim, R., Mahmud H. B & Muntohar, A.S., "Stabilization of Residual soil with Rice husk ash and cement. Original research article construction & Building Material, Volume -19, 2005, Pp.448-453.

[4] Cook, C.J. et al, "Use of rice husk ash to enhance lime treatment of soil." Canadian Geotechnical Journal, 1989, pp. 843-852.

[5] Datta, R.K., et al, "Some alternate binders Based on Rice Husk & other cheap materials". National seminar on Building materials & science & technology, Institute of Engineers (India), Roorkee, April, 1982.

[6] I.S.4332, Test for determination of moisture content-dry density for stabilized mixtures.

[7] Jha J.N. & Gill, K.S., "Effect of Rice husk ash on lime Stabilization". Journal of the Institution of Engineers (India), 2006, Volume 87, page 33-39.

[8] Koteswara Rao. D et al.,"The Effects of ferric chloride and RHA in the stabilization of expansive soils for pavement subgrades."International Journal of Engineering Science & Technology. Volume 2, 2012, Page-146-153.

[9] Zhang MH, Lastra R, Malhotra VM., "Rice husk ash paste and concrete: some aspects of hydration and the microstructure of the interfacial zone between the aggregate and paste. Cement Concrete Research, 1996, vol. -26(6):963–77.

Effects on Intz Type Tank with Code Revision of IS:3370 (1965) To (2009)

Harkomal Kaur,
Assistant Professor
Baba Banda Singh Bahadur Engineering College
Fatehgarh Sahib (Punjab)

H.S Rai
Guru Nanak Dev Engineering College
Gill Road, Ludhiana

Abstract—Water is stored in storage tanks, reservoirs and overhead tank which can be used to store water, liquid petroleum, petroleum products and similar liquids. The load investigation of various reservoirs or tanks is near to the same regardless of the chemical temperament of the product. Tanks are generally designed as crack free structures to eradicate any sort of outflow. Comparative study needed on the theory behind the design of liquid retaining structure. A discussion on the use and change of the code IS: 3370 (part 1& 2) is given in the paper. Overhead tank are used to store water for supplying it to the consumer. BIS has revised the version of IS: 3370 (part 1& 2) after a elongated time from its 1965 version in year 2009. The code is drafted for the water tank. Limit state method is included in this new version. This paper gives the brief study on the design of intz water tank using working stress method and limit state method. Comparative result of IS: 3370 (1965) and IS: 3370 (2009) is specified. This study was conducted in order to compare the design provisions of IS: 3370 (1965) and IS: 3370 (2009). This edition adopts limit state method with these additions. Cracking width of limit state design is limited and second addition is it limits the stresses in steel so that concrete does not reaches in over stressed zone.

Keywords - IS: 3370 (1965) & (2009), Intz Water Tank, Working stress method, limit state method, Design, Crack width

I. INTRODUCTION

In every day usage water is a essential part of life. So water is stored for daily purposes in various forms to use it for daily purposes. Tanks which are constructed above ground are used for the purpose storing water. These tanks are described according to their position as underground on ground overhead tanks. Different shapes of tanks can be constructed circular and rectangular are used most commonly. The tanks can be made of RCC or even of steel. The tanks which are constructed above ground are overhead tanks and are usually elevated from the roof to through the column. As seen in most cases Ground tanks and underground are rectangular or circular in shape but the shape of the Overhead tanks are influenced by the vision of area around and also the design of the construction. Storage tanks are containers that store liquid gases or any other medium Jain, Ashok K (2002). After a long time IS: 3370 is revised from its 1965 version IS: 3370 (Part-I), 1965. In this revision introduction of limit state design is the most important addition.

Limit state design method; found to be has been found to be the best for the design of reinforced concrete structures. There are further two division of limit states- limit state of collapse and limit state of serviceability which involves cracking and deflection. The structure is first analysed and designed under limit state of collapse after that checked under usefulness IS: 3370 (Part-II), 2009.

II. LITERATURE REVIEW

An exhaustive literature review revealed that a minimum amount of research work had been done on this topic.

Tanetal (1966), presented the minimum cost design of reinforced concrete cylindrical water tanks based on the British Code for water tanks, using a direct search method and the (SUMT). The cost function included the material costs of concrete and steel only. The tank wall thickness was idealized with piecewise linear slopes with the maximum thickness at the base.

Thakkar et al. (1974), discussed cost optimization of non cylindrical composite type prestressed concrete pipes based on the Indian code.

Al-Badri (2005), presented cost optimization of reinforced concrete circular grain silos based on the ACI Code (2002).

He proved that the minimum cost of the silo increases with increasing angle of internal friction between stored materials, the coefficient of friction between stored materials and concrete, and the number of columns supporting hopper.

II. PROBLEM FORMULATION

The main objective to study this code is to make engineers aware about the best method available to ensure the best economical and reliable method which can be used to for designing purpose. So to do the comparison study of provisions in IS:3370 (1965) and IS:3370 (2009), Intz type of water tank was chosen since it is widely used for large capacity .

An Intz type water tank of 1million litres (1000 m^3) supported on an elevated lower comprising of 8 columns. The base of the tank is 16 m above ground level. Depth of foundation 1 m below ground level was chosen in this study. M30 grade of concrete and Fe-415 grade of tor steel was used conforming to the stresses specified in IS:3370 and IS 456, 2000. Fe-500 grade of steel may be taken, but it may not be more useful in liquid retaining structures since the permissible stresses in steel is independent of grade of steel as per clause 4.5.3.2 of IS: 3370 (Part 2) 2009. Grade of concrete is taken as M30, as minimum grade of concrete for RCC structures is M30 as per IS: 3370 (Part1) 2009. As per discussion above, the water tank was designed by the following four design methods.

a) Working stress method in accordance IS:3370 (1965)

b) Working stress method in accordance IS:3370 (2009)
c) Limit state design method with crack width calculations and check in accordance IS: 3370 (2009).
d) Limit state design method deemed to satisfy (limiting steel stresses in accordance IS: 3370 (2009).

III. DESIGN METHOD

In past times the design method usually used was working stress method. This method has large number of limitation. Sometimes the limit state method cannot be used due to some technical clinch the working stress method can be used. In liquid retaining structure Limited cracking width calculated by working stress method was prime reason why the Indian Standard IS: 3370 (1965) did not adopt the limit state design method even after adoption by IS; 456–1978. But now, IS:3370 adopted limit state design method in 2009 with the following advantages - limit state design method contemplate the materials according to their properties , and it also treat load according to their load, the structures also fails mostly under limit state and not in elastic state and limit state method also checks for serviceability. There possible intuitions that working stress method will obsolete in coming time IS: 3370 (Part-I), 1965 & IS: 3370 (Part-II), 1965.

IS:3370-2009 adopts limit state design method with precautions. It adopts the criteria for limiting crack width when the structures are designed by considering ultimate limit state and restricts the stresses to 130 MPa in steel so that cracking width is not exceeded this is considered to be deemed to be satisfy condition. This safety ensures that cracking width should be less than 0.2 mm which is quite applicable for the liquids. It clearly shows how the liquid structures all different from other structures IS: 3370 (Part-I), 2009 & IS: 3370 (Part-II), 2009.

IV. GENERAL REQUIREMENT ACCORDING TO IS: 3370 1965 & 2009

Table I. Minimum Cement Content, Maximum water- Cement Ratio and Maximum Grade of Concrete

S No.	Concrete	Minimum Cement Content	Maximum Free Water Cement Ratio	Minimum Grade of Cement
1	Plain concrete	250	0.5	M20
2	Reinforced cement concrete	320	0.45	M30
3	Prestresed concrete	360	0.4	M40

Table II. Comparison of Minimum Reinforcement as per code provision is shown below

IS : 3370 -1965	IS : 3370-2009
A) The minimum reinforcement in walls, floors and roofs in each of two directions at right angles shall have an area equal to 1. 0.3 % of cross sectional area of sections thickness < 100 mm 2. Linearly varying from 0.3 % to 0.2% for thickness 100 mm to 450 mm. 3. 0.2 % for section of thickness > 450mm 4. In concrete sections of thickness >225 mm, two layers of reinforcement be placed one near each face. B) The minimum reinforcement specified above may be decreased by 20 % in case of HYSD bars.	A) The minimum reinforcement in walls, floors and roofs in each of two directions at right angles, within each surface zone shall not be less than 1. 0.35 % of surface zone as shown in for HYSD bars. 2. 0.64 % of surface zone for mild steel bars. B) The minimum reinforcement can be further reduced to 1. 0.24 % for HYSD bars. 2. 0.40 % for mild steel bars. For tanks having any dimension not more than15 m. C) In wall slabs less than 200 mm in thickness, the reinforcement may be placed in one face.

Table III. Comparison of Provisions for Permissible Stresses in Steel

Type of Stress	Permissible Stresses In N/mm^2 IS:3370 -1965		Permissible Stresses In N/mm^2 IS:3370 -2009	
	Plain round mild steel bars	*High strength deformed bars*	*Plain round mild steel bars*	*High strength deformed bars*
Tensile stress in members under direct tension	150	150	115	130
Tensile stress in members under direct tension a) on liquid retaining face b) on face away from liquid for members less than 225 mm c) on face away from liquid for members more than 225 mm	 150 150 125	 150 150 190	115	130
Compressive stress in columns subjected to direct load	125	175	125	140

V. DESIGNS ON BASIS OF CRACK WIDTH

4.1 Working stress method

For No Cracking Criteria,

$$\frac{T}{A_c + (m-1)A_s} \leq \sigma_t$$

$$m = \frac{280}{3\,\sigma_{cbc}}$$

Where, m = Modular Ratio
A_s = Area of steel
σ_t = Allowable tensile stress in concrete
σ_{cbc}= Allowable tensile stress in concrete

4.2 Limit state method

The permissible limit of crack width is 0.2mm. The crack widths due to temperature and moisture effects shall be calculated as given below:

To be effective in distributing cracking, the amount of reinforcement provided needs to be at least as great as given below:

$$\rho_{crit} \geq \frac{f_{ct}}{f_y}$$

Where, ρ_{crit}= critical steel ratio,
f_{ct}= direct tensile strength of the immature
f_y= characteristic strength of the reinforcement.

Table IV. Comparison of provisions for permissible stresses in steel

Grade of concrete	**M25**	**M30**	**M35**	**M40**	**M45**	**M50**
f_{ct}, N/mm^2	1.15	**1.3**	1.45	1.6	1.7	1.8

Maximum spacing of crack

$$S_{max} = \frac{f_{ct}}{f_y} \times \frac{\emptyset}{2\rho}$$

$\frac{f_{ct}}{f_y}$ = ratio of the tensile strength of the concrete to the average bond strength between concrete and steel which can be taken as 2/3 for immature concrete.
$\emptyset$ = size of each reinforcing bar
Width of Fully Developed Crack,

$$W_{max} = S_{max} \times \alpha \times \frac{T_1}{2}$$

Where $\propto$ = Coefficient of thermal expansion of concrete

VI. RESULTS & DISCUSSION

Intz water tank was designed following the provisions of IS:3370 (1965) & (2009) by working stress method and limt state desgin method. The quantities of materials were calculated and have been tabulated in the following section.

The quantities of materials for different components of Intz type water tank for different design theories have been tabulated in Table V, Tables VI, VII, VIII, IX and X present the quantities of materials for Intz type water tank ,respectively.

A comparison of design by working stress method as per IS 3370-1965 and IS 3370-2009 shows that the amount of material remains unchanged. It is further observed that the steel quantity decreases significantly as per IS 3370-2009 in those members where the designed amount of reinforcement is less than the minimum reinforcement. This is because, in IS 3370-2009, the minimum reinforcement is calculated on the basis of the area of cross section of the surface zones and not on the basis of entire cross section as in IS 3370-1965. The steel and concrete quantities for Limit State design Method as per IS 3370-2009 decrease significantly as compared to working stress methods of IS 3370-1965 and IS 3370-2009 because higher permissible stresses are permitted and crack width is checked. The quantities of steel for intz type tank considered in this study was observed to be the maximum for design as per Limit State Method based on Deemed to Satisfy Criteria.

1. TOP DOME

Meridional Thrust = 22.22 kN/m
Circumferential Force =10 kN/m
Meridional Stress = 0.22 N/mm^2
Hoop Stress = 0.10 N/mm^2

Table V. Comparative results of top dome with WSM & LSM

TOP DOME	WORKING STRESS METHOD		LIMIT STATE DESIGN METHOD		
	IS:3370-1965	*IS3370-2009*	*CRACK THEORY*	*CRACK WIDTH*	*DEEMED TO SATISFY*
Thickness	100mm	100mm	100mm		100mm
% age change	----	Nil	Nil		Nil
Area of Steel	300mm^2	175mm^2	120mm^2		130mm^2
% age change	---	-53.16	-50		- 45.8

2. TOP RING BEAM

Hoop Tension = 106.6 KN

Table VI. Comparative results of top ring beam with WSM & LSM

TOP RING BEAM	WORKING STRESS METHOD		LIMIT STATE DESIGN METHOD		
	IS:3370-1965	*IS3370-2009*	*CRACK THEORY*	*CRACK WIDTH*	*DEEMED TO SATISFY*
Area of cross section	62614mm^2	62614mm^2	34500mm^2		34500mm^2
% age change	----	----	-32.61		-32.61
Area of steel	780mm^2	820mm^2	443mm^2	0.06mm	820mm^2
% age change	---	+9.42	-42		+9.42

3. CYLINDRICAL TANK WALL

Max. hoop tension at base of wall = 480 kN/m
Hoop tension at top of wall = 200 kN/m

Table VII. Comparative results of cylindrical tank wall with WSM & LSM

CYLINDRICAL TANK WALL	WORKING STRESS METHOD		LIMIT STATE DESIGN METHOD		
	IS:3370-1965	*IS3370-2009*	*CRACK THEORY*	*CRACK WIDTH*	*DEEMED TO SATISFY*
Base level thickness	350mm	350mm	140mm		140mm
% age change	----	----	-50		-50
Area of steel at base	3200 mm^2	3700 mm^2	1995 mm^2		3700 mm^2
% age change	---	+30.5	-73.21		+30.45
Top thickness	200mm	200mm	100mm	0.16mm	100mm
% age change	---	---	-45.6		-45.6
Area of steel at top	800 mm^2	925 mm^2	500 mm^2		925 mm^2
% age change	---	+36.18	-74		+38.18

4. BOTTOM RING BEAM

Table VIII. Comparative results of bottom ring beam with WSM & LSM

BOTTOM RING BEAM	WORKING STRESS METHOD		LIMIT STATE DESIGN METHOD		
	IS:3370-1965	*IS3370-2009*	*CRACK THEORY*	*CRACK WIDTH*	*DEEMED TO SATISFY*
Area of cross section	720000 mm^2	720000 mm^2	540000 mm^2		540000 mm^2
% age change	----	----	-49.2		-50.1
Area of steel	5320 mm^2	6140 mm^2	3315 mm^2	0.14 Mm	6140 mm^2
% age change	---	+28.4	-31.46		+76.21

5. CONICAL DOME

Table IX. Comparative results conical dome with WSM & LSM

CONICAL DOME	WORKING STRESS METHOD		LIMIT STATE DESIGN METHOD		
	IS:3370-1965	*IS3370-2009*	*CRACK THEORY*	*CRACK WIDTH*	*DEEMED TO SATISFY*
Thickness	600mm	600mm	500mm		500mm
% age change	----	----	-61.1		-61.1
Area of steel	5100mm^2	5885mm^2	3180mm^2	0.19mm	5885mm^2
% age change	---	+32.2	-41.2		+32.2

6. BOTTOM SPHERICAL DOME

Table X. Comparative results of bottom spherical dome with WSM & LSM

BOTTOM SPHERICAL DOME	WORKING STRESS METHOD		LIMIT STATE DESIGN METHOD		
	IS:3370-1965	*IS3370-2009*	*CRACK THEORY*	*CRACK WIDTH*	*DEEMED TO SATISFY*
Thickness	300mm	300mm	200mm		200mm
% age change	----	----	-31		-31
Area of steel	900 mm^2	525 mm^2	642 mm^2	0.17 mm	1506 mm^2
% age change	---	+33.09	-65.03		+213.16

VII. CONCLUSION

According to the result and discussions following conclusions are made.

- Limit State Method was found to be most economical for design of Intz type water tank as the quantity of steel and concrete needed is less as compared to working stress method.
- The thickness of wall and depth of base slab is comes to different for IS 3370:(1965) and IS 3370:(2009) because of the value of permissible stress in Steel (in direct tension, bending and shear) IS 3370:(1965) value of σ_{st} is 150 N/mm^2 and in IS 3370:(2009) σ_{st} is 130 N/mm^2.Water tank is the most important container to store water therefore, Crack width calculation of water tank is also necessary.
- There was no change in size of members for working stress method by IS: 3370 (1965) and IS: 3370 (2009). However, steel requirement decreased in IS: 3370 (2009) for intz type water tank, as the allowable stresses in steel were lower.
- It was found that the provisions of reinforcement through the surface zones in IS: 3370(2009) provides economical and more effective reinforcement by limit state method.

REFERENCES

[1] Al-Badri (2005) "Cost Optimization Of Reinforced Concrete Circular Grain Silo Based On ACI Code (2002), American Concrete Institute Structural Journal, May- June 2006.
[2] Ashok K Jain, *Reinforced Concrete Limit State Design* (Roorkee: Nem Chand &Bros, Roorkee, 2002)
[3] H.J. Mohammed, "Economical Design of Water Concrete Tanks", *European Journal of Scientific Research*,, Vol. 49, 2011
[4] IS 3370 (Part1):1965 concrete structure for storage of liquids-code of practice
[5] IS 3370 (Part2):1965 concrete structure for storage of liquids-code of practice
[6] IS 3370 (Part1):2009 concrete structure for storage of liquids-code of practice
[7] IS 3370 (Part2):2009 concrete structure for storage of liquids-code of practice
[8] IS : 1786 – 1985, Specification for High Strength Deformed Steel Bars and Wired for Concrete Reinforcement
[9] IS : 1786 – 1985, Specification for High Strength Deformed Steel Bars and Wired for Concrete Reinforcement
[10] IS 456:2000 Plain And Reinforced Concrete – Code Of Practice
[11] P.C. Varghese, "Limit State Design of Reinforced Concrete", Second Edition, "*Prentice Hall of India Private Limited",* New Delhi

[12] Sayal & Goel .Reinforced Concrete Structures. New Delhi. S.Chand publication 2004.
[13] Tanetal (1966) "Minimum Cost Design Of Reinforced Concrete Cylindrical Water Tanks Based On The British Code For Water Tanks, Using A Direct Search Method And The (SUMT). Europian Journal Of Scientific Research ISSN 1450 -216XVol.49No.4(2011), pp.510-520.
[14] Thakkar & Sridhar Rao (1974) "Cost Optimization Of Cylindrical Composite Type Prestesses Concrete Pipes Based On The Indian Code", Journal of Structural Engineering 131: 6.
[15] "Treasure of R.C.C.Design"–Sushilkumar "Advance Reinforced Concrete Design" 2nd Edition N. Raju
[16] Vazirani & Ratwani. Concrete Structures. New Delhi. Khanna Publishers.1990.

Possibility of Concrete Demolition Waste and Rubber Tyre Waste in Stone Column to Improve Bearing Capacity of Clayey Soil

Gagandeep Singh
Department of Civil Engineering
Baba Banda Singh Engineering College
Fatehgarh Sahib, Punjab, India

Rakhjinder Singh
Department of Civil Engineering
Baba Banda Singh Engineering College
Fatehgarh Sahib, Punjab, India

Jagseer Singh
Department of Civil Engineering
Gian Jyoti Group of Institutions,
Shambukalan, Banur, Punjab, India.

***Abstract*—Bearing capacity is a very important parameter of the soil. As the construction of the superstructure mainly depend upon foundations of that structure, whole structure has been erected on the soil of suitable bearing capacity. But if that value of bearing capacity is on lower side then improvement of soil can be done. The manner of improvement may be use of piles, piers, cassions and stone columns. Material to be used in stone column are aggregates up to size 100mm. Waste materials generated such as Rubber and Concrete demolition waste can be used as replacement of aggregates.**

In this present study clayey of medium plasticity (CI) used was collected from village lohatbaddi,distt Ludhiana (PB). Concrete demolition waste (CDW) was collected from waste of cubes tested in concrete laboratory. Rubber tyre waste (RTW) in crumbed powder form was collected from Speedways Tyre industry, Transport Nagar, Ludhiana. In this study an attempt was made to use CDW and RTW in improving bearing capacity of the soil. The percentage of RTW: CDW (0:100, 20:80, 40:60, 60:40, 80:20, 100:0) was used in this present study. After the optimization of RTW: CDW (20:80) for single column of L/D ratio 6 [1]. Then this percentage was used for L/D ratios 3, 6 & 10 for the number of columns 1,2,3,4&5 [2].The allowable bearing capacity for L/D = 6 is more than for 3 & 10 [8] and it was maximum for five number of columns. The allowable bearing capacity with five stone columns was 2-3 times the bearing capacity of soil without stone columns.

Keywords*— *(Bearing capacity,stone column, CDW,RTW,MDD)

I. INTRODUCTION

A. Clay

In soft weak clayey soils, the problems are always there which are due to poor strength, high compressibility and permeability of the soil. These sort of soft clays are extensively found in many parts of India and many other countries of world. In these cases where the clayey soil extends up to large depths, it is better and economical to go for stone columns for the stability of soil. Stone column technique is mostly used in recent times for ground improvement of clayey deposits in most of the world. Main function or say purpose of stone column technique is to increase the load carrying capacity of the clayey soil and to stiffen the soft deposits up to the 10 to 15 meters [4]. To support the structures with flexible base, stone columns can be formed in performed bores. The technique is generally used when the large post construction settlement are allowed. However if the settlements are not allowed in recent times, Vibro flotation technique is used to install stone columns.

The stone columns achieve its axial capacity from the passive earth pressure developed due to the bulging of the column and increased resistance to lateral deformation under superimposed surcharged load. The length of stone column is significantly less then length of piles , it is not necessary to rest stone column on very firm bearing stratum as in case of piles.

B. Rubber Tyre Waste (RTW)

Rubber tires are a ductile, non-biodegradable material which will have existence for long period of time without any decay or degradation. Mostly open burning and using as a fuel in some countries in solution of disposal of rubber which is very serious hazard. Tyres can't undergo any bio-degradation even after landfill treatment, material and energy recoveries to alternate to disposal of this, solid waste. Tyre disposal remains problematic issue in the industrialized countries of the world. Globally 1.2 billons of waste tyre rubber were produced every year. It is estimated that 11% of post consumer tyres are exported and 27% are sent to landfill or dumped illegally and only 4% rubber in used for civil engineering projects. About 1000 million tyres end their useful life every year. From total 65% of rubber consumed by the tyres and tubes in the market. Per capita consumption of rubber was 0.8 kg against 14 kg in the developing countries.

C. Concrete Demolition Waste (CDW)

From estimation around about 10-12 million tons of construction waste was generated annually in India. About 55000million cu.m are required for the housing sector and 750million cu.m are required for the road sector. To reduce the demand supply gap, recycling of construction and demolition waste aggregates can be done. 1.3 billion ton of solid waste is generated by the cities across the globe. This number is likely to be increase in 2025 to 2.2 billion ton.

According to 2012 World Bank report the building accounts the half the solid waste generated and half the total solid material used. According to CSE (Centre of Science and Environment) 5.75 billion sq.m of additional floor space has been newly built in India since, 2005. According to TIFAC's (Technology Information Forecasting and Assessment Council's) thumb rule 40-60 kg of CDW/ sq.m is been generated due to new construction in India. From 2005-2013 India produced about 287 million ton of CDW and in 2013 about 50 million from total. As quantity vise CDW is from dams, roads and other projects etc is more than any other solid waste.

II. OBJECTIVES

Followings are the objectives of this study:-

A. *To improve the bearing capacity of clayey soil with use of stone columns[4].*

B. *To make efficient use of Concrete Demolition Waste and Rubber Tyre waste.*

C. *To justify better pattern and Length to Diameter (L/D) ratio of columns.*

III. MATERIALS REQUIRED

A. Clayey Soil

Clayey soil collected and transported from village lohatbaddi & distt Ludhiana (Punjab) was processed in sufficient quantity in the beginning of entire testing program. Soil collected were allowed to dry in the air at room temperature and then hand mixed in dry state by pulverizing it manually to break the lumps with wooden hammer. The soil was dried in oven for 24 hour at 100+ 5 c before use. Then it was allowed to cool at room temperature then the required quantity of soil was taken for various tests to be performed.

B. Concrete Demolition Waste

Concrete Demolition waste sample is collected from concrete laboratory of Civil Engineering Department of the College. The sample that sieved through 5.6 mm sieve and retained at 75 micron sieve is used for the testing procedure. The values of Coefficient of curvature (Cc) and Coefficient of uniformity (Cu) were worked out.

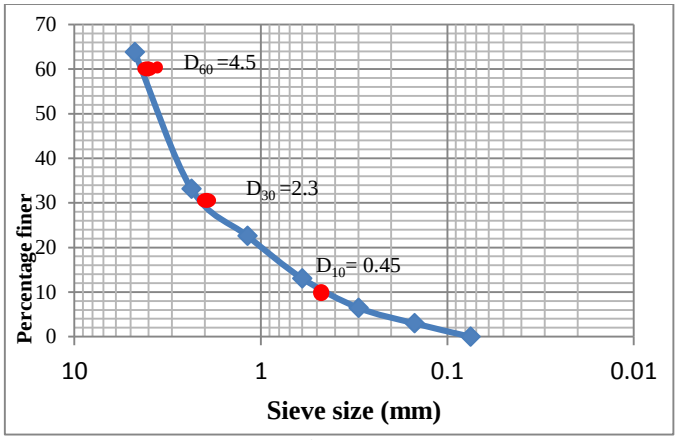

Fig3.1 Sieve analysis of Concrete Demolition Waste

Cc= 2.3 and Cu = 10 (Uniformly well graded demolition waste)

C. Rubber Tyre Waste (RTW)[11]

Rubber tyre Waste sample was collected from the Speedways Tyre Industry, Transport Nagar, Ludhiana(Punjab).Rubber tyre waste in the form of powder that is extracted from waste tyres.

The values of Coefficient of curvature (Cc) and Coefficient of uniformity (Cu) were

- *Cc = 1.53 and Cu = 1.05*

IV. METHODS OF OPERATION

A. Material Processing

Clayey soil collected and transported from village lohatbaddi & distt Ludhiana (Punjab) was processed in sufficient quantity in the beginning of entire testing program. Soil collected were allowed to dry in the air at room temperature and then hand mixed in dry state by pulverizing it manually to break the lumps with wooden hammer. The soil was dried in oven for 24 hour at 100+ 5 c before use. Then it was allowed to cool at room temperature then the required quantity of soil was taken for various tests to be performed.

B. Laboratory tests conducted

On the processed dry soil the following laboratory tests were conducted carefully with the apparatus with precision accuracy.

(1) Liquid limit and plastic limit
(2)Standard proctor test
(3)Plate load test

To determine the liquid limit of this soil under investigation standard Casagrande's apparatus was used and the test was done as pre standard procedure prescribed in IS.2720 (part-1) –2970. Similarly Plastic Limit was determined as per standard test method of I.S2720(part-1)-1970: 2008 took soil about 30 gm and then sieved through 425u I.S sieve and meticulously mixed soil. It was approximately mixed with 10% of water in evaporating dish. It is mixed with fingers thoroughly to make it plastic enough to shape into a small and allowed for some time for maturing. About 10 gm of plastic

soil prepared above and ball is rolled with fingers on a glass plate to form the thread. The water content was increased till the thread because smaller than 3mm without crumbling. The percentage of water was noted each time

Standard Proctor Test

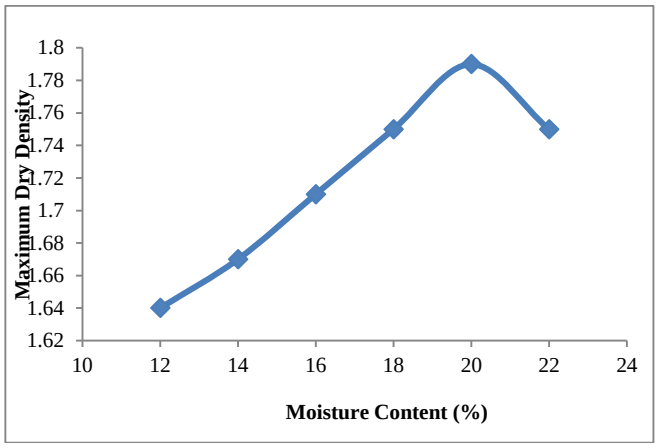

Fig 4.1Maximum Dry Density vs Moisture Content

Pate load test setup and results[6] **:-** The model tests were carried out in a circular test tank of 400 mm length and 300 mm diameter having 24 gauge sheet (5mm thick). Two plates of size 30mm wide and 60 mm long are welded and turned at 90 degree so that tank can be lifted and placed on bearing plate with ease. Bearing plate of 10 mm thickness and 340 mm diameter is placed below the tank. This plate is placed for equal pressure distributions on the bottom face of the tank. Different sizes of plates are used between proving ring and soil in tank. Steel ball is used to transfer the equal pressure on circular plate. Stone column is made with pipe of external 20 mm diameter and length of stone column can we taken by erection of pipe in tank till the marking on pipe touches the soil surface, soil around the pipe was compacted gently.

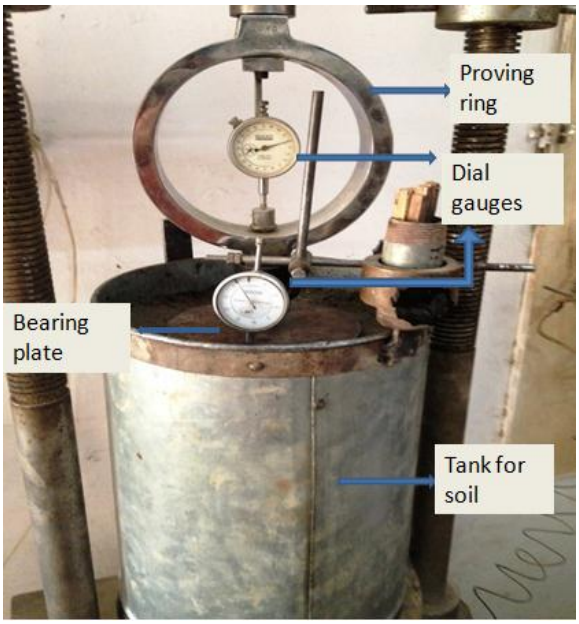

Fig 4.2 Plate Load Test Model

S. No	Number of columns	RTW + CDW (%)	Depth of column (mm)	L/D Ratio	Column Area (cm^2)	Load (kg)	Loaded Area (cm^2)	Ratio of Column Area/Loaded Area)	Allowable Bearing Capacity (kg/cm^2)
1.	None	0 + 0	Nil	Nil	Nil	121	254.34	Nil	0.475
2.	One	0 + 100	120	6	3.14	173	254.34	1.2	0.68
3.	One	20 + 80	120	6	3.14	189.5	254.34	1.2	0.745
4.	One	40 +60	120	6	3.14	160.1	254.34	1.2	0.675
5.	One	60 + 40	120	6	3.14	149	254.34	1.2	0.585
6.	One	80 + 20	120	6	3.14	138.5	254.34	1.2	0.54
7.	One	100 + 0	120	6	3.14	130	254.34	1.2	0.51
8.	One	20 + 80	60	3	3.14	174	254.34	1.2	0.68
9.	One	20 + 80	200	10	3.14	180.5	254.34	1.2	0.705
10.	Two	20 + 80	60	3	6.28	192.7	254.34	2.46	0.755
11.	Two	20 + 80	120	6	6.28	215.3	254.34	2.46	0.845
12.	Two	20 + 80	200	10	6.28	195.4	254.34	2.46	0.765
13.	Three	20 + 80	60	3	9.42	208.5	254.34	3.7	0.82
14.	Three	20 + 80	120	6	9.42	225.8	254.34	3.7	0.885
15.	Three	20 + 80	200	10	9.42	210	254.34	3.7	0.825
16.	Four	20 + 80	60	3	12.56	215.1	256	4.9	0.84
17.	Four	20 + 80	120	6	12.56	247.5	256	4.9	0.965
18.	Four	20 +80	200	10	12.56	202.5	256	4.9	0.79
19.	Five	20 + 80	60	3	15.7	230	254.34	6.2	0.90
20	Five	20 + 80	120	6	15.7	289	254.34	6.2	1.135
21.	Five	20 + 80	200	10	15.7	254	254.34	6.2	1

TABLE 4.3 Variation of Bearing Capacity

RESULT AND DISCUSSIONS

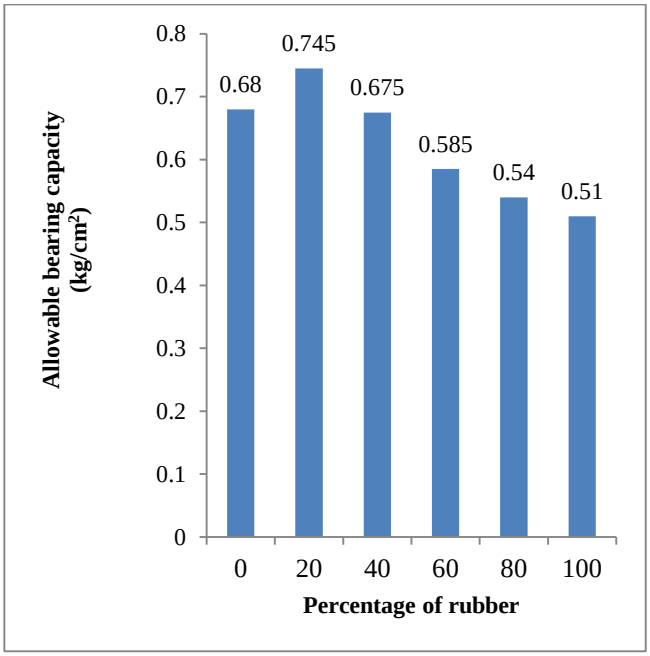

Fig 4.4 Allowable Bearing capacity v/s % of rubber used in stone column

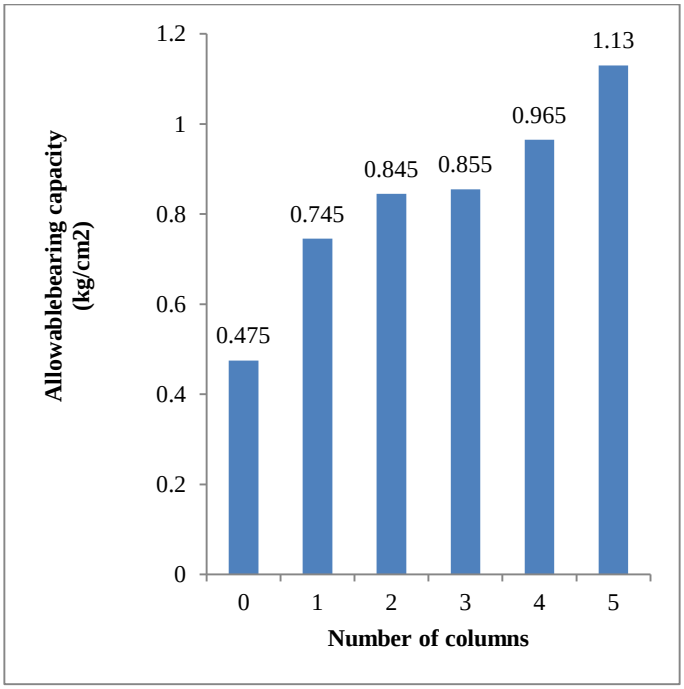

Fig 4.5 Bearing Capacity For (L/d =6) v/s Number of columns

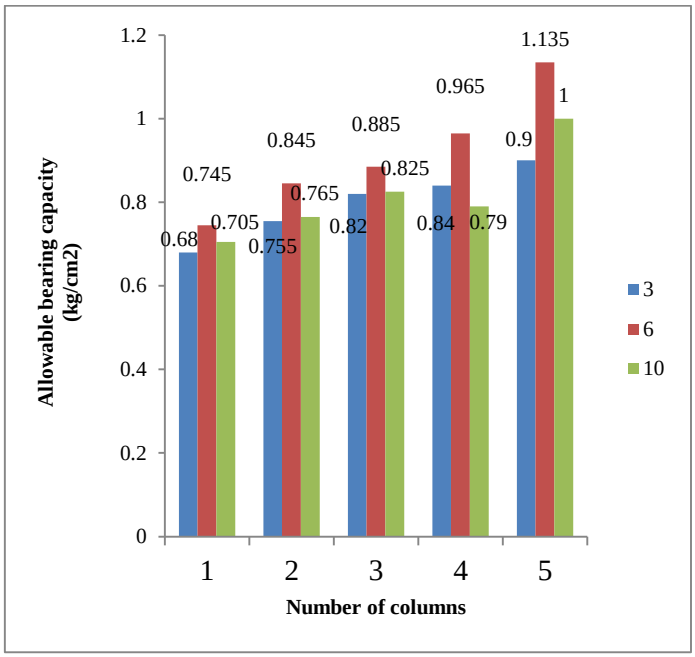

Fig 4.6 Comparison of Allowable bearing capacity for L/D ratios and number of columns

V. CONCLUSION

The value of allowable bearing capacity for single column with different Percentage of rubber and Concrete demolition waste was maximum at (20% rubber + 80% demolition waste) having value 0.745 kg/cm2 with L/D = 6 whereas value of bearing carrying capacity of soil without column was 0.475 Kg/cm2. Allowable bearing capacity decreases with increase in percentage of rubber, this decrease was due to decrease in adhesion of rubber with soil particles and due to compressibility of rubber.

The value of allowable bearing capacity for two columns with L/D ratio 3 is equal to 0.755 kg/cm2 it increases to 0.845 kg/cm2 for L/D equal to 6 and then decreases to 0.765 kg/cm2 at L/D equal to 10. Decrease in allowable bearing capacity after L/D = 6, was due to buckling of stone columns.

The value of allowable bearing capacity for three columns with L/D ratio 3 is equal to 0.82 kg/cm2 it also increases to 0.885 kg/cm2 for L/D ratio 6 and it also decreases to 0.825 kg/cm2 for L/D ratio 10. Similar observation were made in case of Four and five number of columns.

In case of five columns the value of Allowable Bearing Capacity of almost 2.5 times the allowable bearing capacity of virgin soil and about 2 times the allowable bearing capacity of soil with stone column of demolition waste only.

REFERENCES

[1] Nayak, N.V., (1983), " Recent advances in ground improvement by stone column", proceeding of Indian Geotechnical Society Conference., Madras, 1, 19.

[2] Bouassida, m.p debuhan and l. Dormieux (1995) Bearing capacity of a foundation resting on a soil reinforced by a group of column geo-techniques 45, No-1, PP 25,34.

[3] Tan – s.a, muhammad n; karunaratne. G.p. : The role of jute geo-textile / Slurry interface friction on the bearing capacity of clay slurry * geotechnical testing journal 1995/09. 18(3) PP 342-349.

[4] Mayerhoff , G.G And V.V.R.N Sastry (1978) :- Bearing capacity of piles in layered soils ,Part 1 , and part 2, Canadian geotechnical journal, 15, pp 171 -189

[5] Vesic, A.S (1972) Expansion of cavities in infinite soil mass Journal of soil mechanics and foundation Divisions, ASCE, 1972, vol98 , PP 265-290 .

[6] Green Wood , D.A (1970) Mechanical improvement of soils below ground surface ground engineering proceeding conference Organized by the institution of Civil Engineers, London , June 1970 , PP 11-22.

[7] Hughes, J.Mo And N.J Withers (1974) Reinforcing of soft soil with stone columns ground Engineering 7, No-3 PP 42-44 and 47-49

[8] Mckenna, J.M , W.A Eyre And Wolsten Holme (1976) Performance of an embankment supported by stone columns in soft ground treatment by deep compaction conducted by the institution of civil Engineering ,London. 1976 P51

[9] R. Ayothiraman, s. Soumya (2011) Use of Shredded Type Chips as Aggregates in Stone Column : An Experimental Study. (Paper No L-175)

[10] Pradip Das, Dr Sujit Kumar Pal (2013): A Study of the Behavior of Stone Column In Local Soft and Loose Layered Soil.

[11] Kotresh K.M1, Mesfin Getahun Belachew2(2014): Study on Waste Tyre Rubber As Concrete Aggregates.(Vol-3, PP 443-436) (ISSN:2277-1581)

Analytical Investigation on Retrofitting of A Multistoried R.C.C. Framed Building Using Pushover Technique

Guljit Singh
Assistant Professor,
Department of Civil Engineering,
Baba Banda Singh Bahadur Engineering College,
Fatehgarh Sahib, INDIA 140 407

Jagmohan Singh
Assistant Professor,
Department of Civil Engineering,
Baba Banda Singh Bahadur Engineering College,
Fatehgarh Sahib, INDIA 140 407

Simranpreet Singh
Assistant Professor,
Department of Civil Engineering,
Baba Banda Singh Bahadur Engineering College,
Fatehgarh Sahib, INDIA 140 407

***Abstract* - The scope of present study aims at determining the earthquake load carrying of a building and thereby improving its seismic load carrying capacity by providing certain adequate provisions of retrofitting. The performance based seismic engineering technique known has Non-Linear Static Pushover analysis procedure has been effectively used in this regard. The pushover analysis has been carried out using SAP2000, a product of Computers and Structures International. A total of 28 cases for a particular six storey building located in Zone-IV have been analyzed, considering retrofitting of different structural elements, i.e. Beams and Columns, in different combinations as well as at different storey levels. The retrofitting is started from the bottom most storey and subsequently moving towards the top most storey. The response of the building for each case at each storey level is recorded.**

The results of analysis are compared in terms of base shear and storey displacements.

Keywords: Performance-based seismic engineering (PBSE), Retrofitting, nonlinear static pushover analysis, Performance level, Finite element analysis, Sap 2000.

I. Introduction to Pushover Analysis

In Pushover analysis, a static horizontal force profile, usually proportional to the design force profiles specified in the codes, is applied to the structure. The force profile is then incremented in small steps and the structure is analyzed at each step. As the loads are increased, the building undergoes yielding at a few locations. Every time such yielding takes place, the structural properties are modified approximately to reflect the yielding. The analysis is continued till the structure collapses, or the building reaches certain level of lateral displacement.

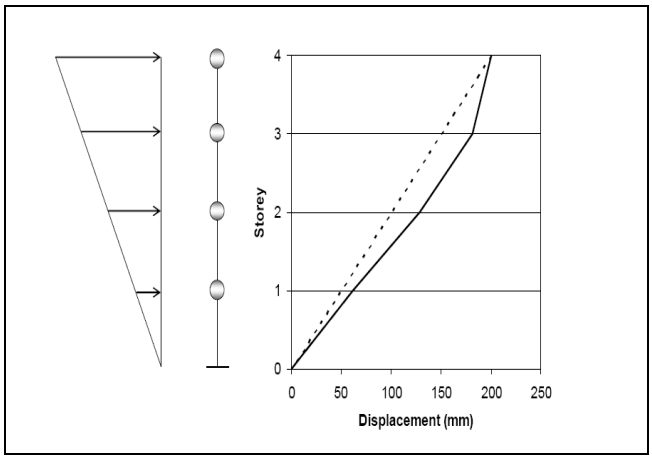

Fig. 1. Inverted Triangular Loading for Pushover

A. Need for Pushover Analysis

Conventionally, seismic assessment and design has relied on linear or equivalent linear (with reduced stiffness) analysis of structural systems. In this approach, simple models are used for various components of the structure, which is subjected to seismic forces evaluated from elastic or design spectra, and reduced by force reduction (or behavior) factors. The ensuing displacements are amplified to account for the reduction of applied forces.

B. Description of Pushover Analysis

The non-linear static pushover procedure was originally formulated and suggested by two agencies namely, federal emergency management agency (FEMA) and applied technical council (ATC), under their seismic rehabilitation programs and guidelines. This is included in the documents FEMA-273, FEMA-356 and ATC-40.

Methods and design criteria to achieve several different levels and ranges of seismic performance are defined in FEMA 273. The four Building Performance Levels are Collapse Prevention, Life Safety, Immediate Occupancy, and Operational. These levels are discrete points on a continuous

scale describing the building's expected performance, or alternatively, how much damage, economic loss, and disruption may occur.[4]

The three Structural Performance Levels and two Structural Performance Ranges consist of:

S-1: Immediate Occupancy Performance Level

S-2: Damage Control Performance Range (extends between Life Safety and Immediate Occupancy Performance Levels)

S-3: Life Safety Performance Level

S-4: Limited Safety Performance Range (extends between Life Safety and Collapse Prevention Performance Levels)

S-5: Collapse Prevention Performance Level

In addition, there is the designation of S-6, Structural Performance Not considered, to cover the situation where only nonstructural improvements are made.

The four Nonstructural Performance Levels are:

N-A: Operational Performance Level

N-B: Immediate Occupancy Performance Level

N-C: Life Safety Performance Level

N-D: Hazards Reduced Performance Level

In addition, there is the designation of N-E, Nonstructural Performance Not Considered, to cover the situation where only structural improvements are made.

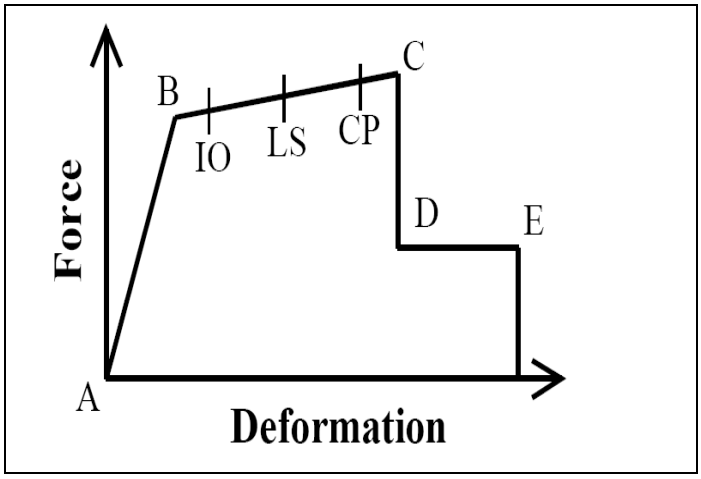

Fig. 2. Force - Deformation Curve [4]

II. PREVIOUS STUDIES

According to Jong-Wha Bai (August 2002), Seismic retrofitting is an effective method of reducing the risks for existing seismically deficient structures. Numerous intervention techniques are available for improving the seismic behavior of RC building structures. It is important to obtain accurate as-built information and analytical data to perform a seismic evaluation of the existing structure and to select the appropriate retrofitting strategy. A number of experimental and analytical studies focused on seismic retrofitting techniques and extensive seismic damage control activities in practice have contributed to the present state of development. Further research should be conducted to improve the selection of appropriate retrofit techniques using criteria based on performance, economy and constructability[16].

According to Gajjar R. K. et al (2002), pushover Analysis results from powerful softwares can be transferred to virtual reality platforms in order to make the outputs more user friendly and easy to understand, besides making it very simple to re-analayze and observe the end results any number of times, till the user is able to grasp the full impact of his final decision. Virtual reality platforms provide a fantastic opportunity as add-on modules to complex analysis software which generally need a high degree of decision and understanding of behaviour of the structure under consideration even prior to modeling it on the desktop. Instant graphical outputs in virtual reality, bring into focus the errors in primary configuration details, in modeling or in designing. The user can therefore afford to make mistakes and correct them at the touch of a few strokes on the keyboard. As the concept is still in its infancy, and as 3D graphics have been hitherto limited to the highly sophisticated domain of movie animation, the computer time and effort required in creating real-life images seem extremely daunting, but are worth the pain if the expense and amount of on-site rehabilitation and on-table interpretation from innumerable tables and numbers, is borne in mind. The concept of VR can then be extended to the web where other stake holders too sitting across the globe can interact and give valuable inputs towards an optimum and robust solution [13].

Chopra et. al (May 2003)**,** laid down the concept of modal pushover analysis (MPA). They analysisd six SAC buildings, each analyzed for 20 ground motions, and their statistical analysis leads to bias and dispersion in the procedure. The results demonstrated that by including a few "modes" (typically two or three), the height-wise distribution of demands estimated by MPA is generally similar to the "exact" results from nonlinear response history analysis. The MPA procedure estimates seismic story-drift demands to a degree of accuracy that should be sufficient for most building design and retrofit applications [15].

Jain et. al (August 2002), carried out pushover analysis for seismic retrofitting of buildings for a flat slab building. The various retrofitting techniques used by them included jacketing of columns only, providing additional beams and providing both columns jacketing and additional beams. They concluded that jacketing or retrofitting of columns result in a much higher drift capacity. The additional beams significantly reduce softening caused by sagging hinges. But they have a comparatively lower drift capacity. However jacketing of both beams and columns result into the best response of the system [12].

III. GENERAL OVERVIEW OF PARAMETRIC STUDY

The main objective of seismic design of buildings is to avoid total catastrophic damage so that structural damages caused, if any, could be repaired after the earthquake event. Static pushover analysis is an attempt by the structural engineering profession to evaluate the real strength of the structure and it promises to be a useful and effective tool for performance based design.

Finally, certain special combinations of retrofitting have been done from the results obtained from the study, so as to get a highly improved response of structure at a relatively cheaper cost.

The following cases (Table I) have been incorporated in the study:

TABLE I. Description of various cases

SR. NO.	CASE NO.	DESCRIPTION OF CASES
1		Original structure
2	1	Retrofitting beams of 1st storey only
3	2	Retrofitting columns of 1st storey only
4	3	Retrofitting beams & columns of 1st storey only
5	4	Retrofitting beams of 1st +2nd storey only
6	5	Retrofitting columns of 1st +2nd storey only
7	6	Retrofitting beams & columns of 1st +2nd storey only
8	7	Retrofitting beams of 1st +2nd+3rd storey only
9	8	Retrofitting columns of 1st +2nd+3rd storey only
10	9	Retrofitting beams & columns of 1st +2nd+3rd storey only
11	10	Retrofitting beams of 1st +2nd+3rd+4th storey only
12	11	Retrofitting columns of 1st +2nd+3rd+4th storey only
13	12	Retrofitting beams & columns of 1st +2nd+3rd+4th storey only
14	13	Retrofitting beams of 1st +2nd+3rd+4th+5th storey only
15	14	Retrofitting columns of 1st +2nd+3rd+4th+5th storey only
16	15	Retrofitting beams & columns of 1st +2nd+3rd+4th+5th storey only
17	16	Retrofitting beams of 1st +2nd+3rd+4th+5th +6th storey only
18	17	Retrofitting columns of 1st +2nd+3rd+4th+5th +6th storey only
19	18	Retrofitting beams & columns of 1st +2nd+3rd+4th+5th +6th storey only

A. Description of a Building

In the present work, a six storied reinforced concrete frame building situated in Zone IV, is taken for the purpose of study. The plan area of building is 12 x 12 m with 3.0m as height of each typical storey. It consists of 4 bays of 3m each in X-direction and Z-direction (3 x 4= 12m). Hence, the building is symmetrical about both the axis. The total height of the building is 18m. The building is considered as a Special Moment resisting frame. The retrofitting of frame elements, i.e. Beams and columns is done in various combinations at all the storey levels. The plan of building is shown in fig. 3; the front elevation is shown in fig. 4 and 3d view in fig. 5.

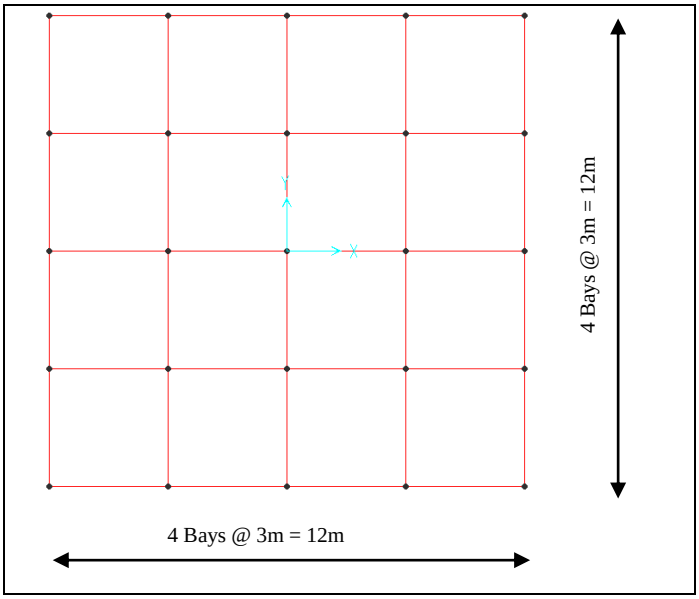

Fig. 3. Plan of Building

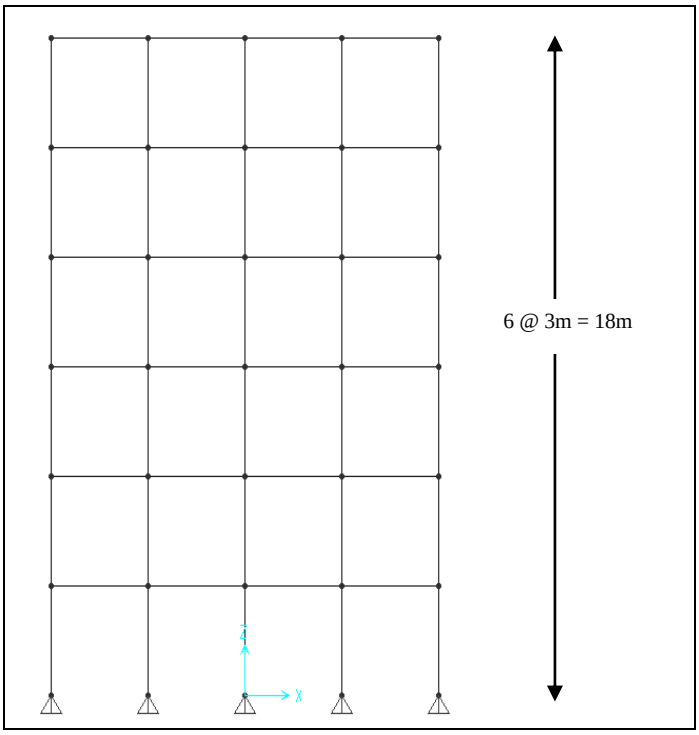

Fig. 4. Elevation of Building

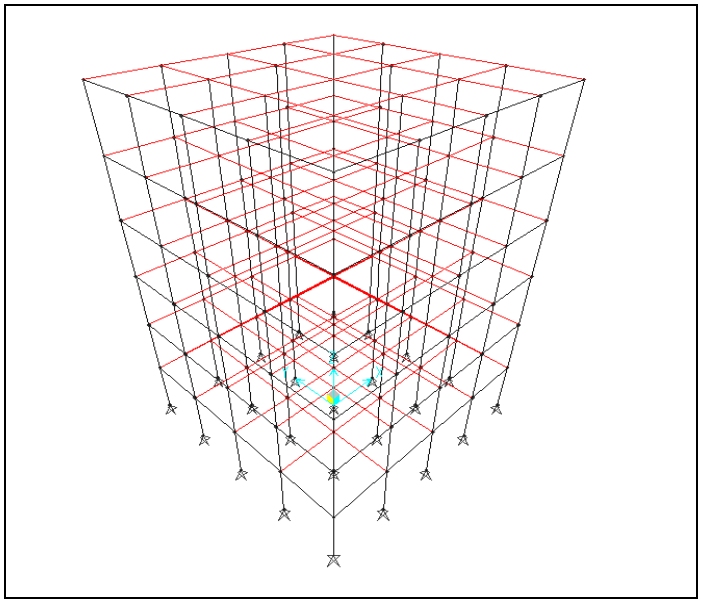

Fig. 5. 3D view of Building

B. *Sectional Properties of Elements*

The sectional properties of elements in case of the original structure are taken as follows:

Size of Column = 450 x 450mm, Size of Beam = 0.230 x 300 mm, Thickness of Slab = 125mm thick

When the structure was retrofitted, the size of columns was increased to 600x600mm, while that of beam was changes to 300x450mm. A nominal percentage i.e. 1% of the increased area can be provided for the retrofitting purposes.

C. *Loads Considered*

The following loads were considered for the analysis of the building. The loads were taken in accordance with IS:875[1][2].

D. *Gravity Loads*

The intensity of dead load and live load at various floor levels and roof levels considered in the study are listed below [9].

- Dead Load

At all Floor Levels

Weight of Slab: 0.125 x 25	= 3.125 kN/m^2
Weight of Screed: 0.050 x 20	= 1.000 kN/m^2
Weight of Floor Finish: 0.025 x 24	= 0.600 kN/m^2
Weight of partition Wall	= 1.000 kN/m^2
Total Dead Load	= 5.725 kN/m^2
Total Dead Load Taken	= 6.0 kN/m^2

A wall load of 12kN/m has been applied to all the outer beams at all the floor levels

- Live Load

Live load at all floor levels = 3.0 kN/m^2

This live load is reduced by 25% for calculating the seismic weight of the structure as per provisions of IS1893:2002(PART 1).

E. *Seismic Loads*

The design lateral force due to earthquake is calculated [11] as follows:

Design horizontal seismic coefficient:

The design horizontal seismic coefficient Ah for a structure shall be determined by the following expressions:-

Ah = Z I Sa 2 R g

Provided that for any structure with T≤0.1 sec. The value of Ah will not be less than Z/2 whatever the value of R/I.

Z= Zone factor

I = Importance factor depending upon the functional use of the structure.

R = Response reduction factor, depending upon the perceived seismic damage performance of the structure.

Sa /g =Average response acceleration coefficient for rock or soil sites.

- Seismic Weight

The seismic weight of each floor is its full dead load plus appropriate amount of imposed load. While computing the seismic weight of each floor, the weight of columns and walls in a storey shall be equally distributed to the floors above and below the storey.The seismic weight of the whole building is the sum of the seismic weights of all the floors.

Design Seismic Base Shear

The total design lateral force or seismic base shear (Vh) along any principal direction is determined by the following expression:-

Vh = AhW

Where W is the seismic weight of the building.

Fundamental Natural Time Period

The approximate fundamental natural time period of vibration (Ts) in seconds of a moment resisting frame building without brick infill panels may be estimated by the following empirical expressions:

TS = 0.075h0.75 for RC framed building

TS = 0.085h0.75 for steel framed building

Where h=Height of the building in meters

For all other buildings, it is given by:-

Tn = 0.09h/√d

Where h=Height of the building in meters

d= base dimension of the building at the plinth level,in meters, along the considered direction of the lateral force.

- Distribution of design force

The design base shear (Vh) computed is distributed along the height of the building as below:

$$Qi = Vh \frac{Wi\ hi^2}{\sum Wi\ hi^2}$$

Where,

Qi = design lateral force at each floor level i

Wi = seismic weight pf floor i.

i = height of floor i measured from the base.

- Design lateral force

The design lateral force shall first be computed for the building as a whole the design lateral force shall then be distributed to the various floor levels. The design seismic force thus obtained at each floor level, shall then be distributed to individual lateral load resisting elements depending on the floor diaphragm action.

IV. PUSHOVER ANALYSIS USING SAP2000

The following steps are included in the pushover analysis. Steps 1to 4 are to create the computer model, step 5 runs the analysis, and steps 6 to 10 review the pushover analysis results.

1. Create the basic computer model (without the pushover data) as shown in Figure 6. The graphical interface of SAP2000 makes this quick and easy task. Assigned sectional properties & applies all the gravity loads i.e. Dead load and Live load on the structure [5].

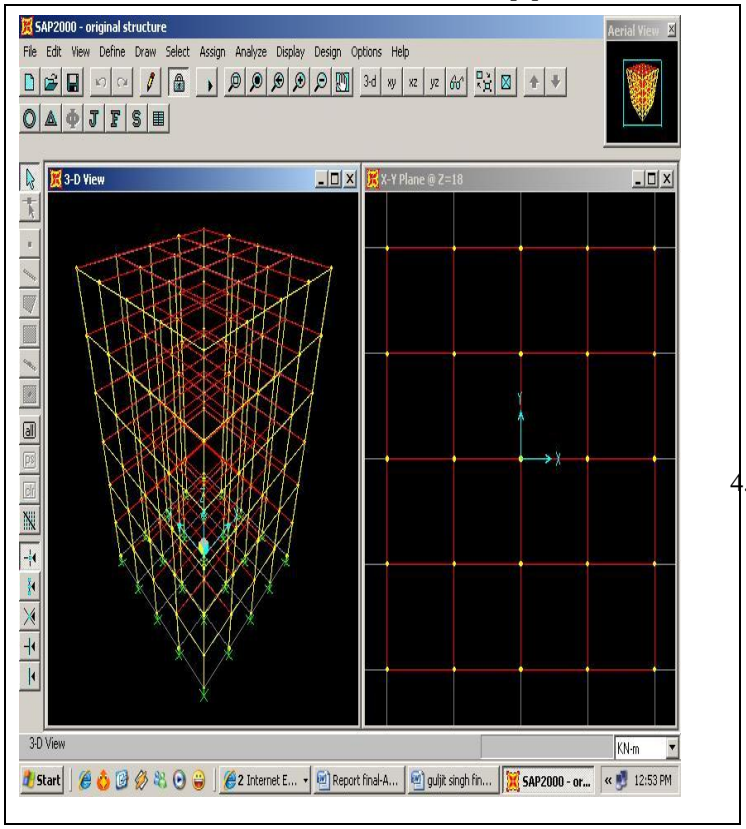

Fig. 6. Basic Model in SAP2000

2. Define properties and acceptance criteria for the pushover hinges as shown in Figure 7. The program includes several built-in default hinge properties that are based on average values from ATC-40 for concrete members and average values from FEMA-273 for steel members. In this analysis, PMM hinges have been defined at both the column ends and M3 hinges have been defined at both the ends of all the beams.

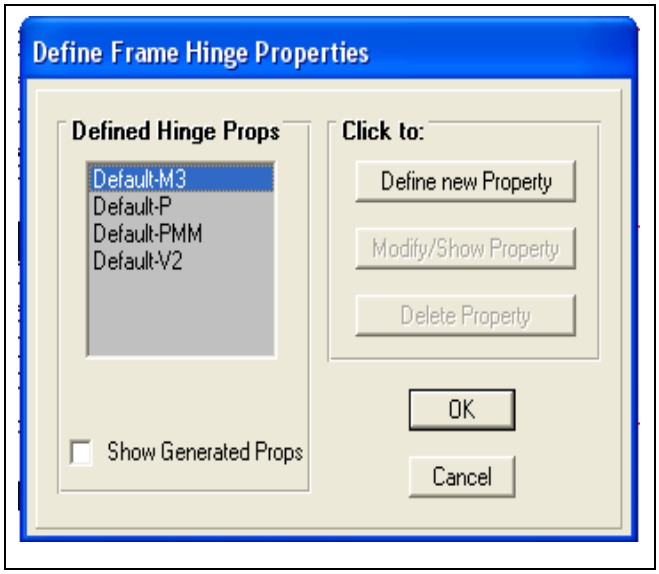

Fig. 7. Defining Hinge Properties

3. Locate the pushover hinges on the model by selecting all the frame members and assigning them one or more hinge properties and hinge locations as shown in Figure 8.

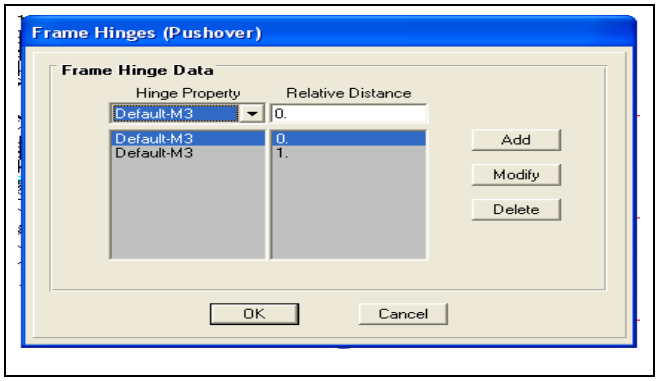

Fig. 8. Assignment of Hinges

4. Define the pushover load cases, figure 9(a) and (b). In SAP2000 more than one pushover load case can be run in the same analysis. Also a pushover load case can start from the final conditions of another pushover load case that was previously run in the same analysis. Typically the first pushover load case was used to apply gravity load and then subsequent lateral pushover load cases were specified to start from the final conditions of the gravity pushover. Pushover load cases can be force controlled, that is, pushed to a certain defined force level, or they can be displacement controlled, that is, pushed to a specified displacement. Typically a gravity load pushover is force controlled and lateral pushovers are displacement controlled. In this case a Gravity load

combination of DL+0.25LL has been used. This combination has been defined as GRAV. The lateral loads have been applied to a case called PUSHPAT.

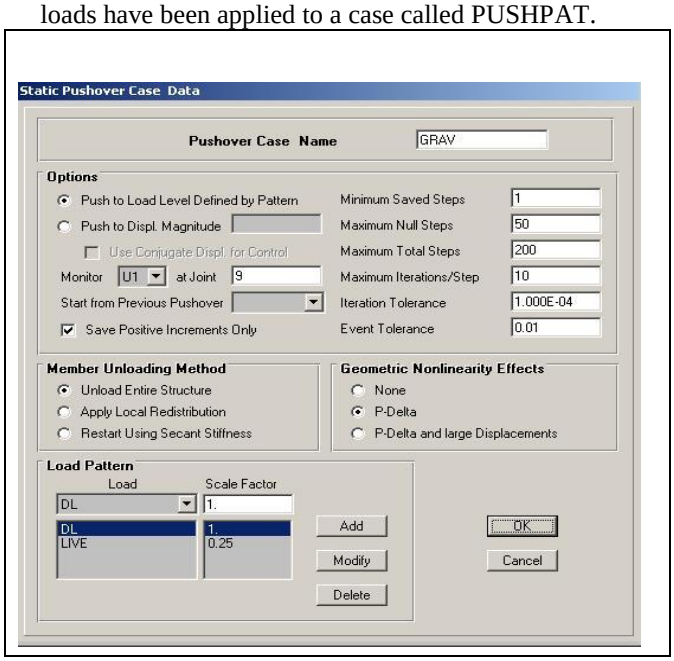

Fig. 9. (a). Defining Pushover Cases

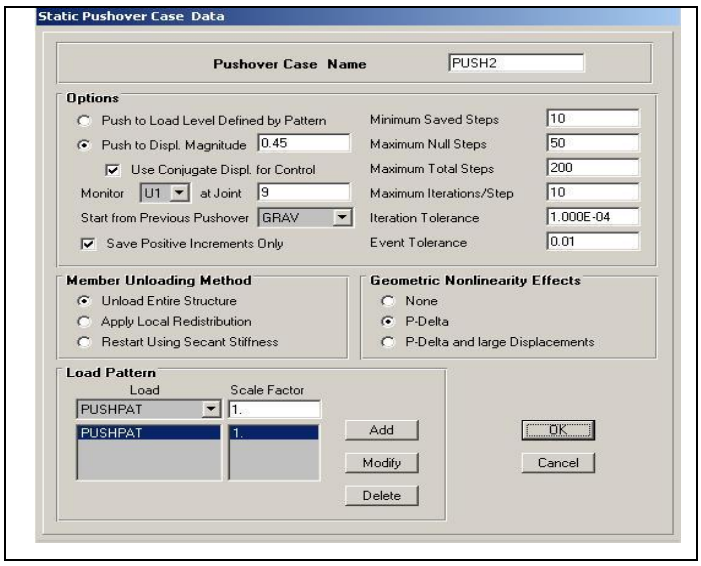

Fig. 9 (b). Defining Pushover Cases

5. Run the basic static analysis. Then ran the static nonlinear pushover analysis.
6. The Pushover curve was made for control nodes at each storey level. This was done by defining a number of pushover cases in the same analysis, and displacement was monitored for a different node in each case.
7. The pushover curve was obtained as shown in Figure 10. A table was also obtained which gives the coordinates of each step of the pushover curve and summarizes the number of hinges in each state (for example, between IO and LS, or between D and E). This table is shown in Figure 11.

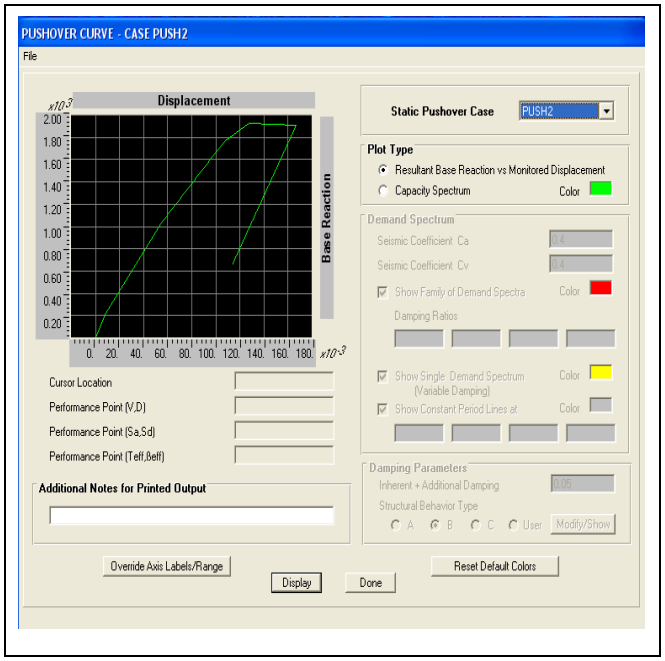

Fig. 10. Pushover Curve

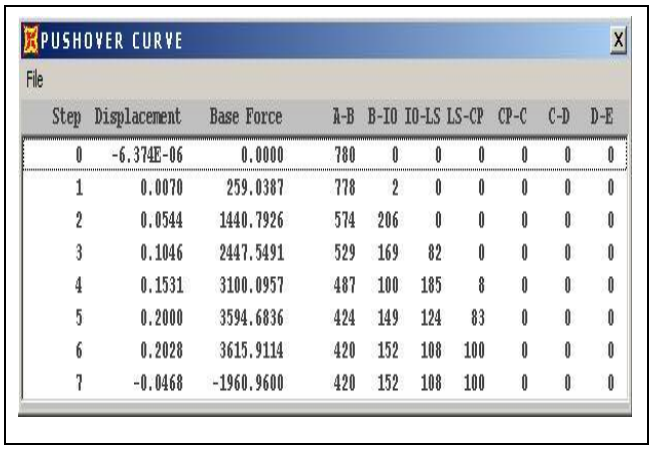

Step	Displacement	Base Force	A-B	B-IO	IO-LS	LS-CP	CP-C	C-D	D-E
0	-6.374E-06	0.0000	780	0	0	0	0	0	0
1	0.0070	259.0387	778	2	0	0	0	0	0
2	0.0544	1440.7926	574	206	0	0	0	0	0
3	0.1046	2447.5491	529	169	82	0	0	0	0
4	0.1531	3100.0957	487	100	185	8	0	0	0
5	0.2000	3594.6836	424	149	124	83	0	0	0
6	0.2028	3615.9114	420	152	108	100	0	0	0
7	-0.0468	-1960.9600	420	152	108	100	0	0	0

Fig. 11. Tabular Data for Pushover Curve

8. The capacity spectrum curve obtained is shown in Figure 12. The magnitude of the earthquake and the damping information on this form can be modified and the new capacity spectrum plot can be obtained immediately. The performance point for a given set of values is defined by the intersection of the capacity curve and the single demand spectrum curve. Also, a table was generated which shows the coordinates of the capacity curve and the demand curve as well as other information used to convert the pushover curve to Acceleration-Displacement Response Spectrum format (also known as ADRS format). See Figure 13.

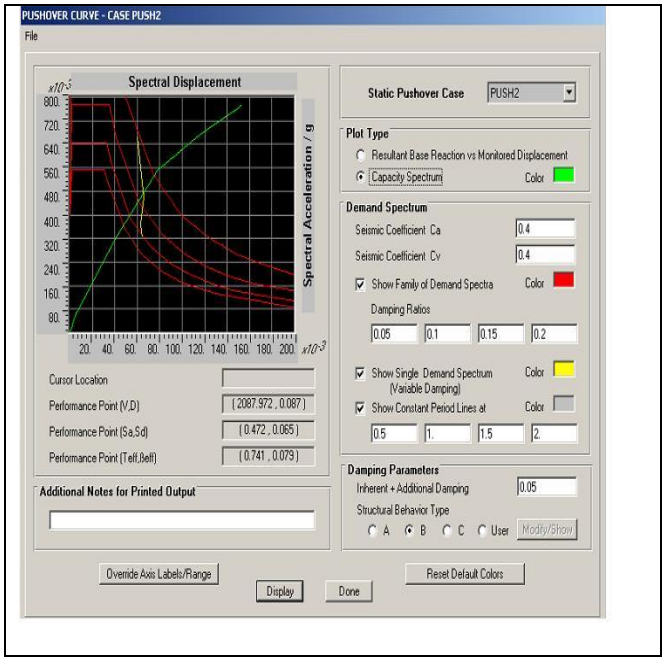

Fig. 12. Capacity Spectrum Curve

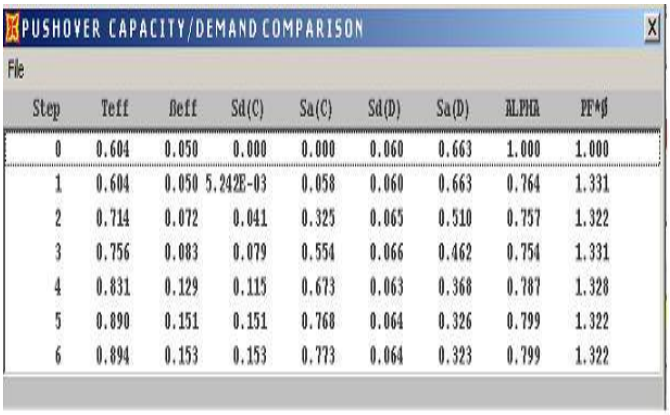

Step	Teff	βeff	Sd(C)	Sa(C)	Sd(D)	Sa(D)	ALPHA	PF*ϕ
0	0.604	0.050	0.000	0.000	0.060	0.663	1.000	1.000
1	0.604	0.050	5.242E-03	0.058	0.060	0.663	0.764	1.331
2	0.714	0.072	0.041	0.325	0.065	0.510	0.757	1.322
3	0.756	0.083	0.079	0.554	0.066	0.462	0.754	1.331
4	0.831	0.129	0.115	0.673	0.063	0.368	0.787	1.328
5	0.890	0.151	0.151	0.768	0.064	0.326	0.799	1.322
6	0.894	0.153	0.153	0.773	0.064	0.323	0.799	1.322

Fig. 13. Tabular Data For Capacity Spectrum Curve

9. The pushover displaced shape and sequence of hinge information on a step-by-step basis was obtained.
10. Output for the pushover analysis can be printed in a tabular form for the entire model or for selected elements of the model. The types of output available in this form include joint displacements at each step of the pushover, frame member forces at each step of the pushover, and hinge force, displacement and state at each step of the pushover [5].

V. RESULTS AND DISCUSSIONS

A. Base Force

The base force for the six-storey building with different combination of element retrofitting at various floor levels is presented in Table 2. The variation of base force for various cases of retrofitting of building is shown in Figure 2.

It is observed that with retrofitting of beams only, there is a very minimal percentage increase in the base force varying from 11.9% to 26.93%, which the structure can carry. However, with the retrofitting of storey columns, there is quite an appreciable gain in the base force carrying capacity of the structure. The percentage change varies from 15.64% to 98.25%. Further it is observed that, retrofitting of columns at 2nd storey there is a decline in the base force capacity, but after 2nd storey, there is predominant increase in base force due to retrofitting of columns only. The combination of retrofitting of beams and columns both, show a consistent increase in base force capacity but it becomes more predominant from 3rd Storey onwards.

TABLE II. COMPARISON OF BASE SHEAR

RETROFITTING LEVEL	CASES	INCREASE IN NO. OF ITERATIONS	BASE SHEAR (KN)	PERCENTAGE INCREASE
Original structure		4	3049.4314	
RETROFITTING UPTO 1st STOREY	CASE 1	5	3415.1372	11.9
	CASE 2	6	3722.8994	22.08
	CASE 3	5	3763.8350	23.42
RETROFITTING UPTO 2nd STOREY	CASE 4	7	3800.3967	24.62
	CASE 5	4	3526.5369	15.64
	CASE 6	6	3543.8384	16.21
RETROFITTING UPTO 3rd STOREY	CASE 7	5	3588.6655	17.68
	CASE 8	4	3689.0637	20.97
	CASE 9	4	3679.8408	20.67
RETROFITTING UPTO 4th STOREY	CASE 10	5	3646.4312	19.57
	CASE 11	8	3848.0723	26.18
	CASE 12	8	5204.1719	70.66
RETROFITTING UPTO 5th STOREY	CASE 13	6	3870.7119	26.93
	CASE 14	6	5983.6665	96.22
	CASE 15	8	6493.8042	112.95
RETROFITTING UPTO 6th STOREY	CASE 16	6	3835.5139	25.77
	CASE 17	6	6045.7153	98.25
	CASE 18	8	6533.5293	114.25

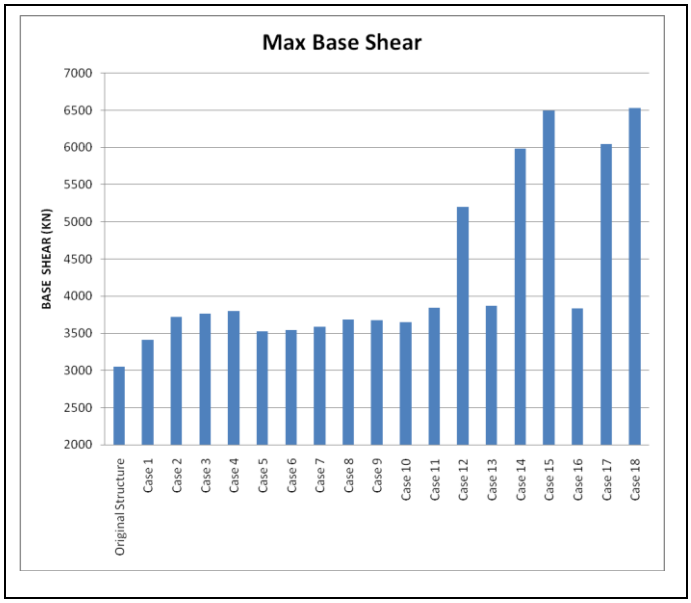

Fig. 14. Variation of Base Shear

B. *Roof Displacement*

The Roof displacement for the six-storey building with different combination of element retrofitting at various floor levels is presented in Table 3. The variation of Roof displacement for various cases of retrofitting of building is shown in Figure 3.

It is observed that with retrofitting of beams only, there is a decrease in the roof displacement upto 4th storey and after 4th storey it got little increased upto5th storey (31.16% to 8.05%) and after 5storey it again decreases to (14.23%). This percentage varies from 31.16% to 8.05%. However, the trends shown by retrofitting of columns only is there is a decrease in the roof displacement upto 2nd storey and after 2nd storey it predominantly increases upto 5th storey and again decreases slightly at 6th storey. The percentage change varies from -8.59% to 102.61%. The combination of retrofitting of beams and columns both, show a consistent decrease in the roof displacement upto 3rd storey and after 3rd storey it predominantly increases upto 5th storey and again decreases slightly at 6th storey.

TABLE III. COMPARISON OF ROOF DISPLACEMENT

RETROFITTING LEVEL	*CASES*	*INCREASE IN NO. OF ITERATIONS*	*ROOF DISPLACEMENTS (mm)*	*PERCENTAGE INCREASE*
Original structure		4	148.9	
RETROFITTING UPTO 1st STOREY	CASE 1	5	169.6	13.90
	CASE 2	6	168.0	12.82
	CASE 3	5	169.6	13.90
RETROFITTING UPTO 2nd STOREY	CASE 4	7	195.3	31.16
	CASE 5	4	136.1	-8.59
	CASE 6	6	124.4	-16.45
RETROFITTING UPTO 3rd STOREY	CASE 7	5	163.3	9.67
	CASE 8	4	143.9	-3.35
	CASE 9	4	115.9	-22.16
RETROFITTING UPTO 4th STOREY	CASE 10	5	160.9	8.05
	CASE 11	8	153.3	2.95
	CASE 12	8	220.1	47.81
RETROFITTING UPTO 5th STOREY	CASE 13	6	177.7	19.34
	CASE 14	6	301.7	102.61
	CASE 15	8	292.1	96.17
RETROFITTING UPTO 6th STOREY	CASE 16	6	170.1	14.23
	CASE 17	6	286.7	92.54
	CASE 18	8	274.3	84.21

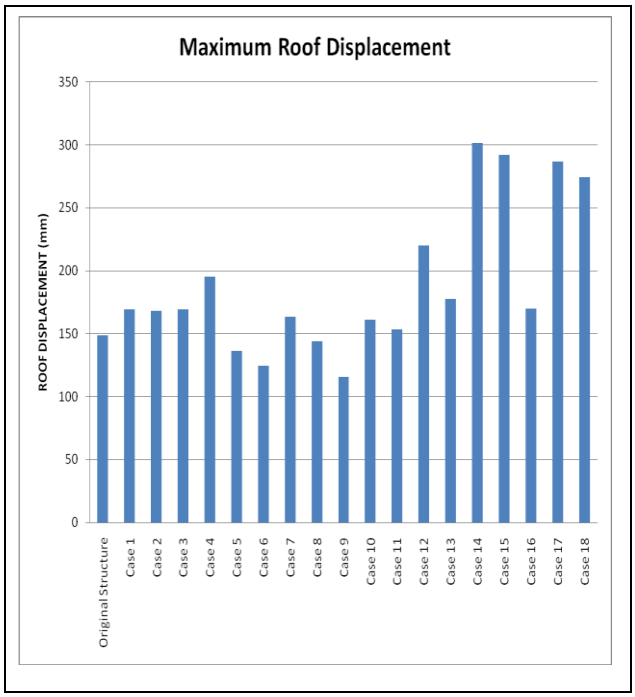

Fig. 15. Variation of Roof Displacement

VI. CONCLUSIONS

Based on the present study, the following conclusions can be drawn:

1. There is a minimal increase in the base shear due to retrofitting of beams only. An increase of only 11.9% to 26.93% is observed when the beams are retrofitted.
2. The retrofitting of columns results into an appreciable gain in base shear. This increase varies from 15.64% to 98.25%. The maximum increase is for the case when all the columns are retrofitted upto 6th storey only.
3. The retrofitting of both beams and columns gives an appreciable increase in the base shear of the structure. This range varies from 16.21% to 114.25%. The maximum value of 114.25% increase is obtained when all the beams as well as columns are retrofitted upto the 6th storey.

4. The retrofitting of beams results into a decrease in the roof displacement upto 4th storey and again got increased at 5th storey and again further decreases at 6th storey of the structure. This decrease varies from 31.16% to 8.05%.
5. The retrofitting of columns results into an appreciable decrease in the maximum roof displacement upto 2th storey and suddenly appreciable increase is seen at 5th storey and again further slightly decreases at 6th storey which the structure can carry without failure. This decrease varies from 102.61% to -8.59%. The maximum roof displacement is observed for the case, when all the columns have been retrofitted upto 5th storey.
6. The retrofitting of both beams and columns in different combinations cause a decrease of 13.90% to -22.16% in roof displacement upto 3rd storey and further increases upto 5th storey from -22.16% to 96.17% in roof displacement and again slightly decreases at 6th storey.

REFERENCES

[1] IS : 875 (Part I) – 1987, " Code of Practice for Design Loads (Other than Earthquake) For Buildings and Structures", Second Revision, Bureau of Indian Standards, New Delhi.

[2] IS : 875 (Part II) – 1987, " Code of Practice for Imposed Loads (Other than Earthquake) For Buildings and Structures", Second Revision, Bureau of Indian Standards, New Delhi.

[3] Applied Technology Council (1996). "Seismic Evaluation and Retrofit of concrete Buildings, Report No. ATC-40", California.

[4] FEMA (1997), "FEMA 273 – NEHRP Guidelines for the Seismic Rehabilitation of Buildings", Federal Emergency Management Agency, Washington DC, USA

[5] SAP2000 (June 1998), "Detailed Tutorial Including Pushover analysis", Computers and Structures Inc., Berkeley, USA.

[6] Ashraf Habibullah and Stephen Pyle (1998), "Practical Three Dimensional Nonlinear Static Pushover Analysis", Structure Magazine, USA.

[7] American Society of Civil Engineers (2000), "Pre-standard and Commentary for the Seismic Rehabilitation of Buildings, FEMA-356", Federal Emergency Management Agency, Washington, D.C.

[8] Farzad Naeim, Hussain Bhatia, Roy M. Lobo, (2000) "Chapter 15, Performance Based Seismic Engineering", Seismic design handbook.

[9] IS 456:2000, "Indian Standard Code of Practice for Plain and Reinforced Concrete", fourth Revision, Bureau of Indian Standards, New Delhi.

[10] Gupta, B. and Kunnath, S.K.(July 2000), "Adaptive spectra-based pushover procedure for seismic evaluation of structures.", Earthquake Spectra, 16(2), pp. 367-391.

[11] IS Code 1893-2002(Part 1) "Criteria for Earthquake Resistant Design of Structures (part 1), General provisions and Buildings, Fifth Revision.

[12] Sudhir K. Jain and T. Srikant (August 2002), "Analysis of seismic retrofitting of buildings, The Indian Concrete journal".

[13] R. K. Gajjar and S. C. Patodi, (2002) "Studying Damage of RCC Columns under Seismic Forces through Virtual Reality", M.E Thesis, The M.S. University of Baroda, Baroda

[14] Durgesh C Rai (2002), "Review of Seismic Strengthening of Buildings", IITK-GSDMA-EQ07-V1.0 11

[15] Anil K. Chopra and Rakesh K. Goel (May 2003), "A modal pushover analysis procedure to estimate seismic demands for buildings: summary and evaluation", Fifth National Conference on Earthquake Engineering, Istanbul, Turkey Keynote Lecture

[16] Jong-Wha Bai (August 2003), "Seismic Retrofit for Reinforced Concrete Building Structures", Mid-America Earthquake Center.

Strength Study of RCC Beams Retrofitted Using Different Fiber Reinforced Polymer (FRP)

Karamjot Singh,
Assistant professor
Department of Civil Engineering,
Baba Banda Singh Bahadur Engineering College
Fatehgarh Sahib, India

Guiljit Singh,
Assistant professor
Department of Civil Engineering,
Baba Banda Singh Bahadur Engineering College
Fatehgarh Sahib, India

Harkomal kaur,
Assistant professor
Department of Civil Engineering,
Baba Banda Singh Bahadur Engineering College
Fatehgarh Sahib, India

***Abstract*—Throughout the world many existing reinforced concrete structure are under need of repair or rehabilitation due to the various deterioration factors like environmental effects, revision in loading standards, seismic retrofitting, corrosion, lack of reinforcement detailing etc leading to failure of bonding between beam-column, increase in deflection limits. As Fiber Reinforced Polymer (FRP) composite incrementing the strength of RCC structures due to its outstanding properties such as high strength to weight ratio, resistance to corrosion and fire, higher fatigue strength and impact energy absorption capacity. This paper focuses exclusively on behaviour of RCC beams strength using the Vinyl-Ester bonded GFRP and Epoxy bonded GFRP wrapped retrofitting. Ultimate load carrying capacity, deflection and cracking are analysis experimental. An effort has been made in this paper to represent the collective contributions of researchers and to focus on the type of beam gaining maximum enhancement in shear strength with use of FRP laminates. The paper also represents the effect of different parameters on the strength of beams strengthened externally with FRP sheets or strips. It was concluded that the wrapping of FRP sheets increases the ultimate load carrying capacity of RCC beams.**

Keywords—FRP; Vinyl Ester Bonded GFRP; Epoxy bonded GFRP; Shear Strength; RCC Beams

I. INTRODUCTION

This Retrofitting of shear concrete elements are accomplished by externally bonding or wrapping steel plates or wires to concrete. This technique has proved to be effective in increasing ultimate strength and stiffness of reinforced concrete elements. In the last decade, the development of strong epoxy glue has led to a technique which has great potential in the field of retrofitting structures. Basically the technique involves pasting steel plates or fiber reinforced polymer (FRP) to the surface of the concrete. These plates then act monolithically with the concrete. FRP can be convenient compared to steel for a number of reasons. These materials have higher ultimate strength and lower density than steel. The installation is easier and temporary support for fixing is not required due to the low weight. They can be formed on site into complicated shapes and can also be easily cut to length on site. FRP composites are different from traditional construction materials such as steel or aluminum. FRP composites are anisotropic (properties apparent in the direction of the applied load) whereas steel or aluminum is isotropic (uniform properties in all directions, independent of applied load). Therefore, FRP composite properties are directional, meaning that the best mechanical properties are in the direction of the fiber placement. Composites are similar to reinforced concrete where the rebar is embedded in an isotropic matrix called concrete. FRP composites possess some outstanding properties such as: resistance to corrosion, good fatigue and damping resistance, high strength to weight ratio, and electromagnetic transparency. FRP has found an increasing number of applications in construction either as internal or as external reinforcement for concrete structures. Civil structures made of steel reinforced concrete are normally susceptible to environmental attacks that lead to the initiation of an electrochemical process which leads to the corrosion of steel reinforcement. Constant maintenance and repairing is needed to enhance the life cycle of those structures.. The use of FRP bars as an internal reinforcement for concrete bridge decks and also girders provides a potential for increased service life, economic and environmental benefits. In this paper beams were retrofitted with 1.2 mm Epoxy bonded GFRP sheets and 0.9 mm Vinyl-Ester bonded GFRP sheets using epoxy resins. In all a total of 6 beams were tested and the respective readings were recorded. The beams were full-wrapped and tested for shear behavior analysis. [1]

II. MATERIAL COMPOSITION

Polymer composites are heterogeneous materials resulting from the combination of different constituents, including high-performance fibers, polymer matrix and various fillers and additives. Fibers exhibit high tensile strength and stiffness and are the main load carrying element. Resin offers high compressive strength and binds the fibers into a firm matrix. Additives help to improve the mechanical and physical properties as well as the workability of composites. Glass fiber reinforced polymer (GFRP) is used for investigation purpose of retrofitting beam. Following are some of the characteristics of this versatile fiber. Glass fiber reinforced polymer (GFRP), also known as glass fiber reinforced plastic is a fiber made of a plastic matrix

reinforced by fine fibers made of glass. The plastic matrix used is epoxy or thermoplastic. The GFRP is the least expensive but has lower strength and significantly lower stiffness compared to other alternatives. The glass fibers are divided into three classes -- E-glass, S-glass and C-glass. The E-glass is designated for electrical use and the S-glass for high strength. The C-glass is for high corrosion resistance, and it is uncommon for civil engineering application. Out of the three fibers, the E-glass is the most common reinforcement material used in civil structures. It is produced from lime-alumina-borosilicate, which can be easily obtained from abundance of raw materials like sand. The fibers are drawn into very fine filaments with diameters ranging from 0.002 to 0.013mm. The glass fiber strength and modulus can degrade with increasing temperature. Although the glass material creeps under a sustained load, it can be designed to perform satisfactorily. The fiber itself is regarded as an isotropic material and has a lower thermal expansion coefficient than that of steel.

TABLE-II FRP Materials

S.no	Constituents	Characteristic
1	Vinyl ester bonded fiber reinforced polymer	Plastic matrix
2	Unsaturated Polyesters	Polymerization of dicarboxylic acid
3	Epoxies	Glycidyl ethers and amines.
4	Vinyl Esters	Workability of the epoxy resins and the Fast curing of the polyesters
5	Polyurethanes	Polyisocyanate and Polyol
6	Phenolics	Phenols and Formaldehyde

III. SPECIMEN AND TEST SET-UP

A. Casting of test Beams

A total of six simply supported beams were tested. All beams were of rectangular cross section 100mm wide and 500mm deep with 2 bars of 8 mm diameter as longitudinal reinforcement at top and 2 bars of 10 mm diameter as longitudinal reinforcement at bottom of beam section. The test specimens were divided into three series, namely, series A for controlled beam, series B for Vinyl Ester Bonded GFRP upto length of L/4 from both ends and at center length of L/2 Epoxy bonded GFRP and series C for Vinyl Ester Bonded GFRP at center length of L/2 from both ends and Epoxy bonded GFRP upto length of L/4 from both ends. Each series consisted of two beams as testing specimens. The material chosen are concrete compressive strength Fck=20 N/mm^2 and the grade of steel chosen is Fe 415 N/mm^2.As to study the increase in the shear strength of the beams after retrofitted with Vinyl Ester bonded Glass Fiber Reinforced Polymer beams are designed in such a manner that they are deficient in shear and hence fail in shear therefore detailing of the shear Reinforcements is done as each 2 Legged 6mm dia stirrups at 90 mm C/C. (Figure-1)

B. Experimental Arrangement

Use All the Six beams are tested under simply supported end conditions .Two point loading is adopted for testing. The testing of beams is done with the help of hydraulic operated jack connected to load cell. The load is applied to the beam with the help of hydraulic jack and the data is recorded from the data acquisition system which is attached with the load cell. The value of deflection is also obtained from the data acquisition system. Out of these six beams 2 are control beam which are tested after 28 days of curing to find out the safe load which is taken as load corresponding to deflection of L/250 i.e. 15 mm. When the beams are tested, shear cracks are seen over the beam which shows that they are failing in shear. Two beams of series A as Controlled Specimens, two beam of series B as Vinyl Ester Bonded GFRP upto length of L/4 from both ends and at center length of L/2 Epoxy bonded GFRP and two beams of series C as Vinyl Ester Bonded GFRP at center length of L/2 from both ends and Epoxy bonded GFRP upto length of L/4 from both end tested for shear. (Figure-2)

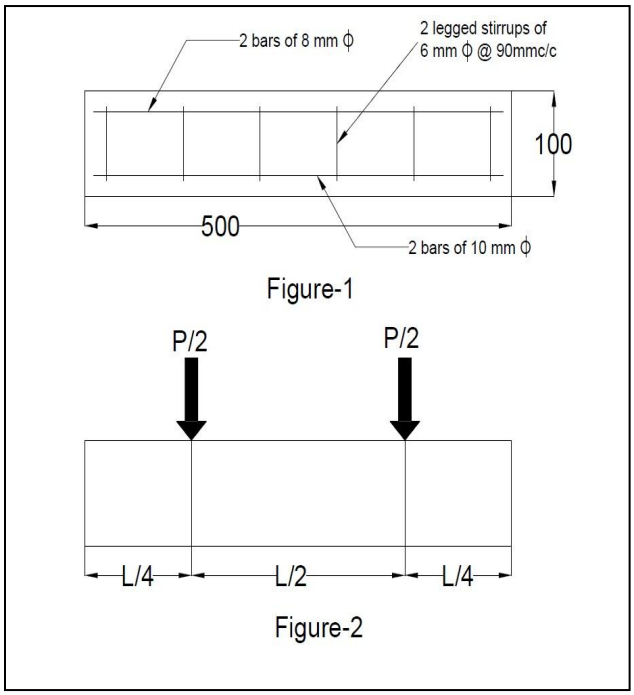

Figure-1:- detailing of beam section

Figure-2:- loading Set-up of beam

C. Retrofitting of the beams

For proper bonding between the beam and the sheets, the surface of the sheets is roughened using brush or using some other roughening materials such as sand paper or hard brush or small chisel. Once the beam surface is roughened, the Vinyl Ester resin is prepared. The Vinyl Ester is prepared in the ratio of 1:5 (1 part of hardener is used with 5 parts of resin). The mixture is then mixed thoroughly. After the Vinyl Ester is mixed complete, the Vinyl Ester is applied to be roughened

end of the sheets using brushes. After the Vinyl Ester is properly applied in the sheets, the sheets are fixed on all the sides of the beams, whose surface was cleaned using a brush. Some pressure is given on the surface for proper fixing of the sheets. Similarly sheets are wrapped on all the faces of the beam for the full wrapping technique. And the same procedure is repeated for applying epoxy bonded GFRP sheets to RCC beams for both full wrapping. After the beam

is completely retrofitted, the beams are kept for drying and setting properly for 24 hours. Figure-3(a), Figure-3(b)

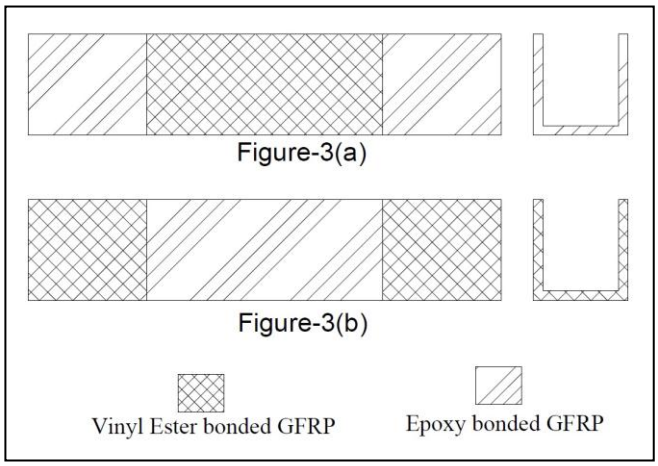

Figure-3(a):-Detailing FRP for Series-B beam

Figure-3(b):- Detailing FRP for Series-C beam

IV. TEST RESULTS AND DISCUSSION

Retrofitted RCC beams, retrofitted using the full wrapping technique has shown an increase by about 15% over the shear strength of normal RCC Beams. The shear strength of the Epoxy bonded GFRP at center and Vinyl ester bonded GFRP retrofitted at both ends of RCC beams; retrofitted using the mix wrapping technique has shown an increase by about 9.47% over the shear strength of normal RCC. The shear strength of the Vinyl ester bonded GFRP at center and Epoxy bonded GFRP retrofitted at both ends of RCC beams; retrofitted using the mix wrapping technique has shown an increase by about 14.2% over the shear strength of normal RCC. First crack strength of the Vinyl ester bonded GFRP retrofitted at center of RCC beams in Shear retrofitted using the mix wrapping technique has shown an increase by about 56.2% over the shear strength of normal RCC Beams. The first crack strength of the Epoxy bonded GFRP retrofitted at center RCC beams in Shear retrofitted using the mix wrapping technique has shown an increase by about 50.2% over the shear strength of normal RCC Beams. It can be concluded that Vinyl Ester bonded GFRP sheets at center and Epoxy bonding GFRP at ends when used for retrofitting performs better in enhances the shear carrying capacity and cracking resistance of the structure as compared to structure retrofitted using Epoxy Bonded GFRP at center and Vinyl ester bonded GFRP at both ends. Generally Vinyl Ester Bonded GFRP at center and Epoxy bonded at both ends gives about 11% of more strength as compared to beam retrofitting using Epoxy bonded GFRP at center.

TABLE-II Percentage increase in load carrying Capacity (%)

Specimen	Load at First Crack (kN)	Failure Load (kN)	Deflection at failure (mm)	Percentage increase in load carrying Capacity (%)
Series-A beam-1	57.5	91.2	5.08	--
Series-A beam-2	62	89.4	5.94	--
Series-B beam- 1	54.5	123.7	6.21	4.98
Series-B beam-2	59.8	120.1	6.16	16.21
Series-C beam-1	64	108.2	5.51	13.24
Series-C beam-2	62	104.2	4.88	9.45

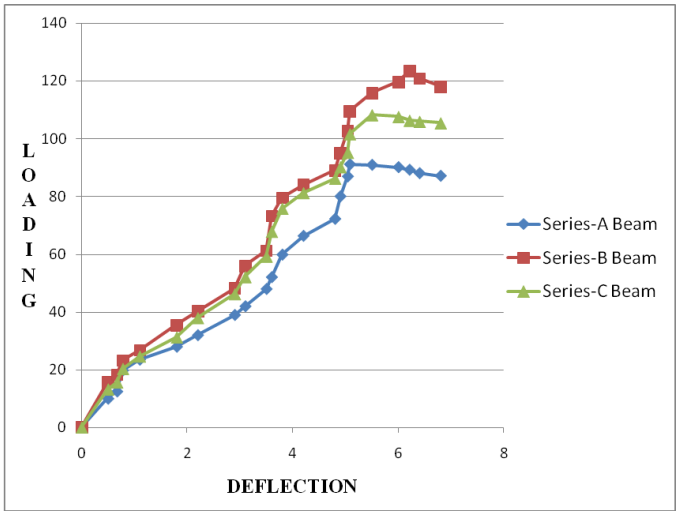

Graph-I Load- Deflection Curves

V. CONCLUSIONS

Based on the test results presented in this study the following conclusions can be drawn.

1. The inclusion of FRP on concrete surface provides better crack control and deformation characteristic of beams.

2. Both the first crack strength and ultimate strength in shear increase in both series of setups. More significant increase was found for the Vinyl Ester Bonded GFRP fiber reinforced beams i.e. series-B because of their increased resistance to propagation of cracks.

3. Shear strength increases with increasing of fiber content
4. The theoretical prediction of ultimate shear strength on the basis of methods used in the study gives results close to the observed values in most of the beams tested.

5. Maximum increase of 56 percent in first cracking load for beam containing 1.25 percent of fibers was observed when compared with beam containing no GFRP.

Also for all the beams tested in this program maximum shear strength was attained in beams reinforced with GFRP

These results support the use of different fiber reinforcement polymer on same beam here Vinyl Ester Bonded GFRP and Epoxy bonded GFRP.

REFERENCES

[1] Tara Sen , H.N.Jagannatha Reddy, Shubhalakshmi B.S "Shear Strength Study of RC Beams Retrofitted Using VinylEster Bonded GFRP and Epoxy Bonded GFRP" *National Institute of Technology, Agartala, Barjala, Jirania, Tripura (West), India, Bangalore Institute of Technology, K.R. Road, Bangalore, India, Dayanand Sagar College of Engineering, Bangalore, India** E-mail of the corresponding author: tara.sen@rediffmail.com (*references*)

[2] Michele BARBATO, Giorgio MONTI, Federico Santinelli," Fiber-Section Fe Of FRP-Strengthened RCCBeam For Seismic Analysis", Structural Engineering Department, UCSD, 9500 Gilman Dr La Jolla, CA, USA ,Dipartimento di Ingegneria Strutturale e Geotecnica, Università La Sapienza di Roma,Via A. Gramsci, 53 – 00197 Roma, Italy

[3] Mohammad Reza Mohammadizadeh, Mohammad Javad Fadaee, And Hamid Reza Ronagh," Improving Torsional Behaviour Of Reinforced Concrete Beams Strengthened With Carbon Fibre Reinforced Polymer Composite", *Iranian Polymer Journal* 18 (4), 2009, 315-327, Received 11 September 2008; Accepted 16 March 2009

[4] Nabil F. Grace," Strengthening Of Negative Moment Region Of Reinforced Concrete Beams Using Carbon Fiber-Reinforced PolymerStrips", *Title No. 98-S33*

[5] J.G. Dai, T. Ueda, Y. Sato1 And T. Ito ,Division Of Built Environment, School Of Faculty Of Engineering,Hokkaido University, Japan, Email: Daijg@Eng.Hokudai.Ac.Jp, P.S. Mitsubishi Construction Co., Ltd., Japan,"

[6] Flexural Strengthening Of Rc Beams Using Externally Bonded FRP Sheets ThroughFlexible Adhesive Bonding", *Proceedings Of The International Symposium On Bond Behaviour Of FRP InStructures (BBFS 2005)* Chen And Teng (Eds) © 2005 International Institute For FRP In Construction

[7] H.C. Wu And P. Sun," Fiber Reinforced Cement Based Composite Sheets For Structural Retrofit",*Proceedings Of The International Symposium On Bond Behaviour Of FRP In Structures (BBFS 2005)* Chen And Teng (Eds) © 2005 International Institute For FRP In Construction.

[8] Robert Ravi.S , Prince Arulraj.G," Experimental Investigation On Behavior Of Reinforced Concrete Beam Column Joints Retrofitted With GFRPAFRP Hybrid Wrapping", *International Journal Of Civil And Structural Engineering*, Volume 1, No 2, 2010

[9] C.A. Zeris," Experimental Investigation Of Strengthening Of Non Ductile Rc Beams Using FRP",*Proceedings Of The 8th U.S. National Conference On Earthquake Engineering*, April 18-22, 2006, SanFrancisco, California, USA. Paper No. 853

[10] M. Z. Jumaat, M. M. Rahman And M. A. Alam, "Flexural Strengthening Of RC Continuous T Beam Using CFRP Laminate: A Review", *International Journal Of The Physical Sciences* Vol. 5(6), Pp. 619-625, June 2010. Available Online At Http://Www.Academicjournals.Org/IJPS. ISSN 1992 - 1950 ©2010 Academic Journals

Structural Analysis of Concrete containing Metakaolin and Cement as partial replacement of Cement

Kamaldeep Kaur
Asstt. Professor,
Department of Civil Engg.
Punjabi University, Patiala, Punjab

Jaspal Singh
Professor,
Department of Civil Engineering
Punjab Agriculture University, Ludhiana

***Abstract*— The use of pozzolanic materials in concrete as partial replacement of cement is gaining wide acceptance in the construction industry. Metakaolin (MK) and fly ash are the pozzolanas, which confirm the requirements of construction industry and are largely available in India. In present study, the results of X-ray diffraction (XRD) analysis of concrete containing metakaolin and fly ash were analyzed. Four samples K0, K4, K8 and K12containing 0%, 7%, 8% and 9% MK (by weight of cement) respectively were analyzed with XRD at the sample age of 1 day.**

Keywords— ***Pozzolanic materials; concrete; metakaolin; fly ash; X-ray diffraction.***

I. INTRODUCTION

Concrete is probably the most extensively used construction material in the world. However, environmental concerns both in terms of damage caused by the extraction of raw material and CO2 emission during cement manufacture have brought pressures to reduce cement consumption by the use of supplementary materials called pozzolanas (1). Typically pozzolanas are used as cement replacements rather than cement additions. Adding pozzolans to an existing concrete improve the workability and strength of concrete (2). Replacing some of the cement with pozzolans preserves the mix proportions. Of all the pozzolanas, metakaolina refined kaolin clay that is fired (calcined) under carefully controlled conditions to create an amorphous aluminosilicate that is reactive in concrete. Like other pozzolans (fly ash and silica fume are two common pozzolans), metakaolin reacts with the calcium hydroxide (lime) by-products produced during cement hydration (3). The use of metakaolin results in considerable enhancement in strength, particularly at the early stages of curing along with the strength at later age (4).

Fly ash produces more cementitious paste as it has a lower unit weight. The greater the percentage of fly ash in the paste, the better lubricated the aggregates are and the better concrete flows. Fly ash reduces the amount of water needed to produce a given slump (5).

When X-rays interact with acrystalline substance (phase), one gets a diffraction pattern. The X-ray diffraction pattern of a pure substance is, therefore, like a fingerprint of the substance. The powder diffraction method is thus ideally suited for characterization and identification of polycrystalline phases (6).Today about 50,000 inorganic and 25,000 organic single components, crystalline phases, and diffraction patterns have been collected and stored on magnetic or optical media as standards (7). The main use of powder diffraction is to identify components in a sample by a search/match procedure. Furthermore, the areas under the peak are related to the amount of each phase present in the sample. X- ray diffraction is now a common technique for the study of crystal structures and atomic spacing.

II. MATERIALS AND METHODS

A. *Cement*

Cement is a fine, grey powder. It is a fine powder produced by grinding Portland cement clinker (more than 90%), a limited amount of calcium sulphate (which controls the set time) and up to 5% minor constituents It is mixed with water and materials such as coarse aggregates and fine aggregates to make concrete. The cement and water form a paste that binds the other materials together as the concrete hardens. It is a material with adhesive and cohesive properties which is capable of bonding mineral fragments into a compact-solid. It is used in the making of concrete with property of setting and hardening, of which when the chemical properties reacts with water. Ordinary Portland cement (OPC) of 43 grade has been used in this study. It was fresh and free from any lumps.

B. *Coarse aggregates*

Materials which are large to be retained on 4.75 mm IS sieve and contain only that much of fine material as is permitted by the specifications are termed as coarse aggregates. The graded coarse aggregate is described by its nominal size i.e. 40 mm, 20 mm, 16 mm and 10 mm. Since the aggregates are formed due to natural disintegration of rocks or by the artificial crushing of rocks or gravel, they derive many of their properties from the parent rocks. These properties are chemical and mineral composition, specific gravity, hardness, strength, pore structure and colour. Some other properties of the aggregates not possessed by the parent rocks are particle shape and size, surface texture, absorption, etc. All these properties may have considerable effect on the quality of concrete. Crushed stone aggregate (locally available) of nominal size 20 mm and 10 mm in the proportion of 50:50 were used throughout the experimental study. The aggregates were washed to remove dust and dirt and are dried to surface dry condition.

C. Fine aggregate

It is the aggregate, most of which passes through a 4.75 mm IS sieve. Sand is generally considered to have a lower size limit of about 0.07 mm. Material between 0.06 mm and 0.002 mm is classified as silt, and still smaller particles are called clay. The fine aggregate may be one of the following types:-

(i) Natural sand
(ii) Crushed stone sand
(iii) Crushed gravel sand

According to size the fine aggregate may be described as coarse, medium nad fine sands. Depending upon the particle size distribution, IS: 383-1970 has divided the fine aggregate into four grading zones. The grading zones become finer from grading zone I to grading zone IV. The sand confirming to zone II was used in this study.

D. Water

Fresh potable, which is free from concentration of acid and organic substances, was used for mixing of concrete.

E. Metakaolin

Metakaolin (MK) is a pozzolanic material. It is a dehydroxylated form of the clay mineral kaolinite. It is obtained by calcination of kaolinitic clay at a temperature between 500°C and 800°C. Between 100 and 200°C, clay minerals lose most of their adsorbed water. Between 500 and 800°C, kaolinite becomes calcined by losing water through dehydroxilization. The raw material input in the manufacture of metakaolin ($Al_2Si_2O_7$) is kaolin clay. Kaolin is a fine, white, clay mineral that has been traditionally used in the manufacture of porcelain. Kaolinite is the mineralogical term that is applicable to kaolin clays. The dehydroxilization of kaolin to metakaolin is an endothermic process due to the large amount of energy required to remove the chemically bonded hydroxyl ions. Above this temperature range, kaolinite becomes metakaolin, with a two dimensional order in crystal structure.

Like other pozzolans (fly ash and silica fume are two common pozzolans), metakaolin reacts with the calcium hydroxide (lime) by-products produced during cement hydration. Calcium hydroxide accounts for up to 25% of the hydrated Portland cement, and calcium hydroxide does not contribute to the concrete's strength or durability. Metakaolin combines with the calcium hydroxide to produce additional cementing compounds. Less calcium hydroxide and more cementing compounds, means stronger concrete. Metakaolin, because it is very fine and highly reactive, gives fresh concrete a creamy, non-sticky texture that makes finishing easier.

F. Fly ash

The fly ash, also known as pulverised fuel ash, is produced from burning pulverized coal in electric power generating plants. During combustion, mineral impurities in the coal (clay, feldspar, quartz, and shale) fuse in suspension and float out of the combustion chamber along with exhaust gases. As the fused material rises, it cools and solidifies into spherical glassy particles called fly ash. It is a fine grained powdery particulate material that is collected from the exhaust gases by electrostatic precipitators or bag filters. Depending upon the collection system, varying from mechanical to electrical precipitators or bag houses and fabric filters, approximately 85–99% of the ash from the flue gases is retrieved in the form of fly ash. Fly ash accounts for 75–85% of the total coal ash, and the remainder is collected as bottom ash or boiler slag.

G. Superplasticizer

Superplasticizers, also known as high range water reducers, are chemicals used as admixtures. These polymers are used as dispersants to avoid particle aggregation, and to improve the flow characteristics of suspensions such as in concrete applications. Their addition to concrete or mortar allows the reduction of the water to cement ratio, not affecting the workability of the mixture, and enables the production of self-consolidating concrete and high performance concrete. This effect drastically improves the performance of the hardening fresh paste. Indeed the strength of concrete increase whenever the amount of water used for the mix decreases.

III. METHODS OF TESTING

A. XRD

In this study, powder method of XRD was used, which is easier to interpret and is capable of high accuracy, especially for determining the spacing of atoms in a solid. In the powder method, monochromatic X-rays are used and the sample is very finely powdered. Detail of samples used in XRD analysis is given in Table 1. The XRD analysis was conducted on the samples at the age of 1 day.

TABLE 1 XRD SAMPLE DETAIL

S. NO.	SAMPLE LABEL	MK	FLY ASH	MEAN COMPRESSIVE STRENGTH AT 1 DAY (MPa)
1	K0	0%	10%	5.27
2	K4	7%	10%	8.73
3	K8	8%	10%	12.80
4	K12	9%	10%	11.24

IV. TEST RESULTS AND DISCUSSION

The powder samples of cement, fly ash, metakaolin, K0, K4, K8 and K12 were analyzed by XRD analysis, indexing of cement was done and the peaks were marked on the basis of ICDD database. The XRD pattern of samples K0, K4, K8 and K12 are given in Figures 1, 2, 3 and 4 respectively.

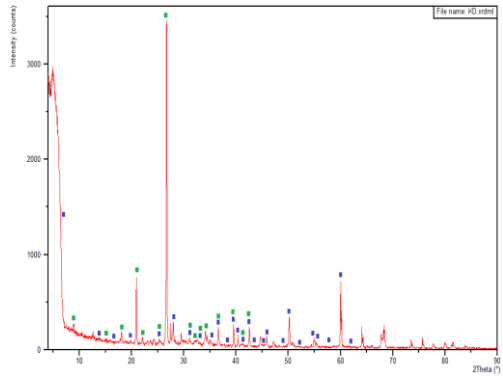

Fig. 1 XRD pattern of K0 (MK 0% and Fly ash 10%)

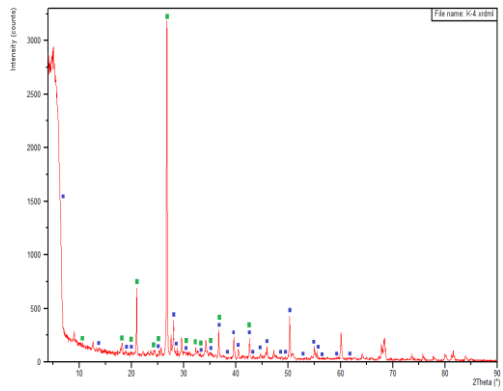

Fig. 2 XRD pattern of K4 (MK 7% and Fly ash 10%)

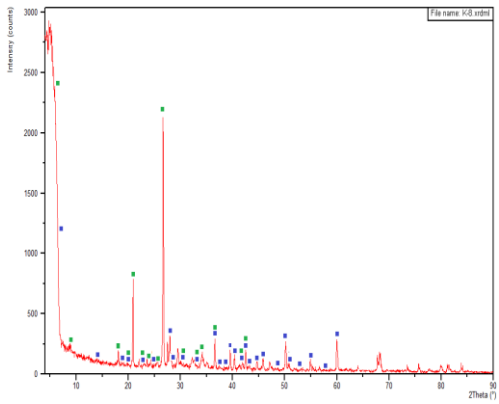

Fig. 3 XRD pattern of K8 (MK 8% and Fly ash 10%)

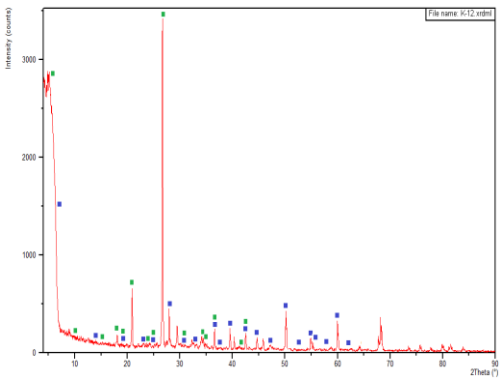

Fig. 4 XRD pattern of K12 (MK 0% and Fly ash 10%)

The XRD pattern indicates that in all samples the phase of Ca(OH)2 SiO2 H2O with a mixed phase of CaO Al2 SiO2 H2O were present. With the increase in the percentage of metakaolin, the phase CaO Al2 SiO2 H2Ois increased but in sample K12 phase CaO Al2 SiO2 H2O is decreased at 9% of metakaolin. Results of compressive strength of samples are shown in Table 1. Here we mentioned earlier the phase CaO Al2 SiO2 H2O decreased at maximum percentage of metakaolin (K12) and as compared with compressive strength of samples, the compressive strength of sample K12 is decreased. Maximum strength gain is at 8% of metakaolin.

REFERENCES

[1] E. Worrell, L. Price, N. Martin, C. Hendriks & L. O. Meida, "Carbon dioxide emissions from the global cement industry," *Annu. Rev. Energy Environ.* Vol. 26 p. 303–29, 2001.

[2] A. Naceri, M. H. Chikouche & P. Grosseau, "Physico-Chemical Characteristics of Cement Manufactured with Artificial Pozzolan (Waste Brick)," *World Academy of Science, Engineering and Technology*. Vol. 52 p. 41-43, 2009.

[3] U. Krajei, I. Janotka, I. Kraus & P. Jamnicky, "Burnt kaolin sand as pozzolanic material for cement hydration," *Ceremic silikaty.* Vol. 51 p. 217-224, 2007.

[4] B. B. Sabir, S. Wild, J. Bai, "Metakaolin and calcined clays as pozzolans for concrete: a review," *Cement & Concrete Comp*, Vol. 23 p. 441-54, 2001.

[5] R. N. Ojha, "Use of fly ash and condensed silica fumes in making concrete," *IE(I) Journal CV*, Vol. 77 p. 170-173, 1996.

[6] C. R. Ward & D. French, "Relation between coal and fly ash mineralogy, based on quantitative X- ray diffraction methods," paper presented at World of coal ash conference, Lexington, Kentucky, USA, 2005.

[7] L. L. Yang, "Synthesis and optical properties of ZnO nanostructure," Thesis, Linkoping university, Sweden, 2008.

[8] A. Torre & M., Aranda, "Accuracy in Rietveld quantitative phase analysis of Portland cements," *J. Appl. Cryst.* Vol. 36 p. 1169-1176, 2003.

[9] K. L. Scrivener, T. Fullmann, E. Gallucci, G. Walenta & E. Bermejo, "Quantitative study of Portland cement hydration by X-ray diffraction/Rietveld analysis and independent methods," *Cement and Concrete RES* Vol. 34 p. 1541-1547, 2004.

[10] A. Palomoa, M. W. Grutzeck & M. T. Blancoa, "Alkali- activated fly ashes-A cement for the future," *Cement and Concrete RES*, Vol. 29, p. 1323-1329,1999.

Use of Waste Ceramic Tile Aggregates as an Alternative Material of Coarse Aggregates in Cement Concrete

Jaspreet Singh
Department of Civil Engineering
GZSCET, Bathinda

Amanpreet Singh Virk
Assistant Professor
Department of Civil Engineering
GZSCET, Bathinda

Gurpreet Singh Bath
Associate Professor
Department of Civil Engineering
GZSCCET Bathinda

***Abstract* - Now a days, Climate change is major international issue. It is the time when governments and consumers have to respond through more environment friendly products and policies. Demand of construction material is increasing day by day and due to which degradation of environment occurs. It is a prime time to explore alternative sustainable construction material from industrial as well as domestic waste. The utilization of waste materials such as slag, fly ash, glass, plastic etc. in concrete manufacturing is significant due to its engineering, environmental, ecological and economic benefits. Thus to achieve the goal of sustainable construction utilization of waste material in concrete is very much helpful. So, this study intends to use of waste ceramic tile aggregates as an alternative material of coarse aggregates in concrete production. In this study, reports are prepared on the basis of performance of three different concrete mixes having different ratio of waste tile aggregates as an alternative material of coarse aggregates. Tests for compressive strength of specimen were carried out at different ages of concrete. From different test results, we concluded that in M-20 and M-25 mixes up to 20% replacement of normal 20 mm coarse aggregate with waste ceramic tile aggregates, there is no significant effect on compressive strength of concrete except M-30 mix. But beyond 20% replacement, compressive strength of cubes started decreasing gradually with increase in the ratio of waste ceramic tile aggregates in concrete.**

Keywords: Environment friendly, compressive strength, waste ceramic tile aggregates

I. INTRODUCTION

In concrete production, a large amount of natural aggregates, water and sand are being consumed. Consequently to minimize the use of natural aggregates researchers have concentrated on the use of various waste materials as alternatives in construction industry, especially in concrete construction. One of the prime research interests is utilization of waste material like slag, fly ash, plastics etc. in concrete construction to achieve the goal of sustainable development (construction). Aggregates consist of 70% to 75% of volume of concrete. So reduce the consumption of natural aggregates, waste ceramic tile or broken tiles as coarse aggregates can be a new scientific sobriety in the field of sustainable concrete. A huge amount of tiles get broken in the tile industries and construction projects. The residual and unused wastes are disposed off into the environment without any commercial return.

Large amount of money is spent for their disposal as well as environmental pollution occurs. Addition of waste material in concrete reduces the cost of construction and more or less maintains the properties of concrete. When we add waste material properly processed, it is effective as construction material and meet the design specifications.

The study focuses on producing concrete of acceptable strength with ceramic tile waste as an alternative material for coarse aggregates and determining the mix ratio of coarse aggregates to achieve the required strength.

II. MAIN OBJECTIVE OF STUDY

- Utilization of waste material properly to provide safeguard to environment
- To strength of concrete by use of waste ceramic tiles as an alternative material of coarse aggregate
- To reduce the waste from the environment
- To find an alternative of aggregates to achieve the sustainable development.
- To reduce the overall environmental effects of concrete production using waste tiles material as partial replacement.

III. LITERATURE REVIEW

Marcio performed experiments on water absorption, modulus of elasticity and compressed stress on the concrete which is made up of ceramic tile aggregates. In concrete casting crushed ceramic blocks were used as coarse aggregates. For 0 to 100 percent replacement specific density of aggregates changes from 2630 to 2310 kg/m^3.When replacement upto 20 percent compression resistance and young's modulus of elasticity was same as the conventional concrete.

Senthamarai concluded that based on strength of ceramic waste aggregates, it can be used effectively as a coarse aggregates in concrete. The crushing value, impact value, abrasion value for natural coarse aggregates 24, 17 and 20

percent correspondingly for ceramic scrap 27, 21 and 28 percent respectively. Ceramic waste tiles do not have much variation with respect to the natural aggregates.
Paulo cachim experimented on use of waste ceramic tile aggregates, collected from ceramic industrial waste from different sources water absorption was 15.81 and 18.91 percent respectively. The more value of water absorption influenced the workability of concrete. In first 2 minutes 75 percent of total absorption takes place and after 5 minutes at least 91 percent of the total absorption occurred.

Medina et al concluded that use of ceramic tile wastes with 4 mm and lower size as fine aggregates in concrete and density of concrete was 2.41 g/cm^3 and compressive strength and split tensile strength were increased due to lower fraction of ceramic waste usage in to the concrete composition.

Pinchatorkittikul and arnonchaipanich experimented that use of ceramic waste as fine aggregates in concrete composition and concluded that the density of concrete casted with 100 percent ceramic waste aggregates was 2.31 g/cm^3 which is 0.07 g/cm^3 lower than with respect to conventional controlled 28 days concrete due to low specific gravity and density of ceramic waste aggregates.
Veerareddy reported on ceramic waste's crushing value and impact value is 24.7 percent and 18.2 respectively. These values were within the permissible limit as per IS 383-1970 code, hence it was safe to use of ceramic tile waste as an alternative material to coarse aggregates.

Correia et al. reported that the recycled aggregates have more water absorption due to higher porosity of recycled aggregated. Due to which there is a need of additional water quantity to make concrete with proper workability. Correiain his previous study of 2006 reported that the abrasion resistance of ceramic aggregates concrete showed even better than the reference concrete in their experimentation work.

Sekar concluded that specific gravity of ceramic coarse aggregates varied between 2.2 and 2.56. These values were effected the density of ceramic aggregate concrete.

Pancheco-Torgail and said jalali experimented the strength and durability of ceramic tile waste concrete as compared to natural aggregate ceramic aggregates have higher value of water absorption.

Medina concluded on utilization of ceramic tile waste as an alternative material of coarse aggregates. It was produced by crushing of sanitary ware and shape curve is same as that of natural aggregates. Irregular shape provided that superior surface area and better bonding was observed in experimentation.

IV. EXPERIMENTAL PROGRAM

Three concrete mix designs M20, M25 and M30 has chosen to carry out the experiments for compressive strength of concrete after replacing the natural coarse aggregates with waste ceramic tile aggregates in proportions of 0%, 5%, 10% and 20%.

Only limited use of tile aggregate in concrete is possible because of tile aggregates are totally flaky in shape. If we used tile aggregates in excess then it will lead to poor strength because of flaky aggregates that tend to brake under pressure.

- Total number of concrete mix designs prepared – 3
- Number of proportions in which tile aggregates eplaced with normal aggregates in each design – 4 (i.e. 0%, 5%, 10% & 20%)
- Therefore, total concrete batches prepared – 12
- Number of concrete batches prepared in a day – 1
- Number of cubes filled in each batch – 6
- Number of cubes casted for each mix design – 24
  i.e.
  For M 20 – 24 cubes
  For M 25 – 24 cubes
  For M 30 – 24 cubes
- Total number of cubes casted including all 3 concrete mix designs – 24+24+24 = 72

TABLE –Material Test Result

Sr. No.	Test	Results
1	Specific Gravity Of Cement	2.74
2	Specific gravity of Coarse Aggregates	2.69
3	Specific gravity of Fine Aggregates	2.70
4	Fineness Modulus of Fine Aggregates	2.17
5	Specific Gravity of Tile Aggregates	2.24
6	Water Absorption of Tile Aggregates	14.8%
7	Impact Value of Tile Aggregates	20%

Table - Comparison of Properties Of Tile Aggregates And Normal Aggregates

Sr. No.	Properties	Normal aggregate	Tile aggregate
1	Shape	Angular	Flaky
2	Texture	Rough	All sides rough except top
3	Water absorption	0.5%	14.8%
4	Impact value	15%	20%
5	Specific gravity	2.69	2.24

RATIOS USED FOR EXPERIMENT

M-20

Cement	Fine Aggregates	Coarse Aggregates	Water
1	2.9	3.40	0.55

M-25

Cement	Fine Aggregates	Coarse Aggregates	Water
1	1.87	3.04	0.50

M-30

Cement	Fine Aggregates	Coarse Aggregates	Water
1	1.64	2.67	0.45

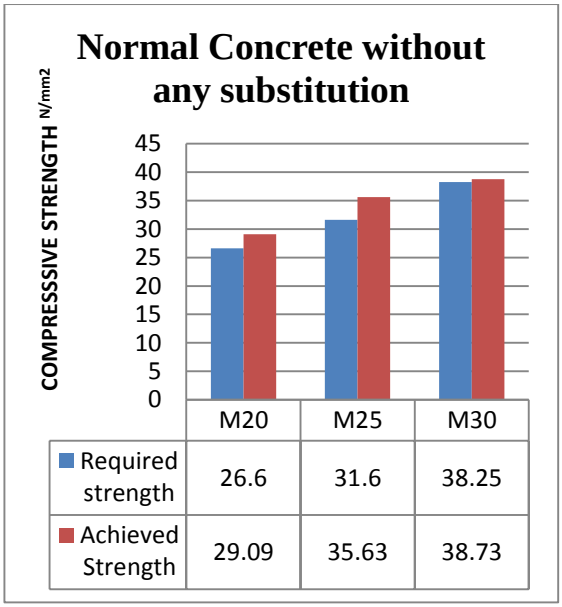

Figure – Different Concrete Grade represents their obtained compressive strength against their required Target Mean Strength.

COMPARISON OF CONCRETE RESULTS

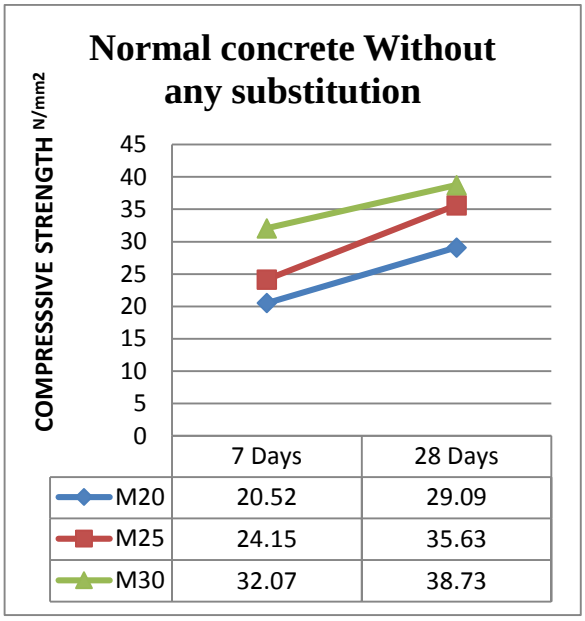

Figure – Different concrete grades without any aggregate replacement and their respective compressive strength at 7 & 28 days.

➢ All three grades shows higher strength than required target mean strength, hence all concrete grades are accepted.

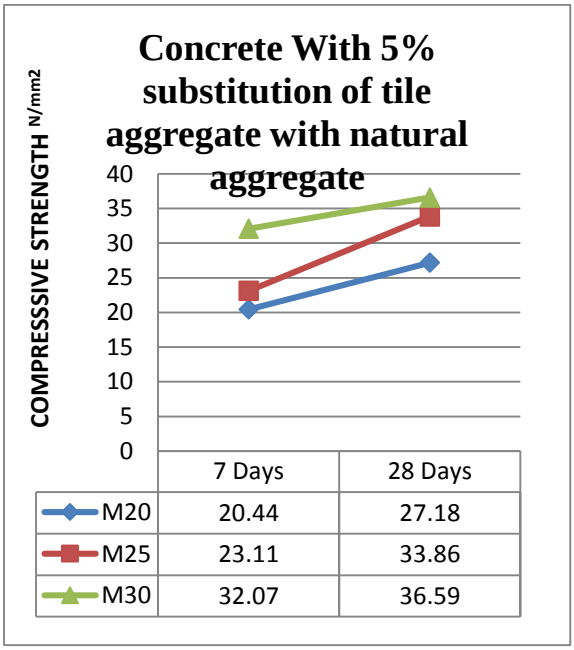

Figure - Different concrete grades with 5% replacement of natural aggregate with tile aggregate and their respective compressive strength at 7 & 28 days.

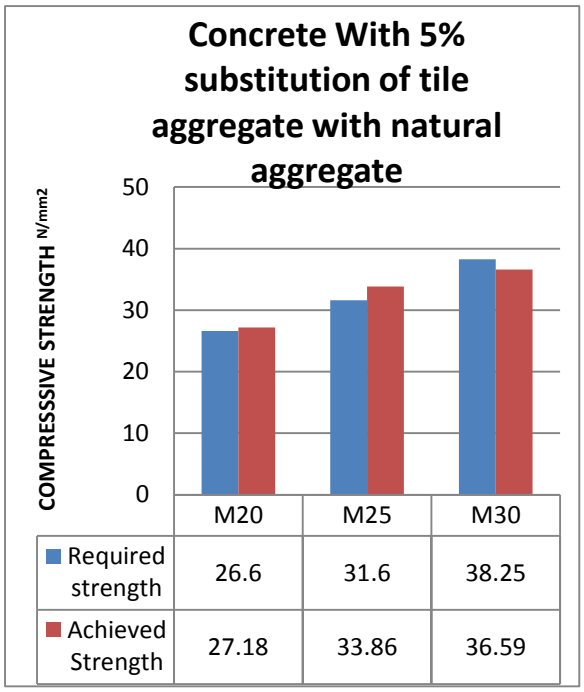

Figure – Different Concrete Grade With 5% Replacement Of Natural Aggregates With Tile Aggregates Represents Their Obtained Compressive Strength Against Their Required Target Mean Strength.

In this case also all concrete grades except M-30 show higher strength than required. M-20 and M-25 are accepted.

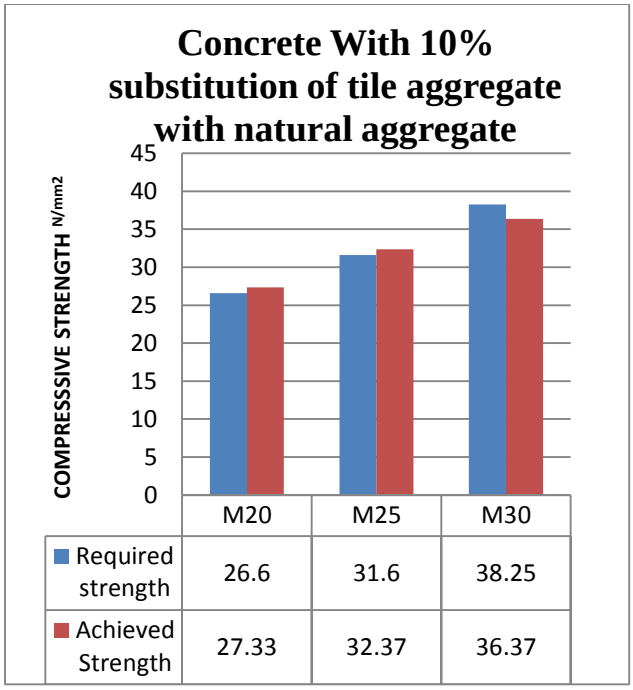

Figure - Different Concrete Grade With 10% Replacement Of Natural Aggregates With Tile Aggregates Represents Their Obtained Compressive Strength Against Their Required Target Mean Strength

Similarly, in this case all grade concrete possess higher strength than required except M-30 and are accepted.

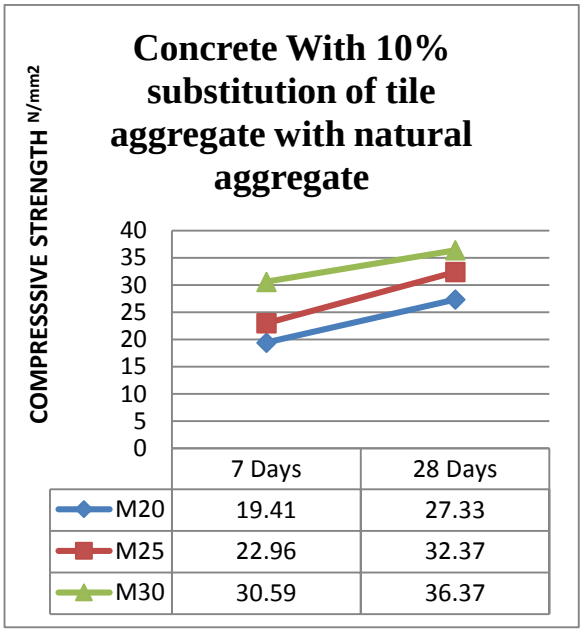

Figure - Different concrete grades with 10% replacement of natural aggregate with tile aggregate and their respective compressive strength at 7 & 28 days.

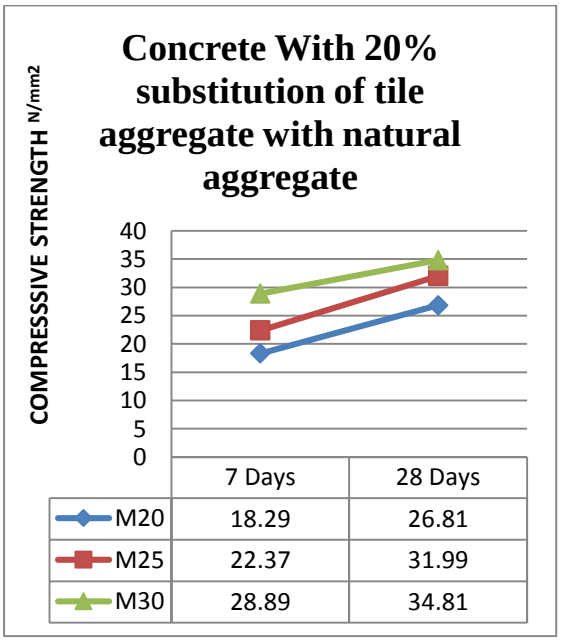

Figure Different concrete grades with 20% replacement of natural aggregate with tile aggregate and their respective compressive strength at 7 & 28 days.

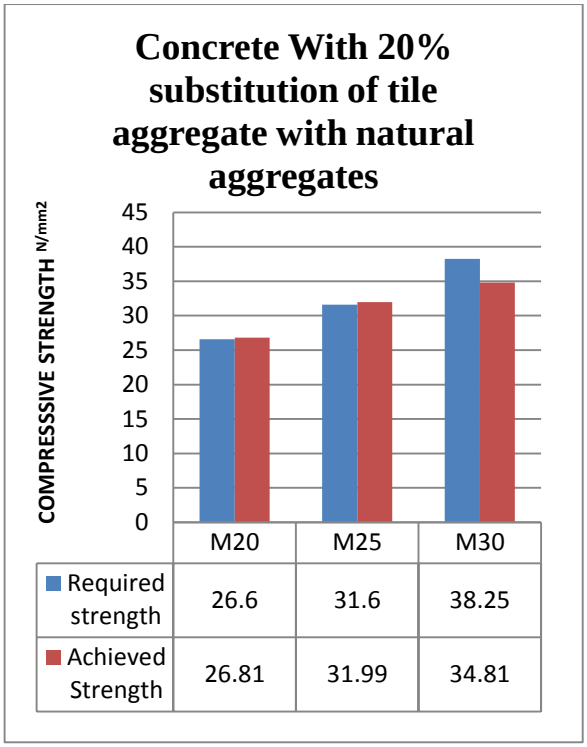

Figure - Different Concrete Grade with 20% replacement of natural aggregates with tile aggregates represents their obtained compressive strength against their Required Target Mean Strength

Here, M 20 & M 25 show acceptable strength but M 30 has lower strength than required. So, M 30 is rejected

Cost Analysis
Total cost of 20 mm aggregates to prepare 1 m^3 M 20 grade concrete –

Total volume of aggregates in M 20 concrete = 0.691 m^3

Total volume of coarse aggregates = 62 % of 0.691

Therefore, 62% of 0.691 = 0.428 (10 mm + 20 mm both)

Volume of 20 mm aggregates in total coarse aggregates = 40%

40% of 0.428 = 0.171 m^3

Now,Price of 1 m^3 of 20 mm natural aggregates = Rs. 1175 (as per CPWD rate analysis 2014)

Price of 0.171 m^3 20 mm natural aggregates

= 1175 × 0.171 = Rs. **200**

Now, Total saving by substituting natural aggregate with tile aggregate in M 20 concrete

Volume of 20 mm aggregates after 20 % replacement with tile aggregates

= 20/100 × 0.171 = 0.0342 m^3

= 0.171 – 0.0342 = 0.1368 m^3

Price of 0.1368 m^3 of aggregates = Rs.162

Total saving on 1m^3 M 20 grade concrete by replacing 20% tile aggregates with normal aggregates = 200 – 162 = Rs. **32**

Hence, total saving on aggregates in terms of rupees to produce 1 m^3 of M 20 grade concrete by using tile aggregates = **16%** (Without including labor and transportation charges)

V. CONCLUSION

Research on the usage of waste construction materials is very important due to the material waste is gradually increasing with the increase in population and increasing of urban development. The reasons that many investigations and analysis had been made on ceramic tile aggregate are because tile aggregates are easy to obtain and their cost is cheaper than the natural aggregates. For natural aggregates mining is needed but tile aggregate can ignore this process.

1. Based upon its properties ceramic tile aggregates are appropriate concrete material which is used as an alternative material to coarse aggregates in concrete.
2. Water absorption, impact value and crushing value are higher than the natural aggregates and specific gravity is lower than natural aggregates.
3. In M20 grade concrete it is possible to replace the 20 percent of normal 20 mm aggregates with waste ceramic tile aggregates.
4. In M30 grade concrete it is not possible even 5 percent replacement of normal 20 mm aggregates with waste ceramic tile aggregates because of less target strength. So it should be avoided.
5. For all concrete mixes as the proportion of tile aggregated increases the strength of concrete decreases gradually which is due to low specific gravity and higher porosity.
6. Use of tile aggregates is more economical than the conventional concrete. 16 percent money can be saved on total amount.

REFERENCES

[1] Advanced Construction Technology System – ACTS By P. G. Ioannou,1 A.M. ASCE, and L. Y. Liu,2 A.M. ASCE.
[2] Binici, Effect of crushed ceramic and basaltic pumice as fine aggregates on concrete mortars properties, Construction and Building Materials 21 (2007) 1191–1197.
[3] Brito J.de., Pereira A.S., Correia J.R., (2005), Mechanical behaviour of non-structural concrete made with recycled ceramic aggregates, Cement & Concrete composites, pp 429-433.
[4] Concrete Technology by M. S. Shetty S. Chand Publishing, page no. 66 – 118.
[5] DUET Journal "Effect of Replacing Natural Coarse Aggregate by Brick Aggregate on the Properties of Concrete" Vol. 1, Issue 3, June 2012.
[6] Freedonia world construction aggregates industry study
[7] International Journal of Civil Engineering Research,ISSN 2278-3652 Volume 5, Number 2 (2014), pp. 151-154,© Research India Publications http://www.ripublication.com/ijcer.htm
[8] International Journal of Civil Engineering Research. ISSN 2278-3652 Volume 5, Number 2 (2014), pp. 151-154.
[9] IS 10262:2009, Indian standard concrete mix proportioning - Guidelines (First revision), Bureau of Indian Standards, New Delhi, India

[10] IS 383 : 1970, Specifications for Coarse and Fine Aggregates from Natural Sources for Concrete (second Revision) Bureau of Indian Standards, New Delhi, India.
[11] IS 456 : 2000, Plain and Reinforced Concrete – Code of Practice (fourth Revision) Bureau of Indian Standards, New Delhi, India.
[12] IS 516 : 1959, Methods of Tests for Strength of Concrete, Bureau of Indian Standards, New Delhi, India.
[13] Journal for scientific and Industrial Research, Vol. 70, May 2011, pp.385-390.
[14] Koyuncu, Y. Guney, G. Yilmaz, S. Koyuncu, R. Bakis, Utilization of Ceramic Wastes in the Construction Sector, Key Engineering Materials Vols. 264-268 (2004) pp 2509-2512.
[15] Mohd Mustafa Al Bakri, H. Kamarudin, Che Mohd Ruzaidi, Shamsul Baharin, R. Rozaimah, Nur Khairiatun Nisa. Concrete With Ceramic Waste and Quarry Dust Aggregates. 5th Annual Conference Management in Construction Researchers Association, 2006: 383-388
[16] Mohini Saxenaa, & Shyam R. Asolekar - Solid wastes generation in India and their recycling potential in building materials.
[17] Pacheco-Torgal, S. Jalali, Reusing ceramic wastes in concrete, Construction and Building Materials 24 (2010) 832–838.

Strength Improvement Studies of Concrete Using Ureolytic Bacteria

Satinder Kaur khattra
Assistant professor,
Civil Engineering Department,
COAE&T, Punjab Agricultural University,
Ludhiana-141004

Urmila Gupta Phutela,
Professor,
School of Energy Studies for Agriculture,
COAE&T,
Punjab Agricultural University, Ludhiana-141004

Manisha Parmar
Department of Microbiology,
College of Basic Sciences and Humanities,
Punjab Agricultural University, Ludhiana-141004

***Abstract*— The "Bacterial Concrete" is a concrete which can be made by embedding bacteria in the concrete that are able to constantly precipitate calcite. The bacterial concrete makes use of calcite ($CaCO_3$) precipitation by bacteria. This phenomenon is called microbiologically induced calcite precipitation. As part of metabolism, some bacterial species like Bacillus pasteurii, Bacillue sphaericus ect. produce urease, which catalyzes urea to produce CO_2 and ammonia, resulting in an increase of pH in the surroundings where Ca^{2+} and CO_3^{2-} ions precipitate as calcite. This microbiologically induced calcite precipitation is highly desirable because the calcite precipitation is pollution free and natural and can be used to improve the compressive strength of concrete specimens, repair cracks in concrete. This paper presents the results of a study carried out to investigate the ability of ureolytic bacteria to enhance the compressive strength of concrete. The urease producing aerobic alkalophilic bacteria *Bacillus subtlis* strain MU12 was used in the present study. Ureolytic bacteria used in the present studies were isolated from various sources like cowshed, poultry farm, milk, soil and pigeon dung. All the isolates were screened for ureolytic activity on the basis of urease test. Four different cell concentration (10^4, 10^5,10^6,10^7 cells/ml) of bacteria were used in making the concrete mixes. Tests were performed for compressive strength of concrete cubes at 7 days, 14 days and 28 days. Inclusion of MU12 @ 10^7 cells/ ml in cement concrete enhanced the compressive strength in 7^{th} and 14^{th} days concrete samples.**

Key Words: Concrete, bacteria, urease, precipitation, ureolytic.

I. . INTRODUCTION

Concrete which forms major component in the construction industry as it is cheap, easily available and convenient to cast. Despite its versatility in construction, it is known to have several limitations. A lot of research has been carried out around the globe to improve properties of concrete. Based on the continuous research carried out around the globe, various modifications have been made from time to time to overcome the deficiencies of cement concrete. The ongoing research in the field of concrete technology has led to the development of special concretes considering the speed of construction, the strength of concrete, the durability of concrete and the environmental friendliness with the use of industrial material like fly ash, blast furnace slag, silica fume, metakeolin etc. Recently a novel technique has been developed by using a selective microbial plugging process, in which microbial metabolic activities promote calcium carbonate (calcite) precipitation. This technique is referred as Microbiologically Enhanced Crack Remediation (MECR)[1]. In this technique urolytic bacteria are used hence the concrete is called Bacterial concrete[2]. The “Bacterial concrete” can be prepared by adding spore forming bacteria in the concrete that are able to continuously precipitate calcite. The basic principle for this process is that the microbial urease hydrolyzes urea to produce ammonia and carbon dioxide and the ammonia released in surrounding subsequently increases pH, leading to accumulation of insoluble calcium carbonate. Bacterial cultures improve the strength of cement sand mortar[3] and crack repair on surfaces of concrete structures[4]. The Calcite precipitation occupies the voids between cement matrixes and therefore leads to denser concrete. The approach does not deplete any natural resources since the bacteria used can be easily reproduced by cultivation process. The use of biological approach in concrete is also considered as a green technology as its production does not involve greenhouse gas emission. Therefore bacterial induced Calcium Carbonate (Calcite) precipitation has been proposed as an alternative and environment friendly way for improvement of strength of building materials[5].

With recent encouraging reports on compressive strength enhancements achieved in conventional concrete through Microbiologically Induced Calcium Carbonate Precipitation (MICCP), the present study was aimed at isolation and characterization of more efficient urease producing bacterial strains for improving the strength of cement concrete.

II. .MATERIALS AND METHODS

Cement:In this experiment 43 grade Ordinary Portland cement is used. The testing of cement is done as per IS 4031-11- 1988 Code the specific gravity of cement found is 3.0.

Fine aggregates: In this experiment the locally available sand is used and the specific gravity of fine aggregate is to be obtained by using the IS 2720 part 3 code. The specific gravity is found 2.65. The fine aggregates used which passes through the 4.75mm sieve.

Coarse aggregates: In this experiment the locally available aggregates are used and the specific gravity of course aggregate is done by using the IS2386 part 3 1963 code. The specific gravity is found 2.82. The coarse aggregates which are used of 20 mm size.

Water:The least expensive but the most important ingredient of concrete is water. The water which was used for mixing concrete was clean and free from harmful impurities such as oil, alkali, acid etc. Portable water was used for making concrete cubes and curing work.

Bacteria: The selected aerobic alkaophilic bacteria *Bacillus subtlis* strain MU12 was used in the present study. The bacteria were grown in B4 broth for about 48 hrs. at 25°C. After growth, the broth was centrifuged at 5000 rpm (rotations per minute) for 20 min. at room temperature. The pellet was suspended in 100 ml distilled water and haemocytometer count was taken. The different concentrations of bacteria were taken to prepare cement concrete made of cement, coarse aggregate, fine aggregate and water (M20-1:1.5:3). The cell suspension was mixed with B4 broth in different concentrations so as to make final concentrations of 10^4, 10^5, 10^6 and 10^7 cells\ml for biodeposition experiment.

Preparation of specimen for compressive strength test:

The cubes were prepared for concrete mix with and without addition of bacteria. The size of the cubes was taken as 150mm x 150mm x150mm. The water to cement ratio was fixed at 0.42 as per standard methods. Control specimens were prepared for 7, 14 and 28 days compressive strength tests in a standard manner according to Indian specifications. Total numbers of 12 cubes were prepared and tested for different days and concentrations.(Fig.1). The cubes were remoulded after 24 hours and subsequently cured in a water bath for 7, 14 and 28 days of compressive strength testing.

Fig1 Casting of cubes

Fig 2 Immersing of cubes in water until tested

Compressive strength Test

Compression test has been conducted confirming to IS 516-1959(5), on the concrete specimens on the universal testing machine in Department of Civil Engineering, PAU Ludhiana on 7^{th}, 14^{th} and 28^{th} days of soaking.(Fig. 2) Test cube, after wiping out the surface moisture, were placed with the cast faces not in contact with the plates of testing machine. Load has been applied at a constant rate of stress equal to 15mpa/min according to the relevant IS code and loading was continued till the dial gauge needle just reverses its direction of motion. The reversal in the direction of motion of the needle indicates that the specimen has failed. The load at which the specimens failed has been recorded. Thus from the results, the compressive strength is obtained.

III. .RESULTS AND DISCUSSION

This study was conducted with the aim of isolating locally urease producing bacteria that could be potentially used in various biocementation processes. Ureolytic bacteria were isolated from various sources like soil (collected from various places Himachal Pradesh, Rajasthan and Punjab), milk, and open air.

Table 1: Isolation of Urease producing bacteria

S. No	Sample Source	No. of Colonies/Plate	No. of Pink Colonies
1	Soil from Cowshed (Rajasthan)	50	Nil
2	Soil from Cowshed (Himachal Pradesh)	100	2
3	Soil from Cowshed (Ludhiana)	60	1
4	Soil (lentil farm, PAU Ludhiana)	40	1
5	Soil (construction site, PAU Ludhiana)	150	1
6	Soil sample (COAET)	60	1
7	Soil from Poultry farm (GADVASU Ludhiana)	150	2
8	Poultry droppings(GADVASU)	90	1
9	Pigeon dung	Morethan 300	1
10	Milk (Unpasteurised)	200	1
11	Milk (Pasteurised)	40	1
12	Air	50	1
13	Garden soil	80	4

Medium used: Urea agar; Temperature 25± 2°C; pH: 7.0; Incubation period, 3-7 days

These samples were serially diluted and one ml of each sample was used to isolate the urease producing bacteria. Colour of the media was observed for urease production as colour change from yellow to pink conformed the urease production(Fig.3). Results from Table 1 shows that a total of 13 samples were used to isolate urease producing bacteria. Approximately, 1500 bacterial colonies were purified from these samples. However, only 17 isolates were urease positive and were able to change the media colour from yellow to pink (Fig. 4).

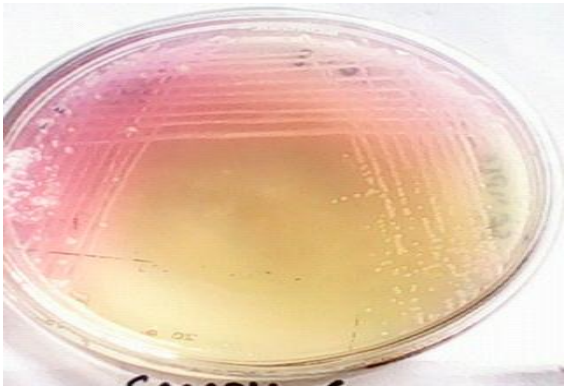

Fig.3: Pink coloured isolate producing

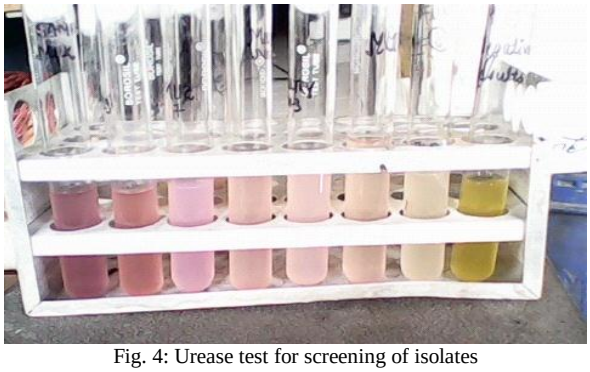

Fig. 4: Urease test for screening of isolates pink colour on urea agar

Comparative Strength

The compressive strength results obtained from the experimental investigations are shown in table 2 and the comparison between the results is presented in form of bar chart. All the values are the average of the three trails in each case in the testing program of this study.

Table 2: Compressive strength of bacterial concrete using Bacillus subtilis

Compressive strength (MPa)				
S.No	Inoculum conc. (cells ml^{-1})	Period of soaking		
		7 Days	14 Days	28 Days
1	Control (without inoculum)	4.66	8.63	26.2
2	10^4	1.18	10.45	14.63
3	10^5	7.99	15.87	20.30
4	10^6	8.08	16.4	20.93
5	10^7	13.00	17.43	21.42
C.D. at 5%		0.88	2.81	2.92

Results from Table 2 indicates that on 7^{th} day, cell concentration of 10^4 cells/ ml showed sudden decrease in the compressive strength. But as cell concentration was increased to 10^5 cells/ ml compressive strength increases from 4.66 MPa (control) to 7.99 MPa. Cell concentration of 10^6 and 10^7 cells/ ml showed further increase in compressive strength to 8.08 MPa and 13 MPa respectively. As cell concentration was increased compressive strength was also increased. Similar trend was observed during 14^{th} day of soaking. However, a decreasing trend in compressive strength was observed during 28^{th} day as compressive strength of cement cubes was decreased as compared to control cubes. The increase in compressive strengths is mainly due to filling of the pores inside the cement mortar cubes with microbiologically induced calcium carbonate precipitation initially[6]. The reduction in the compressive strength after 28 days of curing might be due to reason that survival of microorganisms are greatly influenced by the pH of an environment[7]. The *Bacillus subtilis* strain MU12 did not survived the high pH of concrete and there was a significant loss of compressive strength.

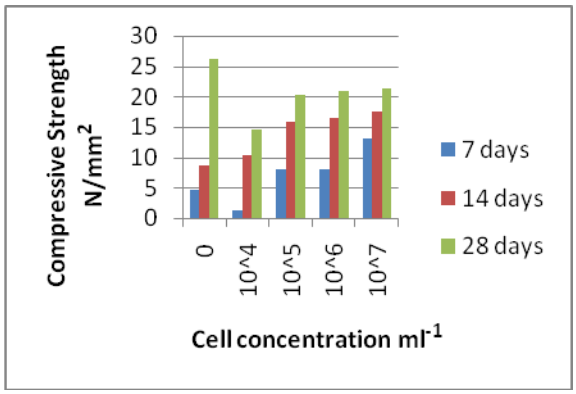

Fig 5. Compressive strength (in MPa) of bacterial concrete with different cell concentrations

IV. . CONCLUSIONS

Out of all isolated cultures developed and tested, it was observed that *Bacillus subtlis* strain MU12 has offered to precipitate calcium carbonate under laboratory conditions. Compressive strength studies have been carried out on concrete cubes by incorporating *Bacillus subtilis* strain MU12 with various concentrations along with control mix. From the strength studies, it was observed that the strength improvement is significantly higher for all concentrations after 7 and 14 days for all concentrations but the strength drastically reduced after 28 days testing as compared with the control concrete. Further studies can be carried out to create an environment for survival of *Bacillus subtlis* strain MU12 and also for higher grades of concrete.

REFERENCES

[1] Meldrum F.C. [2003] "Calcium carbonate in biominerilisation", *Biomimetic chemistry*, 48,187-224.
[2] Dick J., De Windt W., De Graef B., Saveyn H., Vander Meeren P., De Belie N., Verstraete W. [2006]. "Bio-deposition of a calcium carbonate layer on degraded limestone by Bacillus species", *Biodegradation*, 17 (4), 354-367.
[3] Ghosh P., Mandal S., Chattopadhyay B.D., Pal S. [2005]. "Use of microorganism to improve the strength of cement mortar" *Cement and Concrete Research* 35(10), 1980-1983.
[4] Ramachandran S.K., Ramakrishanan V., Bang S.S. [2001]. "Remediation of concrete using microorganisms ACI *Material Journal*, 98, 3-9.
[5] Srinivasa Reddy V, Sreenivasa Rao D, Seshagiri Rao M V, Sasikala Ch. Permeation "Properties of Bacterial Concrete" *Journal of Mechanical and Civil Engineering* (IOSR-JMCE) e-ISSN: 2278-1684 Volume 5, Issue 6 (Mar. - Apr. 2013), PP 08-12
[6] Ghosh P, Mandal (2006) development of bioconcrete material using an enrichment culture of novel thermophilic anaerobic bacteria. *Ind J Exp Biol* **44:** 336- 39.
[7] De Muynck W, De Belie N and Verstraete W (2009) Microbial carbonate recipitation in construction materials: A review *Ecol Eng* doi:10.1016/j.ecoleng.2009.02.006.

Design and Performance Analysis of PID Controller for Automatic Generation Control of an Autonomous Power System

Gurjit Singh
Assistant Professor,
Electrical Engineering Department,
IET Bhaddal, Ropar, India

Vipandeep Kour
Assistant Professor,
Electrical Engineering Department,
IET Bhaddal, Ropar, India

Lakhwinder Singh
Professor,
Electrical Engineering Department,
BBSBEC, Fatehgarh Sahib, India

***Abstract*—Proportional Integral Derivative (PID) controller is a generic feedback controller which is widely used in industrial control system, motor drive, process control, and in instrumentation. It provides simplest and most efficient solution to many real word control problems. However, tuning of PID controller gains is a challenge for researchers and plant operators. In this paper, the design problem of PID controller is formulated as an optimization problem. Particle Swarm Optimization (PSO) technique is used to search the optimum controller gain values. Optimal controller gains are obtained by minimizing the objective function. For evaluating the performance of the proposed PSO based PID and Many Optimizing Liaisons (MOL) based PID controller, a comparison of different frequency domain performance indices were undertaken as objective functions. Independent PID controllers were used for Load Frequency Control (LFC) and Automatic Voltage Regulation (AVR) of a single area power system. The comparison shows that MOL tuned PID controller with Integral Time of Absolute Error (ITAE) as performance index is most efficient in improving the step response of the system.**

Keywords— Automatic Voltage Regulation, Load Frequency Control, PID controller, Particle Swarm Optimization.

I. INTRODUCTION

A power system is prone to instability due to faults and sudden changes in the system load. The faults can be sensed through relays and suitable controlling action can be applied to a particular fault. The variations in load, however, cannot be predicted and eliminated. The sudden changes in load can cause variation in frequency and voltage of the system. Thus, for stable operation of the system, the system generation must equal the system demand. Load Frequency Control (LFC) and Automatic Voltage Regulation (AVR) are two important control mechanisms that help in a minimizing the frequency and voltage variations. LFC is used to maintain the system frequency by controlling the real power flow in the system; AVR is used to maintain the voltage profile of the system by controlling the reactive power flow in the system. Both the LFC and AVR are closed loop control systems and because of the inherent non-linearities present in the power system components and synchronous machines, these control loops are compensated by a controller primarily composed of an integral controller [1-2].

PID controller has three tuning parameters i.e. proportional gain, integral gain and derivative gain. Proper selection of these gain values ensures simplest yet most efficient control [3]. However, the tuning of the controller is quite difficult. Previously various conventional techniques such as Ziegler-Nicholes method, Cohen-Coon method, minimum variance method, gain phased margin method, etc. were used in optimal tuning of the PID controller [4]. These methods were difficult to implement in complex control design. Recently, evolutionary computational algorithms such as Artificial Bee Colony (ABC), Bacterial Foraging Algorithm (BFA), Differential Evolution (DE), Genetic Algorithm (GA), Particle Swarm Optimization (PSO), etc. are used to search for the optimal controller gains of the PID controller. PSO has the advantage that it is a derivative free algorithm which does not require an initial solution to start the algorithm [5].

Particle swarm optimization is a population based, heuristic evolutionary technique based on the movement and intelligence of swarms. It is inspired by the social behavior of bird flocking or fish schooling. In a swarm, birds generally follow the shortest path in a particular direction for searching food. Through social interaction with the bird at best location with respect to the food source, the rest of the birds try to reach that location by adjusting their velocities. This technique was first described by James Kennedy and Russell C. Eberhart in 1995 [6]. Much advancement in PSO has been made since then and different variants of PSO algorithm have been introduced [7-8]. The accepted standard PSO algorithm is the global best model of PSO introduced by Shi and Eberhart [9]. Many Optimizing Liaisons (MOL) is a PSO variant in which the cognitive coefficient of the particle is set to zero. MOL is a simplified form of PSO and is also termed as Social only PSO (S-PSO). The advantage of MOL algorithm when compared with PSO algorithm is that in the former the particle is updated randomly whereas, in later, the particle is updated iteratively over the entire swarm which results in less execution time [10]. Secondly, in MOL the swarm's best position is set to zero, this makes particle not to have any persistence in the previously followed path.

The intent of the paper is to design PSO and MOL based PID controllers with different frequency domain performance indices which has been taken as independent objective functions. PID controllers were used for LFC and AVR loop of a single area power system. A comparison of the results obtained with conventional tuned PID controller, PSO tuned PID controller and MOL tuned PID controller are presented in this paper.

II. LFC AND AVR CONTROL LOOPS

Due to sudden changes in load, the generator observes a momentary speed change, which causes a small change in rotor angle δ. This small change in rotor angle causes variation in real power and leads to variation in the system frequency. The LFC loop compares the new frequency with the old frequency and generates a command signal which is fed to the speed governor. The speed governor regulates the steam input to the turbine by some valve controlling mechanism and there by regulates the turbine mechanical output. This mechanical output when fed to the synchronous generator provides the regulated real power output.

The AVR loop is assigned with maintaining the synchronous generator terminal voltage, which in turn maintains the bus voltage manipulating the reactive power output. This is achieved by controlling the excitation of the field winding of the synchronous generator. The AVR loop continuously senses the terminal voltage; this voltage is rectified, smoothened and compared with a pre-set dc voltage reference. The error voltage, after amplification and shaping is used to control the synchronous generator's field excitation.

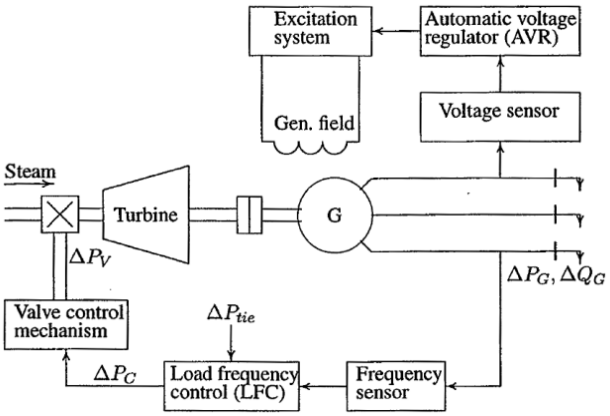

Fig. 1. Schematic diagram of LFC and AVR

The LFC and AVR loops are designed to operate around normal state with small variable excursions. The loops may therefore be modeled with linear, constant coefficient differential equations and can be represented with linear transfer functions [11-12].

A. Linearized model of LFC

LFC requires governor, turbine, inertia and load modeling. The transfer functions of these components can be stated as [13]:

- Governor: The transfer function of governor relates the change in steam valve position (ΔP_V) to change in real power generation (ΔP_g) and is expressed as

$$\frac{\Delta P_V(s)}{\Delta P_g(s)} = \frac{1}{1+\tau_{sg}s} \quad (1)$$

$$\Delta P_g(s) = \Delta P_{ref}(s) - \frac{1}{R}\Delta\omega(s) \quad (2)$$

- Turbine: The transfer function of turbine relates the changes in mechanical power output (ΔP_m) to the changes in steam valve position (ΔP_v) and can be expressed as

$$\frac{\Delta P_m(s)}{\Delta P_v(s)} = \frac{1}{1+\tau_t s} \quad (3)$$

- Inertia & Load: The transfer function of Inertia & Load relates the change in frequency ($\Delta\omega$) to the difference of change in mechanical power (ΔP_m) and change in electrical power (ΔP_e) and can be expressed as

$$\frac{\Delta\omega(s)}{\Delta P_m(s) - \Delta P_e(s)} = \frac{1}{D+2Hs} \quad (4)$$

Thus, the closed loop transfer function relating the load change (ΔP_L) to the frequency deviation ($\Delta\omega$) is

$$\frac{\Delta\omega(s)}{-\Delta P_L(s)} = \frac{(1+\tau_g s)(1+\tau_T s)}{(2Hs+D)(1+\tau_g s)(1+\tau_T s)+\frac{1}{R}} \quad (5)$$

B. Linearized model of AVR

AVR requires amplifier, exciter, generator and sensor modeling. The transfer functions of these components are [13]:

- Amplifier: The transfer function of amplifier relates the amplified voltage (V_R) to the error voltage (V_e) and can be expressed as

$$\frac{V_R(s)}{V_e(s)} = \frac{K_A}{1+\tau_A s} \quad (6)$$

- Exciter: The transfer function of exciter relates the field voltage (V_F) to the amplified voltage (V_R) and can be expressed as

$$\frac{V_F(s)}{V_R(s)} = \frac{K_E}{1+\tau_E s} \quad (7)$$

- Generator: The transfer function of generator relates the terminal voltage (V_t) to the field voltage (V_F) and can be expressed as

$$\frac{V_t(s)}{V_F(s)} = \frac{K_G}{1+\tau_G s} \quad (8)$$

- Sensor: The transfer function of sensor relates the voltage sensed from the generator (V_S) to the terminal voltage (V_t) and can be expressed as

$$\frac{V_S(s)}{V_t(s)} = \frac{K_R}{1+\tau_R s} \quad (9)$$

Thus, the closed loop transfer function relating the generator terminal voltage to the reference voltage is

$$\frac{V_t(s)}{V_{ref}(s)} = \frac{K_A K_E K_G K_R(1+\tau_R s)}{(1+\tau_A s)(1+\tau_E s)(1+\tau_G s)(1+\tau_R s)+K_A K_E K_G K_R} \quad (10)$$

III. PID CONTROLLER TUNING

PID controllers are practical industrial controllers. They are used to improve the dynamic response as well as to reduce or eliminate the steady state error. The controller calculates the error between a measured process value and a desired set point, and this error is reduced by adjusting the controller gains. The gains of a PID controller are: proportional gain (K_P), integral gain (K_I) and derivative gain (K_D). The proportional gain has the effect of reducing the rise time, the integral gain has the effect of eliminating the steady sate error and the derivative gain has the effect of increasing the stability of the system [14]. The Simulink block diagram of a PID controller is shown in fig. 2 and its transfer function is given by,

$$G(s) = K_P + K_I \frac{1}{s} + s.K_D \quad (11)$$

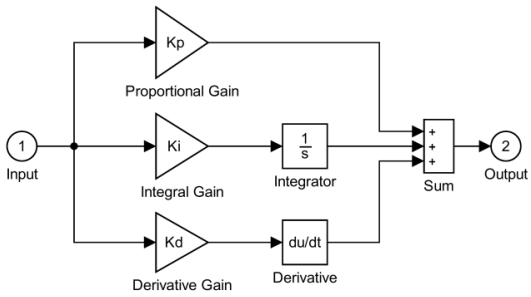

Fig. 2. Simulink block diagram of PID Controller

A. Conventional tuning

The procedure of tuning the PID controller by conventional trial and error method is as follows [15]:

Step 1: Set K_D and K_I to zero. By trial and error, select K_P that results in a stable oscillatory performance. In case of multi input system, select K_P that results near to critical damping.

Step 2: Vary K_D with K_P fixed so as to reduce the oscillations and result in reasonable overshoot and settling time.

Step 3: Vary K_I with K_P and K_D fixed, such that there is zero steady state error in minimum time.

B. Tuning using Particle Swarm Optimization

For the tuning of PID controller, the PSO algorithm generates a random population of the controller gains, then searches for the optimal set of gain values from this random population that minimizes a defined performance index as objective function. Integral of Time multiplied Absolute Error (ITAE), Integrated Absolute Error (IAE), Integral of Time multiplied Square Error (ITSE) and Integrated Squared Error (ISE) are some of the performance indices. ITAE is chosen as the performance index in this study as it can be easily evaluated analytically in the frequency domain [3-5]. The steps involved in implementation of PSO algorithm for tuning of PID controller are [16-17]:

Step 1: Initialize the particles to some linear positions in the range of K_P, K_I & K_D and set their velocities as zero.

Step 2: Evaluate the initial population by simulating the system model with each particle row value as the PID controller value and calculate the performance index for each particle at their corresponding positions.

Step 3: Initialize local minimum (P_{best}) for each particle.

Step 4: Find best particle (G_{best}) in initial particle matrix based on minimum performance index.

Step 5: Start the iteration, iter =1.

Step 6: Update velocities of the particles by the equation:

$$v_{j,g\,(i+1)} = w.v_{j,g\,(i)} + c_1.r_1.[P_{best\,j,g\,(i)} - x_{j,g\,(i)}] + c_2.r_2.[G_{best\,g\,(i)} - x_{j,g\,(i)}] \quad (12)$$

Step 7: Create new particles from the updated velocity.

Step 8: If any of the new particles violate the search space limit, then choose the particle and generate new values within the particle space.

Step 9: Evaluate performance index for each new particle at their respective position by simulating the system model.

Step 10: Update P_{best} and G_{best} based on minimum value between new performance index and old performance index value.

Step 11: Update the G_{best} value and its performance index.

Step 12: Iteration = iteration + 1.

Step 13: If iteration $\leq$ maximum iteration, go to step 6, otherwise continue.

Step 14: The obtained G_{best} is the optimum set of parameters of the PSO-PID controller.

C. Tuning using Many Optimizing Liaisons

In PSO algorithm, the cognitive coefficient (C_1) is set to zero, this results in MOL algorithm. The implementation algorithm of MOL is similar to that of PSO except the fact that C_1=0. Besides this change, the parameters C_2 remains unchanged and the inertia weight is also set similar to PSO. The velocity update equation for MOL algorithm is thus reduced to

$$v_{j,g\,(i+1)} = w.v_{j,g\,(i)} + c_2.r_2.[G_{best\,g\,(i)} - x_{j,g\,(i)}] \quad (13)$$

D. Performance Index

In terms of error signal *e(t)*, the performance indices employed in control system design can be given as:

$$ITAE = \int_0^\infty t.|e(t)|.dt \quad (14)$$

$$IAE = \int_0^\infty |e(t)|.dt \quad (15)$$

$$ITSE = \int_0^\infty t.e^2(t).dt \quad (16)$$

$$ISE = \int_0^\infty e^2(t).dt \quad (17)$$

These are also referred as error functions. These integral performance criteria in the frequency domain have their own advantages and disadvantages [3]. For e.g., a disadvantage of the IAE and ISE criteria is that its minimization can result in a response with relatively small overshoot but a long settling time.

IV. SYSTEM INVESTIGATED

A power system consisting of a thermal generating unit of non-reheat type was considered for the simulation. The performance of the system was observed in terms of dynamic response of the system measured in terms of frequency deviation, Δf and voltage deviation ΔV occurring due to an application of a step load perturbation. The system is brought to its stable sate of operation with the use of PID controller. The Simulink model for the system is shown in fig. 3. The system was observed under a step change in load of 0.1 p.u., speed regulation of R = 3 Hz/p.u. and simulation time of t = 10 seconds. The error signal in the calculation of the performance index is taken as sum of frequency deviation, Δf and Voltage deviation, ΔV. Thus, the performance indices can be stated as:

$$ITAE = \int_0^t t.|\Delta f + \Delta V|.dt \quad (18)$$

$$IAE = \int_0^t |\Delta f + \Delta V|.dt \quad (19)$$

$$ITSE = \int_0^t t.[\Delta f + \Delta V]^2.dt \quad (20)$$

$$ISE = \int_0^t t.[\Delta f + \Delta V].dt \quad (21)$$

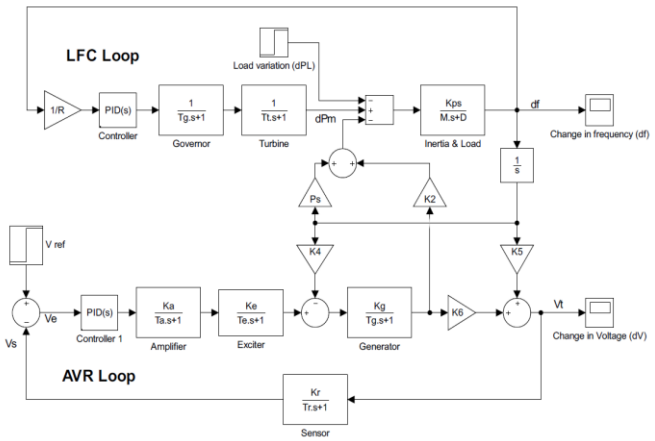

Fig. 3. Simulink model of the system in study

V. RESULTS AND DISCUSSION

A. *Particle Swarm Optimization tuned PID Controller*

Fig. 4 shows the frequency deviations and fig. 5 shows the terminal voltage deviations of the system for different performance indices. Table I provides the comparison of response obtained from different performance indices. The comparison is made in terms of maximum overshoot and settling time of the frequency response and voltage response. Table II shows the values of PSO-PID controller gains obtained from each performance index.

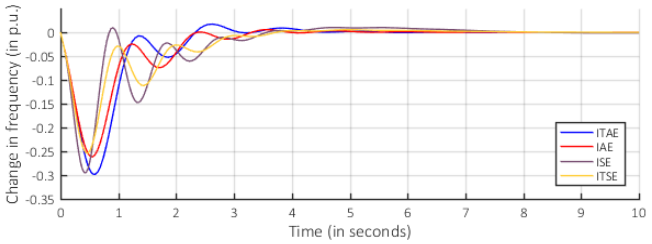

Fig. 4. Frequency deviations for different performance indices (PSO-PID)

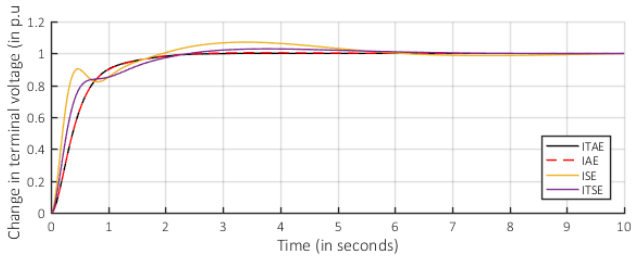

Fig. 5. Terminal voltage deviations for different performance indices (PSO-PID)

TABLE I
COMPARISON OF RESPONSE OBTAINED FROM DIFFERENT PERFORMANCE INDICES (PSO-PID)

Performance Index	LFC Loop		AVR Loop
	Max. Overshoot (p.u.)	*Settling time (s)*	*Settling time (s)*
ITAE	-0.2986	6.650	3.218
IAE	-0.2616	6.983	4.817
ITSE	-0.2537	8.353	7.824
ISE	-0.2951	8.391	10.35

TABLE II
PSO-PID CONTROLLER GAINS OBTAINED FROM DIFFERENT PERFORMANCE INDICES

Performance Index	K_P		K_I		K_D	
	LFC	*AVR*	*LFC*	*AVR*	*LFC*	*AVR*
ITAE	3.19	0.80	2.00	0.38	2.39	0.30
IAE	4.54	0.80	2.00	0.39	2.89	0.30
ISE	5.00	0.80	2.00	0.80	5.00	0.80
ITSE	5.00	0.80	2.00	0.48	4.47	0.50

B. *Many Optimizing Liasons tuned PID Controller*

Fig. 6 shows the frequency deviations and fig. 7 shows the terminal voltage deviations of the system for different performance indices. Table III provides the comparison of response obtained from different performance indices. The comparison is made in terms of maximum overshoot and settling time of the frequency response and voltage response of the single area power system. Table IV shows the values of Many Optimizing Liaisons based Proportional Integral Derivative controller gains obtained from each performance index.

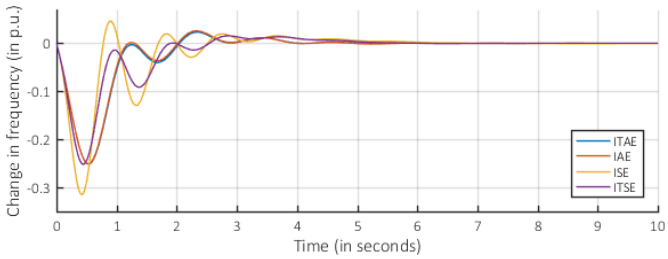

Fig. 6. Frequency deviations for different performance indices (MOL-PID)

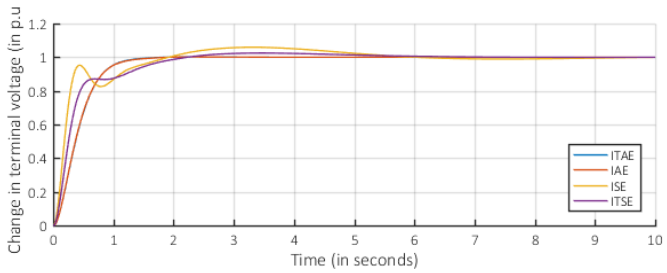

Fig. 7. Terminal voltage deviations for different performance indices (MOL-PID)

TABLE III
COMPARISON OF RESPONSE OBTAINED FROM DIFFERENT PERFORMANCE INDICES (MOL TUNED PID)

Performance Index	LFC Loop		AVR Loop
	Max. Overshoot (p.u.)	*Settling time (s)*	*Settling time (s)*
ITAE	-0.2514	5.833	1.986
IAE	-0.2519	5.871	2.055
ITSE	-0.2519	6.95	7.082
ISE	-0.3153	6.142	9.156

TABLE IV
MOL-PID CONTROLLER GAINS OBTAINED FROM DIFFERENT PERFORMANCE INDICES

Performance Index	K_P		K_I		K_D	
	LFC	*AVR*	*LFC*	*AVR*	*LFC*	*AVR*
ITAE	5.00	0.90	4.57	0.46	3.16	0.29
IAE	5.00	0.90	5.00	0.46	3.20	0.29
ISE	5.00	0.90	5.00	0.89	5.00	0.90
ITSE	5.00	0.90	5.00	0.57	5.00	0.55

C. *Comparison of results obtained from Conventional PID Controller, PSO-PID controller and MOL-PID Controller*

Fig. 8 compares the frequency deviation of the system obtained from PSO-PID controller and MOL-PID controller, and conventional PID controller. Fig. 9 shows the terminal voltage response of the system obtained from PSO-PID controller, MOL-PID controller and conventional PID controller. The ITAE criterion was chosen for comparison as it showed the best result in terms of overshoot and settling time. Table V shows the optimal gains of PSO-PID controller, MOL-PID controller (from using ITAE as performance index) and Conventional PID controller.

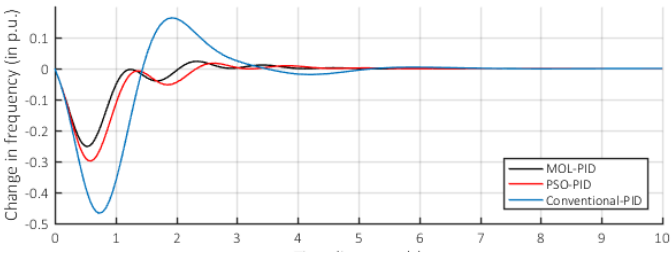

Fig. 8. Comparison of frequency deviation obtained from different tuning methods

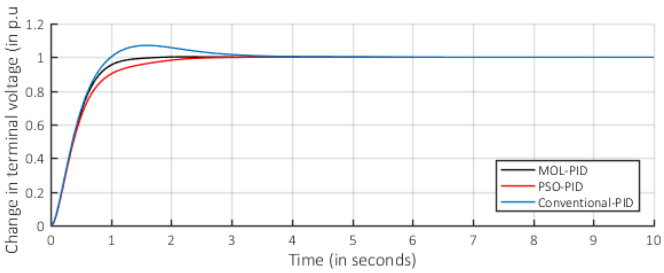

Fig. 9. Comparison of terminal voltage response obtained from different tuning methods

TABLE V
PID CONTROLLER GAINS OBTAINED FROM DIFFERENT TUNING METHODS

Controller	LFC Loop			AVR Loop		
	K_P	K_I	K_D	K_P	K_I	K_D
Conventional PID	0.2	1.5	1.2	0.9	0.6	0.3
PSO-PID	3.19	2	2.39	0.80	0.38	0.30
MOL-PID	5	4.57	3.16	0.90	0.46	0.29

VI. CONCLUSION

The conventional PID controllers results in large settling time, overshoot and oscillations. With use of evolutionary algorithms to tune the PID controllers, the typical characteristics show a faster and smoother response. Table VI provides the comparison of using the conventional tuned PID, PSO-PID controller and MOL-PID controller.

For a LFC system simulated for a step load deviation of 0.1 p.u. and regulation of 3 Hz/p.u., the settling time in the case of MOL-PID controller with ITAE as fitness function is 5.833s with a maximum overshoot of -0.2514 p.u., which is least as compared to the PID controller tuned through PSO algorithm and conventional tuning.

For an AVR system, there is no transient peak, also the MOL algorithm tuned PID controller with ITAE as fitness function gives a very small settling time of 1.986 sec as compared to the PID controller tuned through PSO algorithm and conventional tuning.

Thus the MOL-PID controller with ITAE as performance index results in best performance in terms of reduced overshoot and settling time.

TABLE VI
COMPARISON OF DYNAMIC PERFORMANCE RESULTED FROM USE OF DIFFERENT TUNING METHODS

Tuning Method	Dynamic Response		
	Δf		ΔV
	Max. Overshoot (p.u.)	*Settling time (s)*	*Settling time (s)*
Conventional	-0.467	7.956	6.399
PSO	-0.298	6.650	3.218
MOL	-0.251	5.833	1.986

APPENDIX

The simulation parameters for the Simulink model are provided in table below:

TABLE VII
SIMULATION PARAMETERS CONSIDERED FOR SYSTEM MODEL

LFC Loop Parameters	AVR Loop Parameters
Load change, ΔP_L = 0.1p.u.	Amplifier gain, K_A = 10
Base power = 1000 MW	Amplifier time constant τ_A=0.1
Governor time constant τ_{sg}=0.4s	Exciter gain, K_E = 1
Turbine time constant τ_t= 0.5s	Exciter time constant τ_E =0.4s
Load damping constant, D = 1	Generator gain, K_G = 0.8
Inertia constant H =10 MW/MVA	Generator time constant τ_G=1.4s
Speed regulation, R = 3 Hz/p.u.	Sensor gain K_R = 1
	Sensor time constant τ_R=0.05s

The Particle Swarm Optimization parameters used are:

Population size : 30
No. of iterations : 30
Cognitive coefficient, C_1 : 2
Social coefficient, C_2 : 2
Inertia weight : $0.4 \leq w \leq 0.9$

The Many Optimizing Liaisons parameters used are:

Population size : 30
No. of iterations : 30
Social coefficient, C : 2
Inertia weight : $0.4 \leq w \leq 0.9$

REFERENCES

[1] D. P. Kothari and I. J. Nagrath, "Automatic generation and voltage control," in *Power System Engineering*, 2nd ed., New Delhi, India: Tata McGraw Hill, 2011, pp. 409-430.

[2] H. Saadat, "Power System Control," in *Power System Analysis*, New Delhi, India: Tata McGraw Hill, 2002, pp. 527-569.

[3] Z. L. Gaing, "A particle swarm optimization approach for optimum design of PID controller in AVR," *IEEE Trans. on Energy Convers.*, vol. 19, no. 2, pp. 384-391, June, 2004.

[4] J. F. Nirmal, and D. J. Auxilia, "Adaptive PSO based tuning of PID controller for an automatic voltage regulator system," in *Proc. of IEEE Int. Conf. on Circuits, Power and Computing Technology*, Nagercoil, 2013, pp. 661-666.

[5] Y. Valle, G. K. Venayagamoorthy, S. Mohagheghi, J. C. Hernandez and R. G. Harley, "Particle swarm optimization: Basic concepts, variants and applications in power systems," *IEEE Trans. on Evol. Computation*, vol. 12, no. 2, pp. 171-195, April, 2008.

[6] J. Kennedy and R. C. Eberhart, "Particle swarm optimization," in *Proc. of IEEE Int. Conf. on Neural Networks*, Piscataway, NJ, 1995, vol. IV, pp. 1942-1948.

[7] M. Imran, R. Hashim and N. E. A. Khalid, "An overview of particle swarm optimization variants," in *Proc. of Malaysian Tech. Universities Conf. on Eng. & Tech. (MUCET 2012), Part 4 – Inform. And Commun. Technology*, Malaysia, 2013, pp. 491-496.

[8] Z. H. Zhan, J. Zhang, Y. Li, and H. S. H. Chung, "Adaptive particle swarm optimization," *IEEE Trans. on Syst. Man and Cybern. B, Cybern.*, vol. 39, no. 6, pp. 1362-1381, December, 2009.

[9] Y. Shi and R. C. Eberhart, "A modified particle swarm optimizer," in *Proc. of IEEE Int. Conf. on Evol. Computation*, Piscataway, NJ, 1998, pp. 69-73.

[10] S. Panda, B. K. Sahu, and P. K. Mohanty, "Design and performance analysis of PID controller for an automatic voltage regulator system using simplified particle swarm optimization," *J. of The Franklin Institute*, vol. 349, pp. 2609-2625, July, 2012.

[11] A. Chakrabarti and S. Halder, "Automatic Generation Control," in *Power System Analysis-Operation & Control*, New Delhi, India: Prentice Hall India, 2010, pp. 469-506.

[12] P. Dabur, N. K. Yadav and V. K. Tayal, "Matlab design and simulation of AGC and AVR for multi area power system and demand side management," *Int. J. of Comput. and Elect. Eng.*, vol. 3, no. 2, pp. 259-264, April, 2011.

[13] P. Kundur, "Control of active power and reactive power," in *Power Sys. Satbility & Control*, New York, USA: McGraw Hill, 1994, pp. 581-688.

[14] K. H. Ang, G. Chong and Y. Li, "PID control system analysis, design and technology," *IEEE Trans. on Control Syst. Technology*, vol. 13, no. 4, pp. 559-576, July, 2005.

[15] M. Nagendra, and M. S. Krishnarayalu, "PID controller tuning using simulink for multi area power systems," *Int. J. of Eng. Research & Technology*, vol. 1, no. 7, pp. 1-9, September, 2012.

[16] J. Venkatachalam and S. Rajalaxmi, "Automatic generation of two area interconnected power system using particle swarm optimization," *IOSR J. of Elect. and Electron. Eng.*, vol. 6, no. 1, pp. 28-36, June, 2013.

[17] A. Soundarrajan, S. Sumathi and C. Sundar, "Particle swarm optimization based LFC and AVR of autonomous power generating system," *IAENG Int. J. of Comput. Sci.*, vol.37, no.1, Feb, 2010.

Comprehensive Overview of Research in finding Transfer Capabilities with FACTS devices in India

Divya Gupta
Electrical Engineering Department
Baba Banda Singh Bahadur Engineering College
Fatehgarh Sahib, Punjab, India

Sanjay Jain
Electrical and Instrumentation Engineering Department
Thapar University
Patiala, Punjab, India

***Abstract*—The transmission facilities are the backbone of power system. To keep it delivering with utmost reliability it is very necessary to improve it regularly according to the rising needs. For this either the existing system has to be changed completely again and again or some new devices be added to the existing system so that it keeps on working incessantly and continuously though it will require some extra cost but if it is more advantageous then the decision taken is right. For this, the devices which can be used are FACTS (Flexible AC Transmission Systems) devices. This paper lists the comprehensive overview of research done in various years of these devices and explain how they can improve transfer capabilities along with some practical examples and applications of existing devices in India.**

Keywords—Transfer Capability, FACTS Devices, Congestion Mansgement, Deregulation

I. INTRODUCTION

The answer to the question of reliably and economically transferring power from one point to other is Available Transfer Capability (ATC) [1-3]. It gives the amount of power to be transmitted based on above mentioned grounds. The modern day requirement is to make the access of power open to all. This is fulfilled by Independent System Operator (ISO). It takes the responsibility of making available all the generation data to all the private players so that they can decide their bid based on the data. This system is known as Deregulation. It has changed the structure of power systems to horizontal i.e. VIU (Vertical Integrated Utility) which was acting as a monopoly first is now reduced to horizontal structure containing GENCOs (Generation Companies), DISCOs (Distribution Companies) and TRANSCos (Transmission Companies). ATC is generally linked with transmission facilities. This structure introduces competition among the market players and results in lesser prices which ultimately is advantageous for the consumers. Quality of power received by the consumers is also enhanced. Also they will have more choices now. FERC (Federal Energy Regulatory Commission) had introduced this concept in 1996. Other components linked with ATC are TTC (Total Transfer Capability), CBM (Capacity Benefit Margin) and ETC (Existing Transmission Commitments).

Numerous authors have published regarding the concept. This paper aims at giving insight into the information available about the work done in this area in the past. Section II deals with Transfer capability issues, next section details congestion management, fourth section explains these devices located in India. Fifth section describes how transfer capabilities be improved using FACTS devices. Finally Conclusion and then References are listed.

II. TRANSFER CAPABILITY

ATC is described as

$$ATC = TTC - TRM - ETC - CBM \quad (1)$$

The calculations involved in ATC should take into consideration the points from where the power is extracted, injected and transferred. The power flow conditions which vary with time should be considered in ATC calculations alongwith parallel power flows' path in the network of transmission [4-8]. These calculations should give commercially acceptable outputs which must be accurate and indicate the transfer available for the market. Figure 1 shows the concept of ATC pictorially.

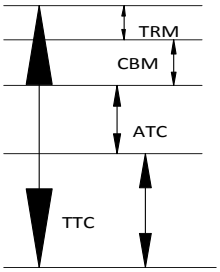

Fig. 1 Concept of ATC

Total Transfer Capability may be defined as per NERC (North America Electric Reliability Council) [9-12] May 1995 notification as the power transferred reliably without violating any limit (such as dynamic stability, thermal and voltage limit) between interconnected network. It is like a vector and hence depends upon direction. If, for example, a simple power system, which is an interconnected one is considered, taking into account three areas viz., receiving, sending and some other area which can be an isolated system etc., then we have to find the value of ATC through the designed path to receiving end from the sending area.

III. CONGESTION MANAGEMENT

Transfer capabilities of power system are often affected by congestion management. It is just like traffic congestion. As we have to devise different methods for easing traffic so that vehicles can go seamlessly. Congestion management is dealt effectively using different Flexible AC Transmission Systems devices (FACTS). The working of these devices depends upon the following equation:

$$P = \frac{V_1 V_2}{X_{12}} \sin(\phi_1 - \phi_2) \quad (2)$$

Where P is the power transferred between buses 1 and 2, V_1 and V_2 are the voltages at these buses respectively. X_{12} is the reactance between them and ϕ_1 and ϕ_2 are the angles respectively.

The only drawback is the cost of these devices which is quite appreciable, but viewing their advantages these can be advised. Many devices come under this category [13-17] viz., UPFC (Unified Power Flow Controller), Series Capacitor, SVC (Static VAR Compensator), STATCOM (Static Compensator) and TCSC (Thyristor Controlled Series Compensator).

Figure 2 gives the comparison of costs of these devices

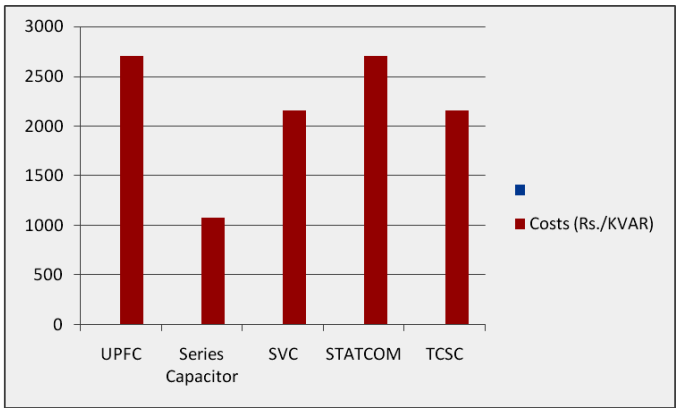

Fig. 2 Comparison of costs of different FACTS Devices

- *UPFC (Unified power flow controller)*

It can be considered as a generalized SSSC [18-20] (Static Synchronous Series Compensator) operated without the constraints of the quadrature relationship stipulated for the injected voltage with respect to the line current equations mentioned below in equations (3) and (4):

$$V_C = -jkXI \quad (3)$$

Where V_C is the injected compensating voltage phasor, I is the line current phasor, X is the series reactive line impedance, k is the degree of series compensation.

$$V_q = \pm jV_q(\varsigma)\frac{I}{I} \quad (4)$$

Where $V_q(\varsigma)$ is the magnitude of the injected compensating voltage ($0 \le V_q(\varsigma) \le V_{qmax}$) and ς is the chosen control parameter.

- *STATCOM (Static synchronous compensator)*

If the SVS is used strictly for reactive shunt compensation, like a conventional static var compensator, the dc energy source can be replaced by a relatively small dc capacitor. It exhibits operating and performance characteristics similar to those of an ideal rotating synchronous compensator, that's why it is called Static Synchronous Compensator. (The term advanced static var compensator or ASVC can also be used).

- *TCSC (Thyristor-controlled series capacitor)*

The two basic schemes of TCSC are first using thyristor switched capacitors and a fixed capacitor in parallel with a thyristor-controlled reactor. In the thyristor-switched capacitor, the degree of series compensation is controlled by increasing or decreasing the number of capacitor banks in series. In the fixed capacitors, thyristor-controlled reactor scheme, the degree of series compensation in the capacitive operating region is increased (or decreased) by increasing (or decreasing) the thyristor conduction period, and thereby the current in the TCR. Minimum series compensation is reached when the TCR is off. The TCR may be designed to have the capability to limit the voltage across the capacitor during faults and other system contingencies of similar effect.

Many authors have penned down their researches [21] based on these devices. This is explained through Figure 3 and 4 based on the years of research. Table 1 lists the properties of different devices.

Table 1 Comparison of Properties of FACTS Devices

Properties of FACTS Devices									
	LSCC	VC	TS	DS	DO	VC	CC	TDV	ARPF
SSSC	√		√	√			√		√
SVC		√	√	√	√	√			
TCBR			√	√	√				
STATCOM		√	√	√	√	√	√		
UPFC		√	√	√	√	√	√		
IPFC		√	√	√	√	√			
IPC	√				√				
TCPST			√	√					√
TCSC	√		√	√			√		√
TSC		√	√	√	√	√	√		
TCR		√	√	√	√	√	√		

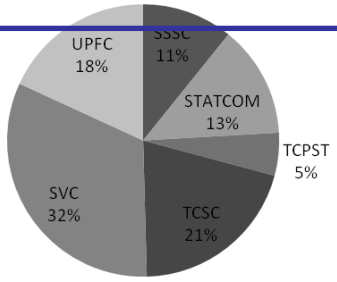

Fig. 3 Percentage of research done in different FACTS devices (1992–2000)

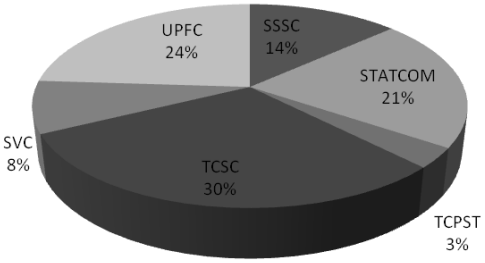

Fig. 4 Percentage of research done in FACTS devices (2001-2016)

IV. LOCATION OF FACTS DEVICES IN INDIA

Many of the FACTS devices have been installed in India. Some of them were installed in 2004 of 400 KV. Others were installed in Lucknow and has been in service since 2007. In 2005 also FACTS devices were installed in Gooty, Anantapur, Andhra Pradesh and in the same year Cuddapah, Rayalseemah, Andhra Pradesh also introduced one. In Sami, Patan, Gujarat and Meerut it got commissioned in 2010. Fixed Series Compensation devices are installed in Lucknow, Bareilly and Unnao. These all devices are commissioned by Power Grid Corporation of India, Limited (PGCIL). The fixed series compensation at Lucknow and Unnao substations are associated with enhancement of transmission capacity in the east-west corridor of the northern region. The devices are located at 400KV Gorakhpur-Lucknow lines at Lucknow Substations, at 400KV Bareilly-Mandolla lines at Bareilly Substations and at 400KV Unnao-Bareilly lines at Unnao Substations. The system used is Fixed Series Capacitors (FSCs). The capacitor ratings are 2 X 189 MVAr FSCs for Lucknow station, 2 X 187 MVAr FSCs for Bareilly station and 2 X 311 MVAr FSCs for Unnao station. The degree of compensation is 30%, 30% and 45% respectively. PGCIL is an Indian Government entity, and is the only agency responsible for transmission of power across the country. In India, where efficiency of power is now 52% approx., the enhancement of transmission capacity will play a vital role in achieving the target. The project focuses on the enhancement of the transmission capacity of northern grid.

Thyristor Controlled Series Capacitor, longest in world is situated in India, installed by PGCIL. It has constructed 475 Km long overhead line from Purnea in the state of Bihar via Muzafarpur to Gorakhpur in state of Uttar Pradesh. This project transmits surplus energy from eastern India to the areas around Delhi where the existing generation capacity can no longer meet demand. For the systems in Purnea and Gorakhpur, two thyristor-controlled series compensation systems and two Fixed compensation systems are installed. Notably, series compensation improves the transmission capacity of the overhead line and ensure stability in the grid. The Light-Triggered Thyristors used are notable for their very high current carrying capacity and blocking voltage. Direct light triggered thyristor make it possible to reduce the number of electronic components in the converter valves by about 80%. A further advantage of this modern thyristor design is that all the firing and monitoring electronics are at earth potential, the equipment is consequently accessible during operation. The purpose of this device is to improve the transmission performance and the reliability of the 400 KV overhead line between Purnea in eastern India and Gorakhpur in the north of the country.

PGCIL installed Purnea FSC, Gorakhpur FSC and Purnea TCSC, Gorakhpur TCSC in New Delhi, India. The capacitor ratings are 24.2Ω / 743MVAr, 3200A nominal current for Purnea FSC and 23.32Ω / 716MVAr, 3200A nominal current for Gorakhpur FSC, 3.03Ω / 3.64Ω / 112 MVAr, 3200A nominal current for Purnea TCSC and 2.92Ω / 3.510Ω / 108MVAr, 3200A for Gorakhpur TCSC. The degree of compensation is 40%, 40%, 5-15% and 5-15% respectively. The thyristor valve data is 125mm light triggered thyristor.

V. TRANSFER CAPABILITIES USING FACTS DEVICES

The introduction of Flexible AC Transmission devices for calculation of Transfer Capabilities enhances the transmission capability and reduces congestion. Various combination of devices can be utilized for this purpose e.g. series compensation, shunt compensation or combination of both. Many methods can be used to calculate this such as ACPTDF, DCPTDF, [22-27] Continuation Power flow etc. many researchers have listed all of these methods as mentioned in the references. Plethora of Intelligent techniques can also be used for the same. The voltage stability improvement can be achieved and losses of power system be reduced by methods like Bacterial Foraging Optimization based location of FACTS devices. Also some applications of Distributed Flexible AC Transmission system can also be performed in power systems. These calculations can be performed on various systems of IEEE like 14 bus etc. using FACTS device with voltage constraints. In deregulated power systems they are far more efficient. Dynamic transfer capability can be enhanced through optimal placement of FACTS controllers. A review of FACTS economic and practical evaluation has revealed their importance. A probabilistic modeling based approach for calculation of total transfer capability using FACTS devices can also be done. Transmission capabilities can be enhanced using TCSC via Artificial Techniques. An application of Hybrid Heuristic approach for ATC enhancement has been observed.

VI. CONCLUSION

The transfer capabilities can well be enhanced utilizing FACTS devices. These devices are good at relieving transmission congestion just like chest congestion and traffic congestion (daily problems faced). The eased out congestion results in better flow of power and quicker response. Also reliability index becomes high. Some tradeoffs are there like the cost of these devices as listed in the paper. Depending upon the real time situations, contingencies and problems, right amount of FACTS devices has to be decided. That is whether the advantage of relieving congestion is more or cost is more. If for some added cost there is reduction in cost in terms of easing of congestion then it will seem beneficial otherwise if the changing of existing lines are giving far more less cost then one is tempted to avoid these devices. So a detailed study into the effectiveness of these devices in power system has to be observed deeply. But if once FACTS devices are involved they are sure to give many beneficial advantages.

REFERENCES

[1] P. Pentayya, P. Mukopadhyay, S. Banerjee and M. K. Thakur, "Contingency Analysis for Eastern Regional Grid of India", *16th National Power Systems Conference*, pp. 359-363, 2010.

[2] North American Electric Reliability Council (NERC), "Available Transfer Capability Definitions and Determination", NERC Report, June 1996.

[3] Q. Morante, N. Ranaldo, A. Vaccaro and E. Zimeo, "Pervasive Grid for Large-Scale Power Systems Contingency Analysis," *IEEE Transactions on Industrial Informatics*, vol. 2, no. 3, August 2006.

[4] G. Sombuttwilailert, B. Eua-Arporn, "A Novel Sensitivity analysis for total transfer capability evaluation." *Proceedings of 22nd IEEE International Conference on Power Industry Computer Applications* 2001, pp. 342–347.

[5] Y. Ou and C. Singh, "Assessment of available transfer capability and margins," *IEEE Transactions on power systems*, vol. 17, no. 2, May 2002.

[6] G. C. Ejebe, J. Tong, J. G. Waight, J. G .Frame, X. Wang, W. F. Tinney, "Available transfer capability calculations." *IEEE transactions on Power System*, 1998, vol. 13, no. 4, pp. 1521–1527.

[7] M. G. Raoot, P. Pentayya and S. Ganguly, "Evaluation of Potential Threats to Grid Security by Contingency Analysis", *WRLDC, Mumbai, National Power System Conference (NPSC)*, Dec. 2008.

[8] N. G. Hingorani and L. Gyugyi, *Understanding FACTS: Concepts and Technology of Flexible AC Transmission Systems*. Wiley-IEEE Press, 1999.

[9] Transmission Transfer Capability Task Force, North American Reliability Council (NERC) Available Transfer Capability Definitions and Determination. Princeton, New Jersey, 1996.

[10] A. Oonsivilai and K. A. Greyson, "Power System Contingency Analysis Using Multiagent Systems", World Academy of Science, Engineering and Technology, 2009.

[11] A.Y. Dewi, S. P. Hadi and Soedjatmiko, "Contingency Analysis of Power System Electrical Operation*", Proceedings of the International Conference on Electrical Engineering and Informatics Institute, Teknologi Bandung, Indonesia,* June 17-19, 2007.

[12] M. Basu, "Optimal power flow with FACTS devices using differential evolution". International Journal of Electrical Power Energy System 2008, vol. 30, no. 2, pp. 150–156.

[13] A. K. Sharma, "Optimal number and location of TCSC and loadability enhancement in deregulated electricity markets using MINLP". *International Journal of Emerging Electrical Power Systems* 2006, vol. 5, no. 1, pp.1–15.

[14] D. Divan, W. Brumsickle, R. Schneider, B. Kranz, R. Gascoigne, D. Bradshaw, M. Ingram, I. Grant, "A distributed static series compensator system for realizing active power flow control on existing power lines." *IEEE transactions on Power Delivery* 2007, vol. 22, no. 1, pp. 642–649.

[15] H. D. Chiang, A. J. Fluek, K S. Shah, N. Balu, "CPFLOW: a practical tool for tracing power system steady state stationery behaviour due to load and generation variations." *IEEE transactions on Power System*, 1995, vol. 10, no. 2, pp. 623–634.

[16] A. J. Wood and B. F. Woolenberg, *Power Generation Operation and Control*, USA, Wiley & sons, 2012.

[17] B.V. Manikandan, P. Venkatesh, S. Charles Raja and A. Srinivasan, *Electrical Power Systems*, PHI Learning Private Limited, Delhi, 2012.

[18] G. C. Ejebe, J. Tong, J. G. Waight, J. G. Flame, X. Wang and W.F. Tinney, "Available Transfer Capability Calculations," *IEEE Transactions on Power Systems*, vol. 13, no. 4, November 1998.

[19] Federal Energy Regulatory Commission (FERC), Open Access Same-Time Information System and Standards of Conduct. Order No. 889, Final Rule, 1996.

[20] A. Kazemi, B. Badrzadeh, "Modeling and simulation of SVC and TCSC to study their limits on maximum loadability point". International Journal of Electrical Power Energy System, 2004, vol. 26, no. 5, pp. 381–388.

[21] R. D. Christie, B. F. Wollenberg and I. Wangstien, "Transmission management in the Deregulated environment". *Proceedings of IEEE*

[22] W. Li, M. Shaaban, Z. Yan, Y. Ni, S. Member, and F. F. Wu, "Available Transfer Capability Calculation with Static Security Constraints," *Power Eng. Soc. Gen. Meet. IEEE*, vol. 1, pp. 306–310, 2003.

[23] N. Sambasivarao, J. Amarnath, and V. Purnachandrarao, "Enhancement Of Available Transfer Capability In Deregulated Powersystem Using Series Facts Device (TCSC)," *Int. J. Eng. Res. Technol.*, vol. 2, no. 11, pp. 192–199, 2013.

[24] L. Min and A. Abur, "Total transfer capability computation for multi-area power systems," *IEEE Trans. Power Syst.*, vol. 21, no. 3, pp. 1141–1147, 2006.

[25] E. de M. Magalhães, A. Bonini Neto, and D. A. Alves, "A Parameterization Technique for the Continuation Power Flow Developed from the Analysis of Power Flow Curves," *Math. Probl. Eng.*, vol. 2012, pp. 1–24, 2012.

[26] B. V. Manikandan, S. C. Raja, P. Venkatesh, and P. S. Kannan, "Available Transfer Capability Determination in the Restructured Electricity Market," *Electr. Power Components Syst.*, vol. 36, no. 9, pp. 941–959, 2008.

[27] V. H. Quintana, C. C. A., and A. C. Z. De Souza, "New Techniques Computations to Speed Using Up Voltage Collapse Tangent Vectors," *IEEE Trans. Power Syst.*, pp. 1380–1387, 1997.

Comparitive Analysis of Lambda Iteration Method and Particle Swarm Optimization for Economic Emission Dispatch Problem

Vipandeep Kour
Assistant Professor,
Electrical Engineering Department,
IET Bhaddal, Ropar, India

Lakhwinder Singh
Professor,
Electrical Engineering Department,
BBSBEC, Fatehgarh Sahib, India

***Abstract* - With the increase in energy demands, it becomes necessary to operate the thermal power plants most economically, which gives rise to Economic Load Dispatch (ELD) problem. The problem of ELD in power system is to plan the power output for each committed generating unit in such a way that operating cost is minimized while meeting load demand, power operating limits. In present scenario, expansion in power generation has resulted to increase in emissions in the environment which is the prime concern for power system planners. In order to get clean energy, emission control has become an important operational objective in addition to minimization of operating cost. The combination of both the objectives i.e. economic dispatch and emission dispatch have resulted in multi-dimensional power system optimization problem called Economic Emission Dispatch (EED) problem. In this paper, EED problem has been solved using Lambda Iteration Method and Particle Swarm Optimization (PSO) technique. Both the solution methodologies have been validated on three generator system and five generator system. Comparative analysis of the results obtained by both the methods has been performed.**

Keywords— Economic Load Dispatch, Economic Emission Dispatch, Lambda Iteration Method, Particle Swarm Optimization.

I. INTRODUCTION

The modern power system is a vast interconnected system in which the main task is to allocate the load demand among participating generators at minimum possible cost. Planning the output of each generator in a power system while minimizing the fuel cost and satisfying various system constrains is termed as economic dispatch. The system constraints include matching the power generation with the load, operating the generators within permissible limits and maintaining system stability. When fossil fuels are burnt, toxic gases are released, such as oxides of carbon, oxides of sulphur and oxides of nitrogen [1]. These gases cause pollution in atmosphere and hence disturb the ecological balance leading to global warming. With the increasing energy production to meet the increasing demands, the emission of pollutants has also increased, thus making the environment unfit for the survival of living beings. To meet clean energy requirement, there is need to minimize the emissions along with the fuel cost which is termed as emission dispatch. While minimizing the emissions, there is need to satisfy the system constraints. When economic dispatch and emission dispatch problems are combined together becomes as Economic Emission Dispatch (EED) problem [2].

Different techniques have been reported in the literature pertaining to solution of economic emission dispatch problem. Senthil *et al.* gave an improved Tabu search algorithm of three generator system, six generator system with emission constraints and thirteen generator system with valve point effect loading [3]. Abido presented a multi-objective evolutionary algorithm for environmental/economic power dispatch problem as non-linear constrained multi-objective optimization problem and used Strength Pareto Evolutionary Algorithm (SPEA) to solve the formed multi-objective problem [4]. In another attempt, Abido also presented a Multi-Objective Particle Swarm Optimization (MOPSO) for environmental/economic dispatch problem [5].

Thakur *et al.* used PSO algorithm to solve the problem of Combined Economic and Emission Dispatch (CEED) with use of penalty factors. The authors focused on reducing NO_2 and SO_2 emissions [6]. Valle *et al.* provided a detailed literature on PSO, its concepts, variants and application in the field of power systems. The authors have performed a vast study on this optimization technique [7]. Arunachalam et al. presented a new approach to solve CEED problem using a Hybrid Particle Swarm Optimization (HPSO) and Firefly algorithm where a multi-objective optimization problem with the valve point effect using a price based penalty factor was solved [8]. Das *et al.* used PSO and Teaching Learning Based Optimization (TLBO) for solution of ELD problem used to find the optimum solution with lowest fuel cost for four different network consisting of three, six, fifteen, and twenty generating units respectively for different load demand. Results obtained using PSO and TLBO are compared with the results obtained using lambda iteration method [9].

Particle swarm optimization is a population based stochastic optimization technique developed by Eberhart and Kennedy in 1995 to optimize nonlinear functions [10]. It is inspired by the social behavior of bird flocking or fish schooling while searching for food. PSO optimizes problem by having a population of particles, moving these particles around in the search space according to simple mathematical formula over the particle's position and velocity. Each particle's movement is influenced by its local best known position and is also guided toward the best known positions in the search space, which are updated as better positions are found by other particles. This moves the swarm toward the best solutions.

Each particle keeps track of its coordinates in the solution space, which are associated with the best solution (fitness) that has been achieved so far by that particle. This value is called personal best, P_{best}. Another best value that is tracked by the PSO is the best value obtained so far by any other particle in the neighborhood of that particle. This value is called G_{best}. The basic concept of PSO lies in accelerating each particle toward P_{best} and the G_{best} locations, with a random weighted acceleration at each time. Each particle tries to modify its position using the following information: current positions, current velocities, distance between the current position and P_{best}, and distance between the current position and the G_{best}.

PSO has a flexible and well balanced method to adapt the global exploration abilities with faster convergence rates [10]. The efficiency of PSO is due to the fact that each particle uses the information of the best particle and improves itself accordingly. PSO has been successfully implemented to solve power system problems including EED and many other multi-objective functions [11-14]. The key objectives of PSO over other optimization techniques can be listed as [15]:

- Unlike other algorithms, it is derivative free algorithm.
- It does not depends on the nature of objective function, i.e. continuity and convexity.
- The solution is not trapped in the local minima.
- It does not require an initial solution to start the algorithm.

In PSO, the individuals of the swarm are not created or destroyed, that is, the population remains stable and the particles follow the path of cooperation over competition. The particles while moving within the search space retains a memory of its best point ever attained. This best position is communicated to all other particles.

The intent of the paper is to implement PSO to optimize EED problem and to compare traditional lambda iteration method with PSO in order to prove the better computational efficiency of later over the former.

II. PROBLEM FORMULATION

A. *Economic Dispatch*

Consider a system of *N* thermal-generating units connected to a single bus-bar serving the electrical load is shown in fig. 1. The input to each unit is F_i. The output of each unit is $P_{gi.}$ The total cost of this system is the sum of the costs of each of the individual units. The essential constraint on the operation of this system is that the sum of the output powers must equal the load demand [16].

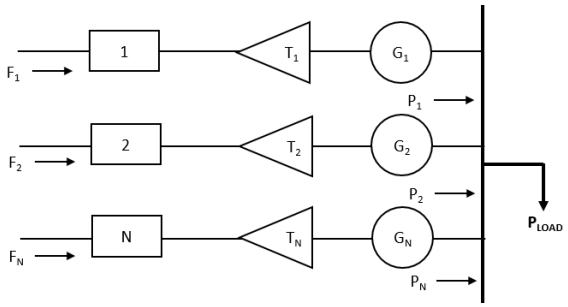

Fig. 1. *N* thermal units committed to serve a load P_{LOAD}

The objective function (F_T) is equal to the total cost for supplying the indicated load (P_{LOAD}). The problem is to minimize function (F_T) subject to the constraint that the sum of the power generated must equal the load. When transmission losses are neglected, the total fuel cost (F_T), is stated as

$$F_T = F_1 + F_2 + \cdots + F_N \quad (1)$$

$$F_T = \sum_{i=1}^{n} F_i(P_{gi}) \quad (2)$$

The operating cost of plant can be represented as shown in fig. 2. This cost is usually approximated by one or more quadratic segments. So, the fuel cost curve is a quadratic curve in active power generation. The fuel cost function without valve-point loading of the generating unit is given by

$$F_i(P_{gi}) = a_i P_{gi}^2 + b_i P_{gi} + c_i \quad \text{Rs/hr} \quad (3)$$

The economic load dispatch problem can be described as an optimization (minimization) process with the following objective function

$$Min \sum_{i=1}^{n} F_T \quad (4)$$

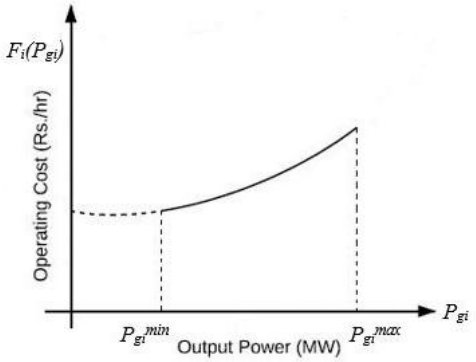

Fig. 2. Operating cost characteristics of fossil fuel fired generator

B. *Emission Dispatch*

Fossil fuels constitute a significant repository of carbon. Burning such fuels, result in the conversion of carbon to carbon dioxide, which is then released into the atmosphere causing an increase in the earth's levels of atmospheric carbon dioxide, which enhances the greenhouse effect and contributes to global warming. Other emissions produced from a generating station are oxides of sulphur and oxides of nitrogen. Sulphur and nitrogen oxides cause smog and acid rain [17-18]. Very tall flue-gas stacks can be built on plants, so that pollutants would get diluted when they are put in the atmosphere. While this helps in reducing local contamination, it does not help in solving the global issues. Total emissions of the system shown in fig. 1 are given by E_T, such that

$$E_T = E_1 + E_2 + \cdots + E_N \quad (5)$$

$$E_T = \sum_{i=1}^{n} E_i(P_{gi}) \quad (6)$$

The emission of the thermal power plant can be formulated as a second order polynomial function as

$$E_i(P_{gi}) = \alpha_i P_{gi}^2 + \beta_i P_{gi} + \gamma_i \quad \text{Kg/hr} \quad (7)$$

The emission dispatch problem can be described as an optimization (minimization) process with the following objective function

$$Min \sum_{i=1}^{n} E_T \quad (8)$$

III. System Constraints

Optimization of a given function is done when certain constraints are being satisfied. The constraints that are considered during the optimization of cost function and emission function formulated in eq. 4 and eq. 8 are:

A. Equality Constraints

The equality constraints are represented by the power balance constraint, that is, the power balance equation, where the total power generation must cover the total power demand and the power loss.

$$\sum_{i=1}^{n} Pgi = P_D + P_{LOSS} \quad (9)$$

B. Inequality Constraints

The inequality constraints are power generation limits of thermal power generators. Upper and lower bounds on the generation of each generator are to be fulfilled and can be expressed as

$$P_{gi}^{\min} \le P_{gi} \le P_{gi}^{\max} \quad (i = 1, 2, \ldots, n) \quad (10)$$

IV. Solution Methodology

The purpose is to solve economic emission dispatch problem using the conventional optimization technique, lambda iteration method, and compare the results obtained by solving the same using PSO algorithm.

A. Lambda Iteration Method

Lambda iteration method is an iterative type of computational technique shown in fig. 3. The optimum operating point of any generator set, within a specified limits, is found using this method.

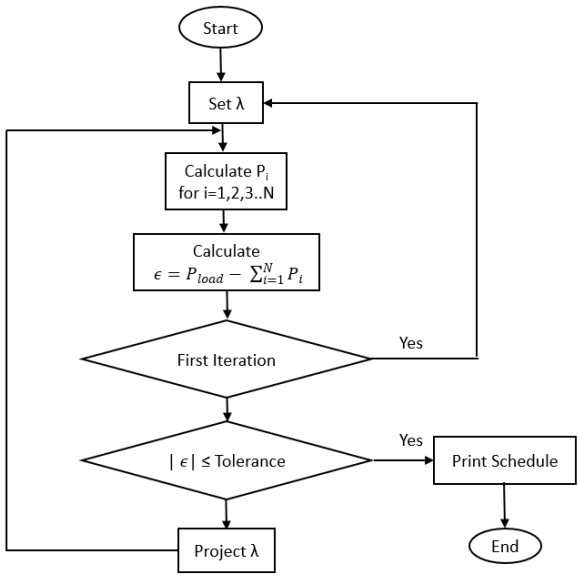

Fig. 1. Lambda iteration method

B. Particle Swarm Optimization

In the PSO algorithm, a random population of particles is created and the optimization is achieved by the movement of particles towards the global best position. The particles update their position and velocity according to their self-experience as well as the social interaction between other particles. Economic emission dispatch problem is solved by implementing PSO.

The modified velocity and position of each particle can be derived using the present velocity and the distance from $P_{best\ id}$ to $G_{best\ d}$ by the velocity and position equations as given in the following equations:

$$V_{id}^{(t+1)} = w.v_{id}^{t} + c_1 r_1 (P_{best\ id} - x_{id}^{t}) + c_2 r_2 (G_{best\ d} - x_{id}^{t}) \quad (11)$$

$$x_{id}^{(t+1)} = x_{id}^{t} + v_{1d}^{(t+1)} \quad (12)$$

Where, x represents the position of particle, v represents velocity of the particle, and the i^{th} particle is denoted as $x_i = (x_{i1}, x_{i2}, \ldots, x_{id})$ in the d^{th} dimensional search space. The previous best position of the i^{th} particle is stored in memory and represented by $P_{best\ i} = P_{best\ i1}, P_{best\ i2}, \ldots, P_{best\ id}$. Also, for a particle, the description of rate of velocity is denoted as $v_i = v_{i1}, v_{i2}, \ldots, v_{id}$. The best position among the P_{best} is represented as $G_{best\ d}$. Fig. 4 shows the flow chart of PSO algorithm.

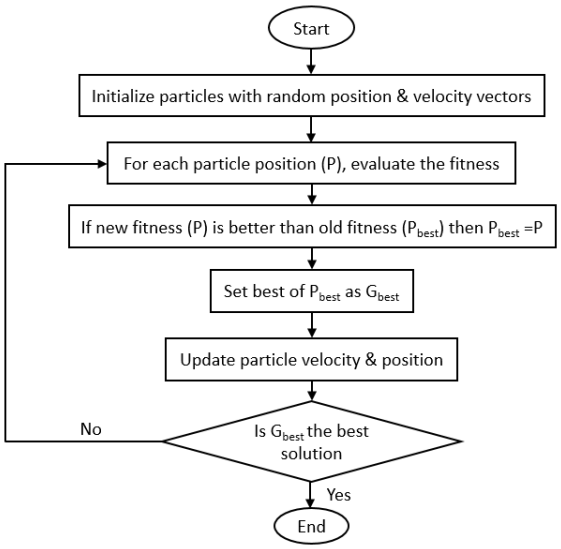

Fig. 2. Basic PSO algorithm

V. Results and Discussion

Economic emission dispatch problem has been solved using lambda iteration method and particle swarm optimization technique. The validity of the proposed techniques has been verified on two generator sets: 3 generator set for a demand of 350, 400 and 450 MW and 5 generator set for a demand of 400, 500 and 600 MW [3][19].

Equations (4) and (8) were solved using the proposed optimization techniques to get desired results for the two generator sets. All the PSO based optimization was done in MATLAB R2015a on 32 bit Intel Core i3 Computer with 2GB RAM with Windows 7 operating system.

A. *Results for 3 Generator Set*

Table 1 shows the values of powers generated and fuel cost in three generator set calculated from Lambda iteration method for economic dispatch. Table II shows the power output and total emissions for emission dispatch calculated from lambda iteration method.

TABLE I
POWER OUTPUT & FUEL COST FOR A 3 GENERATOR SET FOR ECONOMIC DISPATCH CALCULATED FROM LAMBDA ITERATION METHOD

Demand (MW)	P_1	P_2	P_3	Fuel cost (Rs/hr)
350	200.52	94.00	56.32	1487.34
400	200	119.32	81.00	1716.09
450	200	144	106	1957.34

TABLE III
POWER OUTPUT & FUEL COST FOR A 3 GENERATOR SET FOR EMISSION DISPATCH CALCULATED FROM LAMBDA ITERATION METHOD

Demand (MW)	P_1	P_2	P_3	Total Emissions (kg/hr)
350	109.52	96.51	144.4	694.93
400	123.41	109.23	167.32	655.83
450	142.89	127.07	180	753.98

Table III shows the values of powers generated by each of the generator in three generator set calculated from PSO for economic dispatch. Table IV shows the power output of each unit for emission dispatch calculated from PSO.

TABLE IIIII
POWER OUTPUT & FUEL COST FOR A 3 GENERATOR SET FOR ECONOMIC DISPATCH CALCULATED FROM PSO

Demand (MW)	P_1	P_2	P_3	Fuel cost (Rs/hr)
350	182.185	107.258	60.082	1406.273
400	192.716	122.60	84.148	1715.771
450	195.891	142.719	110.775	1956.557

TABLE IVV
POWER OUTPUT & FUEL COST FOR A 3 GENERATOR SET FOR EMISSION DISPATCH CALCULATED FROM PSO

Demand (MW)	P_1	P_2	P_3	Total Emissions (kg/hr)
350	185.636	82.935	81.427	682.891
400	124.3	114	160.751	654.3982
450	143	126.651	179.518	752.412

B. *Results for 5 Generator Set*

Table V shows the values of powers generated and fuel cost in five generator set calculated from Lambda iteration method for economic dispatch. Table VI shows the power output and total emissions for emission dispatch calculated from lambda iteration method.

TABLE V
POWER OUTPUT & FUEL COST FOR A 5 GENERATOR SET FOR ECONOMIC DISPATCH CALCULATED FROM LAMBDA ITERATION METHOD

Demand (MW)	P_1	P_2	P_3	P_4	P_5	Fuel cost (Rs/hr)
400	105.45	69.98	85	30	110.0	1169.19
500	153.99	82.98	85	30	149.23	1418.58
600	187.06	93.48	108.73	30.22	180.6	1632.54

TABLE VI
POWER OUTPUT & FUEL COST FOR A 5 GENERATOR SET FOR EMISSION DISPATCH CALCULATED FROM LAMBDA ITERATION METHOD

Demand (MW)	P_1	P_2	P_3	P_4	P_5	Total Emissions (kg/hr)
400	68.78	55.02	116.95	52.93	106.31	318.99
500	88.40	70.72	139.38	66.01	135.75	451.89
600	118.67	40	173.95	86.17	181.12	670.01

Table VII shows the values of powers generated by each of the generator in five generator set calculated from PSO for economic dispatch. Table VIII shows the power output of each unit for emission dispatch calculated from PSO.

TABLE VII
POWER OUTPUT & FUEL COST FOR A 5 GENERATOR SET FOR ECONOMIC DISPATCH CALCULATED FROM PSO

Demand (MW)	P_1	P_2	P_3	P_4	P_5	Fuel cost (Rs/hr)
400	123.30	61.20	87.23	32.32	91.74	1168.33
500	189.33	70.47	84.78	75.33	80.00	1430.66
600	185.38	93.15	99.69	44.68	175.28	1631.85

TABLE VIII
POWER OUTPUT & FUEL COST FOR A 5 GENERATOR SET FOR EMISSION DISPATCH CALCULATED FROM PSO

Demand (MW)	P_1	P_2	P_3	P_4	P_5	Total Emissions (kg/hr)
400	70.35	53.52	115.34	54.45	105.53	317.32
500	89.58	135.64	135.42	68.53	69.76	450.28
600	116.45	55.64	170.53	88.53	170.45	652.91

C. *Comparison of Results obtained from Lambda Iteration Method and PSO technique*

The results from both the techniques were compared and the comparison results are presented in Table IX for three generator set and in Table X for five generator set.

TABLE IX
COMPARISON BETWEEN LAMBDA ITERATION METHOD & PSO FOR 3 GENERATOR SET

Demand (MW)	Fuel Cost (Rs/hr)		Total Emissions (Kg/hr)	
	Lambda Iteration Method	PSO	Lambda Iteration Method	PSO
200	858.43	858.38	446.08	443.33
250	1060.27	1058.22	472.26	471.70
300	1273.27	1273.21	515.74	510.07

TABLE X
COMPARISON BETWEEN LAMBDA ITERATION METHOD & PSO FOR 5 GENERATOR SET

Demand (MW)	Fuel Cost (Rs/hr)		Total Emissions (Kg/hr)	
	Lambda Iteration Method	PSO	Lambda Iteration Method	PSO
400	1169.19	1168.34	318.99	317.33
500	1418.58	1403.66	451.89	450.28
600	1632.54	1631.85	670.02	652.91

VI. CONCLUSION

In this paper, two optimization techniques (lambda iteration and PSO) have been implemented to solve economic emission dispatch problem and the obtained results have been compared. Lambda iteration method is a conventional method but PSO is a new optimization technique which is a population based search algorithm. PSO shows better results along with fast convergence characteristics hence the optimized results of PSO are better than lambda iteration method. As far as fuel cost is concerned, it is small for three generators set but it is reasonably good for five generators set.

APPENDIX

The Particle Swarm Optimization parameters used are:

Population size : 100
No. of iterations : 80
Cognitive coefficient, C_1 : 2
Social coefficient, C_2 : 2
Inertia weight, w : 1 for 3 gen. set, 1.5 for 5 gen. set

REFERENCES

[1] D.P. Kothari and J.S. Dhillon, Power system optimization, *Prentice Hall of India*, New Delhi, 2011.

[2] L. Singh and J. S. Dhillon, "Interactive fuzzy approach for economic-environmental electric power load dispatch", *IEEE International Conference on Power Systems Technology (POWERCON 2016)*, University of Wollongong, NSW, Australia, September 28 to October 1, 2016, pp. 1-6.

[3] K. Senthil and K. Manikandan 'Economic thermal power dispatch with emission constraint and valve point effect loading using improved tabu search algorithm," *International Journal of Computer Applications*, vol. 3, no. 9, 2010.

[4] M. A. Abido, "Environmental/Economic power dispatch using multi objective evolutionary algorithms," *IEEE Trans. on Power Syst.*, vol. 18, no. 4, pp. 1529-1537, November 2003.

[5] M. A. Abido,"Multi objective particle swarm optimization for environmental/economic dispatch problem," *Elsevier – Electr. Power Res.*, vol. 79, pp. 1105-1113, 2009.

[6] T. Thakur, K. Sem, S. Saini and S. Sharma, "A particle swarm pptmization solution to NO_2 and SO_2 emissions for environmentally constrained economic dispatch problem," in *Proc. of IEEE/PES Transmission & Distribution Conference and Exposition: Latin America*, pp. 1-5, 2006

[7] Y. Valle, G. Venayagamoorthy, S. Mohagheghi, J. C. Hernandez, and R.G. Harley, "Particle swarm optimization: basic concepts, variants and applications in power systems", *IEEE Transactions on Evolutionary Computation*, vol. 12, no. 2, pp. 171-195, April, 2008.

[8] S. Arunachalam, T. AgnesBhomila and M. Ramesh Babu, "Hybrid particle swarm optimization algorithm and firefly algorithm based combined economic and emission dispatch including valve point effect," *Springer Link - Lecture Notes in Computer Science*, vol. 8947, pp. 647-660, 2015.

[9] B. Das and T. K. Sengupta, "Economic load dispatch using PSO and TLBO" in *Micheal Faraday IET Int. Summit*, pp. 212-219, 2015.

[10] J. Kennedy and R. C. Eberhart, "Particle swarm optimization", in *Proc. of IEEE Int. Conf. on Neural Networks*, vol. IV, pp. 1942-1948. IEEE service centre, Piscataway, NJ, 1995.

[11] M. A. Abido, "Multi-objective particle swarm optimization for environmental/economic dispatch problem," *Electrical Power System Research*, vol. 79, no. 7, pp. 1105-1113.

[12] M. R. Al-Rashidi and M. El-Hawary, "Hybrid particle swarm optimization approach for solving the discrete opf problem considering the valve loading effects," *IEEE Trans. on Power System*, vol. 22, no. 4, pp. 2030-2038, 2007.

[13] J. B. Park, K. S. Lee, J. R. Shin and K. Y. Lee, "A particle swarm optimization for economic dispatch with non smooth cost functions," *IEEE Trans. Power system*, vol. 20, no.1, pp .34-42, 2005.

[14] A. Sakthidasan, "Firefly algorithm for economic emission dispatch with normalized objective function," *Int. Journal of Development Research*, vol. 4, no.3, pp. 560-564, 2014.

[15] M. R. Al-Rashidi and M. El-Hawary, "A survey of particle swarm optimization applications in electric power systems," *IEEE Trans. on Evolutionary Computation*, vol. 13, no.4, pp. 913-918, 2009.

[16] A. J. Wood and B. F. Wollenberg, "Characteristics of power generation units," in *Power Generation Operation & Control*, New York, John Wiley & Sons, Inc., pp. 8-11, 1996.

[17] D. P. Kothari, S. K. Maheshwari and K. G. Sharma, "Minimization of air pollution due to thermal power plants," *Journal Institution of Engineering (India)*, vol.EN-57(2), pp.65-68, Feb 1977.

[18] L. Singh and J. S. Dhillon, "Surrogate worth trade off method for economic emission dispatch," *IEEE Power System Conf.*, pp.230-235, 2006.

[19] L. Devi, and O. V. Krishna, "Combined economic and emission dispatch using evolutionary algorithms-a case study," *ARPN Journal of Engineering and Applied Sciences*, vol. 3, no. 6, pp.28-35, 2008.

A Novel Adaptive Neuro-Fuzzy Inference System based MPPT control Multi-Junction PV Cell

Jyoti chaudhary
M.Tech. Power Engineering
Baba Banda Singh Bahadur Engg. College

Gursewak Singh Brar
Professor & Head
BBSBEC, Fatehgarh Sahib,India

Abstract:**In this paper a novel Adaptive Neuro-fuzzy algorithm is proposed based on Inference System for Maximum Peak Power Transfer technique for multi-junction solar cells connected to a grid. The multi-junction solar cells can be supposed to provide better efficiency as opposed to their single junction counterparts. ANFIS based algorithm is designed utilizing neural network and fuzzy logic. The membership functions are formulated using an initial inference and then the weights of the common membership functions are found by using Neural Network. Gradient Learning is utilized for tuning. The firing angle's optimal value is calculated and fed to the Boost converter. The converter output is given to a three phase inverter and the inverter output is connected to a grid. The inverter is controlled using a PWM regulator. The results are compared to that of an incremental conductance technique and it is found that the ANFIS based MPPT performs quite better than its other counterparts in terms of transient state and the magnitude of voltage obtained.**

Keywords: ANFIS, MPPT, PV cell, multi-junction solar cell.

I. INTRODUCTION

Nowadays, consumption of energy is increasing, idea of exploring renewable energy sources are also growing. Due to our limited energy sources, renewable energy sources are the future. Significant processes are made over the later years in development and research of the renewable power systems such as sea, wind, solar energy and wave systems. With these resources, the sun power energy can be used nowadays as most reliable, and environmental friendly energy source. Although sun power energy systems can be suffer with high costs and low efficiencies. To control these problems, maximum power can be extracted from PV panel while using the MPPT methods to optimize an efficiency of all the PV system. The photovoltaic technology can be made attractive option because the features various merits like as low maintenance requirement, environmental friendliness and absence of fuel cost. The efficiency of energy conversion a PV generation system may low because sun power cell exhibits to the nonlinear voltage and current and power versus voltage characteristics. These nonlinear characteristics contain weather functions conditions like as panel temperature and solar insolation. This is used to maintain the maximum power point tracking algorithm, efficient operation which can quick response and extract the maximum power from PV arrays in the real time becomes important in PGSs. Maximum Power Point Tracking, frequently referred to as MPPT, is an electronic system that operates the Photovoltaic (PV) modules in a manner that allows the modules to produce all the power they are capable of. MPPT is not a mechanical tracking system that "physically moves" the modules to make them point more directly at the sun. MPPT is a fully electronic system that varies the electrical operating point of the modules so that the modules are able to deliver maximum available power. Additional power harvested from the modules is then made available as increased battery charge current. MPPT can be used in conjunction with a mechanical tracking system, but the two systems are completely different All types of solar installations will benefit by using MPPT technology. The higher the module operating voltage (Vmp) the more benefit you will gain by using MPPT. Recreational Vehicles (RV) have very limited roof space for solar modules. If you do not tilt the modules, considerable power is lost in the winter months due to the low angle of the sun. Because of these limitations, it is very important to transfer all the power you can by using MPPT technology. For off-grid systems, MPPT will allow you to wire the PV modules in series for high voltage, even up to 600 volts DC! This is extremely beneficial for long wire runs as the higher the operating voltage, the smaller the wire can be for a given length. Several MPPT techniques can be projected and enforced. These strategies are observe and perturb, third open-circuit voltage, progressive conductance, fuzzy logic management, third short-circuit current and ripple correlation management app roaches. Some techniques are aim to attenuate hardware demand that is used to enhance performance which are additionally been projected. Perturb and Observe technique can be displayed to trace the wrong direction beneath for abrupt increase/decrease of the irradiance the result of the irradiance modification can be higher than the [9] perturbation step applied. Moreover, if MPPT algorithmic rule can be slower than speed of the irradiation changes, then most general electrical outlet trailing potency may become lower MPP .Thus, a quick and correct MPPT technique is needed. The wealthy with the numerous MPPT techniques can be supported completely different topologies with various cost, complexness and overall made potency. The hill climbing is Perturb and Observe area unit which is the best-known and commercially used techniques. In HC-MPPT technique, duty cycle can be directly increased or decreased in the fastened steps counting on panel voltage

and power values till utmost electrical outlet has been reached.

The organization of paper is as following. In section II literature review is presented. Proposed methodology is described in section III. The simulation results are seen in section IV. Finally, section V concludes this paper. The block diagram representation of MPPT is as below:

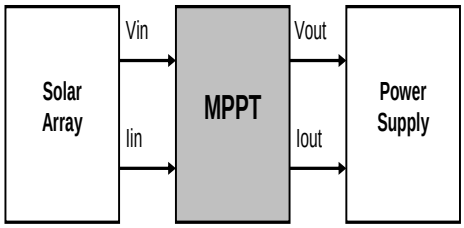

II. LITERATURE REVIEW

In voltage-based MPPT current-based MPPT approaches unit of the measurement is presented. Every unit of measurement can be simple and fast. Hence, these ways can track the low efficiencies for low irradiation levels. In this, Jain and Agarwal et al. [3], a strategy has been projected supported to the analysis and derivation of the I–V characteristics of photo voltaic panel by natural exponent index. This method offers the faster track speed than quality of hill-climbing methodology, the used index is solely to complicate for amount calculation exploitation in an inexpensive 8- or 16-bit lC. In MPPT management rules unit of the measurement can be supported the prediction line which associates the maximum power point and optimum current. One of the parameter got to be non-inheritable through hill-climbing methodology that generates commercially impractical. Kimball and Krein et. al [1]extended previous analog RCC method to the digital domain for MPP track. The projected digital implementation could be plenty of versatile, smaller quantity expensive; ton of durable quite such as analog RCC methodology, inductive and physical phenomenon parasitic elements may have impact on the facility of RCC to drive system toward being MPP. To subsume the exchange between the steady-state performance and so the speed of track, steepest descent methodology, variable step-size ways, parabolic prediction technique measure projected for MPP. The link between the values of panel current and voltage at MPP can be used to accelerate speed of the MPPT algorithmic rule. Panom Petchjatuporn et al [7] introduced most electric receptacle track algorithmic rule exploitation an artificial neural network for energy system. By applying a three layers neural network and few easy activation functions, most electric receptacle of an electrical device is expeditiously tracked .Yuvarajan et al [8] projected proper and fast most electric receptacle track the algorithmic rule for physical phenomenon panel uses electrical circuit voltage and so tangency current of photovoltaic panel. Prof. Dr. Ilhami Colaket al. [9] have curvy three separate farms that supply fifteen emu power for each farm exploitation Mat work Simulink amount analysis code [9]. Energy conversion is performed with the most electric receptacle track algorithms in every device exploitation Perturb and Observe structure S. G. Tesfahunegn et al. [10] designed solar/battery charge controller that mixes every MPPT and over-voltage controls as single operation. Yuncong Jiang et al. [11] has proposed Associate in the analogue most electric receptacle track the controller for physical phenomenon theme that utilized the load current to output power from device [11]. Arash Shafie et al. [12] projected distinctive MPPT algorithmic rule in main for battery charging applications that were thought of the constant voltage kind lots. It is achieved in main with the output current maximization [12]. This method edges from the blessings just like easy current controller and to boot circuit topology independence. Ali F Murtaza et al. [13] addresses the problematic behavior of Perturb & Observe technique and BLOCK DIAGRAM OF MPPT so displays complete distinctive MPPT hybrid technique has combination of the two basic techniques i.e. Perturb & Observe (P&O) [13] and halfway electrical circuit Voltage method therefore transmissible deficiencies found in P&O technique.Ko, S.H. et al. [2]presented Associate in intelligent management methodology for several electric receptacles trailing of physical phenomenon power-driven pump system for long boat within Asian country by exploitation DC-DC boost convertor as shift charger. This method consist the electrical device, a charger supported to the boost, battery, DC-DC converter, small pump. The electrical device has the specification of 75 watts of output power, and 3A of output DC current, 14-18 volts of output DC voltage. The output power of the electrical device uses input power to boost the DC-DC converters the shift charger. To manage the boost convertor heartbeat dimension [2] of the modulation can be applied. B.R.Sanjeeva Reddy et al [14] projected the PWM methods to regulate the output power of boost at the foremost possible price and at controls charging technique of battery. Parameter extraction, model analysis and analysis of boost device square measure incontestable exploitation MATLAB/Simulink model the recent development of the inverters for physical phenomenon AC-modules [4] has been targeted by Soeren et al. [4] The technology can be supported Centralized the Inverters on String Inverters and future on AC-Modules and AC-Cells. In this, target on DC to AC Inverter; power shift system; ability to induce drive voltage and shift power gives between electrical system and energy system.

III. PROBLEM FORMULATION

The problem of drawing maximum power from solar panel which is to be solved using MPPT technique and improvement algorithm needs to be formulated so better performance. A model for the above stated problem needs to be designed. The problem can be briefly summarised as follows. The basic equation can be described mathematically the IV characteristic of PV cell is

$$I_{pv} = I_g - I_S\left(\exp\left(\frac{q(V_{pv} + I_{pv} \cdot R_S)}{nkT}\right) - 1\right)$$

Where, n can be ideality factor, q is electron charge, k can be Boltzmann's constant, T can be temperature in the Kelvin, RS can be equivalent series resistance and Ipv, Ig and Is make the panel current, photo generated current, and saturation currents, respectively.

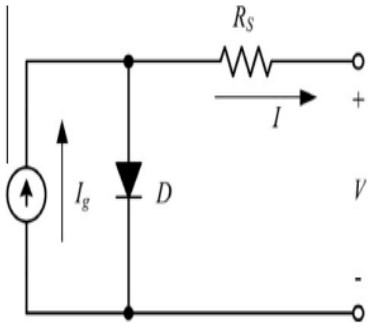

Fig. 1. Equivalent circuit of the PV cell.

In this, MPPT algorithm performance can be measured in dynamic and static ways; static MPPT efficiency can depict the ability of MPPT algorithm to find and hold the MPP under constant environment conditions, where as dynamic MPPT efficiency has been defined the ability in tracking MPP to consider the environmental conditions. The static MPP tracking efficiency gSTATIC is shown as

$$\eta_{STATIC} = \frac{P_O}{P_{MAX}} \times 100\%$$

Where, PO is an average output power that can be attained under the steady state and PMAX may the maximum power of the PV panel which is under the certain environmental conditions. At the locations, where irradiation changes are rapid due to the changes of atmospheric conditions in both dynamic and static MPPT efficiency have to consider. PGSs come with fast MPPT that have larger energy yielding under the modified environments than slow MPP tracking methods. Thus, The MPPT testing cannot be included its performance at different irradiance levels, but also tracks the MPP during transients.

IV. PROPOSED METHOD

It is proposed to use a Neuro-Fuzzy model for improvement of the MPPT technique. A model will be simulated in which the algorithm will be implemented and the controller will be included with the load.To simplify the design procedure, numerical method instead of analytical technique is employed to obtain the EML in this paper. For PV panels, the MPP locus can be defined as the point (VMP, IMP), which expresses a function of panel irradiation at a given operating temperature. When the PGS is subjected to a step change in irradiation level, conventional P&O methods require a few perturbation steps to reach the MPPT value. On the other hand, the operation along the EML is carried out by the fast voltage regulating loop. Thus, the tracking time of the proposed method can be greatly reduced. In addition, this voltage regulating loop is commonly utilized in switching power converters and can simply be implemented using a commercially available pulse-width modulated (PWM) IC in analog form. This paper aims at developing a novel technique based on Neural Network for improved performance of MPPT method for solar cells connected to a grid. The design will be made on SIMULINK of MATLAB and algorithm codes will be written in editor of MATLAB. The Neural Network will be designed using NN-toolbox of MATLAB.

V. RESULTS

This section presents the various results which are obtained using the proposed methodology as given in the previous section. The problem at hand was to develop an MPPT model using ANFIS for multi-junction solar cell connected to a grid. All the simulations have been done in MATLAB R =2013b in a computer having 2.7 GHz processor and 4 GB RAM.

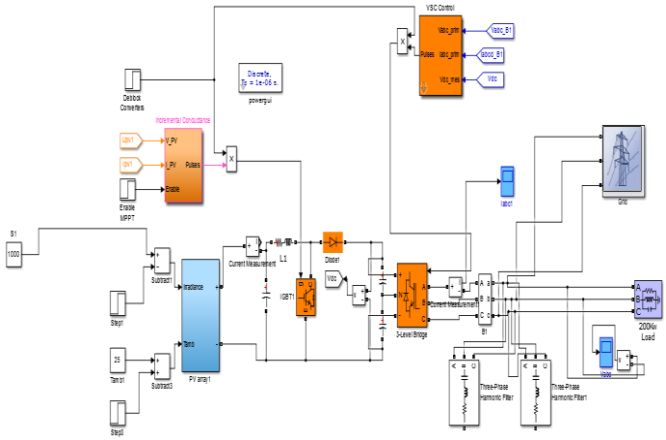

Fig. 2: Representing the overall proposed model

The voltage output is found to be quite close to sine wave as shown in figure 2

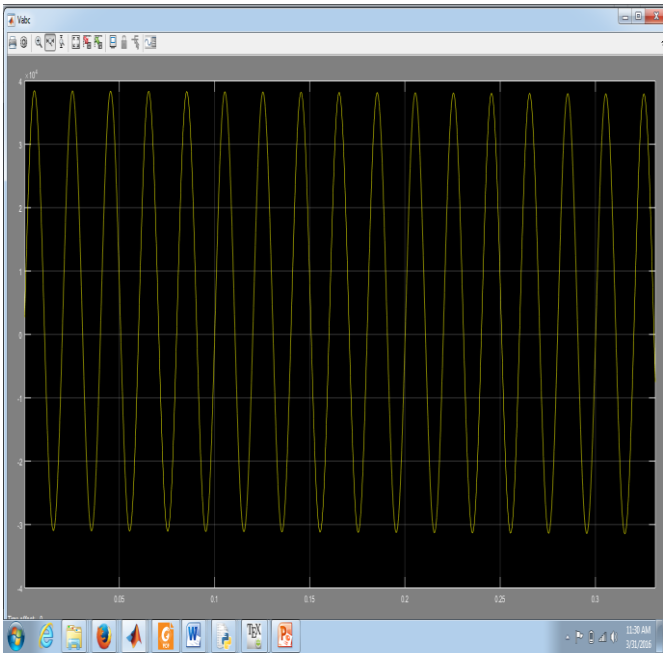

Fig. 3(a): Voltage output of ANFIS based MPPT

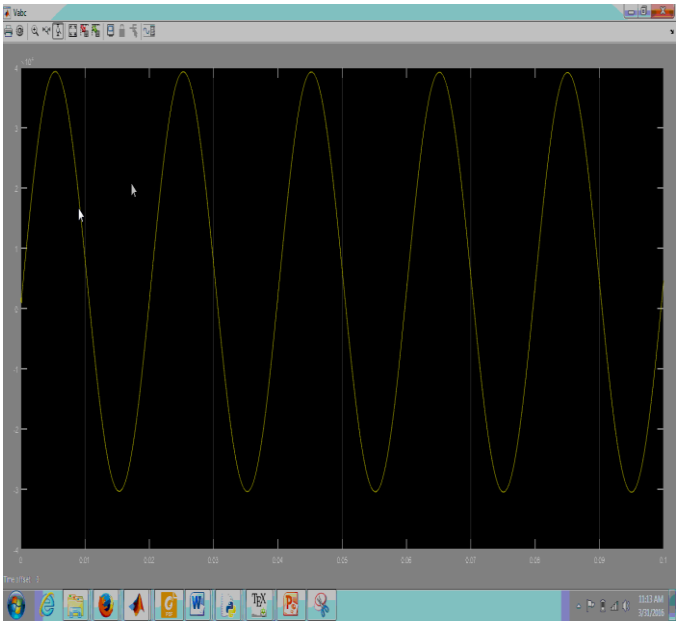

Fig. 3(b): The voltage output of I&C based approach

The voltage obtained using I&C is also analysed using FFT and it is found that the THD content of I&C approach is 0.35% which is more than ANFIS based approach as given in figure 3.

Table1: Showing Comparison of THD

	ANFIS	I&C
THD	0.17%	0.35%

V. CONCLUSION AND FUTURE SCOPE

This paper proposed a novel approach of utilising a neuro-fuzzy approach to solve the MPPT problem in multi-junction photo-voltaic cell connected to a grid using three phase inverter. The multi-junction photovoltaic cell was assumed to provide better output in terms of voltage. The model for adaptive neuro-fuzzy inference system was designed was designed and developed. The neuro-fuzzy model is used to train itself and track the voltage output based on the THD values of the output. The THD of the voltage was fed as input to the neuro-fuzzy model and as it is trained the firing angle of the boost converter connected to it is computed. The solar cell model was designed and given to boost converter. The converter output was analysed. An incremental conductance technique was also implemented for comparison purpose. The result of ANFIS algorithm was found to be quite better than the incremental conductance technique in terms of output voltage magnitude and THD content. The THD content reduces using our proposed approach. Also when the current is compared, the oscillations die out very fast in case of ANFIS algorithm while in I&C approach it is more or less sustained. In future this algorithm can be improved using other techniques and approaches. Also real time implementation of the algorithms can be done and hardware testing can be done. Hybrid with other algorithms can be utilised and the performances can be compared. Also clustering and other gradient learning methods can be utilised and the model can be tested for grid connection.

REFERENCES

[1] Kimball, J.W., Krein, P.T., “Discrete-time ripple correlation controlfor maximum power point tracking”, IEEE Trans. Power Electron. 23, 2353–2362,2008.

[2] Ko, S.H., Chao, R.M., “Photovoltaic dynamic MPPT on a moving vehicle,” Solar Energy 86, 1750–1760,2012.

[3] Jain, S., Agarwal, V., “A new algorithm for rapid tracking of approximate maximum power point in photovoltaic systems”, IEEE Trans. Power Electron. 2, 16–19,2004.

[4] Soeren Baekhoej Kjaer, John K. Pedersen,“Power Inverter Topologies for Photovoltaic Modules – A Review,” *IEEE*, 2002.

[5] V. Salas, M. J. Manzanas,“The Control Strategies for Photovoltaic Regulators Applied to Stand-alone Systems,” *IEEE*, 2002.

[6] Roger Gules, Juliano De Pellegrin Pacheco and HélioLeães Hey, “A Maximum Power Point Tracking System with Parallel Connection for PV Stand-Alone Applications,” *IEEE Transactions on Industrial Electronics*, vol. 55, no. 7, July 2008.

[7] PanomPetchjatuporn, PhaophakSirisuk, “A Solar-powered Battery Charger with Neural Network Maximum Power Point Tracking Implemented on a Low-Cost PIC-microcontroller”, IEEE transaction ,vol,4,no.3,2009.

[8] S. Yuvarajan and JulineShoeb, “A Fast and Accurate Maximum Power Point Tracker for PV Systems,” *IEEE*, 2008.

[9] Prof.Dr.IlhamiColak, Dr.ErsanKabalci and Prof.Dr.GungorBal, “Parallel DCAC Conversion System Based on Separate Solar Farms with MPPT Control,” *8th International Conference on Power Electronics - ECCE Asia*, The ShillaJeju, Korea, May 30-June 3, 2011.

[10] S. G. Tesfahunegn, O. Ulleberg,, “A simplified battery charge controller for safety and increased utilization in standalone PV applications,” *IEEE*, 2011.

[11] Yuncong Jiang, Ahmed Hassan, EmadAbdelkarem and Mohamed Orabi, “Load Current Based Analog MPPT Controller for PV Solar Systems,” *IEEE*, 2012.

[12] ArashShafiei, AhmadrezaMomeni and Sheldon S. Williamson, “A Novel Photovoltaic Maximum Power Point Tracker for Battery Charging Applications,” *IEEE*, 2012.

[13] Ali F Murtaza, Hadeed Ahmed Sher, “A Novel Hybrid MPPT Technique for Solar PV Applications Using Perturb & Observe and Fractional Open Circuit Voltage Techniques”, IEEE,2015.

[14] B.R.Sanjeeva Reddy, P.Badari Narayana,, “MPPT Algorithm Implementation for Solar Photovoltaic module using Microcontroller”,IEEE,2015.

[15] Yang Du and Dylan Dah-Chuan Lu, “Analysis of a Battery-Integrated Boost Converter for Module-Based Series Connected Photovoltaic System,” *The International Power Electronics Conference*, 2010

Heliostat Based Solar Park: Heating and Generation Combined

Neeraj Sharma
Electrical Engineering Department
Baba Banda Singh Bahadur Engineering College,
Fatehgarh Sahib

Hardeep Singh Ryait
Electronics & Communication Engineering Department
Baba Banda Singh Bahadur Engineering College,
Fatehgarh Sahib

R.S. Uppal
Electronics & Communication Engineering Department
Baba Banda Singh Bahadur Engineering College,
Fatehgarh Sahib

***Abstract*— A heliostat (from Helios, the Greek word for sun, and stat, as in stationary) is a device that includes a mirror, usually a plane mirror, which turns so as to keep reflecting sunlight toward a predetermined target (solar panel), compensating for the sun's apparent motions in the sky. Nowadays, most heliostats are used for day lighting or for the production of concentrated solar power, usually to generate electricity. They are also sometimes used in solar cooking. The proposed system would be used to generate the electric power from sunlight and provide thermal energy by heating water for industrial processes like processing food. Its speciality lies in the structural frame consisting of PV cells and water tubes.**

Keywords—Solar, Helistat, Park

Authors have got a grant of 10 lac for this project from DST, New Delhi

I. INTRODUCTION

Renewable energy is defined as energy that comes from resources which are naturally replenished on a human timescale, such as sunlight, wind, rain, tides, waves, and geothermal heat. Renewable energy has the potential in replacing the conventional fuels in four areas namely electricity generation, air and water heating/cooling, motor fuels, and rural (off-grid) energy services. The Sun is the source of energy on Earth, its because of sun that there is change in weather and climate. Efficient and economic harnessing of solar power may be very significant for taking care of today's ever-growing energy needs.

Solar energy can be harnessed by either converting solar energy to thermal energy or by converting solar energy to electricity. Converting solar energy to thermal energy can be for heating purposes or for electricity generation purposes. There has been a new addition which is Photovoltaic/Hybrid technology. Here combination of the two technologies by offering thermal energy and electricity simultaneously from a single solar collector is done.

Solar thermal systems (heating purposes) are usually small scale systems that which meet the heating demands of a facility. Here a fluid, which can be water/water-mixture or air, is circulated through an absorber. The outlet temperature of the fluid is higher than its inlet temperature. Solar systems (generate electricity) are large scale systems involving parabolic trough collectors, Fresnel mirrors or concentrating solar towers to generate heat and then this heat is used to increase the temperature of the running fluid in-turn the heat inside the fluid is converted to electricity using a steam turbine and generator. Other way can be use of photovoltaic modules. An emerging technology, combining the two ways of harnessing solar power is Photovoltaic or Thermal hybrid collectors. This paper investigates the performance of Photovoltaic/Thermal hybrid collectors. Photovoltaic/Thermal hybrid collector consists of a PV layer at the top and an absorber layer beneath it which absorbs heat from the PV layer. For fluid circulation the absorber layer has an inlet and outlet ports. Water or water-ethylene-glycol mixture or air is circulated through the absorber material to extract heat from it.

II. REVIEW

Photovoltaic (PV) module efficiency conversion [1] is affected by environmental changes, particularly by variations in temperature and radiation. There are several devices and techniques that allow a minimization of those effects and changes, by keeping the efficiency conversion at its highest level. Maximum Power Point Tracking (MPPT) and PV cooling systems can provide this efficiency improvement. In this paper it is proposed an association and combination of those systems, with the intent of achieving an even greater efficiency conversion level and also as a suggestion for future works in this area. In [1], a generic model of such system was presented. An exergy analysis was performed [2] to compare a conventional

(1) two panel photovoltaic solar thermal hybrid (PVT x2) system,
(2) side by side photovoltaic and thermal (PV + T) system,
(3) two module photovoltaic (PV) system and
(4) a two panel solar thermal (T x2) system with identical absorber areas to determine the superior technical solar energy systems for applications with a limited roof area. Three locations, Detroit, Denver and Phoenix, were simulated due to their differences in average monthly temperature and solar flux. The exergy analysis results show that PVT systems outperform the PV + T systems by 69% for all the locations, produce between 6.5% and 8.4% more exergy when matched

against the purely PV systems and created 4 times as much exergy as the pure solar thermal system. The results clearly show that PVT systems, which are able to utilize all of the thermal and electrical energy generated, are superior in exergy performance to either PV + T or PV only systems. These results are discussed and future work is outlined to further geographically optimize PVT systems

Concluding their study, they authors found that for solar energy collecting systems with identical absorber areas, PVT hybrid systems surpassed the exergy efficiency of both PV + T (side by side) and purely PV systems in three representative regions in the U.S. The PVT system outperformed the PV + T system by 69% and the Tx2 system by almost 400% in all the locations. Similarly, the PVT system performed 6.5%, 7.2% and 8.4% better than the PV only system for the Detroit, Denver and Phoenix locations respectively. It is clear that for applications with limited roof area PVT systems are superior choices. This research also suggests that greater optimization is required for PVT systems. To further improve the exergy performance of PVT systems, geographical optimization should be further investigated with potential improvements found in the PV material, flow rate and improved thermal loss reductions.

Previous work has shown that high-temperature short-term spike thermal annealing of hydrogenated amorphous silicon (a-Si:H) photovoltaic thermal (PVT) systems results in higher electrical energy output [3]. The relationship between temperature and performance of a-Si:H PVT is not simple as high temperatures during thermal annealing improves the immediate electrical performance following an anneal, but during the anneal it creates a marked drop in electrical performance. In addition, the power generation of a-Si:H PVT depends on both the environmental conditions and the StaeblereWronski Effect kinetics. In order to improve the performance of a-Si:H PVT systems further, this paper reports on the effect of various dispatch strategies on system electrical performance. Utilizing experimental results from thermal annealing, an annealing model simulation for a-Si:H-based PVT was developed and applied to different cities in the U.S. to investigate potential geographic effects on the dispatch optimization of the overall electrical PVT systems performance and annual electrical yield. The results showed that spike thermal annealing once per day maximized the improved electrical energy generation

The electrical and thermal performance of a typical single pass hybrid photovoltaic/thermal (PV/T) air collector was modeled by [4]. They also simulated and analyzed two selected case studies in Iraq. An improved mathematical thermo-electrical model was derived in terms of design, operating and climatic parameters of the hybrid solar collector to evaluate its important characteristics: collector flow and heat removal factors, PV maximum power point and its temperature coefficient, and overall power and efficiency. Unlike previous PV/T thermal models, the present model is obtained with some additions and corrections in radiation and convection heat coefficients for the top loss and for the air duct with more applicable sky temperature correlation. The well-known 5-parameter electrical model of PV module was solved using improved boundary conditions and translation equations for better convergence and accuracy. The voltage temperature coefficient of the PV module was included in the boundary conditions for convergence stability. The module parameters were taken to be dependent on solar radiation and PV cell temperature for improved accuracy. A Matlab computer simulation program is developed to solve the thermo-electrical model. The developed model is verified with previously published experimental results and theoretical simulations; it is proved to be most accurate in respect to percentage errors and correlation coefficients. Different parameters of the PV/T collector such as cell and air temperatures, thermal gain, PV current and voltage, and fill factor have been investigated. The results identified the effects of most important operating conditions such as sky, inlet and cell temperatures, air flow rate and incident solar radiation on the performance of the hybrid collector. The approved model was applied for a winter day (22 January 2011) in Baghdad city and for a summer day (20 May 2011) in Fallujah city. It was found that the electrical, thermal and overall collector efficiencies for the two case studies were 12.3%, 19.4% and 53.6% respectively for the winter day, while that for the summer day were 9%, 22.8% and 47.8%

In its conclusion it was seen that an improved thermo-electrical model was developed for a typical PV/T air based solar collector. The model was verified with previously published results and then applied to two selected cases, winter and summer, in Iraq. No previous study has been found for hybrid PV/T solar collector under Iraq climate. Following are few observations concluded form the study

1.1. Thermal characteristics

1. The gain, efficiency, and collector efficiency and heat removal factors were found to be better in the summer than that in the winter due to lower heat loss coefficient. The thermal gain is considerably higher (2.7 times at mid-day) due to very high solar radiation at the summer of Fallujah city. However, the other characteristics are not much improved due to the relatively high heat loss arise from the dry climate of Fallujah.
2. The variation of thermal efficiency during the day in the winter was larger than that in the summer. This was due to smaller thermal energy is available at low solar radiation (as in the morning and afternoon of winter day) as compared to the electrical energy absorbed and heat loss.
3. The collector flow factor is relatively high for both cases. This indicates that the air flow in the duct is adequate, i.e. the average air temperature is near to the inlet temperature. However, due to high heat loss, the collector efficiency factor was low and consequently the heat removal factor was also low. This indicates that the collector operates, in the winter and the summer, at high cell temperature relative to the inlet temperature. In fact, the heat removal factor can be improved by further increase of duct air velocity; however, this requires higher power air fans.
4. The radiation heat coefficient in the air duct was found to be comparable to the convective heat

coefficient of the fluid (air). This contributes in reducing the collector efficiency factor.

5. It was found that the heat loss is mainly due to top losses from the collector; 70% of these losses are due to the radiation heat transfer from glass to ambient because of low wind speed. The sky temperature affects considerably the radiation losses. The latter are much reduced when sky temperature is closer to the ambient temperature. This condition was applied for the hot moist climate which is not applicable to Iraq climate. This justifies the use of more applicable correlation for sky temperature. In fact, the top losses are very much reduced using a glass cover at appropriate spacing from the PV module.

1.2 Electrical characteristics

1. While the output power in the summer is higher than that in the winter (1.7 times at solar noon); the opposite is true for the efficiency. This is due to the negative temperature coefficient of efficiency. In addition, there is a little variation in the efficiency during the day in the winter and summer due to the relatively small value of its temperature coefficient.
2. To maintain the operation of the PV module at the maximum power point, the electrical load needs to be decreased when the climate changes from winter to summer. This can be achieved using maximum power point tracker.
3. The fill factor is higher in the winter than that in the summer. It is found that the fill factor gives a measure of the maximum electrical efficiency.

1.3 Overall characteristics 1. During the effective hours of the day, the thermal gain and its efficiency are found to be higher than the electrical output power and its efficiency respectively in the winter and summer. However, considering the thermal power conversion factor, the opposite is true. This is due to the high heat loss in the collector. The relative electrical-to-thermal equivalent power and efficiency are higher in the winter than that in the summer. Thus, the overall equivalent efficiency in the winter is higher than that in the summer.

In his paper [5], thermal and electrical performance of PV/T collectors have been analysed and presented for the climate of RAK, UAE. Thermal performance evaluation has been done following the collector output model presented in European standard and electrical performance evaluation is done by analyzing the effect of water circulation on the performance of PV/T collectors. Additionally, a PV/T system has been designed for residential use in UAE and simulated using simulation software Polysun. Power output and requirements of the system along with its financial analysis was also presented. Alternative solar energy systems to PV/T system have been analyzed in terms of power output, specific requirements and financial analyses. Finally, a study is made to reveal the impact of incentives towards sustainable energy systems on the economic feasibility of PV/T systems for residential use in UAE.

In its conclusion, author has observed that by combining thermal and electrical aspects of solar panels, an increase in electrical output is experienced due to the reason that the water circulation through the collector decreases the overall temperature of solar cells, which lead to a performance increase in terms of electricity production. This effect is experienced in the experiments that are conducted on the PV/T module, an increase in electrical output is recorded when there is a flow through the collector in comparison to the case where there is no flow through.

The benefits of PV/T systems are reaped most when there is a demand for both electricity and heat. It is observed that the electricity output of a PV/T collector is already greater than a similar sized PV collector. Adding the thermal output to that, having a PV/T system is most advantageous there is a demand for heat as well besides the increased electricity output. If there is a demand for heat only, having a solar thermal system would be more appropriate due to greater thermal performance and better economic feasibility of solar thermal systems. In case of electricity demand only, designing a PV system would be more suitable due to lower costs although PV/T systems offer better performance in electricity production.

[6]illustrated that , Integrating renewable energy (RE) systems into the built environment and using available rooftop space for solar energy installations provide a number of financial and societal benefits.These benefits include cost savings, increased energy cost security, and reduction of greenhouse gas emissions. Utilization of available rooftop area also provides an opportunity to implement solar energy technologies such as photovoltaic (PV) and solar hot water (SHW) systems to generate electricity and hot water for those buildings. The Project findings are that because of complications in system design and conflicts in installation and commissioning, the process did not deliver results that would be representative of future installations. TRNSYS was used to model the solar thermal system and SolOpt software was used to model the impacts of panel cooling on PV production. The basic system characteristics of the ideal system are outlined below:

- 48 solar thermal collectors installed on the back of typical crystalline silicon PV panels
- 1800 liters of storage
- Typical Office building draw profile (5000 liters/day on weekdays and 0 liter /day on weekend)
- 150-Watt circulation pump
- Standalone boiler provides supplementary heating (electric boiler)
- Tank temperature set point 125 °F
- Mixing valve set point temperature 120 °F

The primary disadvantage of the technology is the lower thermal efficiency, which requires greater surface area to provide an equivalent amount of solar thermal energy. Ultimately, the total system cost must be 30% to 50% lower than the cost of traditional solar thermal systems to be cost competitive. In the future, the technology should be evaluated against a standard solar thermal and separate PV system by an independent energy analyst using an hourly analysis tool. Installations should focus on hotter climates with good local solar incentives, facilities with electric hot water heaters, and high electric rates that can fully capture the benefits of panel cooling and apply the best practices as listed above.

[7] in their paper said that ,Hybrid photovoltaic thermal (PVT) systems consist of PV modules and heat extraction units mounted together. They convert the absorbed solar radiation into electricity and circulating water or air which are heated by cooling the PV modules. The PVT systems using water (PVT/WATER) for heat extraction are more expensive than air type PVT systems and can be used all seasons, mainly in low latitude applications, as water from mains is usually under 20ºC. In this paper they presented the design aspects for the hybrid PVT/WATER systems that can be applied in residential buildings, hotels, etc, aiming to provide electricity and hot water. They suggested the systems are analyzed regarding the design concepts and the electrical and thermal conversion effect for different PV module configurations. Their study was focused to small size PVT/WATER systems that can be applied to one family houses, multiflat residential buildings, small hotels, etc and can be used alternatively to the widespread thermosiphonic solar systems, in stand-alone and mini-grid application of photovoltaics. Additionally, in their study the application of a booster diffuse reflector, which increases the solar radiation on PVT panel aperture surface and overcomes in a way the reduction of the electrical output due to the optical losses from the additional glazing.
Further they concluded that the application of PVT/WATER systems is effective in electrical output, reducing cost pay back time (by 2.5 and 4.5 times regarding that of the typical pc-Si and a-Si PV modules. The addition of the thermal unit for the water heating contributes to a satisfactory total energy output, which is more effective for the pc-Si PVT than for a-Si PVT type systems. The cost pay-back time (of all considered hybrid systems is considered encouraging as they are less than 8 years, with better results for the a-Si type systems (about 5 years).The diffuse reflector increases the electrical and thermal output, but without significant improvement of cost pay-back time. These results show that PVT/WATER systems are of interest for application and wider use of photovoltaics

[8] concluded that Photovoltaic thermal system is better than unique PV module system because the energy can be recycled and the PV module can be cooled to increase the electrical efficiency. In their study, the prostulated that PV/T system that can be installed be PV/T module, storage tank, pump and controller. In the normal distribution of daily solar radiation condition, Water temperature in the storage tank can be heated up to 40 degrees. The PV/T system was found with high thermal efficiency about 35.33 to 47.21% and the electrical efficiency of 12.77 to 14.46%. The results obtained practically indicated that the system thermal efficiency reached 35.33% and photovoltaic conversion efficiency can reach 12.77% during the testing period. The water tank temperature can be risen from 26.2 degree to 40.02 degree.

[9] states that PV modules generate electricity, but the electrical output is only one component of the total energy produced by a photovoltaic array. A typical photovoltaic (PV) module has an ideal conversion efficiency in the range of 15%. The remaining energy produced is heat, which is neither captured nor utilized. This heat increases the operating temperature of the PV modules, which actually decreases their overall performance. Recent scientific testing done in conjunction with the International Energy Agency Task 35 Project at Canada's National Solar Test Facility has shown that it is possible to capture almost two to three times more thermal energy than electricity from a PV array. Panels from various manufacturers were tested under conditions, and the results showed that when PV modules were mounted on top of SolarWall transpired collector panels, the total solar efficiency increased to over 50%, compared to the typical 10 to 15% for PV modules alone. By removing the excess heat generated by the PV modules, the electrical output is increased. Modules can commonly operate at temperatures over 50 degrees C above ambient temperature, resulting in a performance reduction of more than 25%. By dissipating the heat from the module and lowering the operating temperature, significant gains can be made in system performance and the heat can be utilized for practical heating purposes. As a result of these effects, the testing showed that the payback on a PV system that incorporates a thermal component could be reduced by between one third and one half.
Concluding his research, [9] states that **t**est results from the National Solar Test Facility indicate that mounting the PV panels above SolarWall thermal panels will lower the PV panel temperature to an acceptable level. Lowering the cell temperature also increases the power output. The power output for the panels from BP and Evergreen increased at a rate of between 0.4% to 0.5%/ per degree C of lower module temperature. The tests confirmed that the thermal energy was much larger than the electrical energy, between 150% to 400% higher for the crystalline PV panels and as much as 800% higher for the amorphous panels. For example, a 160 Watt PV panel actually produced over 700 Watts of total energy with 540 Watts of thermal energy making up the difference. The solar heat is normally used during the heating season whereas the electrical output is useable over twelve months. Heating air with the transpired collector is cost effective with only 5 - 9 months of utilization and should also be cost effective with PV/T. When space heating is not required, the solar thermal energy can be easily vented. If however, the summer solar heat can also be used for clothes drying, water heating, pool heating or process heating, then the economics improve even more. The tests showed a temperature rise of 6 to 20°C above ambient. If a higher temperature is desired, a two stage solar heating system can be designed with the first stage as PV/T panel system and the second stage a glazed solar panel to receive solar preheated air from the first stage. It is desirable, however, to develop other uses for the heat in the summer months to make a PV thermal system even more cost effective, such as a desiccant cooling system. Utilizing the summer heat will improve the economics of a project and at the same time, recover heat that would otherwise be rejected to the atmosphere. These test results warrant investigating the application of PV/T systems in various geographical areas and climate zones, with and without the various incentives for PV installations. [9] further concluded that all building integrated PV installations should evaluate the benefits of utilizing the rejected heat.

[10] states that a significant amount of research and development work on the photovoltaic/thermal (PVT) technology has been done since the 1970s. Many innovative systems and products have been put forward and their quality evaluated by academics and professionals. A range of theoretical models has been introduced and their appropriateness validated by experimental data. Important design parameters has been identified. Collaborations have been underway amongst institutions or countries, helping to sort out the suitable products and systems with the best marketing potential. This article gives a review of the trend of development of the technology, in particular the advancements in recent years and the future work required. In the summary of this paper they stated that , the performance of various PVT collector types had been studied theoretically, numerically and experimentally for more than three decades. A range of PVT systems and products has been put forward and evaluated by researchers and professionals on various occasions. Their endeavour has been reviewed in this article. Generally speaking, in the early work, the research efforts were on the fundamental theories, the consolidation of the conceptual ideas and the feasibility study on basic PVT collector design configurations. In the 1990s, the PVT studies were more related to the collector design improvement and cost-performance evaluation. There were more rigorous analyses of the energy and mass transfer phenomena on conventional collectors with experimental validation. The ideas of building-integrated design began to emerge and the demonstration projects made available for documentation. In the last decade however, the focus has been generally shifting towards the development of complimentary products, innovative systems, testing procedures, and design optimization.

It was concluded in this paper [11] that the application of PV/T systems is effective in electrical output for lower PV module operating temperature, which corresponds to high thermal energy output, but to lower fluid temperature rise. The results determine the limits of the practical use of PV/T systems and regarding the use of a-Si or pc-Si PV modules, the higher electrical efficiency of pc-Si PV modules make them more effective considering the available area for their installation. The payback time under 10 years for PV/T hybrid systems is an opportunity for a large potential market for the PV industry, as the industry environment needs products that can be marketed without or with lower subsidy support

Solar energy can be converted directly into electric and thermal energy through photovoltaic cells and thermal collectors, respectively [12]. However this conversion, in particular the photovoltaic, has a reduced efficiency. A solution proposed to increase this efficiency is with the hybrid solar structure, which consists in the junction of the photovoltaic panel and the thermal collector in a single module. The paper presents a review of the research in this area, presenting the definitions of the related collectors and results of their characteristics, as well as some ideas for future studies. In their concluding remarks [12] said that the work has presented a review of the available literature on PV/T collectors, mainly of flat plate type. The results show that the PV/T efficiency is sensitive to many variables and a more detailed study seems to be necessary in order to obtain an optimal PV/T collector with improved efficiency and reduced costs, in order to be economically competitive.

The utilization of solar energy can be made by photovoltaic (PV) cells to generate electric power directly and solar thermal (T) panels can be applied to generate heat power. When the utilization of the solar energy is necessary to generate electric power, the option of using T panels [13] in combination with some heat / electric power conversion technology can be a viable solution. The power generated by utilizing the solar energy absorbed by a given area of solar panel can be increased if the two technologies, PV and T cells, are combined in such a way that the resulting unit will be capable of co-generation of heat and electric power. In their paper, combined Photovoltaic / Thermal panels were suggested to generate heat power to produce hot water, while the photovoltaic part is used to obtain electric power mainly for covering the electric power consumption of the system, to supply the electronic control units and to operate pump drives etc. AC and DC supplies are provided by converters for covering self consumption and possibly the need of some household appliances. The development and design of the system was made by extensive use of modelling and simulation techniques. In their paper as part of the simulation studies, they carried out tests to determine the energy balance in the electric energy conversion section of the system and the control structure, assuming stand-alone(SA) operation. In the concluding remarks , [13] conclude that a system suggested for utilizing solar energy for the production of heat and electric energy, based on the application of combined photovoltaic / solar thermal panels, can be operated in parallel or SA mode, but there only SA mode has been studied. The analysis of the complex system requires extensive use of simulation techniques and Matlab / Simulink as well as PSIM models have been described that can be used to study the energy balance of the section connected with the PV part of the combined panels and the operation of the MPPT controller. System have been built and tested by [13[, computer simulation and test results confirm expectations. It can be concluded that the system suggested hereby is technically feasible, however, they concluded that the economy of the solution needs further investigations

The Combined Heat and Power Solar System, or CHAPS system being developed at the Australian National University, has been described as a concentrating parabolic trough system that combines photovoltaic (PV) cells to produce electricity with thermal energy absorption to produce hot water. The first CHAPS prototype is a 25x concentration domestic style system, suitable for hot water and electricity generation for a home. [14] Recently a second CHAPS system prototype has been developed, a 35x concentration single-axis tracking system, designed for installation on the roofs of commercial and light industrial buildings, to contribute to building heating, cooling and power requirements. The development of the CHAPS systems was preceded by PV trough technology development at the ANU

since the mid-1990s, culminating in the commissioning of a 20kW PV trough array at Rockingham, Western Australia, in 2000.It has been concluded by [14] that results from the first CHAPS collector indicate thermal efficiencies around 50% and electrical efficiencies upward of 10% are achievable throughout the sunlight hours of the day. It is expected that recent developments in the design of the receivers and mirrors since the first prototype will further improve both thermal and electrical efficiency.

[15] compared the performance of an integrated photovoltaic and thermal solar system (IPVTS) to a conventional solar water heater and demonstrated the idea of an IPVTS design. A commercial polycrystalline PV module was used for making a PV/T collector. The PV/T collector was used to build an IPVTS. The test results show that the solar PV/T collector made from a corrugated polycarbonate panel can obtain a good thermal efficiency. Their study introduces the concept of primary-energy saving efficiency for the evaluation of a PV/T system. The primary-energy saving efficiency of the present IPVTS exceeds 0.60. This is higher than for a pure solar hot water heater or a pure PV system. The characteristic daily efficiency reaches 0.38 which is about 76% of s the value for a conventional solar hot water heater using glazed collectors. The performance of a sPV/T collector can be improved if the heat-collecting plate, the PV cells and the glass cover are directly packed together to form a glazed collector. The manufacturing cost of the PV/T collector and the system cost of the IPVTS can also be reduced. The present study shows that the idea of IPVTS is economically feasible too.

In their paper [16] , made an attempt to evaluate and compare the energy matrices of a hybrid photovoltaic thermal (HPVT) water collector under constant collection temperature mode with five different types of PV modules namely c-Si, p-Si, a-Si (thin film), CdTe and CIGS. The analysis is based on overall thermal energy and energy outputs from HPVT water collector. The temperature dependent electrical efficiency has also been calculated under composite climate of New Delhi, India. It is observed that c-Si PV module is best alternative for production of electrical power. Maximum annual overall thermal energy and exergy is obtained for c-Si PV module. The maximum and minimum EPBT of 1.01 and 0.66 years on energy basis is obtained for c-Si and CIGS respectively, whereas on exergy basis maximum EPBT of 5.72 years is obtained for a-Si and minimum of 3.44 in obtained for CIGS PV module. EPF and LCCE increase with increasing the life time of the system.

Solar photovoltaic/thermal (PV/T) water collector system was designed and developed at MANIT Bhopal to test its performance by [17]. Solar photovoltaic/thermal (PV/T) system consisted of PV modules coupled with heat extracting media such as water or air. Solar photovoltaic/thermal (PV/T) collector produced both thermal energy and electricity simultaneously. [17] concluded that the electrical efficiency of a PV system drops as its operating temperature rises. Design of solar PV/T system was aimed to reduce the operating temperature of PV modules and to keep the electrical efficiency at sufficient level. This paper presented a performance evaluation of flat plate solar PV/T collector and comparing its performance with the solar PV system. Experiments were conducted with fixed water flow rate of 0.002 kg/sec and different initial water temperature in the outdoor environment. With the proposed design and operating condition the daily electrical efficiency was about 7.57%, the daily thermal efficiency was about 50.1%, and the total efficiency of the system exceeded 73%. The energy saving efficiency of the PV/T system exceeded 68%.The results show that the electrical and thermal performance of the combined PV/T system is much more than that of employing the PV alone. PV/T application can offer sustainable solution for maximizing the solar energy output from building integrated photovoltaic system. This kind of PV/T system is especially suitable for low temperature applications like pre-heating of domestic water.

III. OBJECTIVES OF THE CURRENT RESEARCH

A lot many application are needed to be studied from where the energy can be regenerated, many of such techniques are still unutilized; this is the motivation for envisaging the project. The main objective of the propose project work are:

- Developments of hybrid PVT so that the dual mode of energy can be processed where in water heating along-with electricity can be generated
- Integration of photovoltaic and water heating structure
- Analysis of maximum heat production and electricity generation
- Monitoring of the real time data.

This project will enhance and will provide facilitation for energy harvesting deployment in different scenarios. This project utilizes the direct sunlight as well as diffused sunlight which is being utilized using the heliostat. A 1100 liter tank along with 4 solar panels of 250 W each will be used in this project. A power conditioning unit will be used to monitor and control the flow of power. Sunlight will be directed towards the mirrors and concentrated power will be reflected to the PV cell array structure. The design will be indigenous and have layered structure where first heating will be done and then electricity will be generated via diffused light.

ACKNOWLEDGMENT

The authors acknowledge the support of Department of Science and Technology.

REFERENCES

[1] da Rocha, Nuno M., et al. "A suggestion of combining a PV MPPT algorithm based on temperature control with a PV cooling system." *Industrial Electronics Society, IECON 2014-40th Annual Conference of the IEEE*. IEEE, 2014.

[2] Pathak, M. J. M., P. G. Sanders, and J. M. Pearce. "Optimizing limited solar roof access by exergy analysis of solar thermal, photovoltaic, and hybrid photovoltaic thermal systems." *Applied Energy* 120 (2014): 115-124.

[3] Rozario, Joseph, et al. "The effects of dispatch strategy on electrical performance of amorphous silicon-based solar photovoltaic-thermal systems." *Renewable Energy* 68 (2014): 459-465.

[4] Amori, Karima E., and Hussein M. Taqi Al-Najjar. "Analysis of thermal and electrical performance of a hybrid (PV/T) air based solar collector for Iraq." *Applied Energy* 98 (2012): 384-395.
[5] Kaya, Mustafa. "Thermal and electrical performance evaluation of PV/T collectors in UAE." (2013).
[6] Dean, Jesse, et al. *Photovoltaic-Thermal new technology demonstration*. National Renewable Energy Laboratory (NREL), Golden, CO (United States), 2015.
[7] Tripanagnostopoulos, Y., et al. "Design aspects of hybrid PVT/Water solar systems." *19th European Solar Energy Conference and Exhibition, France*. 2004.
[8] Huang, C. Y., C. H. Sung, and Kun—Lung Yen. "Experimental study of photovoltaic/thermal (PV/T) hybrid system." *Int J Smart Grid Clean Energy* 2.2 (2013): 148-51.
[9] Hollick, John, and Brett Barnes. "PV Thermal Systems; Capturing the Untapped Energy." *PROCEEDINGS OF THE SOLAR CONFERENCE*. Vol. 1. AMERICAN SOLAR ENERGY SOCIETY; AMERICAN INSTITUTE OF ARCHITECTS, 2007.
[10] Chow, Tin Tai, G. N. Tiwari, and Christophe Menezo. "Hybrid solar: a review on photovoltaic and thermal power integration." *International Journal of Photoenergy* 2012 (2012).
[11] Tselepis, S., and Y. Tripanagnostopoulos. "Economic analysis of hybrid photovoltaic/thermal solar systems and comparison with standard PV modules." *Proceedings of the international conference PV in Europe*. 2002.
[12] Ramos, Figueiredo, António Cardoso, and Adérito Alcaso. "Hybrid photovoltaic-Thermal collectors: A review." *Doctoral Conference on Computing, Electrical and Industrial Systems*. Springer Berlin Heidelberg, 2010.
[13] Jardan, Rafael K., et al. "Combined photovoltaic/thermal energy system for stand-alone operation." *Industrial Electronics, 2007. ISIE 2007. IEEE International Symposium on*. IEEE, 2007.
[14] Coventry, J. S., E. Franklin, and A. Blakers. "Thermal and electrical performance of a concentrating PV/Thermal collector: results from the ANU CHAPS collector." *ANZSES Solar Energy Conference*. Newcastle, Australia, 2002.
[15] Huang, B. J., et al. "Performance evaluation of solar photovoltaic/thermal systems." *Solar energy* 70.5 (2001): 443-448.
[16] Mishra, R. K., and G. N. Tiwari. "Energy matrices analyses of hybrid photovoltaic thermal (HPVT) water collector with different PV technology." *Solar Energy* 91 (2013): 161-173.
[17] Rawat, Pratish, and Pardeep Kumar. "Performance Evaluation of Solar Photovoltaic/Thermal (PV/T) System."

Comparative Study and Data Analysis of Combustive Properties of Hydrogen Fuel and Other Conventional Fuels

Vishal Kumar Mittal
Gulzar College of Engineering, Khanna
Punjab, India

Nirbhai Singh
Gulzar College of Engineering, Khanna
Punjab, India

***Abstract*—This paper discusses the environmental issues arise due to the combustion of fossil fuels to get energy for vehicles and compares the various combustive properties of these fuels with the Hydrogen. The industrialization and commercialization plans in the world have improved the living standards but the environment gets depleted. This paper also presents the role of Hydrogen to improve the degrading environmental conditions. The most important need is energy, therefore the process through which this energy is get extracted from the fuel is as much a subject of concern as the energy contained in the fuel. This paper shows how the hydrogen is a better energy carrier and opens the door for sustainable development.**

Key Words — Hydrogen Fuel; Fossil Fuels; Combustive Properties; Carbon Emission; Sustainable Development;

I. INTRODUCTION

The increasing pollution is the major concern of today's world. The transportation is one of the major sector contributing in the pollution. Our transportation sector is heavily dependent on the fossil fuels, the combustion of these fossil fuels to meet our energy demand has declined the quality of air. Carbon dioxide, carbon monoxide, oxides of nitrogen and the particulate matter are the major pollutants which are emitted from the vehicles. The carbon dioxide has contributed to the global warming and the particulate matter ($PM_{2.5}$ and PM_{10}) which remain in air for days and weeks have possessed the bad effects on health and the environment. These fine particles reach to the lungs and cause chronic respiratory diseases such as asthma etc. and on the other hand these fine particles remain for days in air, carried by air to the lakes, rivers etc. making them acidic and also depleting the soil quality. On 21 April, 2016 in Delhi the index value of $PM_{2.5}$ and PM_{10} was 270 which is poor and that of Gurgaon, India was 312 which is very poor. A report suggested that air pollution in India is estimated to kill 1.5 million people every year[1]. According to WHO, India has the world's largest death rate from chronic respiratory diseases and asthma. The oxides of nitrogen has contributed to the tropospheric ozone and increasing temperature is helping in its production. The bad effects on health caused due to the tropospheric ozone are effects on respiratory system causing coughing, throat irritation and uncomfortable sensation in the chest. Reduction in the functioning of lungs, making it more difficult to breathe deeply and vigorously. Ozone makes people more sensitive to allergens, therefore risk of asthma attacks increases. It also causes inflammation and damage to the lining of the lungs.

It also affects plants by slowing down the process of photosynthesis and plant growth as higher concentration of ozone causes the stomata to close down which open to allow carbon dioxide to diffuse in and water to diffuse out, a part of photosynthesis. As ozone is a highly oxidizing gas therefore it directly damages the internal cells of plants.

II. DESCRIPTION

A. Enthalpy of Combustion: Enthalpy of combustion is the amount of energy released during the combustion of 1kg of fuel. It is the measurement of energy to weight ratio. Greater the enthalpy of combustion, better the fuel is.

B. Auto-ignition Temperature: Auto-ignition temperature of a fuel is the lowest temperature at which the fuel gets spontaneously ignited without the presence of a flame or spark. The auto-ignition temperature of fuel tells about how much the fuel is safe. It should be higher than the required temperature of the site, otherwise the fuel gets exploded by itself and become a hazard.

C. Flammability range: Flammability range is the range of concentration of fuel in air that is capable of producing flash of fire in presence of an ignition source. This range lies between the lower flammability range and the upper flammability range.

Lower flammability range is the lowest concentration of gas or vapour in air that is capable of producing a flash in the presence of an ignition source (arc, flame or heat). The concentration of gas in air lower than this will not ignite the mixture. Similarly, the highest concentration of gas or vapour in air that is capable of producing flash in presence of an ignition source is called the upper flammability range. The concentration of gas in air higher than this is too rich to burn. The range between these two limits describe the flammability range of the fuel. This range should be high such that the fuel can be burnt with various fuel to air ratios.

*D. **Minimum Ignition Energy**:* Minimum ignition energy (MIE) is the minimum amount of energy required to ignite a combustible vapour, gas or dust cloud. This energy should be low such that lesser amount of energy will get consumed during the ignition of the fuel.

E.. Diffusivity: Diffusivity of the gaseous fuel is the property by which the fuel gets diffused in air. The greater the diffusivity, lesser the fuel is hazardous. If somehow the fuel gets leaked, due to its diffusive property it gets diffused in air minimizing the fire hazard. Higher the diffusive property more rapidly the fuel gets diffused in air.

F. Flame Speed: The flame speed is the measured rate of expansion of the flame front in a combustion reaction. Higher the flame speed, more closure the engine towards ideal one. With this the efficiency of the engine increases. The unburnt fuel also depends upon flame speed, thus greater the flame speed, the emission of unburnt fuel reduces

G. Combustion products: Combustion is the process of burning of fuel in air. If the products yield during this chemical reaction are non-pollutants, the fuel is said to be clean fuel.

III. RESULT

A. *Enthalpy of Combustion :*

The Fig. 1 describes the enthalpy of combustion of various fuels. The graph depicts that the enthalpy of combustion of hydrogen is around 142 MJ/kg[2] where as that of petrol is around 48 MJ/kg[2], which is around three times that of petrol.

Therefore, the energy to weight ratio of hydrogen is very good i.e. lesser amount of hydrogen will be needed to produce the same amount of energy than the other mentioned fuels.

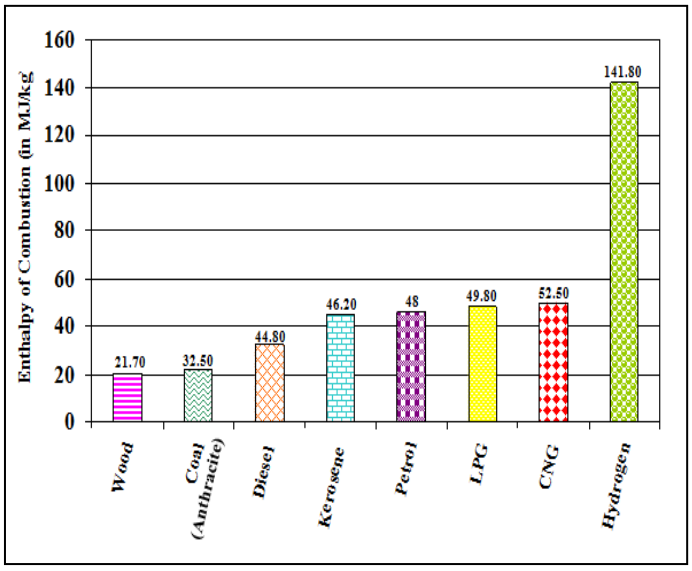

Fig. 1. Enthalpy of Combustion of different fuels

B. *Auto-ignition Temperature :*

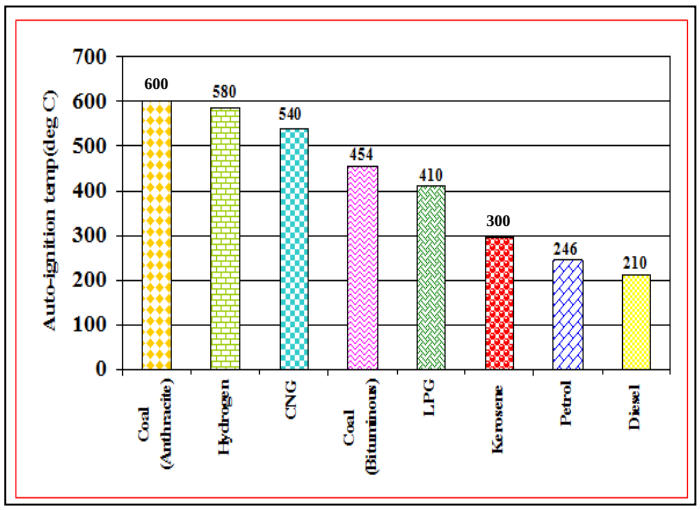

Fig. 2. Auto-ignition Temperature of various fuels

From Fig. 2, we can see that the auto-ignition temperature of hydrogen is around 580^{0}C which is very much higher than diesel, petrol and kerosene. Therefore, hydrogen is much safer fuel.

B. *Flammability range :*

Fig. 3 describes the flammability range of various fuels. As from the graph, hydrogen has maximum flammability range. The vehicle running on hydrogen IC engine can be supplied with various hydrogen to air by volume ratio.

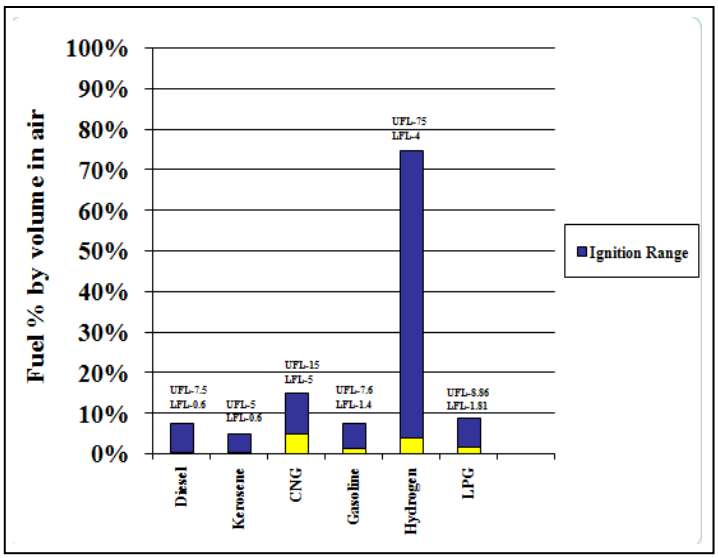

Fig. 3. Flammability range of different fuels

C. Minimum Ignition Energy :

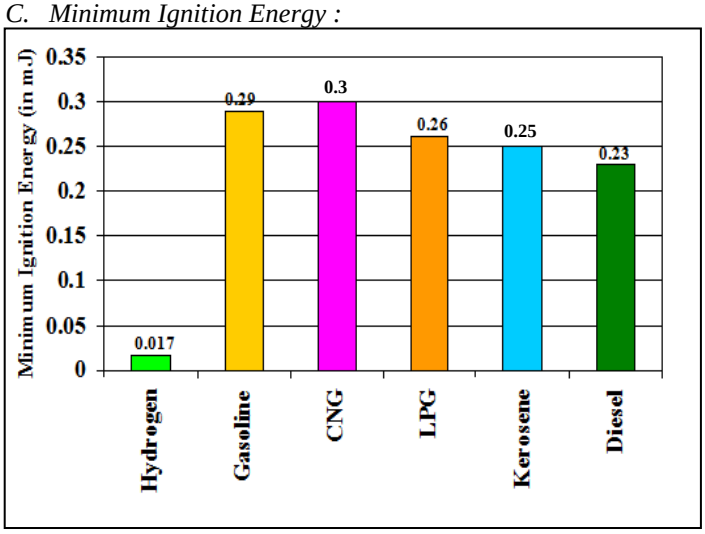

Fig. 4. Minimum Ignition Energy requirement of different fuels

As from Fig. 4, the hydrogen has least minimum ignition energy i.e. 0.017 mJ. Therefore, hydrogen can be ignited easily by giving very low energy.

E. Diffusivity:

Hydrogen has very high diffusivity. The diffusivity of hydrogen is considerably higher than the gasoline. Thus hydrogen favours uniform combustion, hence better efficiency. Also due to its higher diffusivity the possibility of fire hazards due to the leakage of gas are minimum as hydrogen gets dispersed in air quickly.

F. Flame Speed :

It is seen from Fig. 5 that hydrogen has high flame speed, around 2.83 m/s. Thus, engine running on hydrogen fuel has better efficiency than other fuels.

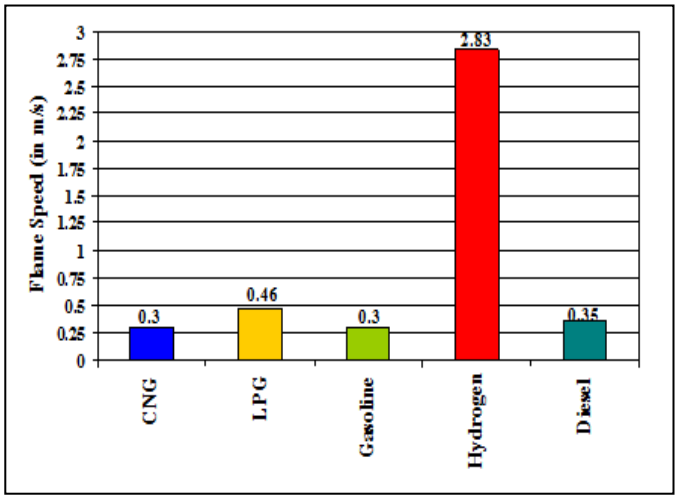

Fig. 5. Flame Speed of different fuels

G. Combustion Products:

When Petrol, Diesel, LPG, CNG etc. are combusted in engine there is emission of Carbon dioxide (CO_2) and other air pollutants like oxides of nitrogen, oxides of sulphur, carbon monoxide and particulate matter. This is because these fuels have carbon in their composition. When hydrogen is combusted, the product is water.

$$2H_2 + O_2 \longrightarrow 2H_2O$$

As from the above chemical equation, there is no emission of pollutant, hence hydrogen is a clean fuel.

IV. CONCLUSION

In today's time, transportation is one of the vital need so we cannot reduce it, we require a clean fuel in place of fossil fuels. One such fuel is hydrogen. Hydrogen has excellent combustive properties. The hydrogen has ability to take the place of fossil fuels, moreover it is far better than other fuels. The more important property is that there is no emission of carbon and other pollutants. Carbon dioxide is mainly responsible for the global warming and the increasing temperature supports the tropospheric ozone production, as there is no emission of these pollutants from the combustion of the hydrogen fuel, a healthy environment can be created.

V. FUTURE SCOPE

Hydrogen is produced through steam reforming[3] process but it is not a clean process. There are also clean methods for the production of hydrogen, such as solar hydrogen production[4], photoelectrochemical process of hydrogen production[5] in which the water is photoelectrochemically splitted into hydrogen gas.

Hydrogen has low energy to volume ratio but high energy to weight ratio. There are methods to reduce the storage and transportation problems of hydrogen such as metal hydride storage technique[6] and carbon adsorption technique[7] which are very much safer techniques of storing hydrogen. The amount of hydrogen stored in vessel filled with the metal hydride can be 2-3 times larger than that in the same vessel filled with the liquid hydrogen. These vessels could be used in vehicles instead of cylinders containing hydrogen gas at high pressure.

ACKNOWLEDGMENT

We would like to extend our gratitude first and foremost to Dr. Arvind Dhingra for his guidance and availing NCERT lab of Guru Nanak Dev Engineering College, Ludhiana, Punjab to carry out research.

REFERENCES

[1] "Ambient (outdoor) air pollution in cities database 2014". WHO. 2014. Retrieved 31 May 2015

[2] Dincer, I. "Technical, environmental and exergetic aspects of hydrogen energy systems". International Journal of hydrogen Energy, Vol. 27, 2002, 265-285

[3] J.R. Rostrup-Nielsen, "Catalytic Steam Reforming", in Catalysis, Science and Technology (J.R. Anderson and M. Boudart, eds.), 5, Springer, Berlin (1984) p. 1.

[4] Kazi Kawser Hussain, Taskin Jamal "Solar PV hydrogen fuel cell system for electrification of remote village in Bangladesh" ICAEE 2015

[5] Alben Cardnas, Cristina Guzman "Development of AC microgrid test bench with hydrogen fuel cell and renewable sources" APPEEC 2016

[6] L.K. Heung, "On-board hydrogen storage system using metal hydride", in T.O. Saetre (editor), Hydrogen Power: Theoretical and Engineering Solutions, 251-256, 1998

[7] G. Eklund, O. von Krusenstierna : Storage and Transportation of Merchant Hydrogen, in International Journal of Hydrogen Energy, Vol. 8, pp. 463-470, 1983

Cost-Benefit Analysis and Emission Reduction of Lighting Retrofits in an Academic Institution

Kuldeep Singh
Electrical Engineering Department,
Assistant Professor at Baba Banda Singh Bahadur
Engineering College, Fatehgarh Sahib, India

Simarpreet Singh
Electrical Engineering Department,
Assistant Professor at Baba Banda Singh Bahadur
Engineering College, Fatehgarh Sahib, India

Abstract **- This study projects electricity savings, cost benefit analysis and emission reduction of lighting retrofits in an academic institution. The cost-benefit is determined as a function of energy savings due to retrofit of more efficient lighting system. The energy savings were calculated based on 25, 50, 75 and 100% of potential retrofits of inefficient lighting in the academic institution. The data used was collected by conducting a survey and by recording the actual load and operating hours of the existing inefficient lighting system at different places in the institution. The study found that, this strategy save a significant amount of energy and money. The study also shows that there is a good potential for reducing carbon emissions by retrofitting the inefficient lighting with efficient lighting.**

I. INTRODUCTION

There has been growing concern about energy consumption and its environmental implications for the last decade. A lot of energy efficient measures are being taken day by day to save energy. Lighting system in any building consumes a substantial part of total electricity consumption. Electric lighting accounts for about 25% of total building energy used by Ghisi and Tinker, 2005. A lighting retrofit means to replace inefficient lighting with the efficient one. Electricity savings over time is significant enough to not only pay for the new lighting, but also produce return on investment. This can be done by either reducing the input wattage or reducing the hours of operation of the lighting to reduce energy consumption. A lot of studies on retrofitting inefficient lighting by reducing input wattage are conducted as presented by Stefano, 2000; Lee, 2000; Guan et al.,1997. This study is also proposed to reduce consumption of electricity by retrofitting of conventional electromagnetic ballasts used with T8 fluorescent tube lights with more efficient electronic ballasts in an academic institution. The electronic ballast can replace electromagnetic ballast without any modification. Fluorescent tube light uses an arc of electricity to create light. This current must be applied in very precise ways to the gases within the tube--normal household electrical current is too erratic and powerful for the fluorescent tube. So the fixture requires a control device known as the ballast, which limits the current and meters it out in cycles that the tube light needs to keep lit.In all fluorescent lighting systems, the ballast provides the proper voltage to start the lamp and then regulates the electric current flowing through the lamp to stabilize output. There are two types of ballasts, the conventional electromagnetic ballasts and the newer electronic ballasts. Electronic ballasts increase lamp-ballast efficacy, leading to increased energy efficiency and lower operating costs. Electronic ballasts are more efficient than magnetic ballasts in converting input power to the proper lamp power, and their operating of fluorescent lamps at higher frequencies reduces end losses, resulting in an overall lamp-ballast system efficacy increase of 15% to 20% as presented by Eley et al., 1993.

One of largest advantages of electronic ballast is the enormous energy savings it provides. This is achieved in two ways. The first is its amazingly low internal core loss, quite unlike old fashioned magnetic ballasts. And second is increased light output due to the excitation of the lamp phosphors with high frequency.The life of FTL with magnetic ballasts is only 5000 burning hours whereas the life with electronic ballast increases up to 20000 burning hours given by Cris Gribbin,2006. This study attempts to calculate potential electricity savings, emission reduction and cost benefit analysis of lighting retrofit and to make a small effort in curbing the global warming.

II. COLLECTED DATA

Sant Longowal Institute of Engineering and Technology is located in Longowal, district Sangrur, Punjab, India. The data used for this study is collected from the institution buildings and comprises of number of fixtures, operating hours per year and wattage of Fluorescent Tube Lights. The building blocks selected for the study are 10 hostels and 5 Instructional blocks, Administration Block, Health Centre, Student Activity Centre and Estate Office. Location details and number of fixtures are provided in Table 1-3. Generally, in SLIET one semester holds for 16 weeks and classes are conducted for 5 days a week excluding Saturdays and Sundays. So number of days of working for instructional blocks is calculated as 160 and operating hours is taken as 6 hours/day. For office buildings the number of days of operation is calculated as 220. This can be calculated as there are 365 days in a year and offices are occupied for 5 days in week so number of days remaining excluding Saturdays and Sundays are 261 and further 20 days are deducted due to holidays and further 20/21 days are taken as reserve for leaves by the individual office occupants. For hostels the number of days of operation is taken as 250 as normally a student resides in the hostel for 8 months (approx.) per year and hours of operation taken is 10 hours per day. The data is collected by conducting survey at all these locations. The uncertainty, sensitivity analyses, life cycle cost and payback period of lighting system can be found by McMahon et al., 2000.

Table.1.Input data for fixtures in Teaching Blocks

Location	No. of fixtures
Electrical and Instrumentation	800
Computer Science	300
Mech. and Workshops	1500
Food and chemical	600
Applied sciences	500
Total	3700

Table.2.Input data for fixtures in Hostels

Items	Details
No. of Hostels	10
Fixtures in Hostel	200
Total	2000

Table.3.Input data for fixtures in Offices

Items	Details
Administration Block	300
Health Centre	20
Estate Office	30
Student Activity Centre	100
Total	450

ABBREVIATIONS USED

AS	annual savings (Rupees)
BS	bill savings (Rupees)
CC	capital costs (Rupees)
CERs	certified emission reductions (tCO_2)
d	discount rate
DO	days of operation in a year
E	electronic ballast lighting system
EC	energy consumption (kWHr)
EC^E	energy consumption with electronic ballast (kWHr)
EC^M	energy consumption with electromagnetic ballast (kWHr)
EF	emission factor
ES	energy savings (kWHr)
GRC	gross return on capital (%)
LL	lamp life (burning hours)
M	electromagnetic ballast lighting system
n	number of years
NF	number of fixtures
NPV	net present value
NRC	net return on capital
OH	operating hours
PC	power consumption (kWHr)
PE	price of electricity (Rs/kWHr)
PF_1	power factor with lighting system M
PF_2	power factor with lighting system E
R	number of replacements
TS	total savings (Rupees)

III. METHODOLOGY

A survey is necessary to determine the potential of retrofit lighting, the operating hours of fluorescent tube lights with electromagnetic ballasts and load taken by one fixture. The data obtained from the survey presented in Tables 4-6 was used to calculate projected electricity savings, emission reductions and cost-benefit analysis of lighting retrofits.

Table.4.Load calculations with electromagnetic ballast for Table 1

Items	Details
Electrical load per fixture	45 W
Operating Hours per day	6
No. of days per year	160
Total fixtures taken	3700
Total electrical load	166.5 kW
Total units consumed/year (kWHr)	159840

Table.5.Load calculations with electromagnetic ballast for Table 2

Items	Details
Electrical load per fixture	45 W
Operating Hours per day	10
No. of days per year	250
Total fixtures taken	2000
Total electrical load	90 kW
Total energy consumed/year (kWHr)	225000

Table.6.Load calculations with electromagnetic ballast for Table 3

Items	Details
Electrical load per fixture	45 W
Operating Hours per days	6
No. of days per year	220
Total number of fixtures	450
Total electrical load	20.25
Total units consumed/year (kWHr)	26730

3.1 Number of Retrofits

Number of retrofits is determined by conducting a survey and it was found that in SLIET there is a practice of using 1X36 W, T8 fluorescent tube light fixture with electromagnetic ballast. So total numbers of fixtures were counted and there is a potential of 6150 lighting retrofits.

3.2 Energy Consumption

Energy consumed by the existing system is calculated by the multiplication of total number of retrofits in each block, power consumption, number of days of operation per year and operating hours of the lighting per day. This can be represented by the following equation. All the calculations are done in according to Mahlia et al., 2004.

$$EC = NF \times PC \times OH \times DO \quad \text{..... (1)}$$

3.3 Energy Savings

Energy savings from retrofitting is the difference between energy consumption of inefficient and efficient lighting. This is given in table 7. This can be calculated using the following equation:

$$ES = EC^M - EC^E \quad \text{..... (2)}$$

Table.7.Predicted electricity consumption and savings

Location	EC^M(kWHr/year)	EC^E(kWHr/year)	Potential of electricity savings (kWHr/year)			
			25% retrofits	50% retrofits	75% retrofits	100% retrofits
Teaching Blocks	159840	127872	7992	15984	23976	31968
Offices	26730	21384	1336.5	2673	4009.5	5346
Hostel	225000	180000	11250	22500	33750	45000
Total	411570	329256	20578.5	41157	61735.5	82314

3.4 Emission reduction

The environmental impact from retrofitting is potential reduction of greenhouse gases which pollutes the environment or other element that caused negative impact on the environment. Carbon emissions can be reduced to some extent by retrofitting the inefficient lighting along with savings in energy. The potential CERs that can be generated from these measures are calculated by taking emission factor of 0.7240 kg of CO_2/kWHr given by the $CO_{2\ Baseline}$ Database for the Indian Power Sector, 2007. The emission reduction is a function of energy savings. The CERs are calculated by the following equation:

$$CERs = \frac{ES \times EF}{1000} \quad \ldots\ldots\ldots\ldots\ldots\ldots\ldots (3)$$

3.5 Gross return on capital

Gross return on capital is a function of total savings from the project and capital costs required for the implementation of the project. It expresses the "annual return" from the project as a percentage of capital cost. This can be calculated from the following equation:

$$GRC = (\frac{TS}{CC}) \times 100 \quad \ldots\ldots\ldots\ldots\ldots\ldots\ldots (4)$$

3.6 Net return on capital

Net return on capital is also a function of total savings from the project and capital cost required for the implementation of the project. It is expressed with the help of following equation:

$$NRC = (\frac{TS - CC}{CC}) \times 100 \quad \ldots\ldots\ldots\ldots\ldots\ldots\ldots (5)$$

3.7 Bill savings

The bill savings of lighting retrofit is a function of energy savings and the average price of electricity. The potential bill savings by lighting retrofit is shown in Table 8 and is calculated by the following equation:

5000 hours whereas with electronic ballast the life increases up to 20000 hours. So, number of replacements will decrease and running cost will also decrease with suggested replacements. The details of number of replacements and running costs are shown in Table 9. Number of replacements can be calculated with the help of following equation:

$$BS = ES \times PE \quad \ldots\ldots\ldots\ldots\ldots\ldots\ldots (6)$$

Table.8.Bill savings and simple payback period for 100% retrofit

Items	Details
Total electricity savings per year (kWHr)	82314
Price of one electricity unit (Rs)	5
Total electricity bill savings (Rs)	411570
Cost of one Electronic Ballast (Rs)	200
Cost of one 36 W TFL 3250 lumens (Rs)	65
Replacement and labor charges per fixture (Rs)	45
Total replacement charges (Rs)	310
Total investment for replacing 6150 ballasts (Rs)	1906500
Simple payback period (years)	4.6

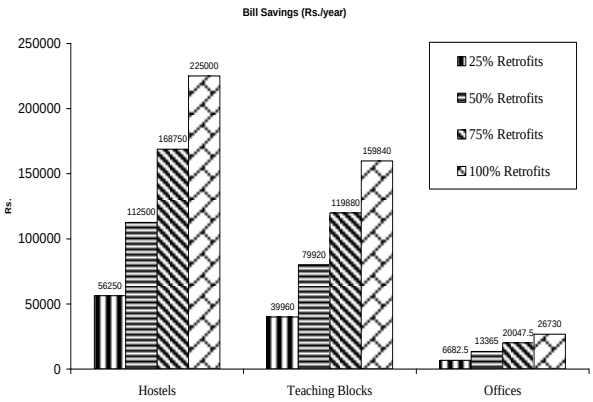

Fig.1. Annual Bill Savings due to lighting retrofit

3.8 Replacements

The replacement of the fixture is a function of rated life of the lamp and actual operating hours of the lamp. The burning hours of FTL with electromagnetic ballast is

$$R = \frac{OH \times DO}{LL \times NF} \quad \ldots\ldots\ldots\ldots\ldots\ldots\ldots (7)$$

Table.9.Comparison of running cost of system M and E

Items	Details	
	M	E
Annual electricity costs (Rs)	21222000	1527840
Lamp life (Burning hours)	5000	20000
Total replacements per year	1829.2	457.3
Replacement cost per FTL	32	65
Total replacement cost/year (Rs)	58534.4	29724.5
Total running cost per year (Rs)	2116384	1676005

Table.10. Predicted emission reduction (tCO_2)

Retrofits	Tons of Carbon Dioxide/year
25%	14.89
50%	29.79
75%	44.69
100%	59.59

3.8 Distribution losses

In an electrical system distribution losses are of great importance towards energy loss estimations. One factor which influences distribution losses is power factor of electrical system. A lot of emphasis is given to improve the power factor of the system to reduce distribution losses. The power factor of electromagnetic ballast is 0.5 only whereas power factor of electronic ballast is as high as 0.95. Reduction in the distribution loss % in kWh when tail end power factor is raised from PF_1 to a new power factor PF_2 will be as given by Mahlia et al., 2004., as give below

$$\left[1-\left(\frac{PF_1}{PF_2}\right)^2\right]\times 100 \quad \ldots\ldots\ldots\ldots\ldots\ldots\ldots\ldots\ldots\ldots (8)$$

3.9 Net present value

Net present value depends on the discount rate. This is calculated for 8%, 9% and 10% discount rate for 10 years. This can be calculated from the following equation:

$$NPV = \frac{AS\times[(1+d)^n-1]}{[d\times(1+d)^n]} \quad \ldots\ldots\ldots\ldots\ldots\ldots\ldots (9)$$

4 RESULTS AND DISCUSSIONS

To calculate energy consumption and potential energy savings by retrofit, it is necessary to have daily average operating hour of lighting in the institution. Based on survey data collected in different locations in the institute the energy consumption and potential energy savings can be calculated. For this study, the calculation is done for 25, 50, 75 and 100% of retrofits. The calculation result is tabulated in Table 7.

It shows that electricity savings of 82314 KWh annually can be achieved by replacing electromagnetic ballasts with energy efficient electronic ballasts in the institution. Table 8 shows the potential bill savings of Rs 411570 per year and the pay-back period is only 4.6 years which is a short term pay-back period as it is less than 5 years. The power factor of the electromagnetic ballasts is only 0.5 whereas the power factor of electronic ballast is 0.95. With retrofitting of electromagnetic ballast by electronic ballasts the power factor of the system will increase which has additional advantage of reduction in distribution losses as if the overall power factor of the system is increased from 0.5 to 0.95 then distribution losses will reduce by 72% which will help the power generating company. Due to reduction of overall load the conductor heating will reduce and thus heat losses will also be lower. As a result, maintenance charges will reduce. With the installation of 36 W T8 energy efficient lamps with 3250 lumens there will be 33% increase in the luminance as compared to the existing lamp of 2450 lumens. Based on potential energy savings per year, the emission reduction can be calculated using Eq. (3). The result is tabulated in Table 10. The predicted annual emission reductions from teaching blocks and hostels is 59.59 tCO_2 with 100% retrofits. The emission reductions with 25, 50 and 75% retrofits are also shown in the Table 10. Net present values with 25%, 50%, 75% and 100% retrofits are also calculated with 8%, 9% and 10% discount rates separately for hostels, offices and teaching blocks which are presented by Figs. 2-5. Figures shows that for 25% retrofits the values are almost same with all the discount rates but with 100% retrofits there is a considerable difference in the values with different discount rates.

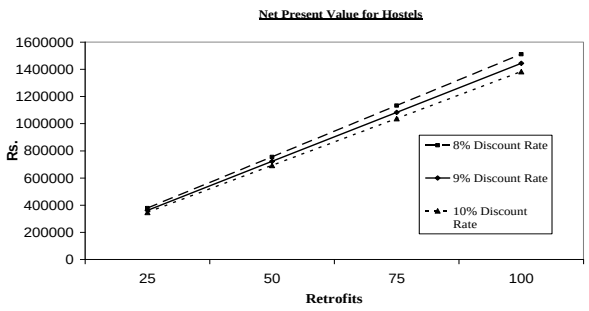

Fig. 2 Net present value for Hostels

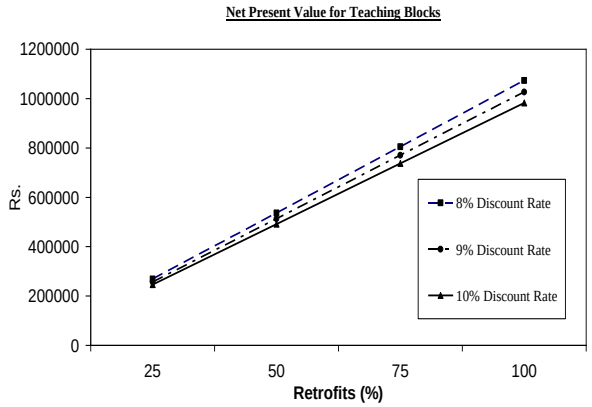

Fig. 3 Net present value for teaching blocks

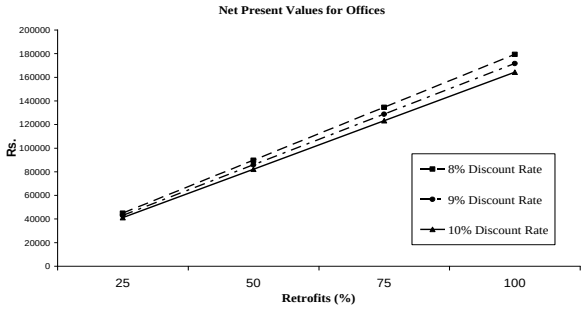

Fig. 4 Net preent value for offices

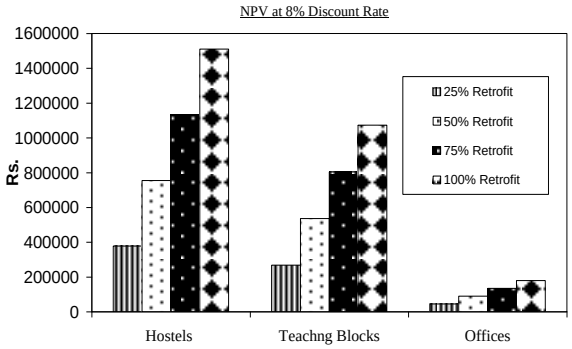

Fig. 5 NPV at 8% discount rate

Gross return on capital and net return on capital are calculated and presented by Fig. 6. It is found that the gross return on investment by retrofitting the lighting in hostels and offices is high which is 362.9 and 191.6 respectively, whereas by retrofitting the lights in teaching blocks the return is not so attractive and is 139.4. Similar is the trend for net return on capital value.

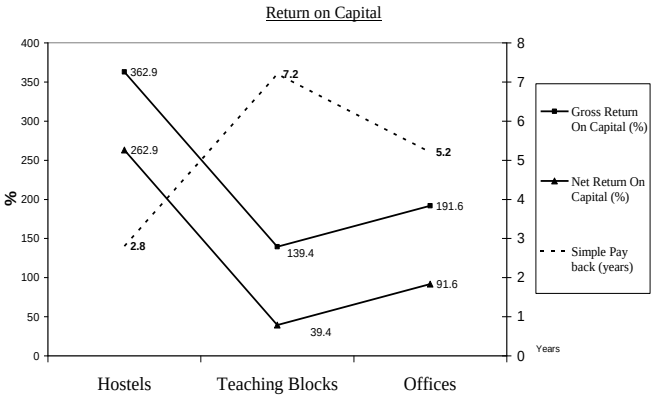

Fig. 6 Return on capital and simple payback period

IV. CONCLUSION

The calculation results show that lighting retrofits have significant impact on the institution electricity consumption. The recommendations based on findings can be considered for implementation in hostels and offices as considerable amount of energy can be saved and the cost benefit analysis shows that these two areas have high return rate. Furthermore, it will result in reduction in emission from power consumed by the institution. It can be concluded that the institution should encourage use of energy efficient lighting instead of inefficient lighting in the institution. A lot of energy can be saved and emission reductions can be achieved if such kinds of measures are adopted by other institutes also, which have hostel facilities.

REFERENCES

[1] Ghisi E, Tinker JA. An ideal window area concept for energy efficientintegration of daylight and artificial light in buildings. Build Environ 2005; 40(1):51–61.

[2] Stefano J.D., Energy efficiency and the environment: the for energy efficient lighting to save energy and reduce carbon dioxide emissions at Melbourne University, Australia, Energy–The International Journal 25 (2000) 823-839.

[3] Lee A.H.W., Verification of electrical energy savings for lighting retrofits using short- and long-term monitoring, Energy Conservation and Management 41 (2000) 1999-2008.

[4] Guan F.M. et al.,1997, Energy efficient lighting in China, Energy Policy 25 (1997) 77-83..

[5] Eley, C. et al., 1993, Advanced Lighting Guidelines: Final Report. Prepared for the U.S. Department of Energy, California Energy Commission, and Electric Power Research Institute, 1993.

[6] Cris Gribbin, National Light Product Information Program, Lighting Answers: T8 Fluorescent life, Volume 9, Issue 1, PP7, June 2006.

[7] McMahon J. et al., 2000, Uncertainty and Sensitive Analysis of Ballast Life-cycle Cost and Payback Period, Lawrence Berkely Laboratory, University of California, Berkeley, 2000.

[8] Mahlia T.M.I., et al., 2004, Cost-benefit analysis and emission reduction of lighting retrofits in residential sector, August 2004.

[9] The $CO_{2\ Baseline}$ Database for the Indian Power Sector, Ministry of Power, Central Electricity Authority (CEA), Version 2, 2007.

Investigation on the Chemical Mist Deposited of Polyethylene Glycol (Peg-400) Assisted Cuo Thin Films

Iqbal Singh
PG Department of Physics,
Khalsa College Amritsar, India

Bikramjeet Kaur
Department of Mathematics,
Thapar University, Patiala, India

***Abstract*—CuO is technologically an important material and in the present study it has been synthesized by forming mist from an aqueous solution of cupric nitrate with PEG-400 using ultrasonic nebulizer sprayed onto glass substrates kept at elevated substrate temperature. The X-ray diffraction study shows the formation of CuO as dominant phase in film samples. The scanning electron microscope images reveal dispersing nature of surfactant that helps to improve porosity in the material. The film sample deposited at substrate temperature of 400℃ comparatively higher response among all samples. The maximum sensitivity was found to be about 6.83% for light impulse of 27800 lux of 40 seconds duration. The sample also shows a repeatable behaviour in response when exposed to a light impulse of 2 seconds. The response of the films for light is almost follows a linear behaviour with time.**

Keywords*— *Photosensor, mist deposition, CuO

I. INTRODUCTION

A photosensor is a device that detects the presence of light energy. Most of the photo sensing devices consist of semiconductor material have ability to possess called photoconductivity in which the electrical conductance of the material varies depending on the intensity of radiation. The most common types of photosensor are the photodiode, the bipolar phototransistor, and the photosensitive field-effect transistor. Photosensors are used in a great variety of electronic devices, circuits, and systems, including fiber optics, optical scanners, wireless LAN, automatic lighting controls, machine vision systems, electric eyes, optical disk drives, optical memory chips, remote control devices.

Thus to synthesize photoactive metal oxide nanoparticles has been attracted considerable attention in last decade. There are various fields where these materials find important applications such as catalyst [1], window material [2], photosensor [3] and gas sensor [4, 5]. CuO being a p-type semiconductor material with a band gap of 1.25-1.51 eV having wide range of applications which makes it promising material in research. This material in the form of nanoribbons [5], nanowires [6, 7], mesoporous dandelion structure [8], urchin-sheet like structure [9], hollow microsphere [10] and nanoneedles [11] etc. has attracted considerable attention due to utilization in diverse technological areas. In the form of a film, it is mainly used in devices like solar cell, window material for solar cell [2], photosensor[7], catalytic sensor [12] and gas sensor [13].

Variety of synthesis techniques like chemical [14], polymer precursor [15], and hydrothermal [16] etc. have been used widely for the preparation of nanocrystalline CuO powder. However, despite the excellent progress in afore mentioned techniques, there is one or more drawback sassociated in their procedure. As no sophisticated instrument is required in chemical precipitation and sol–gel methods and simple processing route, so these methodologies drawn considerable attention [17, 18].High quality CuO films have been deposited by various techniques such as thermal evaporation [19], thermal oxidation [20], spray pyrolysis [21, 22], sol-gel dip coating [23, 24]etc. Among these the spray pyrolysis is preferred over the others routes due to several advantages such as cost effective, easily controllable parameters and most important no vacuum is required [21, 22, 25-28].

Surfactant molecules are widely used for controlling size, shape of grains and acts as polymer which plays an important role in synthesizing self assembled nano as well as micro structures. The surfactant molecules absorb on specific crystal planes and initiate an anisotropic grain growth. PEG as non-ionic surfactant has been widely used in fabricating nanostructured materials by different routes in interesting morphologies with improved properties [29-35]. In its molecules the hydrophilic oxygen atoms are easily linked with the free hydroxyl ions on the surface of colloid particles by hydrogen bonds. The properties of material can be tailored by selecting different types of PEG series. Reference [35] has successfully deposited hexagonal ferrites using PEG 2000 by adopting self propagating combustion technique. Reference [34] have deposit PEG assisted grown ZnO thin films by dip coating method. However as far as the data available, PEG has been widely used in the synthesis of various materials in the powder form but there is no report available related to the deposition of PEG assisted CuO films by using ultrasonic spray pyrolysis technique.

In this paper, the PEG assisted CuO thin films have been synthesized by ultrasonic spray pyrolysis techniques respectively. The samples are systematically characterized and obtained film sample has been tested for white light sensing properties.

II. EXPERIMENTAL

A. Material

All the chemicals (LobaChemie Mumbai) of analytical reagent grade are used as precursors. The solutions are prepared in doubly distilled water. Corning 7059 borosilicate glass slides (2x4 cm^2) are used as substrates and cleaned by standard procedure prior to use.

B. Synthesis process (Ultrasonic spray pyrolysis technique)

The precursor solution for aerosol generation is prepared by dissolving the required amount of $Cu(NO_3)_2{\cdot}3H_2O$ in water to form0.2 M, 100 mL solution. To it10 mL of 0.5M PEG-400 solution is added drop wise with vigorous stirring. The preparative parameters of the ultrasonic spray setup such as nozzle to substrate distance, solution concentration, solution spray rate etc., are optimized to obtain, pin hole free, adherent films and are kept constant in all experiments. The substrate temperature is varied from 300 to 400˚C, in steps of 50˚C using electronic temperature controller (Model DTC303, Selec make) with accuracy of ± 3 ˚C. The substrates are heated to required temperature by a specially designed electrical heater, and the temperature is measured using K type (chromel–alumel) thermocouple. The distance between the nozzle and the substrate after optimization is maintained at 25 cm. The spray rate is fixed at 1 mL per minute. The aerosol is generated using ultrasonic nebulizer (Omron NE-U17), and subsequently passed through glass nozzle using air as carrier gas onto preheated glass substrate. The detailed procedure of film deposition has been already discussed in detail previously [39]. The spray deposited films are named as per terminology indicated in Table I.

TABLE I. Sample codes for the PEG doped CuO thin films

Material powder/film	Substrate temperature	Code
CuO thin film (0.5M PEG-400)	300 ± 3 ˚C	F_1
CuO thin film (0.5M PEG-400)	350 ± 3 ˚C	F_2
CuO thin film (0.5M PEG-400)	400 ± 3 ˚C	F_3

C. Structural analysis

The phase identification of the powder and thin film samples is analyzed by X-ray diffraction (XRD) pattern, taken using X'PertPanlytical diffractometer with Cu Kα radiation (λ = 1.5405 Å , 30mA , 40 kV) in 2θ range from 30-80˚.

Texture coefficient for the thin films is calculated using the equation given as [38, 39]

$$T(hkl)=\frac{I(hkl)}{I_o(hkl)}\left[\frac{1}{n}\sum_{i=1}^{n}\frac{I(hkl)}{I_o(hkl)}\right]^{-1} \quad (1)$$

where I_0 represents the standard intensity, I is the observed intensity of the (hkl) plane and n is the reflection number.

The average crystallite size (D) is obtained from the most prominent peak using Scherrer's formula [36]

$$D=\frac{0.9\lambda}{\beta\cos\theta} \quad (2)$$

where β is the FWHM of the powder, θ the Bragg angle, λ the wavelength of X-ray used.

Lattice parameters ($a \neq b \neq c$, $\alpha = \gamma = 90^\circ \neq \beta$ for monoclinic structure) and the volume of unit cell for the CuO films are calculated using the formulas given below

$$\frac{1}{d^2}=\frac{1}{\sin^2\beta}\left(\frac{h^2}{a^2}+\frac{k^2\sin^2\beta}{b^2}+\frac{l^2}{c^2}-\frac{2hl\cos\beta}{ac}\right) \quad (3)$$

$$V=abc\sin\beta \quad (4)$$

To study the surface topography films, field emission scanning electron micrographs (FESEM) are taken on a JEOL JSM-6700F with a beam voltage of 20 kV.

The film samples have been tested for their response toward white light of different flux by measuring conductance Keysight34410A multimeter. Sensitivity (S %) is defined as the percentage change in conductance when CuO film was exposed to light.

$$S(\%)=\frac{C_l-C_d}{C_d}\times 100 \quad (5)$$

where C_l and C_d are the CuO film conductances measured in light and dark respectively.

III. RESULTS AND DISCUSSION

XRD diffractograms of USP deposited films shown in Fig. 1indicates the film F_1 deposited at substrate temperature of 300 ˚C is found to be amorphous whereas rise in substrate temperature to 350 and 400 ˚C shows characteristic CuO peaks. The strong and sharp diffraction peaks corresponding to CuO phase of(002) and (111)atomic planes appeared at 2θ value of 35.5˚ and 38.7˚ respectively. No peak corresponding to Cu_2O phase has been noticed in the diffraction patterns .It has been noticed that addition of PEG strongly affects the crystallinity of CuO films. Findings from this work suggested that the crystalline CuO films with PEG are successfully deposited at substrate temperature of 350 ˚C. Further characterization of films results for the F_2 and F_3 films are calculated and co-related.

The values of texture coefficient for the F_2 and F_3 are recorded in Table 2. Its value greater than one for the peak located at 35.5˚ and 38.7˚ reveals the preferential orientation of the film. Texture coefficient value for the (002) plane is significantly higher in comparison to (111) plane. This result reveals that CuO particles are anisotropic in shape (non-spherical) [31] and deposited grains tend to possess facet like morphology as directed by the templating nature of surfactant.

TABLE II. Values of the texture coefficient T(*hkl*), lattice constant, *a* (Å), *b* (Å), *c* (Å), *β* (Degree), cell volume (Å^3), crystallite size (*D*) from XRD, particle size from FESEM, F_2 and F_3 samples

Property/ Sample code	**F_2**	**F_3**
T(*hkl*), (002):(111)	2.072:1.928	2.191:1.809
a (Å)	4.699	4.669
b (Å)	3.427	3.420
c (Å)	5.121	5.090
β (Degree)	99.639	97.709
cell volume (Å^3)	81.088	81.062
average Crystallite size (nm) XRD	38	43
SEM (average particle size, nm)	400	160

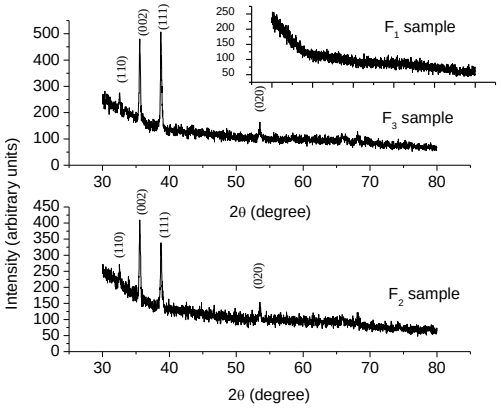

Fig. 1 XRD pattern of the spray pyrolysis deposited CuO thin films of F_1, F_2 and F_3samples

Using Scherrer's formula, average crystallite size of samples has been calculated (Table II) and in case of thin film F_3sample it is 43 nm. The lattice parameters of samples (F_2 and F_3) have been calculated (Table II) and found to be in good agreement with ICDD data card 41-254. The variation in values of lattice parameters and unit cell volume of samples indicates the evidence of strain. The values of lattice parameters for the samples have been found to be lower in magnitude as compared to one those reported for bulk CuO in literature. This implies that lattice structure in spray pyrolysis deposited CuO films having more number of defects.

Fig 2 shows FESEM images of spray deposited F_2 and F_3 films which exhibit uniform, compact, crack free and nano-sized particle agglomerates. Randomly distributed trapezium shaped grains of size 400 nm have been observed in F_2 film sample. F_3 film sample shows comparatively smooth morphology and possess more number of pore channels and possess an interesting morphology on the 100 µm scale, in which spherically shaped particles aggregated to form coin like structures. A numbers of coins appeared on different locations film on the micrograph. The transformation of facets like morphology of particles to spherical might be due to templating nature of the non-ionic, polymer type PEG surfactant used in the synthesis of several porous materials [35]. PEG assisted spray deposited CuO samples shows relatively higher specific surface area, which promises its potential applications.

PEG-400 is a nonionic surfactant and able to acts as a dispersing agent in the reaction. It is one of the most flexible water soluble polymer which has hydrophilic and hydrophobic radicals on the long carbon chains. In aqueous medium its flexible ether linkage makes it less sterically hindered and causing more oxygen atom on polymer chain to combine with the metal ion. The dispersing nature of the surfactant keep the sol particles separated due to long chain of molecules. The surfactant addition causes a reduction in surface tension and slows down growth rate of sol particles. Reference [30] have discussed same concept of the PEG-2000 molecules on the synthesis of ZnO particles by using zinc nitrate and citric acid. Reference [31] observed the similar effect of PEG-600 along with cetylytrimethylammonium bromide (CTAB) in the hydrothermal synthesis of hydroxyapatite.

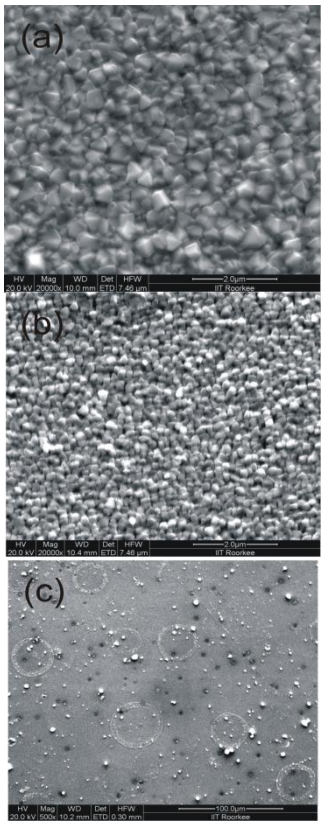

Fig. 2 FESEM images of spray pyrolysis deposited CuO thin films (a) F_2 and (b, c) F_3samples

The PEG assisted CuO thin film has been exposed toward white light from LED source at room temperature (300 K). The time resolved measurements were performed on the F_2film sample when exposed to light of 3420 lux for 2 seconds repeatedly and change in conductance of the film has been observed. The response curve as shown in Fig. 3 shows that F_2 sample after light exposure did not recover its dark conductance and sensitivity was found to be 0.37%. The F_3 sample when exposed to light of 3420 lux it regains its conductance in dark and comparatively higher sensitivity of 0.47 %. Thus F_3 sample explored for photosensing properties for light of 12960 and 27800 lux. The obtained response curves for F_3 samples have been shown in Fig. 4. The sensitivity has been calculated and the maximum sensitivity has been found to be1.62% for light of intensity of 27800 lux.

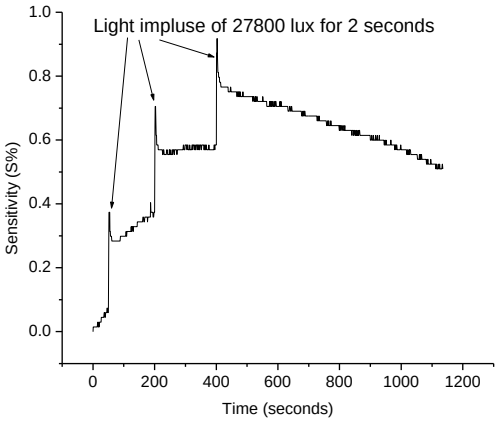

Fig. 4 Response of spray pyrolysis deposited CuO thin film $F_2$for light impulse of 2 seconds for 3420 lux

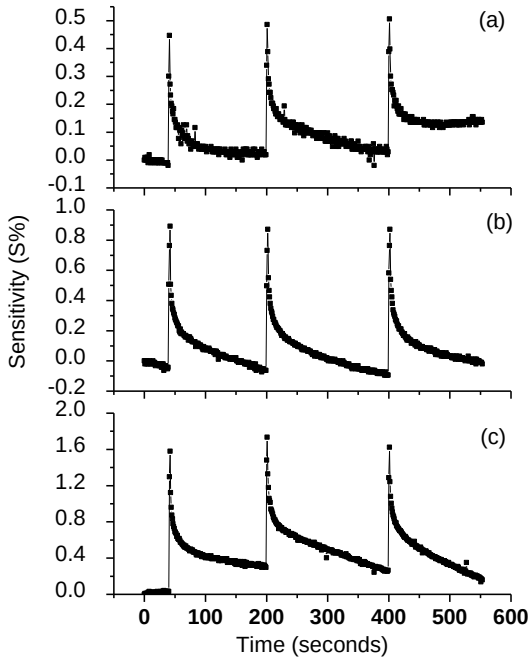

Fig. 4 Response of spray pyrolysis deposited CuO thin film $F_3$for light impulse of 2 seconds for (a) 3420, (b) 12960 and (c) 24900 lux

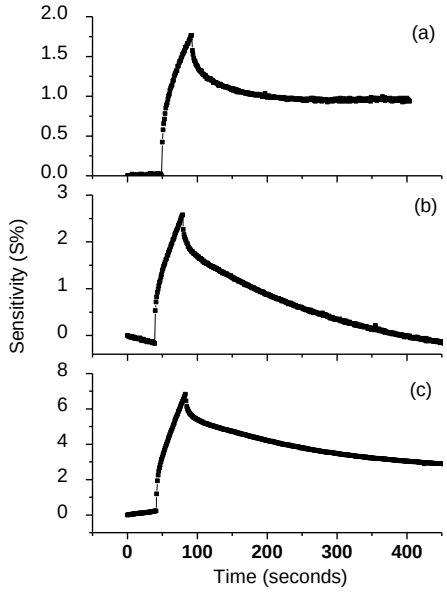

Fig. 4 Response of spray pyrolysis deposited CuO thin film $F_3$for light impulse of 40 seconds for 27900 lux

The F_3film sample has been tested for light impulse of time 40 seconds and obtained response curves are shown in Fig. 5. The calculated sensitivity values for samples F_2 and F_3 for light impulse of 40 seconds is shown in Table III.

The film sample shows almost linear response with light intensity and the corresponding equations for the change in conductance of film in light (C_l) and dark (C_d) with time are tabulated in table 3. The room temperature appreciable light response in case of surfactant assisted thin film sensor may be attributed to the large specific surface area as depicted by FESEM.

TABLE III. Response (S) of samples for light impulse of 40 seconds having different intensity and change in conductance in the light and in dark for F_3 sample

Property	**Light intensity (lux)**	**F_2**	**F_3**
Response (%) for light impulse of 40 seconds	3420	0.80	1.76 $C_l = 0.0167t - 0.689$ (R^2=0.97) $C_d = -0.002t + 0.7241$ (R^2=0.96)
	12960	1.99	2.58 $C_l = 0.0438t - 1.973$ (R^2=0.99) $C_d = -0.0012t + 1.86$ (R^2=0.92)
	27800	2.27	6.83 $C_l = 0.0519t - 2.42$ (R^2=0.99) $C_d = -0.002t + 2.14$ (R^2=0.94)

C_l and C_d correspond to the conductance of the film during light exposure and in dark respectively.

IV. CONCLUSIONS

NanocrystallinePEG-400 doped CuO mist deposited thin films are synthesized by using ultrasonic spray pyrolysis techniques. The average crystallite size has been found to be 43 nm in thin film samples. The lower value of the lattice constants as compared to standard data indicates that the CuO nanocrystallites are subjected to considerable defects in thin film. The defects provide the more active favourable sites for the light capturing. The facets like grains were uniformly distributed on the entire surface of substrate in case of thin film. As a light sensor PEG doped CuO thin films show an appreciable sensitivity of 6.83% at room temperature.

ACKNOWLEDGEMENT

Authors wish to thank UGC for providing financial support in the form of Minor research project, Director IIT Roorkee, STIC, Kochi and RSIC, Panjab University, Chandigarh for providing FESEM, EDAX and XRD facilities. We also gratefully acknowledge Mr. Gurpreet Singh, for his kind assistance in the electrical characterization of the samples.

REFERENCES

[1] S. M. El-Sheikh, F. A. Harraz, K. S. Abdel-Halim, Catalytic performance of nanostructured iron oxides synthesized by thermal decomposition techniqueJ. Alloys Compds.487(1-2) (2009) 716-723

[2] M. Abdel Rafea, N. Roushdy, Determination of the optical band gap for amorphous and nanocrystalline copper oxide thin films prepared by Silar technique. J. Appl. Phys. D 42 (2009) 015413

[3] Q. Kaung, C. S. Lao, Z. Li, Y. Z. Liu, Z. X. Xie, L. S. Zheng, Z. L. Wong, Enhancing the Photon- and Gas-Sensing Properties of a Single SnO_2 Nanowire Based Nanodevice by Nanoparticle Surface FunctionalizationJ. Phys. Chem. C 112 (2008) 11539-11544

[4] J. Zhang, J. Liu, Q. Peng, X. Wang, Y. Li, Nearly monodisperse Cu_2O and CuO nanospheres: Preparation and applications for sensitive gas sensors. Chem. Mater. 18 (2006) 867-871

[5] X. Gou, G. Wang, J. Yang, J. Park, D. Wexler, Chemical synthesis, characterization and gas sensing performance of copper oxide nanoribbons J. Mater. Chem. 18 (2008) 965-969

[6] N. D. Hoa, N. V. Quy, M. A. Taun, N. V. Hieu, Facile synthesis of P-type semiconducting cupric oxide Nanowires and their gas sensing properties Physica E 42(2) (2009) 146-149

[7] J. H. Benjamin, L. Ganhua, C. Junhong, Direct oxidation growth of CuO nanowires from copper containing substrates. J. Nanomater. (2008)830474 91-7

[8] S. Manna, K. Das, S. K. De, Template free synthesis of mesoporous CuO dandelion structures for optoelectronic applications Appl. Mater. Interface 2(5) (2010) 1536-1543

[9] M. Vaseem, A. Umar, S. H. Kim, A. Al-Hajry, Y. B. Hahn, Growth and structural properties of CuO urchin like and sheet like structures prepared by simple solution process Mater. Lett. 62 (2008) 1659-1662

[10] S. Wang, H. Xu, L. Qian, X. Jia, J. Wang, Y. Liu, W. Tang, J. CTAB-assisted synthesis and photocatalytic property of CuO hollow microspheres. Solid State Chem. 182 (2009) 1088-1093

[11] Y. Liu, L. Liao, J. Li, C. Pan, From copper to nanocrystalline CuO nanoneedle array: synthesis, growth mechanism and properties J. Phys. Chem. 111 (2007) 5050-5056

[12] F. Teng, W. Yao, Y. Zheng, Y. Ma, Y. Teng, T. Xu, S. Liang, Y. Zhu, Synthesis of flower like CuO nanostructures as a sensitive sensor for catalyst Sens. Actuat. B 134 (2008) 761-768

[13] Y. Li, J. Liang, Z. Tao, CuO particles and plates: synthesis and gas sensor applications J. Chen, Mater. Research Bull. 43 (2008) 2380-2385

[14] D. Li, Y. H. Leung, A. B. Djurisic, Z. T. Liu, M. H. Xie, J. Gao, W. K. Chan, J. Cryst. Growth 282 (2005)105-111

[15] A. I. Fernandez, A. Calleja, J. M. Chimenos, M. A. Fernandez, X. G. Capdevila, M. Serarra, H. Xuriguera, F. Espiell, Preparation of ultrafine CuO: Comparison of polymer gel methods and conventional precipitation process J. Sol-Gel Sci. Techn.36(2005)11-17

[16] Y. Zhang, S. Wang, Y. Qian, Z. Zhang, Complexing-reagent assisted synthesis of hollow CuO microspheresSolid State Sci.8 (2006) 462-466

[17] L. C. Pathak, T. B. Singh, S. Das, A. K. Verma, P. Ramachandrarao, Effect of pH on the combustion synthesis of nano-crystalline alumina powder Mater. Lett. 57(2) (2002)380-385

[18] J. Zhou, Y. Wang, F. Zhao, Y. Wang, Y. Zhang, L. Yang, Photoluminescence of ZnO nanoparticles prepared by a novel gel-template combustion processJ. Lumin.119(2006) 248-252

[19] G. Papadimitropoulos, N. Vourdas, V. E.Vamvaskas, D. Dava Zoglov, Optical and structural properties of copper oxide thin films grown by oxidation of metal layers,Thin Solid Films515 (2006) 2428-2432

[20] A. H. Jayatissa, K. Guo, A. C. Jayasuriya, Fabrication of cuprous and cupric oxide thin films by heat treatment Appl. Surf. Sci. 255 (20090 9474-9476

[21] J. Morales, L. Sanchez, F. Martin, J. R. Ramos-Barrado, M. Sanchenz, Nanostructured CuO thin film electrodes prepared by spray pyrolysis: a simple method for enhancing the electrochemical performance of CuO in lithium cellsElectrochemicaActa,49 (2004) 4589-4597

[22] S. Kose, F. Atay, V. Bilgin, I. Akyuz, Some physical properties of copper oxide films: the effect of substrate temperature Mater. Chem. Phys. 111 (2008) 351-358.

[23] S. C. Ray, Preparation of copper oxide thin film by the sol–gel-like dip technique and study of their structural and optical propertiesSolar Energy Mater. Solar Cells 68 (2001) 307-312

[24] L. Armelao, D. Barreca, M. Bertapelle, G. Bottaro, C. Sada, E. Tondello A sol–gel approach to nanophasic copper oxide thin filmsThin Solid Films 442 (2003) 48-52

[25] J. H. Lee, B. W. Yeo, B. O. Park, Effects of the annealing treatment on electrical and optical properties of ZnO transparent conduction films by ultrasonic spraying pyrolysisThin Solid Films 457 (2004) 333-337

[26] C. Luyo, I. Fabregas, L. Reyes, J. L. Solis, J. Rodriguez, W. Estrada, R. J. Candal, SnO_2 thin-films prepared by a spray–gel pyrolysis: Influence of sol properties on film morphologiesThin Solid Films 516 (2007)25-33

[27] V. R. Shinde, S. B. Mahadik, T. P. Gujar, C. D. Lokhande, Supercapacitive cobalt oxide (Co_3O_4) thin films by spray pyrolysis Appl. Surf. Sci. 252 (2006) 7487-7492

[28] R. K. Kawar, P. S. Chigare, P. S. Patil, Substrate temperature dependent structural, optical and electrical properties of spray deposited iridium oxide thin filmsAppl. Surf. Sci. 206 (2003) 90-101

[29] X. L. Gou, F. Y. Cheng, Y. H. Shi, L. Zhang, S. J. Peng, J. Chen, P. W. Shen, Shape-Controlled Synthesis of Ternary Chalcogenide $ZnIn_2S_4$ and $CuIn(S,Se)_2$Nano-/Microstructures via Facile Solution RouteJ. Am. Chem. Soc. 128 (2006) 7222-7229

[30] Y. L. Zhang, Y. Yang, J. H. Zhao, R. Q. Tan, P. Cui, W. J. Song, Preparation of ZnO nanoparticles by a surfactant-assisted complex sol–gel method using zinc nitrateJ. Sol-Gel Sci. Techno. 51 (2009) 198-203

[31] M. Salarian, M. Solati-Hashjin, S. S. Shafiei, R. Salarian, Z. A. Nemati, Template-directed hydrothermal synthesis of dandelion-like hydroxyapatite in the presence of cetyltrimethylammonium bromide and polyethylene glycol, Ceram. Int. 35 (2009) 2563-2569

[32] N. Arconada, A. Duran, S. Suarez, R. Portela, J. M. Coronado, B. Sanchez, B. Sanchez, Y. Castro, Synthesis and photocatalytic properties of dense and porous TiO_2-anatase thin films prepared by sol–gelAppl. Catalyst B: Environmental 86(1-2) (2008) 1-7

[33] C. Santato, M. Odziemkowski, M. Ulmann, J. Augustynski, Crystallographically Oriented Mesoporous WO_3 Films: Synthesis, Characterization, and ApplicationsJ. Am. Chem. Soc. 123 (2001) 10639-10649

[34] Z. Liu, J. Li, J. Ya, Y. Xin, Z. Jin, Mechanism and characteristics of porous ZnO films by sol–gel method with PEG templateMater. Lett. 62(8-9) (2008) 1190-1193

[35] M. Han, Y. Ou, W. Chen, L. Deng, Magnetic properties of Ba-M-type hexagonal ferrites prepared by the sol–gel method with and without polyethylene glycol addedJ. Alloy Compds. 474 (2009) 185-189

[36] G. K. Williamson, W.H. Hall, X-ray line broadening from field aluminium and wolfram Acta Mater.1 (1953) 22-31

[37] V.M. Nikale, N.S. Gaikwad, K.Y. Rajpure, C.H. Bhosale, Structural and optical properties of spray-deposited $CdIn_2Se_4$ thin films. J. Mater. Chem. Phys. 78 (2003) 363-366

[38] S. Navaladian, B. Viswanathan, T. K. Varadarajan, R. P. Viswanath,A rapid synthesis of oriented palladium nanoparticles by UV irradiation Nanoscale Res. Lett. 4 (2009) 181–186

[39] R. K. Bedi,I. Singh, CTAB assisted growth and characterization of nanocrystallineCuO films by ultrasonic spray pyrolysis technique Appl. Mater. Interfaces 2(5) (2010) 1361-1368

[40] Y. Feng, M. Zhang, M. Guo, X. Wang, Studies on the PEG-Assisted Hydrothermal Synthesis and Growth Mechanism of ZnO Microrod and Mesoporous Microsphere Arrays on the Substrate Cryst. Growth Des. 10(4) (2010) 1500-1507

Microstructural Studies of Strontium Based Alumino-Borosilicate Glasses for SOFC Applications

Mandeep Kaur
Department of Applied Science
Baba Banda Singh Bahadur Engg College
Fatehgarh Sahib, Punjab, India

Vishal Kumar
Department of Physics
Sri Guru Granth Sahib World University
Fatehgarh Sahib, Punjab, India

Gurbinder Kaur
Department of Physics
Thapar University
Patiala, Punjab, India

Abstract— In the present study, the novel glass series (10+x) CaO-(10-x)-MgO-10SrO-10B_2O_3-20Al_2O_3-40SiO_2 has been synthesized by melt quenching technique. For the stability and good efficiency of the solid oxide fuel cells (SOFCs) at high temperatures, hermetic sealants are required. Glass and glass ceramics offers promising sealant materials due to their adequate properties. Microstructural studies of the glasses (heat-treated at 850^{0}C for 50 h) are done using Scanning Electron Microcopy (SEM) to gain insight of the glass.

Keywords- Solid Oxide Fuel Cell; Glass Sealant; Morphology; Scanning Electron Microscopy.

I. INTRODUCTION

Various research groups over the past few decades are making efforts to develop alternative sources of energy to save world from major threats like global warming, pollution and health hazards. Fuel cell technology is advancing rapidly as a promising alternate energy resource. Fuel cell converts chemical energy of fuels directly into electricity by an electrochemical reaction using oxygen and hydrogen as fuels. Solid oxide fuel cells are very efficient and clean source of energy having least material corrrosion,high efficiency, high relaibility,broad product range capability, high flexibility,environment friendly and electrolyte management problem [1-3]. Generally, two designs of SOFC's are popular: planar and tubular geometries. Although, tubular design is most developed but due to its long current path around the circumference of the cell to interconnect, planar design is preferred because of its short current path resulting in high power density. During the fabrication, an appropriate sealing material is required for planar solid oxide fuel cells (pSOFC) [4-6]. The sealing prevents the mixing of gases and leakage losses at high working temperature of SOFC (800-1000 ^{o}C). Therefore, quality of the sealants must be high, since even small leakages of the fuel into air will result in direct combustion leading to local overheating and thus, affecting and degrading the performance of the cell. Hence, the stringent requirements of the sealing material are high stability over a wide range, good mechanical compatibility with adjacent components, no harmful reactions with adjacent components, good wetting capability, air tightness, matching coefficient of thermal expansion and electrical insulation. Generally, glass and glass ceramics are considered as the most appropriate sealants because of their extensive properties like (i) good thermal expansion match (ii) good wetting ability during sealing (iii) ease to fabricate (iv) can avoid viscous flow and uncontrolled crystallization growth during the operation [7-9].

The present study elucidates the microstructural studies of the strontium based aluminoboro silicate glasses in order to gain insight and in-depth mechanism of the glasses. The scanning electron microscopy is a very powerful tool to investigate the chemical compatibility at the interface and the crystal growth or structure evolution processes. Also, for the stable glass sealants controlled crystallization is required as it leads to favorable microstructure. Thus, SEM analysis has been done in order to study about the crystal growth morphology [10-12].

II. EXPERIMENTAL TECHNIQUES

2.1. Preparation of Glass

The glass series (10+x) CaO-(10-x) MgO-10SrO-10B_2O_3-20Al_2O_3-40SiO_2 (x = 0, 2.5) chosen for the present study were prepared by taking required stoichiometric amounts of different constituent oxides or carbonates of 99.9% purity. Each batch was prepared by mixing an appropriate mole fraction of desired oxide ingredients in acetone medium using mortar and pestle. The powder obtained was melted at 1550 ^{o}C in high resistance furnace. The melt was quenched in air using copper plates. The quenched glass was annealed at 500 ^{o}C in preheated furnace to remove the internal stresses from the glasses. These glass compositions with sample labels are shown in Table 1.

Table 1 Composition (Mol%) Of Glass Constituents

Sample Name	CaO	MgO	SrO	B_2O_3	Al_2O_3	SiO_2
10CaMg	10	10	10	10	20	40
12.5CaMg	12.5	7.5	10	10	20	40

2.2 X-ray studies

The X-ray studies of crystalline phases formed in the 200 h heat-treated glass were analyzed using high-resolution XRD in a Bruker D8 X-ray diffractometer. The XRD voltage was 45 kV and the beam current was 40 mA. The scan time per step was 600 s with CuK_a radiation (λ = 1.5406 A°). The phase identification was done by comparing the experimental diffractgrams to standard patterns complied by the International Centre for Diffraction Data (ICDD).

2.3 Microstructural studies

The interaction study was carried out by heating glasses at 850 ºC for 500 hours before polishing mechanically and etching with dilute HF. Then, these glasses were analyzed under SEM (ZEISS EVO MA-10) to study the microstructures of the glasses.

III. RESULTS AND DISCUSSION

3.1 X-ray Diffraction

The X-ray analysis of both the glass samples 10 CaMg and 12.5 CaMg exhibits very sharp peaks of calcium orthosilicate phase Ca_2SiO_4 (ICDD-00-006-0511) and enstatite phase $MgSiO_3$ (ICDD-01-074-2017) crystalline phases. The formation of these phases can be possibly due to following mechanism:

$$2CaO + SiO_2 \rightarrow Ca_2SiO_4 \quad (1)$$

$$MgO + SiO_2 \rightarrow MgSiO_3 \quad (2)$$

3.2 Microstructural studies

The microstructural studies are very important to gain insight of the glass surface for efficient performance of the fuel cell. The scanning electron microscopy (SEM) is used to study the crystal growth morphology size, surface texture, roughness, and chemical composition of materials. During SOFC operation various chemical reactions can take place due to diffusion of ions at the interface, thus, affecting glass seal and interconnect interface which ultimately impedes fuel cell performance. Therefore, with this analysis the glass surfaces can be analyzed for sealing applications.

Fig. 1(a) shows the microstructure of 10 CaMg glass after 500 h heat treatment at 850^0 C. It exhibits a dense microstructure with crystalline phases, clearly indicating phase formation embedded in amorphous glassy matrix. This phase formation can be possibly due to formation of crystalline peaks of calcium orthosilicate phase Ca_2SiO_4 and enstatite phase $MgSiO_3$ phase which is confirmed by X-ray analysis also [13-15]. Hence, the composite exhibited controlled crystallization. Moreover, the glass is devoid of cracks, pores and pits which makes it suitable to be used as a sealant. Also, Fig. 1(b) shows SEM micrographs for second glass composition. The formation of spherical and needle shaped crystalline phases upon heating could be clearly seen on the glass surface. Also, both the compositions are depicting very clean and smooth surfaces devoid of unwanted delamination, cracks and pores. These results indicates that the glass samples will exhibit good bonding behavior with the interconnect and electrolyte also which is necessary in order to have minimum divtrification and CTE (coefficient of thermal expansion) mismatch between glass/electrolyte interface and glass/interconnect interface. Hence, the glass samples exhibited controlled crystallization, which is a favorable microstructure and further confirms the hermeticity to be used for sealing applications.

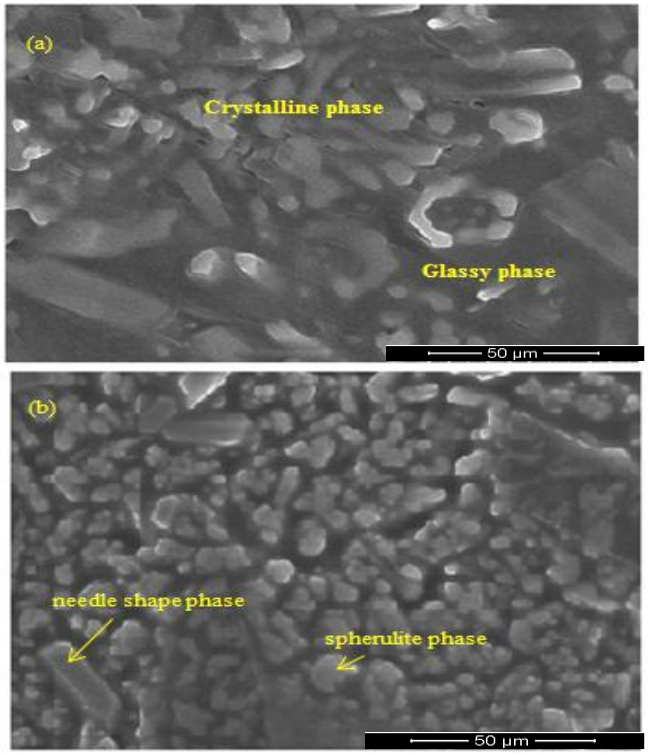

Fig. 1 (a) Microstructure of 10 CaMg glass heat treated at 850^0 C (500 h), (b) Microstructure of 12.5 CaMg glass heat treated at 850^0 (500 h)

IV. CONCLUSION

The microstructural studies has been investigated in (10+x) CaO- (10-x) MgO-10SrO-10B_2O_3-20Al_2O_3-40SiO_2 glasses (x = 0, 2.5) in which SEM micrographs of glass samples 10 CaMg and 12.5 CaMg shows the formation of crystalline phases embedded in amorphous glass matrix which is in well agreement with X-ray analysis. Both the samples exhibits clean and smooth glass surface without any crack or pores in the crystalline phases formed. Hence, the favorable microstructure of the glasses is good for sealing applications.

REFERENCES

[1] R. Mark Ormerod, "Solid oxide fuel cell," The Royal Society of Chemistry, vol. 32,pp. 17-28,2003.

[2] M.SHaile., "Fuel cell materials and components," Acta Materialia, vol. 51, pp. 5981–6000, 2003.

[3] V kumar.,A Arora.,O.P.Pandey., K.Singh., "Studies on thermal and structural properties of glasses as sealants for solid oxide fuel cells,International Journal of Hydrogen Energy, vol. 33,pp. 434 – 438,2008.

[4] Minh. Q. Nguyen, "Solid oxide fuel cell technology-features and applications,Solid StateIonics," vol. 174, pp. 271-277, 2004.

[5] S. P.Jiang, L. Christiansen, B. Hughan and K. Foger," Effect of glass sealant materials on microstructure and performance of Sr-doped $LaMnO_3$ cathodes," J. Mat. Sci. Lett, vol. **20** , pp. 695-697,2001.

[6] S.C Singhal, "Solid oxide fuel cells for stationary, mobile, and military applications," Solid State Ionics, vol.152-153, pp. 405-401,2002.

[7] P.H Larsen., P.F James, "Chemical stability of MgO/CaO/ Cr_2O_3 – Al_2O_3–B_2O_3 phosphate glasses in solid oxide fuel cell environment", J. ofMaterial Science, vol. 33, pp. 2499-2507, 1998.

[8] A.Goel,M.J Pascaul.,J.M.F Ferreia, "Stableglass-ceramic sealants for solid oxide fuel cells: Influence of Bi2O3 doping," Int J. Hydrogen Energy vol. 35, pp.6911-6923, 2010.

[9] K.D Meinhardt,D.-S Kim.,Y-S Chou.,K.SWeil.," Synthesis and properties of a barium aluminosilicate solid oxide fuel cell glass-ceramic sealant,"J.Power sources, vol. 182, pp.188-196, 2008.

[10] T.Jin,K Lu., "Thermal stability of new solid oxide fuel cell/electrolyzer cell seal glass," J. Power sources, vol.195, pp.195-203, 2010.
F. Liu, J. Wu, K. Chen,D. Xue. "Morphology study by using scanning electron microscopy," Microscopy: Science, Technology, Applications and education A. Méndez-Vilas and J. Díaz (Eds.)

[11] G .Kaur, G, Pickrell, Y .Cheng, "Thermal stress simulation and chemical compatibility of glass composite seals with YSZ for solid oxide fuelcells," Int J. Energy Research, vol. 39, pp. 681-695, 2015.

[12] V Kumar, G. Kaur, K.Lu, G. Pickrell, "Interfacial compatibility of alumino-borosilicate glass sealants with AISI 441 and YSZ for different atmospheres," Int J. Hydrogen Energy, vol. 40, pp.1195-1202, (2015).

[13] G. Kaur, D. Homa,, K Singh,O.P Pandey, B.Scott, G.Pickrell," Simulation of thermal stress within diffusion couple of composite seals with Crofer 22APU for SOFC applications," Journal of Power Sources, vol.242, pp.205-21, 2013.

[14] G.Kaur, K. Singh, O.P Pandey, D. Homa, B.Scott, G.Pickrell, "Structural and thermal properties of glass composite seals and their chemical compatibility with Crofer 22APU for solid oxide fuel cells applications", J. Power Sources, vol.240, pp.458-470, 2013.

Effect of Inertia and Constriction Factors on PSO and Quantum Behaved PSO

Gurwinder Singh
Research Scholar,
IKGPTU, Jalandhar

Amarinder Singh
Baba Banda Singh Bahadur Engineering College
Fatehgarh Sahib

***Abstract*—Particle Swarm Optimization (PSO) is characterized as a stochastic optimization algorithm that is based on the behaviour of swarm of birds searching for food. PSO is a very powerful tool for obtaining the optimal solution for complex problems. The algorithm may be modified by varying the various parameters involved and hence new variants of PSO may be obtained that improve the rate of convergence and the diversity of the solutions. In this paper, the basic PSO and the Quantum behaved PSO are compared with the variations of inertia factor and constriction factor applied on the Sphere function and Rosenbrock function.**

Keywords*—Particle Swarm Optimization (PSO), Quantum PSO (QPSO), PSO with Inertia Factor (PSO-In), PSO with Constriction Factor (PSO-Co)

I. INTRODUCTION

Optimization techniques, the techniques to find the best solution for problems, are generally of two types – deterministic and stochastic. Most of the real world problems are stochastic in nature and hence require respective techniques for solution. The stochastic techniques often result in huge computational efforts and hence may fail as the complexity of the problem increases. To deal with such complex problems, bio-inspired stochastic algorithms have been developed and have gained importance because of their computational efficiency. Population based techniques are the meta-heuristic iterative approaches that involve selecting appropriate initial population and operators to produce new set of solutions. PSO algorithm, introduced by Kennedy and Eberhart [1], is based on the simulation of the social behaviour of birds. The algorithm simulates the graceful and unpredictable choreography of swarm of birds. Each individual within the swarm is represented by a vector in the multidimensional search space. This position vector is assigned another vector, called the velocity vector, which determines the next movement of the particle. Each particle updates its velocity based on its current velocity, the individual best position and the global best position explored so far. It has been observed to have good convergence rate and has been applied to many real world optimization problems. PSO seems to have much in common with the Evolutionary Algorithms, however, it differs from these approaches because of the fact that there is no criterion for selecting the population and the population remains the same throughout the iterative procedure. Each particle in the population is attracted to it previous best position and to the global best position attained by the swarm.

One problem with the PSO is that it may fall into the trap of local optima in many optimization problems, since the particles may come close to their previous best and the global best thereby decreasing their dissimilarities. This results in premature convergence, in which case the population needs to be re-initialized to obtain the diversified solutions and hence search for the global optimal solution.

In this paper, basic PSO approach and the Quantum PSO are being compared with emphasis on the Inertia factor and the Constriction Factor. These variants are being applied on the benchmark problems, the Sphere function and the Rosenbrock function to study the convergence of these techniques.

II. BASIC PARTICLE SWARM OPTIMIZATION

PSO remembers both the best position found by all the particles and those obtained by each particle in the search process. For a search problem in an n-dimensional space, a particle represents a potential solution. The velocity v_{ij} and the position x_{ij} of the j^{th} dimension of the i^{th} particle are updated according to equations

$$v_{ij}(t+1)=w.v_{ij}(t)+c_1.rand1_{ij}.(pbest_{ij}(t)-x_{ij}(t)) + c_2.rand2_{ij}.(gbest_{ij}(t)-x_{ij}(t)) \quad (1)$$

$$x_{ij}(t+1)=x_{ij}(t)+v_{ij}(t+1) \quad (2)$$

where i=1,2,... is the particle's index and $X_i=(x_{i1},x_{i2},\ldots,x_{in})$ is the position of the i^{th} particle, $V_i=(v_{i1},v_{i2},\ldots,v_{in})$ is the velocity of the i^{th} particle. The $pbest_i=(pbest_{i1},pbest_{i2},\ldots,pbest_{in})$ is the previous best yielding the best fitness value for the i^{th} particle and $gbest=(gbest_1,gbest_2,\ldots,gbest_n)$ is the global best particle found by all the particles so far. The inertia factor w has been proposed by Shi and Eberhart [2], $rand1_{ij}$ and $rand2_{ij}$ are two random numbers independently generated within the range of [0,1], c_1 and c_2 are two learning factors which control the influence of the social and cognitive components and t=1,2,... represents the iterations.

III. QUANTUM PARTICLE SWARM OPTIMIZATION

In QPSO, the Contraction-Expansion (CE) coefficient α is the most important algorithmic parameter that requires to be adjusted to balance the local and global search of the algorithm during the search process. This work provides an analysis of the impact of the CE coefficient on the behaviour of the particle in both types of the QPSO algorithms and discusses how to select its value for practical usage. Sun, Lai and Wu [3] has discussed both the basic and quantum perspectives of PSO.

A. *Procedure of QPSO*

The procedure of QPSO is similar to that of the PSO algorithm, except that it has different evolution equations In the QPSO algorithm, there is no velocity vector for each particle, and the position of the particle updates directly according to the equations

$$X_{i,n+1}^{j}=p_{i,n}^{j}\pm\alpha|\ X_{i,n}^{j}-p_{i,n}^{j}\ |\ln(1/\ u_{i,n+1}^{j}\ )| \quad (3)$$

or

$$X_{i,n+1}^{j}=p_{i,n}^{j}\pm\alpha|\ X_{i,n}^{j}-g_{i,n}^{j}\ |\ln(1/\ u_{i,n+1}^{j}\ )| \quad (4)$$

where $p_{i,n}^{j}$ is the j^{th} component of the local focus $p_{i,n}$ of particle i at the n^{th} iteration, $u_{i,n+1}^{j}$ is a sequence of random number uniformly distributed on (0,1).

IV. INERTIA FACTOR AND CONSTRICTION FACTOR

A. PSO with Inertia Factor (PSO-In)

Inertia weight maintains a balance between exploring the search space and exploiting the solutions. The Inertia weight determines the contribution of the particle's previous velocity to the current iteration. Shi and Eberhart [2] established that a large inertia weight would facilitate the global search while small inertia weight would facilitate the local search. However, later on, many researchers studied the dynamic inertia weight to improve the convergence of PSO. Eberhart and Shi [4] gave a random inertia weight strategy while Xin, Chen and Hai [5] proposed the linearly decreasing strategy to enhance the efficiency and performance of PSO. In this paper, the linearly decreasing inertia weight has been considered in which the weight is computed by the equation:

$$w=w_{max}+((w_{max}-w_{min})/maxiter)\times\ iter \quad (5)$$

where w_{max} and w_{min} are the maximum and minimum values of the inertia weight that are pre-decided, *iter* represents the number of the current iteration and *maxiter* represents the maximum number of iterations.

B. PSO with Constriction Factor (PSO-Co)

Many researchers have indicated that the PSO often converges significantly faster to the global optimum but has difficulties in premature convergence, performance and diversity loss in the optimization process. In the absence of any restriction of the maximum velocity of the particles, researchers observed that they started oscillating around the optimal solution and the procedure would not reduce the velocity so as to search minutely in the limited search space for the global optimal. Clerc [6] suggested the use of properly defined constriction factor to ensure early convergence of the PSO. The velocity using the PSO with the constriction factor K is given by:

$$v_{ij}(t+1)=K[v_{ij}(t)+c_1.rand1_{ij}.(pbest_{ij}(t)-x_{ij}(t)) +c_2.rand2_{ij}.(gbest_{ij}(t)-x_{ij}(t))] \quad (6)$$

$$K=2/(|2-\varphi-\sqrt{(\ \varphi^2-4\varphi)}|),\ \text{where}\ \varphi=c_1+c_2,\ \varphi>4 \quad (7)$$

The convergence characteristic of the system is controlled by φ that has to be greater than 4. Generally, when the constriction factor is used, c_1 and c_2 are both set as 2.05 and thus φ=4.1. Thus the constriction factor is evaluated to 0.729.

V. BENCHMARK PROBLEMS

The benchmark problems considered in this paper are given by equations (8) and (9).

$$f(x_1,x_2,...,x_n)=x_1^2+x_2^2+...+x_n^2 \quad (8)$$

$$f(x_1,x_2,...,x_n)=\sum(100.(x_{i+1}-x_i^2)^2+(x_i-1)^2) \quad (9)$$

The Sphere function is strongly convex and unimodal function whereas the Rosenbrock function is a non-convex function and have been widely studied as benchmark problems in the theory of evolutionary algorithms.

A. Parameters used

Population Size (M)	20
Maximum Number of Iterations	1000
Search Space	[-100,100]
Acceleration Coefficients (c_1 and c_2)	2.0 (For PSO and PSO-In)
Acceleration Coefficients (c_1 and c_2)	2.05 (For PSO-Co)

During initialization, the current position vector for all the particles are uniformly distributed within the search domain and the initial best position of the particle is set to its initial current position. The fitness value corresponding to each particle is computed followed by the identification of the global best positions. In case of PSO-In, the inertia weight '*w*' should be computed as according to decreasing linearly from 0.9 and 0.4 during the iterative procedure.

B. Iterative Procedure

The procedure of basic PSO, PSO-In and PSO-Co was executed and 50 cases of the final fitness values for each version of the PSO were obtained. The final fitness value for each run of a PSO algorithm was obtained after 1000 iterations of the search process. The average of the 50 best fitness values is known as the mean best fitness value. The standard deviation of the 50 best fitness values is computed for further comparative analysis. The quality of the solution or the fitness value obtained is only one of the aspects that reflect the performance of the algorithms. There are other important factors that may be employed evaluate the algorithms, including the convergence speed of the fitness values. To trace the convergence history of the algorithms, the fitness values at each iteration over 50 runs are averaged and plotted. It is observed that the basic PSO generated poor results even though the Sphere function is a unimodal function whereas PSO-In and PSO-Co generated better results. In particular, the mean best fitness value obtained through PSO-Co is 4.6526×10^{-8} that is extremely close to the optimal solution. Similarly, the solution obtained through the PSO-Co for the Rosenbrock function is extremely close to the optimal solution.

In the similar manner, with the same parameter values and α=0.75, the procedure of QPSO, QPSO-In and QPSO-Co was executed and 50 values of the fitness values were obtained. The graphs of the mean values of the 20 particles of the Sphere function using basic PSO are plotted in Fig. 1-Fig. 3 and those using QPSO are plotted in Fig. 4-Fig. 6. It was observed that the mean best fitness value obtained for Sphere function is 4.9667×10^{-37}.The similar graphs of Rosenbrock function are plotted in Fig. 7-Fig. 9 and Fig. 10-Fig. 12 respectively. The final comparison of the mean values, the standard deviation and the global best of all the three variants for both the Sphere function and Rosenbrock function are given in Table I and Table II.

VI. CONCLUSION

From Table I and Table II, it is easily concluded that the performance of Quantum behaved PSO is much better than the basic PSO because of its characteristic of enhancing the global search ability of the particles. Furthermore, while considering the Constriction Factor, the convergence and the rate of convergence are further improved by a great extent, establishing the significance of both the Quantum behaved PSO and the Constriction Factor while solving the optimization problem for the real world problems. PSO is a potential research topic and has room for considerable amount of modifications and hybridizations.

REFERENCES

[1] J. Kennedy and R.C. Eberhart, "Particle swarm optimization," Proceedings of IEEE International Conference on Neural Networks, pp. 1942-1948, 1995.

[2] Y. Shi and R.C. Eberhart, "A modified particle swarm optimization," Proceedings of IEEE Congress Evolutionary Computation," pp. 69-73, 1998.

[3] J. Sun, C-H. Lai and X-J. Wu, Particle Swarm Optimization: Classical and Quantum Perspectives, CRC Press, 2012.

[4] R.C. Eberhart and Y. Shi, "Tracking and optimizing dynamic systems with particle swarms," Proceedings of the IEEE Congress on Evolutionary Computation, pp. 94-100, 2002.

[5] J. Xin, G. Chen and Y. Hai, " A particle swarm optimizer with multistage linearly-decreasing inertia weight," IEEE Interational Joint Conference on Computational Sciences and Optimization, pp. 505-508, 2009.

[6] M. Clerc and J. Kennedy, "The particle swarm – explosion, stability and convergence in a multidimensional complex space," IEEE Trans. Evolutionary Computation, vol. 6, pp. 58-73, 2002.

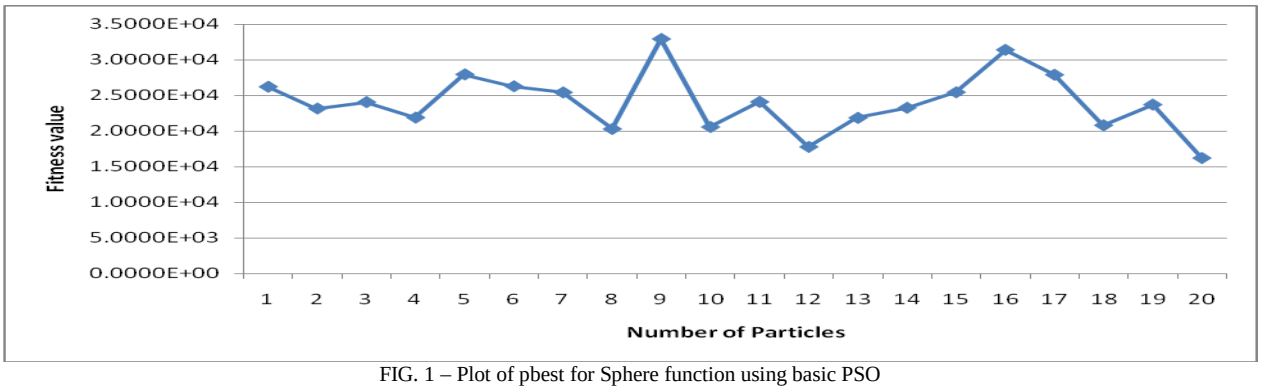

FIG. 1 – Plot of pbest for Sphere function using basic PSO

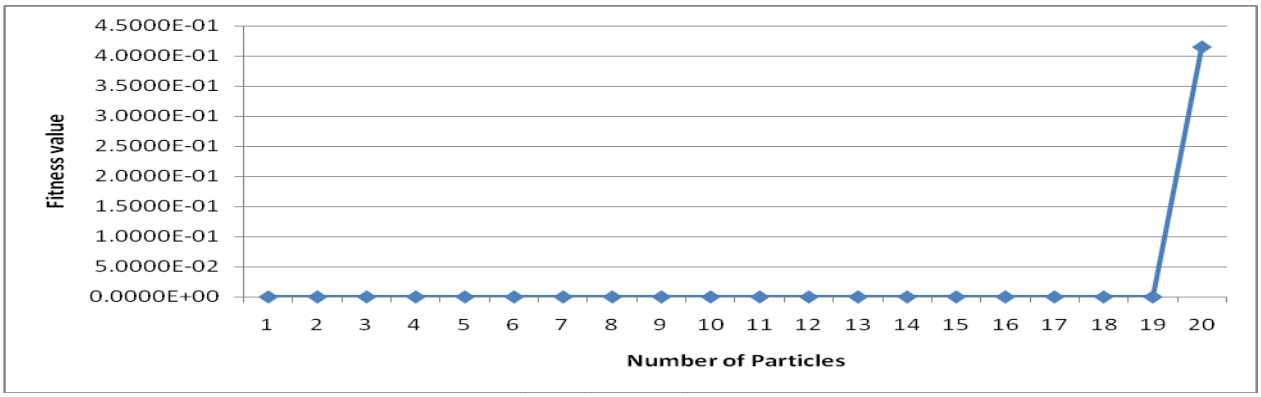

FIG. 2 – Plot of pbest for Sphere function using PSO-In

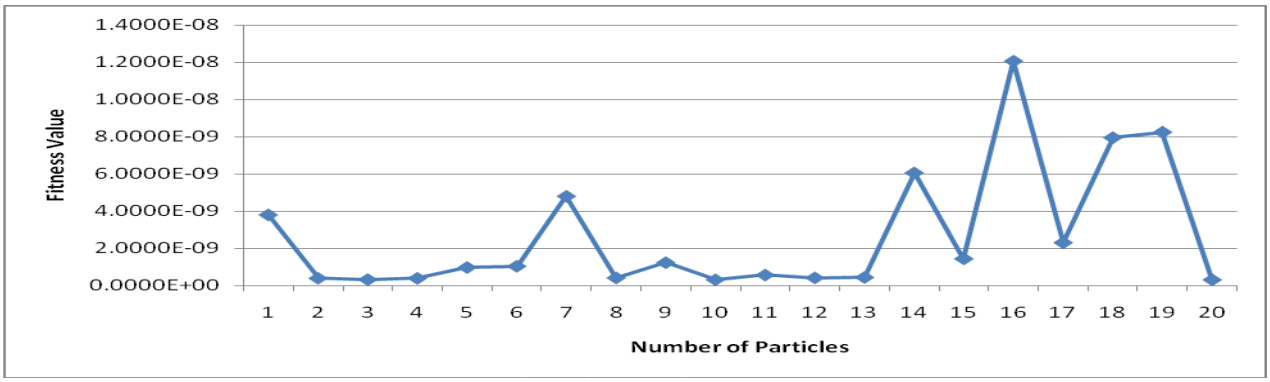

FIG. 3 – Plot of pbest for Sphere function using PSO-Co

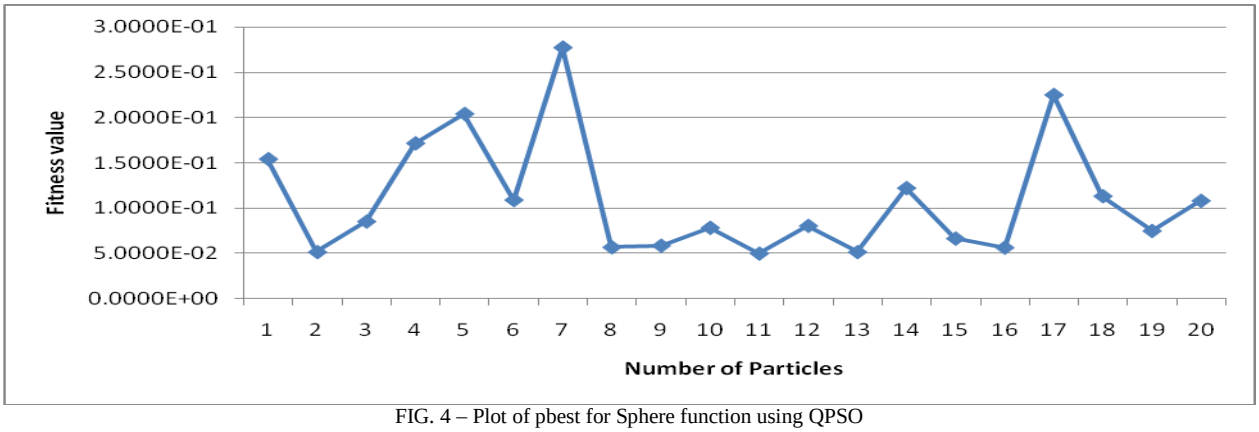

FIG. 4 – Plot of pbest for Sphere function using QPSO

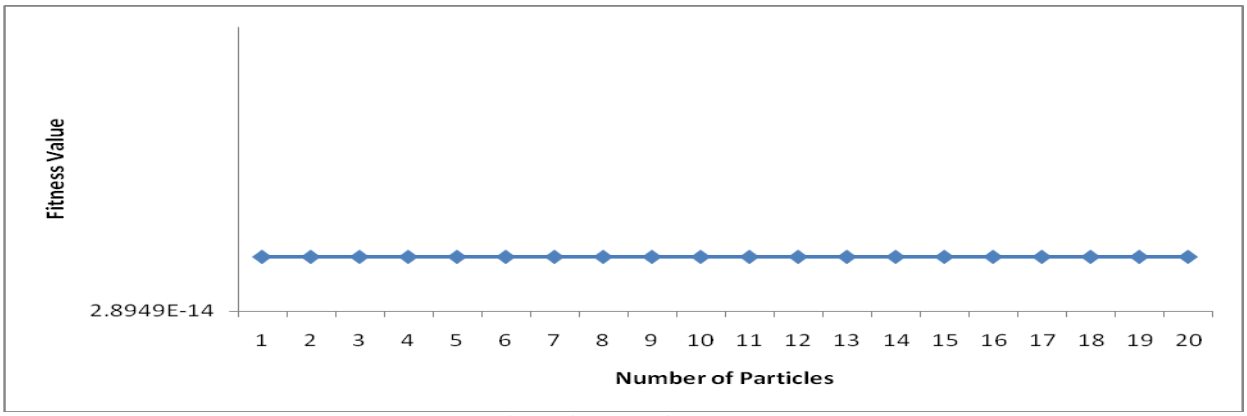

FIG. 5 – Plot of pbest for Sphere function using QPSO-In

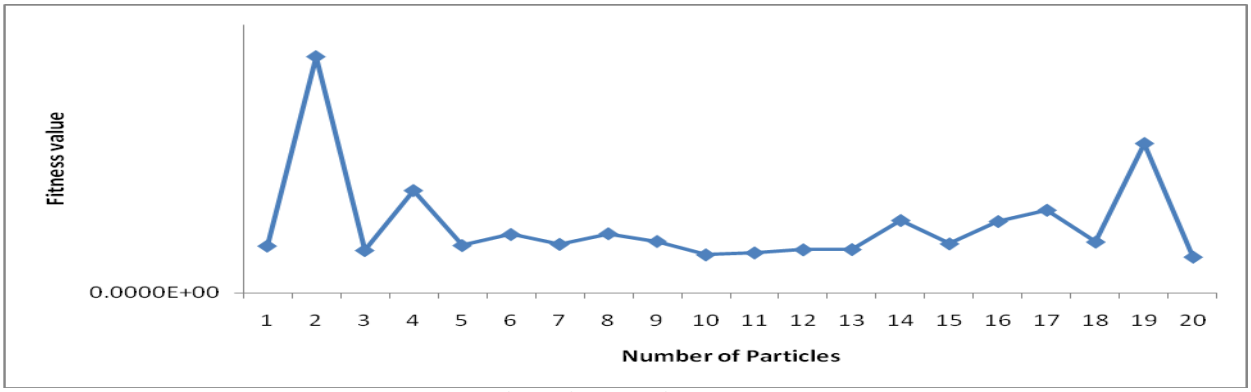

FIG. 6 – Plot of pbest for Sphere function using QPSO-Co

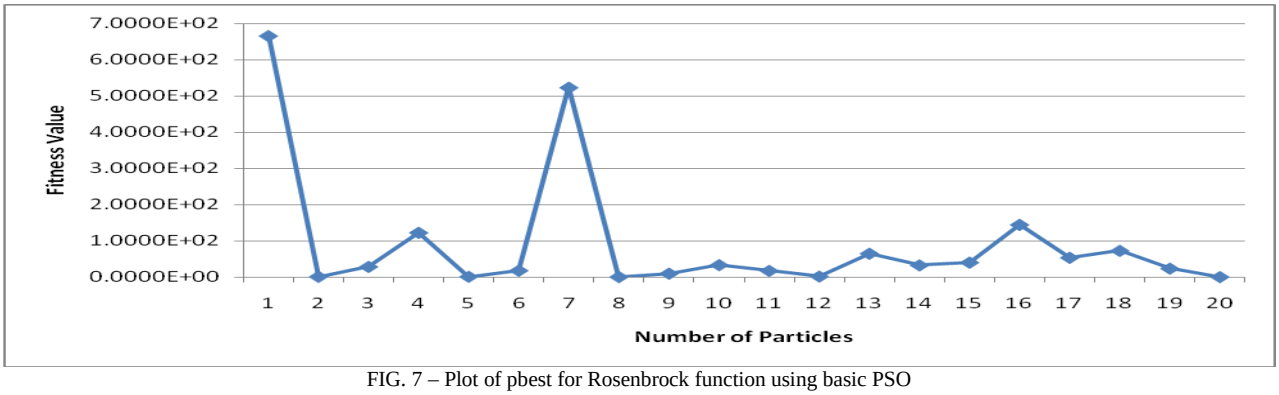

FIG. 7 – Plot of pbest for Rosenbrock function using basic PSO

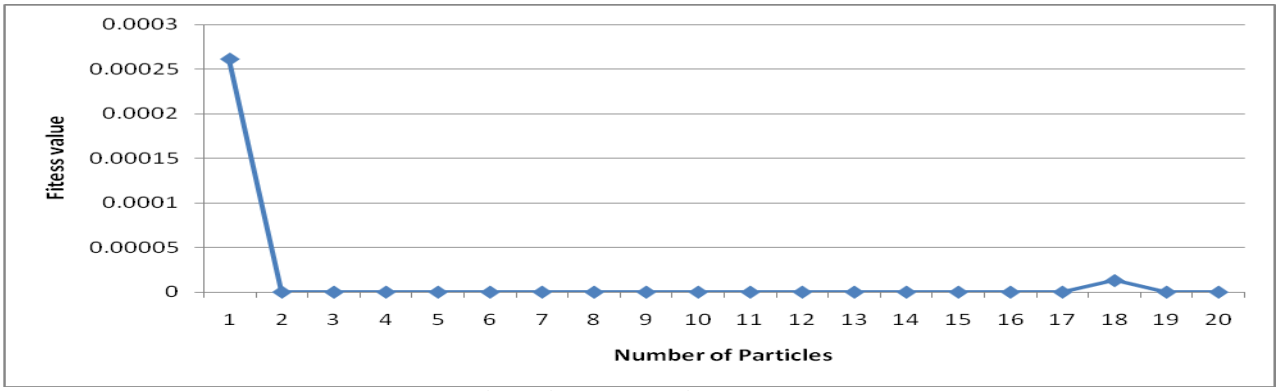

FIG. 8 – Plot of pbest for Rosenbrock function using basic PSO-In

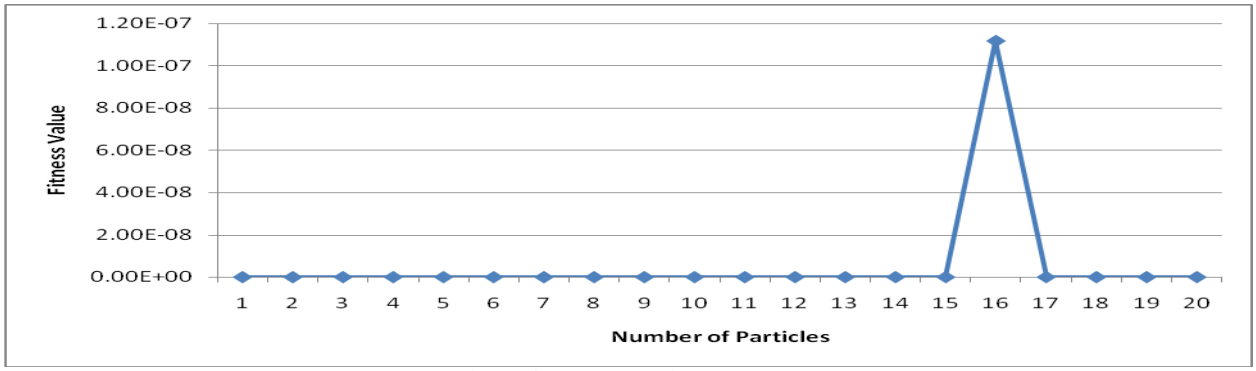

FIG. 9 – Plot of pbest for Rosenbrock function using basic PSO-Co

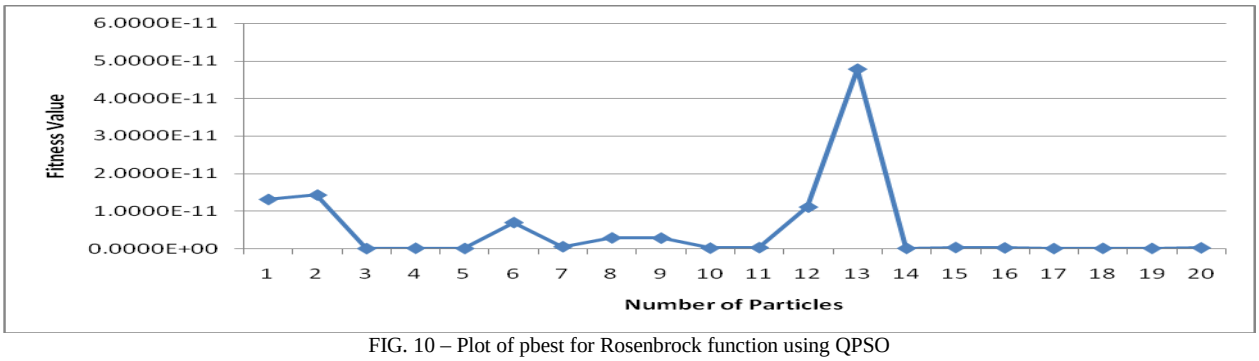

FIG. 10 – Plot of pbest for Rosenbrock function using QPSO

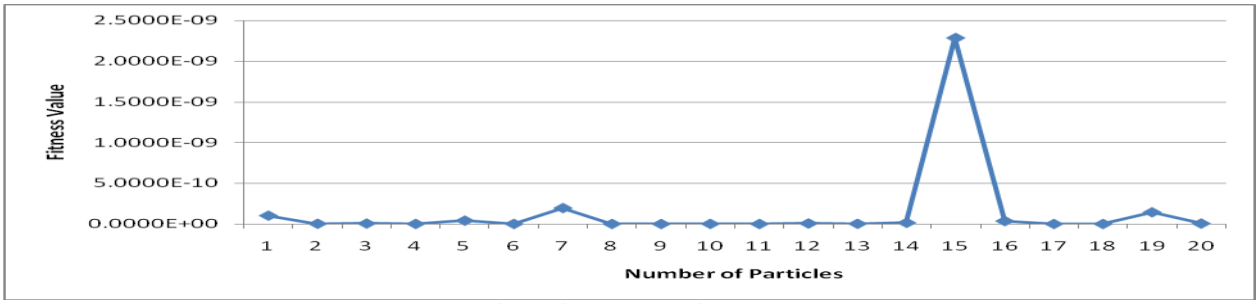

FIG. 11 – Plot of pbest for Rosenbrock function using QPSO-In

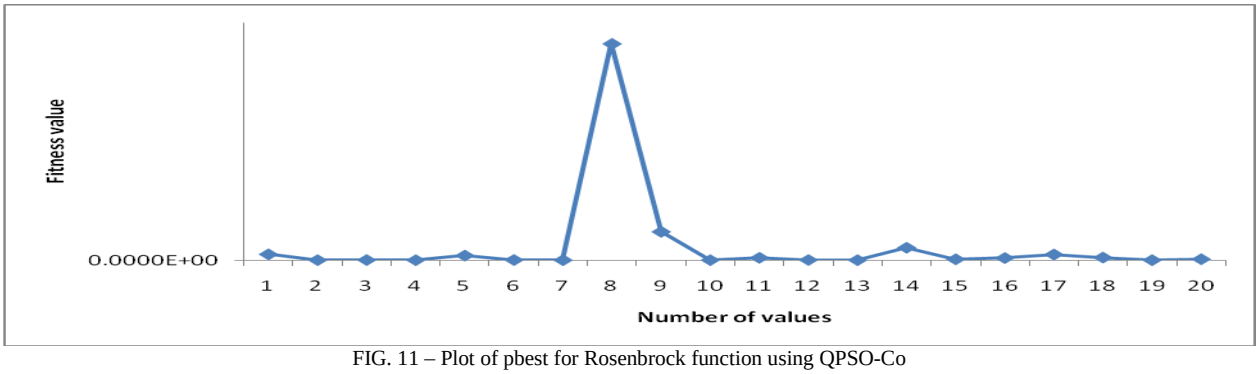

FIG. 11 – Plot of pbest for Rosenbrock function using QPSO-Co

TABLE 3: Mean and Standard Deviation of the Best Fitness Values using basic PSO and QPSO for Sphere Function

	PSO			Quantum PSO		
	Mean	Standard Deviation	Global Best value	Mean	Standard Deviation	Global Best value
BasicPSO	1.3913E+04	2.6379E+03	1.6231E+04	3.3150E-01	3.0730E-01	5.0300E-02
PSO In	4.4914E-07	7.9325E-07	9.1108E-08	205397E-14	8.2150E-014	2.8960E-14
PSO Co	4.6526E-08	1.0754E-07	3.0781E-10	4.9667E-37	1.7747E-36	3.9713E-37

TABLE 4: Mean and Standard Deviation of the Best Fitness Values Obtained using basic PSO and QPSO for Rosenbrock Functions

	PSO			Quantum PSO		
	Mean	Standard Deviation	Global Best value	Mean	Standard Deviation	Global Best value
BasicPSO	2.8489E+00	3.8029E+00	7.0800E-02	1.1043E-04	5.5005E-04	1.2913E-13
PSO In	1.8313E-11	1.2866E-10	1.1585E-17	4.1000E-01	2.8991E+00	2.8051E-14
PSO Co	4.3847E-15	2.6133E-14	1.1590E-20	4.7917E-10	3.1498E-09	9.9911E-25

A Lattice Dynamical Investigation of Raman and Infrared Wavenumbers of Mn_2SiO_4

Harleen Kaur
Dept. of Applied Sciences
Baba Banda Singh Bahadur Engineering College
Fatehgarh Sahib, India

M. M. Sinha
Dept. of Physics
Sant Longowal Institute of Engineering & Technology
Longowal, Sangrur, India

***Abstract*— Wilson's GF matrix method has been applied for the investigation of optical phonons of Mn_2SiO_4 in orthorhombic phase having space group Pbnm using normal coordinate analysis. The calculation of zone center phonons have been made with fifteen stretching and ten bending force constants. The calculated values of Raman and infrared wavenumbers are in good agreement with the experimental values. The contribution of each force constant towards the zone centre phonons has been determined in terms of potential energy distribution.**

Keywords*— Phonon spectra; lattice dynamics; force constant; potential energy distribution.

I. INTRODUCTION

Olivine, $(Mg,Fe)_2SiO_4$, is the major rock-forming mineral in the Earth's upper mantle [1]. The family of olivine compounds, including forsterite (Mg_2SiO_4), fayalite (Fe_2SiO_4), tephroite (Mn_2SiO_4) and solid solutions between them, play a significant role in geosciences since olivines are the most common silicate phases in the Earth's mantle. Manganese orthosilicate, Mn_2SiO_4, the mineral tephroite, has been the subject of structural, crystal, chemical and thermodynamical study because of its petrological and geophysical importance [2]. Apart from its importance in Earth sciences, this family of olivines is potentially significant from technological point of view [3-4]. Silicate olivines show predominant occurence in igneous rock and have been used as an important composition in some refractory materials, grit blasting materials, ceramic pigments, additives in cement concrete, flux and slag conditioner in the steel industry [5-6], and so on.

The study of phonon properties of these minerals is crucial for understanding the phenomenon of phase transition in such compounds. The complete information of the macroscopic behavior of the minerals can be best obtained from a detailed knowledge of microscopic nature and this relation is best made via their vibrational spectra. However, the experimental task required for studying the lattice dynamical behavior and properties of minerals is exigent because of the technical difficulties involved in reproducing the temperature and pressure conditions that are relevant to the Earth's interior and in carrying out controlled experiments at such conditions. Therefore, the theoretical prediction of vibrational properties through accurate modeling is the only feasible solution. It is well known that many interatomic force dependent properties of solids can be described very successfully through harmonic models. Hence, in the present work, the lattice dynamical investigation of Mn_2SiO_4 olivine has been undertaken within the harmonic approximation.

Previous studies reveal that Mg_2SiO_4 and Fe_2SiO_4 olivines have been a subject of thorough study to investigate the lattice dynamical properties both experimentally and theoretically [7-9], but few studies have been conducted to investigate the spectral activity in Mn_2SiO_4. However, none of the observations [10-11] could assign all the observed Raman and infrared modes in Mn_2SiO_4. Also to our knowledge, no theoretical calculation of optical phonons has been made in the orthorhombic phase of Mn_2SiO_4. Hence, in this paper a short range force constant model has been applied to investigate the optical phonons using normal coordinate analysis involving fifteen stretching and ten bending force constants. The theoretically obtained wavenumbers are in very good agreement with the experimental ones. Also, an effort is also made to assign experimental wavenumbers to their respective optical phonon modes. The potential energy distribution (PED) has also been investigated for determining the significance of contribution from each force constant towards the Raman and infrared wavenumbers.

II. THEORY

Mn_2SiO_4, the mineral tephroite, crystallizes in the orthorhombic olivine structure with space group Pbnm (no 62) and D_{2h} symmetry with four formula units. The structure is composed of an almost hexagonally close packed array of oxygen ions. One eighth of the tetrahedral sites are occupied by silicon ions and one half of the octahedral positions are filled with manganese ions. The Mn octahedra have common edges and form chains along the c-axis. Mn ions occupy two crystallographically non-equivalent octahedral positions with different site symmetries, M1 and M2 (as given in Fig 1) with M1 having 4a site and M2 occupying 4c site. The oxygen ions occupy three distinct positions i.e. O1, O2 and O3. Si, O1and O2 reside at 4c and O3 ions occupy 8d site. The crystal structure consists of SiO_4 tetrahedra linked by the divalent manganese cations in six fold oxygen anion coordination. Thus there are twenty eight atoms in primitive cell resulting in eighty four vibrational modes. The detailed analysis of total number of modes at zone centre (k=0) is:

$$\Gamma_{total}= 11A_g+11B_{1g}+7B_{2g}+7B_{3g}+10A_u+10B_{1u}+14B_{2u}+14B_{3u}$$

where $B_{1u}+B_{2u}+B_{3u}$ are acoustical modes, $11A_g$, $11B_{1g}$, $7B_{2g}$ and $7B_{3g}$ are Raman active, $9B_{1u}$, $13B_{2u}$ and $13B_{3u}$ are infrared active and $10A_u$ are inactive modes.

Wilson's GF matrix method [12] has been employed to calculate the Raman and infrared wavenumbers by using normal coordinate analysis. In this method the concept of internal coordinates is being introduced which makes the problem more logical. These internal coordinates includes the parameters like bond distances and angles or interatomic distances. The zone centre modes are determined in terms of kinetic and potential energies of the system. The Kinetic energy T is dependent on geometrical arrangement of the atoms and their masses m_{ij} where as the potential energy V which originate due to interactions within the molecule is defined in terms of force constants F_{ij} .

$$T = \frac{1}{2}\sum_{i=1}^{3N-6}\sum_{j=1}^{3N-6}(G^{-1})_{ij}\ \dot{S}_i\,\dot{S}_j$$

$$V = \frac{1}{2}\sum_{i=1}^{3N-6}\sum_{j=1}^{3N-6}F_{ij}\ \dot{S}_i\,\dot{S}_j$$

where G^{-1} stands for the inverse of the G matrix which is describing the kinetic energies in terms of mass-weighted cartesian displacements and $\dot{S} = \frac{dS}{dt}$. The secular equation for calculating the frequencies is given by $|FG - E\lambda| = 0$

Here G is a matrix connected with the vibrational kinetic energy and F is a matrix of force constants to represent potential energy required for each vibration and thus gives an idea of the bond strength. Molecules are constructed in cartesian coordinates and then transformed to internal coordinates with changes in bond distances and bond angles. Both F and G are symmetrical in nature and E is a unit matrix and λ is related to the frequency ν given by $\lambda = 4\pi^2c^2\nu^2$.

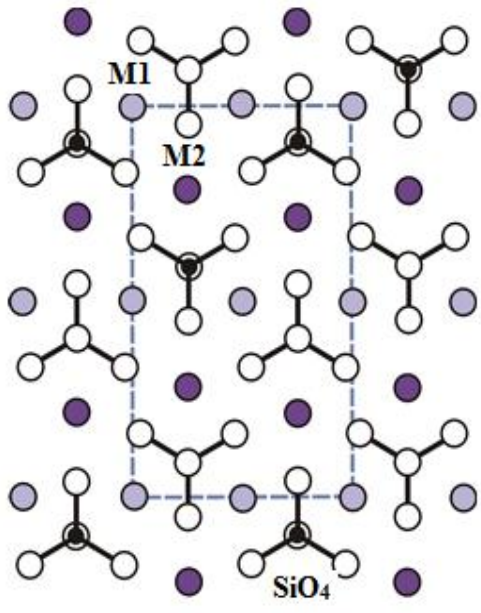

Fig. 1. Unit cell of Mn_2SiO_4 in orthorhombic phase

The present study includes fifteen stretching K_i and and ten bending force constants H_i to formulate F matrix. The short range forces are significant upto certain neighbors and their magnitude generally decreases after the second neighbor interaction. The reason for inclusion of bending forces in our calculations is that the stretching forces only are not sufficient to explain transverse vibrations. Short range stretching forces between nearest neighbors Si-O, Mn-O, O-O and bending forces between O-Mn-O and O-Si-O are used in the present analysis. The input parameters used for the study are masses of the atoms, unit cell dimensions [13], symmetry coordinates and available Raman and infrared frequencies [11].

III. RESULTS AND DISCUSSION

The force constants as given in Table I have been optimized and empirically scaled so as to make the vibrational wavenumbers in good agreement with the observed Raman and infrared numbers.

TABLE I. INTERATOMIC FORCE CONSTANT VALUES (in N cm^{-1})

Force constant	Between atoms	Coordination Number	Distance (Å)/ Angle (degree)	Force constant value
K1	Si-O1	4	1.619	3.812
K2	Si-O3	8	1.639	3.466
K3	Si-O2	4	1.657	3.388
K4	Mn1-O2	8	2.167	0.474
K5	Mn1-O1	8	2.200	0.414
K6	Mn1-O3	8	2.249	0.328
K7	Mn2-O2	4	2.139	0.522
K8	Mn2-O3	8	2.154	0.354
K9	Mn2-O1	4	2.278	0.311
K10	O2-O3	8	2.580	0.638
K11	O1-O3	8	2.753	0.305
K12	O1-O3	8	3.154	0.203
K13	O2-O3	8	3.031	0.172
K14	O2-O3	8	3.358	0.153
K15	O2-O3	8	3.585	0.146
H1	O2-Si-O3	8	103.03	0.423
H2	O3-Si-O3	4	105.53	0.524
H3	O1-Si-O2	4	113.11	0.272
H4	O1-Si-O3	8	115.32	0.179
H5	O3-Mn2-O3	8	87.64	0.156
H6	O3-Mn2-O3	4	115.59	0.182
H7	O1-Mn2-O3	8	90.70	0.156
H8	O3-Mn2-O3	4	68.47	0.484
H9	O2-Mn1-O3	4	108.51	0.212
H10	O1-Mn1-O3	8	84.71	0.159

With the force constants taken as input, the eigen value equation involving 84X84 matrix was solved. It is obvious from Table I that the stretching force constants for Si-O i.e. K1, K2 and K3 show a systematic variation with interatomic distance. The value of K1 is the highest among all corresponding to the smallest interatomic distance Si-O1 in comparison to K2 and K3. For comparison, the results of previous experimental [11] studies are listed in Table II along

with the present calculated results. There is a good agreement between the theory and experimental results thus establishing the validity of present calculations. The potential energy distribution for each normal mode in Mn_2SiO_4 is also investigated and the two dominant contributions from force constant are given in the results. The assignment of specific modes have been made observing the atomic displacements in the eigen vectors.

TABLE II. CALCULATED AND EXPERIMENTAL RAMAN ACTIVE WAVENUMBERS (in cm^{-1}) FOR Mn_2SiO_4

Mode	Expt [11]	Present result	Two dominant contribution as per PED
A_g	935	944	K1-40%, K2-29%
	840	853	K3-57%, K2-24%
	808	812	K1-40%, K2-11%
	575	565	H1-33%, K10-13%
	515	511	H2-48%, K13-9%
	389	408	H3-23%, K13-13%
	291	318	H6-19%, K8-12%
	256.	283	K13-21%, K9-15%
	244	247	K8-30%,K10-15%
	167	182	H7-27%, K7-24%
	124	129	K7-21%, K8-15%
B_{1g}	-	942	K1-41%, K2-30%
	-	858	K3-52%, K2-27%
	820	819	K1-39%, K3-16%
	588	560	H1-31%, K10-14%
	546	530	H2-50%, K13-8%
	393	403	H3-31%, H4-15%
	307	312	K7-18%, H6-15%
	288	273	K9-18%, H8-10%
	271	253	H8-21%, K13-12%
	203	192	H7-28%, H6-14%
	155	168	K7-31%, H7-12%
B_{2g}	-	882	K2-82%, K11-3%
	553	550	H1-43%, K10-24%
	401	427	H4-37%, K12-17%
	319	338	H5-29%, K8-19%
	274	288	K13-21%, K12-13%
	188	186	K8-37%, K9-30%
	119	123	H11-20%, K14-12%
B_{3g}	892	866	K2-84%, K10-4%
	555	548	H1-45%, K10-24%
	378	395	H4-36%, K11-21%
	304	318	H7-26%, K8-28%
	276	279	K9- 29%, K13-14%
	223	226	K8-20%, K15-13%
	137	165	H5-25% , K14-20%

The inferences drawn from the PED are described below: It is quite evident from Table II that the highest frequencies i.e., $944cm^{-1}$, $853cm^{-1}$, $812cm^{-1}$ in A_g mode, $942cm^{-1}$, $858cm^{-1}$, $819cm^{-1}$ in B_{1g} mode, $882cm^{-1}$ in B_{2g} mode and $866cm^{-1}$ in B_{3g} mode has the dominant contribution of Si-O stretching interaction i.e K1, K2 and K3. This result is in confirmation with the inferences drawn by Mouri et al. [10] and Stidham et al. [11]. It has been observed that the M-site cations do not participate in the higher frequency modes. A close look at the reveals that identical results are obtained for the highest infrared wavenumbers in each mode and is attributable mainly due to the Si-O stretching. All the middle order frequencies lying between 400 cm^{-1} to 565 cm^{-1} i.e. $565cm^{-1}$, $511cm^{-1}$, $408cm^{-1}$ in A_g mode, 560 cm^{-1}, $530cm^{-1}$, $403cm^{-1}$ in B_{1g} mode, $550cm^{-1}$, $427cm^{-1}$ in B_{2g} mode and $548cm^{-1}$ and $395cm^{-1}$ in B_{3g} are mainly contributed by O-Si-O bending force constants given by H1, H2, H3 and H4. Thus we find that all the frequencies > 400 cm^{-1} are associated with the internal vibrations within the SiO_4 tetrahedron. The frequencies < 400 $cm^{-1}$are low frequency modes which have the contribution of multiple force constants (K4 to K15 and H5 to H10). These frequencies are due to Mn-O stretching force and O-O repulsive force among SiO_4 tetrahedra. These modes are external vibrations which involve the rotation and translation of SiO_4 tetrahedra and Mn cations. As per our knowledge no other theoretical data is available to compare the calculated infrared Raman and infrared wavenumbers. A precise determination of infrared wavenumbers is required to further establish the present results.

TABLE III. CALCULATED AND EXPERIMENTAL INFRARED ACTIVE WAVENUMBERS (in cm^{-1}) FOR Mn_2SiO_4

Mode	Expt [11]	Present result	Two dominant contribution as per PED
B_{1u}	875	883	K2-81%, K10-4%
	480	500	H1-46%, K10-26%
	430	437	H4-32%, K11-17%
	350	365	H5-22%, K6-20%
	-	306	K5-31%, H10-26%
	300	283	K5-39%, H10-18%
	240	228	H10-34%, K6-17%
	187	172	H9-31%, K13-19%
	-	129	K6-24%, K5-16%
B_{2u}	945	931	K1-45%, K2-33%
	860	884	K3-51%, K2-20%
	816	801	K1-29%, K3-22%
	-	564	H1-30%, K10-11%
	512	514	H2-40%, H10-13%
	454	440	H3-22%, K13-11%
	-	373	K12-18%, K6-14%
	340	322	H9-31%, H10-19%
	276	283	K4-31%, H6-15%
	242	236	H8-26%, K7-23%
	-	198	K7-23%, H7-29%
	157	164	K5-25%, H9-14%
	-	100	H8-24%, H5-16%
B_{3u}	950	934	K1-47%, K2-34%
	912	889	K3-53%, K2-20%
	815	792	K1-30%, K2-19%
	562	550	H1-32%, K10-14%
	490	502	H2-42%, K10-11%
	-	444	H3-22%, K13-14%
	-	378	K5-24%, H10-17%,
	365	341	H10-32%, K7-12%
	297	273	H7-20%, H8-15%
	-	204	K4-33%, H9-24%
	-	188	K6-33%, K5-20%
	177	174	K12-20%, K5-17%
	-	129	K5-22%, K14-15%

IV. CONCLUSION

Normal coordinate analysis has been performed on Mn_2SiO_4 olivine to calculate the Raman and the infrared wavenumbers with twenty five short range force constants. It was found that the higher order frequencies are mainly contributed SiO_4 tetrahedra while the lower frequencies are dominated by Mn atoms. Eigen vectors associated with Raman and infrared frequencies for tephroite has also been determined. The theoretical results are found to be in good agreement with experimental observed values. The contribution of each force constant has been determined from the potential energy distribution towards the different vibrational modes.

REFERENCES

[1] W. Deer, R. Howie and J. Zussman, 1992. An Introduction to the Rock Forming Minerals. John Wiley, New York.
[2] A.M. Dziewonski, A.L. Hales and E.R. Lapwood, "Parametrically Simple Earth Models Consistent With Geophysical Data", Physics of earth and planetary interiors,vol 10 (1), pp. 12–48, 1975.
[3] S. Ni, L. Chou and J. Chang, "Preparation and characterization of Forsterite (Mg2SiO4) bioceramics", Ceram Int., vol 33, pp. 83-88, 2007.
[4] M. Kharaziha and M.H. Fathi, "Improvement of mechanical properties and biocompatibility of forsterite bioceramic addressed to bone tissue engineering materials", J. Mech. Behav. Biomed. Mater., vol 3(7), pp. 530-537, 2010.
[5] R. Pawley, "The reaction talc + forsterite = enstatite +H_2O; new experimental results and petrological implications.", Am. Mineralogist, vol 83 (1), pp. 51–57,1998.
[6] N. Maliavski, O. Dushkin and J. Markina, "Forsterite powder prepared from water soluble hybrid precursor", AIChE J., vol 43 (11A), pp. 2832–2836, 1997.
[7] Y. Kudoh and H.Takeda, "Single crystal X-ray diffraction study on the bond compressibility of fayalite, Fe_2SiO_4 and rutile, TiO_2 under high pressure", Physica B + C, vol 139, pp. 333-336, 1986.
[8] A. M. Hofmeister and K. M. Pitman, "Evidence for kinks in structural and thermodynamic properties across the forsterite- fayalite binary from thin- film IR absorption spectra" , Phys Chem Miner, vol 34, pp. 319-333, 2007.
[9] E. Dachs, C. Geiger, V.von Seckendorff and M. Grodzicki, " A low temperature calorimetric study of synthetic (forsterite-fayalite) {(Mg_2SiO_4-Fe_2SiO_4)} solid solutions: An analysis of vibrational, magnetic and electronic contributions to the molar heat capacity and entropy of mixing", J. Chem Thermodyn, vol 39, pp. 906-933, 2007.
[10] T. Mouri and M. Enami, "Raman spectroscopic study of olivine-group material", Journal of Minerological and Petrological Sciences, vol 103, pp.100–104, 2008.
[11] H.D. Stidham, , J.B. Bates and C.B. Finch,"Vibrational spectra of synthetic single crystal tephroite, Mn_2SiO_4", Journal of Physical Chemistry, vol 80, pp.1226-1234,1976.
[12] T. Shimanouchi, , M. Tsuiboi and T. J. Miyazawa, "Optically active lattice vibrations as treated by the GF-matrix method", Chem. Phys, vol 35, pp.1597-1609, 1961.
[13] K. Fujino, S. Sasaki, Y. Takeuchi and R. Sadanaga, "X-ray determination of electron distributions in forsterite, fayalite, and tephroite", Acta Crystallographica, vol B37, pp. 513-518, 1981.

To Investigate the Role of Thermal Spray Coating in Biomaterials for Combating the Rate of Corrosion In-Vitro

Sarbjit Kaur
Research Scholar
IKGPTU
Kapurthala

Niraj Bala
Mechanical Engg. Deptt.
BBSBEC, Fatehgarh Sahib, India

Charu Khosla
Associate Prof.
Deptt. Applied Sciences
Chitkara University, Banur

Rohit Upadhyaya
Birla institute of Tech. and Sci. Pilani

***Abstract*—A bio-implant is a medical device made to replace and act as a missing biological structure These implants are broadly used in various biomedical applications such as surgical implants, including joints, total hips, knees and dentures. The aim of the present study is to evaluate in-vitro corrosion behavior of uncoated as well as thermal sprayed hydroxyapatite (HAP) coated 316LStainless steel. The economical technique for reducing the rate of corrosion and improves the bioactivity of these existing materials is considered to be Surface modification. Hydroxyapatite (HAP) coatings are used on these alloys to improve the characteristics such as biocompatibility, bone bonding ability and also reduces the toxic effect of bioimplants on living organism. The coating was characterized by electrochemical techniques and SEM/EDS. The results show that after the deposition of the HAP coating, the corrosion resistance of the steel increases. This property of enhanced corrosion resistance is used as a promising technology in biomaterial research and for many clinical applications.**

Keywords: 316L SS, HAP, in-vitro, corrosion, biocompatibility.

I. INTRODUCTION

Biomaterials are used to make devices to implant a part or a function of the body in safe, reliably economically, and physiologically acceptable manner. A huge variety of such devices and materials are used in the treatment of disease or injury including oral and dental implants.

Material of medical instrument, coating, and implant must be corrosion resistant and should tolerate the aggressiveness of biological fluids (blood, urine, lymph, gastric juice, etc.). Long-term exposure of implant material to living tissue should not exert toxic impact. No toxic effect should be observed during even short-term contact of medical instrument with living tissues. Medical instruments should not induce carcinogenesis, mutagenesis, or cytotoxicity during prolonged exposure. The metals or their alloys are not viable to be directly implanted in human body due to corrosion. Due to secretion of some metallic ions (like Fe^{+2}) in vicinity of these organs, it may lead to fibrosis, which is not suitable for body. So the base metal should be coated with materials whose composition be quite similar to that of bones and are biocompatible which may lead to the further growth and development of bones [1]. The coating material should be bioactive and bioresorable. Hydroxyapatite or Calcium phosphate are frequently used for coating. HAP is commonly used as the coating material because it shows bioactivity, bioresorbility, biocompatibility and also the ossoinduction [2].

HAP coating on metallic alloys enhances the bone bonding ability and also improves the biocompatibility and reduces the toxic effect of bioimplants on living organism. The implanted material is accepted to withstand applied physiological forces without any major change. In addition these coatings leads to biocompatibility, provides local source of calcium and phosphate ions required for bone cell to grow [3,4]. Plasma spray technique is generally used for deposition of HAP as a bioceramic but due to the inherent high temperature in the plasma, detrimental effects such as evaporation, phase altercation, residual stress, debonding etc., commonly occur in these coatings. Present study presents a novel approach to deposit HAP at a temperature below its melting point using thermal spray technique. The phase composition of the HAP deposited by the thermal process is identical to that of the powder has been been analysed by SEM/EDS. The HAP Coatings deposited using this process hold enormous potential for improving ossoinduction of bones in wide range of dental and orthopedic implants with technological basis. Hydroxyapatite ($Ca_{10}(PO4)_6(OH)_2$, has been widely used in dental and orthopedic implants, due to its structural and chemical similarity with bone minerals [5-7]. Nowadays, in order to increase the biocompatibility and to improve the performance, surface modification of implants has been carried out successfully. Biological response of the host depends on the primary interactions of biomaterials implanted at biological molecular surfaces. Therefore, the surface morphology influence the compatibility as well as the optimal performance of the implant in body [8].

II. EXPERIMENTAL SET UP

2.1 Feedstock Powder and Substrate

Metals like 316LSS, Ti-6V-4Al are most commonly used alloys as biomaterial. Due to low cost and high corrosion resistance 316LSS is mostly used .It has a very low Carbon content as compared to normal steel. The composition of 316LSS is as follows:

Table I: Chemical composition specification values in % according to ASTM A276 grade

Elements	Percentage
C	≤ 0.03
Mn	≤ 2.0
Si	≤ 1.00
P	0.045
S	≤ 0.030
Cr	16.0-18.0
Mo	2.0-3.0
Ni	10.0-14.0

2.2 Development of Coatings

The Captal 30, HAP powder (Plasma-Biotal, Tides well, UK) of 30µm average particle size was used in this study. The air blasted 316L SS specimens were then coated with the HAP powder using a flame spray system (CERAJET) at Metalizing Equipment Company Private Limited (MECPL), Jodhpur, India**.** CERAJET is a technique of MECPL, chiefly designed for ceramic coatings. In conventional flame spraying systems, the particle velocity is less than 100m/s, however the particle velocity of CERAJET is ≈300m/s and the temperature of oxyacetylene flames is ≈ 2700°C, while in case of plasma spray technique, the temperature is ≈12000^0C, so working temperature is much lower than the plasma spraying technique. The spraying parameters used in coatings are given in Table II.

Table II: Thermal spray process parameters for HAP coatings spraying parameters value.

Spraying parameter	Value
Acetylene flow rate (l/ min^1)	73
Oxygen flow rate (l/min)	44
Air pressure (kg/cm^2)	4.5
Powder feed rate (g/min)	15
Spray distance (cm)	10

2.3 Electrochemical corrosion studies

To analyze the electrochemical corrosion behavior of the uncoated and HAP coated 316LSS specimens, Potentiostat/Galvanostat (Series G-750; Gamry Instruments, Inc. USA), interfaced with a computer and loaded with Gamry electrochemical software DC105, potentiodynamic polarization tests were conducted. Ringer's solution has been used as electrolyte for simulating body fluid (SBF) with chemical composition (in g/l) as, and at pH 7.2.

Table III: Chemical composition of ringer solution

Component	Strength (in g/l)
NaCl	9
$CaCl_2$	0.24
KCl	0.43
$NaHCO_3$	0.2

Before conducting the corrosion studies, each sample was immersed in Ringer's solution (SBF)for 24 hours for stabilization at 37 ± 1˚C, as the normal temperature of the human body, maintained using a heating mantle. The exposed area of the samples in the Ringer's solution was $1cm^2$. A graphite rod served as the counter electrode and a saturated calomel electrode (SCE) as reference electrode, all the potentials were measured with respect to SCE. Fresh Ringer solution was used for each specimen and the scan rate was 1mv/s. The specimen forms the working electrode. Tafel/Elog plots sweeping potential from -250 mV to +250 mV relative to open circuit potential, all the electrochemical tests were carried out on various samples as at least three similar results were required to ensure the reproducibility of the result. Before and after corrosion testing, the specimens were further analyzed by SEM/EDS techniques to analyse the microstructure/ composition and phase formation respectively.

III. RESULTS AND DISCUSSION

3.1 Electrochemical Polarization Behavior

The electrochemical corrosion behaviour of the bare and HAP coated steel was carried out using the procedure discusses in Section 2.3. The potentio-dynamic curves of bare and flame-sprayed HAP coated 316LSS specimens in Ringer's solution (SBF) for 24 hours for stabilization at 37±1˚C temperature (body temperature) were obtained and are shown in Fig. 1 and 2, respectively.

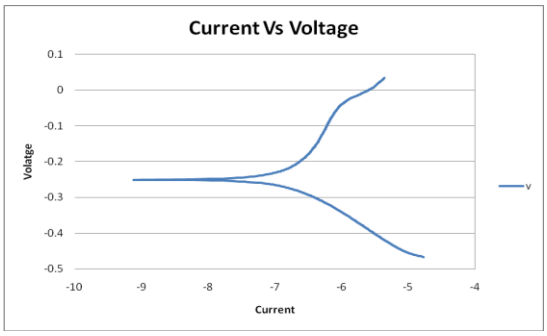

Fig.1 Potentio-dynamic curves of uncoated 316L SS specimens in Ringers solution at 37 ± 1˚C

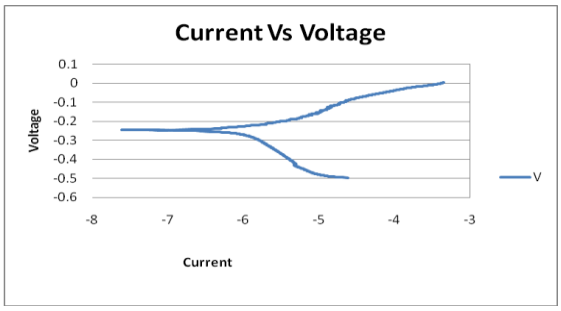

Fig.2 Potentio-dynamic curves of flame-spray HAP coated 316L SS specimens in Ringers solution at 37 ± 1˚C

Table IV: Corrosion parameters of coated and uncoated 316LSS in ringer solution at 37±1°C temperature.

Parametres	Uncoated 316 LSS	HAP coated 316 LSS
ECorr e^{-6} (mV)	-372.1	-245
ICorr (Acm-2)	3.460	1.002
CR e^{-3} (mpy)	1485	451.8

The results of Tafel slope values (Table IV), show that corrosion current density of un-coated 316LSS specimen in Ringer's solution (ICorr = 3.460Acm^{-2}, ECorr= -372.1e^{-6} mV) is higher than of the coated specimen. The polarization curve, for the un-coated 316L SS specimen got shifted towards the right in comparison to the other specimen. The shift of polarization curves of HAP coated 316L SS to lower ICorr values shows a lower tendency towards corrosion in comparison with the uncoated specimen. The higher the corrosion current density (ICorr) at a given potential, more prone is the material to corrode. HAP coatings have shown a minimum corrosion current density (ICorr = 1.002 Acm^{-2}, ECorr = -245e^{-6}mV) as compared to uncoated sample. Corrosion rate (C_R=451.8mpy) of coated sample is lower as compare to uncoated sample (C_R=1485mpy).

3.2 SEM /EDS analysis

The HAP powder was successfully deposited by Flame spray technique on 316L SS. The SEM microstructure of HAP coating on 316LSS has been shown in Fig. 3. As clear from the micrograph the coating show the presence of spherical shaped particles along with well-flattened splats. EDS analysis confirms the presence of Ca, P and O elements in the HAP coated samples. The SEM/EDS micrograph after corrosion testing has been represented in Fig. 4. A comparison of the SEM micrographs of the as-sprayed and exposed HAP coatings showed that the coating has retained its morphology even after exposure to the corrosion testing, which is a positive attribute. Ca and P have been detected as the predominant elements in the coatings.

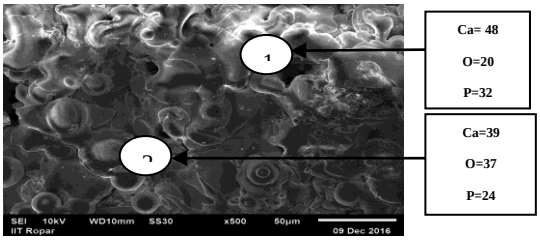

Fig.3 SEM analysis along with EDS point analysis showing the elemental composition of as-sprayed HAP coating on 316LSS.

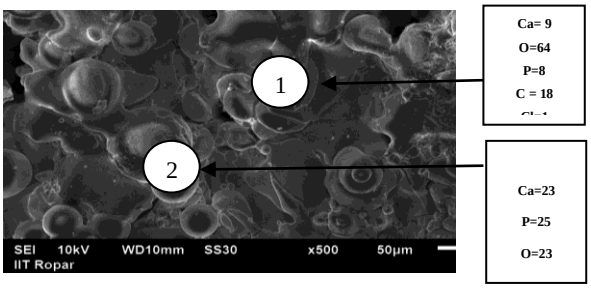

Fig.4. SEM analysis along with EDS point analysis showing the elemental composition of flame-sprayed HAP coating on 316LSS after corrosion testing.

Table V: Ca/P Ratio of flame sprayed HAP coating at selected points.

Fig no	HAP coating	Point 1	Point 2
Fig 3	Ca/P ratio	1.5	1.62
Fig 4	Ca/P ratio	1.12	0.92

The calculated Ca/P ratio from EDS spectra for the flame sprayed HAP coating before and after corrosion testing are tabulated in Table V. The observed different Ca/P ratios confirm the presence of different calcium phosphate compounds in both the HAP coating. The results indicate reduction in Ca/P ratios in the coated specimen after immersion testing. The Ca/P ratio is less in case of sample immersed in ringer solution as O is present in this case.

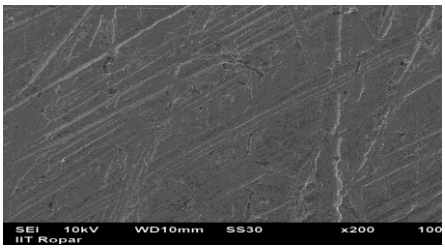

FIG 5. SEM Analysis Of Uncoated 316LSS After Corrosion Testing

In uncoated sample, there are formation of various ferrous oxides. Formation of uniform oxide layer over the surface covers whole the surface. The SEM micrograph for the uncoated 316LSS after corrosion testing has been shown in Fig. 5.

IV. CONCLUSION

In this present paper, a specially designed flame spraying equipment was used to carry out HAP coatings on 316LSS implant material. The following conclusions have been drawn from the study:

A. Using CERAJET flame spraying apparatus, HAP powder was deposited successfully on 316LSS.

B. The electrochemical study revealed an improvement in the corrosion resistance of the 316LSS by deposition of HAP by flame spray technique after immersion in simulated human body fluid.

C. EDS analysis confirmed the presence of the of Ca, P and O in the as-sprayed coating.

D. No cracks were found on the surface of HAP coated specimens even after immersion in Ringer's solution.

The supremacy of O in exposed coatings indicated the onset of oxidation which leads to corrosion. EDS mapping observations confirm that the coating was successful to retain their adherence even after corrosion testing. Future in-vivo studies of flame-spray HAP and 316LSS and further complete analysis of these results can help in assessing their use in clinical applications

V. ACKNOWLEDGMENT

Authors express their earnest thanks to Dr. Harpreet Singh, Associate Professor, School of Mechanical, Materials and Energy Engineering, Indian Institute of Technology, Roopnagar (Punjab) and Metallizing equipment industry, Jodhpur for their kind co-operation during this research work.

REFERENCES

[1] W Bonfield and Tanner K. E. (1997), "Biomaterials: A New Generation", Materials World, Vol. 5, pp 18-20.

[2] L.L Hench CRC Handbook of Bioactive Ceramic Vol. 1s, . (1982), CRC Press, Boca Raton.

[3] Manso M., Jimenez C., Morant C, Herrero P., Mar-Tinez-Duart J.M., "Electrodeposition of Hydroxyapatite Coatings in Basic Conditions", Biomaterials, Vol. 2, pp 1755-1761, 2000.

[4] Haddow D. B., Kothari S., James P. F., Short R.D., "The Formation and Characterization of Sol-Gel Titania Films", Biomaterials, Vol. 17, pp 501-507, 1996

[5] Y. C. Tsui, C. Doyle and T. W. Clyne, Plasma sprayed hydroxyapatite coatings on titanium substrates Part 1:Mechanical properties and residual stress levels, *Biomaterials*, **19**(22), p 2015-2029, 1998.

[6] L. Sun, C.C. Berndt, K.A. Gross, A.K. Material fundamentals and clinical performance of plasma sprayed hydroxyapatite coatings: A review, *J. Biomed. Mater. Res. Part B: Appl. Biomaterials*, **58**(5), p 570 – 592, 2001.

[7] P.K Stephenson, M.A Freeman, P. A Revell, J. Germain, M. Tuke, C.J Pirie. The effect of hydroxyapatite coating on in growth of bone into cavities in an implant, *Journal of Arthroplasty*, **6**(1), p 51-58, 1991.

[8] T. Shirzadian, S. Bagheri, H. Saeidiborojeni, and P. Ghaffari, "The role of biocompatible coatings of biomaterials for creation of direct and appropriate chemical bounding between bioimplant and bone tissue ," vol. 4, no. 39, 2012.

Dynamical Behaviors of Discrete-time Prey-Predator System

Harkaran Singh
Department of Applied Sciences,
Khalsa College of Engineering and Technology,
Amritsar-143001, Punjab, India

H.S. Bhatti
Department of Applied Sciences,
B.B.S.B. Engineering College,
Fatehgarh Sahib, Punjab, India

***Abstract*—In the present study, the dynamical behaviors of discrete-time prey-predator system. Global stability of the model at the fixed points has been discussed. The specific conditions for existence of flip bifurcation and Hopf bifurcation have been derived by using center manifold theorem and bifurcation theory. To analyse our results, numerical simulations have been carried out.**

***Keywords*—Prey-predator system, Center manifold theorem, Flip bifurcation, Hopf bifurcation, Chaos.**

I. INTRODUCTION

The Prey-Predator model is a topic of great interest for many mathematicians and biologists which starts with the pioneer work of Lotka [1] and Volterra [2]. The dynamic relationship between predators and prey living in the same environment will continue to be one of the important themes in mathematical ecology [3-4]. Many authors [5-11] have suggested that the discrete time models are more appropriate than the continuous ones and provide efficient results when the populations have non-overlapping generations. However, there are few articles [12-18] discussing the dynamical behaviors of discrete-time predator–prey models by involving bifurcations and chaos phenomena.

In the present study, we investigated the dynamical behaviors of discrete-time prey-predator model by involving bifurcations and chaos phenomena. This paper is organized as follows: In Section 2, we obtained the fixed points of the discrete-time model and discussed the stability criterion of the discrete-time model at fixed points. In Section 3, the specific conditions of existence of flip bifurcation and Hopf bifurcation have been derived. In Section 4, to analyse our results, numerical simulations have been carried out and further discussion on the period doubling bifurcation and chaotic behavior has been carried out.

The discrete-time prey-predator model [19] is

$$\begin{cases} \frac{dx}{dt} = x(a - cx) - lxy, \\ \frac{dy}{dt} = y(-b - dy) + mxy, \end{cases} \tag{1.1}$$

where x and y represents the densities of prey and predator respectively; a, l, b, m denotes the intrinsic growth rate of prey, capture rate, death rate of predator and the conversion rate respectively; and c, d denotes the intra-specific competition coefficients of prey and predator respectively.

Applying forward Euler's scheme to the system of equations (1.1), we obtain the system as

$$\begin{cases} x \to x + \delta[x(a - cx) - lxy], \\ y \to y + \delta[y(-b - dy) + mxy]. \end{cases} \tag{1.2}$$

II. STABILITY OF THE FIXED POINTS

The fixed points of the system (1.2) are $O(0,0), A\left(\frac{a}{c}, 0\right), B(x^*, y^*)$,

where $x^* = \frac{ad+bl}{lm+cd}, y^* = \frac{am-bc}{lm+cd}$.

The jacobian matrix of (1.2) at the fixed point (x, y) is given by

$$J = \begin{bmatrix} 1 + \delta(a - 2cx - ly) & -l\delta x \\ \delta my & 1 + \delta(-b - 2dy + mx) \end{bmatrix}.$$

The characteristic equation of the jacobian matrix can be written as

$$\lambda^2 + p(x, y)\lambda + q(x, y) = 0, \tag{2.1}$$

where

$$p(x, y) = -trJ = -2 - \delta a + \delta b + \delta x(2c - m) + \delta y(l + 2d),$$

$$q(x, y) = detJ = [1 + \delta(a - 2cx - ly)][1 + \delta(-b - 2dy + mx)] + \delta^2 lmxy$$

Lemma 2.1: Let $F(\lambda) = \lambda^2 + B\lambda + C$. *Suppose that* $F(1) > 0$, λ_1 *and* λ_2 *are roots of* $F(\lambda) = 0$. *Then*

(i) $|\lambda_1| < 1$ *and* $|\lambda_2| < 1$ *if and only if* $F(-1) > 0$ *and* $C < 1$;

(ii) $|\lambda_1| < 1$ *and* $|\lambda_2| > 1$ *(or* $|\lambda_1| > 1$ *and* $|\lambda_2| < 1$*) if and only if* $F(-1) < 0$;

(iii) $|\lambda_1| > 1$ *and* $|\lambda_2| > 1$ *if and only if* $F(-1) > 0$ *and* $C > 1$;

(iv) $\lambda_1 = -1$ *and* $|\lambda_2| \neq 1$ *if and only if* $F(-1) = 0$ *and* $B \neq 0, 2$*;*

(v) λ_1 *and* λ_2 *are complex and* $|\lambda_1| = |\lambda_2| = 1$ *if and only if* $B^2 - 4C < 0$ *and* $C = 1$.

Let λ_1 and λ_2 be the roots of eq. (2.1), which are known as eigen values of the fixed point (x, y). Then (x, y) is called a sink or locally asymptotically stable if $|\lambda_1| < 1$and $|\lambda_2| < 1$. (x, y) is called a source or locally unstable if $|\lambda_1| > 1$ and $|\lambda_2| > 1$. (x, y) is non-hyperbolic if either $|\lambda_1| = 1$ or $|\lambda_2| = 1$. (x, y) is called a saddle if $|\lambda_1| > 1$ and $|\lambda_2| < 1$ (or $|\lambda_1| < 1$ and $|\lambda_2| > 1$). (see [11])

Proposition 2.2. *The fixed point* $O(0,0)$ *is source if* $\delta > \frac{2}{b}$*, saddle if* $0 < \delta < \frac{2}{b}$*, and non-hyperbolic if* $\delta = \frac{2}{b}$.

It has been observed that when $\delta = \frac{2}{b}$, one of the eigen values of the critical point $O(0,0)$ is -1 and magnitude of other is not equal to 1. Thus the flip bifurcation occur when parameter changes in small neighborhood of $\delta = \frac{2}{b}$.

Proposition 2.3. *There exists different topological types of* $A\left(\frac{a}{c}, 0\right)$ *for possible parameters.*

(i) $A\left(\frac{a}{c}, 0\right)$ *is sink if* $bc > am$ *and* $0 < \delta < min\left\{\frac{2}{a}, \frac{2c}{bc-am}\right\}$.

(ii) $A\left(\frac{a}{c}, 0\right)$ *source if* $bc > am$ *and* $\delta > max\left\{\frac{2}{a}, \frac{2c}{bc-am}\right\}$.

(iii) $A\left(\frac{a}{c}, 0\right)$ *is non-hyperbolic if* $\delta = \frac{2}{a}$ *or* $\delta = \frac{2c}{bc-am}$ *and* $bc > am$.

(iv) $A\left(\frac{a}{c}, 0\right)$ *is saddle for all values of the parameters, except for that which lies in (i) to (iii).*

The term (iii) of proposition 2.3 implies that the parameters lie in the set

$$F_A = \left\{(a, b, c, m, \delta), \delta = \frac{2}{a}, \delta \neq \frac{2c}{bc-am} \text{ and } bc \neq am, a, b, c, m, \delta > 0\right\}.$$

If the term (iii) of proposition 2.3 holds, than one of the eigen values of the fixed point $A\left(\frac{a}{c}, 0\right)$ is -1 and magnitude of other is not equal to 1. The point $A\left(\frac{a}{c}, 0\right)$ undergoes flip bifurcation when the parameter changes in small neighbourhood of F_A.

Proposition 2.4. *When* $am > bc$*, there exists different topological types of* $B(x^*, y^*)$, where $x^* = \frac{ad+bl}{lm+cd}, y^* = \frac{am-bc}{lm+cd}$ *for all possible parameters.*

(i) $B(x^*, y^*)$ *is sink if either condition (i.1) or (i.2) holds:*

(i.1) $0 < \delta < \frac{N-\sqrt{M}}{(ad+bl)(am-bc)}, M \geq 0.$

(i.2) $0 < \delta < \frac{N}{(ad+bl)(am-bc)}$, $M < 0,$

where $N = acd + adm + bcl - bcd$ and $M = N^2 - 4(ad + bl)(am - bc)(lm + cd)$.

(ii) $B(x^*, y^*)$ *is source if either condition (ii.1) or (ii.2) holds:*

(ii.1) $\delta > \frac{N+\sqrt{M}}{(ad+bl)(am-bc)}$, $M \geq 0.$

(ii.2) $\delta > \frac{N+\sqrt{M}}{(ad+bl)(am-bc)}$, $M < 0.$

(iii) $B(x^*, y^*)$ *is non-hyperbolic if either condition (iii.1) or (iii.2) holds:*

(iii.1) $\delta = \frac{N\pm\sqrt{M}}{(ad+bl)(am-bc)}, M \geq 0.$

(iii.2) $\delta = \frac{N\pm\sqrt{M}}{(ad+bl)(am-bc)}, M < 0.$

(iv) $B(x^*, y^*)$ *is saddle for all values of the parameters, except for that which lies in (i) to (iii).*

From lemma (2.1), it has been observed that one of the eigen values of the fixed point $B(x^*, y^*)$ is -1 and magnitude of other is not equal to 1, if the term (iii.1) of proposition 2.4 holds. The term (iii.1) of proposition 2.4 may be written as follows:

$$F_{B1} = \left\{(a, b, c, d, l, m): \delta = \frac{N-\sqrt{M}}{(ad+bl)(am-bc)}, M \geq 0, am - bc > 0, a, b, c, d, l, m > 0\right\}, \quad F_{B2} = \left\{(a, b, c, d, l, m): \delta = \frac{N+\sqrt{M}}{(ad+bl)(am-bc)}, M \geq 0, am - bc > 0, a, b, c, d, l, m > 0\right\},$$

where $N = acd + adm + bcl - bcd$ and $M = N^2 - 4(ad + bl)(am - bc)(lm + cd)$.

From lemma (2.1), it has been observed that the eigen values of the fixed point $B(x^*, y^*)$ as a pair of conjugate complex numbers with modulus 1, if the term (iii.2) of

proposition 2.4 holds. The term (iii.2) of proposition 2.4 may be described as follows:

$$H_B = \left\{(a,b,c,d,l,m): \delta = \frac{N}{(ad+bl)(am-bc)}, M < 0, am - bc > 0, a,b,c,d,l,m > 0\right\}.$$

III. BIFURCATION BEHAVIOR

In this section, we study the flip bifurcation and Hopf bifurcation at the fixed point $B(x^*, y^*)$.

III.1 FLIP BIFURCATION

Consider the system (1.2) with arbitrary parameter $(a_1, b_1, c_1, d_1, l_1, m_1, \delta_1) \in F_{B1}$, which is described as follows:

$$\begin{cases} x \to x + \delta_1[x(a_1 - c_1 x) - l_1 xy], \\ y \to y + \delta_1[y(-b_1 - d_1 y) + m_1 xy]. \end{cases} \quad (3.1)$$

Eq. (3.1) has fixed point B(x^*, y^*), whose eigen values are $\lambda_1 = -1, \quad \lambda_2 = 3 - \frac{\delta_1(a_1c_1d_1 + a_1d_1m_1 + b_1c_1l_1 - b_1c_1d_1)}{(l_1m_1 + c_1d_1)}$ with $|\lambda_2| \neq 1$ by proposition (2.4), where $x^* = \frac{a_1d_1 + b_1l_1}{l_1m_1 + c_1d_1}$, $y^* = \frac{a_1m_1 - b_1c_1}{l_1m_1 + c_1d_1}$ and

$$\delta_1 = \frac{N_1 - \sqrt{M_1}}{(a_1d_1 + b_1l_1)(a_1m_1 - b_1c_1)}.$$

where $N_1 = a_1c_1d_1 + a_1d_1m_1 + b_1c_1l_1 - b_1c_1d_1$ and $M_1 = {N_1}^2 - 4(a_1d_1 + b_1l_1)(a_1m_1 - b_1c_1)(l_1m_1 + c_1d_1)$.

Consider the perturbation of (3.1) as below:

$$\begin{cases} x \to x + (\delta_1 + \delta^*)[x(a_1 - c_1 x) - l_1 xy], \\ y \to y + (\delta_1 + \delta^*)[y(-b_1 - d_1 y) + m_1 xy], \end{cases} \quad (3.2)$$

where $|\delta^*| \ll 1$ is a limited perturbation parameter.

Let $u = x - x^*$ and $v = y - y^*$.

After transformation of the fixed point $B(x^*, y^*)$ of map (3.2) to the point (0, 0), we obtained

$$u \to a_{11}u + a_{12}v + a_{13}uv + a_{14}u^2 + b_{11}\delta^*u + b_{12}\delta^*v + b_{13}\delta^*uv + b_{14}\delta^*u^2 \quad \text{and} \quad v \to a_{21}u + a_{22}v + a_{23}uv + a_{24}v^2 + b_{21}\delta^*u + b_{22}\delta^*v + b_{23}\delta^*uv + b_{24}\delta^*v^2, \quad (3.3)$$

where

$$a_{11} = 1 + \delta_1[a_1 - 2c_1x^* - l_1y^*], \quad a_{12} = -l_1\delta_1x^*, \quad a_{13} = -l_1\delta_1, \quad a_{14} = -c_1\delta_1,$$

$$b_{11} = a_1 - 2c_1x^* - l_1y^*, \quad b_{12} = -l_1x^*, \quad b_{13} = -l_1, \quad b_{14} = -c_1,$$

$$a_{21} = m_1\delta_1y^*, \quad a_{22} = 1 + \delta_1[-b_1 - 2d_1y^* + m_1x^*], \quad a_{23} = m_1\delta_1, \quad a_{24} = -d_1\delta_1,$$

$$b_{21} = m_1y^*, \quad b_{22} = -b_1 - 2d_1y^* + m_1x^*, \quad b_{23} = m_1, \quad b_{24} = -d_1.$$

Consider the following translation:

$$\begin{pmatrix} u \\ v \end{pmatrix} = T\begin{pmatrix} \tilde{x} \\ \tilde{y} \end{pmatrix},$$

where $T = \begin{pmatrix} a_{12} & a_{12} \\ -1 - a_{11} & \lambda_2 - a_{11} \end{pmatrix}$.

Taking T^{-1} on both sides of eq. (3.3), we get

$$\begin{pmatrix} \tilde{x} \\ \tilde{y} \end{pmatrix} \to \begin{pmatrix} -1 & 0 \\ 0 & \lambda_2 \end{pmatrix}\begin{pmatrix} \tilde{x} \\ \tilde{y} \end{pmatrix} + \begin{pmatrix} f(u,v,\delta^*) \\ g(u,v,\delta^*) \end{pmatrix}, \quad (3.4)$$

where

$$f(u,v,\delta^*) = \frac{[a_{13}(\lambda_2 - a_{11}) - a_{12}a_{23}]uv}{a_{12}(\lambda_2+1)} + \frac{[a_{14}(\lambda_2 - a_{11})]u^2}{a_{12}(\lambda_2+1)} - \frac{a_{12}a_{24}v^2}{a_{12}(\lambda_2+1)} + \frac{[b_{11}(\lambda_2 - a_{11}) - a_{12}b_{21}]\delta^*u}{a_{12}(\lambda_2+1)} + \frac{[b_{12}(\lambda_2 - a_{11}) - a_{12}b_{22}]\delta^*v}{a_{12}(\lambda_2+1)} + \frac{[b_{13}(\lambda_2 - a_{11}) - a_{12}b_{23}]\delta^*uv}{a_{12}(\lambda_2+1)} + \frac{[b_{14}(\lambda_2 - a_{11})]\delta^*u^2}{a_{12}(\lambda_2+1)} - \frac{a_{12}b_{24}\delta^*v^2}{a_{12}(\lambda_2+1)},$$

$$g(u,v,\delta^*) = \frac{[a_{13}(1+a_{11}) + a_{12}a_{23}]uv}{a_{12}(\lambda_2+1)} + \frac{[a_{14}(1+a_{11})]u^2}{a_{12}(\lambda_2+1)} + \frac{a_{12}a_{24}v^2}{a_{12}(\lambda_2+1)} + \frac{[b_{11}(1+a_{11}) + a_{12}b_{21}]\delta^*u}{a_{12}(\lambda_2+1)} + \frac{[b_{12}(1+a_{11}) + a_{12}b_{22}]\delta^*v}{a_{12}(\lambda_2+1)} + \frac{[b_{13}(1+a_{11}) + a_{12}b_{23}]\delta^*uv}{a_{12}(\lambda_2+1)} + \frac{[b_{14}(1+a_{11})]\delta^*u^2}{a_{12}(\lambda_2+1)} + \frac{a_{12}b_{24}\delta^*v^2}{a_{12}(\lambda_2+1)},$$

$$u = a_{12}(x + y), \quad \text{and} \quad v = -(1 + a_{11})x + (\lambda_2 - a_{11})y.$$

Applying center manifold theorem to eq. (3.4) at the origin in limited neighborhood of $\delta^* = 0$. The center manifold $W^c(0,0)$ can be approximately presented as:

$$W^c(0,0) = \left\{(\tilde{x}, \tilde{y}): \tilde{y} = a_0\delta^* + a_1\tilde{x}^2 + a_2\tilde{x}\delta^* + a_3{\delta^*}^2 + O((|\tilde{x}| + |\delta^*|)^3)\right\},$$

where $O((|\tilde{x}| + |\delta^*|)^3)$ is a function with at least third order in variables$(\tilde{x}, \delta^*)$.

By simple calculations for center manifold, we have

$$a_0 = 0,$$

$$a_1 = \frac{[a_{13}(1+a_{11}) + a_{12}a_{23}](1+a_{11}) - a_{12}a_{14}(1+a_{11}) - a_{24}(1+a_{11})^2}{(\lambda_2+1)(\lambda_2+3)},$$

$$a_2 = \frac{-[b_{11}(1+a_{11}) + a_{12}b_{21}]a_{12} + [b_{12}(1+a_{11}) + a_{12}b_{22}](1+a_{11})}{a_{12}(\lambda_2+1)^2},$$

$$a_3 = 0.$$

Now, consider the map restricted to the center manifold $W^c(0,0)$ as below:

$h: \tilde{x} \to -\tilde{x} + h_1\tilde{x}^2 + h_2\tilde{x}\delta^* + h_3\tilde{x}^2\delta^* + h_4\tilde{x}\delta^{*2} + h_5\tilde{x}^3 + O((|\tilde{x}| + |\delta^*|)^4)$, (3.5)

where

$h_1 = \frac{1}{(\lambda_2+1)}\{-(1+a_{11})[a_{13}(\lambda_2 - a_{11}) - a_{12}a_{23}] + a_{12}a_{14}(\lambda_2 - a_{11}) - a_{24}(\lambda_2 - a_{11})^2\}$,

$h_2 = \frac{1}{(\lambda_2+1)}[b_{11}(\lambda_2 - a_{11}) - a_{12}b_{21}] - \frac{1}{a_{12}(\lambda_2+1)}(1 + a_{11})[b_{12}(\lambda_2 - a_{11}) - a_{12}b_{22}]$,

$h_3 = \frac{1}{(\lambda_2+1)}\{[a_{13}(\lambda_2 - a_{11}) - a_{12}a_{23}](\lambda_2 - 2a_{11} - 1)a_2 + 2a_{12}a_{14}(\lambda_2 - a_{11})a_2 + a_{24}(1 + a_{11})(\lambda_2 - a_{11})a_2 + [b_{11}(\lambda_2 - a_{11}) - a_{12}b_{21}]a_1 - [b_{13}(\lambda_2 - a_{11}) - a_{12}b_{23}](1 + a_{11}) + a_{12}b_{14}(\lambda_2 - a_{11}) - b_{24}(1 + a_{11})^2\} + \frac{1}{a_{12}(\lambda_2+1)}[b_{12}(\lambda_2 - a_{11}) - a_{12}b_{22}](\lambda_2 - a_{11})a_1$,

$h_4 = \frac{1}{(\lambda_2+1)}[b_{11}(\lambda_2 - a_{11}) - a_{12}b_{21}]a_2 + \frac{1}{a_{12}(\lambda_2+1)}(\lambda_2 - a_{11})[b_{12}(\lambda_2 - a_{11}) - a_{12}b_{22}]a_2$,

$h_5 = \frac{1}{(\lambda_2+1)}\{[a_{13}(\lambda_2 - a_{11}) - a_{12}a_{23}](\lambda_2 - 2a_{11} - 1)a_1 + 2a_{12}a_{14}(\lambda_2 - a_{11})a_1 + a_{24}(1 + a_{11})(\lambda_2 - a_{11})a_1\}$.

According to Flip bifurcation, the discriminatory quantities γ_1 and γ_2 are given by:

$\gamma_1 = \left(\frac{\partial^2 f}{\partial\bar{x}\partial\delta^*} + \frac{1}{2}\frac{\partial f}{\partial\delta^*}\frac{\partial^2 f}{\partial\bar{x}^2}\right)\Big|_{(0,0)}$,

$\gamma_2 = \left(\frac{1}{6}\frac{\partial^3 f}{\partial\bar{x}^3} + \left(\frac{1}{2}\frac{\partial^2 f}{\partial\bar{x}^2}\right)^2\right)\Big|_{(0,0)}$.

After simple calculations, we obtain $\gamma_1 = h_2$ and $\gamma_2 = h_5 + h_1^2$.

Analyzing above and the flip bifurcation [20], we write a theorem similar to [11] as below:

Theorem 3.1. If $\gamma_2 \neq 0$, and the parameter δ^* alters in the limiting region of the point (0, 0), then the system (3.2) passes through flip bifurcation at the point $B(x^*, y^*)$. Also, the period-2 points that bifurcate from fixed point $B(x^*, y^*)$ are stable (resp., unstable) if $\gamma_2 > 0$ (resp., $\gamma_2 < 0$).

III.2 HOPF BIFURCATION

Consider the system (1.2) with arbitrary parameter $(a_2, b_2, c_2, d_2, l_2, m_2, \delta_2) \in H_B$, which is described as follows:

$$\begin{cases} x \to x + \delta_2[x(a_2 - c_2x) - l_2xy], \\ y \to y + \delta_2[y(-b_2 - d_2y) + m_2xy] \end{cases} \quad (3.6)$$

(3.6) has fixed point $B(x^*, y^*)$, where $x^* = \frac{a_2d_2+b_2l_2}{l_2m_2+c_2d_2}$, $y^* = \frac{a_2m_2-b_2c_2}{l_2m_2+c_2d_2}$ and $\delta_2 = \frac{(a_2c_2d_2+a_2d_2m_2+b_2c_2l_2-b_2c_2d_2)}{(a_2d_2+b_2l_2)(a_2m_2-b_2c_2)}$.

Consider the perturbation of (3.6) as follows:

$$\begin{cases} x \to x + (\delta_2 + \delta)[x(a_2 - c_2x) - l_2xy], \\ y \to y + (\delta_2 + \delta)[y(-b_2 - d_2y) + m_2xy], \end{cases} \quad (3.7)$$

where $|\delta| \ll 1$ is small perturbation parameter.

The characterization equation of map (3.7) at $B(x^*, y^*)$ is given by $\lambda^2 + p(\delta) + q(\delta) = 0$,

where

$p(\delta) = -2 + \frac{(\delta_2+\delta)(a_2c_2d_2+a_2d_2m_2+b_2c_2l_2-b_2c_2d_2)}{(l_2m_2+c_2d_2)}$,

$q(\delta) = 1 - \frac{(\delta_2+\delta)(a_2c_2d_2+a_2d_2m_2+b_2c_2l_2-b_2c_2d_2)}{(l_2m_2+c_2d_2)} + \frac{(\delta_2+\delta)^2(a_2d_2+b_2l_2)(a_2m_2-b_2c_2)}{(l_2m_2+c_2d_2)}$

Since the parameter $(a_2, b_2, c_2, d_2, l_2, m_2, \delta_2) \in H_B$, the eigen values of $B(x^*, y^*)$ are a pair of conjugate complex numbers $\bar{\lambda}$ and λ with modulus 1, where

$\bar{\lambda}, \lambda = \frac{-p(\delta) \mp i\sqrt{4q(\delta) - p^2(\delta)}}{2}$.

Now we have

$|\lambda| = (q(\delta))^{1/2}$,

$l = \frac{d|\lambda|}{d\delta}\Big|_{\delta=0} = \frac{(a_2c_2d_2+a_2d_2m_2+b_2c_2l_2-b_2c_2d_2)}{2(l_2m_2+c_2d_2)} > 0$.

When δ varies in small neighborhood of $\delta = 0$, then $\bar{\lambda}, \lambda = \alpha \mp i\beta$.

Hopf bifurcation requires that when $\delta = 0$, $\bar{\lambda}^n, \lambda^n \neq 1$ $(n = 1, 2, 3, 4)$ which is equivalent to $p(0) \neq -2, 0, 1, 2$.

Since the parameter $(a_2, b_2, c_2, d_2, l_2, m_2, \delta_2) \in H_B$, therefore $p(0) \neq -2, 2$. We only require that $p(0) \neq 0, 1$, which leads to

$(a_2c_2d_2 + a_2d_2m_2 + b_2c_2l_2 - b_2c_2d_2)^2 = j(l_2m_2 + c_2d_2)(a_2d_2 + b_2l_2)(a_2m_2 - b_2c_2), j = 2,3.$ (3.8)

Let $u = x - x^*$ and $v = y - y^*$.

After transformation the fixed point $B(x^*, y^*)$ of map (3.7) to the point (0, 0). We have

$u \to u + (\delta_2 + \delta)[a_2u - 2c_2x^*u - l_2y^*u - c_2u^2 - l_2v(u + x^*)]$ and $v \to v + (\delta_2 + \delta)[-b_2v - 2d_2y^*v + m_2x^*v - d_2v^2 + m_2u(v + y^*)$ (3.9)

After that we discuss the normal form of (3.9) when $\delta = 0$.

Consider the following translation:

$\begin{pmatrix} u \\ v \end{pmatrix} = T \begin{pmatrix} \tilde{x} \\ \tilde{y} \end{pmatrix}$, where $T = \begin{pmatrix} 0 & 1 \\ \beta & \alpha \end{pmatrix}$.

Taking T^{-1} on both sides of (3.9), we get

$$\begin{pmatrix} \tilde{x} \\ \tilde{y} \end{pmatrix} \to \begin{pmatrix} \alpha & -\beta \\ \beta & \alpha \end{pmatrix} \begin{pmatrix} \tilde{x} \\ \tilde{y} \end{pmatrix} + \begin{pmatrix} \tilde{f}(\tilde{x}, \tilde{y}) \\ \tilde{g}(\tilde{x}, \tilde{y}) \end{pmatrix}, \quad (3.10)$$

where

$\tilde{f}(\tilde{x}, \tilde{y}) = \frac{\delta_2}{\beta}[\alpha c_2u^2 + (\alpha l_2 + m_2)uv - d_2v^2]$,

$\tilde{g}(\tilde{x}, \tilde{y}) = -\delta_2[c_2u^2 + l_2uv]$,

$u = \tilde{y}$ and $v = \beta\tilde{x} + \alpha\tilde{y}$.

According to Hopf bifurcation, the discriminatory quantity k is given by

$$\boldsymbol{k = -Re\left[\frac{(1-2\bar{\lambda})\bar{\lambda}^2}{1-\lambda}\varphi_{11}\varphi_{20}\right] - \frac{1}{2}\|\varphi_{11}\|^2 - \|\varphi_{02}\|^2 + Re(\bar{\lambda}\varphi_{21})}, \quad (3.11)$$

where

$$\boldsymbol{\varphi_{20} = \frac{1}{8}[\tilde{f}_{\tilde{x}\tilde{x}} - \tilde{f}_{\tilde{y}\tilde{y}} + 2\tilde{g}_{\tilde{x}\tilde{y}} + i(\tilde{g}_{\tilde{x}\tilde{x}} - \tilde{g}_{\tilde{y}\tilde{y}} - 2\tilde{f}_{\tilde{x}\tilde{y}})]},$$

$$\boldsymbol{\varphi_{11} = \frac{1}{4}[\tilde{f}_{\tilde{x}\tilde{x}} + \tilde{f}_{\tilde{y}\tilde{y}} + i(\tilde{g}_{\tilde{x}\tilde{x}} + \tilde{g}_{\tilde{x}\tilde{y}})]},$$

$$\boldsymbol{\varphi_{02} = \frac{1}{8}[\tilde{f}_{\tilde{x}\tilde{x}} - \tilde{f}_{\tilde{y}\tilde{y}} + 2\tilde{g}_{\tilde{x}\tilde{y}} + i(\tilde{g}_{\tilde{x}\tilde{x}} - \tilde{g}_{\tilde{y}\tilde{y}} + 2\tilde{f}_{\tilde{x}\tilde{y}})]},$$

$$\boldsymbol{\varphi_{21} = \frac{1}{16}[\tilde{f}_{\tilde{x}\tilde{x}\tilde{x}} + \tilde{f}_{\tilde{x}\tilde{y}\tilde{y}} + \tilde{g}_{\tilde{x}\tilde{x}\tilde{y}} + \tilde{g}_{\tilde{y}\tilde{y}\tilde{y}} + i(\tilde{g}_{\tilde{x}\tilde{x}\tilde{x}} + \tilde{g}_{\tilde{x}\tilde{y}\tilde{y}} - \tilde{f}_{\tilde{x}\tilde{x}\tilde{y}} - \tilde{f}_{\tilde{y}\tilde{y}\tilde{y}})]},$$

On solving (3.11), we obtain the value of $\boldsymbol{k}$.

Analyzing above and Hopf bifurcation [20], we write a theorem similar to [11] as below:

Theorem 3.2. *If the condition (3.8) holds,* $\boldsymbol{k \neq 0}$ *and the parameter* $\boldsymbol{\delta}$ *alters in the limited region of the point (0, 0), then the system (3.7) passes through Hopf bifurcation at the point* $\boldsymbol{B(x^*, y^*)}$. *Moreover, if* $\boldsymbol{k < 0}$ *(resp.,* $\boldsymbol{k > 0}$*), then an attracting (resp., repelling) invariant closed curve bifurcates from the fixed point* $\boldsymbol{B(x^*, y^*)}$ *for* $\boldsymbol{\delta > 0}$ *(resp.,* $\boldsymbol{\delta < 0}$*).*

IV. NUMERICAL SIMULATIONS

To verify the theoretical analysis, we draw the bifurcation diagrams, largest Lypunov exponents and phase portraits for the system (1.2). This shows the complete dynamical behavior and the global stability of prey-predator system at the fixed points. We discuss bifurcation in following cases:

Case 1: In this case, we draw the bifurcation diagram of the model (1.2) taking $\boldsymbol{a = 3.7,\ b = 1,\ c = 2,\ d = 0.9,\ l = 1, m = 0.9}$, the initial value of $\boldsymbol{(x, y) = (0.86, 0.63)}$ and $\boldsymbol{\delta}$ covering [0.5, 0.9]. From Fig. 4.1 (a), we see that from the fixed point $\boldsymbol{(1.6037, 0.4925)}$, flip bifurcation appears at $\boldsymbol{\delta = 0.6848}$ having $\boldsymbol{\gamma_1} = -7.1235$ and $\gamma_2 = 18.8$ and $(a, b, c, d, l, m) = (3.7, 1, 2, 0.9, 1, 0.9) \in F_{B1}$. It shows that the Theorem 3.1 is correct.

The phase portraits in the Fig. 4.2 shows that there are chaotic sets at $\delta = 0.79, 0.8$. Moreover, the Largest Lypunov exponents corresponding to $\delta = 0.79, 0.8$ are positive that confirm the chaotic sets.

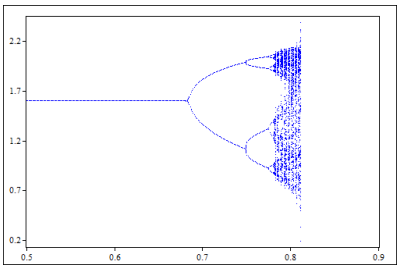

Fig.4.1.(a)

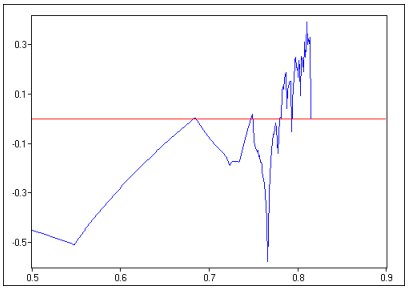

Fig. 4.1. (b)

Fig. 4.1 (a) Bifurcation diagram of system (1.2) with δ covering [0.5, 0.9], a = 3.7, b = 1, c = 2, d = 0.9, l = 1, m = 0.9, the initial value of (x, y) = (0.86, 0.63), where horizontal axis, vertical axis presents δ, x respectively. (b) Largest Lyapunov exponents related to 4.1 (a).

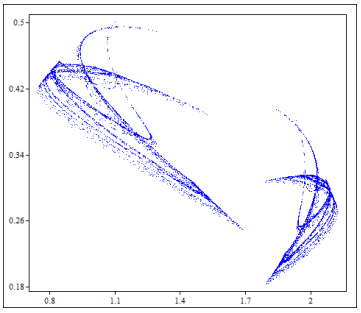

$\delta = 0.790$

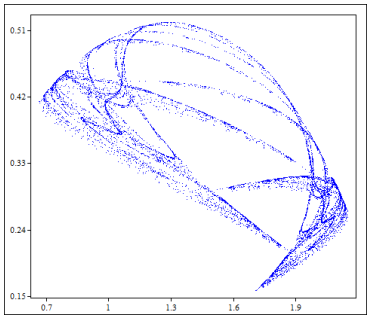

$\delta = 0.8$

Fig. 4.2. Phase portraits for several values of δ corresponding to Fig. 4.1 (a) where horizontal axis, vertical axis presents x, y respectively.

Case 2: In this case, we draw the bifurcation diagram of the model (1.2) taking $a = 1,\ b = 0.9,\ c = 0.4,\ d = 0.7,\ l = 0.5, m = 1$, the initial value of $(x, y) = (0.7, 0.3)$ and δ covering [1, 1.4]. We see from Fig. 4.3 (a) that from the fixed point $(1.4743, 0.8205)$, Hopf bifurcation emerges at $\delta = 1.2336$ with $\alpha = 0.28192$, $\beta = 0.95943$, $k = -0.3669$ and $(a, b, c, d, l, m) = (1, 0.9, 0.4, 0.7, 0.5, 1) \in H_B$. It shows that the Theorem 3.2 is accurate.

From the Fig 4.3(a), it has been observed that when $\delta < 1.2336$, the fixed point $(1.4743, 0.8205)$ of the system (1.2) is stable. At $\delta = 1.2336$ the fixed point loses its stability and as δ exceeds from 1.2336, an invariant circle generates.

The largest Lyapunov exponents in Fig. 4.3(b) shows that for the parameter $\delta \in (1, 1.2336)$, the Lyapunov exponents are negative. For $\delta \in (1.2336, 1.34200)$, some Lyapunov exponents are positive and some negative, it means that there exist stable period windows in chaotic region.

The phase portraits in Fig. 4.4, shows that a smooth invariant circle bifurcates from the fixed point $(1.4743, 0.8205)$. There appears an invariant circle for some values of δ and its radius becomes larger with the growth of δ e.g. when δ varies from 1.2336 to 1.23787. There appears a closed curve for some values of δ and its shape changes with the growth of δ e.g. when δ varies from 1.25123 to 1.342.

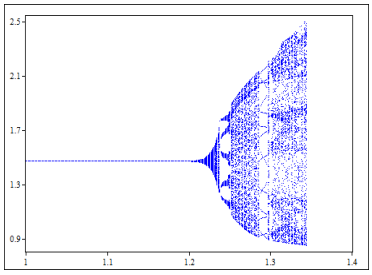

Fig. 4.3(a)

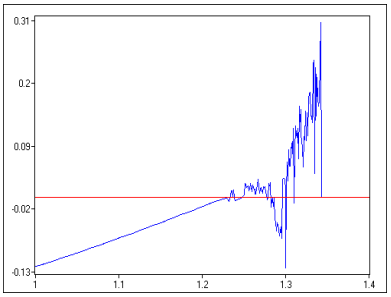

Fig. 4.3(b)

Fig. 4.3(a) Bifurcation diagram of system (1.2) with δ covering [1, 1.4], a = 1, b = 0.9, c = 0.4, d = 0.7, l = 0.5, m = 1 the initial value of (x, y) = (0.7, 0.3), where horizontal axis, vertical axis presents δ, x respectively. (b) Largest Lyapunov exponents related to (a).

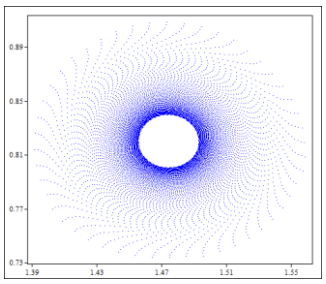

δ = 1.2336

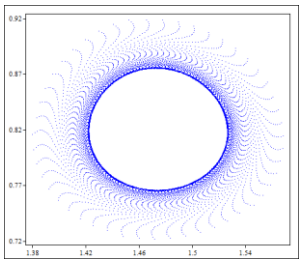

δ = 1.2378

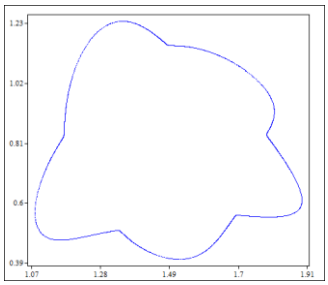

δ = 1.25123

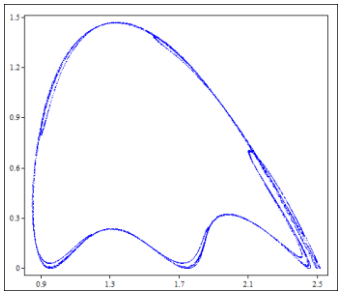

$\delta = 1.342$

Fig. 4.4. Phase portraits for several values of δ related to Fig. 4.3 (a) where horizontal axis, vertical axis presents x, y respectively.

V. CONCLUSIONS

In this paper, we investigated the dynamical behaviors of discrete-time prey-predator model in the closed first quadrant R_+^2. Global stability of the model at the fixed points has been discussed. The map undergoes flip bifurcation and Hopf bifurcation at the fixed point under specific conditions, when δ varies in small neighbourhood of F_{B1}or F_{B2} and H_B . Numerical simulations display cascade of period doubling bifurcation, chaotic sets in case of flip bifurcation, and smooth invariant circle and closed curves in case of Hopf bifurcation. The complexity of dynamical behaviors is confirmed by computation of Lyapunov exponents.

Further, Liu et al. [19] for corresponding continuous predator-prey model concluded that the system is globally asymptotically stable under certain conditions, whereas we observed that the discrete system has a rich and complex dynamical behavior than the continuous system.

REFERENCES

[1] A.J. Lotka, Elements of Physical Biology, Williams and Wilkins, Baltimore, 1925.
[2] V. Volterra, Fluctuations in the abundance of species considered mathematically, Nature 118 (1926) 558–560.
[3] A.A. Berryman, The origins and evolution of predator–prey theory, Ecology 73(5) (1992) 1530-1535.
[4] R.M. May, Stability and Complexity in Model Ecosystems, Princeton University Press, Princeton, NJ, 1973.
[5] R.P. Agarwal, Difference Equations and Inequalities: Theory, Method and Applications, Monogr. Textbooks Pure Appl. Math., Vol. 228, Dekker, New York, 2000.
[6] R.P. Agarwal, P.J.Y. Wong, Advance Topics in Difference Equations, Kluwer Acad. Publ., Dordrecht, 1997.
[7] H.I. Freedman, Deterministic Mathematics Models in Population Ecology, Dekker, New York, 1980.
[8] J.D. Murray, Mathematical Biology, Springer-Verlag, New York, 1989.
[9] C. Celik, O. Duman, Allee effect in a discrete-time predator-prey system, Chaos, Sol. and Frac. 40 (2009) 1956-1962.
[10] K. Gopalsamy, Stability and Oscillation in Delay Differential Equations of Population Dynamics, Mathematics and its Applications, Kluwer Acad. Publ., Dordrecht, 74 (1992).
[11] X. Liu, D. Xiao, Complex dynamic behaviors of a discrete-time predator-prey system, Chaos, Sol. and Frac. 32 (2007), 80-94.
[12] Y. Chen, S. Changming, Stability and Hopf bifurcation analysis in a prey–predator system with stage-structure for prey and time delay, Chaos, Sol. and Frac.38 (4) (2008) 1104–1114. [13] X. Liu, D. Xiao, Complex dynamic behaviors of a discrete-time predator–prey system, Chaos, Sol. and Frac. 32 (2007) 80–94.
[13] Z. Hu, Z. Teng, L. Zhang, Stability and bifurcation analysis of a discrete predator–prey model with nonmonotonic functional response, Nonlinear Anal.: Real World Appl. 12 (2011) 2356–2377.
[14] C.H. Zhang, X.P. Yan, G.H. Cui, Hopf bifurcations in a predator-prey system with a discrete delay and a distributed delay, Nonlinear Anal.: Real World Appl. 11 (2010) 4141-4153.
[15] Z. Jing, J. Yang, Bifurcation and chaos in a discrete-time predator-prey system, Chaos, Sol. and Frac. 27(2006), 259-277.
[16] Z. He, X. Lai, Bifurcation and chaotic behavior of a discrete-time predator–prey System, Nonlinear Anal.: Real World Appl. 12 (2011) 403–417.
[17] S. Gakkhar, A. Singh, Complex dynamics in a prey predator system with multiple delays, Commun. Nonlinear Sci. Numer. Simulat., 17 (2012) 914-929.
[18] M. Liu and K. Wang. Persistence, extinction and global asymptotical stability of a non-autonomous predator–prey model with random perturbation. Applied Mathematical Modelling, 36(11):5344–5353, 2012.
[19] J. Guckenheimer, P. Holmes, Nonlinear oscillations, dynamical system and bifurcation of vector fields, Springer-Verlag, New York, 1983.